

MODERN ASPECTS OF ELECTROCHEMISTRY

No. 16

Edited by

B. E. CONWAY

*Department of Chemistry
University of Ottawa
Ottawa, Ontario, Canada*

RALPH E. WHITE

*Department of Chemical Engineering
Texas A&M University
College Station, Texas*

and

J. O'M. BOCKRIS

*Department of Chemistry
Texas A&M University
College Station, Texas*

PLENUM PRESS • NEW YORK AND LONDON

The Library of Congress cataloged the first volume of this title as follows:

Modern aspects of electrochemistry. no. [1]

Washington, Butterworths, 1954-

v. illus., 23 cm.

No. 1-2 issued as Modern aspects series of chemistry.

Editors: no. 1- J. Bockris (with B. E. Conway, No. 3-)

Imprint varies: no. 1, New York, Academic Press.—No. 2, London , Butterworths.

1. Electrochemistry—Collected works. I. Bockris, John O'M. ed. II. Conway, B. E. ed. (Series: Modern aspects series of chemistry)

QD552.M6

54-12732 rev

ISBN 0-306-42024-4

©1985 Plenum Press, New York
A Division of Plenum Publishing Corporation
233 Spring Street, New York, N.Y. 10013

All rights reserved

No part of this book may be reproduced, stored in a retrieval system, or transmitted, in any form or by any means, electronic, mechanical, photocopying, microfilming, recording, or otherwise, without written permission from the Publisher

Printed in the United States of America

LIST OF CONTRIBUTORS

BRIAN E. CONWAY
Department of Chemistry
University of Ottawa
Ottawa, Ontario K1N 9B4, Canada

S. EFRIMA
Department of Chemistry
Ben-Gurion University of The Negev
Beer-Sheva, Israel 84105

YU. YA. GUREVICH
A. N. Frumkin Institute of Electrochemistry
Academy of Sciences of the USSR
Moscow, USSR

A. HAMELIN
Laboratoire d'Electrochimie Interfaciale du CNRS
92195 Meudon Cedex, France

YU. V. PLESKOV
A. N. Frumkin Institute of Electrochemistry
Academy of Sciences of the USSR
Moscow, USSR

HALINA S. WROBLOWA
Ford Motor Company
Scientific Research Laboratory
Dearborn, Michigan 48121

HOWARD L. YEAGER
Department of Chemistry
University of Calgary
Calgary, Alberta T2N 1N4, Canada

RICHARD S. YEO
Pinnacle Research Institute
Cupertino, California 95014

Preface

This volume of the *Modern Aspects of Electrochemistry* series contains six chapters: four are on topics of current fundamental interest in the subject and two deal with more technological aspects of electrochemistry.

In Chapter 1, Antoinette Hamelin deals with the topic of characterization of the double layer at well-defined single-crystal faces of solid metals. She also gives valuable instructions for the preparation and characterization of single-crystal faces of known orientation and index which will be very useful to many workers in this field, especially those who are just entering it as novices or to those whose crystals are not always too accurately characterized! Most of the work reported is concerned with crystal faces of gold and silver which this author has specialized in studying. It is her work in recent years that has taken experimental studies of double-layer behavior well beyond the conventional area of research at liquid mercury.

Chapter 2, by B. E. Conway, deals with a curious fundamental but hitherto little-examined problem in electrode kinetics: the real form of the Tafel equation with regard to the temperature dependence of the Tafel-slope parameter b , conventionally written as ' $b = RT/\alpha F$ ', where α is a transfer coefficient. He shows, extending his 1970 paper and earlier works of others, that this form of the relation for b rarely represents the experimental behavior for a variety of reactions over any appreciable temperature range. Rather, b is of the form $RT/(\alpha_H + \alpha_S T)F$ or $RT/\alpha'F + K$, where α_H and α_S are enthalpy and entropy components of the transfer coefficient (or symmetry factor for a one-step electron transfer reaction), and K is a temperature-independent parameter, the apparent limiting

value of b for some systems at $T = 0$. These forms for b , required by the observed experimental behavior, imply that fundamental aspects of the charge transfer and activation process in electrode reactions are not at all fully understood yet. This chapter deals with various possible interpretations of the observed T dependence of b , including the topic of potential dependence of the *entropy* of activation of electrode processes.

The electrochemistry of semiconductors has played a major part in the development of modern electrochemistry, especially in recent years with regard to photoelectrochemical energy conversion using illuminated semiconductor electrodes. Drs. Pleskov and Gurevich of the Institute of Electrochemistry, Moscow, contribute an important chapter (3) on "New Problems and Prospects" in this field. Readers will find that their chapter gives a thorough account of the current directions of development in this field, as well as some of the difficulties and new areas of research in this subject.

Surface-enhanced Raman scattering has been regarded, in some ways, as the spectroscopic "Godsend" to electrochemists trying to characterize submonolayer quantities of adsorbates at electrode interfaces. Professor S. Efrima presents, in Chapter 4, a monumental and thoroughly referenced survey of the vast literature on this topic that has grown in the past 14 years or so. He presents a "personal view" of this intriguing and often controversial subject, and attempts to distil out for the electrochemist what is of quantitative significance in the many contributions that have been made on this topic. He concludes by critically reviewing the various, not always mutually exclusive, theories of the origin of the SERS effect.

Dr. Halina S. Wroblowa, in Chapter 5, gives a valuable comparative account of the current state of the art in development of batteries for vehicular transportation. The Laboratory at Ford, through Kummer, has been the "prime mover" in high-energy and power-density battery development, especially in the field of sodium-sulfur battery systems. Dr. Wroblowa herself has, for some years, been an active researcher in this field at Ford, so she brings to bear on this topic substantial experience and an authentic critical judgment of the viability of various systems that have been engineered over the past 10-15 years, including the latest developments.

The volume ends with a chapter on "Structural and Transport Properties of Perfluorinated Ion-Exchange Membranes" by Dr. Richard S. Yeo and Professor Howard L. Yeager. The development of such membranes has revolutionized the electrochemical technology of the chlorine-caustic industry and also has been of great value in the engineering of water electrolyzers, organic preparation cells and some designs of fuel cells. This chapter is not only of technological interest in the above areas but deals in some detail with fundamental problems of ion association, aggregation, membrane structure and ion transport in the solution-invaded, locally hydrophobic medium which these polymers provide in membranes.

University of Ottawa
Texas A&M University
Texas A&M University

B. E. Conway
Ralph E. White
J. O'M. Bockris

Contents

Chapter 1

DOUBLE-LAYER PROPERTIES AT *sp* AND *sd* METAL SINGLE-CRYSTAL ELECTRODES

A. Hamelin

I. Introduction	1
II. Historical	3
III. Structure of Metals	4
1. Basis of Crystallography	4
2. The Stereographic Projection	6
3. Determination of Crystallographic Orientation	10
4. Models of Crystal Surfaces	15
5. Structure of Metal Surfaces	23
IV. Preparation of Single-Crystal-Face Electrodes	28
1. Growing Single Crystals	28
2. Cutting the Crystal	32
3. Polishing and Isolating the Face of Interest	33
4. Final Surface Preparation	36
5. <i>Ex Situ</i> Check of State of Electrode Surface	37
6. <i>In Situ</i> Check of State of Electrode Surface	38
V. Electrochemical Results	43
1. The pzc's	45
2. The Solution Side of the oHp	50
3. The Metal Side of the oHp	58
4. The Roughness Factor	94
5. Conclusions	96
References	98

Chapter 2

THE TEMPERATURE AND
POTENTIAL DEPENDENCE OF
ELECTROCHEMICAL REACTION RATES, AND
THE REAL FORM OF THE TAFEL EQUATION

Brian E. Conway

I.	Introduction	103
	1. Scope and Significance of this Article	103
	2. Preliminary Definitions	104
	3. The Tafel-Slope Parameter b	106
II.	Origin of Potential Dependence of Electrochemical Reaction Rates and the Conventional Role of Tem- perature	107
	1. Theoretical Representations of Rates of Electrode Processes	107
	2. Relation of β to α	115
III.	The Experimental Situation Regarding the Temperature Dependence of Tafel Slopes	116
	1. General Remarks	116
	2. Documentation and Examples of the Experimentally Observed Dependence of b on T and the Behavior of α with T	117
IV.	Theoretical Discussion	132
	1. Interpretation of the Case Where α is Proportional to T	132
	2. General Case	134
	3. A Question About the Electrical Energy Term βVF in the Rate Equation	135
	4. Temperature-Dependent Orientation of Solvent Dipoles in the Inner Region of the Double Layer and the Entropy of Activation	138
	5. Tafel Slopes and Proton Tunneling	143
	6. Behavior of α with Temperature on the Basis of Electron and Particle Transfer Treatment of Ulstrup	147
	7. Nonlinear Potential Dependence of Electrochemical Reaction Rates	148

8. Expansion of the Helmholtz Layer with Temperature	155
9. Effects of Specific Adsorption of Anions	156
10. Tafel Slopes for Reactions Proceeding in Multistep Pathways	160
11. Tafel Slopes in Relation to Exchange Current Densities i_0	164
12. Electrode Area and Tafel Slopes	167
V. Problems with Evaluation of Heats of Activation When α is Temperature Dependent	168
1. Derivation of the Apparent Heat of Activation at the Reversible Potential	168
2. α and the Relation between Real and Apparent Heats of Activation	175
3. Experimental Evidence for the Potential Dependence of the Entropy of Activation, ΔS^\ddagger	178
VI. Conclusions and Final Remarks	182
References	185

Chapter 3

ELECTROCHEMISTRY OF SEMICONDUCTORS: NEW PROBLEMS AND PROSPECTS

Yu. V. Pleskov and Yu. Ya. Gurevich

I. Introduction	189
II. Characteristic Energy Levels in the Electrode/Electrolyte Solution System	190
1. The Electrochemical Potential of Electrons in the Solution Containing a Redox Couple	191
2. Relationship between the Energy Scale and the Scale of Electrode Potentials	196
3. Determination of the Reorganization Energy of a Solvent	199
III. Specific Features of the Structure of the Semiconductor/Electrolyte Interface	201
1. The Electrical Double-Layer Model	201

2. Potential Distribution: "Pinning" of Band Edges and/or the Fermi Level at the Surface	206
3. Determination of the Flat-Band Potential	210
IV. Quasithermodynamic Approach to the Description of Photoelectrochemical Processes	216
1. Quasi-Fermi Levels	216
2. Description of the Most Important Types of Photoelectrochemical Reactions	218
3. Photocorrosion and Stability	228
4. The Limits of Applicability of the Quasi-Fermi Level Concept in Photoelectrochemical Kinetics: Alternative Approaches	232
V. New Applications	236
1. Photoelectrochemical Conversion of Solar Energy	236
2. Laser Etching of Semiconductors	239
3. The Ion-Selective Field-Effect Transistor	243
4. Characterization of Semiconducting Materials	245
VI. Concluding Remarks	245
References	247

Chapter 4

SURFACE-ENHANCED RAMAN SCATTERING (SERS)

S. Efrima

I. Introduction	253
II. SERS Experimental Studies	255
1. Estimate of the Enhancement Factor	256
2. Surface Preparation	271
3. Some Molecules and SERS Behavior	291
4. Metals (or Solids) which Exhibit SERS	307
5. Excitation Profiles	312

III. Theoretical Models of SERS	322
1. General	322
2. Resonance Models (RE)	325
3. Electric Field and Emission Enhancement Mechanisms (LFE)	336
4. Dyes in SERS—Theory	344
IV. What is “the” SERS Mechanism?	348
1. General	348
2. “The” SERS Mechanism	349
V. SERS—A Useful Tool	350
References	357

Chapter 5

BATTERIES FOR VEHICULAR PROPULSION

Halina S. Wroblowa

I. Introduction	371
1. General Remarks	371
2. Battery Classification	372
II. EV Battery Requirements	373
1. Performance-Related Requirements	375
2. Cost-Related Requirements	384
3. Safety and Environmental Impact	389
III. Characteristics of Individual Systems	391
1. The Lead/Acid Battery	391
2. The Nickel-Iron Battery	396
3. Zinc Batteries	399
4. High-Temperature Batteries	409
5. Rechargeable Lithium Batteries	417
6. Conducting Polymer Systems	418
7. Metal-Air Batteries	420
IV. Comparative EV Battery Characteristics	423
References	427

Chapter 6

STRUCTURAL AND TRANSPORT PROPERTIES OF
PERFLUORINATED ION-EXCHANGE MEMBRANES

Richard S. Yeo and Howard L. Yeager

I. Introduction	437
1. Historical Background of Ion-Exchange Membrane Cells	437
2. Requirements of High-Performance Membranes	438
3. Development of Perfluorinated Ionomer Membranes	439
4. Types of Applications	440
5. The Scope of this Review	441
II. Microstructure	441
1. Structural Studies of Ionomers	441
2. Eisenberg's Theory	443
3. Ions in Perfluorinated Ionomers	445
4. Structural Models of Nafion	447
5. Solvation Phenomena	450
III. Ion and Water Diffusion	459
1. Diffusional Properties in Dilute Solution Environments	460
2. Diffusion Properties in Concentrated Solution Environments	465
IV. Transport Properties under Industrial Electrolysis Conditions	470
1. Characteristics of Perfluorinated Chlor-Alkali Membranes	471
2. Membrane Permselectivity in a Chlor-Alkali Cell	472
3. Interpretation of Permselectivity as a Function of Membrane Properties and Cell Parameters	475
V. Conductivity and Permeability in Membranes	479
1. Conductivity in Pure Water—Solid Polymer Electrolyte Systems	480
2. Conductivity in Acidic Electrolytes	482
3. Conductivity in Alkaline Electrolytes	485
4. Conductivity of Nafion in Protic Solvents	489

Contents

xv

5. Permeation of Molecular Species	490
VI. Conclusion	496
References	497
<i>Index</i>	505

Double-Layer Properties at *sp* and *sd* Metal Single-Crystal Electrodes

A. Hamelin

*Laboratoire d'Electrochimie Interfaciale du CNRS,
92195 Meudon Cedex, France*

I. INTRODUCTION

Writing such a chapter on solid metal electrodes is a challenge when, at every moment, the latest developments of surface science give rise to new possibilities and new results in this area of electrochemistry. However, an attempt will be made to give an "up-to-date snapshot" of the state of affairs for the double layer at single-crystal electrodes of metals which are not of the transition series.

Already in this *Modern Aspects of Electrochemistry* series the theory and status of data for electrochemical double layers (dl) were detailed,¹⁻³ but the sections devoted to results obtained with solid electrodes and their discussion were brief. Some aspects of the dl on polycrystalline metals, such as the potential of zero charge (pzc), were described.⁴ In this series a chapter was also devoted to the metal-gas interface⁵; certainly the comparison of this interface with that at an electrode is fruitful, although the local electric field in the latter case can be varied far more easily.

Other basic books have dealt with dl properties without giving extensive discussion of the dl at solid electrodes.⁶⁻⁹ Although at the end of the 1960s and beginning of the 1970s some reliable results had been obtained on polycrystalline metals, their analysis suffered from the uncontrolled complexity of the surface structure.

This can be easily understood: When a potential is applied to an electrode the surface is an equipotential but the different grains (of different structures) at the surface have different densities of charge; e.g., for a given potential the density of charge can be zero for certain patches of the electrode, positive for others, and negative for other ones (as long as the patches are large enough to create their own local electrochemical dl).

It will be useful to emphasize the practical aspects of the problem which are twofold: the solution side and the metal side. On the solution side at the interphase, a level of impurities which does not interfere with dl measurements over the time scale of a mercury-drop lifetime, which is 4 s, could completely hinder observations of significant current-potential curves [$i(E)$] or meaningful differential capacity-potential curves [$C(E)$] at a solid metal electrode which will stay 2, 3, or 4 h in the same solution. Not only must the water, salts, and glassware be kept clean, but also the gas used to remove oxygen and the tubing for the gas. Of course, conditions are less drastic for studies of strong adsorption than in the case of no adsorption; also bacteria develop less in acid solutions than in neutral ones (which cannot be kept "uncontaminated" more than one or two days). This aspect will not be discussed in this chapter.

The metal side of the electrochemical interphase must also be rigorously controlled. For crystal faces, this includes not only the chemical state but also the physical state of the top layers of atoms at the surface (layers: 0, 1, 2 at least). Each metal brings specific difficulties—e.g., one oxidizes in air, another does not; one has a low melting point, another a high melting point; one is hard, another is soft, etc. Practical requirements which are satisfactory for one metal are not necessarily valid for another one. This aspect of the problem is the subject of this chapter.

Both sides of the interface must be rigorously clean for observations of the dl. The beginner will ask, "How can I know that my interphase is clean?" He or she will be able to answer this question by: observation of the $i(E)$ curve in the dl range of potential; observation of the contribution of the diffuse part of the dl on the $C(E)$ curves in dilute solutions (in the case of no specific adsorption); comparison of the $i(E)$ and $C(E)$ curves; observing the stability of these two curves; etc. Comparison with the results

published for polycrystalline electrodes of one metal gives indications of what should be observed at faces of this metal (as long as they were obtained with great care). Furthermore, as *ex situ* and nonelectrochemical *in situ* methods become increasingly available in laboratories, they will contribute to the control and understanding of the electrochemical interphase.

II. HISTORICAL

A review paper¹⁰ published in 1983 gives all references for dl work at *sp* and *sd* metal faces up to July 1982, since then, numerous other papers were published.

As in any rapidly developing field, many publications can claim little more than being the first to examine such faces of a particular metal in given conditions. All publications except one (Ref. 11) deal with results obtained in the aqueous solvent; all publications except two (Refs. 12 and 13) deal with results obtained at room temperature. Faces of only seven nontransition metals were studied (Ag, Au, Cu, Zn, Pb, Sn, and Bi). Only for gold has a large number of high-index faces been studied in order to give a general view of the influence of the crystallographic orientation (*co*) of the electrode surface; these faces are distributed only on the three main zones of the unit projected stereographic triangle (see Section III.2), so it would be interesting to make faces having *co*'s which are inside this triangle.

From 1956 to the end of the 1960s dl properties were studied by conventional electrochemical methods, but during the last decade a number of results obtained by optical measurements or other physical methods were published. It is sometimes difficult to determine whether a paper pertains to the study of dl properties or to the study of the metal surface properties in the presence of the electrochemical dl. All are of interest to electrochemists who work with metal faces.

Anyway, experimental results on well-defined faces of non-transition metals are more and more numerous every year; their understanding is related to the theories developed not only from results obtained on mercury but also from knowledge of solid surfaces.

III. STRUCTURE OF METALS

1. Basis of Crystallography

The essential characteristic of a single crystal is the periodic nature of its structure. Its atomic structural arrangement can be related to a network of points in space called the *lattice*. The coordinates of a given point in a lattice (or atom in a structure) are referred to as the crystal axes, for instance, for the cubic system, axes at right angles to each other. Seven different systems of axes are used in crystallography and there are seven crystal systems. The axes form the edges of a parallelepiped called the *unit cell* which is the fundamental building block of the crystal. The unit cell has a definite atomic arrangement with lattice points at each corner and, in some cases, lattice points at the center of the face or at the center of the volume.

Most of the metals crystallize in the cubic system (face centered, body centered). Zn and Cd crystallize in the hexagonal system, Bi in the rhombohedral system, and Sn in the tetragonal system. In this chapter emphasis will be placed on the cubic system, for Au, Ag, Cu, Pb, and so forth, are face-centered-cubic metals (fcc).

Miller indices are universally used as a system of notation for faces of a crystal. The orientation of the plane of a face is given relative to the crystal axes and its notation is determined as follows:

1. Find the intercepts on the axes.
2. Take their reciprocals.
3. Reduce to the three (or four for the hexagonal close-packed (hcp) system[†]) smallest integers having the same ratio.
4. Enclose in parentheses, e.g., (hkl) .

All parallel planes have the same indices. Negative intercepts result in indices indicated with a bar above. Curly brackets signify a family of planes that are equivalent in the crystal—the six different

[†] A system of rectangular axes could also be used for hcp structure; a four-axes system is preferred where three axes are drawn on the basal hexagon and the fourth axis perpendicularly. Therefore, four Miller indices are necessary to give the position of a plane: $\{0001\}$ is the basal plane, $\{1\bar{1}00\}$ the prism plane, and the third apex of the unit projected stereographic triangle (see Section III.2) is $\{11\bar{2}0\}$.

faces of a cube, for instance, or the family of planes $\{110\}$ which is

$$\{110\} = (110) + (011) + (101) + (\bar{1}10) + (1\bar{1}0) + (0\bar{1}1) \\ + (01\bar{1}) + (10\bar{1}) + (\bar{1}01) + (\bar{1}\bar{1}0) + (\bar{1}0\bar{1}) + (0\bar{1}\bar{1})$$

All these planes have the same atomic configuration. For pure metals the high level of symmetry allows us to write indifferently parentheses or curly brackets. The Miller indices of some important planes of the cubic and the hexagonal close-packed systems are given in Fig. 1.

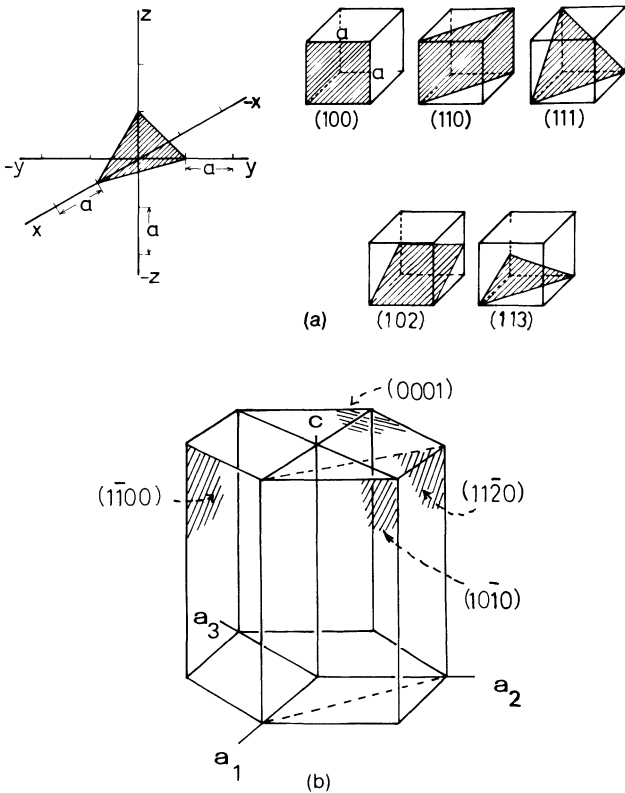


Figure 1. (a) The three rectangular axes and the (111) plane for the cubic system. Some important planes and their Miller indices for the cubic system are shown. (b) The four axes and some important planes for the hexagonal close-packed system.

Any two nonparallel planes intersect along a line; they are planes of a *zone* and the direction of their intersection is the zone axis. A set of crystal planes which meet along parallel lines is known as planes of a zone. The important zones in a crystal are those to which many different sets of planes belong. On a crystal the faces of a zone form a belt around the crystal. Zones are useful in interpreting X-ray diffraction patterns (see Section III.3). Zones are denoted $[hkl]$.

For a detailed study of Section III, the reader can refer to a universally accepted textbook—Reference 14.

2. The Stereographic Projection

The angular relationships among crystal faces (or atomic planes) cannot be accurately displayed by perspective drawings; but if they are projected in a stereographic way they can be precisely recorded and then clearly understood.

Let us assume a very small crystal is located at the center of a reference sphere (atomic planes are assumed to pass through the center of the sphere). Each crystal plane within the crystal can be represented by erecting its normal, at the center of the sphere, which pierces the spherical surface at a point known as the *pole* of the

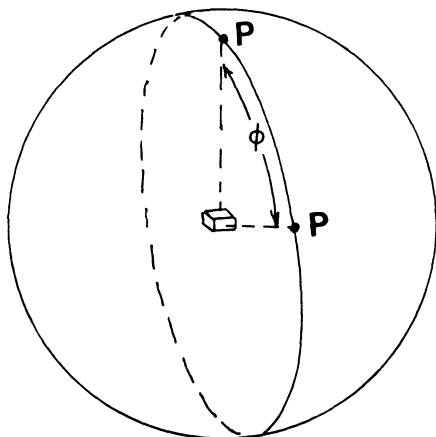


Figure 2. Angle ϕ between two poles measured on a great circle.

plane. The angle between any two planes is equal to the angle between their poles measured on a great circle of the sphere (in degrees) as in Fig. 2.

As it is inconvenient to use a spherical projection to determine angles among crystal faces or angular distances of planes on a zone, a map of the sphere is made, so that all work can be done on flat sheets of paper.

The simple relation between the reference sphere and its stereographic projection (its map) is easily understood, by considering the sphere to be transparent and a light source located at a point on its surface (see Fig. 3). The pattern made by the shadows of the poles which are on the hemisphere opposite to the light source, falls within the basic circle shown on the figure. The other hemisphere will project outside the basic circle and extend to infinity. To represent the whole within the same basic circle the light source is put on the left and the screen tangent to the sphere on the right side; the points of this latter hemisphere are distinguished from those of the first by a notation such as plus and minus. All plotting can be done by trigonometric relationships directly on graph paper.

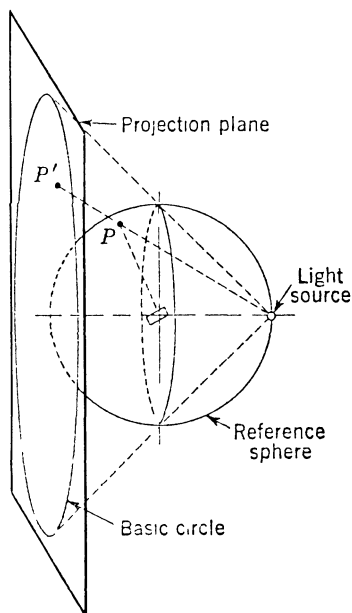


Figure 3. Stereographic projection. Pole P of the crystallographic plane projects to P' on the projection plane (Ref. 14).

The projection of the net of latitude and longitude lines of the reference sphere upon a plane forms a stereographic net—the Wulff net (Fig. 4). The angles between any two points can be measured with this net by bringing the points on the same great circle and counting their difference in latitude keeping the center of the projection at the central point of the Wulff net.

Stereographic projections of low-index planes in a cubic crystal and in a hcp crystal are given in Fig. 5. Only one side of the projection is visible; thus it must not be forgotten that “below” (001) there is (00 $\bar{1}$), “below” the planes of the {111} family represented on Fig. 5a there are the ($\bar{1}\bar{1}\bar{1}$), ($1\bar{1}\bar{1}$), ($11\bar{1}$), and ($\bar{1}1\bar{1}$) planes, and so on for other families of planes. This fact must be kept in

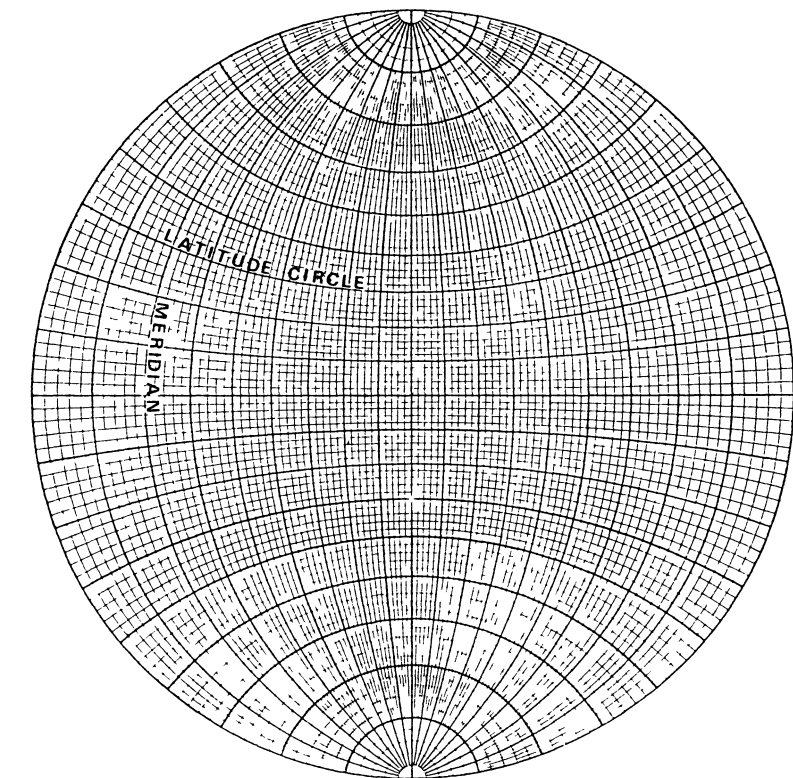


Figure 4. Stereographic net, Wulff or meridional type, with 2° graduation (Ref. 14).

mind when assessing the faces to simulate an “ideal” polycrystalline surface from three or more families of faces.¹⁵

For electrochemists using single-crystal electrodes, the high level of symmetry of the crystal of pure metals allows all types of planes to be represented on a single triangle—the *unit projected stereographic triangle*. The co of a face is represented by a single point; therefore the azimuthal orientation is not specified. When important, the azimuth is added; it is denoted $[hkl]$. Any co can be represented on the unit projected triangle; this is done for faces of high indices on a figure presented in Section III.4.

Some of the most important angles between the faces are given in Table 1.

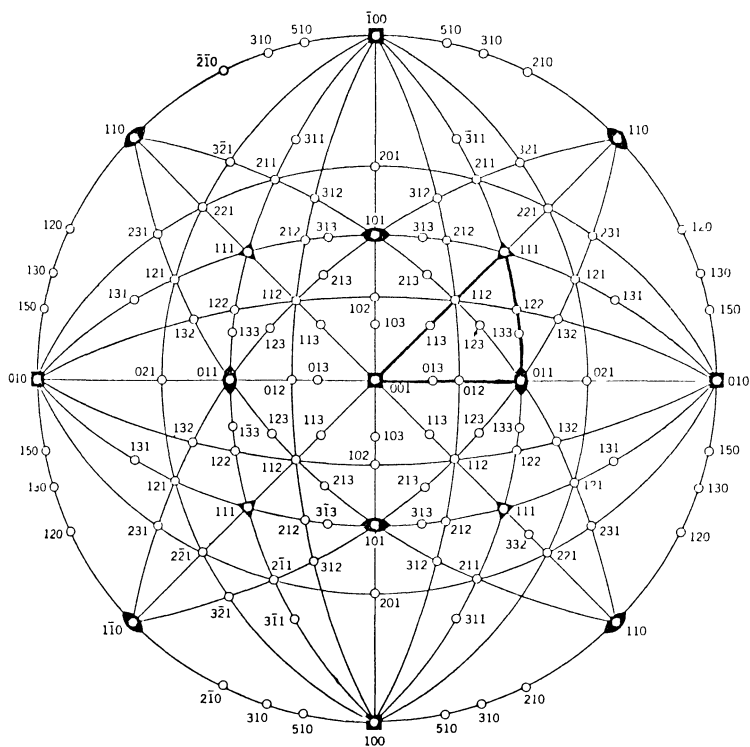


Figure 5 (a) Standard (001) stereographic projection of poles and zones circles for cubic crystals (after E. A. Wood, *Crystal Orientation Manual*, Columbia Univ. Press, New York, 1963).

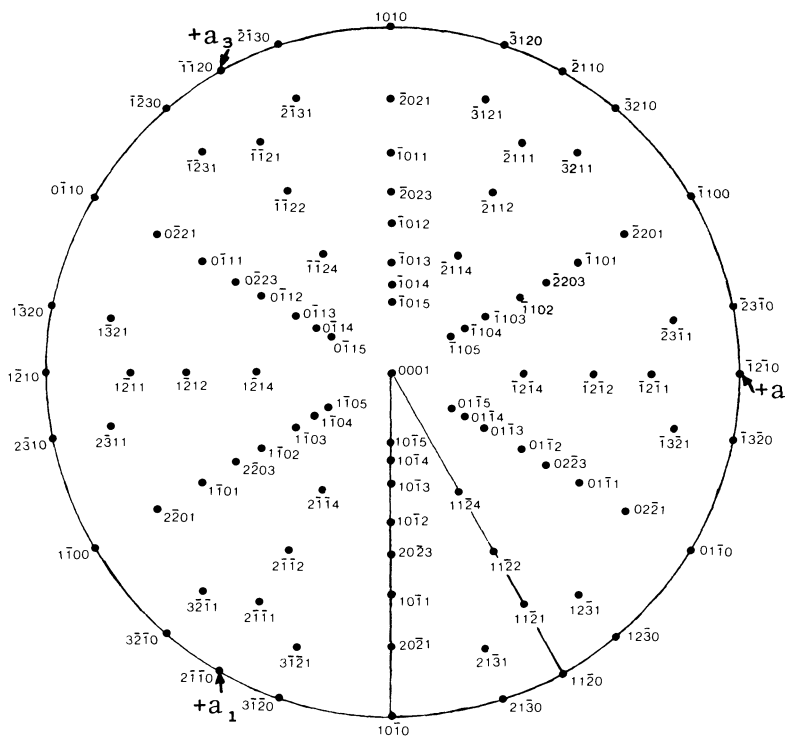


Figure 5. (b) Standard (0001) projection for zinc (hexagonal, $c/a = 1.86$) (Ref. 14).

3. Determination of Crystallographic Orientation

The diffraction of X-rays by a crystal, i.e., by a three-dimensional grating, is analogous to the diffraction of light by a one-dimensional grating. When the incident and scattered rays make equal angles with the atomic plane there is reinforcement—the atomic plane behaves like a mirror that is reflecting a portion of the X-rays. The geometry of the lattice determines entirely the direction of the reflected beams, i.e., the reflected beams are governed by the distribution of atoms within the unit cell following Bragg's law and the Laue equations.¹⁴

By using these principles the electrochemist has only to find out the co of a piece of metal which was recognized as being an

Table 1
Symmetries and Angular Specifications of Principal Index Faces of Single Crystals

Face of reference	(100)			(111)			(101)		
Symmetry of the spots around this face	Fourfold			Threefold			Twofold		
Angles between the zones intersecting at this face	$[0\bar{1}0][0\bar{1}1] = 45.00^\circ$ $[0\bar{1}0][0\bar{3}1] = [001][0\bar{1}3] = 18.30^\circ$ $[0\bar{1}0][0\bar{2}1] = [001][0\bar{1}2] = 26.56^\circ$			$[10\bar{1}][01\bar{1}] = 60.00^\circ$ $[10\bar{1}][21\bar{3}] = [01\bar{1}][12\bar{3}] = 19.10^\circ$ $[10\bar{1}][11\bar{2}] = 30.00^\circ$			$[010][\bar{1}01] = 90.00^\circ$ $[010][\bar{1}41] = 19.46^\circ$ $[\bar{1}01][\bar{3}23] = [010][\bar{1}31] = 25.23^\circ$ $[\bar{1}01][\bar{1}11] = [010][\bar{1}21] = 35.26^\circ$ $[\bar{1}01][\bar{3}13] = 13.26^\circ$		
	$[0\bar{1}0]$	$[0\bar{1}1]$	$[0\bar{3}1]$	$[10\bar{1}]$	$[01\bar{1}]$	$[11\bar{2}]$	$[\bar{1}01]$	$[010]$	$[\bar{1}11]$
Angles between the face of reference and the low-index faces or the low-index zones	601 9.46°	711 11.41°	913 19.36°	545 5.76°	655 5.03°	534 11.53°	717 5.76°	605 5.18°	817 6.41°
	501 11.31°	611 13.26°	813 21.58°	323 10.03°	433 7.96°	957 13.13°	515 8.05°	403 8.13°	615 8.95°
	401 14.03°	511 15.78°	713 24.30°	535 12.27°	755 9.45°	423 15.23°	414 10.13°	302 11.31°	514 10.90°
	301 18.43°	411 19.46°	613 27.80°	212 15.80°	322 11.41°	735 18.08°	727 11.41°	503 14.05°	413 13.95°
	502 21.80°	311 25.26°	513 32.30°	737 18.41°	533 14.41°	312 22.20°	313 13.26°	201 18.43°	312 19.10°
	201 26.56°	733 31.21°	413 38.50°	525 19.46°	955 16.58°		525 15.80°	703 21.80°	523 23.41°
	503 30.85°	211 35.26°		313 22.00°	211 19.46°		737 16.86°	502 23.20°	734 25.28°
	302 33.41°	533 41.08°		515 27.21°	733 23.51°		212 19.46°	301 26.40°	211 30.00°
	705 35.51°	322 43.31°		101 35.26°	311 29.50°		535 22.98°	401 30.96°	
	403 36.86°	755 45.28°					323 25.23°	501 33.68°	
	605 39.81°	433 46.66°						601 35.53°	
	101 45.00°	111 54.73°						100 45.00°	

individual crystal (see Section IV.2); the metal crystal system and the crystal parameters can then be found in handbooks.

The most convenient method for determining the *co* of an individual crystal is the *back-reflection Laüe method*. This method requires only simple equipment: the crystal is positioned in a goniometer head (or any instrument which provides adjustable orientation) and a flat X-ray film in a lightproof holder is mounted normal to the X-ray beam. The film must be at a precise distance R from the crystal (3, 6, or 12 cm) (Fig. 6).†

The interpretation of the photograph obtained after about 20 min, is carried out‡ by making use of a chart developed by Greninger¹⁶ (Fig. 7), a standard projection of the crystal system (Fig. 5 for the cubic system), and a table of the angles between the different faces (Table 1 for the cubic system).

For planes in a given zone, which form a belt around the crystal, a cone of reflected X-rays cuts the film along a hyperbola. The closest approach of the hyperbola to the center of the film is equal to $R \tan 2\phi$, where ϕ is the angle of inclination of the zone axis (to the plane of the film). When the zone axis is parallel to the film the hyperbola degenerates into a straight line passing through the center of the film. A back-reflection pattern of a fcc crystal (gold) is shown in Fig. 8. The circle at the center is due to the punched hole necessary for the pinhole collimator of the incident X-ray beam. The spots on one row (a hyperbola) are reflections from various planes of one zone.

First, attention is directed only to hyperbolas densely packed with spots and to spots which lie at the intersections of these hyperbolas. These spots correspond to low-index planes: (100), (110), and (111) (for the fcc system). Their symmetry—easily observed—allows indices to be tentatively assigned to them. The assigned indices are checked by reading the angles between the planes (the spots) on a zone (a hyperbola) using Table 1. A Grenin-

† Tungsten target X-ray tubes are convenient for this work. Place a small piece of metal on the lower right-hand side of the black paper which covers the film, so as to have a guidemark on the film.

‡ The film must be read from the side on which the reflected rays were incident. When, after developing, the film is dry, it is advisable to reproduce it on tracing paper using ink. Then the supposed zones and angles are drawn with pencil so that they can be easily erased if mistaken.

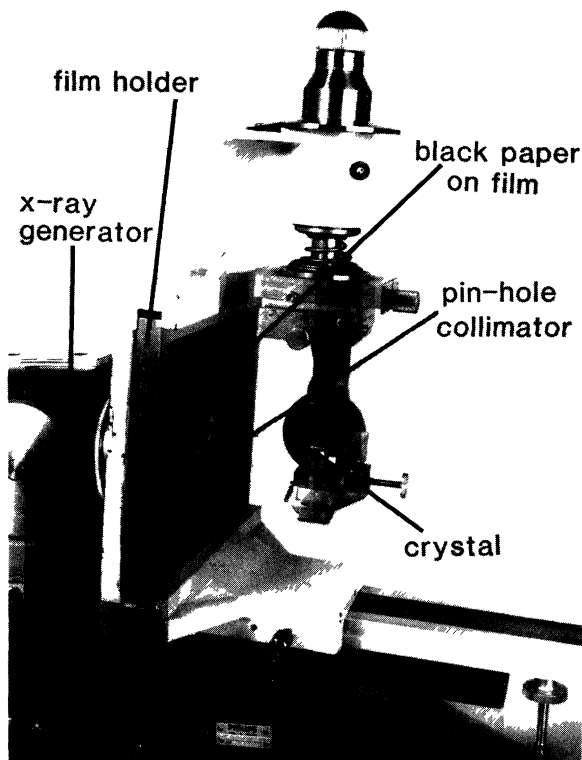


Figure 6. An X-ray goniometer for the Laue back-reflection method (CNRS, France).

ger chart is used for reading angular relations on back-reflection films (for a crystal at a 3-cm distance from the film; see Fig. 7).

Keeping the center of the traced pattern (reproducing the spots and axes of the film) carefully to the center of the chart, any row of spots can be made to coincide with one of the hyperbolas extending horizontally across the chart by turning it through an angle α , where α is the azimuthal angle. ϕ is determined directly from the chart (Fig. 8).

By tilting the position of the crystal by the angles α and ϕ , any plane (any chosen co) can be set parallel to the film (perpendicular to the X-ray beam). Then another photograph gives a pattern

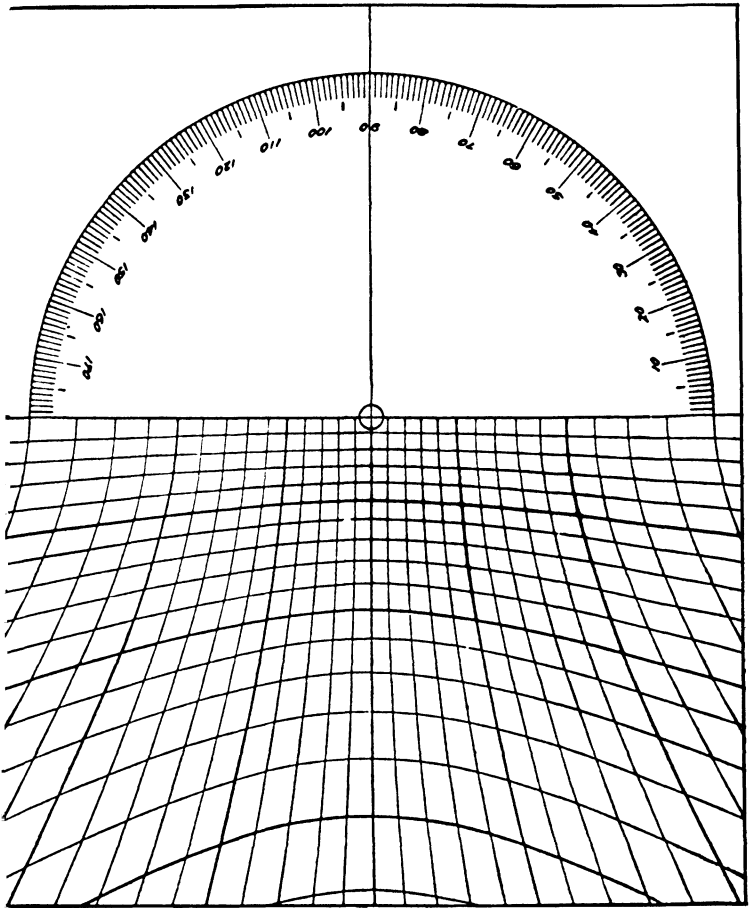


Figure 7. Chart for back-reflection photographs printed in the size for a 3-cm distance from specimen to film and graduated in 2° intervals (Ref. 14).

with the chosen co at its center; the prominent zones and the sets of indices assigned to the spots must coincide with a standard stereographic projection having the chosen co at its center. Then the crystal must be cut parallel to the film to have the desired face of a precise co .

The technique described above for crystal orientation is one of the simplest; others are used in crystallography laboratories.

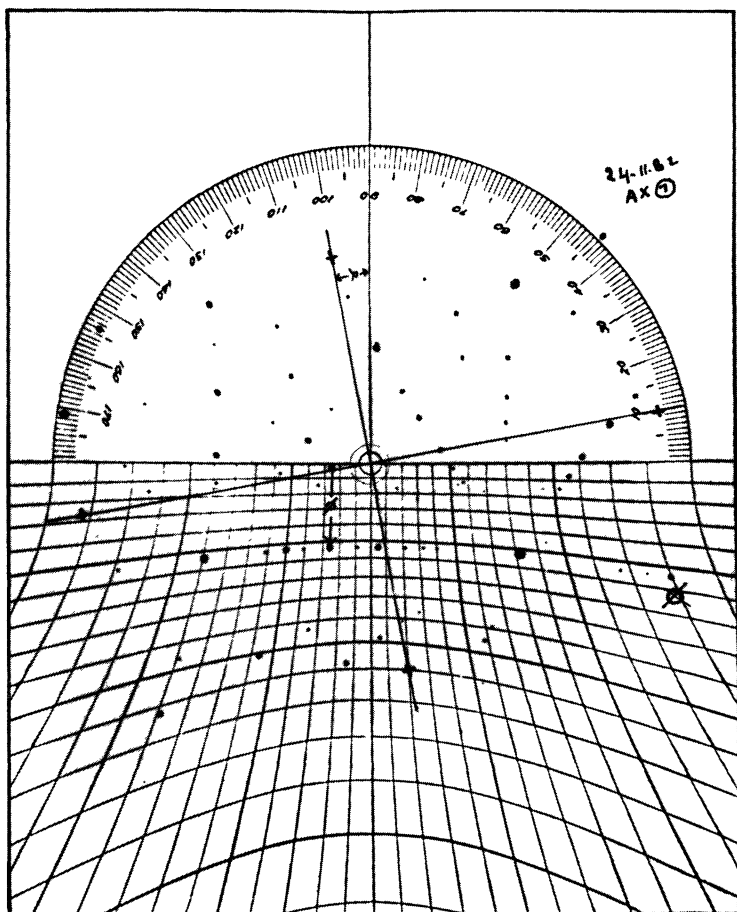
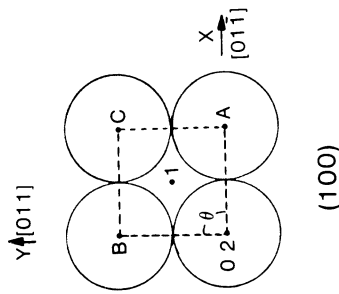
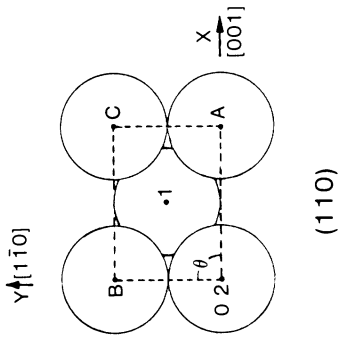
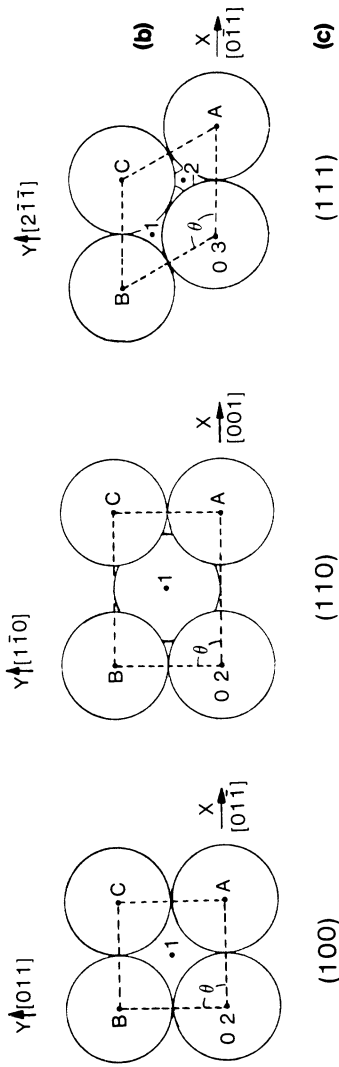
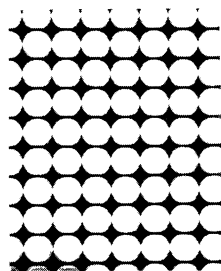
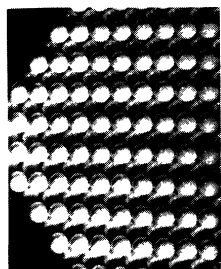
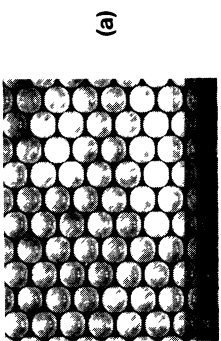


Figure 8. Back-reflection pattern of a gold crystal drawn on tracing paper superimposed on a Greninger chart.

4. Models of Crystal Surfaces

An *atomically flat surface* is the surface of an ideal crystal when cut by a plane. The ideal-half-crystal is made of semiinfinite regular arrays of atoms. The orientation of the dividing plane can be specified by a set of Miller indices (see Section III.2). Assuming that the metal atoms are hard spheres, any atomically flat surface can be represented by *ball models*.



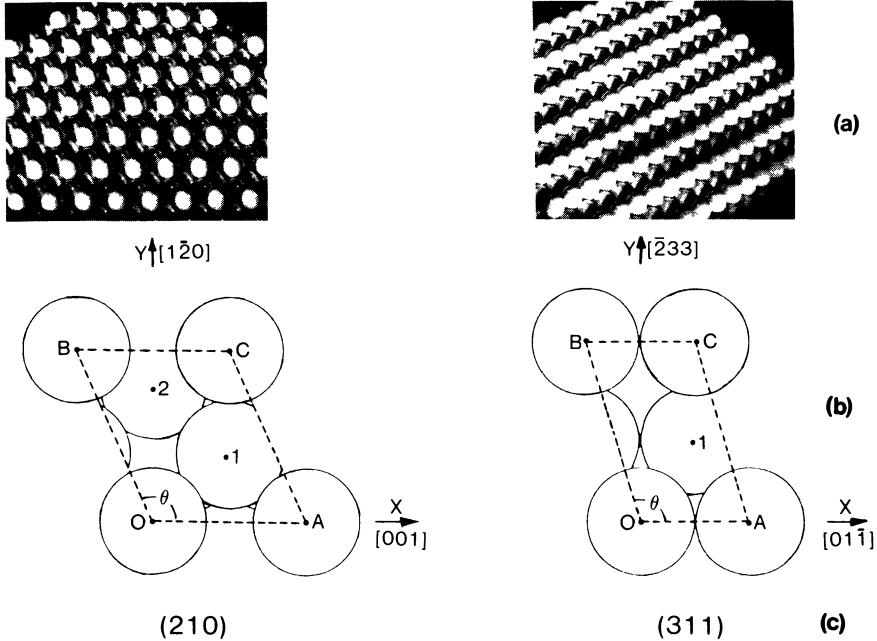


Figure 9. Ball models for five faces of the fcc system (Ref. 17). (a) Photographs. (b) Drawings looking normally at the model. The center of each surface atom which lies on, or inside, the unit-cell boundary is marked with a dot; in some cases this is all that can be shown of that atom. 0, 1, 2 are the number of the layer of atoms (0, 2 implies that one atom lies directly behind the other). (c) Miller indices.

For the fcc and hcp systems, the bulk of the crystal has a close-packed structure. By inserting (theoretically) a dividing plane and removing the unwanted balls from one side of this, a surface model is produced. For our metals the model is made of balls of one size, the diameter being a measure of the spacing between nearest-neighbor atoms. Figure 9 shows the ball models of the five faces of Fig. 1, for the fcc system. These models give an overall picture of the crystal surfaces, but for detailed work the precise disposition of the atoms is necessary; it is also given on Fig. 9. The shape and dimensions of the unit cell of surface is drawn by means of dotted lines on the drawings.

The *unit cell* of the surface can be defined either by considering only the outermost plane of surface atoms, or by considering, in a more realistic interpretation, all atoms which have less than their full complement of neighboring atoms. For the fcc system, an atom in the bulk metal has 12 nearest-neighbor atoms (its coordination is 12); the number of surface atoms of given coordination for the five faces of Fig. 9 is given in Table 2. It can be easily understood that, in the fcc system, a surface atom of coordination n has $12 - n$ "broken bonds". This is just a description based on the geometrical concept of "bonds"; no physical reality can be ascribed to it.

A surface (hkl) can be represented by its outward normal \mathbf{h} (having h, k, l components); a bond can be specified by a vector \mathbf{u} (having u, v, w components). For the fcc structure, an atom may have 12 nearest-neighbor bonds, but only six of these can give positive scalar products $\mathbf{h} \cdot \mathbf{u}$ for h within the unit triangle. For a

Table 2
Numbers of Surface Atoms of Given
Coordination in Unit Cells of Various
Single-Crystal Faces for the fcc System

Face	Coordination					
	6	7	8	9	10	11
(100)	0	0	1	0	0	0
(110)	0	1	0	0	0	1
(111)	0	0	0	1	0	0
(210)	1	0	0	1	0	1
(311)	0	1	0	0	1	0

particular \mathbf{h} ,

$$\mathbf{h} \cdot \mathbf{u}_a \geq \mathbf{h} \cdot \mathbf{u}_b \geq \mathbf{h} \cdot \mathbf{u}_c \geq \mathbf{h} \cdot \mathbf{u}_d \geq \mathbf{h} \cdot \mathbf{u}_e \geq \mathbf{h} \cdot \mathbf{u}_f \geq 0$$

The ordered subset of bonds $\mathbf{u}_a, \dots, \mathbf{u}_f$ is termed the *bond order* appropriate to the particular \mathbf{h} . If \mathbf{h} is visualized as moving over the unit projected stereographic triangle, then the bond order changes at certain points thus dividing the unit triangle into *regions* (such that the bond order is fixed within a region but changes on passing to an adjacent region). For the fcc structure five regions may be considered on the triangle (Fig. 10a). For the electrochemists, up to now, it is not necessary to go into further details of bond orders; they are given in *An Atlas of Models of Crystal Surfaces*.¹⁷

For the fcc system for each of the three families of planes $\{111\}$, $\{100\}$, and $\{110\}$ there is only one type of site where an atom could be added in the nearest-neighbor position; they are called *singular faces* (Fig. 9). Atomically flat surfaces nearly parallel to a singular face are called *vicinal faces*. The vicinal faces can be described by the composition of *terraces* of singular faces and by *monoatomic steps* (Fig. 11). The monoatomic steps are either densely packed in atoms or kinked. This model is called the *TLK model* (terrace, ledge, kink) and it can be easily extended to all faces on the three main zones of the unit triangle.

These faces are called *stepped faces*. For instance, the (221) face which is 15.79° from the (111) face on the zone from (111) to (110) is made of terraces (111) oriented and monoatomic steps denoted (111) [(111) steps] because they have threefold symmetry like the (111) face (Fig. 9). For the (211) face, which is 19.46° from the (111) face on the (111)-(100) zone, there are also (111) terraces and densely packed steps but denoted (100) because they have fourfold symmetry like the (100) face (Fig. 9). For the (310) face, which is 18.43° from the (100) face on the (100)-(110) zone the terraces are (100) oriented and the monoatomic steps which are made of kinks are denoted (110) (Fig. 11).

Accepting this TLK model, a very convenient *notation* was proposed for stepped surfaces (see Appendix of Ref. 18). Thus a stepped surface is called $n(h_t k_t l_t) - (h_s k_s l_s)$, where $(h_t k_t l_t)$ represents the co of the terraces, $(h_s k_s l_s)$ represents the step face, and n denotes the width of the terraces in number of atoms. For instance, (221)

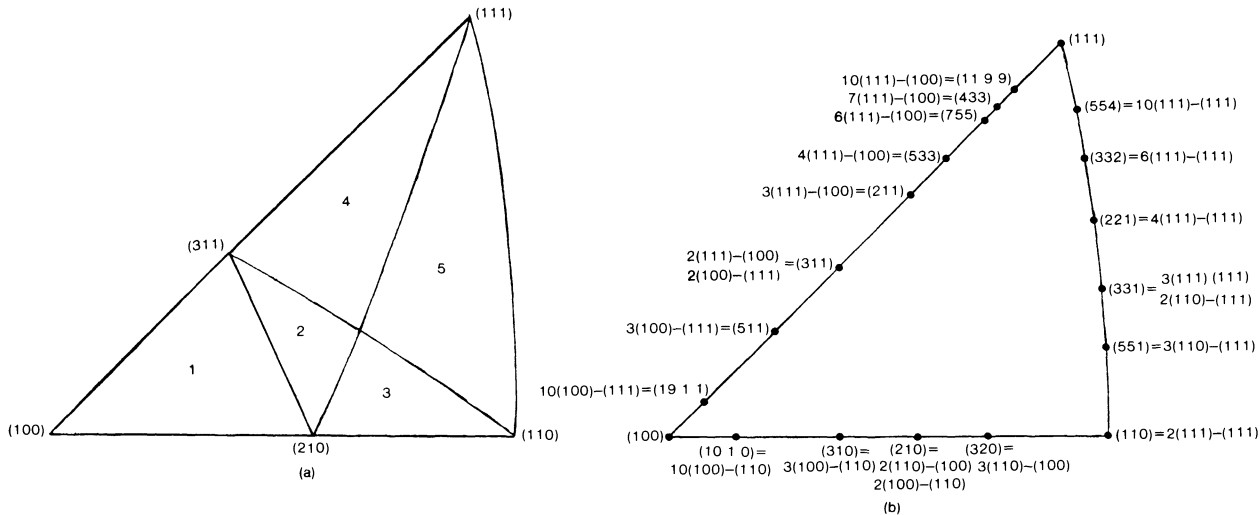


Figure 10. Unit stereographic triangle for the fcc structure with the (100) face at the center of the projection. (a) Regions which correspond to different bond orders (Ref. 17):

region	1	2	3	4	5
bond order	$abcdef$	$abcdcf$	$abcefd$	$abecdf$	$abecfd$

(b) Accepting the notation of Lang *et al.*,¹⁸ namely $n(h,k,l) - (h_s k_s l_s)$, where (h,k,l) represents the terrace, $(h_s k_s l_s)$ represents the step face, and n measures the width of the terrace in number of atoms.

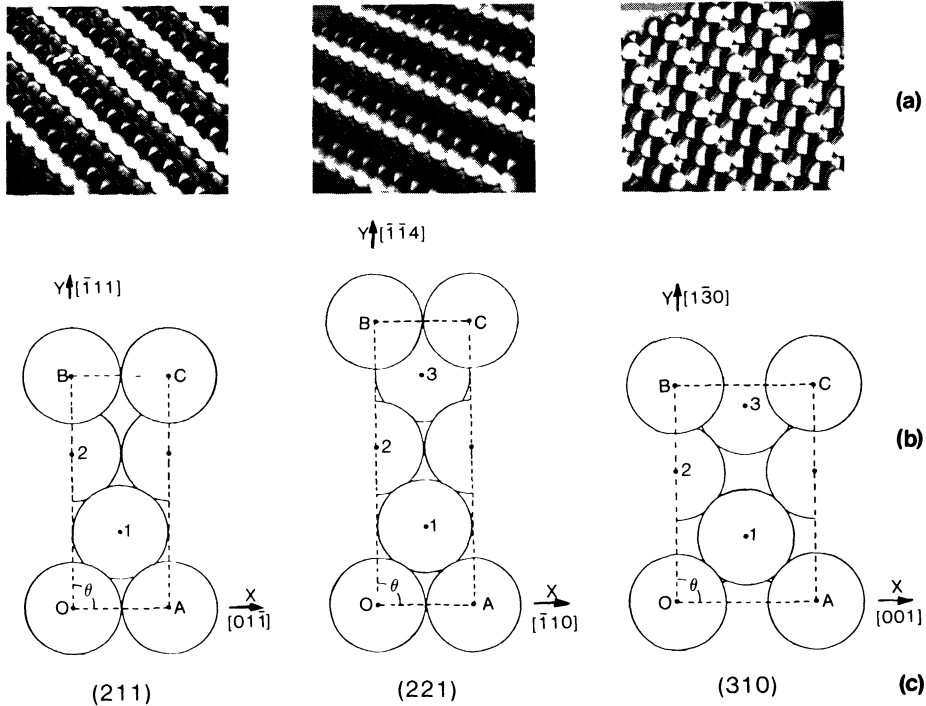


Figure 11. Models for the (221), (211), and (310) faces of the fcc system. Comments are the same as for Figure 9.

is 4(111)-(111) because the terraces for an ideal (221) face are four atoms wide and the terraces and steps are both (111) oriented. Most of the faces which have been used by electrochemists are represented on the unit projected stereographic triangle of Fig. 10b with their Miller indices and their notation as stepped faces. Each of the three sides of the triangle seems to be made of two sections where there are systematic changes of the composition of the surface. The (311) and (210) faces appear as "turning points" on the (111)-(100) and (100)-(110) zones, respectively. But the (331) face on the (111)-(110) zone cannot be considered a turning point because the (110) face itself is made up of small terraces which are (111) oriented and steps which are (111) oriented; in fact, (110) is 2(111)-(111). Therefore, for the fcc system, on the three main zones five sections are observed for the bond-order notation. But when

Table 3
Types of Stepped Surfaces in Cubic System

Stepped-surface designation	Miller indices	Angle of cut from terrace along zone line toward step
$n(111)-(111)$ Example: 9(111)-(111)	$(n, n, n - 2)$ (997)	$\tan^{-1}\left(\frac{2\sqrt{2}}{3n - 2}\right)$ 6.45°
$n(111)-(100)$ Example: 10(111)-(100)	$(n + 1, n - 1, n - 1)$ (11, 9, 9)	$\tan^{-1}\left(\frac{2\sqrt{2}}{3n - 1}\right)$ 5.57°
$n(100)-(111)$ Example: 10(100)-(111)	$(2n - 1, 1, 1)$ (19, 1, 1)	$\tan^{-1}\left(\frac{\sqrt{2}}{2n - 1}\right)$ 4.25°
$n(100)-(110)$ Example: 9(100)-(110)	$(n, 1, 0)$ (910)	$\tan^{-1}\left(\frac{1}{n}\right)$ 6.34°
$n(110)-(111)$ Example: 5(110)-(111)	$(2n - 1, 2n - 1, 1)$ (991)	$\tan^{-1}\left(\frac{\sqrt{2}}{2(2n - 1)}\right)$ 4.49°
$n(110)-(100)$ Example: 9(110)-(100)	$(n, n - 1, 0)$ (980)	$\tan^{-1}\left(\frac{1}{2n - 1}\right)$ 3.37°

generalizing the mathematical formulas, as shown in Table 3, six sections have to be considered.

For stepped surfaces in the cubic system, the designation, Miller indices, and the "angle of cut from the terrace along the zone line toward the step" are related, as shown in Table 3 (for the six sections, six examples are given). Any face can be imagined with this model.

One may ask if these ideal faces actually exist. The evidence is that they do not exist; even at thermal equilibrium there are disorders at the surface and more kinks are present than necessary for the average specified *co*. However, we shall see that this model does fit in with some experimental results of dl studies; it explains other electrochemical results, such as lead underpotential deposition on gold faces.¹⁹

5. Structure of Metal Surfaces

(i) Atomic Aspects

At present the detailed knowledge of the outermost layers of a *clean* metal surface is based on electron spectroscopy or scattering of neutral atoms. Low-energy electron diffraction (LEED) and helium (for instance) scattering give structural information about the top of the surface in ultrahigh vacuum (UHV). Are the surfaces observed in UHV close to the models described in Section III.4?

In some cases they are, but for platinum, iridium, and gold a *reconstruction* of the first outermost layer of atoms was observed for some faces of simple indices. Of these three metals, only *gold* is within the scope of this chapter. Numerous papers were written about the surface reconstruction of gold which, however, happens only under certain conditions of cleanliness and temperature.

It is conventional to describe the real surface by a notation which compares it with the ideal one.²⁰ The surface net is indexed with respect to the bulk net as a $p \times q$ unit cell. A top layer, which is just a bulk termination, is denoted 1×1 .

The Au(100) face surface is approximated by a 20×5 (or 1×5) unit cell; this implies a bond-length reduction of a few percent. Then there is a mismatch between the topmost layer and the substrate (the bulk) that would increase the strain energy at the surface. A buckling of the surface is accepted as an explanation of

some LEED observations. At least four different surface structural models were proposed.

The Au(111) face, which is the closest packed fcc structure, is known to have the lowest surface energy among all possible fcc crystal faces. The clean Au(111) face surface was first approximated to be a $\sqrt{3} \times \sqrt{3} \cdot R30^\circ$ unit cell.²¹ A model with a uniaxially contracted top hexagonal layer was proposed²² and a charge-density-wave (CDW) structure was also proposed as an explanation of the LEED observations.²²

The Au(110) face surface has a 1×2 structure suggested^{21,23-25} to consist probably of alternately missing rows producing micro-facets having the close-packed arrangement of the (111) face.

This notation is extended to the case of a foreign substance on a well-defined substrate—for instance, for oxygen on copper,²⁶ $\text{Cu}(100) + c(2 \times 2)\text{O}$ (c stands for centered mesh), and for gold on silver,²⁷ $\text{Ag}(111) + p(1 \times 1)\text{Au}$ (p stands for primitive mesh).

It seems that for *all clean metals* the case of stepped faces is different from that of low-index faces. The monoatomic steps would be stabilized by repulsive forces; therefore they would be less stable for a large width of terrace than for a small width of terrace.²⁸

In this section we have tried to show that the surface may not be a perfect bulk termination structure. But do these reconstructions exist at an electrochemical interphase as they are observed in UHV? Probably not; but with the variation of the electric field at the interphase and with the adsorption and desorption of ionic (or neutral) substances, some reconstruction of the surface may occur.

(ii) *Electronic Aspects*

Up to now we have considered only the positive ions of the metals, neglecting the electron distribution. For *sp* and *sd* metals the “jellium” model is accepted as a good representation of this distribution: the positive ions are immersed in a “gas” of approximately uniform density of free electrons. The attraction of the positive and negative charges holds the structure together and balances the repulsive forces of the positive (or negative) charges for one another. The moving electrons are subjected to a periodically varying potential as a result of the presence of the ions in the lattice. (The moving electron behaves as if it were a system of waves

diffracted by crystal planes.) The electrons are described by Bloch functions associated with waves extending throughout the entire crystal.

The reader is referred to textbooks^{14,29} for further information.

At the *surface*, the electron density dies off gradually, the electrons spilling over the positive-ion lattice. The charge density is negative on the outer side and predominantly positive just inside the metal (when there is a deficiency of electrons); an electric double layer is created. The dipole moment of this double layer will vary with the nature of the metal and with the ϕ_0 for a given metal.

This last point is well within the scope of this chapter because the variation of the electronic work function with the ϕ_0 for a given metal is due to this double layer. The electronic work function represents the difference in energy between the highest normally occupied electronic energy level inside the metal and the state of an electron at rest outside the uncharged surface. The work function of a metal depends both on its bulk properties and on the characteristics of its surface, the latter being influenced by the surface atomic structure. The magnitude of the double-layer dipole moment was computed for several metals and it varies from tenths of a volt to several volts;³¹ for different ϕ_0 's of a given metal it can vary by amounts which are sizable fractions of itself.

In addition to the wave functions of uniform amplitude throughout the crystal, wave functions may exist which have appreciable amplitude only in the surface region; they represent localized electronic states at metal surfaces.

For an *actual surface* the positive charge is not uniformly distributed over a half-space. For steps at the surface or corrugated surfaces (on an atomic scale), the contours of constant electronic density have ridges and valleys corresponding to those of the distribution of positive ions at the surface but they are smoother and less bumpy.

Smoluchowski³⁰ attempted to calculate the "smoothing." For the most closely packed crystal faces, more complete smoothing is expected and the constant electron density contours are fairly flat; this lowers the double-layer moment (negative corrections to values without smoothing). The amount by which the "smoothing" decreases the double-layer moment will be greater the rougher (on

an atomic scale) the surface. Smoluchowski demonstrated that for peaks and valleys a few atom spacings apart enough smoothing will occur to make the rougher crystal faces have the lower work function. In summary, all irregularities will tend to lower the work function because each irregularity creates a point dipole with its positive direction outward.³¹

In electrochemical conditions, a change of density of charge at the metal surface, i.e., a change of potential, produces a shift of the electron distribution.

(iii) *Surface Energy Aspects*

The increase in energy associated with an increase in the surface area of a metal arises from the fact that surface atoms have fewer neighbors than bulk atoms and hence contribute less to the total binding energy of the crystal. Surface free energies γ were calculated assuming short-range interactions for binding one surface atom with either its nearest or its second-nearest-neighbor (and so on) atoms.³² The contour lines of constant free energy, based on the nearest broken-bond model, for a fcc crystal are shown (Fig. 12) only in a unit projected stereographic triangle.³² Obviously, there is one turning point on the (111)-(100) and (100)-(110) zones and monotonic variations on the (111)-(110) zone as we observed (see Fig. 10).

When using the TLK model, the surface free energy is calculated by adding the surface free energy for the terraces and the line free energy of the steps.³³ Then the variations of the surface free energy with the ϕ can be drawn (it is called a γ plot). In the neighborhood of singular faces [such as (100) and (111) for the fcc system], an inward-pointing cusp is observed and maxima are observed for the roughest faces [the (210) face for the fcc system, for instance; see Fig. 12].

These theoretical predictions are confirmed by experiment but very few results are available at the present time.

As we shall see, not only will the atomic aspect of the face surfaces be reflected by electrochemical results but the electronic and surface energy aspects as well, the three being related as would be expected.

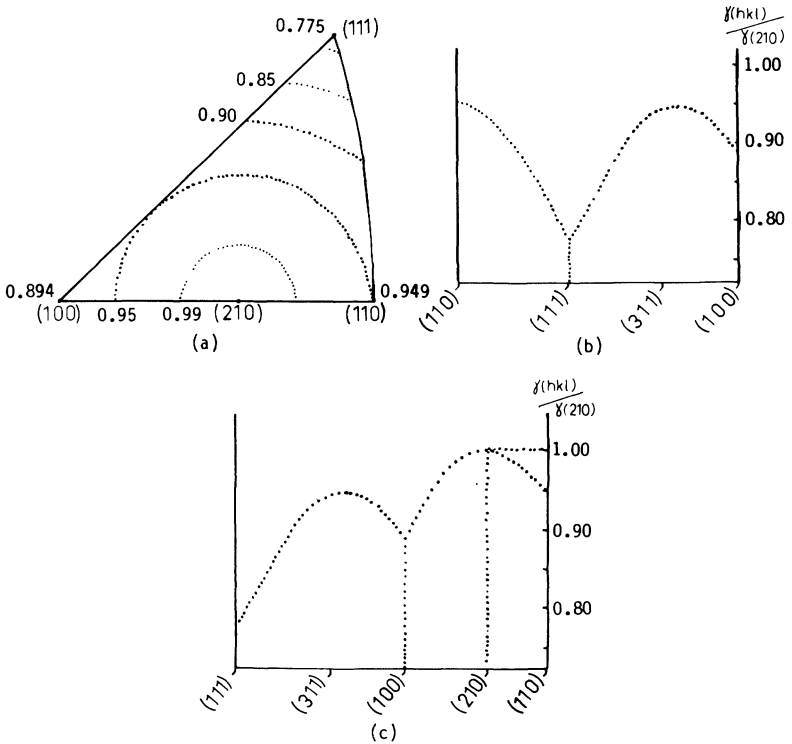


Figure 12. For a fcc crystal (from Ref. 32): (a) contour lines of the surface free energy γ based on the nearest-neighbor broken-bond model and (b) and (c) corresponding γ plots—the horizontal axis is scaled taking into account the angular distances between the faces; the free surface energy relative to the (210) face is plotted on the vertical axis.

In electrochemical conditions, in the case of no adsorption, when the density of charge is zero at the metal surface the work function is linearly related to the potential, and the pzc varies with the co in parallel with the γ plot (see Section V.1).

(iv) Defects

Even in the best crystals some defects exist; they are a necessary consequence of the thermodynamic equilibrium of the crystal. At

room temperature, at least 10^6 – 10^7 cm^{-2} dislocation lines exist⁵ at a metal surface which has a density of atoms of about 10^{15} cm^{-2} .

Actual crystals which have been manipulated have certainly more defects; furthermore, evidently, they have edges which are not sharp on an atomic level.

For advanced studies of the subjects of Section III.5 and the notation, the reader may refer to the chapter of Oriani and Johnson⁵ in this series.

IV. PREPARATION OF SINGLE-CRYSTAL-FACE ELECTRODES

1. Growing Single Crystals

Books about crystal-growing procedures are available.^{34–36}

It is difficult to assess the relative merits of the different methods used for growing crystals on account of the following factors:

1. The choice of the shape of the crystal (cylinder, disc, thin layer) depends on the techniques which will be used. (Thin layers are necessary for resistance measurements of the surface layer during electrochemical adsorption, while some optical measurements require large surface areas.)
2. Some facilities are available in one laboratory but not in others.
3. An incidental advantage, which can be useful for electrochemists, is the “perfect” surface found on crystals grown from the vapor or from electrolytic solutions.
4. What is possible for one metal might be impossible for another.

The metal crystal growth could take place from:

1. The metal melt.
2. The metal vapor.
3. Metal electrolyte solutions.

These different possibilities will be illustrated by examples used in electrochemistry.

(i) *Growth from the Metal Melt*

This is by far the most important technique. A seed is formed in the melt or added but the solid–melt interface must remain planar

during solidification from the seed. Methods developed from this principle are:

1. The crystal-pulling method.³⁷
2. The Bridgman method.
3. The zone-melting method.
4. The floating-zone method.

Hitherto, the last two methods have not been used by electrochemists. They have either melted the tip of a wire so as to obtain a small sphere which in some cases is a single-crystal (platinum) or used a modified Bridgman method.

For the Bridgman method the melt is contained in a crucible (graphite for gold or silver); the freezing must commence at a point—used as a seed—from which the solidification proceeds (a conical tip of the crucible produces a “natural” but uncontrolled selection of the seed). The solidification proceeds either by moving the crucible or by regulating the temperature gradient, i.e., the rate of movement of the freezing plane. This last possibility was used for gold, silver, and copper, for example.

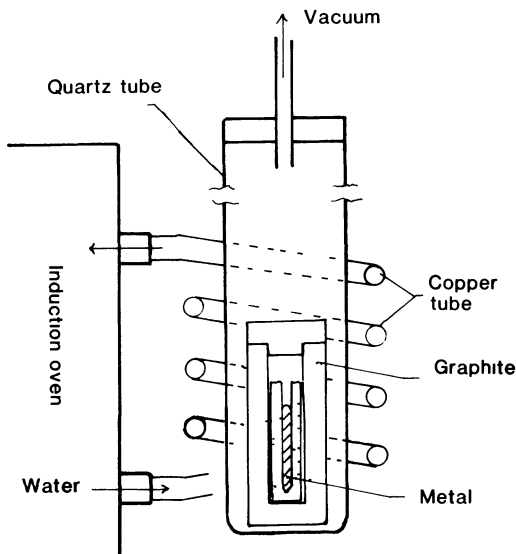


Figure 13 One of the possible ways of growing a gold (or silver) crystal in a crucible placed in the helix of an induction oven

For gold or silver, the graphite crucible was placed in a quartz tube; the quartz tube was positioned in the helix of an induction oven; and the tube was evacuated (Fig. 13) and the temperature gradient regulated. Mechanical vibrations must be avoided during solidification (2–20 min for a cylinder 20 mm long). The experimenter has to know whether the sample is an individual crystal or not when it is removed from the crucible. Its macrostructure (its general gross structural distribution in the whole) has to be determined. Therefore the ingot has to be macroetched†; then grain boundaries, if they exist, are visible to the naked eye.

The size of the crystal thus obtained may be 2–20 mm in diameter and 5–200 mm in length.

(ii) *Growth from the Metal Vapor*

The collector [polished glass, cleaved mica, (100) face of a sodium chloride crystal, face of a metal, face of the metal] is maintained at a temperature below the melting point of the metal (in vacuum or in a neutral gas) so that crystal nuclei can be formed. The area of the film can reach several square centimeters.

The metal is either evaporated or sputtered, so that either very thin layers or thicker layers are obtained. In the following paragraphs, some examples are given.

Thin layers of gold, evaporated on polished glass (10–80 nm thick) give *monooriented polycrystalline electrodes*; the film is made of grains, the surfaces of which are (111) faces. The [111] axes of the grains are nearly perpendicular to the substrate and the azimuthal orientation is random.

Layers of gold (100–150 nm thick) sputtered on cleaved mica give *monooriented polycrystalline electrodes*. The grains are a few tenths of micrometers in area; they are (111) oriented, but the azimuthal orientation is random. Since the whole electrode surface is not made of one grain, there are grain boundaries. At present the contribution of these to dl parameters does not seem important. The behavior of these layers is close to that of massive conventional single crystals which are (111) oriented.³⁸

† Macroetching is done by dipping the ingot in an etching reagent (for gold a few seconds in warm aqua regia, for silver a few seconds in tepid 50% nitric acid, etc.) and rinsing.

Heteroepitaxial layers of gold (100–150 nm thick) evaporated on cleaved mica give *nearly monooriented crystalline electrodes*; with big (111)-oriented grains (a few micrometers to a few tenths of a micron in area), nearly no azimuthal disorientations are observed at the surface. Their electrochemical behavior is close to that of massive conventional single crystals.³⁸

Heteroepitaxial layers of gold sputtered on polished (100) faces of sodium chloride crystals were made. The first deposited layers of gold on the substrate have its topography—they are gold *single crystals which are (100) oriented*. A supplementary deposit of gold (about 2 μm thick) makes them “easy” to manipulate and to remove from the NaCl crystal. The first layer built on the substrate was used as an electrode surface for dl measurements; the results are close to those of massive conventional single crystals which are (100) oriented.³⁹

Homoepitaxial layers of one metal on a substrate of the same metal improve the quality of the surface.

The surfaces grown from the metal vapor do not require cutting and polishing. However, isolation of the face of interest and electric contact must be ensured.

(iii) Growth from Metal Electrolyte Solutions

The question of why electrochemists have so seldom used a technique which is their own is of interest. First, only the faces of the lowest surface energies can be obtained [the (111) and (100) faces for the fcc system]. Second, if an epitaxial growth is observable on some metals it is not on others. Up to the present, dl measurements were done on faces grown from the metal electrolyte solutions only in the case of silver.^{40–42} These silver faces were grown in glass or Teflon capillaries on a substrate which was a massive silver crystal grown from the melt (oriented, cut, and polished according to the desired face).

After electrolytic growth, only one crystal face fills the section of the capillary. The surface of the face consists of terraces and growth steps; by convenient cathodic treatment, one can change the growth-step density and can thus partly modify the atomic surface structure of the electrode although its co remains unchanged.^{40–42}† The possibility to change this density at will is the

† Screw dislocation free faces are obtained.

main advantage of this type of electrode. It should be emphasized that, by this method, the imperfections of the surface seem to be minimized. Furthermore, the influence of these atomic irregularities on dl measurements was studied by using silver (111) and (100) faces with a definite growth-step density ($2-20 \cdot 10^4 \text{ cm}^{-1}$).

The working area of these electrodes is a few tenths of a square millimeter.

2. Cutting the Crystal

Crystals grown from the melt are removed from the crucible and have to be recognized as individual crystals [see Section IV.1(i)] before being oriented by the X-ray back-reflection Laue method (see Section III.3). At the end of this procedure, the desired co is perpendicular to the X-ray beam; therefore the crystal must be cut perpendicularly to this beam.

The cutting can be done either with a saw (thread saw, with carborundum, electrolytic saw, spark erosion), or by elimination of part of the crystal by abrading (grinding on emery paper of fine grade, for instance, or spark erosion). The position of the crystal when cutting and the angle of cut have to be maintained with precision. Either the crystal has to be left in the goniometer or some precise guidemark has to be drawn on the crystal.†

Any face of determined co can be obtained by this method and thus the variation of dl parameters can be investigated from a general viewpoint; but a disturbed layer is made at the surface which has to be removed by polishing (see Section IV.3).

In some cases the cylindrical crystal (of small diameter) can be cleaved successfully in liquid nitrogen along the most densely packed face. This is the case for the basal face of zinc⁴⁴; then no polishing is necessary.

† If the desired face, which is elliptical in shape, is parallel to the film and the major axis of its ellipse horizontal, a guide mark (a thin line) can be drawn horizontally on the crystal, i.e., along the major axis. In the holder (Teflon or another material) a hole of the diameter and the cut angle of the crystal is driven. A line, as a guidemark, is also drawn along the major axis of the elliptical hole (at the surface of the holder). The lines drawn on the crystal and on the holder are brought into coincidence. The bulging part of the crystal is then abraded flat. The crystal must sometimes be fixed in the holder with a wax melting below 100°C . This technique was used for gold crystals.⁴³

To introduce a personal comment, it is surprising that this part of the work is considered as a menial task and every time, when visiting a laboratory, I asked to see how the crystals were cut, I felt that I was being indiscreet. However, any error introduced at this stage will entail errors in the electrochemical results.

3. Polishing and Isolating the Face of Interest

After cutting along the desired crystal face, the surface is left with a disturbed layer on top. The physical state of the electrode surface must be that of an atomically flat face described above (see Section III.4). Therefore the experimenter must try, by all means available, to create a disturbed layer as thin as possible, or absent. Elimination of this disturbed layer can be done either directly by electrochemical polishing (e.g., possible for silver) or by mechanical polishing, followed by electrochemical or chemical polishing.

(i) *Mechanical Polishing*

Any book of metallography provides good information for this step of preparation of the surfaces.

The choice of the ingredients used for mechanical polishing (felt or cloth, alumina powder or diamond paste, etc.) is dictated by the hardness of the metal and its chemical properties. Soft metals (such as gold) are more difficult to polish than hard metals because the polishing material can possibly be "buried" into the metal and consequently modify the chemical composition of the electrode surface (see Section IV.6).

Mechanical polishing is generally first done with fine emery paper. Care must be taken to work across the lines (scratches) formed on the surface by continual random rotation of the sample. Then alumina powders of different grades (on different felts) or diamond pastes of different grades (on different cloths) are used to remove, as well as possible, the disturbed layer.† A mirror finish should be observed; for instance, no trace of the lines due to the polishing should appear when observation is magnified 20 times.

† A lapping wheel is generally used; the sample can be held by hand but an automatic apparatus is now available.

The elimination of the disturbed layer can be checked by X-ray photographs.

However, electrochemistry takes place on the outermost layer of atoms which was in contact with the products; therefore annealing, chemical or electrochemical polishing, and then further annealing are necessary.†

(ii) Electrochemical (or Chemical) Polishing of the Face

Books have been published about electrochemical and chemical polishing.⁴⁶ Of course, the procedure depends on the nature of the metal, the size of the electrode, and the skillfulness of the experimenter.

Only the face of interest must be in contact with the polishing bath; therefore the isolation of the face (see further: resin, O-ring, and holder) is necessary. Creeping of polishing solution between the crystal and the isolating material could round the edge of the face and change the geometric working area; therefore creeping must be avoided.

Electrochemical or chemical polishing, whatever is the rinsing procedure, leaves traces of chemicals at the surface (cyanide in the case of gold or silver, for instance). These polishing stages are followed either by annealing or by one of the final surface preparations (see Section IV.4).

(iii) Isolating the Face of Interest

The problem is to leave only the face of interest in contact with the solution and to do it in such a way that the geometric working area can be known and to avoid contamination of the face which could not be removed by a final preparation (see Section IV.4). Of course, creeping between the holder and the walls modifies the working geometric area of the electrode and then other co's than the desired one are in contact with the solution.

The crystal was often positioned in a Teflon holder (which has been thoroughly cleaned) and the face was limited with a RTV

† For silver, we succeeded in making good electrochemical dl measurements after mechanical polishing just by annealing and cooling in argon and putting the crystal in contact with the solution without contact with air.⁴⁵

(room-temperature vitrification) silicone resin (Fig. 14a). Polythene dissolved in toluene is also used. In any case, it should be a noncontaminating material. When using films, a viton O-ring can be positioned on the face (Fig. 14b); this type of holder was also used for faces of large geometric area. For crystals grown in capillaries no further isolation is necessary.

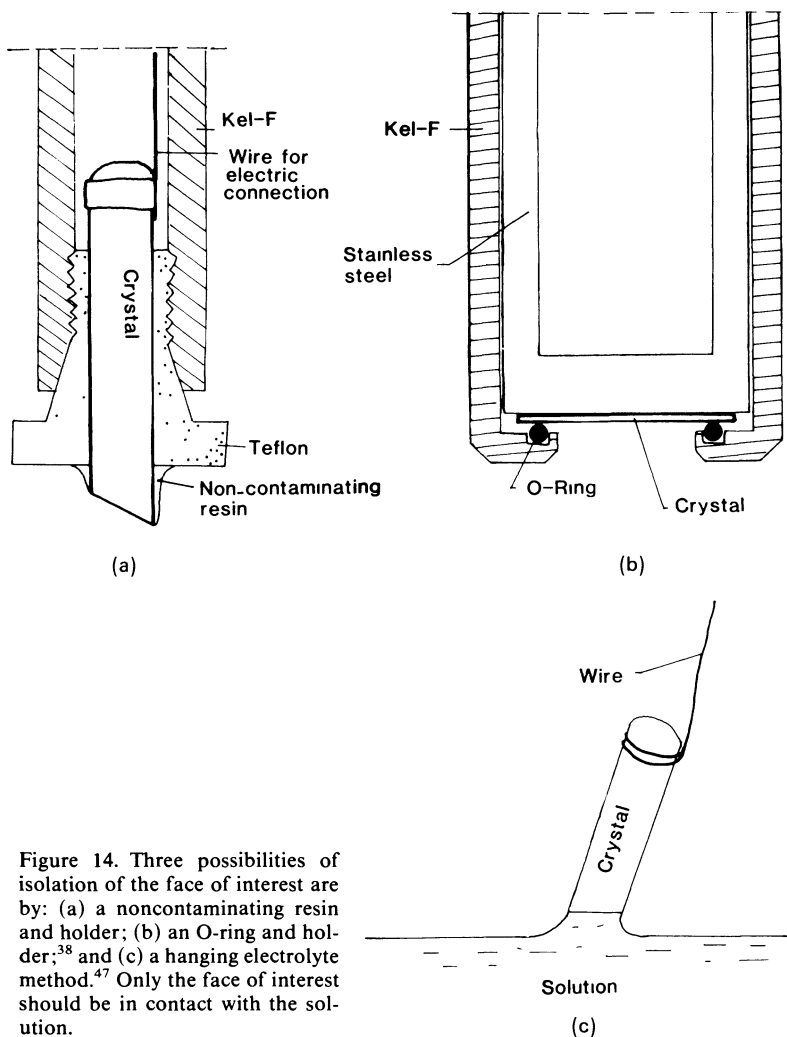


Figure 14. Three possibilities of isolation of the face of interest are by: (a) a noncontaminating resin and holder; (b) an O-ring and holder;³⁸ and (c) a hanging electrolyte method.⁴⁷ Only the face of interest should be in contact with the solution.

Where the "hanging electrolyte" method is used,⁴⁷ no isolating material is necessary; just after annealing the crystal in a torch (town gas and oxygen) and cooling it in a clean medium (water⁴⁸ or argon⁴⁵) and touching the surface of the solution, a noncontaminated interphase can be obtained without any interference of the co's of the walls of the crystal (which have to be dry and smooth) (Fig. 14c).

Once more, for each metal, solvent, and chosen technique, the sequence of procedures will differ.

4. Final Surface Preparation

The final aim is to have an electrochemical interphase *chemically clean* both on the solution side (water, chemicals, gas) and on the metal side (no oxide, no sulfide, no traces of the polishing solutions), and *physically well-defined* at the outermost layer, or layers, of atoms being as they are in the bulk metal in a plane parallel to the surface. We shall discuss two examples.

1. For silver faces, mounted as in Fig. 14a, before each series of dl measurements a few seconds of electrochemical polishing are necessary; therefore traces of cyanide are left at the surface which are not eliminated by rinsing thoroughly with solvent (very pure water). In the aqueous solvent, excursions, in a range of potentials more negative than the double-layer region, produce a slight hydrogen evolution as a consequence, which carries the impurities existing at the metal surface away into the volume of the solution, if the latter is stirred. Then the solution has to be renewed. This procedure can be applied several times until the $C(E)$ curves are stable and satisfactory. Of course, one must avoid by all means excessive hydrogen evolution which could substantially disturb the first layers of atoms of the electrode surface or work the resin loose.

It must be pointed out that oxides formed on silver cannot be reduced electrochemically.

2. For gold faces, mounted as in Fig. 14a, no annealing and cooling as described in Section IV.3(iii) is possible. In the aqueous solvent a slight hydrogen evolution could be used (as for silver, with the same disadvantages, although electrochemical polishing was not done at this stage). But for gold, with no or slight adsorption, a monolayer of oxide can be completed at the surface and removed

electrochemically in the aqueous solvent; the formation and removal of this oxide layer can be used as a cleaning procedure. Do these formations and removals of oxide disturb the outermost layer of gold atoms? Yes, if the variation of the applied potential with time is fast (more than 100 mV s^{-1}),⁴⁹ but it does not seem to be the case for slow sweep rate (20 mV s^{-1}). For the (100) face, comparison of $C(E)$ curves obtained after numerous cycles of formation and removal of oxide and obtained just after annealing and cooling [see Section IV.3(iii)] are identical.⁵⁰ If there is ionic adsorption (bromide, iodide solutions), there is oxidation of the anion before oxidation of gold and this final preparation has to be done in another solution (perchloric acid, for instance) before dl study of ionic adsorption.

For each metal and each solvent a final preparation of the face has to be adopted. In some cases this final surface preparation is at the same time a check of the quality of the electrochemical interphase.

5. *Ex situ* Check of State of Electrode Surface

Ex situ checking of the electrode surface is done first by optical microscopy, electron microscopy, and scanning microscopy. When a UHV chamber is available in the laboratory then more sophisticated methods can be used, although the state of the surface in vacuum is not necessarily what it is in contact with a solvent at the electrochemical interphase.† However, the new powerful methods used to provide information on the chemical state of surfaces, namely, AES (Auger electron spectroscopy) and XPS (X-ray photoelectron spectroscopy) [also called ESCA (electron spectroscopy for chemical analysis)], and on the physical state of the uppermost region of the surface, namely, LEED (low-energy electron diffraction) and RHEED (reflection high-energy electron diffraction), are certainly of great help for the electrochemist working on single-crystal-face electrodes. The “gap” between observations in the UHV chamber and observation at the electrochemical interphase due to transfer is smaller every day, although it may never be completely

† After the present chapter was submitted, studies on emersed electrodes consisting of single crystal faces were published; they give information on the dl.

closed. Therefore conclusions drawn from observations in UHV can, to some extent, be valid for the electrochemical situation.

The reader can refer to References 5 and 51-53 for further information.

6. *In situ* Check of State of Electrode Surface

In fact, all that follows in this chapter could be considered, in a way, as an "*in situ* check" of the electrode surface, because, while observing the desired electrochemical dl parameters, questions of the chemical cleanliness of the electrode surface (and of the interphase[†]) and the physical state of the outermost layer of atoms at the metal surface are always open.

In situ checks are absolutely necessary. Either they are provided by the experimental electrochemical results themselves or by other methods such as optical techniques.

For instance, at the present, by optical measurements (by *in situ* electroreflectance) it was shown that the symmetry properties of the crystal faces were not perturbed by contact with aqueous solutions. For *copper*, all faces studied present their azimuthal anisotropy with respect to the plane of polarization of the incident light, except for (100), (111), (211), and some neighboring faces of (111) for which no azimuthal anisotropy is observed.⁵⁴ For *silver*, the twofold symmetry of the (110) face was observed: the electroreflectance spectra at normal incidence differ markedly when the electric field vector of light is parallel or perpendicular to the surface atomic "rails." This is not the case for the (111) and (100) faces⁵⁵ which have higher symmetry. For *gold*, no azimuthal anisotropy was observed for the (111) and (100) faces with respect to the plane of polarization of the incident light, while the (110) and (311) faces present an azimuthal anisotropy.^{56,57} It does not necessarily mean that the outermost layer of surface atoms is 1×1 , because a surface reconstruction such as 1×2 for Au (110) would have the same symmetry order as 1×1 . These are already studies of the metal surface in the presence of the electrochemical dl.

[†] For further discussion of techniques required for obtaining ultraclean conditions, see the chapter by H. A. Kozłowska in *Comprehensive Treatise of Electrochemistry*, Ed. by E. Yeager, J. O'M. Bockris, and B. E. Conway, Plenum Press, New York, 1984, Vol. 9.

Most electrochemistry laboratories have no optical setup and therefore are limited to electrochemical observations. Furthermore, the potentialities of $i(E)$ curves and $C(E)$ curves seem larger every day; this means that under rigorously clean and well-defined conditions, the wealth of information contained in these curves is not yet fully exploited.

For any metal in a given solution, at a given temperature, the range of potential E over which *only* a change (with potential applied) of the electrostatic charge on the metal (and correspondingly in solution) is observable, is the “*dl region*.”

In the dl region, comparison of the $i(E)$ and $C(E)$ curves can be used as a first test [one should be able to deduce one from the other, the current being only capacitive, ($i = C dE/dt$)]. The shape of the minimum (corresponding to the capacity of the diffuse part of the electrochemical dl) on the $C(E)$ and $i(E)$ curves (Fig. 15) for the case of no adsorption in dilute solution, is another criterion; it should not be too different than that observed for mercury, but its position in the range of potential can be completely different. The shape of the adsorption peak is another criterion (in the case of adsorption); it should be sharp and reproducible. Of course, the stability and reproducibility of the curves are important and should be observed not only in the dl region but over all the range of potential explored.

On the $i(E)$ curves, the dl region is limited at negative potential by a faradaic current corresponding to the reduction of the solvent (or of the cation); the observation of the foot of the wave of this current gives an indication of the cleanliness of the interphase. Undoubtedly, a steep foot of the wave of current (Fig. 16) is indicative of a cleaner (or less dirty) surface than a curve that rises slowly because the electrochemical reaction rate is slowed down by some impurities (for instance, carbonaceous species) at the surface. Slight hydrogen evolution will clean the surface; but care must be taken to avoid strong hydrogen evolution which could modify the outermost layer of metals atoms irreversibly.

On the $i(E)$ curve the dl region is limited at positive potentials by oxidation—either of the anion, the solvent, the metal, or of impurities. For some metals, oxidation of the metal occurs at potentials less positive than oxidation of the solvent. When the oxygenated compound formed can be totally reduced at the

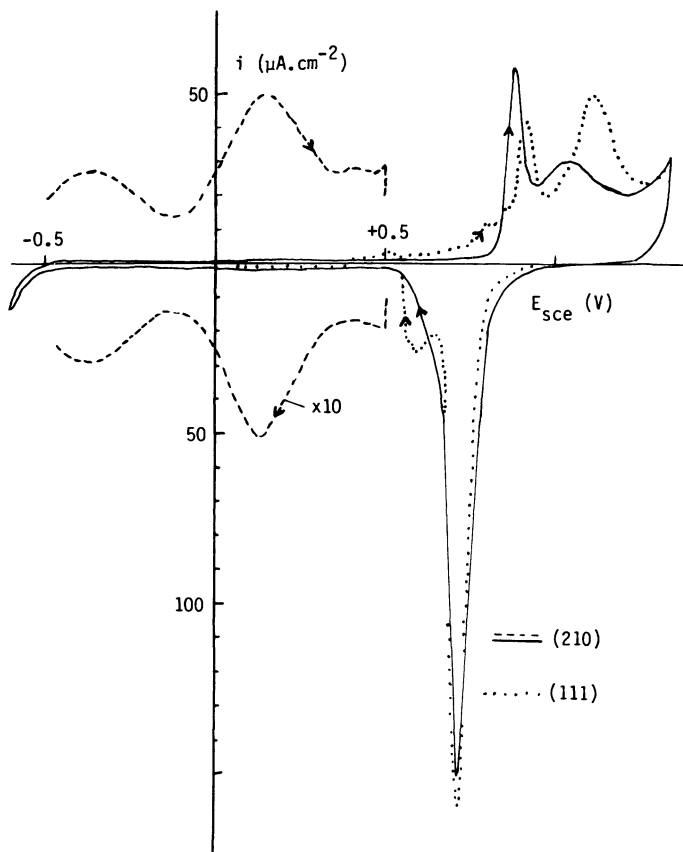


Figure 15. $i(E)$ curves for the (111) and (210) faces of gold in contact with an aqueous solution of KBF_4 (10 mM); sweep rate = 20 mV s^{-1} , temperature = 25°C , and pH = 3.5. For the (210) face, in the dl region, the $i(E)$ curve enlarged 10 times shows clearly the shape of the $C(E)$ curve, in particular, the minimum corresponding to the contribution of the diffuse part of the dl.⁵⁸

electrochemical interphase, the observation of the currents of oxidation and reduction (number, shape and position of the peaks) gives some indications; thus, the sharper (the less rounded) the peaks are the cleaner the interphase is, and the more details are observable the cleaner the surface is (then the structural details of the surface are available for bonding). This is the case for gold in solutions

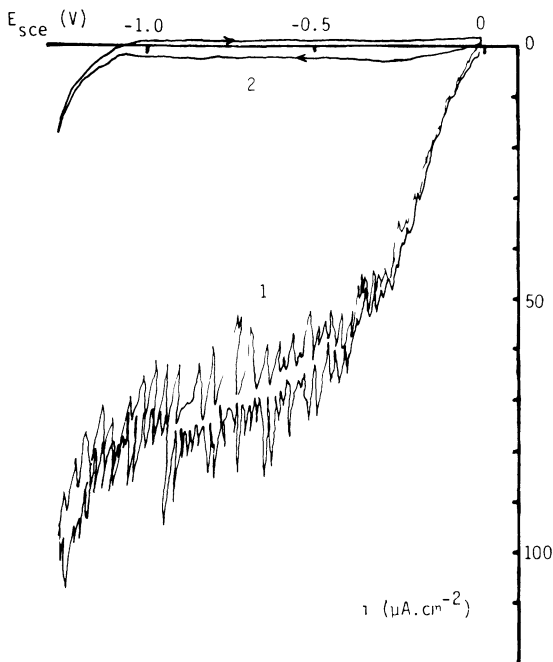


Figure 16. $i(E)$ curves for the (311) face of silver in a stirred aqueous solution of NaF (5 mM); sweep rate = 20 mV s^{-1} . Curve 1 represents a partially deaerated solution and curve 2 a deaerated solution at a temperature of 21°C ; the beginning of the reduction of the solvent is visible on curve 2.

without strong specific adsorption (Fig. 15). Cyclic voltammetry is a convenient technique in this case; $i(E)$ curves give information on the physical state of the surface because the number, the potentials, and the shape of the oxidation peaks, in a given solution, are characteristic of each co.⁵⁹ Formation of monolayer of oxide and reduction processes of gold faces can clean the surface; performed at too high a sweep rate (larger than 100 mV s^{-1}) they can modify the metal surface irreversibly and then change the co.⁴⁹ Worse still may be potential steps, but the effect of these on the outermost-layer surface atoms has not been carefully studied.

When some electroactive species exist in solution or at the surface of the metal, in the range of potential corresponding to the

dl region, a current due to the electrochemical reaction is observed. For instance, the observation of the current corresponding to reduction of oxygen (from the air) in aqueous solution on gold (or silver) electrodes gives a good indication of the cleanliness of the interphase; the foot of the wave should be steep (as for solvent reduction), while in stirred solution the current should be diffusion controlled (Fig. 16).

We consider next another example. Years ago, gold faces were cut, mechanically polished—either with “alumina” or with “diamond paste”—and then electropolished. No AES was available to check the final chemical state of the faces. When solutions containing only ions, which adsorbed slightly, were deaerated with *nitrogen*, curves for all samples were of the type exemplified by the solid line of Fig. 17. When *molecular hydrogen* was bubbled in these solutions, for samples prepared with “alumina”, curves were of the type shown in curve 1 of Fig. 17; for samples prepared with “diamond paste”, curves were typically as shown in curve 2 of Fig. 17. The results obtained with the faces polished with “alumina” were comparable (as far as oxidation of molecular hydrogen is concerned) to the results observed with a gold sphere obtained by just melting a gold wire.⁶⁰ The results of the faces polished with “diamond paste” (although also electrolytically polished) showed that some constituents of the so-called “diamond paste” remained buried in the gold, which is a soft metal, and were responsible for the catalytic oxidation of molecular hydrogen. Nevertheless, the pzc's observed for all these faces were satisfactory when nitrogen was used to deaerate the solutions, and comparable to the ones observed with samples prepared with “alumina”.

These examples are given to show that sometimes great experimental experience and acumen are necessary to detect the cause of unexplained results and their origin may be in one of the steps of surface preparation.

For other materials, other types of arguments should be developed, according to the known properties of the electrode.

The author must apologize for talking more about gold and silver than about other metals; but it should be pointed out that too much work on other metals is being published without giving significant detail on the preparation of the crystal faces and the checking of the state of their interphases. Therefore, it is not possible

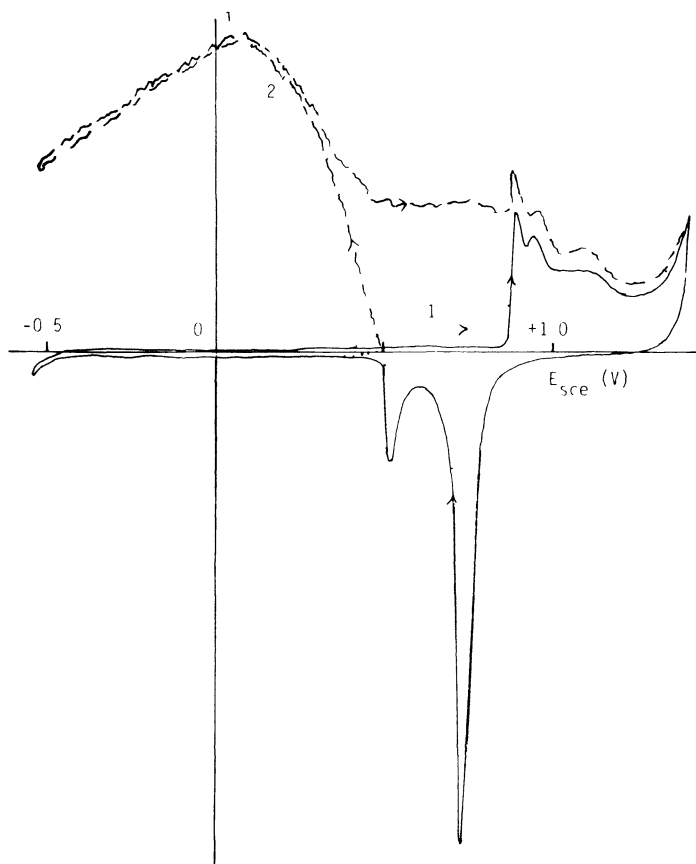


Figure 17. $i(E)$ curves for two different samples of the (110) face of gold in stirred HClO_4 (10 mM): deaerated with nitrogen (solid line) and deaerated with hydrogen (dotted line represents sample 1 and dashed line represents sample 2). Temperature = 22°C ; sweep rate = 20 mV s^{-1} .

to describe the techniques that may have been used with those other metals.

V. ELECTROCHEMICAL RESULTS

The range of potential in which *only* the change of the electrostatic charge on the metal (and correspondingly in solution) is observable,

is the *dl region*; it depends in a given solution, at a fixed temperature, on the nature of the metal.

From experimental observations in a given medium *the dl region is nearly the same for all co's of a given metal* and for a polycrystalline electrode of this metal in the same medium, it depends on the chemical nature of the metal. In this region the interphase is "ideally polarized" or "blocked"; in an equilibrium situation the thermodynamic analysis of the *dl* behavior can be performed in this potential region.⁶

Although the shortage of data for the *dl* on single-crystal faces was already pointed out,¹⁰ we may note that:

1. No results concerning cadmium, indium, etc., are known.
2. Nearly all measurements have been obtained at "room temperature."
3. Nearly all experiments were carried out in aqueous solvent.
4. In most cases only the three low-index faces were studied; only for gold has a large number of high-index faces been investigated, etc.

Some trends in our current understanding of *dl* can be discussed.

Considering the way in which the ions present in solution interact with the electrode, a successful approach was developed for liquid metal electrodes: the solution side of the *dl* was divided by a plane parallel to the electrode surface—the "outer Helmholtz plane" (oHp). On the solution side of the oHp, only long-range interactions obeying classical electrostatic and distribution laws arise; this is the so-called diffuse layer [long-range interactions are described by the Gouy–Chapman (G–C) theory]. On the metal side of the oHp, short-range interactions as well as long-range ones exist. These short-range interactions change the solvent properties, while interactions between the ions and the metal electrode take place. This is the so-called inner part of the *dl* (Stern or Helmholtz layer). It has a thickness of molecular dimensions. The whole *dl* is represented by the Gouy–Chapman–Stern (G–C–S) model.

When there is substitution of the solvent molecules, by an organic neutral substance, in the double-layer region the adsorption–desorption of this substance can usually be observed on the $C(E)$ curves.

When using this approach for different crystal faces, one might expect that the diffuse layer will probably not be influenced by atomic arrangement of the surface for a given metal, while the co will strongly influence the inner part of the dl. But the contribution of the diffuse part of the dl varies with the density of charge at the electrode surface, according to the G-C theory, and the density of charge at a given potential imposed to the electrode depends on the co. Therefore we have to discuss first the influence of the co on the solution side of the oHp; then we will discuss short-range interactions on the metal side of the oHp and the validity of the G-C-S model. However, for the sake of clarity, it is better first to analyze the pzc values published in the literature¹⁰ and then to consider the behavior of the solution and the metal sides of the oHp. Separation of the results into those for conditions with and without specific adsorption has been avoided because many borderline cases are observed.

Some monographs may be found useful in connection with this section; see References 3, 6, and 9.

1. The pzc's

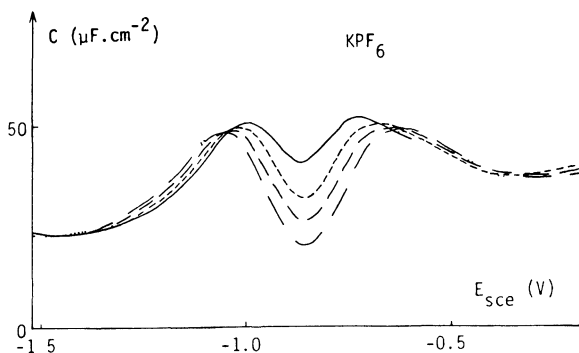
Most of the pzc values published in the literature were determined by observation of the minimum due to the contribution of the diffuse part of the dl to the $C(E)$ curves. See, for instance for Ag(100), Ref. 62 and Fig. 18. However, depending on the metal, for a given solvent and for given ions, the potential at which the density of charge is zero at the metal surface may be in the dl region for all co's or for only some of them, or for none of them. When a pzc cannot be obtained by this direct method, an indirect method has to be used,† as was the case for copper‡⁶³ and zinc.⁶⁴

Most of the pzc values are summarized (Fig. 19) as a function of the melting point of the metal⁶⁵; the length of the solid lines show to what extent the pzc varies with the co for each metal.§ It

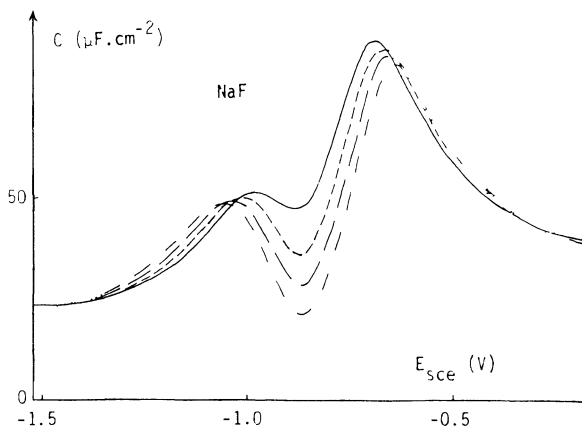
† The scraping method cannot be used for crystal faces obviously.

‡ Although it seems possible to obtain the pzc by a direct method for copper (111) and (100).

§ For gold, the extent the pzc varies is given here for 10 mM NaF; it is smaller in 10 mM HClO₄.



(a)



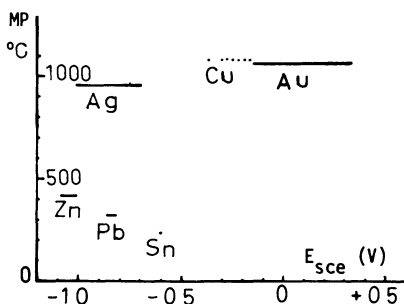
(b)

Figure 18. $C(E)$ curves for the (100) face of silver in aqueous solutions of (a) KPF_6 and (b) NaF for different concentrations of electrolyte: (—) 100, (---) 40, (— · — ·) 20, (— · · · — · · ·) 10, and (· · · ·) 5 mM. Sweep rate = 5 mV s^{-1} ; frequency = 20 Hz (Ref. 62)

is clear that the co influences largely the pzc for high-melting metals and has little or no influence for low-melting metals. This is probably due to the mobility of the surface atoms at room temperature for low-melting metals.

As the pzc (in the case of no adsorption) is linearly related to the electronic work function of the metal surface^{66,67} and as the

Figure 19. Anisotropy of the pzc of different metals as a function of their melting point; the solid lines show to what extent the pzc varies with the ϕ_0 for each metal.⁶⁵ Bismuth, which is a semimetal, is not plotted.



work function depends on the metal surface double-layer dipole moment [see Section III.5(ii)] which varies with the ϕ_0 , the pzc should vary with the ϕ_0 as the work function. Unfortunately, the general influence of the ϕ_0 was experimentally shown for the electronic work function for copper⁶⁸ and for the pzc for gold; however, the parallelism of these two experimental variations is excellent.⁶⁹

The relative surface energy [see γ plot of Section III.5(iii) for the fcc system; Fig. 12] varies with the ϕ_0 ; the comparison established between the relative surface energy [relative to the (210) face for the fcc system] and the pzc of gold faces is surprisingly good if we keep in mind that the former parameter is calculated from a model (in the nearest-neighbor broken-bond approximation) [see Section III.5(iii)] and the latter parameter is experimental¹⁰ (Fig. 20).

As foreseen from the discussion of Section III.5, the contributions to the surface potential from the “overspill” of the electrons perpendicularly to the metal surface and the “smoothing” by a lateral flow of electrons from high-ionic-density regions to low-ionic-density ones, explain the decrease of the electronic work function and the pzc from smooth to atomically stepped surfaces.

Obviously, the most densely packed face should have the most positive pzc because it has the highest work function, and the roughest face on an atomic scale should have the most negative pzc because it has the lowest electronic work function. This is observed experimentally for metals.

When there are irregularities (on an atomic scale) at the metal surface, they should lower the work function and shift the pzc negatively. It was observed experimentally that monoatomic steps

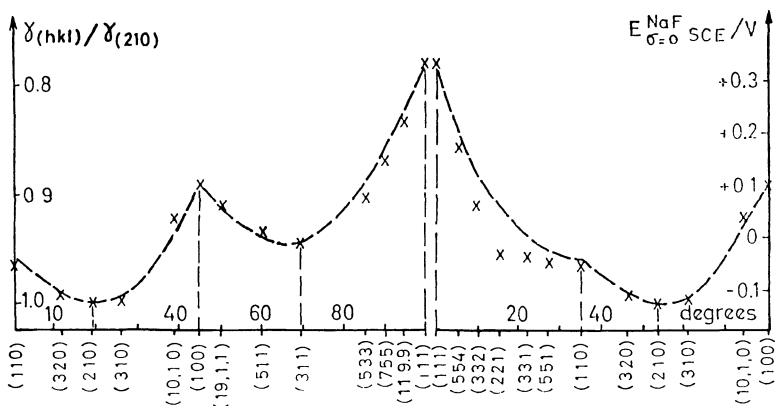


Figure 20. Variation of the relative surface energy (---) and pzc (x) of gold faces in 10 mM NaF at room temperature⁶⁹ with the θ plotted as a continuously varying parameter. Here (hkl) is a family of planes.¹⁰

on terraces of singular faces shift the pzc negatively. For a (100) face of gold, the 1×1 atomic arrangement [see Section III.5(i)] should have a more negative pzc than a reconstructed one more densely packed in atoms, if both can exist at the electrochemical interphase.

This anisotropy of the pzc tends to increase with the melting point of the metal. Therefore the influence of atomic steps and irregularities is less observable in electrochemical results obtained with low-melting metals than for results obtained with high-melting metals.

When adsorption takes place, if the adsorbate is positively charged it lowers the work function but the pzc is shifted positively with increasing concentration of adsorbate; if the adsorbate is negatively charged it raises the electronic work function but the pzc is shifted negatively with increasing concentration [see Fig. 21 for adsorption of Cl^- on Ag (110)⁷⁰]. There is no longer a parallelism between the pzc and work-function data. In vacuum the adsorbate is part of the surface and, for instance, positively charged adsorbate allows the electrons to leave more easily from the metal surface (it lowers the work function) and the surface dipole is oriented toward the vacuum (Fig. 22a). At the electrochemical interface the surface dipole is oriented toward the metal (Fig. 22b) because for a

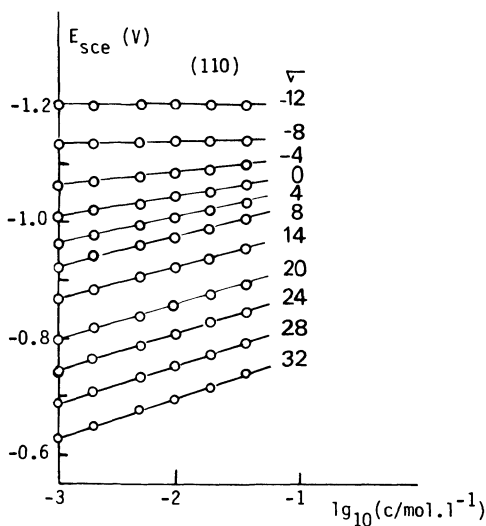


Figure 21. Variations of the potential with the logarithm of the concentration of the electrolyte at constant density of charge at the metal surface for the (110) face of silver in solution x mM NaCl + $(40-x)$ mM NaF.⁷⁰

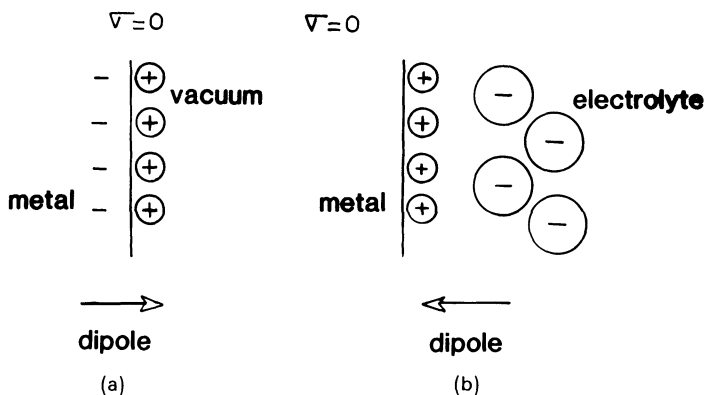


Figure 22. Representation of (a) the metal-vacuum interface and (b) metal-electrolyte interface in the case of adsorption of a positively charged species.

positively charged adsorbate negatively charged ions come into the dl to ensure electric neutrality of the interfacial region.

Considering the whole set of pzc values published,¹⁰ there are some discrepancies and some inconsistencies; how much are they due to poor control of the surface's actual structure and cleanliness is the question.

2. The Solution Side of the oHp

The variations of the capacity of the diffuse part of the dl with the potential at the electrode surface has the shape of a hyperbolic cosine (G-C theory for a symmetrical electrolyte); the minimum of capacity corresponds to zero-charge density on the metal. This density of charge corresponds to a potential imposed on the electrode. This potential of zero charge (pzc) varies with the co (see Section V.1).

The solution side of the oHp, in the case of no (or slight) adsorption and for dilute solutions, gives rise to a depression on the experimental $C(E)$ curves, deepening with the dilution of the solution (Fig. 18). Even if the density of charge is uniformly distributed at the metal surface, the shape of the experimentally observed depression is not exactly a hyperbolic cosine because of the contribution of the inner part of the dl (see Section V.3). Furthermore, complete nonspecific adsorption exists only for a very small number of systems and over restricted potential ranges. The contribution of the diffuse part of the dl (the hyperbolic cosine) appears on the $C(E)$ curves (for low concentrations of the solution) more distinctly when:

1. The adsorption is weak (or nonexistent).
2. The inner-layer capacity existing on the metal side of the oHp is high in this range of potential.
3. The concentration of the ions in solution is low (Fig. 18).

All of this is summarized in one well-known relation⁷¹:

$$1/C = 1/C^i + 1/C^d(1 + d\sigma^i/d\sigma) \quad (1)$$

where C^i is the inner-layer capacity, C^d the diffuse-layer capacity (if C^d is very large, $1/C = 1/C^i$), σ the charge on the metal surface, and σ^i the charge due to adsorbed ions. (If $d\sigma^i/d\sigma = 0$, $1/C = 1/C^i + 1/C^d$; if $d\sigma^i/d\sigma = -1$, $1/C = 1/C^i$).

The last two parameters are definitely on the metal side of the dl, but they also influence the contribution of the diffuse part to the total dl capacitance.

All this is clear as long as the charge is uniformly distributed on the surface of the solid metal electrode (as it is for mercury) and then the thermodynamic analysis can be reasonably carried out.†

But if there are *defects* on the metal surface (dislocation lines, pits due to electropolishing, etc.) the charge is not uniformly distributed on the surface. The influence of these irregularities will be all the more visible on the $C(E)$ curves when their relative area is larger and their pzc is far from the pzc of the atomically smooth part of the electrode (or more generally if their contribution arises in a range of potential in which the curve corresponding to the smooth part of the electrode does not have a large feature which could mask it).

This last point requires some comments. Small pits (on a smooth face) can be represented by a combination of monoatomic steps and kinks¹⁵ (see Section III.4). Therefore their behavior, if they are large enough, is close to that of the roughest face on an atomic scale. Also their interference will be more visible, on the $C(E)$ curves, for an atomically smooth face than for an atomically rough one. For instance, their effect is more visible in the fcc system, for the (111) face than for the (210) face. On the contrary, for the fcc system, a small facet, (111) oriented will alter the $C(E)$ curve of a rough face more than that of a smooth face.

When making low-index faces, a slight disorientation, which could be due to cutting (see Section IV.2), will create some steps and kinks. The contribution of these could be noticeable in the electrochemical results.

These ideas on the effects of nonuniformity of charge density on the $C(E)$ curves were checked years ago for an extreme case—polycrystalline silver in dilute sodium fluoride solution‡¹⁵ (Fig. 23)—in the following way. For a *model* polycrystalline electrode,

† The work required at a solid metal surface to form a unit area of new surface by stretching under equilibrium conditions is not equivalent to the surface tension and for some faces is obviously an anisotropic quantity (see p. 21 of Ref. 9).

‡ Later it was shown that there was a slight adsorption of the fluoride ion on silver electrodes,⁶² but this does not alter the conclusions.

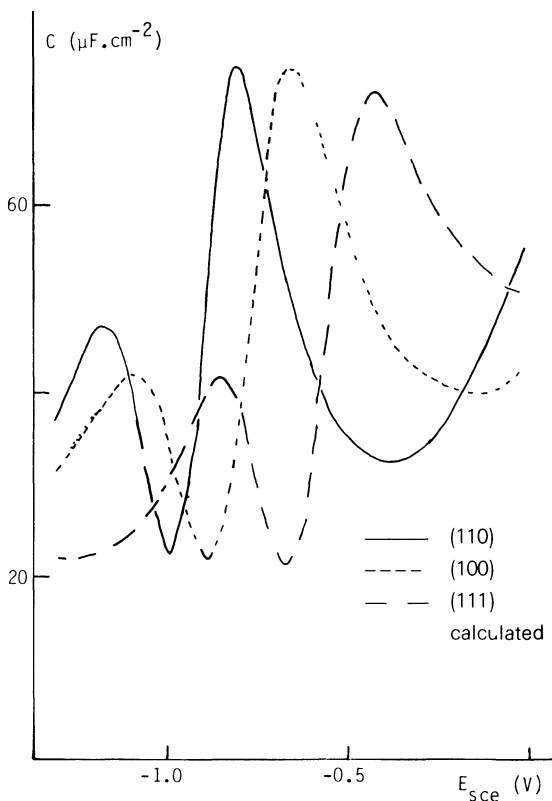


Figure 23 Experimental $C(E)$ curves for silver (111), (100), and (110) faces in 10 mM NaF (frequency of the alternating signal = 20 Hz, sweep rate = 10 mV s^{-1}) and calculated $C(E)$ curve for a *model* polycrystalline electrode¹⁵

made up of *only* the three faces of simplest indices, according to the stereographic projection (Fig. 5), there are at the surface 46% (110) oriented, 23% (100) oriented, and 31% (111) oriented; the calculated $C(E)$ curve [taking into account these proportions for the contributions of the three experimental curves of the (110), (100), and (111) faces and assuming a parallel capacitor equivalent circuit] is very close to that observed experimentally for polycrystalline silver. The following features are to be noted:

1. The diffuse-layer minimum is broader than for low-index faces (on which charge can be thought of as uniformly distributed).
2. The capacity minimum is very close to that of the (110) face, because the diffuse-layer minima for the (100) and (111) faces appear in ranges of potential where the two other faces have high capacity values.
3. The capacity peak for positive density of charge is less high than for low-index faces (Fig. 23).

For *high-index faces* a number of steps and kinks are necessary for the average specified co . They alter the distribution of charge at the surface [see Section III.5(ii)] and on the $C(E)$ the part of the curves which reflects the contribution of the diffuse part of the dl. Unfortunately, the study of high-index faces was performed *only* for gold. For this metal, "secondary" effects⁷² were observed[†]; they have to be discussed first for low-index faces and are as follows:

1. For the (100) face, there is an influence of the negative limit of the explored range of potential on the pzc and on the hysteresis existing between both sweeps of the $C(E)$ curves⁷³ (Fig. 24).

2. For the (111) face, no influence of the negative limit arises but an hysteresis of the $C(E)$ curves in the range of potential of the pzc⁷² is observed, the origin of which is at slightly positive density of charge (Fig. 25).

3. For the (110) face, there is no hysteresis and no effect of the range of potential explored but a secondary effect was also observed. It is easier to observe in concentrated solutions and in the case of specific adsorption (see Section V.2); it does not seem to alter the contribution of the diffuse part of the dl on the $C(E)$ curves.⁷²

These secondary effects are less and less important as the co 's of gold faces are further from those of the low-index faces. They will be discussed in more detail in Section V.3(ii).

Besides these "secondary effects" there is slight adsorption of the fluoride ion on gold⁷⁴ and most of the studies for high-index faces were done in fluoride. Last, but not least, the dl region for gold [for which the $C(E)$ curves should show no dispersion over

[†] They were not observed for silver faces and are not mentioned in the literature for other sr metals

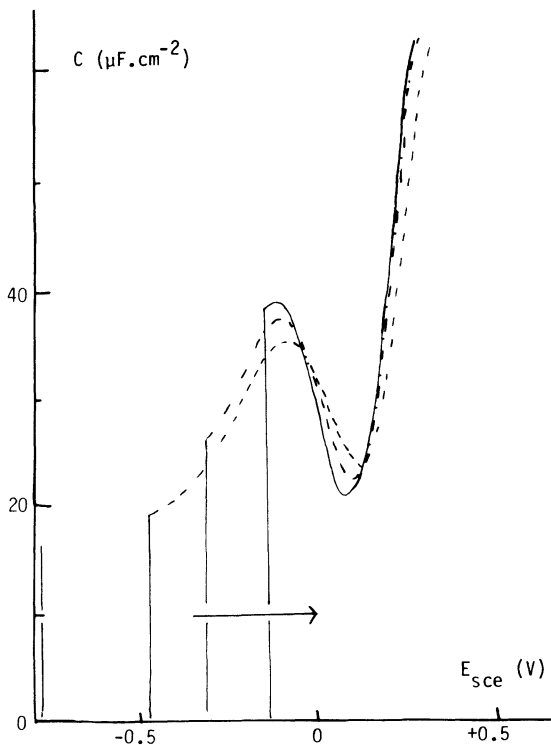


Figure 24. $C(E)$ curves for the (100) face of gold in 10 mM NaF (frequency of the alternating signal = 20 Hz; sweep rate = 10 mV s^{-1}) for different negative limits of the range of potential explored.⁷³

a large range of frequency] is difficult to define (see Fig. 26a). These observations explain the $C(E)$ curves of the three faces of lowest indices (Fig. 26b).

However, for *high-index gold faces*, the contribution of the diffuse part of the dl appears clearly. For the sake of clarity, the potential scales for the different $C(E)$ curves⁷⁵ have been aligned to the pzc's (all pzc's are "at zero") and the capacity minima are adjusted so that the scale for capacity is given $\pm 5\%$ (Fig. 27). Obviously, for the (210) and (311) gold faces, the depression on the $C(E)$ curves is narrow and nearly the same as for the (110)

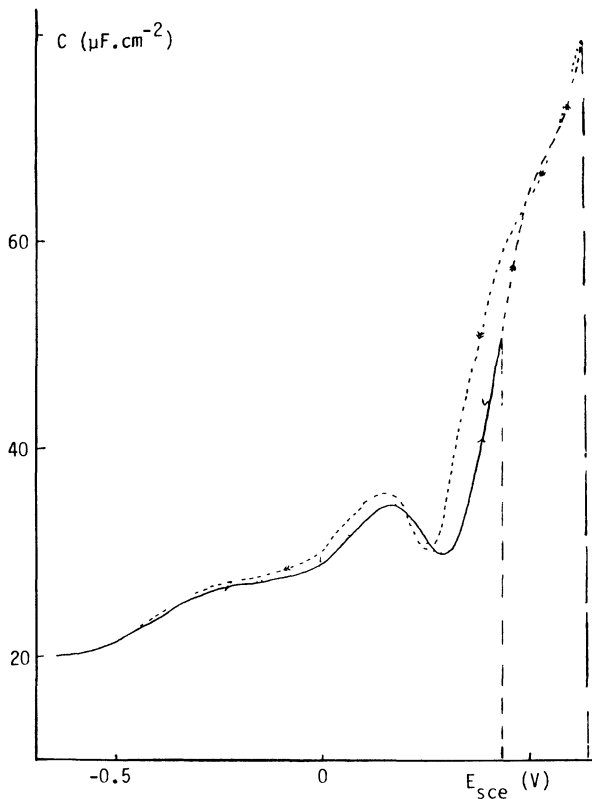


Figure 25. $C(E)$ curves for the (111) face of gold in 10 mM KBF_4 (frequency of the alternating signal = 20 Hz; sweep rate = 10 mV s^{-1}) for two positive limits of the explored range of potentials.⁵⁸

face. For faces which have the most positive pzc's there is already interference of some faradaic process for the positive density of charge; this is the case for (533) and (755) (Fig. 27a) and (332) (Fig. 27b). However, for a systematic change of surface structure, (311), (211), and (533) [which are 2(111)-(100), 3(111)-(100), 4(111)-(100)], the capacity depression becomes broader and broader as the charge density seems to be less uniformly distributed. The same explanation would be valid for the series (110), (551)

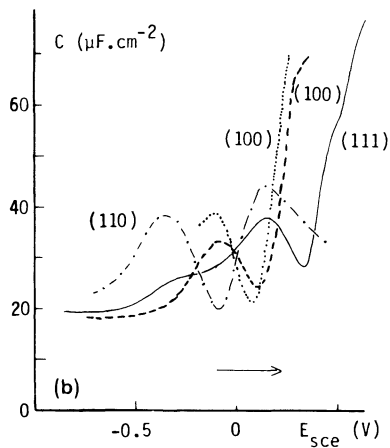
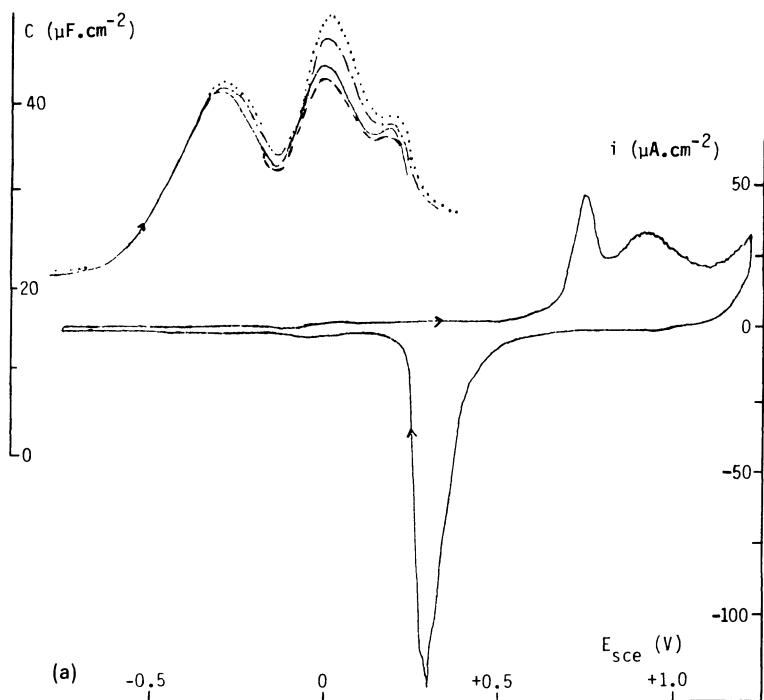


Figure 26. (a) $C(E)$ curves for a (210) gold face in 40 mM NaF: (· · · · ·) 15, (— · — ·) 20, (—) 40, and (— — —) 80 Hz; sweep rate = 10 mV s^{-1} . Cyclic voltammogram of the face in 10 mM NaF; sweep rate = 20 mV s^{-1} .⁷⁴ (b) $C(E)$ curves for the (111), (100), and (110) faces of gold in 10 mM NaF (frequency of the alternating signal = 20 Hz; sweep rate = 5 mV s^{-1}) for the positive sweeps, without correction for the roughness factor. For (100), curves are given for two different negative limits.

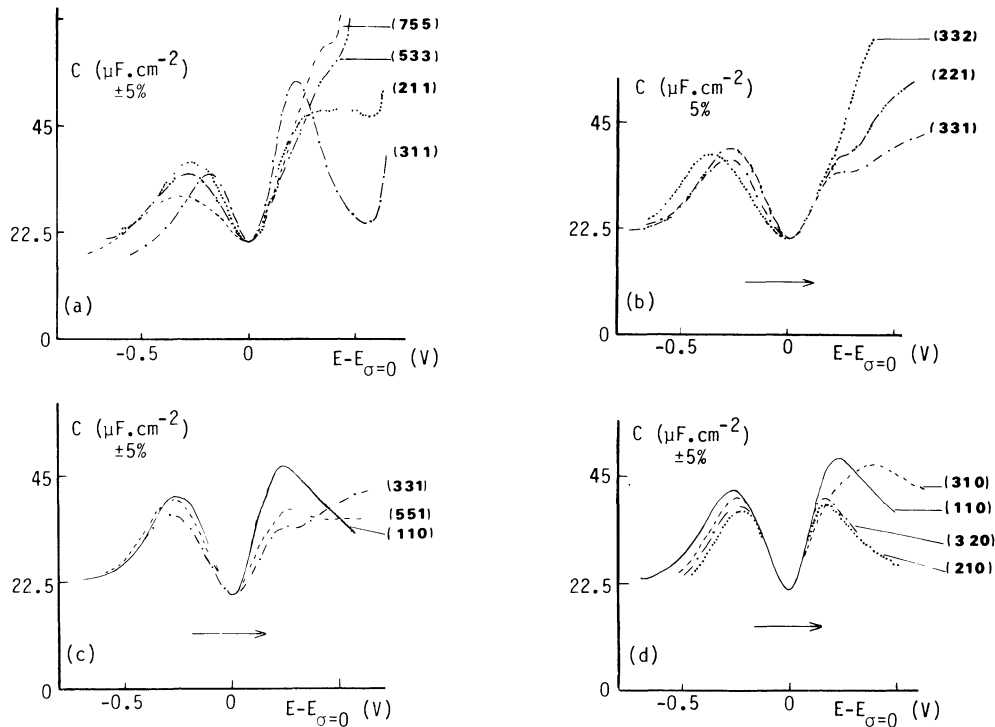


Figure 27. (a), (b), (c), and (d) $C(E)$ curves for different faces of gold in 10 mM NaF. Sweep rate = 5 mV s^{-1} ; frequency of the alternating signal = 20 Hz.⁷⁵ For atomic arrangement of the faces, see Figures 9–11.

[which is 3(110)-(111)], and (331) [which is 2(110)-(111)] (Fig. 27c). For atomically very rough faces the "smoothing" effect (see Section III.5) is such that the density of charge has nearly the same uniform distribution at the surface; this would be the case for (110), (210), (320), and (310) (Fig. 27d), and (311) (Fig. 27a) which show a capacity depression of the same shape on the $C(E)$ curves.

Therefore it seems that, in some cases, the atomic nonuniformity of the surface entails a distortion of the shape of the $C(E)$ curves in the part due to the contribution to the diffuse part of the dl[†]; then blind application of the G-C-S theory would be a mistake, but for low-index faces (and furthermore for low-melting metals) the application of the G-C-S theory is not questionable, as long as it is used in a *true* dl region.

3. The Metal Side of the oHp

On the metal side of the oHp, there is the so-called inner layer (the compact layer, or Stern or Helmholtz layer) which is a molecular-diameter thick and in which short-range interactions as well as long-range interactions exist.

When there is no adsorption, only solvent molecules are present in this layer. Then the variation of the inner-layer capacity *vs.* charge density gives information on the metal-solvent interactions [see Section V.3(i)]. The short-range interactions change the solvent properties.

When there is ionic adsorption, there are ions on the metal side of the oHp (substitution for the water molecule). These metal-ion interactions cannot be described by the G-C theory [see Section V.3(ii)]; they alter the metal-solvent interactions.

When there are organic neutral substances on the metal side of the oHp, there is also substitution of solvent molecules by neutral molecules and metal-neutral substances interactions are observed, they could also alter the metal-solvent interactions; in some cases the adsorption-desorption peaks can be observed [see Section V.3(iii)].

These three cases will now be briefly reviewed.

[†] The possible nonuniform distribution of charge for some faces is controlled, whereas for polycrystals nonuniform distribution of charge is uncontrolled.

(i) *Metal-Solvent Interactions*

Although, obviously, there is a continuous change of structure and composition in the dl, from the metal surface to the bulk of the solution, the model which has explained successfully many results for mercury, was assumed to be valid for other metals. In the case of *no adsorption* this model leads to the conclusion that the variations of the inner-layer capacity C^i with charge density σ should be independent of the concentration of the ions in solution. In the case of no adsorption, there are only solvent molecules on the metal side of the oHp. Only for *water* are there available results on metal crystal faces.

For *bismuth* faces these water-metal interactions are represented by the $C^i(\sigma)$ curves of Fig. 28.⁷⁶ At significantly negative charges, C^i depends very little on the co, while at zero and positive charge density the most densely packed (atomically) face has lower values. No correction for the roughness factor (see Section V.4) was performed when plotting these results.

For *silver* faces, years ago,¹⁵ these $C^i(\sigma)$ curves were found, for the three faces of lowest indices, to be nearly independent of the concentration of the fluoride ions (after correction for the

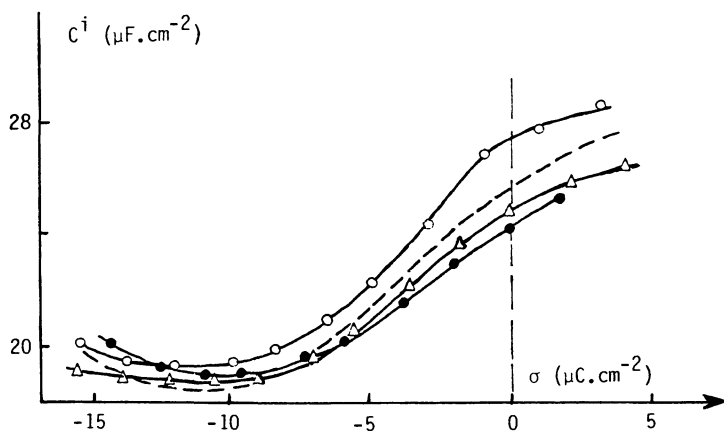


Figure 28. $C^i(\sigma)$ curves for bismuth faces: (○) (111) face; (△) (01 $\bar{1}$) face; (●) (2 $\bar{1}\bar{1}$) face, and (---) polycrystalline bismuth. From experimental results in KF solutions.⁷⁶

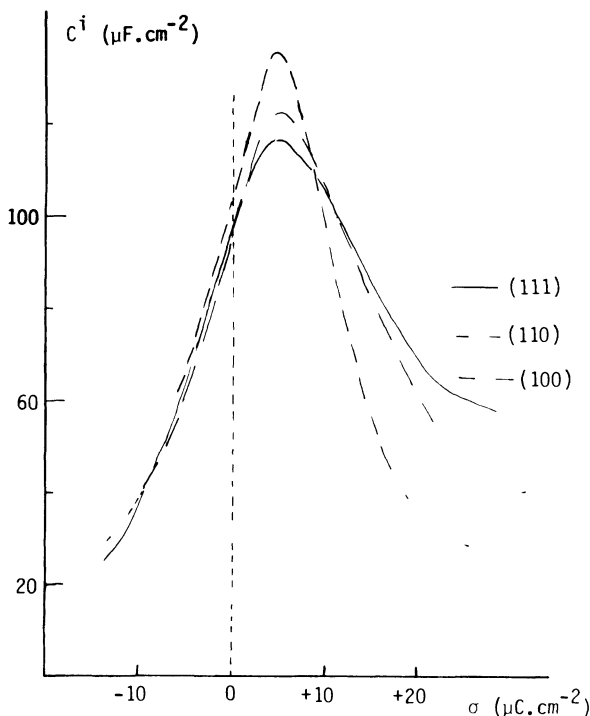


Figure 29. $C^i(\sigma)$ curves for silver faces (111), (100), and (110) from experimental results in NaF solution corrected by the roughness factor.¹⁵

roughness factor) (Fig. 29). For negative-charge density, the variations are identical. For zero charge and small positive charges, the most densely packed face has the lowest value (the contrary was observed by other authors⁷⁷). Later, it was shown that there is slight adsorption of fluoride ions⁶² and the absence of influence of the concentration of the ions in solution was demonstrated for the (100) and (110) faces of silver in KPF_6 ^{62,78} (Fig. 30) (after correction for the roughness factor[†]). Therefore the model is valid at least for these faces of silver. This is why we have divided Section V into two subsections on the solution side and the metal side of the oHp.

[†] For the (100) face the curves are also corrected for incomplete dissociation of KPF_6 .⁶²

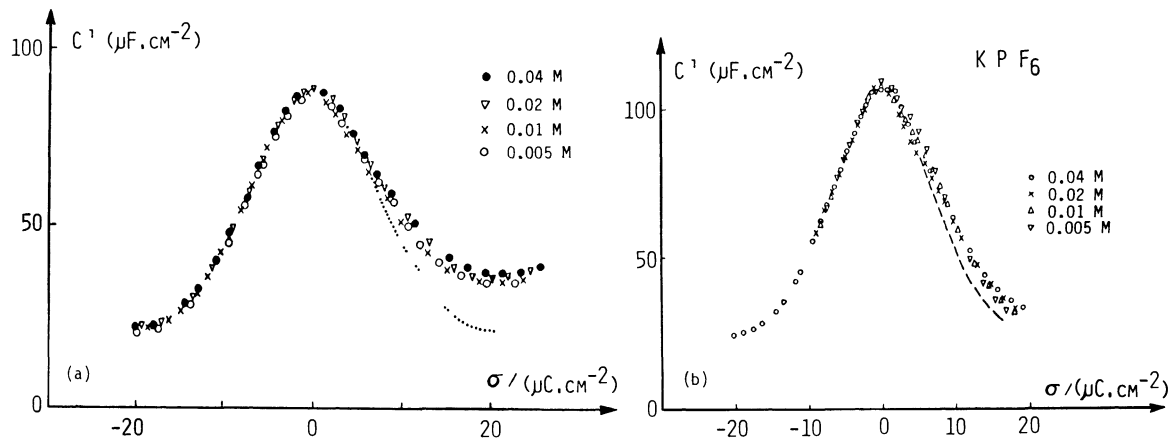


Figure 30. $C'(\sigma)$ curves for silver faces from results in KPF_6 solutions: (a) (100) face corrected for roughness factor and incomplete dissociation of the electrolyte⁶² and (b) (110) face corrected for the roughness factor only.⁷⁸

Although $C'(\sigma)$ curves were published for *gold* faces^{73,74} they were not found to be independent of the concentration of the ions in solution; this can be due either to specific adsorption of ions or to the existence of some faradaic process in the range of potentials used, i.e., this range of potential was not really a "dl region," or the G-C-S theory is adequate at low but not at higher concentrations. Unfortunately, the corrections proposed for the G-C-S theory have not yet been used by practicing electrochemists.

From so few results it is difficult to draw precise conclusions on the influence of the co on the metal-solvent interactions. It was foreseen⁷⁹ that $\Delta g(\text{dip})$, the change of the contribution to the metal-solution electrode potential drop due to preferential orientation of water dipoles, increases as the work function of the metal surfaces decreases, i.e., is larger for the (110) face than for the (100) face (of the fcc system); this was observed for silver faces in KPF_6 (Fig. 30).

(ii) *Metal-Ion Interactions*

Most papers published on single-crystal-face behavior¹⁰ deal with this situation because most ions adsorb on solid electrodes of *sp* and *sd* metals. Adsorption depends on the nature of the ions and the metal, the interaction between ions and solvent in the dl,[†] the interactions between electrode metal and solvent, and the influences of these interactions on each other. All this exists already for electrodes which are not single-crystal faces, but the situation is complicated by the fact that the charge is distributed at the surface in an uncontrolled way. This is not the case for single-crystal faces for which the strength of adsorption, as well as its variation with charge density at the electrode surface, could depend on the atomic structure of the face which is the electrode. However, despite these complications, some progress has and can be made.

Any species, the surface excesses of which are not totally described by the diffuse-layer theory, are said to be specifically adsorbed. σ' , the quantity of charge, that cannot be accounted for by the diffuse-layer model, is the charge at the electrode surface

[†] The ions are no more in a symmetrical situation as they are in the bulk of the solution.

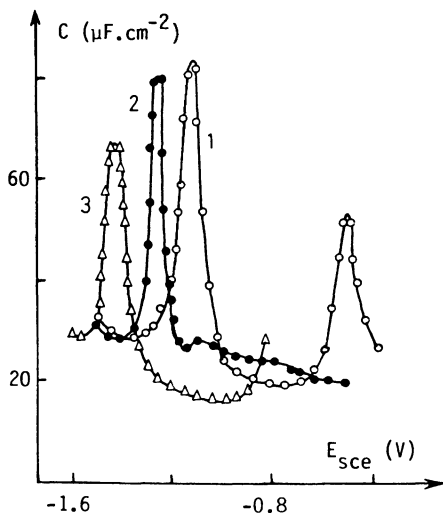


Figure 31. $C(E)$ curves for copper faces in 50 mM Na_2SO_4 + 5 mM TBAI: curve 1, (111), curve 2, (100); and curve 3, (110).⁸¹

due to the specifically adsorbed ions; for anions

$$\sigma^i = zF\Gamma^- - zF\Gamma^{-d} \quad (2)$$

where z is the valence of the anion, F the Faraday constant, Γ^- the anion relative surface excess, and Γ^{-d} the anion relative surface excess in the diffuse layer.

For faces of a given metal, the phenomenology of specific adsorption is the following.†

(a) Type of ions

Alkali and alkaline-earth cations have less tendency to adsorb than anions on metal faces, as was observed on other metal electrodes. However, in general, large cations do adsorb; Cs^+ was demonstrated to adsorb on $\text{Ag}(100)$.⁸⁰ TBA^+ was demonstrated to adsorb on $\text{Cu}(111)$, $\text{Cu}(100)$, and $\text{Cu}(110)$ ‡^{63,81} (Fig. 31) and on

† The effect of temperature on specific adsorption was not studied on single-crystal faces.

‡ It was used as an indirect method to determine the pzc's.

Zn(0001), Zn(10 $\bar{1}$ 0), and Zn(11 $\bar{2}$ 0).^{82,83} For TBA⁺, there is a possibility of forming cation-anion pairs which may be considered as approximating to neutral molecules in their adsorption behavior [see Section V.3(iii)]. Underpotential deposition (UPD) of a foreign metal on crystal-face substrates is an extreme case of the adsorption of cations; then the adsorbate becomes part of the substrate surface. Therefore it is not included in the dl properties of single-crystal faces. However, as for the understanding of adsorption of anions on stepped faces, comparison with these results is very helpful, some results for UPD of lead on gold faces will be given in the paragraph on stepped faces.

(b) *Dependence on charge density*

The amount of specifically adsorbed ions increases with increasing density of charge of the opposite sign on the electrode (although negative ions begin to adsorb already at low negative-electrode-charge densities). When experimental results are precise enough and when the dl region is sufficiently extended, $\sigma^i(\sigma)$ curves can be plotted for different crystal faces at a given concentration of anion in solution (Figs. 32a-32c).

The variations of the strength of the metal-to-ion interaction depend on the atomic structure of the face and of the charge density on the face. At low charge densities on the face, for silver for instance (Fig. 32c), the charge density due to adsorbed anions is larger for the (111) face than for the (100) face, which is not the same at high charge densities (Fig. 32a).

Comparison of faces is difficult; when reading papers attention must be paid to the fact that some authors corrected their results by a roughness factor (see Section V.4) and others did not.

(c) *Effect of concentration of anions in solution*

For a given face of a metal at a given charge density, the amount of adsorbed ions increases with concentration of the ion in solution. The way the amount of adsorbed ions increases with bulk concentration is described by an isotherm.

The practicing electrochemist observes on the $C(E)$ curves, with increasing concentration of the anion in solution, progressive disappearance of the contribution of the diffuse part of the dl and

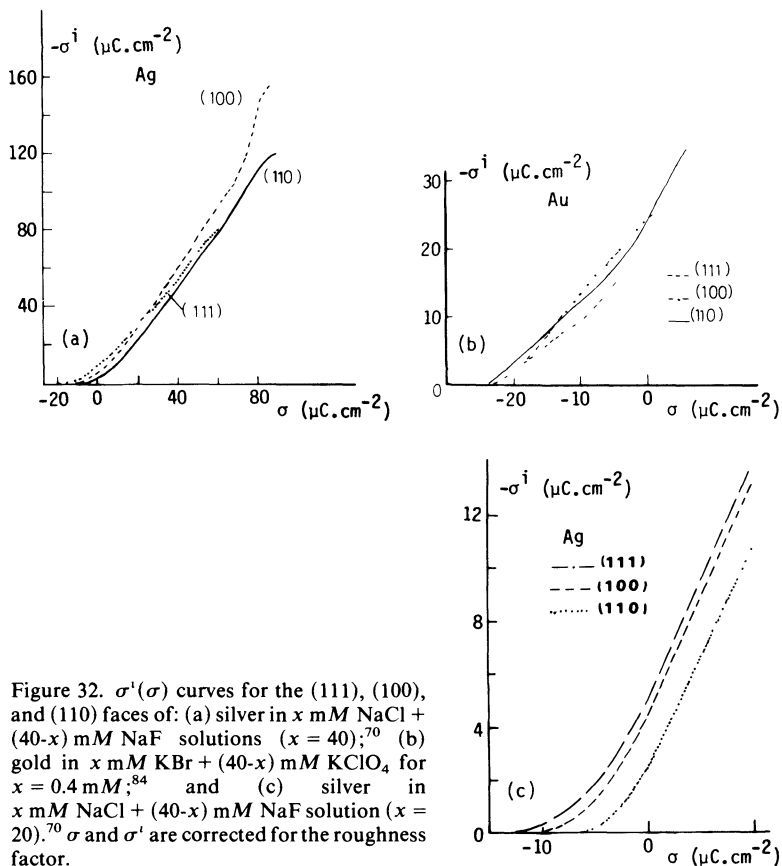


Figure 32. $\sigma'(\sigma)$ curves for the (111), (100), and (110) faces of: (a) silver in x mM NaCl + $(40-x)$ mM NaF solutions ($x = 40$);⁷⁰ (b) gold in x mM KBr + $(40-x)$ mM KClO_4 for $x = 0.4$ mM;⁸⁴ and (c) silver in x mM NaCl + $(40-x)$ mM NaF solution ($x = 20$).⁷⁰ σ and σ' are corrected for the roughness factor.

a negative shift of the adsorption capacity peaks (Fig. 33). A criterion used for comparison of different faces of one metal for adsorption has been the disappearance, with increasing concentration, of the contribution of the diffuse part of the dl. Another criterion was the shift of potential $\Delta E = \Delta(E_{\sigma=0,x} - E_{\sigma=0,y})$ (assuming no adsorption of y and x being the adsorbate), at a given concentration. Generally, according to these criteria, for different faces of one metal, at zero-charge density, adsorption of anions tends to be the strongest on the face with the most densely packed atoms.[†]

[†] From results obtained in the case of coadsorption of anions and neutral molecules, other information can be obtained [see Section V.3(iii)].

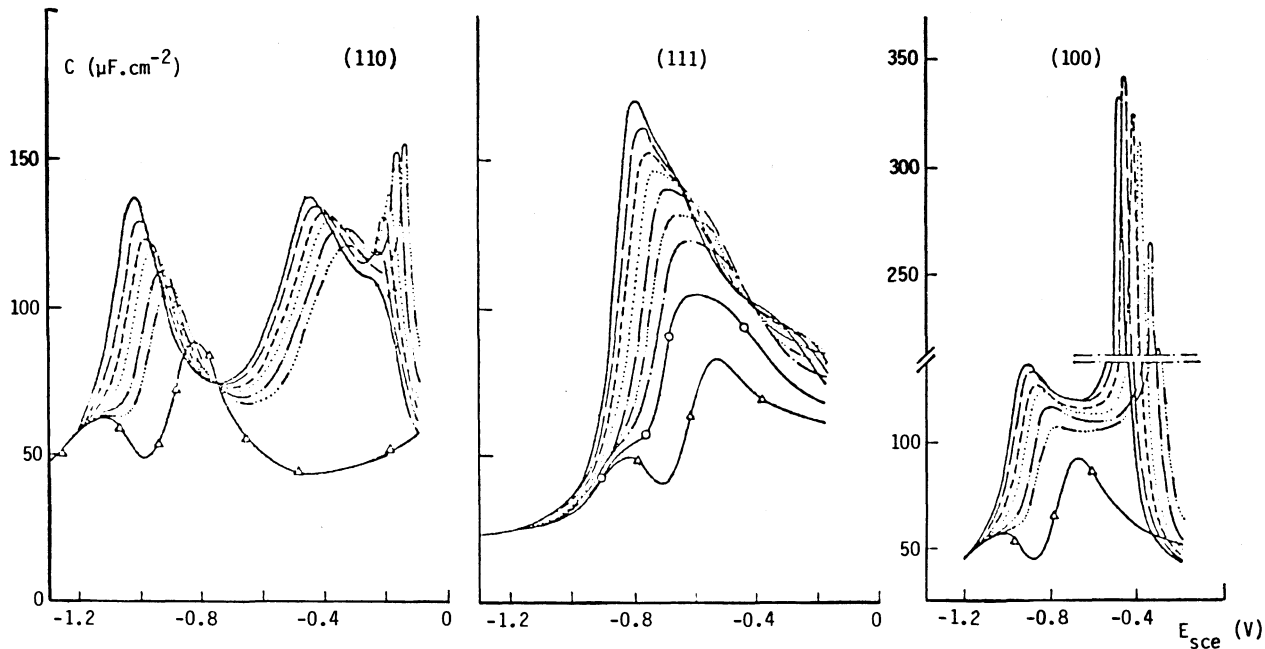


Figure 33. $C(E)$ curves for the (111), (100), and (110) faces of silver in x NaCl + $(40-x)$ mM NaF for $x = (\Delta)$ \circ , (\circ) 0.2, $(-\cdot-)$ 0.5, $(-\cdots-)$ 1, $(-\cdots-)$ 2, $(\cdots\cdots)$ 5, $(---)$ 10, $(- - -)$ 20, and $(-)$ 40. Sweep rate = 10 mV s^{-1} ; frequency = 20 Hz .⁷⁰

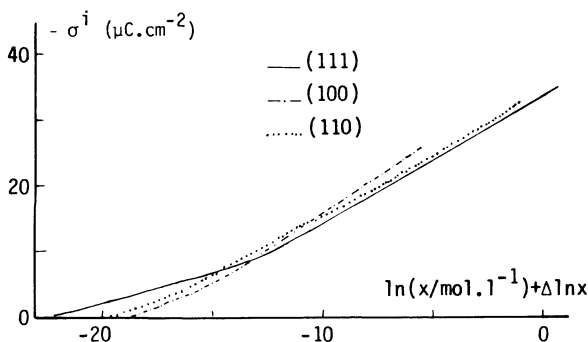


Figure 34. Composite curves of $\sigma^i(\ln x)$ built on the isotherm at $\sigma = 0$, for faces of gold in x mM KBr + $(40-x)$ mM KClO₄ solutions.⁸⁴ $\Delta \ln x = f(\sigma)$.

By building on the isotherm at zero charge, a composite curve can be obtained; for instance, for faces of gold⁸⁴ the results are as given in Fig. 34. Are the differences between these results of the different faces significant?

(d) Effect of the size of the ions

The bigger the ion is, the more it tends to adsorb at the electrode.† This is also true for single-crystal faces. For instance, for gold faces, the shift of the dl region for the sequence of anions F⁻, Cl⁻, Br⁻, and I⁻ is to more negative potentials together with higher and higher values of the capacity of the adsorption peaks and decrease of their widths (Figs. 35 and 36). This is in agreement with expectations and with what is observed for polycrystals. Furthermore, the shift in potential is the same for all faces: the relative adsorption strengths are the *same* for all faces of one metal.

(e) Analysis of the $C(E)$ curves

Most of the studies of anion adsorption on metal faces were done by $C(E)$ curves. According to the method used to obtain these curves, there are slight differences. For the bridge method, it

† The strength of adsorption is also connected with the hydration of the ions: small ions like F⁻ tend to retain their primary hydration sheaths so that they adsorb weakly or not at all.¹⁰⁶ Electronic factors involved are the donating ability of the electron pair and the polarizability.

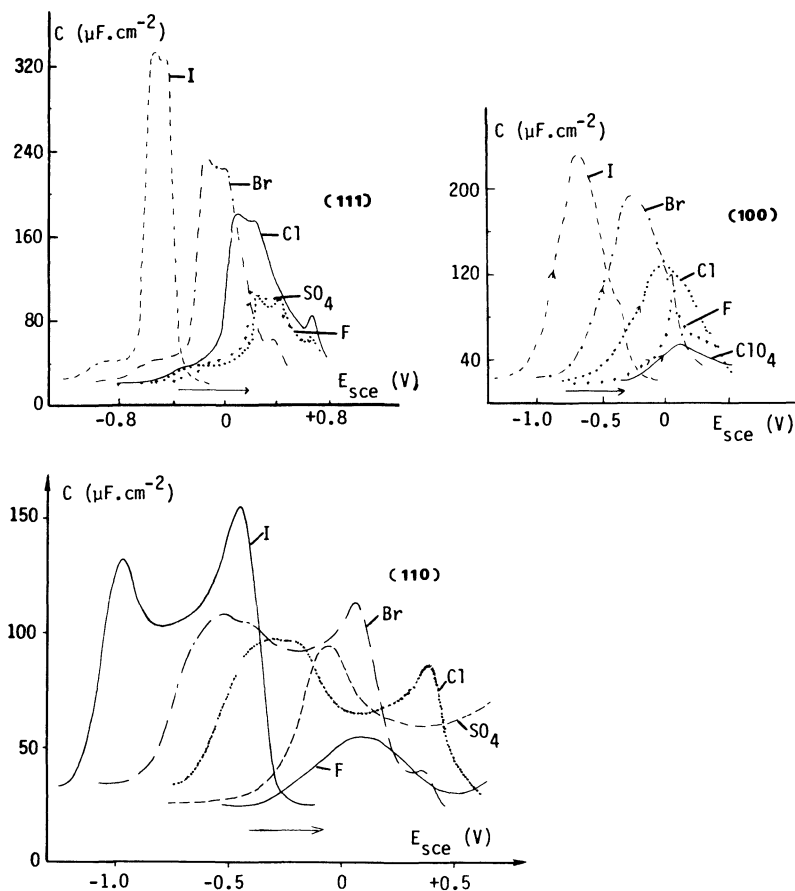


Figure 35. $C(E)$ curves for different anions in solutions for the (111),⁸⁵ (100)⁷² and (110)¹⁰ faces of gold. For KI, KBr, and KCl, concentration of the electrolyte is 100 mM, frequency of the alternating signal is 80 Hz, and sweep rate is 5 mV s⁻¹. For K₂SO₄, the same items are 200 mM, 130 Hz, and 100 mV s⁻¹, respectively; for NaF, 500 mM, 20 Hz, and 5 mV s⁻¹; and for HClO₄, 1000 mM, 20 Hz, and 10 mV s⁻¹.

is necessary to remain several minutes at one potential in order to balance the bridge. Therefore the results can be affected by adsorption of impurities (which is a slow process). For the sweep method, one has to be careful that the interphase is in adsorption equilibrium. In both cases an alternating signal is used for the measurements.

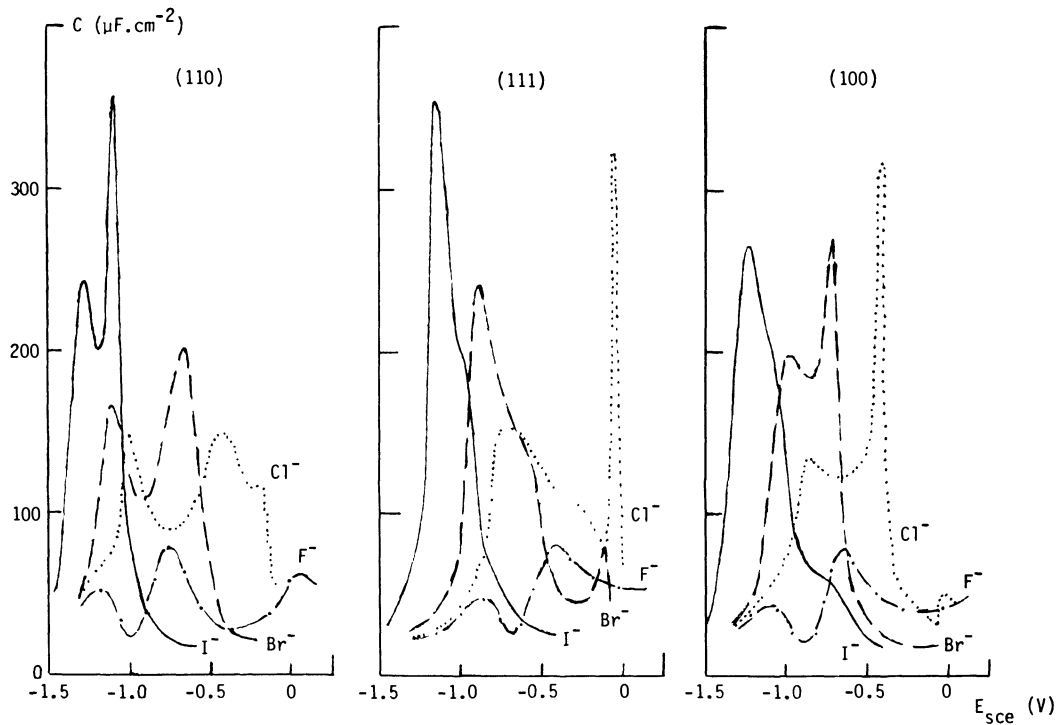


Figure 36. $C(E)$ curves for the (111), (100), and (110) faces of silver for different anions in 10 mM solutions. Frequency = 80 Hz; sweep rate = $10 \text{ mV s}^{-1.70}$.

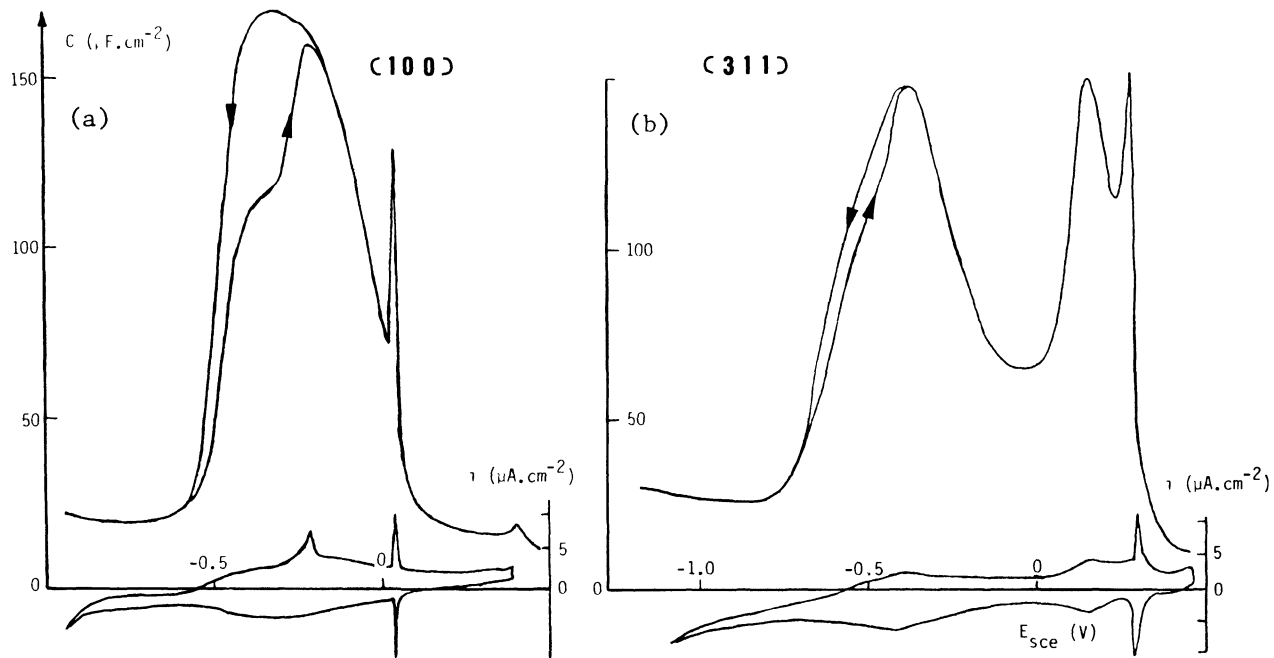


Figure 37. $C(E)$ curves for the (a) (100) and (b) (311) faces of gold in 2 mM bromide solution (frequency = 20 Hz, and sweep rate = 5 mV s^{-1}) and corresponding $i(E)$ curves (sweep rate = 20 mV s^{-1}).¹⁰

For an ideal-polarized electrode, the capacity values should be, in a large range, independent of the frequency of this alternating signal.

For a given metal in a given medium, the shape of the $C(E)$ curves differs significantly from one face to the other—quite distinctive patterns are observed experimentally (Figs. 35–37). A general pattern (number, relative amplitude of the capacity peaks, and their relative positions in the range of potential) is observed at a given face for different sizes of the anions[†] (Figs. 35 and 36).

The origin of these peaks can be discussed. Obviously, when metal-ion interactions are weak, the effects of the metal-solvent interactions should still be observable. On the contrary, when the metal-to-ion interactions are strong, the metal-solvent interaction effects become obscured. Intermediate cases will be difficult to analyze.

Three capacity peaks may be observed in the dl region: for some co's they merge, then one peak can be only a shoulder on another peak. We now discuss some cases.

1. For *silver*, in chloride solution, a complete thermodynamic analysis was done for the (110) face (Fig. 33).⁷⁰ The most negative peak (which shifts negatively with increasing concentration of anions) was shown to be possibly due to orientation of water molecules in the inner layer and is derived from the one observed without adsorption [see Section V.3(i)]. The middle peak occurs in the range of half-coverage and has been interpreted as being caused by the usual type of adsorption effect. The third very narrow capacity peak appears at more positive potentials where the chloride coverage is almost complete; it diminishes with increasing concentration of Cl^- (Fig. 33) and it is frequency dispersive. It could be due to reorganization of the adsorbate or charge transfer.[‡]

2. For much stronger adsorption, for which we have some quantitative data, the metal-to-ion interactions are much stronger. This is the case of bromide or iodide on *gold* faces. This is clear from the charge due to adsorbed ions at charge-density zero on the metal; for bromide, in a 1.25 mM solution, it is about $5 \mu\text{C cm}^{-2}$

[†] Furthermore, when comparing the same face of two different metals (crystallizing in the same system) the general patterns are nearly the same; therefore conclusions obtained for one metal might be cautiously extended to another.⁷⁰

[‡] Later it was demonstrated that fluoride ion (used in this mixed solution) adsorbs also on silver; these conclusions are, however, still valid and they can be extended to adsorption of bromide ion on silver.⁸⁶

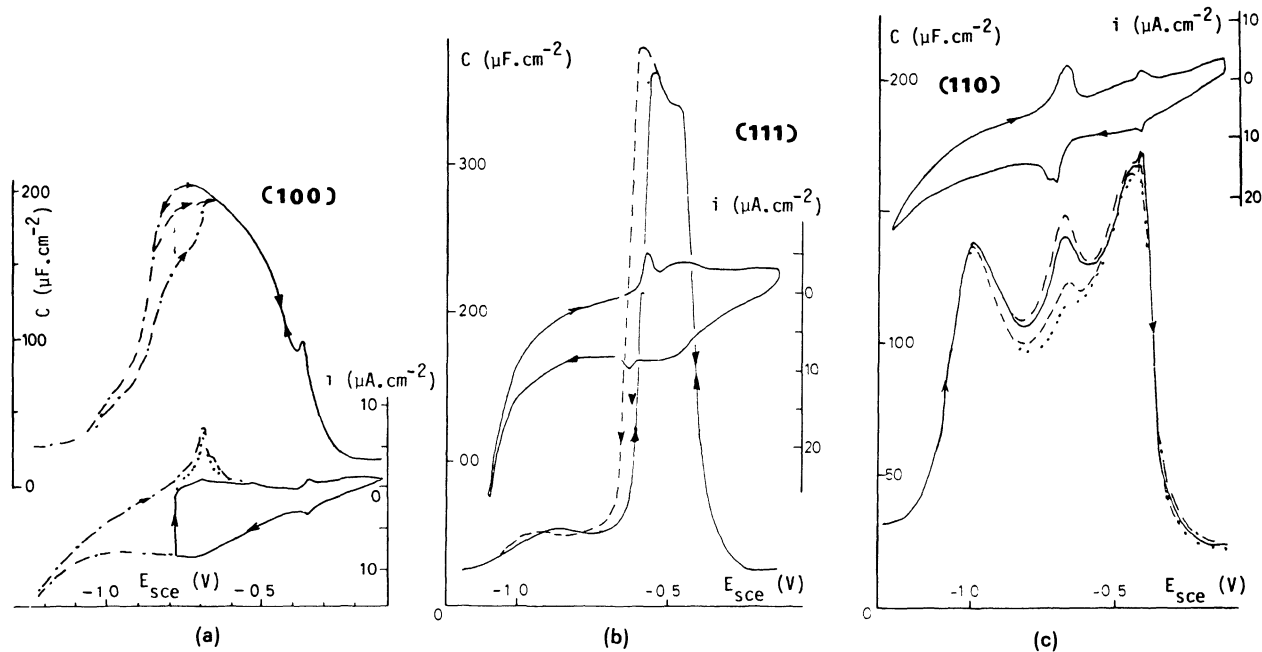


Figure 38. $C(E)$ curves for gold faces for continuous cycling; KI (concentration = 100 mM, sweep rate = 3 mV s^{-1} , and frequency = 20 Hz) and corresponding $i(E)$ curves (sweep rate = 17 mV s^{-1}). (a) (100) face for three negative limits of the range of potential explored; $i(E)$ curve for a stop of 30 s at -0.78 V ($\cdots\cdots$) is added for comparison.⁷² (b) (111) face for two positive limits of the range of potential explored.⁷² (c) (110) face for different frequencies of the alternating signal: ($-\cdot-\cdot-$) 12, ($—$) 20, ($---$) 40, and ($\cdots\cdots$) 80 Hz.⁷²

for Ag(110)⁸⁶, and about $25 \mu\text{C cm}^{-2}$ in an only 0.4 mM solution for Au(110).⁸⁴ Then the peak observed at the most negative potential is no longer due only to water reorientation but also to adsorption of anions.

The middle peak, which is connected to the inflection point of the isotherm, appears clearly for all faces, while the third peak, in the most positive part of the potential range of the dl region, is visible for some faces. For the (111) face, the general pattern (Figs. 35 and 36) is that of a huge double peak—which corresponds to the middle peak (its double shape is not yet explained).

The results of Fig. 37 can be discussed as follows; for the (100) gold face one peak is a shoulder on another and for the (311) face the three peaks are visible (the cyclic voltammograms are given for comparison [in fact, they are a $C(E)$ curve at very low frequency]).

The understanding of the $C(E)$ curves for gold faces is complicated by the “secondary effects” (already described for slight adsorption in dilute solutions; see Section V.2):

a. For the (100) face of gold, for all anions, hysteresis of the $C(E)$ curves, which diminishes when the negative limit of the explored range of potential is shifted positively (Fig. 38a), is observed. This effect is still visible for the (311) face which is 25.26° from (100) (Fig. 37). For all anions at the point at which the $C(E)$ curves of positive and negative sweeps merge, the difference of density of charge, $\Delta\sigma_{\text{hyst}}$, is nearly that of the extra peak observed on the cyclic voltammogram, $\Delta\sigma_{\text{peak}}^+$, at these potentials.⁷² Is this due to strong adsorption of the anions, reconstruction of the adsorbate and/or the substrate?

b. For the (111) face of gold, for all anions, an hysteresis of the $C(E)$ curves, which is not influenced by the negative limit of the explored range of potentials, but diminishes when the positive limit of the explored range of potentials is limited, was observed, as shown in Fig. 38b. It could be explained as for (100).

c. For the (110) face of gold, for most anions, in addition to the general phenomena described for all faces, an extra frequency-dispersive peak is observed [clearly visible from 12 to 60 Hz in KI solution (Fig. 38c)]; it was explained either by surface reconstruction⁷² or complexation of the gold face⁸⁷ or reconstruction of the adsorbate.⁸⁴ It remains open to question.

Understanding of the $C(E)$ of gold faces is easier when considering the influence of the co in a general way; to systematic changes of co correspond systematic changes of the pattern of the $C(E)$ curves for anion adsorption (see further).

3. For sulfate ions, which adsorb less than chloride ions on *gold* faces, only the more negative part of the $C(E)$ patterns is in the dl region (Fig. 35); oxidation of the gold surface occurs for all faces before complete coverage by sulfate ions (this is clearly visible for Au(110), Fig. 35). This example shows that *it is not always possible to see a dl region, which extends from the region of potentials in which there is no metal-ion interaction, all the way to the region of complete coverage of the surface by the adsorbed ions.*

(f) *Influence of systematic changes of the co on the $C(E)$ curves*

High-index faces were studied only for *gold*. For chloride on gold, which adsorbs less than bromide on gold, the three peaks are

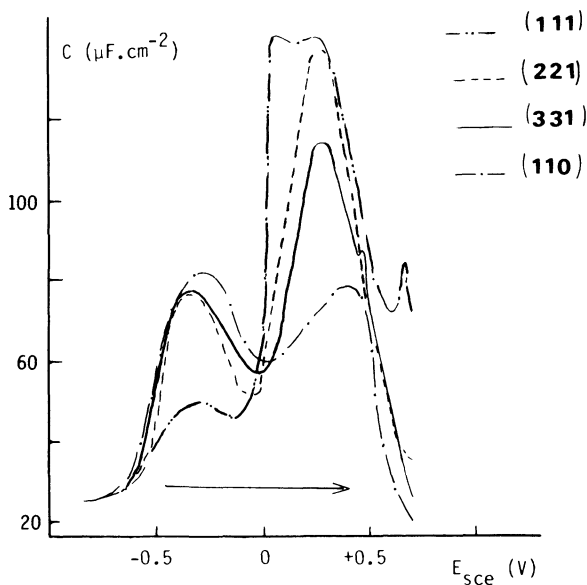


Figure 39. $C(E)$ curves for gold faces on the (111)-(110) zone, in 10 mM KCl solutions. Frequency = 12 Hz; sweep rate = $17 \text{ mV s}^{-1.88}$.

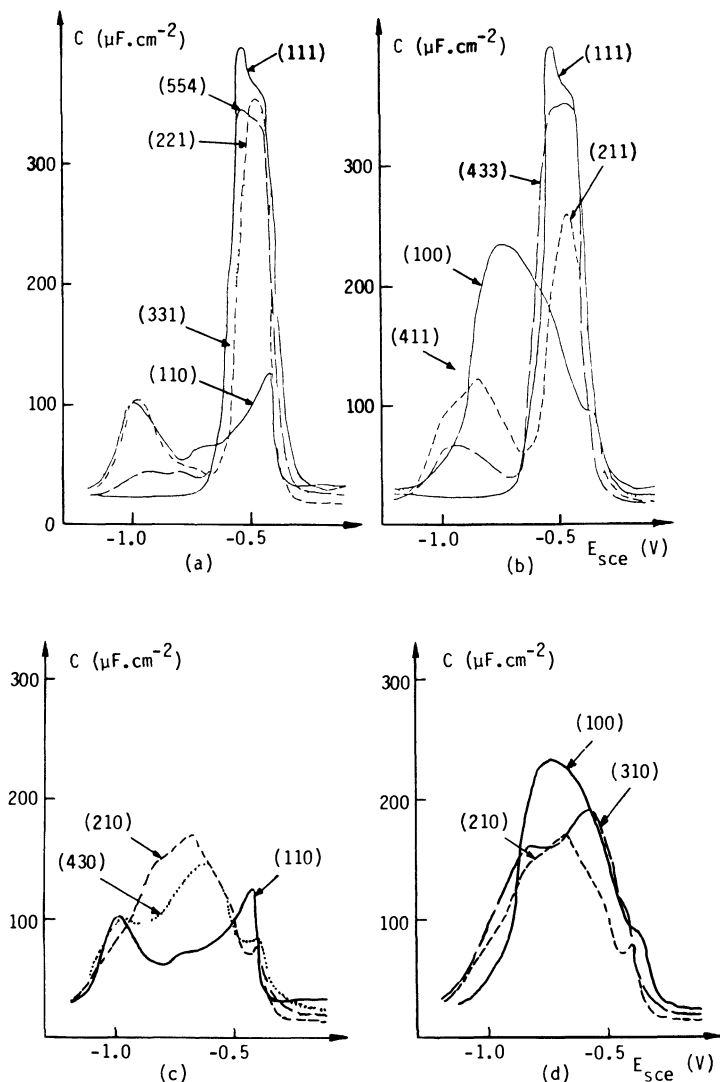
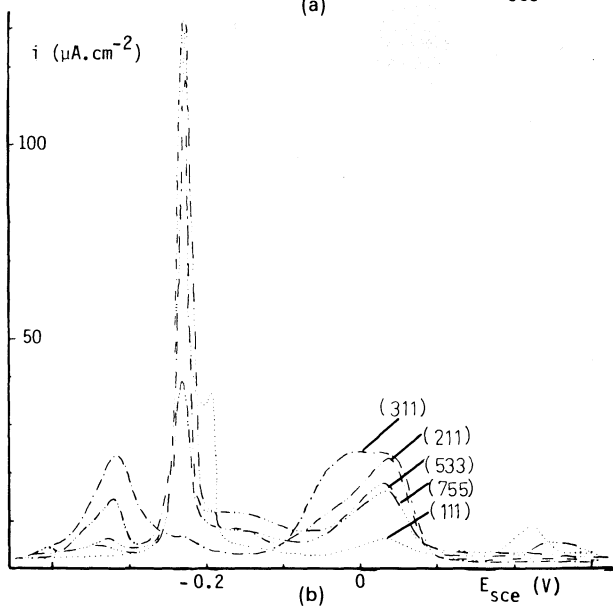
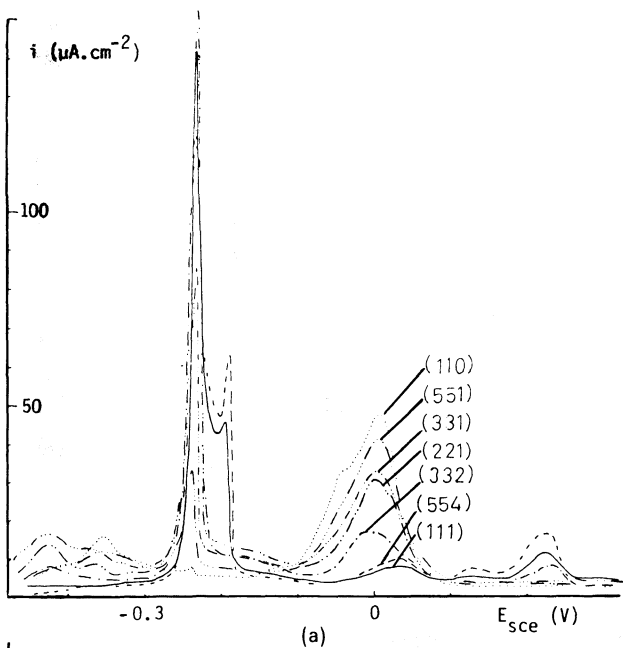


Figure 40. $C(E)$ curves for iodide adsorption on gold faces distributed on the three main zones of the projected unit stereographic triangle (concentration = 100 mM KI, frequency = 80 Hz, and sweep rate = 3 mV s^{-1}): (a) (111)-(110) zone; (b) (111)-(100) zone; (c) from (110) to (210) on the (100)-(110) zone; and (d) from (210) to (100) on the (100)-(110) zone.⁸⁹



Double-Layer Properties at Metal Electrodes

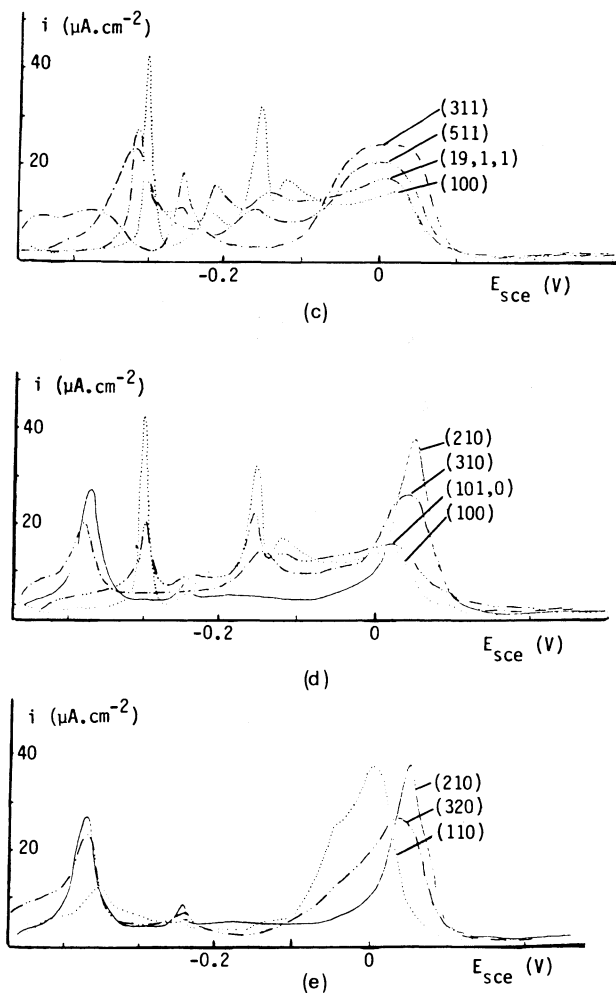


Figure 41. Voltammograms for stripping of lead adsorbed on gold faces the co's of which are on: (a) the (111)-(110) zone; (b) the (111)-(311) section of the (111)-(100) zone; (c) the (311)-(100) section of the (111)-(100) zone; (d) the (100)-(210) section of the (100)-(110) zone; and (e) the (210)-(110) section of the (100)-(110) zone. Sweep rate = 20 mV s^{-1} ; $10 \text{ mM HClO}_4 + 1 \text{ mM PbF}_2$ solutions deaerated with nitrogen and stirred. Although the UPD of oxygen was also included in each cycle, this is not shown on the figure because it occurs at more positive potentials. Deposition and stripping profiles of lead are similar for nearly all faces.

visible on the $C(E)$ curves for some faces. For systematic changes of the co on the (111)–(110) zone (making stepped faces; see Section III.4) (Fig. 39), a systematic change of the $C(E)$ curves was observed for the first time:⁸⁸ the more negative capacity peak increases with the number of atomic steps at the gold surface; in parallel, the middle peak decreases and the more positive peak shifts negatively. The most negative capacity peak seems connected to adsorption of chloride ion on monoatomic steps at the surface and the middle peak to adsorption on the terraces (see TLK model, Section III.4).

For iodide adsorption on gold faces,⁸⁹ metal-to-ion interactions are very strong because the anion is very large. The middle peak for the (111) face (Fig. 35) has (as for chloride, bromide, and concentrated sulfate or fluoride) the shape of a double peak; this shape remains unexplained. The most positive peak is not observable for most of the faces (probably charge transfer takes place over all the potential region observed). The situation is such for iodide adsorption on gold faces that, for faces distributed on the three main zones of the stereographic triangle⁸⁹ (see Fig. 10b), the more negative capacity peak increases systematically as the number of monoatomic steps at the gold surface increases (Fig. 40), while the middle peak decreases (i.e., increases with the width of the terraces at the gold surface) and the most positive peak is hardly noticeable and only in some cases. The evolution of the general pattern of the $C(E)$ curves with systematic changes of the structure of the faces was explained by the TLK model (see Section III.4).^{88,89}

The case of iodide adsorption on gold can be fruitfully compared to that of lead adsorption on gold faces¹⁹ which takes place with complete charge transfer,⁹⁰ i.e., by so-called underpotential deposition (UPD).

For faces distributed on the three main zones of the projected unit stereographic triangle (see Section III.2), systematic changes of the co exist; they were described by the TLK model (see Section III.4). As in fact the three main zones have to be divided into five sections to observe monotonic variations of the surface energy (Fig. 12) and monotonic changes of surface notation (Fig. 10), it is not surprising that the results for UPD of lead on gold faces have to be divided into five groups to observe monotonic changes: from (111) to (110) (Fig. 41a), from (111) to (311) (Fig. 41b), from (311)

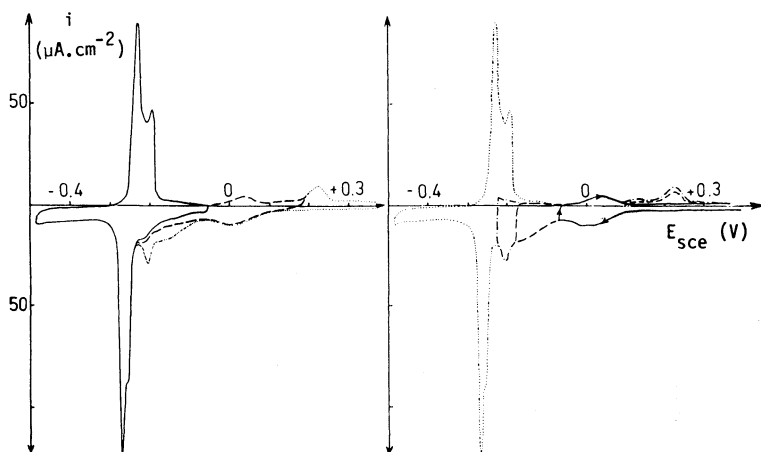


Figure 42. Cyclic voltammograms for the (111) face of gold. Sweep rate = 20 mV s^{-1} ; $10 \text{ mM HClO}_4 + 1 \text{ mM PbF}_2$ solutions deaerated with nitrogen and stirred, for different ranges of the potential scan. Although not shown on the figure, the formation of a monolayer of oxidized compounds was included in each cycle.

to (100) (Fig. 41c), from (100) to (210) (Fig. 41d), and from (210) to (110) (Fig. 41e). For an increase of the density of monoatomic steps at the electrode surface, the large positive peak increases; correspondingly, as the width of the terraces diminishes, the large negative peak decreases. Obviously, the TLK model is valid, although several details of these curves are not yet completely explained.

The TLK model is valid as well for anion adsorption as for lead UPD; furthermore other features are observed in both cases—for instance, for the (111) face of gold, the huge double peak with its hysteresis (Fig. 42). Thus it can be understood that such features are directly connected to the gold surface structure and properties.

From this paragraph on the general influence of the co, and ideas developed previously, it can be understood that comparison of interactions for two different metals can be done only for the same co of two metals crystallizing in the same system, if that!

(g) Influence of growth steps on the $C(E)$ curves

Only for the (100) and (111) faces of *silver* was the influence of growth-step density [see Section V.1(iii)] on the $C(E)$ curves

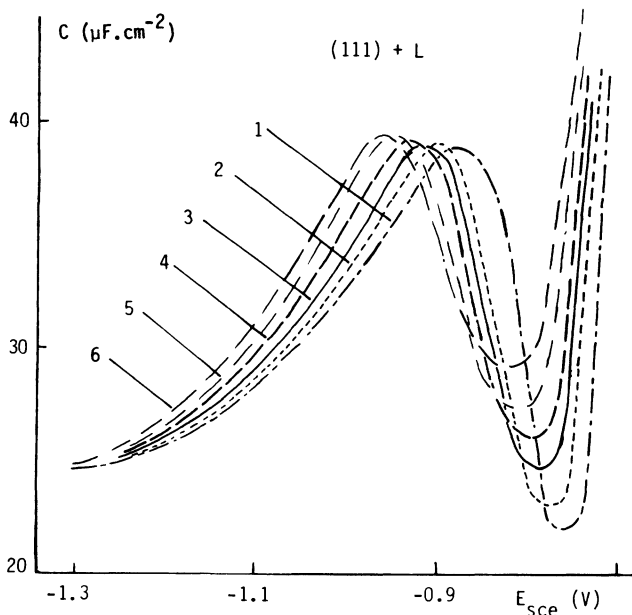


Figure 43. $C(E)$ curves of an electrolytically grown (111) face of silver for different growth-step densities L in 5 mM Na_2SO_4 : curve 1, $L = 2.0 \times 10^4 \text{ cm}^{-1}$; curve 2, $L = 4.2 \times 10^4 \text{ cm}^{-1}$; curve 3, $L = 7.0 \times 10^4 \text{ cm}^{-1}$; curve 4, $L = 9.2 \times 10^4 \text{ cm}^{-1}$; curve 5, $L = 12.3 \times 10^4 \text{ cm}^{-1}$; curve 6, $L = 15.3 \times 10^4 \text{ cm}^{-1}$. $C(E)$ curves obtained by bridge method at 210 Hz.⁹²

examined. Although, in fluoride solution, this parameter does not influence the pzc and the $C(E)$ curve of the (100) face⁹¹ and of the (111) face,⁹² in sulfate solution it is not the same. The shift to more negative potentials of the capacity minima (Fig. 43) was explained by adsorption of sulfate ions on the growth steps and not on the flat terraces which are (100) or (111) oriented. The value of the capacity at the minimum of the curves increases with the density of growth steps for the same reason. Sulfate ion would adsorb on growth steps but not on terraces in the case of silver, according to these results.

(h) Energy of adsorption

Besides this phenomenological review of the metal-to-ion interactions, some values for the influence of the co on the free energy

of adsorption (referred to as zero charge on the metal and standard states: 1 mol dm^{-3} in solution and 1 ion cm^{-2} on the surface) are given: for iodide on Bi (111), (01 $\bar{1}$), and ($\bar{2}$ 11), 112, 116, and 114 kJ mol^{-1} ;⁹³ for bromide on Au (111), (100), and (110), 120, 123, and 122 kJ mol^{-1} ;⁸⁴ and for chloride on Ag (111), (100), and (110), 100, 95, and 93 kJ mol^{-1} .⁷⁰ None of the authors was so audacious as to give experimental uncertainty of these values!

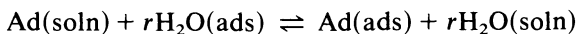
In this section, an attempt was made to give some clear trends for the metal-ion interactions for better understanding of already published results and future research.

(iii) *Neutral Molecules–Metal Interactions*

The reader may refer to Chapter 8 of Reference 9 for general background material.

For the electrochemical study of adsorption of an uncharged species, a base electrolyte is necessary. When neither the anion nor the cation of the base electrolyte adsorbs at the metal electrode, the simplest situation is achieved. When one of the ions of the base electrolyte adsorbs, it not only changes the chemical potential of the neutral substance but also the structure of the dl, decreasing (or increasing) the adsorption of the neutral molecule. Most of the time it is supposed that the ions of the base electrolyte do not adsorb at the electrode. But this is not always the case and furthermore the anion adsorbs in a different way on the different faces of one metal (see Section V.3). For some metal faces, studies of neutral-molecule adsorption may be complicated by the fact that the anion of the base electrolyte, as well as the neutral molecule, adsorb at least at the most densely packed faces. But if the adsorption-desorption capacity peak occurs in a range of potential in which the charge due to adsorbed anions is very small, the analysis of the adsorption of the neutral species is valid in this range.

Neutral adsorbate molecules replace solvent molecules on the metal side of the oHp according to the quasichemical equation:



Ad refers to the adsorbate and r is the number of water molecules replaced by one molecule of adsorbate.

This simple relation corresponds to a complicated phenomenon, because the solubility of the salt may be changed in the interfacial region (more than in the bulk solution) and both activity coefficients of the salt and the neutral substance are altered. The modifications of these may be different on the different faces.

We shall discuss only the case in which the adsorbate retains its chemical individuality, then adsorbed molecules are those which are in solution.

Electrode-adsorbate, electrode-solvent, and adsorbate-solvent interactions (which are no more as they are in the bulk solution) are involved in the process of adsorption; the first two depend directly on the density of charge at the metal surface.

For data obtained at equilibrium of adsorption on faces, thermodynamic analysis is possible and is more valid than for polycrystalline electrodes because the distribution of the charge density is controlled (uniform) at the electrode surface (see Sections V.1 and V.2).

As for polycrystalline electrodes, adsorption of neutral species on faces depends on the nature of the metal, and adsorbate and on the different interactions mentioned above. The surface excess Γ and the coverage θ , as well as their variations with charge density at the electrode surface, can depend on the atomic arrangement of the face.

For faces of a given metal, the phenomenology of adsorption of neutral substances is the following.

(a) *Effect of temperature*

Only for *bismuth* faces has the temperature effect been studied (for cyclohexanol adsorption in 50 mM/ Na_2SO_4 and H_2SO_4 aqueous solutions) from 281 to 321 K.¹³ The different behavior of the (111) face from that of the (01 $\bar{1}$) and (2 $\bar{1}\bar{1}$) faces, suggested that the chemical interactions between bismuth atoms and cyclohexanol are reinforced by temperature for the two last faces but that, for (111), there is only physical adsorption. This could explain why Γ_{max} (surface excess at saturation) diminishes with increasing temperature for (111) and increases for the two other faces. Bismuth crystallizes in the rhombohedral system, the (111) face is less densely packed in atoms than the two other faces, and bismuth is a semimetal, not a metal.

(b) *Dependence on potential*

Representation of the variations of the surface excess with the potential of the electrode is more usual than with charge density. Generally, only one part at the expected $\Gamma(E)$ curve is observable in the dl region. For instance, for cyclohexanol adsorption on zinc faces, comparison of the three low-index faces for one concentration of cyclohexanol in 100 mM KCl + 0.1 mM H₂SO₄ is represented in Fig. 44;⁹⁴ the surface excess is the highest for the most densely packed face.

(c) *Effect of the concentration of adsorbate in solution*

With increasing concentration of adsorbate in solution, for a given charge or a given potential, the surface excess increases. Comparison of the coverages for different concentrations of cyclohexanol, at the potential of maximum adsorption, for different faces of zinc (Fig. 45)⁹⁴ show that the situation is complex: at low concentrations coverage is higher for a nondense face, while at higher concentration of adsorbate the coverage is higher for the most densely packed face. For lead the similarity of the coverage-concentration variations for the (111), (110), and (112) faces but not for the (100) face, in the case of adsorption of cyclohexanol,⁹⁵ is surprising. How much this is due to experimental uncertainty or poor control of the surface state remains an unanswered question.

The effect of the concentration of adsorbate was observed for gold faces for the case of diethyl ether adsorption.⁹⁶ It is represented

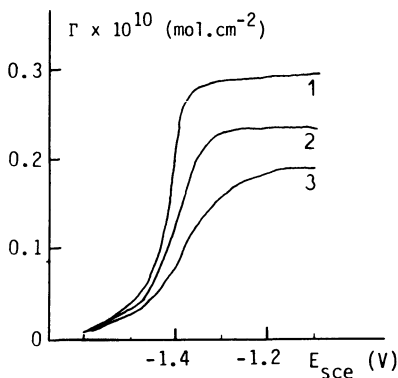


Figure 44. Surface excess of cyclohexanol at zinc faces as a function of potential: curve 1, (0001), curve 2, (10 $\bar{1}$ 0), and curve 3, (11 $\bar{2}$ 0) at constant concentration 150 mM in 100 mM KCl + 0.1 mM H₂SO₄.⁹⁴

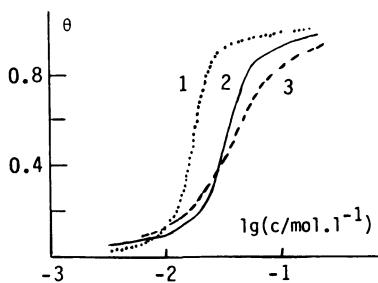


Figure 45. Coverage as a function of concentration for adsorption of cyclohexanol at zinc face: curve 1, (0001), curve 2, (10 $\bar{1}$ 0), and curve 3, (11 $\bar{2}$ 0) at potential of maximum adsorption.⁹⁴

by the variations of the surface pressure[†] with concentration (Fig. 46). Surface pressure increases with concentration for all faces. The composite curves represented in Fig. 46 were based on the surface pressure *vs.* concentration curve observed for the potential for the maximum of adsorption ($\Delta \ln c$ is the quantity that the surface pressure curve, for a given potential, has to be shifted to be superimposable on that corresponding to the potential of maximum adsorption). This work was done in 10 mM NaF; the fluoride may adsorb, for instance, more on the (111) gold face than on the (110) face. However, analysis from the capacity peak in the negative range of

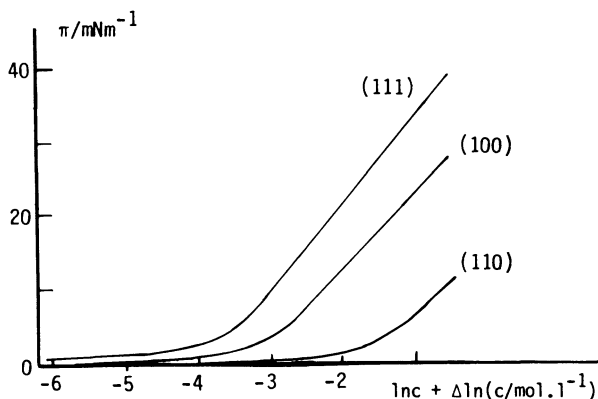


Figure 46. Surface pressure *vs.* concentration curves for adsorption of diethyl ether on gold faces (in 10 mM NaF).⁹⁶

[†] By integration of the charge-potential plots, the difference between the surface tension at zero coverage and at a given coverage is obtained; it is the surface pressure.

potential or from densities of charge *vs.* potential curves (obtained by chronocoulometric method) in a range of potential which corresponds to this peak is valid.

(d) *Effect of the structure of the nonionic adsorbate*

For the (0001) face of zinc, a systematic change of the chain length of the adsorbate was analyzed. For *n*-propyl, *n*-butyl, and *n*-amyl alcohols (in 100 mM KCl + 0.1 mM H₂SO₄), the coverage varies with the concentration (at potential of maximum adsorption), as shown in Fig. 47.⁹⁷

For the three alcohols, the two-capacitor model (see further) is valid. The attraction constant (in the Frumkin isotherm) and the maximum surface excess vary with the chain length as for mercury and polycrystalline cadmium. The adsorption energy of the alcohol increases with chain length for Zn (0001), mercury, and cadmium.

From the preceding discussion it is easy to understand that the phenomenology on crystal faces is qualitatively the same as for a polycrystalline electrode.

(e) *Analysis of the C(E) curves*

As adsorption of a nonionic substance at a metal electrode proceeds by replacement of solvent molecules at the surface by the adsorbate, following the G-C-S model, it is sufficient to consider the inner-layer capacity:⁹⁸

$$1/C' = d\varphi_i/d\sigma = (\partial\varphi_i/\partial\sigma)_\Gamma + (\partial\varphi_i/\partial\Gamma)_\sigma(d\Gamma/d\sigma)_c \quad (3)$$

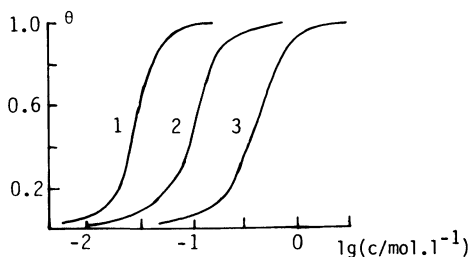


Figure 47. Coverage as a function of concentration for: curve 1, *n*-C₃H₇OH, curve 2, *n*-C₄H₉OH, and curve 3, *n*-C₅H₁₁OH at potential of maximum adsorption on the (0001) face of zinc.⁹⁷

where φ_i is the potential drop in the inner layer. Each term of the equation varies with the quantity adsorbed and the density of charge on the metal. When the adsorption is maximum, $d\Gamma/d\sigma = 0$; then all the effects of adsorption are described by the first term of Eq. (3) and C^i is a minimum.

For single-crystal faces, as for all metal electrodes, in the potential region where adsorption of neutral species prevails, the capacity is decreased (surface tension is diminished). When the dl region is large enough, adsorption-desorption capacity peaks are observable on both sides of the maximum of adsorption; they are due to the second term of Eq. (3) (Fig. 48). In some cases, only the adsorption-desorption capacity peak which occurs in the more negative range of potential of the dl region is observable because oxidation of the metal face takes place at more positive potentials (Fig. 31). By changing the base electrolyte, the range of potential of the dl region may be shifted; then the range of observation of the $C(E)$ curves is extended and, in some cases, both adsorption-desorption capacity peaks are observable (in different base electrolytes) (Fig. 49). If thermodynamic analysis of the adsorption process from the $C(E)$ curves is planned, coincidence of the $C(E)$ curves in base electrolyte and for different concentrations of the neutral substance should be observed in the dl region in order to give the integration constant. For most metal faces only this coincidence and one adsorption-desorption peak were observable.

In the range of potentials of an adsorption-desorption capacity peak, the extent of adsorption changes so rapidly with potential that the superposition of an alternating signal (for measurements) of different amplitude or frequency produces different values of the differential capacity.† Therefore, the potential of the adsorption-desorption capacity peak and potential (or density of charge) at the maximum of adsorption are often used as parameters characterizing adsorption because they are less subject to error.

From a *model*¹⁰⁰ based on the summation of capacitance due to adsorbate ($\theta = 1$) and solvent ($\theta = 0$), the charge density is

$$\sigma = \sigma_{\theta=0}(1 - \theta) + \sigma_{\theta=1}(\theta) \quad (4)$$

† Here the case of equilibrium adsorption is discussed; of course, the amplitude of the capacity peak depends also on the *rate* and potential dependence of the adsorption process.

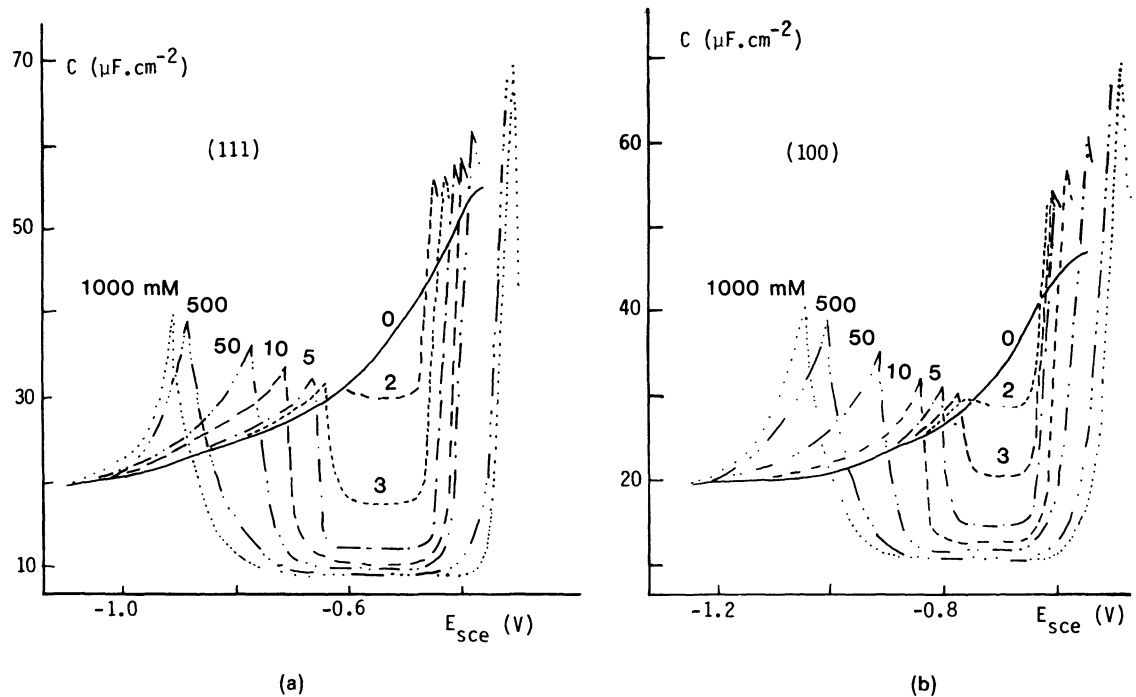


Figure 48. $C(E)$ curves for adsorption of *n*-isobutanol (in 50 mM Na_2SO_4) on silver faces: (a) (111) and (b) (100) for seven different concentrations although nine were investigated by the authors. $C(E)$ curves obtained by bridge method at 210 Hz.⁹¹

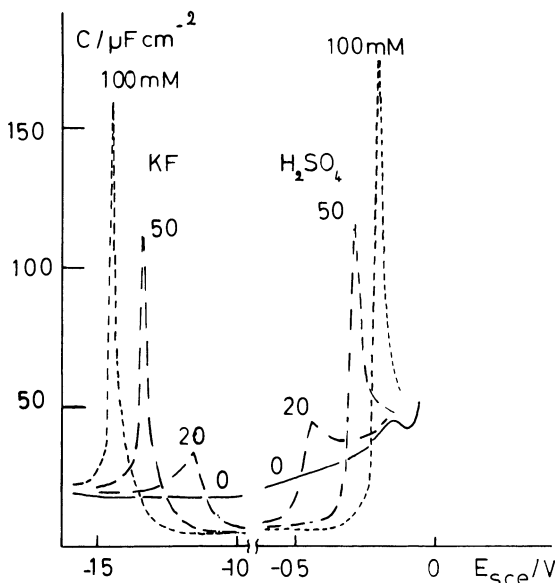


Figure 49. $C(E)$ curves for the (111) face of bismuth in two different base electrolytes (100 mM KF and 50 mM H_2SO_4) for different concentrations of cyclohexanol. $C(E)$ curves obtained by bridge method at 210 Hz.⁹⁹

For this two-capacitors-in-parallel model,

$$C = C_{\theta=0}(1 - \theta) + C_{\theta=1}(\theta) + (\sigma_{\theta=1} - \sigma_{\theta=0})(d\theta/dE)_c \quad (5)$$

The third term of the right-hand-side of Eq. (5) is always positive. This model is often used for comparison with experimental results.

Let us examine three cases:

1. For isobutanol adsorption on *silver* (111) and (100) faces (in 50 mM K_2SO_4)⁹¹ (Fig. 48), obviously the two adsorption-desorption capacity peaks are observable in the dl region on both sides of the maximum of adsorption. The capacity peak at negative potentials shifts negatively with increasing concentration of isobutanol while the capacity peak at positive potentials shifts positively. For a given concentration of adsorbate, the maxima of the capacity peaks are observed at less negative potentials for the (111) than for the (100) face, probably because the pzc of (111) is

less negative than that of (100).† The attraction constant and the standard (standard states are not quoted) free energy of adsorption (at zero charge) were found to be independent of the co. The same observations were made for adsorption of *n*-hexyl alcohol at these silver faces.⁹¹

2. For cyclohexanol adsorption on the three faces of lowest indices of zinc (in 100 mM KCl + 0.1 mM H₂SO₄), $C(E)$ curves are given in Fig. 50.^{97,101} Obviously, only one of the adsorption-desorption peaks is observable in the dl region. These results were shown to fit the two-parallel-capacitors model (dashed lines). For a given concentration of adsorbate, the potentials of the peak and of the maximum of adsorption shift in the same order as the pzc's in base electrolyte. From the complete analysis of the curves, all adsorption parameters were found to be co dependent.‡

3. For adsorption of pyridine on silver faces (in 100 mM NaF), the $C(E)$ curves are given in Fig. 51¹⁰² for three concentrations (although the authors published data for five concentrations). It is clear that the peak observed on the $C(E)$ curve in base electrolyte still shows on the $C(E)$ curves of (111) silver face. It disappears for the higher concentrations at the (100) silver face and disappears already for the lowest concentration at the (110) silver face. If this capacity peak is due to fluoride adsorption, ion-silver interactions are stronger on (111) than on (100) than on (110); if the capacity peak observed in base electrolyte is due to water-silver interactions, these are stronger on (111) than on (100) than on (110); if the capacity peak is due to water-silver interactions on (110) and to fluoride-silver interactions on (100) and (111), then there is adsorption of fluoride ion through the film of pyridine on the (111) face.§ In such a case, although the situation is clearer for single-crystal faces than for polycrystalline silver (Fig. 51d), the analysis of the $C(E)$ curves and determination of the adsorption parameters are difficult. But the adsorption-desorption capacity peak increases with concentration of adsorbate and shifts negatively

† The same sequence of co was observed for adsorption of TBAI on faces of copper in 50 mM Na₂SO₄ (Fig. 31).⁸¹

‡ For adsorption of TBAI on zinc faces, the adsorption parameters are also dependent on the co.

§ As was observed for sulfate adsorption on a gold (111) face through pyridine⁸⁵ (Fig. 52).

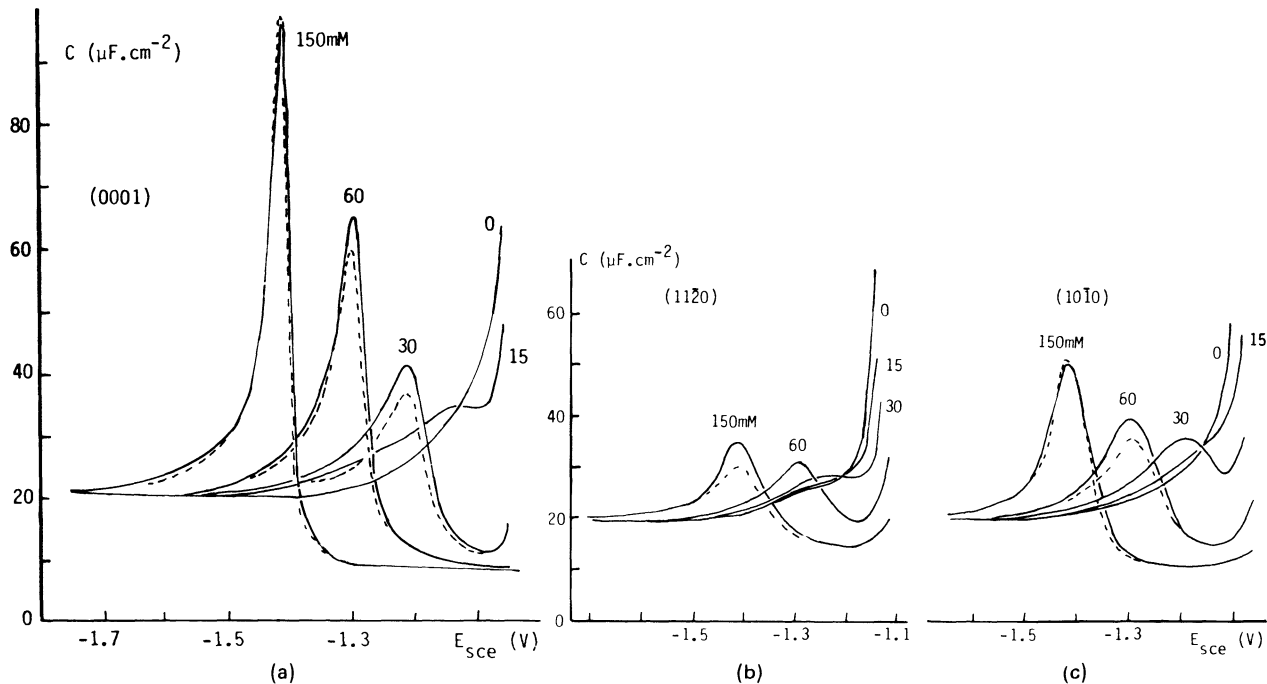


Figure 50. $C(E)$ curves for adsorption of cyclohexanol (in 100 mM KCl + 0.1 mM H_2SO_4) on faces of zinc, (a) (0001), (b) $(11\bar{2}0)$, and (c) $10\bar{1}0$, for five different concentrations although the authors investigated a greater number of concentrations. Curves calculated from Eq. (5) represented by dashed lines.^{97,101}

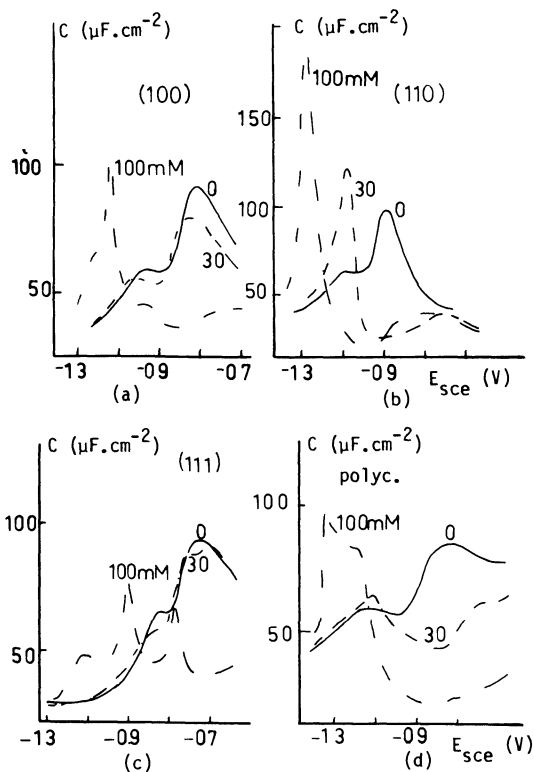


Figure 51. $C(E)$ curves for silver faces and polycrystalline silver for adsorption of pyridine for three concentrations although the authors studied 5 concentrations. Frequency = 40 Hz; sweep rate = 4 mV s^{-1} .¹⁰²

as is generally observed; however, its complicated shape, for (111) for instance, is not yet explained.

From these three examples and the disparity of the studied systems, it is difficult to draw conclusions. One could conclude that for a given metal and adsorbate the adsorption capacity peak shifts in the same way as the pzc in the range of potential and that its shape is simpler for single-crystal faces than for a polycrystalline electrode. This is not always the case—for instance, for adsorption of pyridine on gold faces⁸⁵ the capacity peaks are not distributed in the same range of potentials as the pzc's and the capacity peak

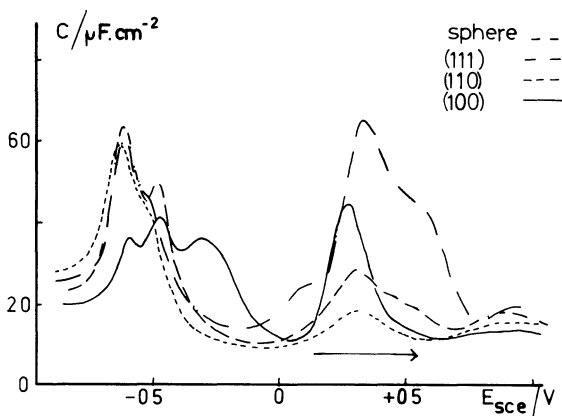


Figure 52. $C(E)$ curves for adsorption of pyridine (in 200 mM K_2SO_4) on gold faces⁸⁵ and polycrystalline gold sphere¹⁰³. Concentration of pyridine = 6.15 mM, frequency = 380 Hz, and sweep rate = 25 mV s⁻¹.

of the (100) face⁸⁵ has a more complicated shape than that of a polycrystalline sphere¹⁰³ (Fig. 52).

(f) Coadsorption of anions and neutral molecules

A base electrolyte is always necessary for study of adsorption of neutral molecules. We have already mentioned that in some cases an extra capacity peak appears at potentials less negative than the adsorption-desorption capacity peak and that it could be due to ion-metal interactions through the film of adsorbate or to very strong solvent-metal interactions. For extreme cases of coadsorption, e.g., pyridine on silver faces in KCl electrolyte¹⁰² and pyridine on gold faces in K_2SO_4 electrolyte,⁸⁵ a capacity peak at a less-negative-charge density than the capacity peak due to adsorption of neutral molecules could be explained in such a way. These studies can give information on the nature of the capacity peaks observed in pure electrolyte, i.e., how much they are due to solvent reorientation or to anion adsorption (Fig. 51).

Another puzzling cases of coadsorption is that observed for adsorption from 300 mM $n-C_5H_{11}OH$ (in 50 mM Na_2SO_4) on faces of silver on which a well-controlled density of growth steps exists;

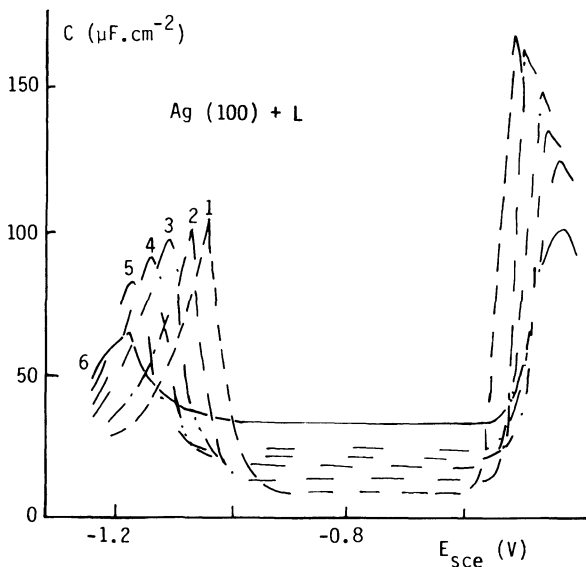


Figure 53. $C(E)$ curves for adsorption of 300 mM *n*-amyl alcohol (in 50 mM Na_2SO_4) on the (100) face of silver with different densities of growth steps: curve 1, $L = 1.5 \times 10^4 \text{ cm}^{-1}$; curve 2, $L = 2.7 \times 10^4 \text{ cm}^{-1}$; curve 3, $L = 5.9 \times 10^4 \text{ cm}^{-1}$; curve 4, $L = 8.1 \times 10^4 \text{ cm}^{-1}$; curve 5, $L = 19.8 \times 10^4 \text{ cm}^{-1}$; and curve 6, $L = 30 \times 10^4 \text{ cm}^{-1}$. $C(E)$ curves obtained by bridge method at 210 Hz.⁹¹

the capacity at the maximum of adsorption increases with the density of growth steps (Fig. 53).⁹¹ This effect does not exist when the electrolyte is 100 mM KF.⁹¹ It was explained that there is adsorption of sulfate ions on the growth steps[†] and adsorption of the organic molecules on the smooth atomic terraces and that fluoride does not adsorb on the growth steps. The most puzzling observation remains that, in the case of sulfate used as base electrolyte, the adsorption equilibrium of the organic molecules was established only after 1.5–3 h, while it was established in 10 min when the base electrolyte was fluoride.

[†] Adsorption of sulfate ion on growth steps of (111) and (100) faces was already mentioned in Section V.3(ii).

4. The Roughness Factor

Practicing electrochemists who, for years, have worked with dropping or hanging mercury drops never had to face this problem, because the roughness factor for the very smooth surface of the mercury is unity. On the contrary, for solid electrodes, the surface is never perfectly smooth and a roughness factor has to be introduced in calculations.

It was proposed, for determination of the roughness factor, that the value of the capacity at very negative density of charge (where there is no longer adsorption of anions) be compared to that of mercury. This does not take into account that at such negative density of charge there are metal-solvent interactions and these are not only metal specific but also face specific.

In the case of no adsorption of ions and complete dissociation of the electrolyte, it is possible to determine the roughness factor by observation (at constant density of charge, for instance, zero) of the inverse of the slope of the variations of $1/C$ (C is the capacity observed experimentally) as a function of $1/C^d$ (C^d is the capacity of the diffuse layer calculated according to the G-C theory), for different concentrations of electrolyte¹⁰⁴ (Fig. 54).† This so-called Parsons-Zobel plot gives the capacity of the inner layer by extrapolating to infinite concentration. Slight adsorption or incomplete dissociation of the electrolyte will vitiate the determination of the roughness factor by this method.‡ This was discussed in detail for the (100) silver face in KPF_6 .⁶²

Another way of determining the roughness factor was proposed by Valette and Hamelin¹⁵ when there is no adsorption. For this case,

$$R(C)^{-1} = (C^d)^{-1} + (C')^{-1} \quad (R = \text{roughness factor}) \quad (6)$$

The plot of $C'(\sigma)$ (σ charge density) has to be made for several supposed values (for instance, 1.00, 1.05, 1.10, etc.) of R . For unity (obviously a too-small value) the diffuse-layer part is compensated too much and gives rise to a sharp maximum on the $C'(\sigma)$ curve

† It was already mentioned for gold faces of Fig. 21 that blind application of the G-C theory is obviously a mistake.

‡ Of course, nonuniform distribution of the charge density at the surface of the electrode (as for a polycrystalline electrode) spoils this plot.^{15,105}

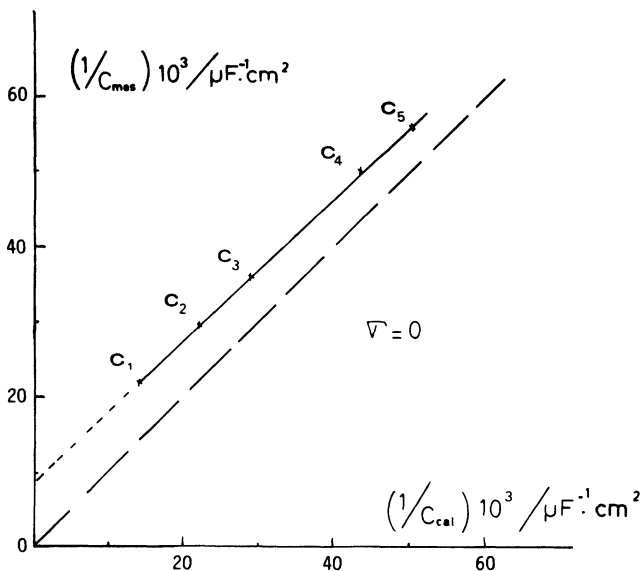


Figure 54. Plot of reciprocal of experimental measured capacity vs. reciprocal of calculated diffuse-layer capacity at constant charge zero, for different concentrations of solution: $C_1 > C_2 > C_3 > C_4 > C_5$.

for density of charge around zero. For a too-high value of R , the contribution of the diffuse part of the dl is not compensated enough and a minimum appears on the $C'(\sigma)$ curves. The Valette-Hamelin method postulates that the variations of C' vs. σ are monotonic around zero charge. The value of R is adjusted to obtain such behavior (Fig. 55).

Most of the time the experimenter has to use these two last methods to have an idea of the situation.

When reading papers, one must pay attention to how the roughness factor was determined, if it was used for correction of the curves, and if some other corrections, for example, for incomplete dissociation of the electrolyte, were also made.

It is hoped that in the near future other more convincing methods will be proposed to disentangle the roughness factor from the effect of defects which introduce also the effect of other co's.

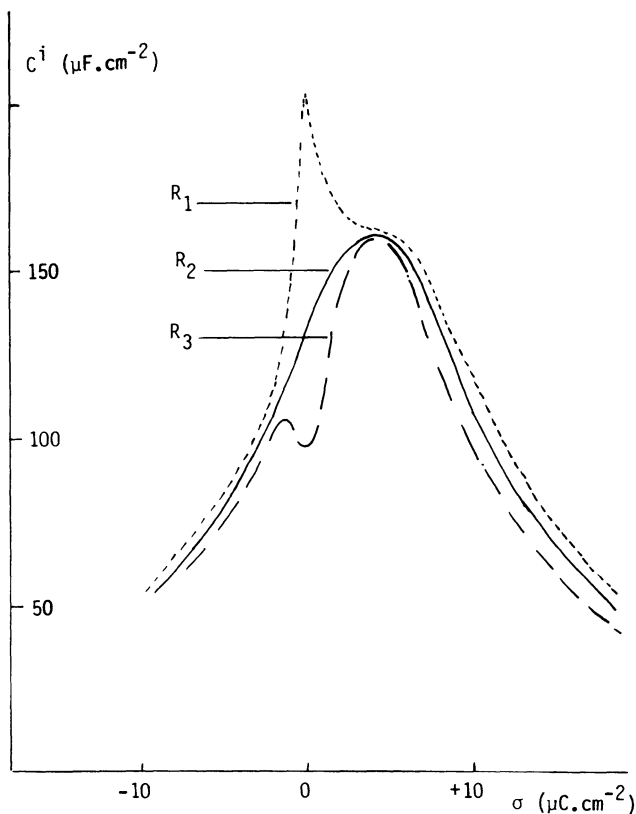


Figure 55. $C^i(\sigma)$ curves for different values of the roughness factor: $R_1 < R_2 < R_3$. R_2 is in agreement with the postulated monotonic shape of the curve.

5. Conclusions

1. Sections V.1-V.4 were not written as a bibliographical review of electrochemical results on metal crystal faces. Possibly, the present author has not quoted some excellent papers and may have put too much emphasis on results that are not always reliable. The works, which are not in the references, were, however, used to determine the general trends described for the behavior of single-crystal faces. In some cases the trends were not clear or were not able to be detected.

All results were analyzed with the help of the G-C-S model for the interfacial region, although for this model the surface is assumed to be "flat" down to an atomic level and its atomic arrangement is not taken into consideration. This last parameter should be a crucial one in the model of this region.

2. The status of data at the beginning of 1984 is as follows. For the pzc, the situation is well advanced (Figs. 19 and 20) and the anisotropy of this parameter for high-melting metals is in agreement with the knowledge of the structure of the metal surface.

For the inner-layer capacity and its variations with charge density at the metal surface, results are very scarce and much debated. It seems that, in aqueous solutions without specific adsorption, C' is maximum not far from zero-charge density (Figs. 28-30); on single-crystal metal faces, the general shape of the curve would include only one maximum and would be nearly symmetrical.

For adsorption, the phenomenology is qualitatively what it is for polycrystalline electrodes. Of course, the shift of the pzc with the σ_0 (which increases with the melting point of the metal) entails differences which are not entirely reduced when the experimental results are analyzed as a function of charge density at the metal surface. Anyway, analysis of adsorption (especially for high-melting metals) is more valid for metal single-crystal faces than for polycrystals (which have a patchy, uncontrolled density-of-charge distribution at their surface).

3. Comparison (and therefore understanding) of the results would be easier if authors had some respect for the IUPAC recommendations and were thoughtful enough to mention such things as the reference electrode when giving a potential, in the text and on all figures, and the standard states when quoting a free energy of adsorption.

4. Theoreticians who wish to use published experimental data on single-crystal metal faces should consider that experimental interfacial electrochemistry on solid metal faces is still in its infancy and a sizeable proportion of the results are meaningless, even when they are printed. They should read carefully Sections IV.2-IV.5 and ponder. Then the great difficulties faced by the experimenters will be clear to them.

ACKNOWLEDGMENTS

The author is pleased to acknowledge her indebtedness to the Centre National de la Recherche Scientifique (France). She is also grateful for comments, discussions, and corrections from Dr. R. Parsons who thoroughly went over the entire manuscript written in a language which is not her mother tongue. Also thanks are due to Dr. M. Bonnemay for suggesting, in 1955, the importance of work with metal single-crystal electrodes.

REFERENCES

- ¹ R. Parsons, Equilibrium properties of interfaces, in *Modern Aspects of Electrochemistry*, Ed. by J. O'M. Bockris and B. E. Conway, Butterworths, London, 1954, Vol. 1, Chap. 3.
- ² A. N. Frumkin and B. B. Damaskin, Adsorption of organic compounds at electrodes, in *Modern Aspects of Electrochemistry*, Ed. by J. O'M. Bockris and B. E. Conway, Butterworths, London, 1964, Vol. 3, Chap. 3.
- ³ R. Reeves, The electric double-layer, the current status of data and models with particular emphasis on the solvent, in *Modern Aspects of Electrochemistry*, Ed. by J. O'M. Bockris and B. E. Conway, Butterworths, London, 1974, Vol. 9, Chap. 4.
- ⁴ R. S. Perkins and T. N. Andersen, Potential of zero-charge of electrodes, in *Modern Aspects of Electrochemistry*, Ed. by J. O'M. Bockris and B. E. Conway, Butterworths, London, 1969, Vol. 5, Chap. 3.
- ⁵ R. A. Oriani and C. A. Johnson, The metal-gas interphase, in *Modern Aspects of Electrochemistry*, Ed. by J. O'M. Bockris and B. E. Conway, Butterworths, London, 1969, Vol. 5, Chap. 2.
- ⁶ P. Delahay, *Double-Layer and Electrode Kinetics*, Interscience, New York, 1965.
- ⁷ D. Mohilner, The electric double layer, in *Electroanalytical Chemistry*, Ed. by A. J. Bard, Marcel Dekker, New York, 1966, Vol. 1.
- ⁸ J. O'M. Bockris and A. K. N. Reddy, *Modern Electrochemistry*, Plenum Press, New York, 1970, Vol. 2, Chap. 7.
- ⁹ The double-layer, in *Comprehensive Treatise of Electrochemistry*, Ed. by J. O'M. Bockris, B. E. Conway, and E. Yeager, Plenum Press, New York, 1980, Vol. 1, Chapters 1-5 and 8.
- ¹⁰ A. Hamelin, T. Vitanov, E. Sevastianov, and A. Popov, *J. Electroanal. Chem.* **145** (1983) 225.
- ¹¹ K. L. Anni, Yu. I. Erlich, and U. V. Pal'm, *Double-Layer and Adsorption on Solid Electrodes*, Tartu University, EESTi, USSR, 1981, vol. VI, p. 5.
- ¹² F. Silva, A. Hamelin, and R. Parsons, Extended Abstracts, 34th ISE Meeting Erlangen (Germany) 1983, p. 930.
- ¹³ E. I. Lust, M. P. Pyaroyaya, and U. V. Pal'm, *Double-Layer and Adsorption on Solid Electrodes*, Tartu University, EESTi, USSR, 1981, Vol. VI, p. 228.
- ¹⁴ C. S. Barret and T. B. Massalski, *Structure of Metals: Crystallographic Methods, Principles and Data*, McGraw-Hill, London, 1966.

- ¹⁵ G. Valette and A. Hamelin, *J. Electroanal. Chem.*, **45** (1973) 301.
- ¹⁶ A. B. Greninger, *Trans. AIME* **117** (1935), 61; see also *Z. Krist.* **91** (1935) 424.
- ¹⁷ J. F. Nicholas, *An Atlas of Models of Crystal Surfaces*, Gordon and Breach, New York, 1965.
- ¹⁸ B. Lang, R. W. Joyner, and G. A. Somorjai, *Surf. Sci.* **30** (1973) 454.
- ¹⁹ A. Hamelin, *J. Electroanal. Chem.* **165** (1984) 167.
- ²⁰ E. A. Wood, *J. Appl. Phys.* **35** (1963) 1306.
- ²¹ J. Perdureau, J. P. Biberian, and G. E. Rhead, *J. Phys. F* **4** (1974) 798.
- ²² M. A. Van Hove, R. J. Koestner, P. C. Stair, J. P. Biberian, L. L. Kesmodel, I. Bartos, and G. A. Somorjai, *Surf. Sci.* **103** (1981) 189.
- ²³ W. Moritz and D. Wolf, *Surf. Sci.* **88** (1979) L29.
- ²⁴ S. H. Overbury, W. Heiland, D. H. Zehner, S. Datz, and R. S. Thoe, *Surf. Sci.* **109** (1981) 239.
- ²⁵ M. Manninen, J. K. Nørskov, and C. Umrigar, *Surf. Sci.* **119** (1982) L393.
- ²⁶ L. MacDonnel, D. P. Woodruff, and K. A. R. Mitchell, *Surf. Sci.* **45** (1974) 1.
- ²⁷ F. Soria, J. L. Sacedon, P. M. Echnique, and D. Titterington, *Surf. Sci.* **68** (1977) 448.
- ²⁸ J. Lapujolade, private communication.
- ²⁹ C. Kittel, *Introduction to Solid-State Physics*, J. Wiley, New York, 1968.
- ³⁰ R. Smoluchowski, *Phys. Rev.* **60** (1941) 661.
- ³¹ C. Herring, *Metal Interfaces*, ASM, 1952.
- ³² J. K. MacKenzie, A. J. W. Moore, and J. Nicholas, *J. Phys. Chem. Solids* **23** (1962) 185.
- ³³ C. Herring, *Phys. Rev.* **82** (1951) 87.
- ³⁴ W. D. Lawson and S. Nielsen, *Preparation of Single Crystals*, Butterworths, London, 1958.
- ³⁵ A. Chernov, E. Guvargizov, and H. Bagdasarov, *Modern Crystallography, Vol. III, Crystal Growth*, Moscow Science Publ., Moscow, USSR, 1980.
- ³⁶ W. Bardsley, D. L. J. Hurlle, and J. E. Mullin, *Crystal Growth: A Tutorial Approach*, North-Holland, Amsterdam, 1979.
- ³⁷ J. Czochralski, *Z. Phys. Chem.* **92** (1918) 219.
- ³⁸ J. Lecoeur, C. Sella, L. Tertian, and A. Hamelin, *C. R. Acad. Sci., Ser. C* **280** (1975) 247.
- ³⁹ J. Lecoeur, C. Sella, and J. C. Martin, *C. R. Acad. Sci., Ser. C* **287** (1978) 447.
- ⁴⁰ E. Budevski, W. Bostanov, Z. Stoinov, A. Kotzeva, and R. Kaishev, *Elektrokhimiya* **3** (1967) 856.
- ⁴¹ E. Budevski and W. Bostanov, *Electrochim. Acta* **9** (1964) 477.
- ⁴² E. Budevski, W. Bostanov, T. Vitanov, Z. Kotzeva, and R. Kaishev, *Phys. Status Solidi* **13** (1966) 577; *Electrochim. Acta* **11** (1966) 1697.
- ⁴³ A. Hamelin and A. Katayama, *J. Electroanal. Chem.* **117** (1981) 221, see Appendix.
- ⁴⁴ Tza Chuan-Sin and Z. Iofa, *Dokl. Akad. Nauk. SSSR* **131** (1960) 137
- ⁴⁵ A. Hamelin and L. Dubova, unpublished results.
- ⁴⁶ W. J. McG. Tegart, *The Electrolytic and Chemical Polishing of Metals in Research and Industry*, Pergamon Press, London, 1956.
- ⁴⁷ D. Dickertmann, F. D. Koppitz, and J. W. Schultze, *Electrochim. Acta* **21** (1976) 967.
- ⁴⁸ J. Clavilier, R. Faure, G. Guinet, and R. Durand, *J. Electroanal. Chem.* **107** (1980) 205.
- ⁴⁹ J. Lecoeur, C. Sella, J. C. Martin, L. Tertian, and J. Deschamps, *C. R. Acad. Sci., Ser. C* **281** (1975) 71.
- ⁵⁰ A. Hamelin and J. Lipkovski, unpublished results.

- ⁵¹ B. G. Baker, Surface analysis by electron spectroscopy, in *Modern Aspects of Electrochemistry* Ed. by J. O'M. Bockris and B. E. Conway, Plenum Press, New York, 1975, Vol. 10, p. 93.
- ⁵² M. A. Van Hove and S. Y. Tong, *Surface Crystallography by Leed*, Springer-Verlag, Berlin, 1979.
- ⁵³ P. F. Kane and G. B. Larrabee, *Characterization of Solid Surfaces*, Plenum Press, New York, 1976.
- ⁵⁴ R. Kottz and H. J. Lewerenz, *Surf. Sci.* **78** (1978) L233.
- ⁵⁵ T. E. Furtak and D. W. Lynch, *J. Electroanal. Chem.* **79** (1977) 1.
- ⁵⁶ C. Nguyen van Huong, C. Hinnen, J. Lecoecur, and R. Parsons, *J. Electroanal. Chem.* **92** (1978) 239.
- ⁵⁷ R. Kofman, R. Garrigos, and P. Cheyssac, *Surf. Sci.* **101** (1980) 231.
- ⁵⁸ A. Hamelin and Z. Borkowska, *J. Electroanal. Chem.* **189** (1985) 85.
- ⁵⁹ A. Hamelin and M. Sotito, *C. R. Acad. Sci., Ser. C* **271** (1970) 609.
- ⁶⁰ J. Clavilier and C. Nguyen van Huong, private communication.
- ⁶¹ C. Nguyen van Huong, C. Hinnen, and J. Lecoecur, *J. Electroanal. Chem.* **106** (1980) 185.
- ⁶² G. Valette, *J. Electroanal. Chem.* **138** (1982) 37.
- ⁶³ H. Hennig and V. V. Batrakov, *Elektrokhimiya* **15** (1979) 1833.
- ⁶⁴ V. V. Batrakov, B. B. Damaskin, and Yu P. Ipatov, *Elektrokhimiya* **10** (1974) 144; see also Yu P. Ipatov and V. V. Batrakov, *Elektrokhimiya* **12** (1976) 1174.
- ⁶⁵ A. Hamelin, Extended Abstracts No. 711, 163rd Meeting of The Electrochemical Society, San Francisco, Calif., May 1983.
- ⁶⁶ A. N. Frumkin, *J. Colloid Sci.* **1** (1946) 290.
- ⁶⁷ S. Trasatti, *J. Electroanal. Chem.* **33** (1971) 351.
- ⁶⁸ L. Peralta, Y. Berthier, and J. Oudar, Fourth Colloquium of Physics and Chemistry of Solid Surface, Antibes 06160, France, September 1978 [*Le Vide* (1978) 83].
- ⁶⁹ J. Lecoecur, J. Andro, and R. Parsons, *Surf. Sci.* **114** (1982) 320.
- ⁷⁰ G. Valette, A. Hamelin, and R. Parsons, *Z. Phys. Chem. (N.F.)* **113** (1978) 71.
- ⁷¹ M. A. V. Devanathan, *Trans. Faraday Soc.* **50** (1954) 373.
- ⁷² A. Hamelin, *J. Electroanal. Chem.* **142** (1982) 299.
- ⁷³ A. Hamelin and A. LeLan, *C. R. Acad. Sci., Ser. II* **295** (1982) 161.
- ⁷⁴ A. Hamelin, *J. Electroanal. Chem.* **138** (1982) 395.
- ⁷⁵ J. P. Bellier and A. Hamelin, unpublished results.
- ⁷⁶ U. V. Pal'm, M. P. Pyaroyaya, and M. A. Salve, *Elektrokhimiya* **13** (1977) 873.
- ⁷⁷ T. Vitanov, A. Popov, and E. S. Sevastyanov, *J. Electroanal. Chem.* **142** (1982) 289.
- ⁷⁸ G. Valette, *J. Electroanal. Chem.* **122** (1981) 285.
- ⁷⁹ S. Trasatti, Extended Abstracts No. 701, 163rd Meeting of The Electrochemical Society, San Francisco, Calif., May 1983.
- ⁸⁰ T. Vitanov, A. Popov, and E. S. Sevastyanov, *Elektrokhimiya* **11** (1975) 170.
- ⁸¹ V. V. Batrakov and H. Hennig, *Elektrokhimiya* **13** (1977) 259.
- ⁸² V. V. Batrakov and Yu. I. Ipatov, *Elektrokhimiya* **11** (1975) 1287.
- ⁸³ V. V. Batrakov and B. B. Damaskin, *J. Electroanal. Chem.* **65** (1975) 361.
- ⁸⁴ C. Nguyen Van Huong, C. Hinnen, and A. Rousseau, *J. Electroanal. Chem.* **151** (1983) 149.
- ⁸⁵ A. Hamelin, *J. Electroanal. Chem.* **144** (1983) 365.
- ⁸⁶ G. Valette, *J. Electroanal. Chem.* **132** (1982) 311.
- ⁸⁷ J. P. Bellier, *J. Electroanal. Chem.* **140** (1982) 391.
- ⁸⁸ A. Hamelin and J. P. Bellier, *J. Electroanal. Chem.* **41** (1973) 179.
- ⁸⁹ A. Hamelin and J. P. Bellier, *Surf. Sci.* **78** (1978) 159.

- ⁹⁰ A. Hamelin and J. Lipkowski, *J. Electroanal. Chem.* **171** (1984) 317.
- ⁹¹ T. Vitanov and A. Popov, *Trans. SAEST* **10** (1975) 5.
- ⁹² T. Vitanov and A. Popov, *J. Electroanal. Chem.* **159** (1983) 437.
- ⁹³ U. V. Pal'm and M. P. Pyar'noya, *Elektrokhimiya* **16** (1980) 1599.
- ⁹⁴ Yu. P. Ipatov and V. V. Batrakov, *Elektrokhimiya* **11** (1975) 1717.
- ⁹⁵ L. P. Kmelevaya, A. V. Tchijov, B. B. Damaskin, and T. I. Vainblat, *Elektrokhimiya* **16** (1980) 257.
- ⁹⁶ J. Lipkowski, C. Nguyen van Huong, C. Hinnen, R. Parsons, and J. Chevalet, *J. Electroanal. Chem.* **143** (1983) 375.
- ⁹⁷ Yu. P. Ipatov, V. V. Batrakov, and V. V. Shalaginov, *Elektrokhimiya* **12** (1976) 286.
- ⁹⁸ R. Parsons, *Proc. R. Soc., London, Ser. A* **261** (1961) 79.
- ⁹⁹ U. V. Pal'm and M. P. Pyar'noya, *Elektrokhimiya* **14** (1978) 1070.
- ¹⁰⁰ A. N. Frumkin, *Z. Phys.* **35** (1926) 792.
- ¹⁰¹ Yu. Ipatov and V. V. Batrakov, *Elektrokhimiya* **11** (1975) 1282.
- ¹⁰² M. Fleischmann, J. Robinson, and R. Waser, *J. Electroanal. Chem.* **117** (1981) 257.
- ¹⁰³ M. Petit, C. Nguyen van Huong, and J. Clavilier, *C. R. Acad. Sci. Ser. C* **266** (1968) 300.
- ¹⁰⁴ R. Parsons and F. G. R. Zobel, *J. Electroanal. Chem.* **9** (1965) 333.
- ¹⁰⁵ I. A. Bagotskaya, B. B. Damaskin, and M. D. Levi, *J. Electroanal. Chem.* **115** (1980) 189.
- ¹⁰⁶ B. E. Conway, in *Ionic Hydration in Chemistry and Biophysics*, Elsevier, Amsterdam, 1981, Chap. 32, p. 637.

The Temperature and Potential Dependence of Electrochemical Reaction Rates, and the Real Form of the Tafel Equation

Brian E. Conway

Department of Chemistry, University of Ottawa, Ottawa, Ontario K1N 9B4, Canada

I. INTRODUCTION

1. Scope and Significance of this Article

The Tafel equation $\eta = a + b \ln i$, where b , the so-called Tafel slope, conventionally written in the form $b = RT/\alpha F$, where α is a charge transfer coefficient, has formed the basis of empirical and theoretical representations of the potential dependence of electrochemical reaction rates, in fact since the time of Tafel's own work.¹ It will be useful to recall here, at the outset, that the conventional representation of the Tafel slope as $RT/\alpha F$ arises in a simple way from the supposition that the free energy of activation ΔG^\ddagger becomes modified in an electrochemical reaction by some fraction, ~ 0.5 , of the applied potential expressed as a relative electrical energy change ηF , and that the resulting combination of ΔG^\ddagger and $0.5\eta F$ are subject to a Boltzmann distribution in an electrochemical Arrhenius equation involving an exponent in $1/RT$. Hence we have the conventional role of T in $b = RT/\alpha F$, as will be discussed in more detail later.

Despite the almost universal adoption of the form in which b is written above and the implicit assumption therefore that b is proportional to temperature T , there now exists a sufficient number

of qualitative exceptions to this assumed behavior that a major reassessment of the form of the Tafel equation is required with regard to the way T enters into the behavior of the potential dependence of rates.

Conway *et al.*² in 1970 made the first detailed study of this situation experimentally and also discussed comparatively several pertinent theoretical aspects of this problem regarding the commonly observed actual behavior where α is itself a function of T or b is represented as a $f(T)$ in some way other than by the conventional definition given above. Notwithstanding the treatment of this problem in Ref. 2, already some 14 years ago, very little attention has been given to it since, except in discussion contributions of Yeager at meetings (see p. 129) and some private communications between Gileadi and the present author and others during the past year. This situation is surprising since the problem of the proper form of the temperature dependence of Tafel's b factor is central in the understanding of effects of potential on electrochemical reaction rates and the molecular mechanism of activation in charge-transfer processes.

This paper examines this whole problem in a comprehensive way and reports some new examples of nonconventional behavior of b with respect to temperature.

First, we establish some preliminary definitions and summarize the historical background.

2. Preliminary Definitions

Conventionally, the Tafel equation represents the potential dependence of electrochemical reaction rates, expressed as currents (I) or current densities (i), according to the following empirical relation:^{1,2}

$$\eta = a + b \ln i \quad (1)$$

where η is an overpotential defined as the difference of electrode/solution potential difference, V , when a current of $i \text{ A cm}^{-2}$ is passing from that, V_n , when the electrode process is at equilibrium: $i = 0$, $\eta = 0$. The net current density i can be defined generally as the difference of forward (\vec{i}) and backward (\tilde{i}) components:

$$i = \vec{i} - \tilde{i} \quad (2)$$

and, at equilibrium, this leads to the definition of the exchange current density, i_0 :

$$i_0 = \vec{i}_{(\eta=0)} = \vec{i}_{(\eta=0)} \quad \text{when } i = 0 \quad (3)$$

This definition, using Eq. (1), leads to an alternative form of the Tafel equation, written exponentially as

$$i = i_0 \exp(\eta/b) \quad (4)$$

from which it is evident that $a = -b \ln i_0$. Conventionally, η is taken positive for an anodic reaction with b positive.

Initially, the parameter b which defines the slope of the η vs. $\ln i$ relation (the "Tafel slope" for this relation) was taken as an empirical quantity, usually found to be a multiple or simple fraction of RT/F .

Tafel's original work in 1905¹ was concerned with organic reactions and H₂ evolution at electrodes, and Eq. (1) was written as an empirical representation of the behavior he first observed. A particular value of $b = RT/2F$ has come to be associated specifically with Tafel's name for the behavior of the cathodic H₂ evolution reaction (h.e.r.) when under kinetic control by the recombination of two (adsorbed) H atoms following their discharge from H₃O⁺ or H₂O in a prior step.³ Such kinetic behavior of the h.e.r. is observed under certain conditions at active Pt electrodes⁴ and in anodic Cl₂ evolution at Pt.⁵ (We note here, in parentheses, that an alternative origin for a Tafel slope of $RT/2F$ for the h.e.r. at Pt has been discussed by Breiter⁴ and by Schuldiner⁶ in terms of a quasiequilibrium diffusion potential for H₂ diffusing away from a very active Pt electrode at which H₂ supersaturation arises).

The empirical representation of electrode process rates according to a relation such as Eq. (1) or its exponential form, Eq. (4), takes into account that, for many electrode processes, $\ln i$ is linear in η over an appreciable range ($> \sim 0.2$ V say) of potentials. More will be said about this later with regard to specific examples; however, it must be stated here that for some processes such as rapid redox reactions⁷ (high i_0 values) and some organic electrode reactions,⁸ a quadratic term in η may also arguably appear in Eq. (4), giving a curved η vs. $\ln i$ relation, the observation of which has been claimed experimentally. Such behavior follows theoretically (see Section IV.7) from a harmonic potential energy rep-

resentation, e.g., of Marcus,⁹ of the course of the energy change of the reaction along its reaction coordinates rather than from the anharmonic representation used in earlier works.¹⁰⁻¹²

3. The Tafel-Slope Parameter b

While the form of the Tafel equation with regard to the potential dependence of i is of major general interest and has been discussed previously both in terms of the role of linear and quadratic terms in η ⁷⁻⁹ and the dependence of the form of the Tafel equation on reaction mechanisms,¹³ the *temperature dependence* of Tafel slopes for various processes is of equal, if not greater general, significance, as this is a critical matter for the whole basis of ideas of "activation" and "reorganization" processes¹⁴ in the kinetics of electrode reactions.

The conventional form of b , which follows from the recent IUPAC recommendation for the so-called transfer coefficient[†] α , is

$$b = RT/\alpha nF \quad (5)$$

where n is the electron charge number for the reaction. In terms of the derivative of the current I with potential V , $\alpha/\nu = (RT/nF)(\partial \ln I/\partial V)_{T,P,C}$ where ν is the stoichiometric number.[‡] For simplicity, in some of the material that follows, we shall write the conventional form of b (with n and $\nu = 1$) simply as $b = RT/\alpha F$, i.e., with the commonly assumed linear dependence on T . This form for b , with the transfer coefficient α to be discussed in Section II with respect to its possible linear dependence on T , is, however, rarely found to be followed² experimentally, so that very basic ideas, extant and accepted for many years, about the mechanism of activation and potential dependence of electrochemical rates are

[†] In this article, the symbol β is used for the barrier symmetry factor and α for the charge transfer coefficient. For a $1e$ process, $\beta \equiv \alpha$ in the usual way (see Section II.2). In various places in the text, where generality is implied and the process concerned is not necessarily a $1e$, single-step reaction, the transfer coefficient α is written. In the latter case, e.g., when charge transfer is involved in a rate-controlling desorption step, a β factor is included in the relevant value of α (see p. 115).

[‡] Introduction of the stoichiometric number ν , with α and n , in b is sometimes confusing. Some discussion of this matter is to be found in Ref. 13 and in Gileadi's contribution in Chapter 8 of the present author's monograph, *Theory and Principles of Electrode Processes*, Ref. 25.

put at issue. Attention was first directed to this rather remarkable situation in the paper by Conway *et al.* in 1970.²

The main purpose of this paper is to examine the real temperature dependence of the Tafel-slope parameter b for various processes and to discuss the mechanisms of activation in electrode processes in the light of the observed behavior of b as a function of temperature.

Before proceeding to direct attention to the real temperature dependence of Tafel slopes as found experimentally for a number of systems, it will be necessary to review the conventional behavior usually assumed and describe its theoretical and historical origins. The remarkable contrast of the behavior actually observed, to be described in Section III, to that conventionally assumed will then be apparent and thus the present major gap in our understanding of the fundamental aspect of potential dependence of electrode reaction rates will be better perceived.

II. ORIGIN OF POTENTIAL DEPENDENCE OF ELECTROCHEMICAL REACTION RATES AND THE CONVENTIONAL ROLE OF TEMPERATURE

1. Theoretical Representations of Rates of Electrode Processes

Here, for obvious reasons, we confine the discussion to activation-controlled processes thus avoiding complications due to concentration and nucleation overpotentials which are not relevant to the present discussion.

The first attempts at deriving a theoretical rate equation for a heterogeneous electrochemical process involving only electron transfer were given by Gurney¹⁵ and Gurney and Fowler.¹⁶ Gurney's treatment recognized the essential quantum-mechanical aspect of electron transfer at electrodes, a feature rather neglected subsequently for some 30 following years. The electron transfer rate was calculated in terms of the integral of the product of probabilities of electron states, and acceptor or donor states as functions of their energy distributions. A quantum-mechanical tunneling of electrons was involved. This paper provided the basis of later treatments of electron transfer but did not explicitly give an account of the

significance of the α parameter in b [Eq. (5)]; in fact, α is added somewhat as an "afterthought" (as a parameter $\gamma = 1/\alpha$) in this otherwise important and seminal paper.

Almost simultaneously, Erdey-Gruz and Volmer¹⁷ and Butler¹⁸ wrote a generalized kinetic equation for a one-electron transfer process corresponding to the form of Eq. (2), namely

$$i = i_0\{\exp(\alpha\eta F/RT) - \exp[-(1 - \alpha)\eta F/RT]\} \quad (6)$$

which took into account: (1) both the forward and backward reaction directions of the process corresponding to net i ; and (2) the exponential potential dependence of the forward and backward current components through the transfer coefficients α and $1 - \alpha$, respectively. [The representation in Eq. (6), with the α and $1 - \alpha$ factors, only applies to the one-electron process considered here and in the original papers. More complex relations must be written for multielectron, multistep processes; see Ref. 13. For the one-electron case in Eq. (6), $\alpha \equiv \beta$, the symmetry factor (see Section II.2).]

From Eq. (6), it is obvious that for appreciable polarizations where $i \gg i_0$, the Tafel equation in the form of Eq. (4) is obtained so that b is defined as $RT/\alpha F$, as in Eq. (5). This is the essential origin of the conventional representation of b in terms of a transfer coefficient α .†

While the derivative $d\eta/d \ln i$ is used commonly to characterize the dependence of current density on potential and is referred to as the Tafel slope, $b = RT/\alpha F$, we suggest that there is some advantage to using its reciprocal, $d \ln i/d\eta = \alpha F/RT$, as this corresponds directly to the exponential term in the electrochemical free energy of activation [Eq. (9)]. Then *reciprocal* Tafel slopes‡ can conveniently be referred directly to factors that affect the activation process in charge transfer reactions [Eqs. (4) and (9)].

A more explicit physical significance of the α factor and the potential-dependence functions $\alpha\eta F/RT$ or $(1 - \alpha)\eta F/RT$ in Eq. (6) is given when the energy course of the reaction is represented

† A useful general review on the topic of transfer coefficients has been given by Bauer¹⁹ but does not cover the important question of temperature dependence of b or α discussed in the present paper.

‡ If a name is required for this reciprocal quantity, it might be suggested that it be called the "Lefat" slope.

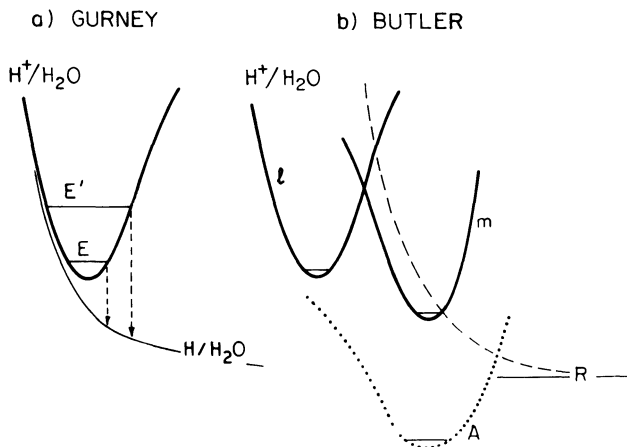


Figure 1. Potential energy profile diagrams for a charge transfer process as in H^+ ion discharge with coupled atom transfer (based on representations by Gurney¹⁵ and Butler²¹. In (b), curve l represents the H^+/H_2O proton interaction potential and m that for discharged H with the metal M . R is the repulsive interaction of H with H_2O and A the resultant interaction curve for H with M .

in terms of a potential (or free) energy profile or surface diagram (Fig. 1). Such an approach was given qualitatively in the papers of Gurney¹⁵ and Horiuti and Polanyi,²⁰ and more quantitatively in Butler's 1936 paper²¹ where the importance of metal-to-H adsorption energy as well as solvational interactions in the kinetics of the h.e.r. was also deduced. This paper, it may be noted, provided the foundation for future work on the dependence of "electrochemical catalysis" on electrode properties, e.g., the role of H adsorption energy and work function. Historically, it should be noted that the role of solvational activation in the kinetics of electrode reactions was already recognized in papers by Gurney,¹⁵ Gurney and Fowler,¹⁶ and Butler²¹ (Butler also introduced quantitatively the effect of chemisorption energy, as mentioned above, e.g., of H in the h.e.r.), and was given more detailed treatment in various papers of Bockris with Parsons and with Conway in the 1950s. The solvational activation factor is what became known later as the "reorganization energy" in Marcus's representations¹⁴ of the activation process.

A formally more explicit representation of the effect of electrode potential and associated role of temperature on electrochemical reaction rates follows from the transition-state theory applied by Glasstone *et al.*²² soon after the appearance of Butler's paper.²¹ The rate constant k of a chemical process is written as

$$k = \kappa \frac{kT}{h} \exp(-\Delta G^{\ddagger}/RT) \quad (7)$$

where k is Boltzmann's constant and κ a transmission coefficient for passage of activated complexes, \ddagger , over the energy barrier; κ is normally taken as near 1.

For an electrochemical rate process, the rate constant \bar{k} is determined by an electrochemical free energy of activation, $\Delta \bar{G}^{\ddagger}$, related to ΔG^{\ddagger} , the "chemical" free energy of activation, by

$$\bar{k} = \kappa \frac{kT}{h} \exp(-\Delta \bar{G}^{\ddagger}/RT) \quad (8)$$

where

$$\Delta \bar{G}^{\ddagger} = \Delta G^{\ddagger} - \beta VF \quad (9)$$

and β is a barrier symmetry factor, analogous to Brønsted's α factor in linear free-energy relationships and V is the metal/solution potential difference across part of which electron transfer normally takes place. The significance of β is illustrated in the well-known way by reference to the working diagram, Fig. 2, which shows how an electrical energy VF applied to the initial state of an electron transfer reaction, e.g., $\text{H}_3\text{O}^+ + e + \text{M} \rightarrow \text{MH}_{\text{ads}}$, changes the relative energy of the transition state by $(1 - \beta)VF$ and hence the activation energy for the forward direction of the process by βVF as in Eq. (6).[†] For a symmetrical barrier, based on two approximately anharmonic potential energy curves (cf. Refs. 10 and 21), as shown schematically in Fig. 2, it is obvious that $\beta \approx 0.5$ over an appreciable range of change of V . For the H_2 evolution reaction at Hg, the range of constancy of β is surprisingly large (cf. the work of Nürnberg). For a barrier based on harmonic curves (see p. 150), β is not constant with changing V .

[†] Equation (6) is written in a general way with a transfer coefficient α . Here $\alpha \equiv \beta$ (see later discussion in Section II.2).

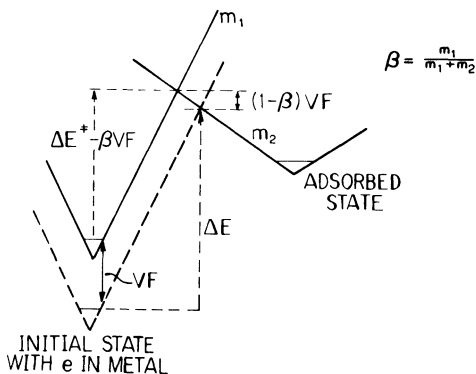


Figure 2. Working diagram showing how the “linear free-energy relationship,” common in electrode process kinetics, arises from changes in electrode potential. β is a symmetry factor. An extreme case of an anharmonic oscillator energy profile is shown in schematic form (cf. Ref. 25). This representation assumes changes in V affect only the energy of electrons in the initial state at the Fermi level.

The principles involved in expressing β in this way are evidently quite analogous to those that define Brønsted's α factor²³ (cf. Ref. 2). However, one matter requires special mention: in the case of electrode reactions, the free-energy change of the initial state of a cathodic electrochemical reaction or of the final state of an anodic one associated with a change of potential has, in previous work, been almost entirely attributed to the *change the Fermi level* of electrons:

$$\Phi_V = \Phi_{V=0} \pm eV \quad (10)$$

Thus the form of the energy hypersurface itself is not normally considered to vary with the potential or corresponding field across the double layer. Hence the effect of potential in electrode kinetics has usually been represented simply by “vertical movement” on the energy axis of potential energy curves without much or any change of their shape.[†] However, we shall see that the conclusions

[†] In a recent paper by Kuznetsov, discussed later on p. 153, some change of shape is attributed to the interaction of medium fluctuations on the partially charged, transferred H atom in the case of the h.e.r.

of the present paper and of recent new experimental work in this Laboratory (see p. 179) indicate that the *entropy* of activation of some electrode processes is materially dependent on electrode potential in addition to the usual effect of potential on the *energy* of activation through changes in the electron Fermi level energy (Eq. 10). Thus electrode potential evidently can have a substantial effect on the structure and/or solvational environment of the reacting molecular species in the interphase as reflected in this entropy function, in addition to changing the energy of electrons.

In Brønsted linear free-energy relations for homogeneous acid/base proton transfers, modification of pK 's of a series of acids reacting with a given base normally changes not only the depth of the proton's energy but also the shape of the potential energy curve for its transfer since force constants for BH^+ bonds are approximately proportional to bond strength, hence pK 's, reflecting Badger's rule. Because the main effect of electric energy change is on Φ_V (Eq. 10), the "linear free-energy relations" for electrode processes (Tafel behavior) are often linear over wider ranges of energy change (but below, of course, those corresponding to approach to the diffusion-controlled limit²⁴) than are Brønsted relations for acid/base processes over comparable ranges of pK ; see e.g., Refs. 23 and 24.

Introduction of Eq. (9) into \bar{k} [(Eq. (8))] gives

$$\bar{k} = \kappa \frac{kT}{h} \exp[-(\Delta G^{\ddagger} - \beta VF)/RT] \quad (11)$$

Equation (11) is the transition-state equation for electrochemical rates (i is, of course, proportional to \bar{k} and concentration of reactants in the double layer at the electrode interface in the usual way²⁵) and is obviously equivalent to the Tafel equation in exponential form [Eq. (4)]. From Eq. (11) it is seen that the Tafel slope for a simple electron transfer process is $RT/\beta F$, i.e., b is linear in temperature. We shall return later to a more critical examination of Eq. (11) insofar as energy and entropy components of the free energy of activation are concerned.

It was mentioned that manipulation of energy profile diagrams (Fig. 2) gives a simple significance to β . However, this is a grossly oversimplified representation since the course of activation in a charge transfer process involves intermolecular and orientational

fluctuations in the solvation shell of the reacting ion or molecule at the electrode, as well as some physical transfer of an atom down a single reaction coordinate in the case of atom transfer reactions, as with anodic Cl_2 evolution, metal deposition, or the h.e.r. (in the latter case, the atom transfer component may be nonclassical²⁶⁻²⁸).

Other representations^{19,25} of the significance of β must accordingly be included here.

In the case of multicoordinate redox processes, Hush²⁹ has suggested that β can be represented as the fractional charge transferred when the transition-state configuration is attained: for symmetrical redox reactions such as $\text{Fe}(\text{CN})_6^{3-}/\text{Fe}(\text{CN})_6^{4-}$ or $\text{Fe}(\text{aq})^{3+}/\text{Fe}(\text{aq})^{2+}$, β is then obviously 0.5 except for any asymmetry that may be introduced by a different degree of specific adsorption of the ox (oxidized) form from the red (reduced) form of the conjugate redox pair.³⁰ This representation, now no longer believed to be correct (cf. Marcus^{9,14}), also gives an indication of how β is related to the way in which the transition-state configuration may be more similar to the initial state than to the final state, or vice versa, in the case of unsymmetrical redox pairs. The potential energy diagram representation also gives similar indications, as may be seen for limiting cases of highly exoenergetic or highly endoenergetic electron transfers.

Alternatively, in a related qualitative sense, β can be interpreted as measuring^{25,35} fractionally "how far along" the reaction coordinate is the transition state attained and hence over what fraction of the potential difference, ΔV , across the Helmholtz layer does the electron charge have to be transferred to this transition state. This interpretation is related to the "half-jump distance" characterizing activated charge transfer across, e.g., oxide films.³¹

For symmetrical processes, each of these ways of representing the significance of β gives the latter quantity a value of 0.5. However, the unsymmetrical processes, the different representations do not lead to identical values of β for a given reaction; note that atom transfer processes are normally highly unsymmetrical, so how β is considered from the theoretical point of view is especially important for such types of electrode reaction.

The significance of β as a measure of the fraction of the interface p.d. involved in the formation of activated complexes is formally explained as follows. In terms of a supposed quasiequili-

brium between initial-state ions i and transition-state complexes \ddagger in a discharge reaction,

$$\mu_i + zF\psi_1 = \mu_i^\ddagger + zF\phi^\ddagger$$

where ψ_1 is the potential at the outer Helmholtz plane and ϕ^\ddagger is the local potential in the compact double layer at which activated complexes begin to pass over to product configurations. $\Delta G^{\circ\ddagger}$ is defined as

$$\mu_i^\ddagger - \mu_i \quad \text{and} \quad \mu_i^{\circ\ddagger} - \mu_i^\circ + RT \ln(c^\ddagger/c_i) = -zF(\phi^\ddagger - \psi_1)$$

Then $\phi^\ddagger - \psi_1$ may be written as some fraction β of $\phi_M - \psi_1$, where ϕ_M is the electrode metal Galvani potential. The same result, but not having the same physical significance, is obtained if a fraction β of a unit e charge is envisaged as being transferred to \ddagger as it is formed from the initial state.²⁹ This representation is not, however, consistent with that shown above in terms of local potential ϕ^\ddagger ; nor can both types of representation be introduced simultaneously since then evidently β would be 0.25!

It is clear from the foregoing proposition that β could be $\frac{1}{4}$, that a representation of the approach to the transition state in terms of traversal of a charged reactant particle across an electrical potential profile to ϕ^\ddagger (approximately half the p.d. $\Delta\phi$ across the Helmholtz layer) cannot be combined with an adiabatic readjustment of electron distribution giving (cf. Hush²⁹) a charge of approximately $e/2$ on the transition state for a one-electron transfer process. Thus, the representation of the process of attainment of the transition state in which activation of the reacting particle takes place through solvation-shell reorganization and/or ligand coordination-shell distortions in the case of ionic redox reactions or, for atom transfer processes, through a coupled bond stretching and solvation-shell reorganization, implies that the transfer of the electron takes place by a tunneling process, as proposed by Gurney,¹⁵ to (or from) the reactant particle when the latter has attained, multidimensionally, the required transition-state configuration so that a radiationless electron transition arises in the usually supposed manner.

The discussion given above serves to indicate that the question of "how" the electron transfer event actually takes place, if such a microscopic and normally nonclassical process can be considered in those terms, is not yet fully answered.

2. Relation of β to α

In Section II.1 the transfer coefficient α was introduced in the usual general way in relation to the definition of b , the Tafel slope. In electrode reaction mechanisms involving two or more consecutive steps, the dependence of a time-invariant current density on potential must be evaluated by one of the following:

1. The steady-state method in which differential equations are set up defining the time dependence, $d[x]/dt$, of concentrations of intermediates x involved in the process. In the steady state, $d[x]/dt = 0$ giving a rate equation containing potential-dependent terms.

2. Using the quasiequilibrium hypothesis, for steps prior to the rate-determining one, to enable an explicit relation between (surface) concentration of x species and potential to be substituted in a rate equation for the velocity of the rate-determining step which itself may or may not be directly dependent on potential.

Normally,^{25,32} method 1 does not give a rate equation that leads to a simple explicit expression for potential dependence of the current density and hence no simple-valued Tafel slope arises. Numerical evaluations of the dependence of $\ln i$ on η can, however, usually be made, e.g., for a range of assumed or evaluated rate constants. Bockris³² has given the most sophisticated application of method 1, using Christiansen's approach;³³ the multistep O_2 evolution reaction was taken as an example. It must be stated that experimentally meaningful results from this method only arise after limiting assumptions are made about relative values of the rate constants for the component steps (in forward and backward directions) and associated surface coverages by adsorbed intermediates. Usually, the assumptions required to derive the electrode-kinetic behavior for the limiting cases are equivalent to those that are adopted in the quasiequilibrium method 2; then, the Tafel slopes for most kinetically significant cases can be evaluated "by inspection" after a little experience with writing the equations.

For a reaction scheme involving n charge transfer events prior to the rate-determining step (for most electrode reactions $n \geq 3$), the Tafel slopes work out to be

$$b = RT/(n + \beta)F \quad (\text{i.e., } \alpha = n + \beta) \quad (12)$$

or

$$b = RT/nF \quad (\text{i.e., } \alpha = n) \quad (13)$$

depending on whether [Eq. (12)] or not [Eq. (13)] charge transfer is involved in the final rate-controlling step. "Chemically" controlled rate-determining steps thus have Tafel slopes determined by *even* fractions of RT/F , while those that involve a charge transfer process in the rate-controlling step have slopes that are *odd* fractions of RT/F , depending on the value n and of β . It will be important for the subsequent discussion to note that processes of the former type [slopes characterized by Eq. (13)] are independent of any barrier symmetry factor or of its possible temperature dependence.

Possible values of b for steps in the h.e.r. have been discussed by various workers and the limiting cases have been considered in detail by Bockris,¹³ Parsons,³ and Conway;³⁴ similar treatments have been given for the O_2 evolution reaction,³² the Kolbe reaction,³⁶ and some metal-deposition processes.³⁵

Finally, here it should be noted formally that α is, of course, identical with β in cases where the initial step in a reaction sequence is a one-electron charge transfer process and is itself the rate-controlling process. Also b can be related to the total number of electrons passed in the overall reaction or in the rate-controlling step through α and the stoichiometric number ν . This matter has, however, been treated in various earlier works by, e.g., Horiuti and Ikusima,³⁷ Bockris,¹³ and Gileadi,³⁸ and so need not be examined again here since no involvement of the temperature variable arises apart from that in b itself.

III. THE EXPERIMENTAL SITUATION REGARDING THE TEMPERATURE DEPENDENCE OF TAFEL SLOPES

1. General Remarks

Contrary to common belief, the Tafel equation as represented by Eqs. (1) or (4), with b given by Eq. (5), virtually *never* represents the electrode-kinetic behavior of electrochemical processes (except probably simple ionic redox reactions that have minimal chemical coupling of one kind or another, p. 125) in particular with reference

to: (1) the supposed linear proportionality of b to T (i.e., α is a constant, temperature-independent parameter); and/or (2) the *form* of b with respect to T . These experimental facts are central to the topic of the present paper.

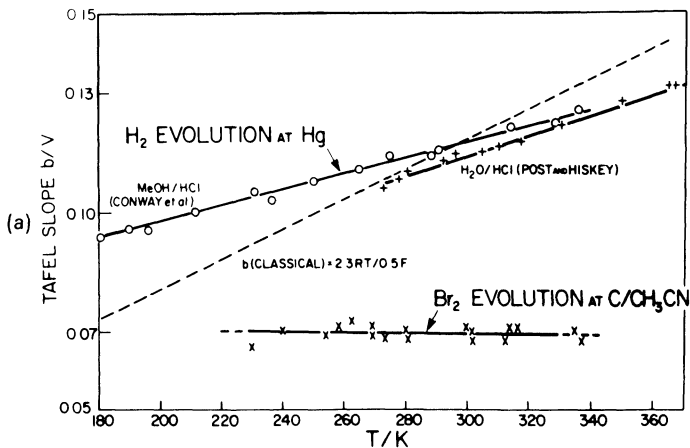
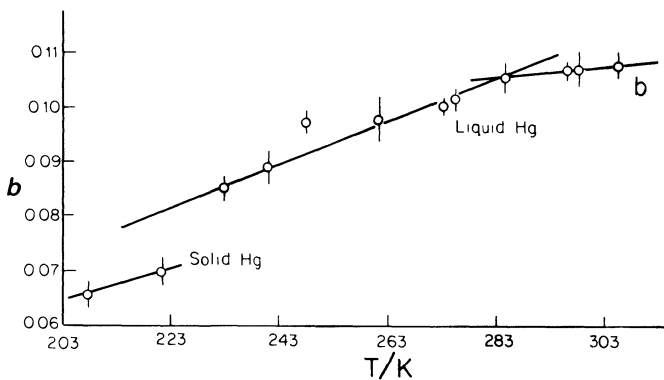
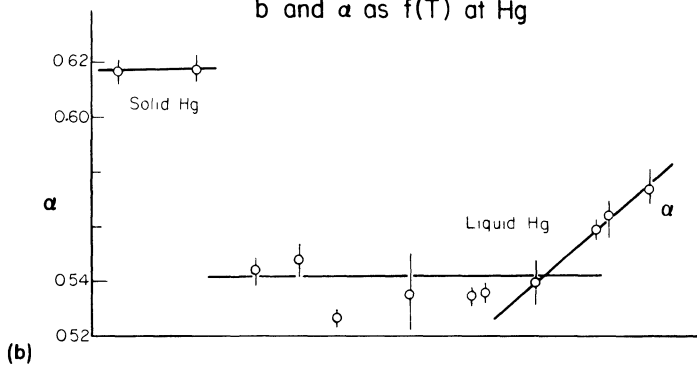
In this section the bases of the above remarks are documented from previous literature and from new results recently reported.

2. Documentation and Examples of the Experimentally Observed Dependence of b on T and the Behavior of α with T

(i) *The H₂ Evolution Reaction at Hg*

Historically, the h.e.r. has often been taken as a prototype process for discussions of the principles of electrode kinetics;^{13,17,18,20,21,34} however, the behavior of this process at various metals is far from that represented by Eqs. (1) or (4) with (5). For the h.e.r. at Hg, four sets of relevant data that are to be considered reliable from the point of view of system purity and experimental technique,^{39,40} and cover a wide range of temperature, are available for discussion: the work of Post and Hiskey⁴¹ in aqueous HCl; the work of Conway *et al.*² in methanolic HCl from 173 to 353 K; the work of Bockris *et al.*⁴³ in methanolic HCl above and below the mp of Hg; and the work of Conway and Salomon⁴² in methanolic HCl and MeOD/DCI, also down to low temperatures.

Following the first indication in the work of Stout⁴⁸ that b can be independent of temperature, Bockris and Parsons,¹¹ and Bockris *et al.*⁴³ showed that a similar effect arose in the h.e.r. at Hg in methanolic HCl between 276 and 303 K; below these temperatures, b apparently varied in the conventional way with T . However, the derived α values showed a considerable spread. Variations of the temperature effect in b were discussed in terms of the possible influence of impurities but an overall assessment of all other, more recent, observations of the dependence of b on T for various types of reactions leads to the conclusion that the "unconventional" dependence is *not* due to some incidental effect of impurities. In fact, in another paper, Bockris and Parsons¹¹ suggested that the temperature dependence of β for the h.e.r. at Hg arose because of expansion of the inner region of the double layer with temperature. They also noted that, formally, for b to be independent of T , the entropy of activation should be a function of electrode potential,

b and α as f(T) at Hg

but the matter was not pursued further until the treatment of Conway *et al.*² referred to in more detail elsewhere in this article.

In Fig. 3a, the Tafel slopes from these authors' works are plotted comparatively as a function of temperature T . It is evident that the Eq. (5) for b as $f(T)$, commonly assumed, is not followed, and the T dependence of b is fitted² by an equation of the form

$$b = \frac{RT}{\beta'F} + K \quad (14)$$

rather than that of Eq. (5) with $\alpha \equiv \beta$. (Note, that for Hg, almost all authors, with the exception of Horiuti,⁴⁴ agree that the rate-controlling step in H_2 evolution at Hg from acidic solutions is the discharge of the hydronium ion, H_3O^+ , or the related species $H_9O_4^+$, so that $\alpha \equiv \beta$; cf. Section II.) The data of Bockris *et al.*⁴³ are somewhat different (Fig. 3b) and β appears to be dependent on T over part of the T range investigated.

Thus from Refs. 2, 41, and 42, b has a temperature-independent component, K , which for the h.e.r. at Hg has the value 40 mV. Here, in Eq. (14), β' is the symmetry factor which must be evaluated from the derivative of b with respect to T ; thus

$$db/dT = R/\beta'F \quad (15)$$

so that

$$\beta' = (R/F)[1/(db/dT)] \quad (16)$$

The data of Fig. 3a show that β' is *constant* with T but has a value appreciably different from 0.5 ± 0.05 usually obtained using Eq. (5) at $T \approx 298$ K. It is evident, and important to note, that for the h.e.r. results at Hg it is incorrect to evaluate β from Eq. (5) at some particular values of T since, in fact, that equation erroneously represents the form of b with T ; it is Eq. (14) that must be employed, using Eq. 16.

It is certainly a remarkable coincidence that β evaluated from Eq. (5) at the "laboratory temperature" ~ 298 K comes out very

Figure 3. (a) Tafel slopes b for the h.e.r. at Hg in aqueous and methanolic acid solutions as a function of temperature (from data of Post and Hiskey, Conway *et al.*,² and Conway and Salomon⁴²). Comparison with behavior for Br_2 at graphite also shown (see Fig. 8). (b) Tafel slopes b for the h.e.r. at liquid and solid Hg from the results of Parsons and Bockris¹¹ in methanolic HCl (from Ref. 43).

near the conventionally "expected" value of 0.5; a similar point has been emphasized by Yeager *et al.*^{45b} (see below) with regard to his results for O₂ reduction at Pt in H₃PO₄ over a wide temperature range. However, it evidently just is a coincidence since it is quite evident that the true " β ", written as β' in Eq. (14), must be evaluated from Eq. (16) rather than from Eq. (5). If β is evaluated from Eq. (5) it has an *apparent* temperature dependence, the origin of which is clear if Eq. (5) is coupled with Eq. (14), which truly represents the results of Fig. 3a, namely

$$b = \frac{RT}{\beta F} \equiv \frac{RT}{\beta' F} + K \quad (17)$$

Then β is evidently given by

$$1/\beta = 1/\beta' + KF/RT \quad (18)$$

or

$$\beta = \beta'/(1 + \beta'KF/RT) \quad (19)$$

so that β is apparently T dependent; thus it is seen that β apparently increases with T as has been noted empirically in some earlier works using Eq. (5) with experimental b values. We emphasize again that the symmetry factor for the h.e.r. at Hg must be evaluated from Eq. (14); then the true β , written as β' , is found to be *independent* of T and the Tafel slope has the form represented by Eq. (14) which is fundamentally different from that normally assumed [Eq. (5)]. We shall comment on possible nontrivial explanations for the form of Eq. (14), including the significance of K , in Section IV.

(ii) The H₂ Evolution Reaction at Ni

Conway *et al.*² also studied the h.e.r. at Ni under high-purity conditions in methanolic HCl over a wider range of temperature. Under these conditions, the "Tafel lines" appear as two linear segments,[†] the slopes of each of which depend on T as shown in Fig. 4. Comparative data for the D₂ evolution reaction (d.e.r.) from MeOD/DCl are shown in Fig. 5.

[†] In aqueous HCl, lines with a small degree of curvature are usually observed with $b = 0.10 \pm 0.005$ V at 298 K.

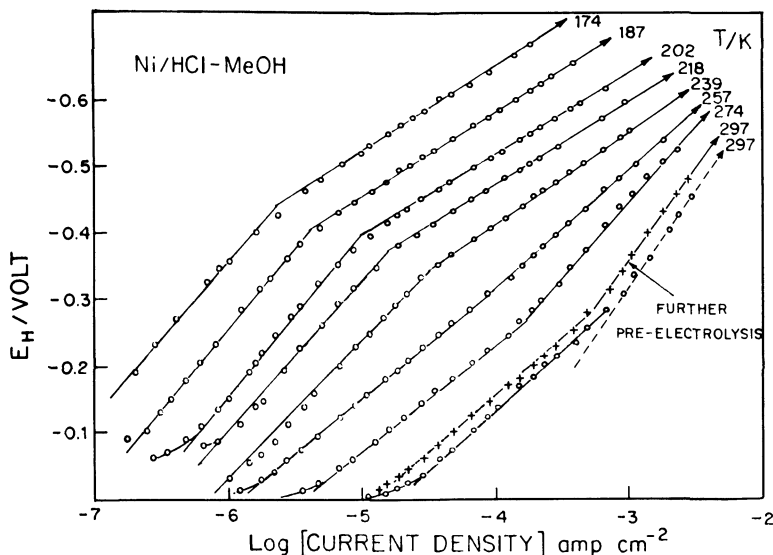




Figure 4. Tafel relations for the h.e.r. at Ni in methanolic HCl over a wide range of temperature (from Ref. 2). Note that upper-region slopes increase with increasing T , while lower-region slopes decrease for the *same* electrode process.

The two linear Tafel regions at Ni in methanolic HCl vary with T in a continuous and complementary way: one has a slope that increases with T while the slope of the other simultaneously decreases with T (Fig. 4), so there is a singular temperature at which the Tafel relation is one line over the whole c.d. range.² The directions of change of the slopes of the two Tafel lines at each temperature, other than at the singular temperature, correspond apparently to reaction mechanisms that are consecutive () or parallel (). However, we believe, based on new data obtained from potential-decay experiments,⁷⁷ that the two regions correspond to desorption mechanisms in the h.e.r. taking place through different populations of adsorbed H which have different dependencies of their coverage on T and η .

It is evident that the T -dependence of b again does not follow that conventionally assumed [Eq. (5)] and, moreover, for the same reaction at the same metal, Ni, the two Tafel-line segments have slopes that vary in *opposite* directions with temperature; Fig. 4 shows that this is a systematic variation and not the result of some

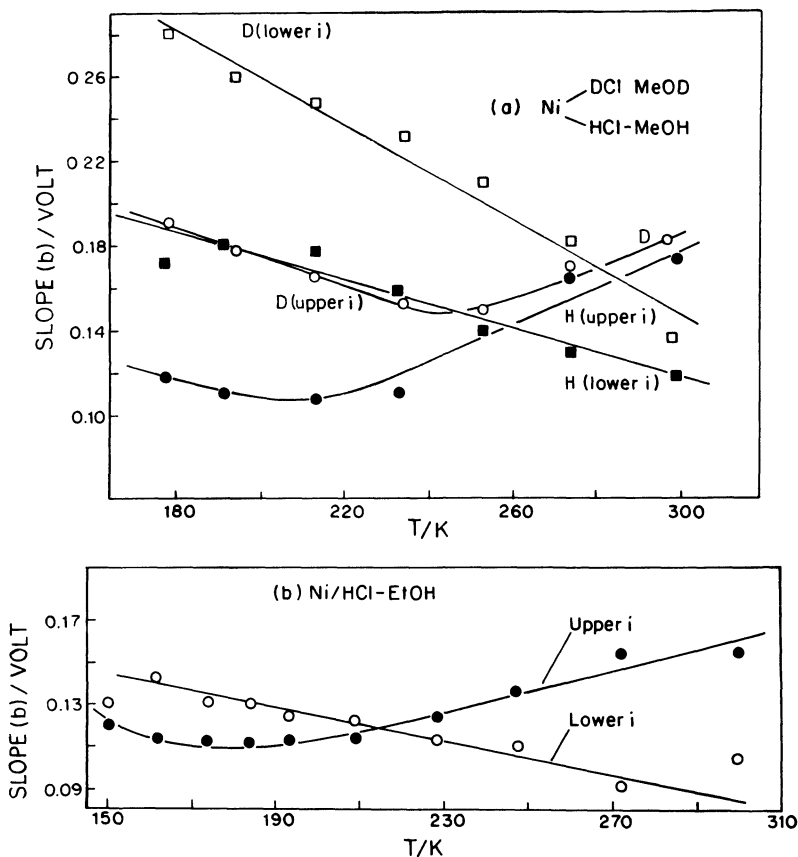


Figure 5. Tafel slopes for the d.e.r. at Ni in *d*-methanolic DCl over a wide range of temperature in comparison with those for the h.e.r. in ethanolic HCl (from Ref. 2).

arbitrary comparison of the behavior at say just two different temperatures. It is interesting that in methanolic HClO_4 , made up from the 70% aqueous acid, so that the methanolic solution contains an unavoidable small mole fraction of H_2O , two Tafel regions are not observed. Hence the behavior in anhydrous methanolic HCl may be connected with anion adsorption effects in that solvent [see Section IV.9]. As will be discussed in that section, the influence of temperature on the effects of adsorbed anions on the kinetics of

an electrode process must always be recognized as a possible reason for unconventional temperature variation of Tafel slopes, unless conditions otherwise preclude the possibility of such effects, e.g., as at Hg at appreciable overpotentials in the h.e.r. where anion adsorption is known to be insignificant.^{93,94}

(iii) *The H₂ Evolution Reaction at Cd*

Data for the h.e.r. at Cd were also found² to behave unconventionally.

(iv) *The H₂ Evolution Reaction at Electrocatalytic Ni–Mo Alloys*

Recently, much interest has centered on the electrocatalytic behavior of Ni–Mo alloys[†] (prepared electrolytically or by thermal reduction of oxide or molybdate mixtures) for cathodic H₂ evolution in alkaline-water electrolyzers or as cathodes in electrolytic Cl₂ cells. The h.e.r. at these electrode materials exhibits⁴⁶ remarkably low Tafel slopes, in the range 22–26 mV, at elevated temperatures, ~363 K. This is one of the reasons for their excellent behavior as electrocatalysts for the h.e.r. However, the Tafel slopes exhibited by these materials depend on temperature in a most unusual way, *decreasing* with increasing temperature, as do some of the results at Ni² (Fig. 4).

The η vs. \ln [current-density] relations (Fig. 6) exhibit two linear regions (as with Ni under certain conditions—see Fig. 4), each of which has a slope that decreases with T as shown in Fig. 7. This is not seemingly due to some change of mechanism as temperature is increased since the decrease of the slopes with T is evidently (see Fig. 7) a continuous one for both regions of the $\ln i$ vs. η relations as is seen from Fig. 7.

This behavior must correspond to variation of α with a power of $T > 1$ in the relation $b = RT/\alpha(T)F$ in order for b to decrease with increasing T , or b is of the form $b = K' - cT$ for the particular case where b decreases linearly with T as in some experiments.

† There is some question whether these are true equilibrium metallic alloys (it is unlikely) and also what is the state of Mo—is it metallic or in the form of MoO in a Ni-metal host structure.

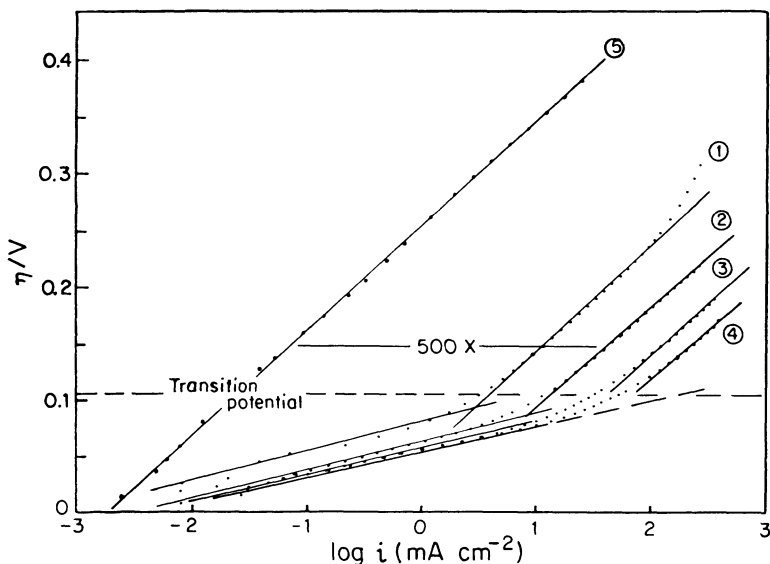


Figure 6. Tafel relations for the h.e.r. at Ni-Mo electroplated electrocatalysts at several temperature curves (1-4), 341, 319, 298, and 278 K, compared with behavior of metallic nickel (curve 5) (Real apparent area factor for Ni-Mo coated electrode $450 \times$); electrolyte is 1.0 M aqueous KOH (from Ref. 46, see also Fig. 19).

(v) Redox Reactions at Electrodes Involving Werner Complex Ions

The behavior of b as $f(T)$ for ionic redox reactions at electrodes, especially those processes that involve only outer-sphere changes of state, and both red and ox species which are not specifically adsorbed, is of great interest. From some of Weaver's work^{107,108} information on the dependence of b on T for such reactions is available and some attempts have been made, e.g., by Parsons and Passeron,⁷ to establish if the potential-dependent factor in the electrochemical rate equation in fact includes a quadratic term in η as well as the usual linear one; however, this is a different question (cf. Ref. 8) related to the harmonicity or, otherwise, of the fluctuations involved in the activation process.¹⁴

Later in this article, we refer to Weaver's work^{107,108} on the evaluation of real entropies of activation of some one-electron redox reactions of complex metal ions at Hg, and corresponding data on

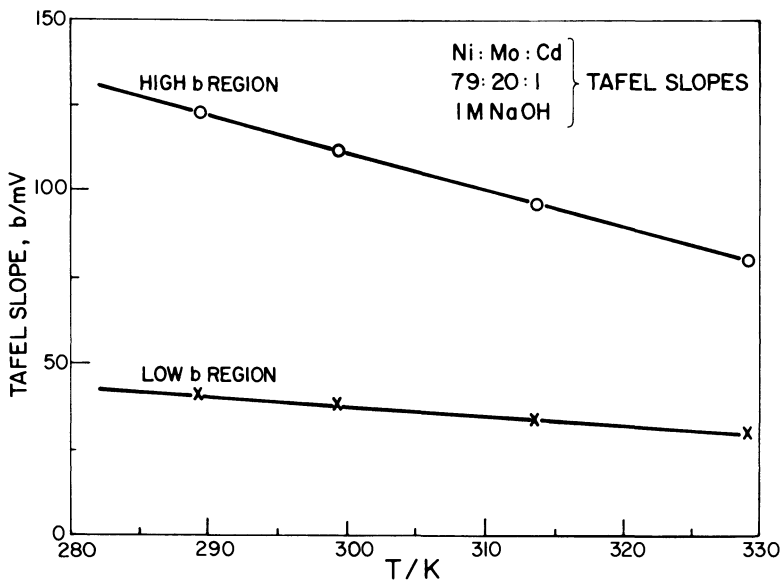


Figure 7. Decrease of slope b for h.e.r. at Ni-Mo electrocoated cathodes with temperature: (○) upper c.d. region, and (×) lower c.d. region (from Ref. 46).

temperature variation of the transfer coefficient. These results are of great interest.

The problem with redox reactions of this type is that their rate constants are usually too large for regular steady-state techniques to be reliably applied. α or β then have to be determined through the reaction order or by some method such as Faradaic rectification. Usually, such methods require evaluation of the double-layer behavior in order to make "double-layer corrections." This is often an unsatisfactory business, especially when corrections would be required over a range of temperatures. We conclude that for this important class of electrochemical reactions more data for examination of $b(T)$ or $\alpha(T)$ are required. However, for certain ionic redox reactions that are sufficiently slow, Weaver¹⁰⁷ has been able to evaluate α as $f(T)$ from Tafel plots over a range of 0.3 ~ 0.4 V: α is in fact found to be *independent* of T for these cases (see p. 179), an important result.

The Tafel-slope behavior as $f(T)$ for solvated electron formation⁴⁷ in, e.g., liquid NH_3 or HMPA solutions would be another interesting case for investigation.

(vi) Anodic N_2 Evolution from N_3^- -ion at Pt

Probably the earliest, well-documented case of unconventional behavior of the Tafel slope with temperature was reported by Stout⁴⁸ for the anodic evolution of N_2 from discharge of azide ion at Pt in aqueous solutions. The overall reaction is



but detailed steps in the reaction have not been characterized; presumably the N_3^\bullet radical is an intermediate but whether its decomposition to N_2 is homogeneous or heterogeneous is as yet unknown and the question of recombination to give an unstable (and probably chemically unlikely) N_6 species is unresolved.

For the azide discharge reaction at Pt, b in Eq. (5) is found to be *independent* of T so that α itself is apparently *linear* in T ! This case can be regarded qualitatively as different from that for the h.e.r. at Hg or limitingly as a special case of Eq. (14) where $K \gg RT/\beta'F$. Theoretical aspects of this type of case will be treated in Section IV.

Although very little is known about the surface electrochemistry of the azide discharge reaction, analogies with the situation in Cl^- or $R.COO^{-36}$ discharge from aqueous solutions would suggest that N_3^- is discharged at Pt on a surface covered or partially covered by discharged OH or O species (cf. Ref. 49) with possible coadsorption of N_3^- ion (regarded as a pseudohalogen). Then the state of surface oxidation of the Pt and the temperature dependence of the state of surface oxidation will determine, in part, the temperature dependence of the Tafel slope of the N_3^- discharge process. That a process occurring on a surface oxide is involved is indicated by the unusually high Tafel slopes of $\sim 4RT/F$ (as in the Kolbe reaction³⁶) characteristic (cf. Refs. 50 and 51) of charge transfer across a barrier-layer film. Competition between specific adsorption of N_3^- and electrodeposition of OH and O species⁴⁹ may be expected in this reaction. In this case, it is difficult to assign any single reason for the independence of b on temperature. Qualitatively, α tends to become smaller with increasing film thickness but greater with increasing film conductivity. The surface electrochemistry involved (cf. Ref. 49) is obviously complex and little is known about its temperature dependence except that surface

oxidation of Pt is facilitated, as may be expected, by elevation of temperature;⁵² the charge transfer characteristics of the oxide film are not, however, known as a function of temperature, but conductance measurements were made by Shibata and Sumino⁵³ at room temperature for thin and thick films in the absence of Cl^- or pseudohalide ions.

(vii) Anodic O_2 Evolution at Pt

In studies of the O_2 evolution reaction at Pt from aqueous H_2SO_4 , it is found that the Tafel slopes determined for the steady-state kinetics of this reaction at several temperatures do not correspond to the conventionally expected behavior according to Eq. (5), so that α is somewhat temperature dependent as in the case of Section III.2, (ii). However, more work on this case is required, taking into account the temperature dependence of oxide-film growth, etc.

(viii) Anodic Br_2 Evolution from Br^- in CH_3CN Solution

In an experiment designed to determine if unconventional temperature dependence of Tafel slopes (where α seems to be itself linear in T) originates in some way on account of the temperature dependence of the structure^{54,55} of associated solvents such as H_2O and MeOH (cf. Ref. 2) in the electrode/solution interphase or of orientation of solvent dipoles of the structured solvent, Conway *et al.*² determined b for anodic Br_2 evolution at graphite from Br^- ion in CH_3CN over an 80 K temperature range: b was found to be 70 ± 7 mV and independent of T over the whole temperature range covered so that α is again, for this case, independent of T (Fig. 8a). Since CH_3CN , although a strongly polar solvent, is generally considered to be "unstructured" in the sense that H_2O or MeOH are, it can be concluded that it is unlikely that the temperature dependence of α can be directly attributed to changes of structure of the solvent in the double layer or of the structural factor⁵⁵ in the solvation of the reactant ion. Recent results from this laboratory on anodic Cl_2 evolution at Pt also show that b ($=0.04$ V in this case, prior to a limiting current) is almost independent of T . This result is surprising since two complicating aspects of the electrode-kinetic behavior must be involved: temperature dependence of Cl^-

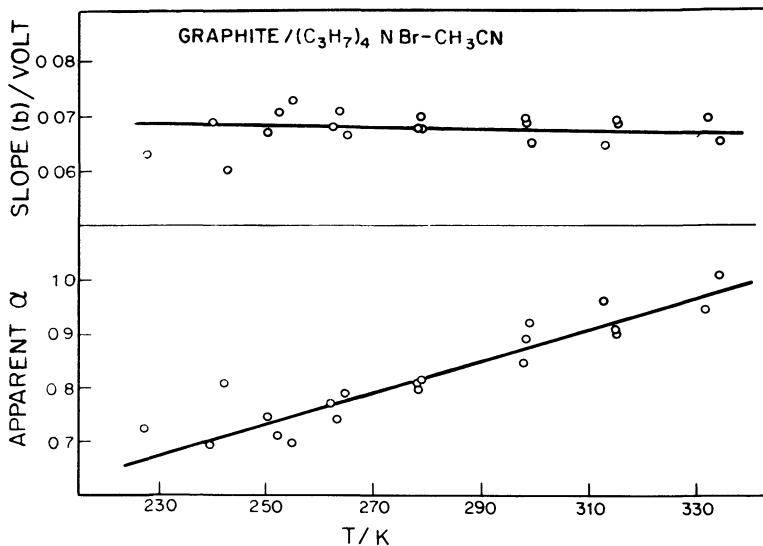


Figure 8a. Independence of b on T and linear variation of α with T for anodic Br_2 evolution from $(n\text{-Pr})_4\text{NBr}$ at pyrolytic graphite anodes (from Ref. 2).

ion adsorption that is also potential dependent,⁵ and temperature and potential dependence of surface oxide coverage.

More recent work in this laboratory with Wilkinson (to be published) on the Br_2 evolution reaction in CH_3CN gave somewhat different results from those of Ref. 2 when glassy carbon was used as the anode. Low Tafel slopes (0.065 at 298 K) were again observed but b was not, in this case, found to be independent of T [Fig. 8b, (i)]. In fact, the derived α values [Fig. 8b, (ii)] tend to become constant with T for $T < 267$ K while they decrease with T above that temperature. This is the trend expected from Eq. (24) as $\mu T < \lambda$ at sufficiently low T values, depending on the magnitude of μ .

The difference in behavior of pyrolytic graphite, examined in Ref. 2, and the glassy carbon investigated in this more recent work, is probably done to the different electrocatalytic surfaces that these materials present. Thus, impedance measurements we have made indicate little adsorption pseudocapacitance for adsorbed Br^+ species at glassy carbon whereas, at pyrolytic graphite, an adsorption capacitance is measurable. The results depend on edge or basal-plane exposure.

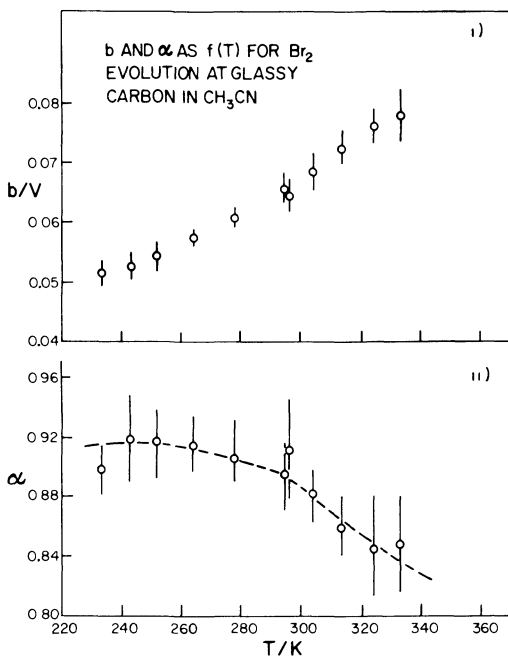


Figure 8b. Tafel slope, b , and transfer coefficient, α , for the Br_2 evolution reaction at glassy carbon in CH_3CN from 0.4 M $(n - \text{C}_3\text{H}_7)_4\text{NBr}$ with 0.2 M Br_2 over a range of temperatures: (i) values of b ; (ii) values of α .

(ix) Cathodic O_2 Reduction in H_3PO_4 at Pt over a Wide Range of Temperature

Appleby^{45a} and, later, Yeager *et al.*^{45b} have found interesting cases of unconventional temperature dependence of b for O_2 reduction at Pt and Os in H_3PO_4 over a 115 and 220 K range of T , respectively. The experimental behavior for Pt^{45b} is shown in Fig. 9. This case is important as it gives not only another example of unconventional temperature dependence of the Tafel slope ($\alpha \propto T$), but also shows that this type of behavior arises for a reduction reaction as well as for oxidation reactions where the properties of surface oxide films that can vary with temperature may complicate the situation. Using this example of the independence of b on T , Yeager has reemphasized⁵⁶ the importance of the whole question

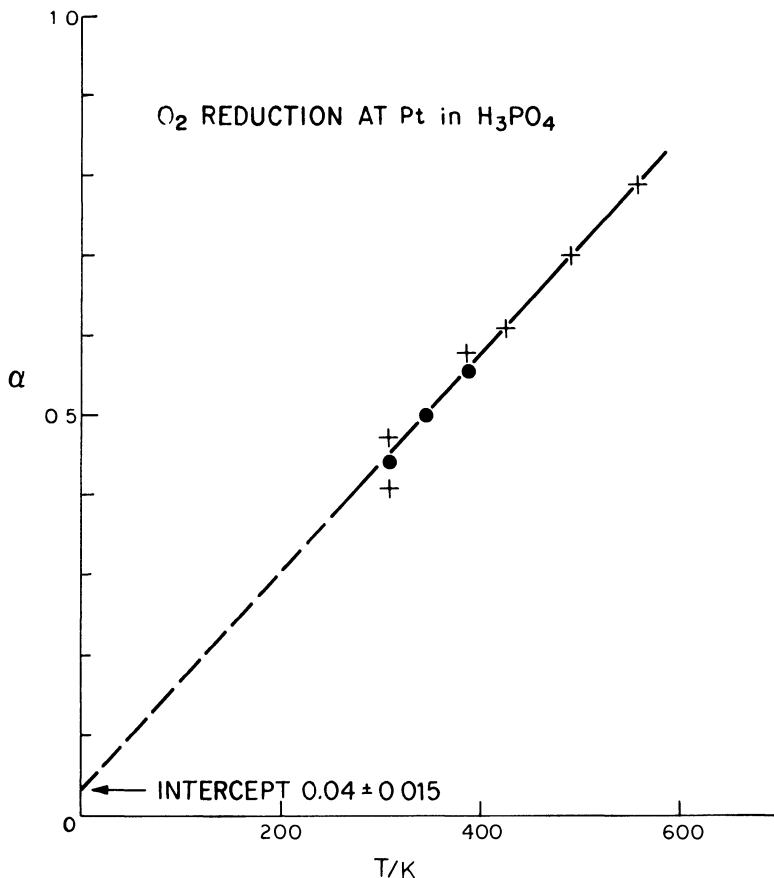


Figure 9. Behavior of the Tafel slope for O_2 reduction in H_3PO_4 as a function of temperature (from Yeager *et al.* Ref. 45b).

of temperature dependence of α for the basic understanding of the potential-assisted activation process in electrode kinetics.

(x) Reduction of Nitro Compounds

Recent unpublished work by Evans^{102b} (see Ph.D. Thesis, 1982, by R. A. Petersen, Chemistry Department, University of Wisconsin, Madison, Wisconsin) has shown that for reduction of $C_2H_5NO_2$ at a hanging Hg drop over a temperature range of ~ 40 K, α is sensibly

constant with a value of 0.45 ± 0.03 . This is evidently one of the few cases where the conventional form of the Tafel equation applies with b linear in T . It would be interesting to know if the Tafel slope is correspondingly constant with potential or not (cf. Ref. 8 for reduction of other nitro compounds).

(xi) General Comment Regarding Independence of b with T

When b is observed to be independent of temperature, b is formally either equal completely to the constant K in Eq. (14) or α is linearly proportional to T in the relation $b = RT/\alpha(T)F$. For such cases, it is unproductive to try to evaluate $1/\alpha$ or $1/\beta$ by taking the derivative of b with respect to T in the way that can usefully be done for the h.e.r. behavior at Hg^2 to which Eq. (14) applies. Physically, the two situations are not necessarily identical but cannot be experimentally distinguished except in a case where say $\alpha(T) = \alpha_0 + \gamma T$ rather than $\alpha(T) = \gamma T$. The latter form implies, of course, that $\alpha \rightarrow 0$ as $T \rightarrow 0$; this is close to the behavior actually observed² for Br^- discharge at carbon in acetonitrile referred to in Section II.

(xii) Phenomenological Conclusions from the Experimental Behavior

It is useful, at this point, to summarize the phenomenological conclusions from the experimental data referred to above.

1. The form of the Tafel-slope parameter b for the h.e.r. at Hg is not $b = RT/\beta F$ with β a constant near 0.5 but is rather $b = RT/\beta' F + K$ or $RT/(\lambda - \mu T)F$ (cf. Eq. 24), so that the form of the Tafel equation is not that commonly assumed. This conclusion is based on results of three different groups of workers.

2. For the H_2 evolution reaction at other metals, the deviation from the conventional form of b is even more striking, and α or β may be $f(T)$, usually linear.

3. For other electrode reactions such as the anodic N_2 and O_2 evolution processes, and O_2 reduction, b approaches the form $b = RT/\alpha(T)F$, where α varies more or less linearly with T making b almost independent of T .

4. Anodic Br_2 evolution at C from Br^- in CH_3CN behaves as in case 3.

5. For the h.e.r. at special Ni-Mo electrodes, α apparently even decreases with increasing T , as is also found for one of the h.e.r. processes at Ni in MeOH.

6. Two types of cases can be limitingly distinguished where (i) $b = RT/\beta'F + K$ so that b is still linear with T , β' is a constant, and K is a T -independent component of b , and (ii) $b = RT/\alpha(T)F$ and α is proportional to T [$\alpha(T) = \gamma T$] so that b is independent of T (cf. cases 1 and 3 above).

7. A final and very important general phenomenological conclusion is that the conventional form of the Tafel equation with slope $b = RT/\alpha F$ with α constant is rarely observed at least for those cases where adequate and reliable T -dependence studies of the electrode kinetics have been made (cf. Yeager⁵⁶). Simple ionic redox reactions seem, however, to be an exception.⁸⁶

8. The previous conclusion means that existing conventional representations of the activation process according to an electrochemical Arrhenius type of equation involving the Boltzmann factor $1/kT$ are seriously inadequate and fail to represent the real kinetic behavior of most electrode reactions from the important point of view of temperature effect—a central aspect of most evaluations of kinetics of chemical processes.

9. Since b values for simple electron-transfer-controlled processes are approximately of the correct magnitude at 298 K, taking $\beta \approx 0.5$, it is clear that the temperature factor in the experimental behavior must be entering the electrochemical Arrhenius expression in more or less the conventional way, i.e., as a $(kT)^{-1}$ term. However, since b is often found to be independent of T , it is clear that there must be another compensating temperature-dependent effect, namely an approximately linear dependence of α or β on temperature in the Tafel slope, $b = RT/\alpha(T)F$. The experimental results for a variety of reactions, summarized in Section III, show that this is a general effect. Reduction of $C_2H_5NO_2$ is an exception while reduction of other nitro compounds takes place with substantial potential dependence of α .⁸

IV. THEORETICAL DISCUSSION

1. Interpretation of the Case Where α is Proportional to T

We have seen that this case arises for several reactions. Agar⁸² was the first to point out that such behavior could arise if the electrode

field mainly influenced the *entropy of activation* rather than the energy, as was usually assumed. Conway *et al.*² in their paper in 1970 developed this explanation further and provided more experimental examples of “unconventional” variation of b with T , i.e., where some T -dependent component of α was involved, as will be shown below.

The electrochemical free energy of activation is formally $\Delta\bar{G}_\eta^{\circ\ddagger} = \Delta G^{\circ\ddagger} - \alpha\eta F \equiv (\Delta H_{\eta=0}^{\circ\ddagger} - \alpha\eta F) - T\Delta S^{\circ\ddagger}$. However, more generally, the Tafel-slope factor should be regarded as originating from the total derivative with respect to potential of $\Delta\bar{G}_\eta^{\circ\ddagger}$. To illustrate this, we write the electrical energy factor which modifies the activation energy by changing the Fermi level as a fraction λ (≈ 0.5) of ηF . Then, writing a fraction λ for β in Eq. (9) and for overpotential η ,

$$\begin{aligned} d(\Delta\bar{G}_\eta^{\circ\ddagger}/d\eta) &= d(\Delta G^{\circ\ddagger})/d\eta - (d/d\eta)(\lambda\eta F) \\ &= d(\Delta H^{\circ\ddagger})/d\eta - T(d/d\eta)(\Delta S^{\circ\ddagger}) - \lambda F \end{aligned} \quad (21)$$

i.e., $\Delta S^{\circ\ddagger}$ for the reaction may be potential dependent, a situation that may well arise in structured solvents⁵⁵ such as water[†] where hydrated ions are intimately associated⁵⁷ with the co-plane of oriented water molecules in the inner region of the double layer.

We write the two derivatives in Eq. (21) as λF (from the electric potential term in $\Delta\bar{G}_\eta^{\circ\ddagger}$) and μF (from the $\Delta S^{\circ\ddagger}$ term). Then

$$d(\Delta\bar{G}_\eta^{\circ\ddagger})/d\eta = \lambda F + \mu TF \quad (22)$$

In terms of the usual empirical factor α , $d(\Delta\bar{G}_\eta^{\circ\ddagger})/d\eta$ is written as $-\alpha F$. Therefore

$$\alpha F = \lambda F + \mu TF \quad (23)$$

Thus, in the general case, α is seen to have a T -independent component λ (the term corresponding to the conventional behavior) and a second component, μT , giving rise to temperature dependence. This result was also derived by Yeager *et al.*^{45b} From Eq. (23), introducing[‡] the Boltzmann factor $1/RT$ [cf. Eq. (11)], the

† Thus many thermodynamic and kinetic properties of aqueous systems are “entropy controlled” as much as “energy controlled,” a fact first noted by Butler⁵⁸ many years ago.

‡ It may be noted that there is also always a preexponential T term in kT/h that appears in the transition-state equation for the rate constant. However, here we neglect the influence of this factor on the temperature dependence of electrode reaction rates considered here as is usual practice except over wide ranges of T .

Tafel slope is seen to be

$$RT/\alpha F \equiv RT/(\lambda F + \mu TF)^\dagger \quad (24)$$

If μTF is sufficiently larger than λF as a limiting case, it is seen that

$$RT/\alpha F \equiv RT/\mu TF \equiv R/\mu F \quad (25)$$

or, as written earlier, $\alpha(T) = \gamma T \equiv \mu T$. Thus, this case can evidently arise, as was shown in Ref. 2, if under certain conditions the increase of electrode potential has its principal effect on ΔS^{ot} rather than ΔH^{ot} or ΔE^{ot} (see footnote \dagger below).

2. General Case

While the above treatment (cf. Ref. 2) gives a basis for temperature-independent Tafel slopes, such as are observed, it must be recognized that the special conditions that are required for this case to arise ($\mu TF \gg \lambda F$) are physically rather improbable. Thus, in a charge transfer process, there will *always* be an electrical energy change $\pm VF$ or $\pm \eta F$ of the initial or final state due to the effect of potential on the Fermi level according to Eq. (10) given earlier, and it is this effect that gives rise to the familiar βVF term in the electrochemical Arrhenius equation or the λF term in Eq. (23). Therefore it is difficult, if not impossible, to see how this factor could ever be negligible in comparison with the effect of changing potential or corresponding interphase field on ΔS^{ot} , which leads to the μTF term in Eq. (23). Hence the general form of b might be [cf. Eq. (24)] $RT/(\lambda + \mu T)F$ but hardly just $R/\mu F$, although the latter form is what experiment requires for some reactions.

It is seen that the general form for b derived above, taking into account both λ and the entropy derivative μF , is not either identical with the experimental behavior² at Hg where $b = RT/\beta'F + K$. The general case above is rather of the form $R/(\lambda F/T + K')$ which is not in any way reducible to, or reconcilable with, the experimental Eq. (14) for b for the h.e.r. at Hg.

The problem is further illustrated in the case of the h.e.r. at Hg by writing the observed Tafel slope, $b = RT/\beta'F + K$, as a corresponding "Lefat-slope" factor (see p. 108) in the exponential

\dagger It is seen that this equation leads to the conventional temperature dependence of b at sufficiently low T , while at high T , b becomes independent of T .

of the electrochemical Arrhenius equation: it is $\eta/(RT/\beta'F + K)$ or $\beta'\eta F/(RT + K\beta'F)$; or alternatively, $(\beta'\eta F/RT)/(1 + K\beta'F/RT)$. [Compare $(\lambda + \mu T)\eta F/RT$ for the general case treated above through the ΔS^{\ddagger} factor.] The h.e.r. case [Eq. (14)] does not seem to correspond to the situation where a linear dependence of α on T originates from a field effect on ΔS^{\ddagger} ; the behaviors are mathematically different. However, a plot of b^{-1} vs. T^{-1} also seems to fit the same data.

At this point in the discussion, the very difficult problem and important nature of the linear temperature dependence of α is clearly perceived and its general significance for electrode kinetics hardly requires reemphasis, although, as Yeager has noted,⁵⁶ little attention has been paid to this problem previously or to the published analysis of main aspects of it in Ref. 2.

3. A Question About the Electrical Energy Term βVF in the Rate Equation

As referred to earlier, the usual representation of effects of electrode potential on electrochemical reaction rates is through a modulating term βVF operating on ΔG^{\ddagger} [Eq. (11)]. [Taking account of double-layer structure, this term is written as $\beta(V - \psi_1)F$, where ψ_1 is the diffuse-layer potential, but this is a trivial difference in the present context.] Change of potential, $\pm V$, modifies the Fermi level energy by $\pm eV$ as in Eq. (10). In the usual transition-state treatment, this quantity, modified by the factor β , appears in the Arrhenius-Boltzmann exponent $[-(\Delta G^{\ddagger} - \beta VF)/RT]$. It is from this exponent that the conventional Tafel-slope quantity b arises, linear in T .

Since the exponential can be written identically as $\exp(-\Delta G^{\ddagger}/RT) \exp(\beta VF/RT)$, this implies that the electrical energy quantity is also Boltzmann distributed. However, it could be argued that since it is electrons in the metal at the Fermi level that are involved, the term $\exp(\beta VF/RT)$ should in some way be written as a Fermi-Dirac factor rather than a Boltzmann factor. The forms of such a term would be $P(E) = 1/\{1 + \exp[(E - E_F \pm VF)/kT]\}$. Introduction of such a probability factor into the equation for electron transfer rate is to be found in Gerischer's treatment⁸⁸ (see below). The effect of this is a broad-

ening of the distribution of electron energies around E_F to an extent of the order of kT . Note that a correspondence with the Boltzmann function only arises when $E \gg E_F$ or at very low T ; these conditions are not always approached in most electrode-kinetic experiments.

In the original treatment of Gurney,¹⁵ the current was expressed as the integral of the product of electrolyte and electron energy distribution functions but with the electronic one written as a Boltzmann factor, $\exp(-\Delta E/kT)$. The symmetry factor was introduced intuitively in terms of the shift of intersection point of energy profiles in relation to change of electrode potential, i.e., of the Fermi-level energy (cf. Butler⁸⁷).

While Gurney¹⁵ referred in his treatment of electrochemical charge transfer to the Fermi distribution function for electronic states in the metal, he did not, however, pursue the consequences of using this function in preference to a Boltzmann distribution. In Gerischer's treatment⁸⁸ of redox reactions, also referred to by Schultze and Vetter^{89,90} in their treatments of the role of electron tunneling in O_2 evolution and other redox process at oxide-covered (Pt) electrodes, the Fermi distribution was explicitly used in the current-potential function which is written (cf. Gurney¹⁵ and Gerischer⁸⁸) as

$$i = e \int_{-\infty}^{+\infty} D_M(E)[f(E_F - E)]D_{El}(E)[f(E - E_F)]\nu(E) dE \quad (26)$$

where e is the electronic charge, $D_M(E)$ and $D_{El}(E)$ are the distribution functions (D) of the electron states in the metal M and the electrolyte redox reagent El ., and $\nu(E)$ is the electronic, tunnel-transfer, frequency factor. The number of unoccupied electronic states in the metal is given by $D_M(E)[f(E_F - E)]$ and in the redox system by $D_{El}(E)[f(E - E_F)]$, where, respectively, the f is the Fermi function

$$f(E_F - E) = [1 + \exp(E_F - E)/kT]^{-1} \quad (27a)$$

or

$$f(E - E_F) = [1 + \exp(E - E_F)/kT]^{-1} \quad (27b)$$

As in the usual way, the current density i is potential dependent mainly on account of a shift of the Fermi level E_F of the metal relative to the effective "Fermi level" of the electrolyte redox

system,⁹¹ i.e., as given by the shape of the electronic distribution function for the latter species. E_F is potential dependent according to $E_F = E_F^\circ(\phi_M = 0) \pm e\phi_M$. In the above kind of treatment, the temperature dependence of the current is usually attributed to a change of $D_{\text{El}}(E)$ with T , corresponding to (classical) thermal activation of surrounding ions and molecules. The quantum-mechanical electron tunneling probability $\nu(E)$ at constant energy E is independent of T .

The significance of the so-called Fermi level for a solution redox system is not altogether clear, but it has recently been critically examined by Bockris and Khan⁹¹ in relation to the vacuum energy level of the electron(s) involved.

From the above, it seems clear that a Fermi-type distribution for the electronic energy levels in the metal should certainly be employed in the representation of electrode reaction rates as a function of potential and hence enters into how the Tafel slope or transfer coefficient is expressed, including its relation to T .

In relation to the above, it is useful to note here the well-known limiting cases of the Fermi function:

- For $E \gg E_F$, $f(E - E_F) \rightarrow \exp[-(E - E_F)/kT]$ (the Boltzmann function).
- For $E = E_F$, $f(E - E_F) = \frac{1}{2}$.
- For low enough T , $f(E - E_F) \rightarrow \exp[-(E - E_F)/kT]$ as in (a), but for a different reason ($T \rightarrow 0$ rather than $E \gg E_F$).

From the form of the Fermi function, it is seen that when it is used for an electrode process where E_F is modulated according to $E_F = E_F^\circ \pm Ve$, the Ve term does not simply factorize from the Fermi equation giving a normal Tafel relation even with an empirically included β factor (cf. Gurney¹⁵), since

$$\begin{aligned} f(E - E_F) &= 1/\{1 + \exp[(E - E_F \pm Ve)/kT]\} \\ &= 1/\{1 + \exp[(E - E_F)/kT] \exp(\pm Ve/kT)\} \end{aligned}$$

Factorization of a term in $\exp(\pm Ve/kT)$ from such a function can only be made when the \exp term in the combined argument is $\gg 1$. So long as the Ve term remains in the \exp in the denominator of the Fermi function, i.e., so long as conditions obtain where such a function applies, it is unclear how, in the general case, a β factor

should enter into this function, multiplying V_e , as it does when the conventional Boltzmann form of the current equation is written.

The question of how the β factor enters in relation to the applicability of the Fermi-Dirac distribution in electron transfer processes appears to require further exploration. The problem arises from the way change of Fermi-level energy is assumed just to shift the potential energy surface up or down by VF and hence cause a change of $(1 - \beta)VF$ in the transition-state energy according to the Brønsted principle.

4. Temperature-Dependent Orientation of Solvent Dipoles in the Inner Region of the Double Layer and the Entropy of Activation

A possible effect of the state of orientation of solvent dipoles in the inner region of the double layer, as a function of potential and temperature, on the temperature dependence of Tafel slopes was suggested in Ref. 2. Reacting ions or molecules, especially in the case of the h.e.r., are intimately involved^{55,57} in solvational interactions with the inner-region solvent dipoles, so the temperature-dependent state of the latter region could lead to effects on the Tafel slope. It would be anticipated that these effects might also be associated with the entropy of activation (Section IV.1).

We have shown earlier (cf. Ref. 2) how, in a formal way, an apparent temperature dependence of α or a temperature-independent component of the Tafel slope could arise if the entropy of activation rather than, or as well as, the energy of activation is affected in a linear way by electrode potential [see Eqs. (21) and (23) and Agar in Ref. 82]. This could arise by the electrode field having an effect on the solvent structure in the double layer, with a corresponding influence on the entropic component of the free energy of solvent reorganization around the discharging reagent ion or molecule.

Several theories have been proposed in the past 20 years for changing solvent polarization in the double layer with electrode potential. One of the most useful has been that of Mott and Watts-Tobin⁵⁹ and the development of it by Bockris *et al.*⁶⁰ The model represents the inner region of the double layer in terms of two-states of orientation of solvent dipoles, parallel and antiparallel, $\uparrow\downarrow$, to the electrode field across the interphase, analogous to the

Ising model of paramagnetization. Variants of this model, taking account of three states of dipole orientation, $\uparrow \rightarrow \downarrow$, or of clusters, have been treated more recently.^{61,62} Especially with electrochemical reactions involving a change of state of H bonding, or complete elimination or creation of a charge, may it be expected that the potential-dependent solvent dipole orientation in the double layer would have an influence on entropy of activation of the electrode process and its response to changes of temperature.

Conway *et al.*² examined this question in terms of the BDM (Bockris-Devanathan-Müller) two-state model⁶⁰ of solvent dipole orientation. The dipole polarization, expressed as a surface potential contribution, g_{dip} , is given by

$$g_{\text{dip}} = \frac{4\pi\mu N_T}{\epsilon} \tanh\left(\frac{\mu E}{kT} - Y \frac{Uc}{kT}\right) \quad (28)$$

where Y is the orientation distribution expressed as $(N_{\uparrow} - N_{\downarrow})/N_T$ for $N_T = 10^{15}$ water dipoles cm^{-2} ; c is half the two-dimensional effective coordination number for the solvent in the interphase, μ is the dipole moment of water, ϵ the electronic plus atomic dielectric constant of water⁶⁰ (~ 6), and E the interphasial field. In BDM, this is taken as $4\pi q_M/6$, with $\epsilon = 6$, for surface charge densities q_M on the electrode. g_{dip} can be calculated as $f(q_M)$ for various lateral interaction energies U in Eq. (28). The results are shown in Fig. 10.

It is interesting that while g_{dip} decreases, as expected, with increasing T for $U = 0$, it can *increase* with T if U is appreciable. This is because g_{dip} is always smaller with increasing U for a given polarizing q_M value, but the effect of U is diminished at higher T so g_{dip} can increase with T when $U \neq 0$. Several examples are shown in Fig. 11 for g_{dip} as $f(T)$ for various Uc/k values.

These results mean that the solvent environment of a discharging ion on the inner side of the outer Helmholtz plane can be quite substantially modified toward a state of orientational saturation depending on q_M and T . The entropy of activation of a process involving change of charge number is closely associated with changing state of solvation in formation of the transition state. Hence it can be seen, at least qualitatively, how an influence of potential on solvent dipole orientation in the inner layer could be transmitted as a potential or field effect on the entropy of activation. This

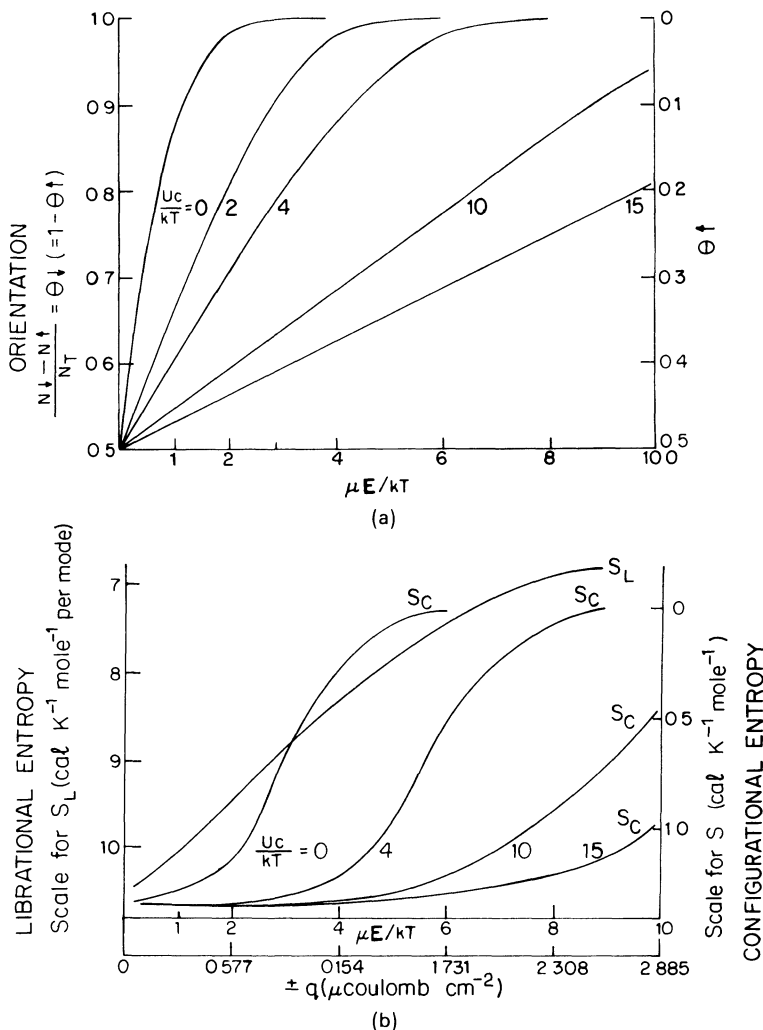


Figure 10. (a) The orientation distribution function $(N_{\uparrow} - N_{\downarrow})/N_T$ for an oriented two-state array of dipoles in the Mott and Watts-Tobin/BDM model (Refs. 59 and 60) for various values of the interaction parameter Uc/kT in Reference 60 [see Eq. 28]. (b) The configurational entropy s_C and the librational entropy S_L for the two-state model of solvent orientation of electrodes as a function of q_M (corresponding to data in Fig. 10a). (From B. E. Conway and L. G. M. Gordon, *J. Phys. Chem.* 73 (1969) 3609.)

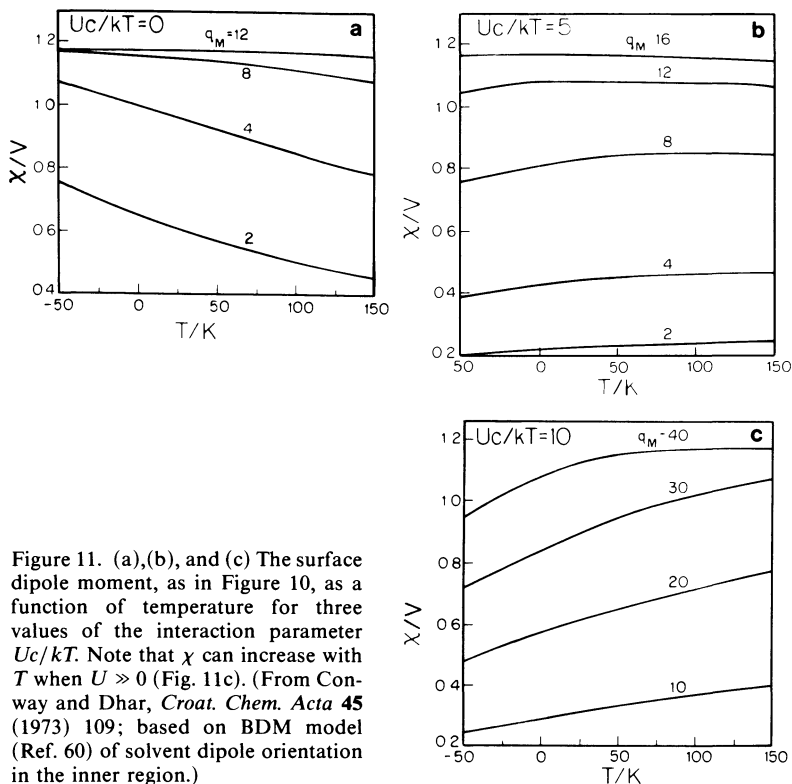


Figure 11. (a), (b), and (c) The surface dipole moment, as in Figure 10, as a function of temperature for three values of the interaction parameter Uc/kT . Note that χ can increase with T when $U \gg 0$ (Fig. 11c). (From Conway and Dhar, *Croat. Chem. Acta* **45** (1973) 109; based on BDM model (Ref. 60) of solvent dipole orientation in the inner region.)

influence of potential, as shown above, will be temperature dependent in a way determined by the magnitude of lateral interactions between solvent molecules in the double layer.

It may be anticipated that the effect of temperature on solvent dipole orientation at a given electrode charge or potential will have a larger influence on the reorganization energy for large, weakly solvated ions than for more strongly solvated ones having higher charge density (larger charge/radius ratio⁵⁵).

Expressed in another way, the microscopic structure of the profile of potential difference ΔV between the metal electrode and the solution will be dependent on q_M and g_{dip} , the latter being itself determined by q_M and Uc/kT ; we assume here for convenience, an absence of the diffuse layer p.d., $\Delta\psi_1$, i.e., for an excess of

nonspecifically absorbed electrolyte, so that $\Delta V \approx \Delta\phi_1$, the p.d. across the compact layer to the outer Helmholtz plane, a region of thickness d .

According to Mott and Watts-Tobin's representation,⁵⁹

$$\Delta\phi_1 = q_M / K_0 - \frac{N_T\mu}{\epsilon_0} \tanh\left(\frac{\Delta\phi_1\mu}{dkT}\right) \quad (29)$$

where K_0 is the vacuum (or electronic polarizability) capacitance of the inner region, i.e., $\epsilon/4\pi d$. The field $\Delta\phi/d$ can also be expressed as

$$E = \Delta\phi/d = 4\pi(q_M - q_{\text{dip}}) \quad (30)$$

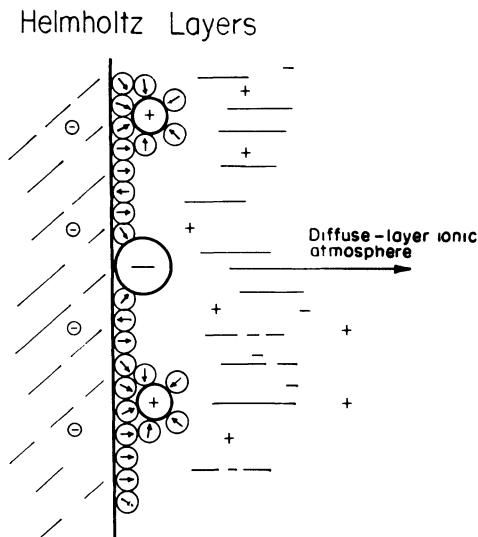
where q_{dip} , the charge density associated with the inner side of the oriented array of solvent dipoles, is given by the implicit equation

$$q_{\text{dip}} = N_T\mu \tanh[4\pi(q_M - q_{\text{dip}})\mu/kT] \quad (31)$$

Physically, q_{dip} is the reactive polarization of the dipole layer in response to the electrode charge density q_M (compare the representation in Ref. 60).

For a given metal solution p.d., $V \approx \Delta\phi_1 = \text{constant}$, the g dipole term will decrease with increasing T (U here taken as 0) so that the p.d. component due to net charge on the electrode will tend to decrease in order to maintain required constancy of $\Delta\phi_1$ (the assumed constant potential condition). For constant q_M , on the other hand, a corresponding increase of $\Delta\phi_1$ would have to take place. For finite and significant U , opposite trends would evidently arise. Thus, the components of electrical potential difference across the inner region at a given q_M will change with increasing temperature. Qualitatively, it may be seen how this effect might change β with temperature, noting that one physical interpretation of β is that it represents^{25,35} the fraction of ΔV ($\approx \Delta\phi_1$) traversed by the reactant ion as its configuration attains that of the transition state.† A fuller microscopic picture would have to take into account: (1) the location of the electric dipole "within" the oriented layer of solvent molecules in relation to their van der Waals envelope size; and (2) the finite size of the ions, the loci of which constitute the outer Helmholtz plane (see Fig. 12).

† The origin of this representation was shown on p. 111 (cf. Ref. 25).



Double-Layer with Hydrated Ions and Oriented Solvent Molecules

Figure 12. Diagram of inner region of the double layer showing outer Helmholtz (OHP) plane with oriented solvent dipoles interacting with electrostatically adsorbed solvated ions [schematic; based on Stern-Grahame model (Ref. 95); BDM model (Ref. 60) includes an extra layer of solvent dipoles between the metal surface and OHP of cations].

5. Tafel Slopes and Proton Tunneling

In electrochemical proton transfer, such as may occur as a primary step in the hydrogen evolution reaction (h.e.r.) or as a secondary, followup step in organic electrode reactions or O_2 reduction, the possibility exists that nonclassical transfer of the H particle may occur by quantum-mechanical tunneling. In homogeneous proton transfer reactions, the consequences of this possibility were investigated quantitatively by Bernal and Fowler⁶³ and Bell,^{26a} while Bawn and Ogden^{26b} examined the H/D kinetic isotope effect that would arise, albeit on the basis of a primitive model, in electrochemical proton discharge and transfer in the h.e.r.

More detailed calculations of these effects were given later by Christov²⁸ and Conway,²⁷ who calculated proton tunneling probabilities through an Eckart barrier, the height of which was varied with potential. This gave a Tafel relation, as shown in Fig. 13, for proton transfer at a cathode for the case of complete tunneling control. In practice, both classical and nonclassical transfer occur in parallel⁶⁴ to relative extents dependent on temperature.

The Tafel slope at low potentials, for *pure* tunneling control, has a higher value than for the classical case and the Tafel relation is nonlinear. These calculations²⁷ were based on Bell's method^{26a} of integrating tunneling probability over the height of the barrier, allowing for a Boltzmann-distributed range of initial states from which the H tunneling can occur. An appreciable D-isotope effect is predicted^{26b,27} for the Tafel slope for pure tunneling transfer of H or D although, in practice, D⁺ discharge will tend to occur with a relatively greater classical transfer probability⁶⁴ than that for H⁺, again depending on temperature. Experimentally, appreciably greater slopes for D transfer than for H have not been observed^{42,65} in the h.e.r.

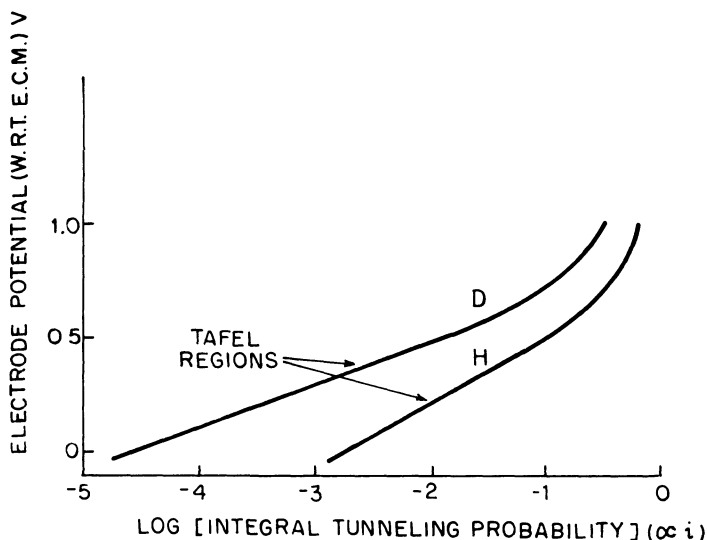


Figure 13. Tafel relation arising from complete proton tunneling control in the h.e.r. (from Conway,²⁷).

An important treatment of electrochemical proton discharge and H transfer was given by Levich *et al.*⁶⁶ who combined the model of hydration-shell reorganization^{9,14} with quantum-mechanical transfer of H from a solvationally activated state (Fig. 14).† Krish-talik⁶⁷ has described some comparative experiments on H transfer from H₂O in a nonaqueous solvent and from excess water, the aim of which was to distinguish between the role of hydration-shell reorganization and O-H bond breaking in the mechanism of the activation process in the step of discharge and atom transfer in the h.e.r. It was claimed that the results supported the Levich model which differs substantially in emphasis from some earlier treatments.^{11,12,21} The problems involved were examined⁶⁸ at a recent Faraday Discussion.

Inspection of the model and treatment by Levich *et al.*⁶⁶ shows that it does not differ in principle from the earlier quantum-mechanical treatments of rates of H transfer evaluated by Bell's method;^{26a} there, an initial Boltzmann activation of the hydrated proton to various levels (in his treatment, a continuum of levels was considered but activation into a discrete quantized sequence can easily be handled in a similar way to that given in Conway and Bockris's calculations⁶⁹ on homogeneous proton transfer in conductance) was assumed from each of which there was a probability of quantum-mechanical H leakage through an energy barrier determined (see Refs. 11, 12, and 21) by the energetics of hydration of the proton (including the main term for the interaction: $\text{H}_2\text{O} + \text{H}_g^+ \rightarrow \text{H}_3\text{O}^+$) on the one hand and the adsorptive bonding behavior of H to the metal (cf. Ref. 21) on the other. It is evident that Levich's model and calculation is a more generalized treatment of the earlier calculations^{26,27} in which a combination of classical activation and

† This treatment arose from these authors' belief that because the quantum for OH vibration ($\sim 40 \text{ kJ mol}^{-1}$) was $\gg kT$, no activation of bond vibrations, that could account for electrochemical proton discharge and transfer, was possible. Thus, the activation energy should correspond to fluctuations in the hydration shell of H_3O^+ but the bond-breaking process is a proton tunneling transition. Objections¹⁰¹ to this model are based on the fact that: (1) energy is always available, e.g., at a value $\sim h\nu_{\text{OH}}$, Boltzmann distributed with a probability $\exp(-h\nu_{\text{OH}}/kT)$, as in the Arrhenius equation for the rate constant of any process where the condition $\Delta E^\ddagger \gg kT$ is often involved; and (2) in H-bonded solvents, OH vibrations are coupled with librations and intermolecular modes giving a wide manifold of states within which activation can arise—cf. the known^{102a} heat-capacity behavior of $\text{H}^+(\text{aq})$.

a) Model of Levich et al.

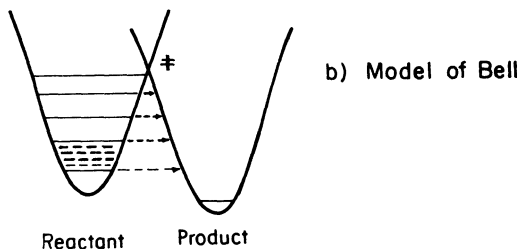
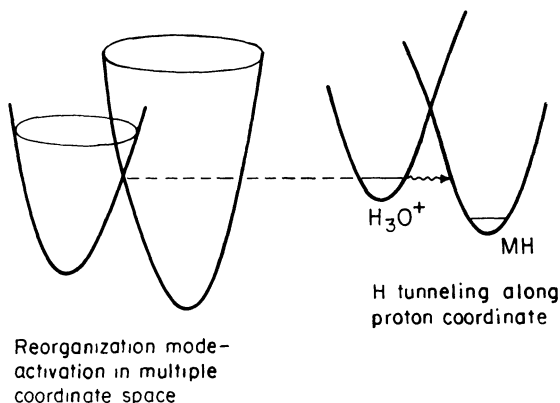


Figure 14. Potential energy diagram for solvation-shell activation of the hydrated proton coupled with quantum-mechanical H^+ neutralization and transfer $a \rightarrow b$ at an electrode: (a) after Levich *et al.*⁶⁶ and (b) comparison with Bell's 2(a) approach and others (Ref. 26b).

quantum-mechanical H transfer was envisaged but it was proposed, and has been perceived apparently incorrectly, as a new treatment. Levich's model is illustrated in Fig. 14.

Unfortunately, the quantum-mechanical tunneling approach does not lead to any better understanding of why α should be temperature dependent in many reactions, if only for the reason that in most of the cases where such behavior is observed, the reactions involve heavy particles for which quantum effects are negligible. O_2 reduction, however, could be quantumly controlled if

a proton transfer step were rate controlling in the reaction sequence of reduction to H_2O , as investigated by Yeager.

In the h.e.r. case at Hg, where b is of the form $RT/\beta'F + K$, it was suggested² that the T -independent component, K , of b (the intercept at $T = 0$ K of a plot of b vs. T) might be connected with a residual, nonclassical, H^+ transfer rate that was potential dependent at the absolute zero. However, since the rate, expressed as i , always involves a *reciprocal* form of b (the Lefat slope), namely,

$$i = i_0 \exp(-\eta/b) = i_0 \exp[-\eta\beta'F/(RT + \beta'FK)] \quad (32)$$

it is unclear how K could characterize a T -independent rate due to H tunneling (that would have to be in parallel with the classical transfer rate) since the exponent of Eq. (32) cannot be expressed as the sum of two terms.

6. Behavior of α with Temperature on the Basis of Electron and Particle Transfer Treatment of Ulstrup

Ulstrup⁷⁰ has recently given a treatment of the possible variation of α with temperature according to theories of electron transfer. On this basis, α is expected to increase weakly with temperature over a sufficiently wide range of T but the calculated effect is very small. It originates from the fact that⁷⁰ the nature of the motion of the discrete molecular or continuum solvent modes is converted from nuclear tunneling at low T to classical, thermally activated motion at elevated temperatures. The distribution of solvent modes which enters into the solvent reorganization energy is replaced by Ulstrup by the behavior of a dielectric medium with an optical dielectric constant ϵ_0 and an effective static dielectric constant ϵ_{eff} . When the solvent modes are dominant, and as long as potential-dependent work terms are disregarded, the T -effect on α arises essentially from variation of ϵ_{eff} with temperature. If ϵ_{eff} is identified with the bulk static dielectric constant of the solvent, the effect is deduced to be insignificant for common hydroxylic solvents. On the other hand, it is concluded that if ϵ_{eff} is determined by the short-range limiting "infrared" dielectric constant to a considerable extent, i.e., when spatial dispersion effects are important, α may exhibit a detectable T -dependence. In the range of T from 150 to 300 K, α varies only by 2-6%.

These effects, while of fundamental interest, are altogether too small in relation to experiment where α typically varies by $\sim 50\%$ over such a range of T (but note that the lowest temperatures as attained in the works of Conway *et al.* were ~ 173 K). Obviously, an effect of a much more substantial and radical kind must be operative to keep b approximately constant and α linear in T over a wide range of T in several important electrochemical reactions. The effect is not a subtle minor one, although its origin is elusive, as is apparent from the foregoing material.

7. Nonlinear Potential Dependence of Electrochemical Reaction Rates

(i) Nature of the Effects

Constancy of β (or α) over some appreciable range of potential is quite generally expected when potential energy surfaces intersect over the anharmonic, linear region, as with Morse functions. When one curve crosses the other, or both curves cross each other near the zero-point energy levels(s), which is usually in a harmonic region of small displacement along the reaction coordinate, then β will become dependent on the electrical energy displacement, ΔVF , associated with change of energy of the electrons at the Fermi level. This situation was treated in the paper by Despić and Bockris³⁵ on metal-ion discharge. It is also the basis of the predicted quadratic dependence of \ln [rates] of electrochemical processes on potential according to Marcus theory where the energy barrier is assumed to be determined by potential energy surfaces (profiles) in the *harmonic* approximation which applies, however, only to processes having small activation energies (cf. the harmonic behavior[†] of the Morse function for small vibrational displacements).

The origin of potential dependence of β was treated by Despić and Bockris³⁵ in terms of the geometry of crossing of potential energy profile sections of the potential energy surface for ion discharge. Using Morse functions to represent the course of energy changes of the initial and final states of the reaction along a

[†] However, in Marcus's treatments, the harmonic behavior corresponds usually to fluctuations in long-range dielectric polarization and/or solvation-shell interactions.

unidimensional reaction coordinate, these authors derived a rather complex expression for β in terms of the equilibrium initial and final energies of the system, the overall energy change ΔE_0 , (in the reaction step), the relative position of the transition state along the reaction coordinate, and the anharmonicity constants a of the pseudodiatomic states involved. Their calculation was similar to that of Conway and Bockris⁶⁹ for the effect of changing heat of adsorption in the H_2 evolution reaction.

The expression derived by Despić and Bockris gives a potential dependence of β , especially when initial- and final-state profiles cross asymmetrically (see Fig. 15), i.e., when ΔE_0 is either a large exothermic or endothermic quantity, so that the transition state is, respectively, either close in configuration to the final state or to the initial state. The Tafel relation is consequently nonlinear; simulated Tafel relations were calculated³⁵ showing this behavior.

From their representation of the origin of a possible potential dependence of β , it is possible to perceive factors, e.g., those that

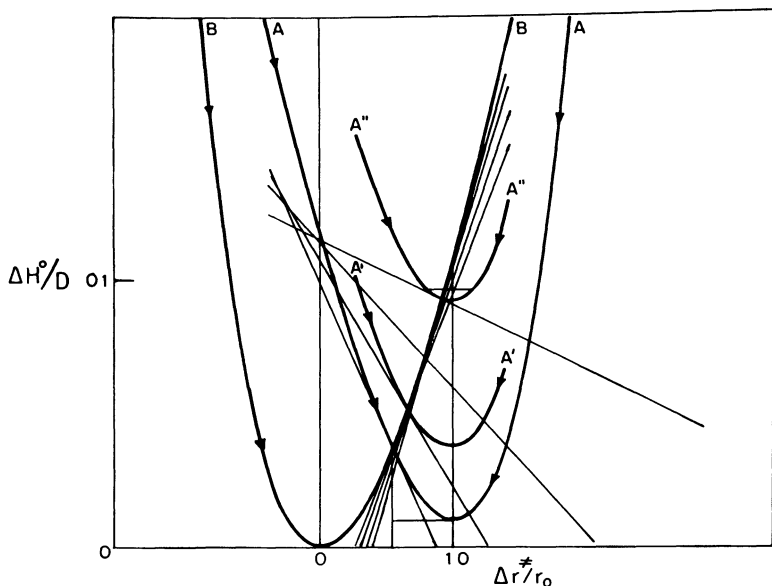


Figure 15. Crossing of potential energy curves leading to potential dependence of β (after Despić and Bockris,³⁵).

determine the desolvation potential energy curve, that could also give rise to a corresponding temperature dependence of β , although it is not obvious how this would be the linear one often indicated experimentally.

This paper also identified how β could be represented in terms of the configuration of the transition state along the reaction coordinate in relation to that of the initial state; that is, $\beta = r^\ddagger/\Delta r_0$, where r^\ddagger is the "distance" of the transition-state configuration along the reaction coordinate and Δr_0 is the total "distance change" in the reaction (this basis of expressing β is to be found first in Ref. 11). As we mention elsewhere in this chapter, this definition of β is not necessarily²⁵ identical with that made in terms of energy changes associated with changes of electrical potential. Coincidence, or otherwise, of these representations depends on the geometry assumed for the potential energy curves (surfaces), e.g., anharmonic or harmonic, and the magnitude of ΔE^\ddagger relative to ΔE_0 . Also, of course, multidimensionality of the function for the energy of the system renders the representation of β in terms of r^\ddagger and Δr_0 seriously oversimplified as is now generally recognized for an ionic redox reaction where no net atom transfer process, coupled with electron transfer, takes place.

Finally, we note here that the representation of the potential dependence of β in the diagram in Despić and Bockris's paper³⁵ (their Fig. 14) implies ultimately that activationless discharge will set in, as treated by Krishtalik.⁸³ Then, of course, the process becomes entirely diffusion limited. Correspondingly, barrierless discharge would arise at the other extreme.

Two consequences of the energy barrier arising from harmonic potential energy surfaces or profile sections are: (1) that the activation energy involves a term in $\frac{1}{4}$ of the solvational reorganization energy associated with charge transfer; and (2) that the electrical energy factor in η or V includes a second-order term in η^2 or V^2 . Since the effect of potential on reaction rates is intimately associated with the role of temperature (Sections II and III), it will be useful to show briefly how the quadratic term in potential, that use of harmonic potential energy curves predicts, arises in the electrochemical Arrhenius equation: it is simply the result of a coordinate-geometry treatment of two intersecting parabolas.

According to the Marcus theory, the electrochemical rate constant k_v is written as

$$-\frac{RT}{F} \ln k_v + \frac{RT}{F} \ln Z_{el} = n\phi + \frac{\lambda}{4F} + \frac{\Delta V - \phi}{2} + \frac{F}{4\lambda} (\Delta V - \phi)^2 \quad (33)$$

where k_v is the potential-dependent rate constant, Z_{el} a heterogeneous collision frequency, n the number of electrons in the charge transfer process (usually 1), λ the reorganization energy,† ϕ the potential difference between the reaction site and the solution (\approx the ψ_1 diffuse-layer potential), and ΔV is the electrode potential. The apparent transfer coefficient $\alpha = -(RT/F) d \ln k_v / d(\Delta V)$ and is hence given by

$$\alpha_{app} = n \frac{d\phi}{d\Delta V} + \left(1 - \frac{d\phi}{d\Delta V}\right) \left(0.5 + \frac{F}{2\lambda} (\Delta V - \phi)\right) \quad (34)$$

Savéant and Tessier⁸ gave two ways of expressing the transfer coefficient:

$$\bar{\alpha} = 0.5 + \frac{F}{2\lambda} (\Delta V - \phi) \quad (35)$$

and

$$\alpha = 0.5 + \frac{F}{4\lambda} (\Delta V - \phi) \quad (36)$$

so that

$$2\alpha = 0.5 + \bar{\alpha} \quad (37)$$

and

$$\bar{\alpha} = \left(\alpha_{app} - n \frac{d\phi}{d\Delta V}\right) / \left(1 - \frac{d\phi}{d\Delta V}\right) \quad (38)$$

α_{app} is obtained, of course, from the experimental dependence of $\ln k_v$ or \ln [current density] on ΔV .

† For the convenience of readers who may not be familiar with the definitions given in Marcus's papers, λ , the reorganization energy, is the energy change that the particle undergoing electron transfer would experience if its change of state took place from the initial-state energy surface to the final-state one, but in an unchanged configuration on the reaction coordinate. Then the solvational part of ΔE^\ddagger is $\lambda/4$.

The potential dependence of the predicted and experimental transfer coefficients can be compared by means of

$$\frac{d\bar{\alpha}}{d\Delta V} = \frac{F}{2\lambda} \left(1 - \frac{d\phi}{d\Delta V} \right) \quad \text{or} \quad \frac{d\alpha}{d\Delta V} = \frac{F}{4\lambda} \left(1 - \frac{d\phi}{d\Delta V} \right) \quad (39)$$

The "chemical" component of the rate constant is expressed in the usual way as $k_c = Z_{el} \exp(-\lambda/4RT)$.

It will be noted from the above that no unconventional temperature dependence of α arises explicitly in this treatment; however (see below), a T -dependence of α could arise from the λ^{-1} factor in Eq. (34).

The experiments of Savéant and Tessier⁸ aimed to establish whether α was potential dependent. k_V was obtained as $f(\Delta V)$ over a ΔV range of ~ 0.5 – 1.0 V for reduction of three nitro compounds on Hg in anhydrous acetonitrile and dimethylformamide. Under those conditions, the products of the electron transfer process are anion radicals. k_V is convincingly potential dependent and α_{app} decreases with increasing negative potential: $d\alpha_{app}/d\Delta V \approx 0.46 \text{ V}^{-1}$. These results give the clearest evidence hitherto published for a quadratic dependence of rates on potential but their interpretation is not without ambiguity since the adsorption of the reactant molecules and their orientation, which will affect the ΔS^\ddagger , are potential dependent if substitutional adsorption arises, as it probably does at the Hg/solution interface.⁶⁰ For the organic compounds used, nitrodurene and nitromesitylene, adsorption is almost certainly significant since it is known that benzene is adsorbed at Hg, e.g., from methanol as well as from water. In relation to Savéant's results,⁸ it is interesting that in work on reduction of $\text{C}_2\text{H}_5\text{NO}_2$ at Hg, Evans^{102b} has shown that α is clearly *constant* over a temperature range of ~ 60 K. The solvent in that work was acetonitrile. This is evidently one of the few cases where the conventional form of the Tafel equation, with b proportional to T [cf. Eq. (5)], is followed.

(ii) Consequent Temperature Dependence of α

From Eq. (34), it is seen that α_{app} is a function of λ in the case where quadratic terms in the Tafel relation [Eq. (33)] are significant. It is interesting that this situation could evidently give

rise to a temperature dependence of α since, in most liquids, the reorganization energy will be temperature dependent, especially in structured solvents. If λ is taken as a *free-energy* term, then it is clear that $|\lambda|$ will *decrease* with increasing temperature since entropies of ionic solvation are always negative (cf. the Born and other treatments of the thermodynamics of ionic solvation⁵⁵). In Eq. (34), this means that the second term $0.5 + (F/2\lambda)(\Delta V - \phi)$ will increase. This is the direction required for consistency with experiment. However, it is important to recognize that such an effect would arise *only* for processes that exhibit a quadratic term in the potential dependence of $\ln[\text{rates}]$. For some ionic redox reactions,⁸⁶ and especially for the h.e.r.,^{10,11} the activation behavior is *anharmonic*, so an effect through the λ^{-1} term will not arise [see Eq. (33)]. Then recourse must be had to other potential-dependent effects, that are also a function of temperature, to explain the variation of α with T as was discussed in Section IV.4 with regard to e.g., solvent dipole orientation in the electrode interphase.

Based on careful work on $\text{Fe(III)(C}_2\text{O}_4)_3$ reduction, Sluyters¹¹⁶ considers that the *potential* dependence of α , observed with certain electrode processes, really arises from kinetic complications and that the transfer coefficient for the elementary step of charge transfer is constant at ~ 0.5 . However, the work of Hupp and Weaver⁸⁶ on the $\text{Cr(OH}_2)_6^{2+/3+}$ system demonstrated a relation between the temperature and potential dependence of the rates, and showed that at overpotentials of *ca.* 0.7 \sim 0.9 V the potential dependence of rate arises extensively from the entropic factor (p. 133). It was also shown that the Marcus theory was able to predict a potential dependence of ΔS^\ddagger comparable to or $>$ that of ΔH^\ddagger when the system has a large entropic asymmetry, i.e., a large net reaction entropy change.

(iii) *Linear Relations between $\ln i$ and Overpotential—the Common Behavior*

While we have seen that experiments indicate that α or β are functions of electrode potential for one or two reactions,^{7,8} the most common kinetic behavior over quite large ranges of potential is a linear relation between η and $\ln i$, so that α or β are usually constant with varying potential, e.g., as with the h.e.r. at Hg.² Qualitatively,

this has usually been attributed to variations of the energy of the transition state over a range where anharmonicity of vibrations or other fluctuations of energy obtains, as with Morse functions for atom transfer reactions^{11,12,69} (cf. also Ref. 101 referred to below) when ΔH^\ddagger is greater than $\sim 20\%$ of the dissociation energy or less than $\sim 60\%$ of it.

In a recent interesting paper by Kuznetsov,¹⁰⁵ constancy of α or β over a wide range of η has been attributed, through quantum-mechanical calculations, to the change of shape of the free-energy surface as a function of the coordinates of the molecules of the solvent medium. This effect arises, it is supposed, on account of the partial charge on the transferred H atom, which becomes adsorbed as a product of the proton discharge process, being dependent on these coordinates. The change of shape of the free-energy surface is due physically to the change of the interaction of the adsorbed atom with the medium polarization in the process of activation. Calculations were made of the variation of α with overall free-energy change ΔG_R in the process for two models of the electronic state of the adsorbed H atom at a metal electrode: (1) Anderson's model¹⁰⁶ for the electronic energy of an ad-atom in relation to electron energy levels in the metal; and (2) the LCAO (linear combination of atomic orbitals) approximation describing the electronic energy of an adsorbed atom in a two-level approximation. It is concluded that α or β actually vary little with ΔG_R , though small but significant changes do arise.

Since two of the factors involved in the relation between α or β and the free-energy charge in the reaction, treated in this work, can be temperature dependent, qualitatively it follows that a variation of α or β with T could, to some extent, arise. However, a satisfactory quantitative evaluation of the possible effect would be rather difficult to achieve on the basis of Kuznetsov's treatment.

Considerable attention has been given, e.g., in various works of Lorenz and Schultze to the extent to which charge transfer is complete in the electrosorption of various species at electrodes, e.g., ad-atoms in UPD and with ions that are specifically adsorbed. If the extent of charge transfer in such processes (the "electrosorption valency") is temperature dependent, this would provide another contribution to the apparent variation of α with T in terms of changing charge distribution. However, almost all existing data

on electrosorption valency are at one temperature only so the results of such an effect must remain speculative.

**(iv) Limiting Cases of the Activation Processes:
“Barrierless Discharge”**

The situation where so-called “barrierless discharge” (the barrier height then really corresponds to an activation energy equal to the endothermicity of the reaction) arises has been treated in some detail in a number of papers by Krishtalik.⁸³ It is claimed that the transition from a regular activated process ($\beta \approx 0.5$) to the “barrierless” condition ($\beta = 1$) can be observed in some processes, e.g., the h.e.r. at Hg at very low current densities, although in Bowden and Grew's¹⁰³ careful work such effects are not apparent. There are practical experimental problems that make observation of this effect not always unambiguous, e.g., double-layer corrections and anion adsorption effects near the pzc (potential of zero charge). Also, as noted by Krishtalik himself,⁶⁷ when the barrierless condition is established, the back-reaction is activationless so it proceeds at its maximum, diffusion-limited† rate which complicates the observation of the desired, forward, barrierless process.

The actual situation involving barrierless discharge is not altogether clear when finite temperatures obtain, for then transitions to some excited vibrational states in the product species could be barrierless, while transition to the ground-state, zero-point, energy level may not be.

8. Expansion of the Helmholtz Layer with Temperature

A further possible cause of a variation of β with temperature is expansion of the double layer with increasing T . If the potential energy surfaces cross symmetrically over a range of energies with changing total length of the reaction coordinate (associated with increasing double-layer thickness), then no expansion effect on β will arise. This corresponds to linear anharmonic behavior. On the other hand, if the intersection region is one where the surfaces have changing and unequal derivatives, then some variation of β with

† In certain cases, it is conceivable that the reaction might still be limited by an unfavorable entropy of activation.

double-layer thickness would be anticipated, and hence with T . This situation corresponds to one potential energy surface being near either the zero-point (harmonic) limit or the dissociation limit at the region of intersection; these are extreme cases, not altogether probable in reality.

From the existing data, e.g., from Grahame's work in 1958, for double-layer capacitance behavior of the Hg/solution interface as a function of temperature, for a sufficiently negatively charged Hg surface (absence of specific adsorption of anions), it seems that the capacity C is virtually *independent* of temperature. Hence it is unlikely that the observed unconventional dependence of b on T could arise in some way from a temperature-dependent change of mean thickness d of the double layer expressed as $d = \epsilon/4\pi C$. Of course, the effective ϵ of the inner region may also vary with temperature at a given surface charge density, q_M , on the electrode metal surface; generally, it will tend to decrease, except in the saturation limit when $\pm q_M$ is large.

Bockris and Parsons,¹¹ however, in an early discussion of possible effects on α of changing double-layer thickness with temperature, concluded that such an effect could account approximately for the variation of α with T that was observed over a certain temperature range in their work. This question evidently remains to be settled by further experiments.

9. Effects of Specific Adsorption of Anions

The presence of adsorbed anions in the double layer has at least five distinguishable effects on the rate of an electrode process:

1. The potential profile across the double layer is modified,⁹⁵ including the value of the diffuse-layer potential, ψ_1 , for a given metal/solution p.d., $\Delta\phi$.
2. The location of the transition state within the double layer can be modified from that in the absence of specifically adsorbed anions.
3. Correspondingly, the potential ϕ^\ddagger at this location is usually modified.
4. The transition state suffers interactions with the adsorbed anions that alters its activity coefficient (Parsons⁹⁶).

5. The interaction of the transition state with oriented solvent molecules in the inner layer is dependent on the charge density of anions adsorbed through the co-sphere/solvent co-plane overlap and resulting interaction effect (Conway⁵⁷).

Especially, for an anodic reaction, the specific adsorption of anions can be important, for then the anion can be the primary electrochemical reagent in those processes that involve anion discharge, e.g., halogen evolution from Cl^- , Br^- , or I^- (usually strongly adsorbed anions), carboxylation (in the Kolbe reaction), or N_3^- in anodic N_2 evolution.⁴⁸ OH^- in oxygen evolution is not normally regarded as strongly adsorbed although it may interact with oxide films on anodes in aqueous media or be part of the surface structure of an oxyhydroxide film, e.g., with NiO.OH .

Factors (1) to (5) above are known in one way or another to affect the kinetics of an electrode reaction including, in most cases, the Tafel slope. Since the anion adsorption is normally temperature dependent owing to the usually finite enthalpy of adsorption (most chemisorptions are energy as well as entropy controlled in their thermodynamics), it follows that anion effects could give rise to unconventional temperature dependence of α .

We next consider a few cases individually.

(i) Hg

Although the h.e.r. has been studied extensively at Hg, a relatively small amount of work has been done on the temperature dependence of the kinetics of this reaction and previous temperature studies (with a few exceptions) were concerned mainly with obtaining electrochemical activation energies and, consequently, a relatively small temperature range was used. In the work of Conway *et al.*,² Conway and Salomon,⁴² and Post and Hiskey⁴¹ in 0.1 *N* aqueous solution, referred to earlier, b was found to vary with T but not according to Eq. (5) (Fig. 3a). The work of Bockris and Parsons³⁹ on the h.e.r. at Hg in solutions of aqueous 0.1 *N* HCl, 0.1 *N* HCl + MeOH, and 0.1 *N* HCl + H_2O + MeOH mixtures over the temperature range 0 to $\pm 40^\circ\text{C}$ gave b values that were, however, independent of temperature over a short range of T but also dependent on T over a different range of T .

In aqueous medium at the high η values involved in most steady-state studies at Hg, specific adsorption of Cl^- ions in dilute

HCl is not indicated by electrocapillary and capacitance studies⁹²⁻⁹⁵ nor in the work of Post and Hiskey.⁴¹ Similarly, in alcoholic solutions of HCl, specific adsorption of Cl^- does not appear to be significant at the potentials used in that work,^{2,42} although nearer the pzc specific adsorption of Cl^- is greater⁹² than it is in aqueous HCl at the same concentrations. Hence the dependence of b on T shown in Figure 3 for Hg and represented by Eq. (17) with $\beta = 0.71$ and $K = 0.04$ is unlikely to be the result of specific adsorption of Cl^- and an explanation of the forms of Eq. (17) or $b = RT/\alpha(T)F$ must therefore be sought in other terms.

At high acid concentrations, however, the kinetic results are undoubtedly complicated by anion adsorption,^{93,94} particularly for halides; interpretation of the kinetics (b and $\log i_0$) in terms of H tunneling²⁶⁻²⁸ or other factors is then difficult and special models must be introduced. For example, anion effects on the location of the H^+ ion in the initial state and anion interactions with the transition state⁹⁶ have been considered.

From a treatment of Parsons,⁹⁶ it is possible to show approximately how a temperature-dependent apparent contribution to β can arise for specific adsorption. If adsorbed anions affect the activity coefficient of the activated complex, then the relative change of rate constant k with coverage θ by the anions is given by

$$\ln(k/k_0) = 2B\theta \quad (40)$$

where k_0 is the rate constant in the absence of adsorption of anions and resulting interactions with the activated complex and B is the second virial coefficient in the equation of state for the ad-species. If θ is approximately linear in electrode potential ϕ (constant inner-layer capacity contribution C), then⁹⁶

$$\ln(k/k_0) = 2BC\phi \quad (41)$$

The overall rate expression will then involve an exponential factor in ϕ of the form $\exp(-\beta\phi R/RT) \exp(-2BC\phi)$, i.e., $\exp(-\phi F/RT)(\beta + 2BCTR/F) \equiv \exp(-\beta'F/RT)$. The apparent symmetry factor β' is hence composed of the normal β plus a temperature-dependent term involving the interaction parameter B and a capacity term C characterizing the potential dependence of coverage of the adsorbed anions. This is of the correct form required to explain cases where b varies anomalously with T for anion adsorption.

(ii) Ni

The results in Fig. 4 for Ni in alcoholic HCl are considered together with those of Bockris and Potter⁹⁷ in dilute aqueous acid and alkaline solutions. The Tafel lines for Ni in the alcoholic solutions consistently show two linear regions both for the protium and deuterium solvents (CH_3OD , $\text{C}_2\text{H}_5\text{OD} + \text{DCl}$). Changes of slope were not, however, observed in a similar study carried out in methanol + HClO_4 solutions. This proves that the anion of the electrolyte can have a qualitative effect on the potential dependence of the electrode reaction rate as well as on its i_0 value. However, in this work, the methanolic HClO_4 contained a small quantity of H_2O from the 70% HClO_4 (aq) used to make up the CH_3OH solutions.

Reasonably linear Tafel relations were observed at all temperatures (down to low T) and the b values corresponded closely to those obtained for the high c.d. region at Ni in the alcohol + HCl solutions. The (b, T) plot (Fig. 5) shows that b decreases linearly with T down to the lowest temperature attained i.e., -89°C). This behavior is to be contrasted with that shown in Fig. 4 for the chloride solutions.

On the basis of these results, it may be argued that the lower Tafel lines at Ni in aqueous HCl represent the kinetics of the h.e.r. at a Ni surface with specifically adsorbed Cl^- (cf. Ref. 92), while the upper line (which has b similar to that for the HClO_4 solution at Ni) represents the kinetics in the absence of specific adsorption. That the Cl^- ion may have more of a kinetic effect than it does at Hg probably arises since: (1) overpotentials at Ni are nearer the pzc than they are at Hg for c.d. $> 10^{-6} \text{ A cm}^{-2}$; and (2) H is appreciably adsorbed at the Ni electrode surface and its coverage and binding energy may hence be sensitive to coadsorption of Cl^- (cf. the results of Breiter⁹⁸ at Pt). Similar conclusions apply to Pt. The results of Bockris and Potter⁹⁷ over a small temperature range in aqueous HCl indicate that b is almost independent of T . Since this result was observed in 0.001 and 0.01 N HCl, and in dilute KOH, it seems justified to regard it as also applying to the h.e.r. in the absence of specific adsorption of anions.

The lower Tafel region at Ni and the whole behavior at Pt thus seem consistent with anion adsorption effects since: (1) the Tafel slope (at Ni) becomes changed at higher potentials and then varies

more normally with T ; and (2) for ascending changes of T at Pt, it is found that b remains almost constant with T as low T^2 but suddenly changes at ~ 270 K, whereas for descending changes of T , b , both for the h.e.r. and d.e.r. continuously increases with decreasing T . Similarly, in the Br_2 e.r. (Fig. 8), b is independent of T and, since this is an anodic reaction, Br^- adsorption may be expected.

(iii) Lead and Cadmium

More complex relationships between hydrogen overpotentials and specific anion adsorption are observed for these metals⁹⁹ and slow anion adsorption is indicated;¹⁰⁰ e.g., η is lowered in HCl and HBr solutions as the concentration is increased.

We conclude that changing anion adsorption at electrodes with temperature can, in some cases, lead to unconventional behavior of Tafel's b coefficient; but this is not the only reason for such anomalies, especially in cathodic reactions where potential ranges for appreciable currents are negative to the pzc of the electrode material concerned.

Conclusions about an intrinsic variation of α or β with T , or the applicability of Eq. (17), must be based on experiments where temperature-dependent anion adsorption effects are minimized or absent, as ensured by appropriate choice of chemistry of the system or of the electrochemical conditions. A favorable choice is not always easy to achieve; suitable systems are limited.

10. Tafel Slopes for Reactions Proceeding in Multistep Pathways

It is well known^{3,13,25,32,34} that when an electrochemical reaction proceeds in a multistep pathway with the steps *in series*, the Tafel slope observed for the $\log i$ vs. η relation depends on the partial reaction sequence, and the state and potential dependence of adsorption of intermediates [see Eqs. (12) and (13)]. Various values of b for the reaction, $< RT/0.5F$, can arise depending on: (1) which step determines the rate of the overall reaction; and (2) the conditions of coverage of the electroactive intermediate (H in the h.e.r.) in the reaction and the potential dependence of that coverage. Values $> RT/0.5F$ ($\beta = 0.5$) sometimes arise with reac-

tions proceeding at barrier-layer films which exhibit non-Ohmic charge transfer through them.^{50,51}

When steps other than simple electron transfer are rate controlling, the forms of the overall rate equation that then can be deduced are assumed to arise on account of potential dependence of coverage by a reaction intermediate (X) in the main reaction sequence given by

$$\theta_X = \frac{K_X C_R \exp(VF/RT)}{1 + K_X C_R \exp(VF/RT)} \quad (42)$$

where R is the reactant from which adsorbed X is discharged. θ_X or $1 - \theta_X$ terms which appear in the kinetic equation for the rate-controlling step then have limitingly the respective forms: $K_X C_R \exp(VF/RT)$ or $[1 + K_X C_R \exp(VF/RT)]^{-1} \doteq (K_X C_R)^{-1} \exp(-VF/RT)$ when V is large. Thus VF/RT terms arise limitingly as components in the rate-equation expressions giving the Tafel slopes having the forms written in Eqs. (12) or (13). The T factor thus appears in a normal way.

In the case when discharge is not rate controlling, so that, for example, in the h.e.r., atom-ion desorption step characterizes the mechanism, we have

$$\frac{d \ln i}{d\eta} = \frac{\beta F}{RT} + \frac{d \ln \theta}{d\eta} = \frac{\beta F}{RT} + \frac{1}{\theta} \frac{d\theta}{dV} \quad (43)$$

$d\theta/dV = 1/q_1$ multiplied by the capacitance, C_H due to the adsorbed electroactive H species in the h.e.r., where q_1 is the charge for monolayer coverage of those H species (not necessarily the strongly bound H that is observed in underpotential deposition (u.p.d.) experiments at Pt). We see that the Lefat slope is, in general, composed of two component terms, one from the charge transfer factor and the other from the potential dependence of coverage; each gives rise to an inverse dependence of b^{-1} on T or a more complex function of T (see below). For the Langmuir case we find

$$\frac{d \ln i}{d\eta} = \frac{\beta F}{RT} + \frac{F}{RT} \frac{1}{1 + K_X C_X \exp(VF/RT)} \quad (44)$$

This relation gives the regular Tafel slope for this mechanism of $b = RT/(1 + \beta)F$ only when $K_X C_X \exp(VF/RT) \ll 1$. Under other conditions it is seen that $b = (d\eta/d \ln i)$ will not be simply propor-

tional to T so that α will be apparently T -dependent. The range of potentials over which this conclusion will be valid is, however, strictly limited. A wider range will apply when the g factor in the Temkin-type isotherm [see Eq. (45)] is appreciable ($gRT \approx 5 \sim 10 RT$ in energy). Such conditions are treated as follows.

For the so-called "Temkin" case, the adsorption isotherm equation for θ_X is written with an $\exp(g\theta_X)$ term in it,^{71,72} i.e., for the condition where K is θ -dependent [$K = K_0 \exp(-g\theta_X)$],

$$(\theta_X/1 - \theta_X) \exp(g\theta_X) = K_0 C_R \exp(VF/RT) \quad (45)$$

The rate equation must then be written correspondingly with similar $\exp(g\theta_X)$ or $\exp(\beta g\theta_X)$ terms, where g is an interaction or heterogeneity parameter (as specifically in Temkin's original treatment) characterizing the variation of energy of adsorption of X with coverage. Then, for example, for the atom-ion desorption mechanism in the h.e.r., the Tafel slope is given by

$$\frac{dV}{d} \ln i = \frac{RT}{F} \left/ \left(\beta + \frac{1 - \theta}{1 + g\theta(1 - \theta)} \right) \right. \quad (46)$$

which, for $\theta = 0$, becomes the usual value $RT/(1 + \beta)F$. For H adsorbing metals, b can be reasonably constant with η or V if $g \gg 0$ but varies less with T than is usually assumed.

It should be remarked here that except perhaps for OH and O species on noble metals, the adsorption energy of an intermediate is rarely distributed in a linear way with coverage; thus for submonolayer chemisorption, states with *discretely* different adsorption energies are the rule rather than the exception, so that a continuous exponential function in ' $g\theta$ ' is usually less than realistic as a basis for writing an electrochemical adsorption isotherm equation. When terms such as $\exp(g\theta)$ are included, this introduces a further implicit T -dependent quantity since really $\exp(g\theta) \equiv \exp(r\theta/RT)$, i.e., g is a $f(T^{-1})$.

Various limiting cases have been worked out in the literature for several well-known electrode processes: the H_2 , O_2 , Cl_2 evolution reactions and the Kolbe reaction, as well as O_2 reduction and some electroorganic oxidation processes with simple molecules. The general conclusions can be summarized as follows:

1. When the rate-controlling step involves an electron transfer, b has the form $b = RT(n + \beta)F$ [Eq. (12)].

2. When the rate-controlling step involves a "chemical" process, b has the form $b = RT/nF$ [Eq. (13)] (or ∞ for a chemically controlled limiting current as in molecule dissociation or H recombination as $\theta_{\text{H}} \rightarrow 1$), where n is an integer characterizing the number of quasiequilibrium charge transfer steps that precede the rate-controlling step.

It will be noted that properties of the barrier-to-electron transfer do *not* enter into the determination of b for "chemically controlled" rate-determining steps provided the quasiequilibrium hypothesis applies adequately to the steps prior to the rate-controlling one, which may not always be the case. This means practically that the exchange rate in the pre-rate-determining steps must be at least 10 times the net velocity of the rate-controlling step at all overpotentials.

In practice, judging by the numerical variety of Tafel-slope values that are observed but do not accord exactly with theoretically predicted limiting cases, it is generally not adequate to assume that the conditions required for the limiting values to arise according to Eqs. (12) or (13) are met. Then, of course, rather arbitrary dependences of b or α on T can arise and do not have any special fundamental significance.

Gileadi has pointed out in a private communication⁷³ that the b values for chemically controlled processes, e.g., the value $RT/2F$ for ad-atom recombination in the h.e.r. or for Cl_2 evolution under certain conditions,⁵ must follow the normally expected T -dependence, i.e., b is *linear* in T and α is then independent of T . This is because no e -barrier properties are involved in determining b for such cases. This is an important point but difficult to exemplify unambiguously from experimental data since $b = RT/2F$ for the h.e.r. is only observed at Pt and its significance for that case, with respect to recombination control, has been questioned^{4,6} (diffusion of H_2 from the electrode can give the same behavior). For Cl_2 evolution, where recombination control is indicated under same conditions,^{5,49} the behavior is complicated by T -dependent Cl^- adsorption and surface oxidation of the anode metal, e.g., Pt. In fact, this is probably a complication in all anodic reactions in aqueous media, including the discharge of N_3^- at Pt,⁴⁸ which provided the first example of α being temperature dependent. It is surprising that in our recent studies of anodic Cl_2 evolution at Pt,

where the Tafel slope at lower current densities is ~ 38 mV, i.e. $\ll \sim 2.3RT/(1 + 0.5)F$, the slopes are again independent of T yet this slope would be expected to be of the form $RT/(1 + \beta)F^\dagger$ so that even if β were linear in T , b would still be T -dependent.

11. Tafel Slopes in Relation to Exchange Current Densities i_0

It is often found that electrochemical processes that take place in a multistep sequence (see Section IV.7) exhibit Tafel slopes that have relatively high values (~ 120 mV) when the i_0 values are large. This behavior is important in evaluations of trends of electrocatalytic activity for a given electrochemical process at a series of electrode materials.⁴⁶ Practically, it is evident that a reaction proceeding by a rate-controlling pathway with a *low* Tafel slope, e.g., 29 or 42 mV ($2.3RT/2F$ or $2.3RT/3F$ at $T = 298$ K say), may well have a better operating polarization performance⁴⁶ in terms of η at say 200 mA cm^{-2} than another process with a higher i_0 but also a greater b value, say 120 mV. This is illustrated qualitatively in Fig. 16.

It is quite clear from general principles of electrode kinetics that, for a reaction which proceeds by two or more steps *in series*, there will arise a sequence of Tafel-line segments in the relation shown in Fig. 17. Thus, the step "furthest down" the reaction step sequence tends to be rate controlling at the lowest current densities. This will also be the step with the smallest Tafel slope as can be shown by treating the kinetics of the sequence by the quasiequilibrium method or the steady-state method, taking into account potential dependence of surface concentrations of the (adsorbed) intermediates (cf. Refs. 13, 25, 32, and 34). Thus, in the three-step sequence illustrated in Fig. 17, there is a progressive increase of the $\ln i_0$ values of the segments *and* an associated increase in b values. In the example schematically given, it is clear that had step III remained rate controlling up to high current densities, better electrode performance would have been realized at practical, elevated current densities, despite the lower i_0 value. In practice, of

[†] Yokoyama and Enyo⁷⁴ have recently argued that Cl_2 evolution at Pt is controlled by the kinetics of discharge of Cl^- but this is not supported by the Tafel-slope behavior or the reaction order (cf. 76) when adsorption effects involving Cl^- ion are taken into consideration.⁷⁵

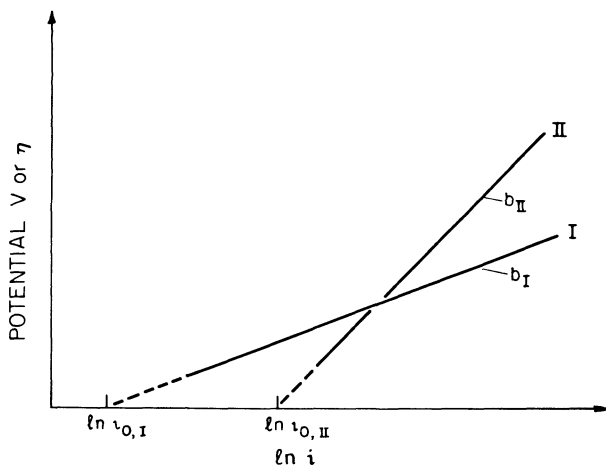


Figure 16. Illustrating relative polarization performance of two processes at an electrode having two possible $\ln i_0$ and corresponding b values, I and II. Process I gives better polarization performance at high c.d. despite its lower i_0 value.

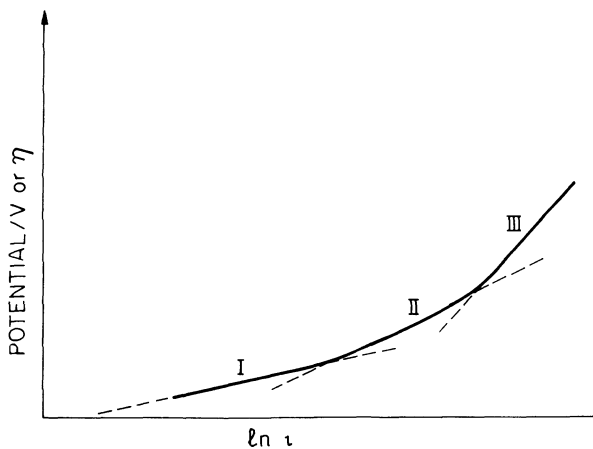


Figure 17. Sequence of Tafel regions for a hypothetical three-stage series electrode process as overpotential η is increased at constant temperature (schematic).

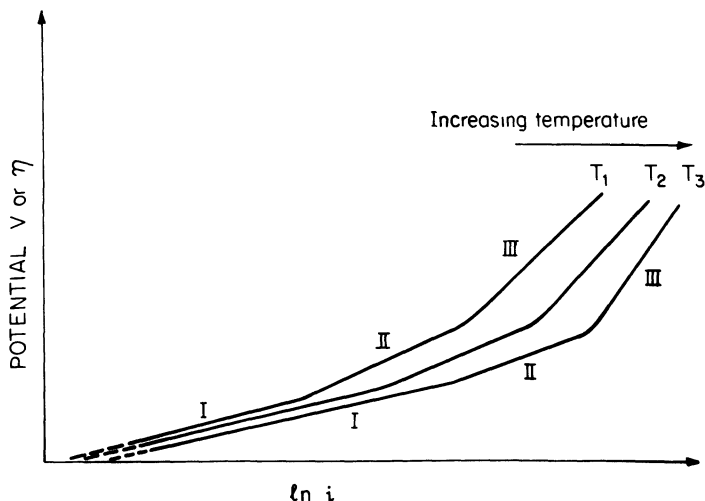


Figure 18. Sequence of Tafel regions of a three-stage series electrode process, as in Figure 17, with increasing temperature, $T_1 \rightarrow T_2 \rightarrow T_3$, assuming the steps have different activation energies (schematic).

course, various cases can arise, depending on the kinetic behavior of the sequential steps of the reaction.

Temperature is an important aspect of the above type of behavior since the steps in a multistep sequence are usually associated with different activation energies. Then the step with the lower activation energy tends to control the kinetics at the higher temperature in a *series* reaction sequence (see Fig. 18).

An interesting example of this behavior has recently been observed in our own work on the kinetic behavior of the h.e.r. at high activity Ni-Mo-Cd cathode materials.¹⁰⁴ These electrodes give remarkably low overpotentials (<100 mV) for cathodic H_2 evolution at a practical c.d. of ~ 200 mA cm⁻² but only at an elevated temperature of 80–90°C. The reason is clear as is seen from the graph of the actual Tafel lines for one of these electrode materials in aqueous NaOH at various temperatures (Fig. 6). The Tafel relations show two, or sometimes three, segments but the low c.d. region (II) has a low Tafel slope in the range 23–29 mV. It is superseded by a region (I) of greater slope (~ 120 mV) at higher c.d.'s which, however, is associated with a larger (apparent) heat of activation. Hence this region moves relatively more to higher

c.d.'s at elevated temperatures, leaving the low-slope region (advantageous for good electrode performance) to characterize the kinetics under the latter conditions. Hence relative performance is much enhanced at elevated temperature. Note that the slope of the upper region line I does not change very much with T , thus providing another example of α being temperature dependent. The two regions are associated with measurably different⁷⁷ behaviors of the H intermediate; possibly sorbed H as an hydride is involved⁴⁶ as well as two-dimensionally adsorbed H.

12. Electrode Area and Tafel Slopes

Recent work on the h.e.r. at high-area electrode materials, e.g., Raney-Ni type preparations by Tilak,⁷⁸ seems to indicate that low Tafel slopes are exhibited at such materials in comparison with the behavior of the same metal in bulk form. This is not just a matter that arises on account of the lower real c.d.'s that can be achieved at high-area porous materials since at corresponding low current densities at the bulk metal, e.g., Ni, there is *not* an indication of a change of Tafel slope from the usually observed value of ~ 100 mV (298 K) to a lower value within ~ 100 mV from the reversible H_2/H^+ or $\text{H}_2/\text{H}_2\text{O}$, OH^- reversible potentials. An example is shown in Fig. 19 from the work of Tilak.⁷⁸

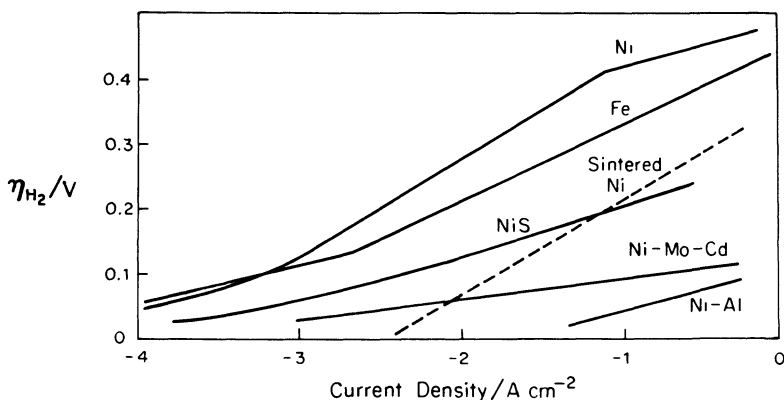


Figure 19. Comparison of Tafel relations for the h.e.r. at various Ni electrode preparations, and Fe, having varying real to apparent area ratios; $T = 343$ K (from Tilak⁷⁸).

The behavior at high area, porous cathode materials is, in fact, the opposite of that normally predicted for a porous electrode, namely that the Tafel slope, for a given process, will be twice the value at the corresponding bulk metal plane surface. Hence the observed behavior must be due to some intrinsic difference in the adsorption behavior of H and/or the kinetics of the h.e.r. under such conditions.

Bearing in mind that low Tafel slopes for the h.e.r. are usually associated with a mechanistic step involving a potential-dependent state (H coverage or degree of H sorption) of the H [see Eq. (43) or (44)], it is tempting to suggest that the interesting behavior of the h.e.r. at high-area active metal cathode materials is associated with a special state of the H intermediate⁴⁶ which is promoted by the disordered state of the metal in Raney-type materials or electrodeposited composites such as Ni-Mo-Cd. Here it is useful to recall that special catalytic effects are observed with metal-atom cluster materials as recently investigated, e.g., by Ozin and Power⁷⁹ and Messmer and Salahuf.⁸⁰

This is an area of much practical importance for research and development in electrolyzer technology; more work is currently required for elucidation of the behavior of high-area porous and composite electrode materials with regard especially to the values of Tafel slope and conditions under which *low* b values can be achieved for H₂, O₂, and Cl₂ evolution reactions, thus minimizing activation overpotential energy losses in high current-density operations.

V. PROBLEMS WITH EVALUATION OF HEATS OF ACTIVATION WHEN α IS TEMPERATURE DEPENDENT

1. Derivation of the Apparent Heat of Activation at the Reversible Potential

Normally, as may be seen from Eq. (11), evaluation of ΔH^\ddagger can be made from plots of $\ln k$ vs. $1/T$ or, taking account of any double-layer effects, from $\ln i_0$ vs. $1/T$. This gives the apparent heat of activation at the reversible potential. The real but experimentally undeterminable ΔH^\ddagger at $\eta = 0$ differs from the apparent value by

$\alpha \Delta H^\circ$, where ΔH° is the heat change in the single electrode reaction involved. This problem was first treated by Temkin⁸¹ (see Section V.2).

As is well known, the apparent heat of activation evaluated experimentally is dependent on η , as follows from Eq. (11). Following the form of that equation, the exchange current density i_0 can be written in an abbreviated practical form as

$$i_0 = k_0 \exp(-\Delta H_r^{\circ\ddagger}/RT) \quad (47)$$

where $\Delta H_r^{\circ\ddagger}$ represents the (apparent-see below) heat of activation at $\eta = 0$ (reversible condition 'r'). At other current densities, i_η , for $\eta > 0$, is

$$i_\eta = k_0 \exp(-\Delta H_\eta^{\circ\ddagger}/RT) = k_0 \exp[-(\Delta H_r^{\circ\ddagger} - \alpha\eta F)/RT] \quad (48)$$

where α may or may not be a function of T in the above equations, k_0 is written to include a temperature-independent molal reactant concentration but this is a trivial point. For simplicity here, it is assumed in Eq. (48) that η does not affect $\Delta S^{\circ\ddagger}$ in k_0 (see p. 131).

For processes that obey the conventional form of the Tafel equation with $b = RT/\alpha F$, the $\Delta H^{\circ\ddagger}$ evaluated at various η is simply given by

$$\Delta H_\eta^{\circ\ddagger} = \Delta H_r^{\circ\ddagger} - \alpha\eta F \quad (49)$$

for the case where no quadratic term in η is involved. However, when α is $f(T)$ in Eq. (48), it is clear that this must be taken account of when $\Delta H_\eta^{\circ\ddagger}$ for various η 's is evaluated from $d \ln i_\eta / d(1/T)$. Conway and MacKinnon⁸² first examined this problem in relation to their paper on $b(T)$ with Tilak.²

It is useful to show the results of their illustrative calculations of the consequences of b not being simply $RT/\alpha F$, with α constant, by evaluating $\Delta H_r^{\circ\ddagger}$ for various cases corresponding to the several forms of b as $f(T)$ encountered experimentally. For this purpose, $\Delta H_r^{\circ\ddagger}$ is taken arbitrarily as 41.8 kJ mol^{-1} and corresponding i_0 values can be calculated for various temperatures. Corresponding i values at various η and for various temperatures can be evaluated from the Tafel equation in the form $\log i = \log i_0 + \eta/2.3b$, where b is taken as one of the four possible forms encountered experimentally:

Case 1: $b = RT/\beta F$ with $\beta = \text{constant} = 0.5$ – the classical expression for b with conventional T -dependence. (For this case, $\Delta H_r^{\circ\ddagger}$ should be recovered without complications. This is just a reference example).

Case 2: $b = RT/\beta' F + K$, where $K = 0.04$ V and $\beta = 0.71$ as for Hg^2 (this corresponds to $b = 0.116$ V at 298 K).

Case 3: $b = RT/\alpha(T)F = R/\gamma F = \text{const}$, independent of T , as observed for a number of electrode processes exemplified in Section III.

Case 4: $b = K' - RT/\beta F$ or $b = RT/\alpha(T)F$ with $\alpha = \gamma T^m$, where $m > 1$ so that b decreases as T increases.

For each of the cases listed above, $\Delta H_r^{\circ\ddagger}$ and $\Delta H_\eta^{\circ\ddagger}$ can be recovered⁸² from the calculated $\ln i_\eta$ vs. $1/T$ taking account of the form of b as $f(T)$. The following methods may be used:

1. $\Delta H_r^{\circ\ddagger}$ is recovered from $d \ln i_0/d(1/T) = -\Delta H_r^{\circ\ddagger}/R$. This is the usual and most convenient way of obtaining the heat of activation at $\eta = 0$.
2. $\Delta H_\eta^{\circ\ddagger}$ is recovered at various η from $d \ln i_\eta/d(1/T) = -(\Delta H_r^{\circ\ddagger} - \alpha\eta F)/R$.
3. From $(d\eta/dT)_i = -\Delta H_\eta^{\circ\ddagger}/\alpha FT$.
4. From $(d\eta/d \ln T)_i = -\Delta H_\eta^{\circ\ddagger}/\alpha F$.

The latter two derivatives give, of course, $\Delta H_\eta^{\circ\ddagger}$ values for respective η values corresponding to the i_η values at which the derivatives are evaluated.

The results of the illustrative calculations, made in these various ways, may be compared as shown in Fig. 20 for plots of the $\log i_\eta$ vs. i/T type. Fig. 21–22 show η , vs. $\log T$ plots (method 4) for cases 1–3.

In Case 1, treated by the conventional method (1), linear electrochemical Arrhenius plots result with slopes that decrease in the expected way with increasing η . Case 2 gives curvature in such plots as does case 4 (but with the curvature in the opposite direction). Case 3, with α linear in T , as often found, gives $\log i_\eta$ vs. $1/T$ plots that are *parallel* for various η values so that the $\Delta H_\eta^{\circ\ddagger}$ values that are recovered are apparently *independent* of η . This is an interesting and significant case. The behavior of Case 3 follows obviously from Eq. (48) when $\alpha = \gamma T$ since then the exponent in Eq. (48) only involves the term $\Delta H_r^{\circ\ddagger}/RT$ as a T -dependent quantity so that a common $\Delta H_r^{\circ\ddagger}$ is recovered for all η values. For Case 4,

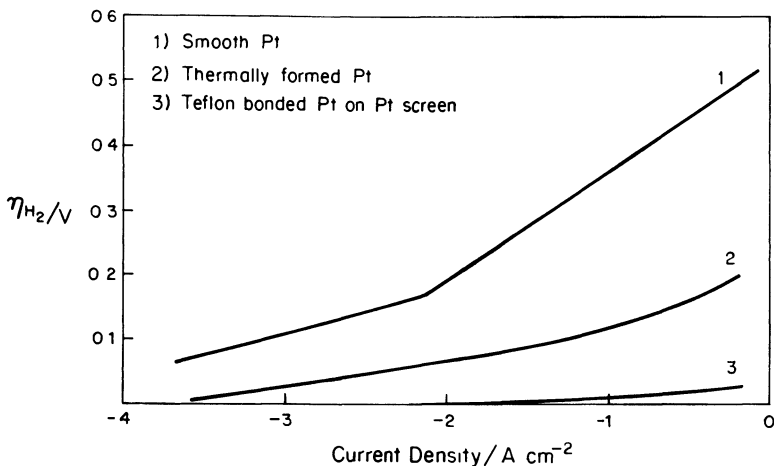


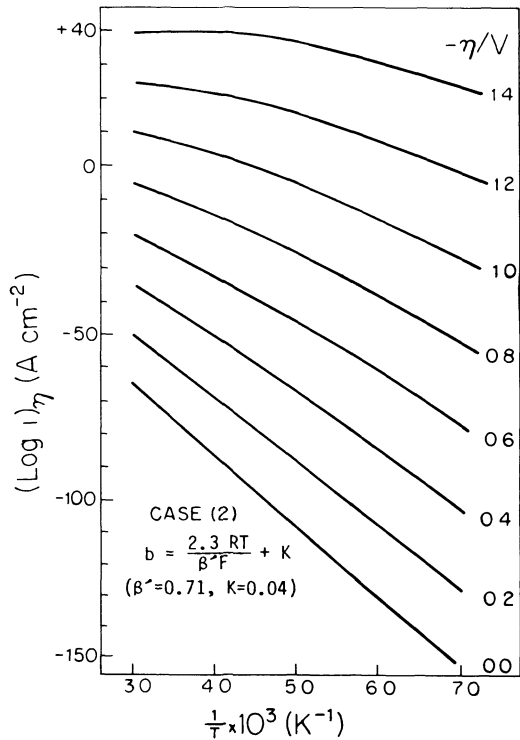
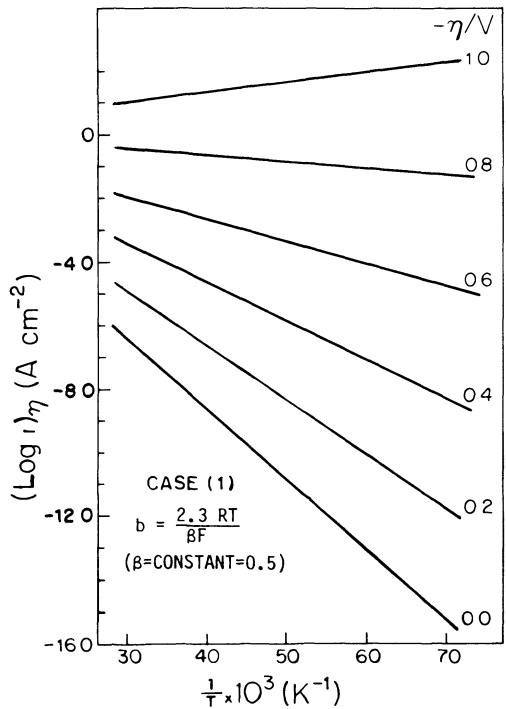
Figure 20. Comparison of Tafel relations for the h.e.r. at three types of Pt: smooth Pt and two high-area materials (from Tilak⁷⁸).

$\Delta H_{\eta}^{\circ\ddagger}$ evidently increases (!) with increasing η when b decreases linearly with T ; this is also a case sometimes encountered experimentally.

It is interesting to note that when conditions corresponding to case 3 apply, as shown in Fig. 21c, no condition of activationless discharge (cf. Krishtalik⁸³) would be reached according to experimental evaluations of $\ln i_{\eta}$ as $f(1/T)$ for various increasing η values. However, at a *given* constant T , such a condition should still (theoretically) be attainable when ηF becomes sufficiently large. In case 1, activationless discharge *does* formally arise as is seen in Fig. 21a when $\log i_{\eta}$ becomes parallel to the $1/T$ axis. This condition arises, of course, at an overpotential η^* determined by the limit $\Delta H_r^{\circ\ddagger} - \alpha\eta^*F = 0$. The line for $-\eta = 1.0\ V$ in Fig. 21a is physically fictitious.

Results for other cases are to be found in Reference 82.

For the conventional case where $\Delta G^{\circ\ddagger}$ is modified by an electrical energy $-\alpha\eta F$ with increasing potential and $\alpha \neq f(T)$, increase of $T \ln i_0$ to an extent dependent on $\Delta H_{\eta=0}^{\ddagger}$ [cf. Eq. (48)]. However, b also increases in proportion to T so a series of Tafel lines arises for increasing temperatures as shown schematically in



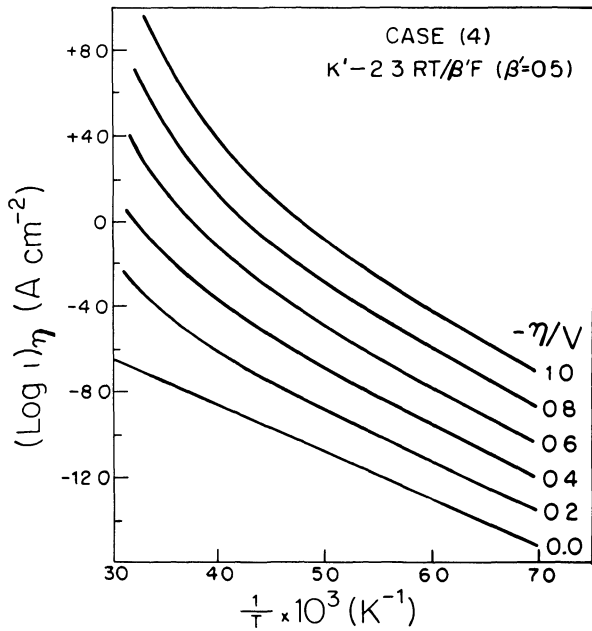
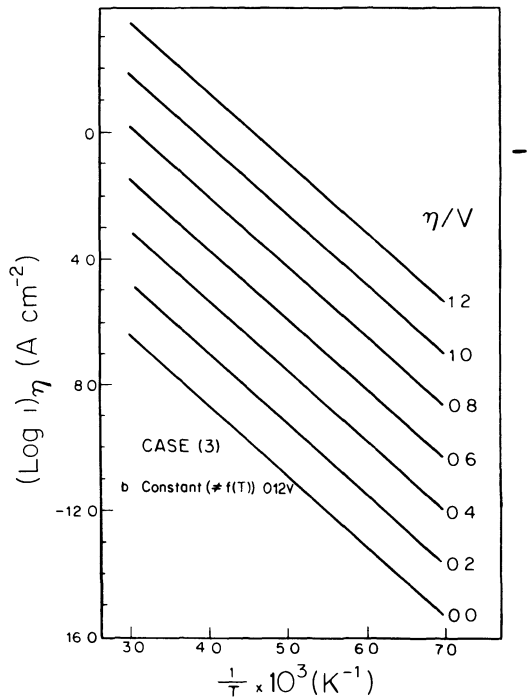


Figure 21 (a)-(d) Results of illustrative calculations for evaluation of heat of activation of an electrode process from plots of $\log i_\eta$ vs $1/T$ for cases 1-4

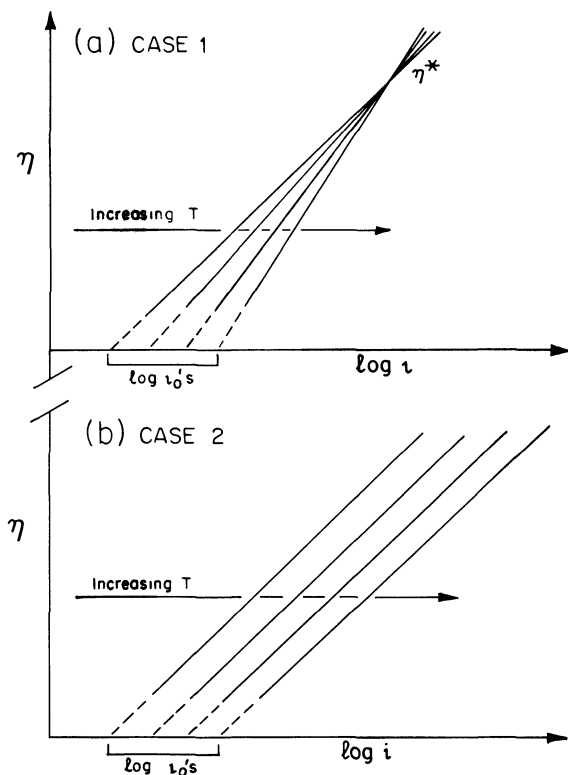


Figure 22. (a) Tafel relations for a process with a finite heat of activation ($\log i_0$ dependent on T) and a b value linear in T (conventional case, schematic) and (b) as in part a but for α proportional to T (b independent of T) (schematic).

Fig. 22a[†]; these lines evidently cross at some potential η^* so that i_{η^*} is then independent of T , i.e., $\Delta H_{\eta^*}^\ddagger = 0$. This evidently corresponds to the condition of activationless discharge considered by Krishtalik⁸³ and referred to above for the case of increase of η (at a given T) to a limit corresponding to $\Delta H^\ddagger = 0$, i.e., when $\alpha\eta F = \Delta H_{\eta=0}^\ddagger$, assuming α is not $f(\eta)$; actually it probably always is, over

[†] We are indebted to Mr. D. Wilkinson in our laboratory for useful discussions on this point.

a sufficient range of η , as shown by Despić and Bockris³⁵ (but contrast the h.e.r. case).

For the case where the conventional form of the Lefat slope applies $b^{-1} = \alpha F/RT$ with α independent of T , it is easy to show that a family of Tafel relations obtained (Fig. 22a) at various temperatures intersect at a common overpotential η^* given by

$$\eta^* = \log \left(\frac{i_{0, T_1}}{i_{0, T_2}} \right) / \frac{\alpha F}{R} \left(\frac{1}{T_2} - \frac{1}{T_1} \right)$$

since $\log(i_{0, T_1}/i_{0, T_2})$ is determined by the quantity $(-\Delta H^\ddagger/2.3R)(1/T_1 - 1/T_2)$, it is clear that η^* will be a common intersection point for *all* temperatures. Thus, at this potential, the apparent ΔH^\ddagger is zero. These conclusions depend, of course, on the usual assumption that ΔH^\ddagger itself is approximately independent of T if the T range is not too large.

From the foregoing, it also follows that when b^{-1} is of the form $(\gamma T + c)F/RT$ (cf. p. 133) there will be no common η^* point since the term $b_{T_1}^{-1} - b_{T_2}^{-1}$ is then $(F/R)(\gamma T_1 + c)/T_1 - (\gamma T_2 + c)/T_2$, which will not cancel with the term $1/T_1 - 1/T_2$ from the difference of $\log i_0$ values at any two temperatures.

In the limiting case of $\alpha(T) = \gamma T$, Tafel lines will remain *parallel* with increasing T so that no crossing point as in Fig. 22a will ever be reached; this is indicated in Fig. 22b. $di_\eta/d(1/T)$ will then be finite (hence $\Delta H_\eta^\ddagger > 0$) at *all* potentials but, for a given T , increase of η will decrease ΔH^\ddagger from its zero- η value in the usual way, eventually leading to activationless discharge.

Care must therefore be taken in interpreting apparent activation energies as $f(\eta)$ from electrochemical Arrhenius plots when $\alpha = \gamma T$, i.e., when b is independent of T .

2. α and the Relation between Real and Apparent Heats of Activation

In any practical electrochemical experiment the absolute, but unknown, metal/solution p.d. at the reference electrode must normally vary with temperature on account of the single interface reaction entropy change. This leads to the now well-known situation that measurements of i_η or i_0 as a function of temperature can never give the true or "real" heat of activation for the electrode process. This was first pointed out by Temkin⁸¹ who showed that

only an *apparent*[†] heat of activation (which we have called $\Delta H_{\eta}^{\circ\ddagger}$ or $\Delta H^{\circ\ddagger}$ above) can be derived from electrochemical Arrhenius plots. Similar limitations apply to the evaluation of volumes of activation, $\Delta V^{\circ\ddagger}$.³⁰

The relation between Temkin's energy of activation quantity, $W^{\circ\ddagger}$, i.e., at zero metal-solution p.d. (V), and the apparent one $\Delta H^{\circ\ddagger}$ (referred to by Temkin as the "real" heat of activation) that is both experimentally measured and practically significant, i.e., as obtained from the reciprocal temperature coefficient of $\ln i_0$, $d \ln i_0 / d(1/T)$, is conveniently derived (cf. Refs. 25, 81) as follows. $\ln i_0$ is written as

$$\ln i_0 = \ln k_0 - (\Delta W^{\circ\ddagger} - \alpha V_r F) / RT \quad (50)$$

where V_r is the value of V when the reaction is at equilibrium ($i = 0$; $\eta = 0$) and α is the transfer coefficient, taken for this case to be independent of T . Noting that the reversible potential V_r is expressible for say a $1e$ process as $\Delta G_r = -FV_r$, where ΔG_r is the free-energy change in the single electrode interface reaction under study and $\Delta G_r = \Delta H_r - T\Delta S_r$, $\ln i_0$ can be written further as

$$\ln i_0 = \ln k_0 - \left[\Delta W^{\circ\ddagger} - \alpha F \left(\frac{T\Delta S_r}{F} - \frac{\Delta H_r}{F} \right) \right] / RT \quad (51)$$

Hence, obtaining the heat of activation in the usual way from $d \ln i_0 / d(1/T)$, it is found that[‡]

$$d \ln i_0 / d(1/T) = -(\Delta W^{\circ\ddagger} - \alpha \Delta H_r) / R \quad (52)$$

[†] Sometimes this quantity is referred to, somewhat misleadingly, as the "real" heat of activation as it is the quantity that is accessible experimentally. However, it is obviously not the "true" heat of activation of the process that would be measurable if a constant electrode/solution p.d. could actually be maintained as temperature is varied in the experiment to evaluate the heat of activation. In this respect, it is seen that the apparent, experimentally measurable, heat of activation of an electrode process does not have the same significance as the $\Delta H^{\circ\ddagger}$ quantity for a simple homogeneous chemical reaction.

The problem of the variation of reference-electrode potential can, of course, be avoided if the reference electrode is kept at constant T while the temperature of the working electrode is varied. However, then a thermal diffusion junction p.d. is introduced that depends on the temperature difference, as is well known.

[‡] In deriving the result in Eq. (52) from Eq. (50), it is usually assumed that over relatively small ranges of T , ΔH_r itself does not vary with T , i.e., $\Delta C_{p,r}$ is small. This is not always the case, however, for reactions involving change of charge in hydroxylic, structured solvents (see Ref. 55).

or

$$\Delta H_r^{\ddagger} = \Delta W^{\circ\ddagger} - \alpha \Delta H_r \quad (53)$$

ΔH_r is the enthalpy change in the single interface reaction under study in the $\ln i_0$ vs. T experiment but cannot directly be determined in a thermodynamically rigorous manner. However, with some extrathermodynamic assumption about evaluation of individual heats of ionic solvation,^{55,84} estimates of ΔH_r can be made but they are never very satisfactory. Uncertainties are 20–35 kJ mol⁻¹. However, non-isothermal cell measurements offer an approximate way of obtaining $\Delta W^{\circ\ddagger}$.

When α or β is a function of temperature, or b is given by Eq. (17), the simple additive relation between $\Delta W^{\circ\ddagger}$ and ΔH_r , given in Eq. (53) does not arise. The case where α is linear in T , namely $\alpha(T) = \gamma T$, as found for a number of processes experimentally, is of special interest with regard to evaluation of the true heat of activation, $\Delta W^{\circ\ddagger}$.

In this case we introduce $\alpha(T)$ as γT in Eq. (51) which becomes

$$\ln i_0 = \ln k_0 - \frac{\Delta W^{\circ\ddagger}}{RT} - (\gamma T \Delta H_r - \gamma T^2 \Delta S_r^0) / RT \quad (54)$$

giving

$$d \ln i_0 / d(1/T) = -\Delta W^{\circ\ddagger} / R - \gamma T^2 \Delta S_r^0 = -\Delta H_r^{\circ\ddagger} / R \quad (55)$$

assuming, as previously, that ΔH_r is not a function of T . Thus the experimentally accessible apparent activation energy $\Delta H_r^{\circ\ddagger}$ is now $\Delta W^{\circ\ddagger} + \gamma T^2 \Delta S_r^0$ (note that γ has the units T^{-1} and is experimentally measurable). This quantity is of interest since the ΔS_r^0 for the single interface reaction is much more reliably determinable^{55,84} than the corresponding ΔH_r . Thus, ΔS_r^0 will normally involve, among other accurately known thermodynamic quantities: (1) the absolute standard partial molar entropy of a single type of ion; and (2) the entropy of electrons in the electrode metal. Single-ion entropies required in (1) are now known by at least one more-or-less reliable extrathermodynamic method⁸⁴ to within ± 1 e.u. (± 1.2 kJ mol⁻¹ for $T \Delta S^\circ$ at 298 K) and the entropy of electrons is usually justifiably assumed to be $0 \pm < 1$ e.u. due to the low heat capacity⁸⁵ of the degenerate “electron gas” in metals. Hence $\Delta W^{\circ\ddagger}$ can be derived for this case with a reliability of ~ 1.5 kJ mol⁻¹ which is *very much*

better than would be the case where ΔH_r was required, as in Eq. (53). For that case, the uncertainty is at least $\pm 28 \text{ kJ mol}^{-1}$ based on the much larger uncertainty of absolute ionic heats of hydration.⁸⁴

Reliable evaluation of $\Delta W^{\circ\ddagger}$ would also then lead to an estimate of absolute entropies of activation for those electrode processes that are characterized by temperature-independent Tafel slopes, e.g., for anodic Br_2 evolution at C,² O_2 reduction at Pt,^{45a,45b} and N_2 evolution from the N_3^- at Pt.⁴⁸

3. Experimental Evidence for Potential Dependence of the Entropy of Activation, ΔS^\ddagger

(i) ΔS^\ddagger for Ionic Redox Reactions

We have referred earlier to the requirement^{2,11,82} that the entropy of activation of an electrode process be potential dependent if β is found to be dependent on temperature.

In recent important papers, Weaver¹⁰⁷⁻¹⁰⁸ and Weaver *et al.*¹⁰⁹ have made interpretations of the free energy of activation of some ionic-complex redox reactions in terms of their entropic as well as enthalpic components. His approach has been to combine regular kinetic measurements over a range of temperatures which give, in the usual way, the apparent heat of activation, with nonisothermal emf (electromotive force) measurements on thermocells[†] involving the potential of the reference electrode at different temperatures. Within the limitations that (1) the entropy of transfer of electrons, ΔS_e , involved in the cell reaction at the two temperatures is small enough to give a negligible $T\Delta S_e$ over the range of T involved in the measurements and (2) that the thermal diffusion potential at the boundary of the two solutions at different temperatures in the thermocell is small, or can be corrected for, this approach enables the "real" heat of activation (i.e., the ΔH^\ddagger free from an incidental effect of variation of electrode potential with T) to be distinguished fairly reliably from the apparent value in a more or less quantitative

[†] A treatment of the thermodynamic background of thermocell measurements may be found in the present author's (2) in Vol. 1 of this series, 1954, which refers to the earlier original work of Eastman, Crockford, and Hall, and Tyrell and Hollis on this topic.

way. Then, from the observed free energies of activation, the $T\Delta S^\ddagger$ component or the corresponding frequency factor can be evaluated and related to the solvational, steric, and other properties of the conjugate redox pair, and examined for any dependence on potential.

In this work, ΔS^\ddagger values, corrected for coulombic double-layer effects,¹¹⁰⁻¹¹³ were found¹⁰⁷ to be both large and sensitive to the ligand structure around the metal ion [Cr(III), Co(III) complexes, and $\text{Eu}(\text{H}_2\text{O})_n^{3+}$, and $\text{V}(\text{H}_2\text{O})_6^{3+}$] in outer-sphere redox reactions at Hg. Ammine, anionic, aquo, and other simple ligands were involved.¹⁰⁷⁻¹⁰⁹ These observations of specificity in the kinetic parameters, to ligand structure, must be considered in relation to the expectations of long-range polarization activation theory ("polaron theory") but the behavior observed is, in fact, what may be expected on the basis of more "molecular" pictures of the activation process and the role of short-range effects and solvent structure, taking into account ligand-specific effects that determine the "thermodynamic part" of the barrier.

Of special interest for the topic of the present chapter is the observation of Weaver¹⁰⁷ that while the "double-layer-corrected" ΔS^\ddagger quantities are ligand sensitive, they are found to be independent of potential. This is not the case for the atom and electron transfer process involved in the hydrogen evolution reaction at Hg studied by Conway, *et al.*,¹¹⁴ where an appreciable potential dependence of ΔS^\ddagger is observed, corresponding to "conventionally anomalous" variation of the Tafel slope with temperature. Unfortunately, in the work with the ionic redox reactions, as studied by Weaver, it is only possible to evaluate the variation of the transfer coefficient or symmetry factor with temperature with a limited variety of redox pairs since Tafel slopes, corresponding to any appreciable logarithmic range of current densities, are not always easily measurable. Alternatively, evaluation of α or β from reaction-order determination requires detailed double-layer studies over a range of temperatures.

It is interesting also that the ΔS^\ddagger quantities are approximately one-half of the corresponding overall reaction entropies as was found for the corresponding ΔV^\ddagger and ΔV° quantities in the work of Conway and Currie¹¹⁵ on kinetic studies at high hydraulic pressures.

(ii) ΔS^\ddagger for the Hydrogen Evolution Reaction

In work on the hydrogen evolution reaction at Hg from $\text{CF}_3\text{SO}_3^-\text{H}_3\text{O}^+$ (where the proton is present only as the unhydrated H_3O^+ ion) and from $\text{CF}_3\text{SO}_3\text{H}$ in excess water (where the proton is present as the fully hydrated ion H_9O_4^+), Conway *et al.*¹¹⁴ directly derived the real entropies of activation for proton discharge at Hg by means of kinetic measurements at various temperatures employing a nonisothermal cell, i.e., with a reference H_2/H^+ electrode at constant, ambient temperature. These measurements give, within a good approximation (see Ref. 107), the true heat of activation free from effects of incidental variations of the reference electrode potential (cf. Temkin⁸¹), so that the entropy of activation or the corresponding frequency factor can be evaluated.

By applying this approach to rates measured at a series of overpotentials, the potential dependence of what we have referred to above as the "true" heat of activation and the entropy of activation, ΔS_ϕ^\ddagger at constant potential, ϕ , was evaluated for proton discharge from the above two media. The important conclusion that was reached from the results is that ΔS_ϕ^\ddagger (or equivalently ΔS_η^\ddagger (since these ΔS^\ddagger functions differ only by a constant quantity) is dependent on potential for the h.e.r. at Hg, as shown in Fig. 23.

From these results, we have evaluated,¹¹⁴ using Eq. (23), the values of λ and μT as follows for the h.e.r.: in 1M aq. $\text{CF}_3\text{SO}_3\text{H}$, $\lambda = 0.22$, $\mu T = 0.28$ with the overall $\alpha \equiv \beta = 0.5$ while in the monohydrate melt, $\lambda = 0.77$, $\mu T = -0.07$, with the overall $\beta = 0.77$. Note that μ has the units T^{-1} .

It is of considerable interest that the h.e.r., which involves both atom and electron transfer, shows this effect quite clearly (Fig. 23), while for ionic redox reactions involving supposedly only outer-shell reorganization in the activation process, Weaver's results¹⁰⁷ show that there is little or no dependence of ΔS_ϕ^\ddagger on potential. This difference implies that there is a qualitative difference between the activation processes in an atom transfer process such as the h.e.r. and in ionic redox processes where a state of hydration- or ligand-shell interaction is *maintained* in the electron transfer process while, in atom transfer processes, the state of hydration and ionic charge is *eliminated* in the electrode reaction. These results lend some support to the view we have expressed elsewhere⁶⁸ that the activa-

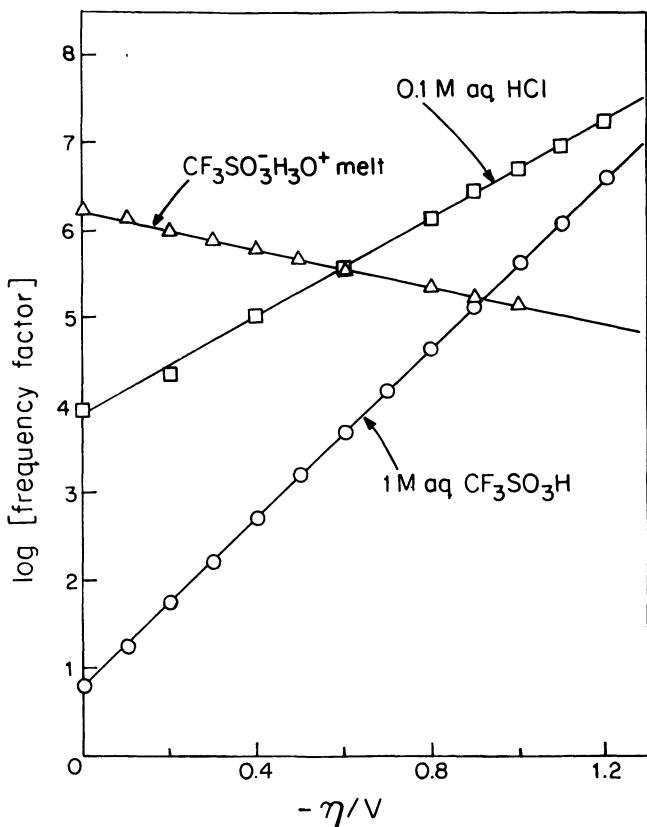


Figure 23. Evaluation of dependence of Arrhenius frequency factor or entropy of activation on electrode potential for the h.e.r. from H_3O^+ in $\text{CF}_3\text{SO}_3\text{H}_3\text{O}^+$ melt and from aqueous H^+ in 1 M aqueous $\text{CF}_3\text{SO}_3\text{H}$ [from Conway *et al.* (to be published)]; see D. F. Tessier, Ph.D Thesis, University of Ottawa, 1985.

tion process in the discharge step of the h.e.r. is not that of outer hydration-shell reorganization (as in an ionic redox reaction) as has been proposed by Levich *et al.*⁶⁶ but rather a more intimate neutralization and transfer, closely coupled with the desolvation process as treated in earlier papers^{39,69} on this question.

Since the effect of potential on ΔS^\ddagger for the h.e.r. is evidently quite substantial, it seems reasonable to suggest that it arises from potential dependence of the solvent-structure environment (e.g.,

H bonding and potential dependence of ion concentrations in the double layer⁵⁷) of the transition state in the interphase rather than, e.g., from changes in anharmonicity or OH-bond frequency with potential, which could lead only to small changes of ΔS^\ddagger .

It is curious that the striking deviations of electrochemical kinetic behavior from that expected conventionally, which are the subject of this review, have not been recognized or treated in the recent quantum-mechanical approaches, e.g., of Levich *et al.* (e.g., see Refs. 66 and 105) to the interpretation of electrode reaction rates. The reasons for this may be traced to the emphasis which is placed in such treatments on (1) quantal effects in the *energy* of the system and (2) continuum modeling of the solution with consequent neglect of the specific solvational- and solvent-structure aspects that can lead, in aqueous media, to the important *entropic* factor in the kinetics and in other interactions in water solutions.⁵⁵ However, the work of Hupp and Weaver,⁸⁶ referred to on p. 153, showed that the results could be interpreted in terms of Marcus theory, with regard to potential dependence of ΔS^\ddagger , when there was a substantial net reaction entropy change in the process.

VI CONCLUSIONS AND FINAL REMARKS

1. Review of the experimental literature shows that the Tafel equation written in the conventional form $\ln i = \ln i_0 + \alpha\eta F/RT = \ln i_0 + \eta/b$, with α constant, is rarely obeyed in the sense that b is not linearly dependent on T , so that α is apparently temperature dependent; the latter dependence is usually quite large, e.g., 25% over a 150 K range of T .
2. Approximate *independence* of the Tafel slope b on T is the "rule rather than the exception" in electrode kinetics of a variety of processes.
3. The situation summarized in remarks 1 and 2 implies that quite fundamental aspects of electron transfer associated with thermal activation and solvation changes in electrochemical charge transfer reactions are not yet well understood. Indeed, the problem suggests that the foundations of electrode kinetics, commonly regarded as

- well understood, are, in fact, not yet adequately formulated.
4. For the h.e.r. at Hg, several series of experimental results show that it is not because β is dependent on T that b is not equal to $RT/\beta F$ but rather that $b = RT/\beta' F + \text{const.}$ in certain cases.
 5. For some processes, b may even decrease with T .
 6. If the entropy of activation, ΔS^\ddagger , as well as the electrochemical energy of activation, is potential or field dependent, it can be shown that the Lefat slope b^{-1} will contain a temperature-independent component, so that α or β is apparently linear in T . In the general case, b^{-1} will contain both temperature-dependent and temperature-independent components. The case where b is entirely constant with T requires, formally, that it is only the *entropy* of activation that is potential dependent—a situation that is difficult to understand on the basis of current and established ideas on the role of electrode potential in influencing rates of heterogeneous charge transfer reactions through changes of the Fermi level.
 7. It is possible to understand how a potential or field effect on ΔS^\ddagger could originate from the influence of the known field-dependent solvent orientation in the inner region of the double layer on the solvation-shell reorganization in the activation process through solvation co-sphere/solvent co-plane interaction. Quantitative formulation of this effect has not yet been made.
 8. Specific adsorption of anions can give rise to unconventional temperature dependence of Tafel slopes on account of the temperature dependence of the ion adsorption and consequent changes of the structure and electric potential profile across the double layer where the transition state is established.
 9. Complex reaction sequences can also give rise to unconventional temperature dependence of α since then α involves potential dependence of surface coverages of adsorbed intermediates.
 10. When α is $f(T)$, complications arise in electrochemical Arrhenius plots for evaluation of the apparent ΔH^\ddagger ; then

ΔH^\ddagger is found to depend on potential in an unconventional manner.

11. For the case of reactions for which α is linear in T , the absolute heat of activation of the electrode process can be quite reliably derived from the experimental variation of $\ln i_0$ with $1/T$. This is not the case when the conventional behaviour obtains ($b = RT/\alpha F$; $\alpha = \text{const.}$).
12. Fluctuation theory can only account for a very small variation of α or β with T . The experimental variation is much larger, indicating the importance of other effects, such as the influence of the field effect on entropy of activation.
13. The relatively large influence of temperature on α or β suggests that temperature dependence of solvent structure is an important factor in the effect, especially in associated solvents such as H_2O , H_3PO_4 , etc.
14. Further measurements need to be made on the temperature and potential dependence of the rates of *simple ionic redox reactions* at electrodes with proper corrections for double-layer effects at various temperatures, so that the temperature dependence of β for an elementary electron transfer reaction, without chemisorption and coupled atom transfer, would become better known. This is an essential requirement for progress in understanding the true significance of the temperature effects on electrode-kinetic behavior; reliable experiments will not, however, be easy to accomplish and will require parallel double-layer studies over a range of temperatures.
15. For certain ionic redox reactions, it appears that conventional behaviour *does* arise, i.e., β is independent of T . The case of T -dependence of β probably arises when there is some strong coupling in the reaction with the electrode surface either when atom transfer occurs or a reactant ion solvation or ligand shell is shared with the solvation co-plane of the electrode surface, the condition of which is potential or surface-charge dependent.
16. In a proper representation of electron transfer rates (cf. Gerischer⁸⁸) the Fermi-Dirac distribution must be used to express the occupancy of electron energy states in the

metal as a function of T , relative to the Fermi level. This introduces a nonclassical temperature effect, i.e., differing from that given by the Boltzmann function, except under the limiting conditions for which the Fermi-Dirac distribution goes over to the Boltzmann distribution.

ACKNOWLEDGMENTS

Acknowledgement is made to the Natural Sciences and Engineering Research Council of Canada for support of theoretical work on the problem of variation of α with T which is, in part, reported in this chapter. The author is also grateful to professors J. O'M. Bockris, E. Gileadi and M. Weaver, and Dr. J. Appleby, to whom this chapter was circulated prior to publication, for their comments. Thanks are due also to Professor E. B. Yeager for provision of data on O_2 reduction in phosphoric acid and for material related to Eq. (24) in this chapter; to Dr. R. P. Bell, F.R.S., for helpful discussion in correspondence on the question of temperature dependence of Brønsted coefficients; to Professor D. F. Evans for provision of unpublished data on nitro-compound reduction; and to Messrs. D. F. Tessier and D. Wilkinson in our laboratory for helpful discussion on various points.

The author also gratefully acknowledges award of the Killam Senior Research Fellowship of the Canada Council for 1983-1985 during the tenure of which this work was carried out.

REFERENCES

- ¹ J. Tafel, *Z. Phys. Chem.* **50** (1905) 641.
- ² B. E. Conway, D. J. MacKinnon, and B. V. Tilak, *Trans. Faraday Soc.* **66** (1970) 1203.
- ³ R. Parsons, *Trans. Faraday Soc.* **47** (1951) 1332.
- ⁴ M. W. Breiter, *J. Electrochem. Soc.* **109** (1962) 549.
- ⁵ B. E. Conway and D. M. Novak, *J. Electroanal. Chem.* **99** (1979) 133.
- ⁶ S. Schuldiner, *J. Electrochem. Soc.* **109** (1962) 550.
- ⁷ R. Parsons and E. Passeron, *J. Electroanal. Chem.* **12** (1966) 524; see also J. E. B. Randles and D. R. Whitehouse, *Trans. Faraday Soc.* **64** (1968) 1376.
- ⁸ J. M. Savéant and D. Tessier, *J. Electroanal. Chem.* **65** (1975) 57; *J. Phys. Chem.* **81** (1977) 2192, and **82** (1978) 1723; see also *Faraday Discuss. Chem. Soc.* **74** (1982) 57.
- ⁹ R. A. Marcus, *Ann. Rev. Phys. Chem.* **15** (1964) 15.
- ¹⁰ B. E. Conway and J. O'M. Bockris, *J. Chem. Phys.* **26** (1957) 532.
- ¹¹ J. O'M. Bockris and R. Parsons, *Trans. Faraday Soc.* **45** (1949) 916; **47** (1951) 914.

- ¹² B. E. Conway and J. O'M. Bockris, *Can. J. Chem.* **35** (1957) 1124.
- ¹³ J. O'M. Bockris, *Modern Aspects of Electrochemistry*, Ed. by J. O'M. Bockris, Butterworths, London, 1954, Vol. 1, p. 180.
- ¹⁴ R. A. Marcus, *J. Chem. Phys.* **24** (1956) 966; **26** (1957) 862. See also K. J. Laidler, S. Gladstone, and H. Eyring, *J. Chem. Phys.* **7** (1939) 1053.
- ¹⁵ R. W. Gurney, *Proc. R. Soc. London, Ser A* **134** (1932) 137.
- ¹⁶ R. W. Gurney and R. H. Fowler, *Proc. R. Soc. London, Ser A* **136** (1932) 378; see also R. H. Fowler, *Trans. Faraday Soc.* **28** (1932) 368.
- ¹⁷ T. Erdey-Gruz and M. Volmer, *A. Phys. Chem.* **150** (1930) 203; **162** (1932) 53.
- ¹⁸ J. A. V. Butler, *Trans. Faraday Soc.* **19** (1924) 729; **28** (1932) 379.
- ¹⁹ H. Bauer, *J. Electroanal. Chem.* **16** (1968) 419.
- ²⁰ J. Horiuti and M. Polyanyi, *Acta Physiochim. U.R.S.S.* **2** (1935) 505.
- ²¹ J. A. V. Butler, *Proc. R. Soc. London, Ser A* **157** (1936) 423.
- ²² S. Glasstone, K. J. Laidler, and H. Eyring, *J. Chem. Phys.* **7** (1939) 1053.
- ²³ J. N. Brønstead and N. L. Ross-Kane, *J. Am. Chem. Soc.* **53** (1931) 3624; see also R. P. Bell, *Acid-Base Catalysis*, Clarendon Press, Oxford, 1941 and R. P. Bell, *The Proton in Chemistry*, second edn., Chapman and Hall, London, 1973.
- ²⁴ M. Eigen, *Discussions Faraday Soc.* **39** (1965) 1.
- ²⁵ For example see B. E. Conway, *Theory and Principles of Electrode Processes*, Ronald Press, New York, 1964 or J. O'M. Bockris in Ref. 13.
- ²⁶ R. P. Bell, *Proc. Soc. London, Ser. A* **139** (1933) 466. ^b C. E. H. Bawn and G. Ogden, *Trans. Faraday Soc.* **30** (1934) 432.
- ²⁷ B. E. Conway, *Can. J. Chem.* **37** (1959) 178.
- ²⁸ St. G. Christov, *Electrochim. Acta* **4** (1961) 194; **4** (1961) 306; **9** (1964) 575.
- ²⁹ N. S. Hush, *J. Chem. Phys.* **28** (1958) 962; *Trans. Faraday Soc.* **57** (1961) 557.
- ³⁰ B. E. Conway and J. C. Currie, *J. Phys. Chem.* **125** (1978) 257.
- ³¹ L. Young, *Anodic Oxide Films*, Academic Press, New York, 1961.
- ³² J. O'M. Bockris, *J. Chem. Phys.* **24** (1956) 817.
- ³³ C. A. Christiansen, *Z. Phys. Chem.* **B33** (1936) 145; **B37** (1937) 374.
- ³⁴ B. E. Conway, in *M.T.P. International Review of Science, Vol. 6, Electrochemistry*, Ed. by J. O'M. Bockris, Butterworths, London 1973, Chap. a, pp. 41-113.
- ³⁵ A. R. Despić and J. O'M. Bockris, *J. Chem. Phys.* **32** (1960) 389.
- ³⁶ A. K. Vijh and B. E. Conway, *Chem. Rev.* **67** (1967) 623.
- ³⁷ J. Horiuti and M. Ikusima, *Proc. Imp. Acad. Tokyo* **15** (1939) 39.
- ³⁸ E. Gileadi, in Reference 25, Chapter 8, p. 262.
- ³⁹ J. O'M. Bockris and R. Parsons, *Trans. Faraday Soc.* **44** (1948) 860; **45** (1949) 916.
- ⁴⁰ A. M. Azzam, J. O'M. Bockris, B. E. Conway, and H. Rosenberg, *Trans. Faraday Soc.* **46** (1950) 918.
- ⁴¹ B. Post and C. F. Hiskey, *J. Am. Chem. Soc.* **72** (1950) 4203.
- ⁴² B. E. Conway and M. Salomon, *J. Chem. Phys.* **41** (1964) 3169; *Disc Faraday Soc.* **39** (1965) 223.
- ⁴³ J. O'M. Bockris, R. Parsons, and H. Rosenberg, *Trans. Faraday Soc.* **47** (1951) 766.
- ⁴⁴ J. Horiuti, Chapter 2, p. 17, *Transactions Symposium on Electrode Processes, 1959*, The Electrochemical Society, Wiley, N.Y., 1961.
- ^{45a} A. J. Appleby, *J. Electrochem. Soc.* **117** (1970) 1158 and **117** (1970) 641; see also *J. Electroanal. Chem.* **27** (1970) 325 and **24** (1970) 97.
- ^{45b} E. Yeager, D. Scherson, and B. Simić-Glavaski, Extended Abstracts of the Spring Meeting of The Electrochemical Society, San Francisco, Calif. (1983), p. 1043.
- ⁴⁶ B. E. Conway, H. Angerstein-Kozłowska, M. A. Sattar, and B. V. Tilak, *J. Electrochem. Soc.* **130** (1983) 1825.
- ⁴⁷ B. E. Conway, in *Modern Aspects of Electrochemistry*, Ed. by J. O'M. Bockris and B. E. Conway, Plenum Press, New York, 1982, Vol. 7, Chap. 2, p. 83.

- ⁴⁸ H. P. Stout, *Trans Faraday Soc.* **41** (1945) 64.
- ⁴⁹ B. E. Conway and D. M. Novak, *J. Chem. Soc., Faraday Trans 1* **75** (1979) 2454; **77** (1981) 2341.
- ⁵⁰ J. J. MacDonald and B. E. Conway, *Proc. R. Soc. London, Ser. A* **269** (1962) 419.
- ⁵¹ R. E. Meyer, *J. Electrochem. Soc.* **107** (1960) 847.
- ⁵² D. Gilroy and B. E. Conway, *Can. J. Chem.* **46** (1968) 875.
- ⁵³ S. Shibata and M. P. Sumino, *Electrochim. Acta* **20** (1975) 739; see also *Electrochim. Acta* **22** (1977) 175 and *J. Electroanal. Chem.* **89** (1978) 37.
- ⁵⁴ J. Morgan and B. E. Warren, *J. Chem. Phys.* **6** (1938) 666.
- ⁵⁵ B. E. Conway, *Ionic Hydration in Chemistry and Biophysics*, Elsevier, Amsterdam, 1981, Chaps. 3 and 23.
- ⁵⁶ E. Yeager, *Discussion Remarks in Proceedings of Symposium on Electrocatalysis*, Vol. 84-12, Spring Meeting of The Electrochemical Society, San Francisco, Calif. 1980 publication (The Electrochemical Soc. Inc., 1984).
- ⁵⁷ B. E. Conway, *J. Electroanal. Chem.* **123** (1981) 81.
- ⁵⁸ J. A. V. Butler, *Chemical Thermodynamics*, Macmillan Co., London 1962, p. 389; see also I. M. Barclay and J. A. V. Butler, *Trans. Faraday Soc.* **34** (1938) 1445.
- ⁵⁹ N. F. Mott and R. J. Watts-Tobin, *Phil. Mag.* **7** (1962) 483.
- ⁶⁰ J. O'M. Bockris, M. A. V. Devanathan, and K. Müller, *Proc. R. Soc. London, Ser. A* **274** (1963) 55.
- ⁶¹ R. W. Fawcett, *Isr. J. Chem.* **18** (1979) 3.
- ⁶² R. Parsons, *J. Electroanal. Chem.* **59** (1975) 229.
- ⁶³ J. D. Bernal and R. H. Fowler, *J. Chem. Phys.* **1** (1933) 515.
- ⁶⁴ J. O'M. Bockris and D. B. Matthews, *Modern Aspects of Electrochemistry*, Ed. by J. O'M. Bockris and B. E. Conway, Plenum Press, New York, 1971, Vol. 6, p. 230.
- ⁶⁵ B. E. Conway, *Proc. R. Soc. London, Ser. A* **256** (1960) 128; **247** (1958) 400.
- ⁶⁶ V. G. Levich, R. Dogonadze, and A. Kuznetsov, *Electrochim. Acta* **13** (1968) 1025; **15** (1970) 353. For more recent reviews, see R. R. Dogonadze and A. M. Kuznetsov, *Itogi Nauki i Tekhniki, Ser. Phys. Chem. Kinetics*, Vol. 2, 1973 and Vol. 5, 1978, VINITI, Moscow; and R. R. Dogonadze and A. M. Kuznetsov, *Progr. Surf. Sci.* **1** (1975) 1; and *Elektrokhimiya* **3** (1967) 739.
- ⁶⁷ L. I. Krishtalik, Electron and proton transfer, *Faraday Discuss. Chem. Soc.* **74** (1982) 205.
- ⁶⁸ Electron and proton transfer, *Faraday Discuss. Chem. Soc.* **74** (1982).
- ⁶⁹ B. E. Conway and J. O'M. Bockris, *J. Chem. Phys.* **31** (1959) 1133.
- ⁷⁰ J. Ulstrup, *Electrochim. Acta* **29** (1984) 1377.
- ⁷¹ J. G. N. Thomas, *Trans. Faraday Soc.* **57** (1961) 1603.
- ⁷² E. Gileadi and B. E. Conway, *J. Chem. Phys.* **39** (1963) 3420.
- ⁷³ E. Gileadi, private communication in discussion at Ottawa, (Summer 1983).
- ⁷⁴ T. Yokoyama and M. Enyo, *J. Electroanal. Chem.* **136** (1982) 185.
- ⁷⁵ B. E. Conway and D. M. Novak, *J. Electroanal. Chem.* **136** (1982) 191.
- ⁷⁶ M. Enyo and T. Yokoyama, *Electrochim. Acta* **15** (1970) 1921.
- ⁷⁷ B. E. Conway, L. Bai, and D. F. Tessier, *J. Electroanal. Chem.* **161** (1984) 39.
- ⁷⁸ B. V. Tilak, *J. Electrochem. Soc.* (in press).
- ⁷⁹ G. A. Ozin and W. J. Power, *Ber Bunsenges. Phys. Chem.* **82** (1978) 93; see also G. A. Ozin, *Acc. Chem. Res.* **10** (1977) 21; and G. A. Ozin, *Faraday Discuss. Chem. Soc. Diatomic Metal-Metal Clusters* **14** (1980) 7.
- ⁸⁰ R. P. Messmer and D. R. Salahub, *Comput. Chem. Educ. Res. (Proc. Int. Conf.)* 3rd 1976, Ed. by E. V. Ludena, Plenum Press, N.Y., (1977) p. 171. *Chem. Abstr.* **89**, (1978) 89721; see also R. P. Messmer and D. R. Salahub, *Chem. Phys. Lett.* **51** (1977) 84.

- ⁸¹ M. I. Temkin, *Z. Fiz. Khim* **22** (1948) 1081.
- ⁸² B. E. Conway and D. J. MacKinnon, *J. Electrochem. Soc.* **116** (1969) 1665; see also J. N. Agar, *Discussions Faraday Soc.* **1** (1947) 84 and *Ann. Rept. Chem. Soc., London* (1938).
- ⁸³ L. I. Krishtalik, *Elektrokhimiya* **6** (1970) 507; see also L. I. Krishtalik, *Electrode Reactions; The Mechanism of the Elementary Act*, Nauka, Pub. Moscow, (1979).
- ⁸⁴ B. E. Conway, *J. Solution Chem.* **7** (1978) 721.
- ⁸⁵ J. C. Slater, *Introduction to Chemical Physics*, McGraw-Hill, N.Y., (1939), Table 29-2, p. 478.
- ⁸⁶ M. J. Weaver and F. C. Anson, *J. Phys. Chem.* **80** (1976) 1861; P. D. Tyma and M. J. Weaver, *J. Electroanal. Chem.* **111** (1980) 195, see also R. Hupp and M. J. Weaver, *J. Phys. Chem.* **88** (1984) 6128.
- ⁸⁷ J. A. V. Butler, *Electrocapillarity*, Methuen, London, 1940, p. 138.
- ⁸⁸ H. Gerischer, *Z. Phys. Chem. N.F.* **26** (1960) 223; **26** (1960) 325.
- ⁸⁹ K. J. Vetter and J. W. Schultze, *Ber. Bunsenges. Phys. Chem.* **77** (1973) 945.
- ⁹⁰ J. W. Schultze and K. J. Vetter, *Electrochim. Acta* **18** (1973) 889.
- ⁹¹ J. O'M. Bockris and S. U. M. Khan, *Appl. Phys. Lett.* **42** (1983) 124; *J. Phys. Chem.* **87** (1983) 2599.
- ⁹² R. Parsons and M. A. V. Devanathan, *Trans. Faraday Soc.* **49** (1953) 673.
- ⁹³ A. N. Frumkin, *Advanced Electrochemistry and Electrochemistry Engineering*. Ed. by P. Delahay and C. Tobias, Wiley, N.Y., 1961, Vol. 1, p. 65.
- ⁹⁴ S. Jofa and A. N. Frumkin, *Acta Physicochim. URSS* **10** (1939) 473.
- ⁹⁵ D. C. Grahame, *Chem. Rev.* **41** (1947) 441.
- ⁹⁶ R. Parsons, *J. Chim. Phys.* **49** (1952) C82; *J. Electroanal. Chem.* **21** (1969) 35.
- ⁹⁷ J. O'M. Bockris and E. C. Potter, *J. Chem. Phys.* **20** (1952) 614.
- ⁹⁸ M. W. Breiter, *Ann. N.Y. Acad. Sci.* **101** (1963) 709.
- ⁹⁹ A. N. Frumkin, *Advanced Electrochemistry and Electrochemistry Engineering*, Ed. by P. Delahay and C. Tobias, Wiley, N.Y., 1963, Vol. 3, p. 287.
- ¹⁰⁰ Y. M. Kolotyrkin, *Trans. Faraday Soc.* **55** (1969) 455.
- ¹⁰¹ B. E. Conway, discussion remarks to paper by L. I. Krishtalik, *Faraday Discuss. Chem. Soc. London*, **74**, 1982, Electron and Proton Transfer.
- ^{102a} Th. Ackermann, *Discussions Faraday Soc.* **24** (1957) 180.
- ^{102b} D. Evans, Private communication; see R. Petersen, Ph.D thesis in chemistry, University of Wisconsin, Madison, 1982.
- ¹⁰³ F. P. Bowden and P. Grew, *Discussions Faraday Soc.* **1** (1947) 86.
- ¹⁰⁴ B. E. Conway and L. Bai, *Proceedings of the Fifth World Hydrogen Energy Conference*, Toronto, Canada, 1984, Pergamon Press, N.Y. 1984.
- ¹⁰⁵ A. M. Kuznetsov, *J. Electroanal. Chem.* **159** (1983) 241.
- ¹⁰⁶ See, e.g., J. P. Muscat and D. M. Newns, *Progr. Surf. Sci.* **9** (1978) 1.
- ¹⁰⁷ M. J. Weaver, *J. Phys. Chem.* **83** (1979) 1748.
- ¹⁰⁸ M. J. Weaver, *J. Phys. Chem.* **80** (1976) 2645.
- ¹⁰⁹ E. L. Yee, R. J. Cave, K. L. Guyer, P. D. Tyma, and M. J. Weaver, *J. Am. Chem. Soc.* **101** (1979) 1131.
- ¹¹⁰ M. J. Weaver and F. C. Anson, *J. Am. Chem. Soc.* **97** (1975) 4403; *Inorg. Chem.* **15** (1976) 1871.
- ¹¹¹ M. J. Weaver and T. L. Sattesberg, *J. Phys. Chem.* **81** (1977) 1772.
- ¹¹² T. L. Sattesberg and M. J. Weaver, *J. Phys. Chem.* **82** (1978) 1784.
- ¹¹³ M. J. Weaver, *J. Electroanal. Chem.* **93** (1978) 231.
- ¹¹⁴ B. E. Conway, D. F. Tessier and D. Wilkinson, *J. Electroanal. Chem.* (to be published).
- ¹¹⁵ B. E. Conway and J. C. Currie, *J. Electrochem. Soc.* **127** (1978) 257.
- ¹¹⁶ J. Sluyters, *J. Electroanal. Chem.* **146** (1983) 263; **176** (1984) 297.

Electrochemistry of Semiconductors: New Problems and Prospects

Yu. V. Pleskov and Yu. Ya. Gurevich

*A. N. Frumkin Institute of Electrochemistry, Academy of Sciences of the USSR,
Moscow, USSR*

I. INTRODUCTION

Electrochemistry of semiconductors is now in a state of outliving its "second youth." This direction of electrochemical physics, which emerged more than a quarter of the century ago, developed especially intensively at the beginning of the 1960s when its scientific foundations were laid down and methods of surface treatment of semiconductor materials were designed, which found application in the technology of semiconductor devices.¹ Electrochemistry of semiconductors did not retire into itself; on the contrary, the results obtained in this field made it possible to look in a new way at such concepts, common for electrochemistry as a whole, as the zero-charge potential, exchange current, the transfer coefficient of an electrochemical reaction, etc. Later, however, interest in the problems of electrochemistry of semiconductors dropped significantly, mainly because practical applications proved to be more difficult than was expected.

A new surge of activities in this field (which is being continued now) arose after the beginning of the 1970s when the possibility had been found of employing semiconductor electrodes for solar energy conversion via photoelectrolysis of water with hydrogen production. At present, when, on the one hand, the danger of the depletion of natural resources becomes more and more acute and, on the other, growth of environmental pollution increases, wide

attention² has been drawn to potentially important "liquid junction solar cells" which are ecologically pure and utilize renewable energy. Research and development effort in the "solar-semiconductor" field has led to considerable development in electrochemistry of semiconductors. At the same time, progress made in electrochemistry of semiconductors has proved to be rather useful for electrochemistry as a whole. For example, the study of semiconductor electrodes has resulted in comprehensive development of such general problems as the concept of the electrochemical potential of electrons in the solution, the relationship between the "physical" energy scale and the "electrochemical" scale of electrode potentials, etc. These problems constitute the content of first sections of this review.

In the following sections we consider new problems in electrochemistry and photoelectrochemistry of semiconductors proper, such as "Fermi-level pinning" at the surface of a semiconductor electrode (as an alternative to the more common "band-edge pinning"), the quasithermodynamic description of electrode reactions—in particular the concept of quasi-Fermi level and the limits of its applicability—and so on. In these sections we also consider briefly the principles of certain of the most up-to-date practical applications of electrochemistry of semiconductors.

Information concerning the physics of semiconductors and their surfaces can be found, for example, in References 3 and 4; general problems of electrochemistry of semiconductors are discussed in References 1, 5, and 6. Finally, all these problems are considered in greater detail in a monograph of the authors.⁷

Notations used in this review are in accord with the IUPAC electrochemical nomenclature, but only with the exception that the electrode potential is denoted by φ instead of E , because, in semiconductor physics, the symbol E conventionally denotes the energy characteristics (such as, for example, the band-edge energies E_c and E_v , and the band gap E_g).

II. CHARACTERISTIC ENERGY LEVELS IN THE ELECTRODE/ELECTROLYTE SOLUTION SYSTEM

The thermodynamically correct description of energy characteristics of electrons in electrochemical systems is a rather important prob-

lem both in purely methodological and practical respects. In particular, the concept of the electrochemical potential of electrons in a solution which contains a redox couple, is essential for the understanding of the laws governing electrochemical and photo-electrochemical processes. Next, the reorganization energy of a solvent affects significantly the kinetics of reactions which involve charge transfer. Finally, the electron energy levels, which are directly related to the oxidized and reduced components of the couple, determine the quantitative characteristics of the corresponding electron currents.

1. The Electrochemical Potential of Electrons in the Solution Containing a Redox Couple

Consider an electrode immersed in a solution, which contains a redox couple taking part in a reversible electron exchange reaction



Here ox and red denote the oxidized and reduced forms of the substance (e.g., Fe^{3+} and Fe^{2+}) in the solvated state, and n is the number of electrons transferred in the electrode reaction. Under thermodynamic equilibrium, the following relation holds:

$$\tilde{\mu}_{\text{ox}} + n\tilde{\mu}_e = \tilde{\mu}_{\text{red}} \quad (2)$$

where $\tilde{\mu}_{\text{ox}}$ and $\tilde{\mu}_{\text{red}}$ are the electrochemical potentials of the redox couple components in the solution (per mole), and $\tilde{\mu}_e$ is the electrochemical potential of electrons in the electrode. The quantities $\tilde{\mu}_{\text{ox,red}}$ can be represented in the form

$$\tilde{\mu}_{\text{ox,red}} = RT \ln c_{\text{ox,red}} + z_{\text{ox,red}} \mathcal{F} \phi + \mu_{\text{ox,red}}^\circ \quad (3)$$

Here R is the universal gas constant, T the absolute temperature, $c_{\text{ox,red}}$ are the concentrations (the activities in a more general case) of the ox and red reactants in the solution, $z_{\text{ox,red}}$ are their charge numbers, \mathcal{F} is the Faraday constant, ϕ is the electric potential, and $\mu_{\text{ox,red}}^\circ$ are constants independent of $c_{\text{ox,red}}$ and ϕ .

Taking into account Eqs. (2) and (3), we can calculate the equilibrium electrode potential φ^0 , which corresponds to reaction (1) occurring on an electrode:

$$\varphi^0 = \varphi_0^0 + \frac{RT}{n\mathcal{F}} \ln \frac{c_{\text{ox}}}{c_{\text{red}}} \quad (4)$$

where φ_0^0 is the standard electrode potential in a given solution; φ_0^0 depends on the difference $\mu_{\text{ox}}^{\circ} - \mu_{\text{red}}^{\circ}$ and, thereby, on the nature of the electrode reaction and also on the choice of the reference electrode.

It is rather important that if thermodynamic equilibrium is established, in accordance with Eq. (1), we can introduce the concept of the electrochemical potential of electrons in the electrolyte solution, $\tilde{\mu}_e^{\text{el}}$, which is in no way related to the presence of the electrode itself. The fact is that within the framework of thermodynamics, a specific mechanism, through which an equilibrium is established, does not play any role, so one may assume, in particular, that electron exchange between ox and red proceeds without any electrode involved. In this case, $\tilde{\mu}_e^{\text{el}}$ for reaction (1) is given by

$$\tilde{\mu}_e^{\text{el}} = \frac{1}{n} (\tilde{\mu}_{\text{red}} - \tilde{\mu}_{\text{ox}}) \quad (5)$$

where $\tilde{\mu}_{\text{red}}$ and $\tilde{\mu}_{\text{ox}}$ are taken at the potential $\phi^{\text{el},b}$ of the bulk electrolyte solution. Since the quantities $\tilde{\mu}_{\text{red,ox}}$ depend only on the properties of the ox and red reactants and the solvent, $\tilde{\mu}_e^{\text{el}}$ is in no way related to the nature of the electrode and does not depend on its interface structure. Moreover, it is the quantity $\tilde{\mu}_e^{\text{el}}$ which determines the electrochemical potentials of electrons in a given electrode under equilibrium conditions. In particular, this electrochemical potential has the same value for any electrode which is in equilibrium with a given redox couple.

The above considerations show how important it is to find a relationship between $\tilde{\mu}_e^{\text{el}}$ and the characteristic parameters of a redox couple. To this end, we shall consider a solution containing one red particle. Denoting the most probable thermodynamic energy of the electron level of the red particle by E_{red}° and that of the ox particle by E_{ox}° , we shall analyze, following papers,^{8,9} the thermodynamic cycle (a-d) shown in Fig. 1 [in Eq. (1), $n = 1$ is assumed for simplicity):

- a. An electron is instantly transferred from a solvated red particle (from the level E_{red}°) to the level E_{vac} . Here E_{vac} is the potential energy of an electron in vacuum, more precisely, in the vapor phase in a close proximity of the electrolyte surface, yet beyond the action limits of purely surface forces.

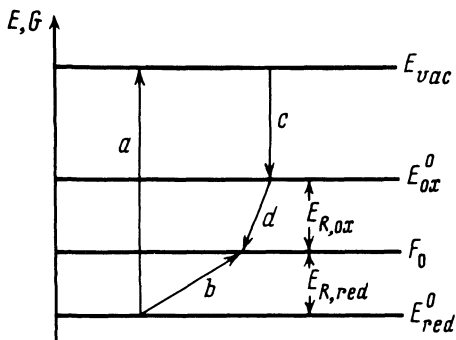


Figure 1. Determination of the position of energy levels of an electron in the solution containing a redox couple. E is the internal energy and G is the free energy.

- b. The state of the solvent near the red particle, which has now become the ox particle, changes, corresponding to the thermodynamic equilibrium of the ox particle in the solution.
- c. The electron from the level E_{vac} is instantly transferred to the ox particle formed (to the level E_{ox}°) without any change in the state of the solvent.
- d. A certain rearrangement of the solvent occurs around the red particle formed; as a result, the whole system returns to the initial equilibrium state.

In this cycle, the changes in the internal energy of the system taking place at stages a and c characterize the depths of the levels E_{red}° and E_{ox}° with respect to E_{vac} ; these changes are also equal to the ionization energy of the red particle and the electron affinity of the ox particle in the solution. The energy characteristics corresponding to stages b and d represent reorganization energies of the solvent, $E_{R,red}$ and $E_{R,ox}$, related to the red and ox particles.

For the process considered here, the quantities $E_{R,red,ox} > 0$ are the absolute value of energies (free energies to be exact), which are necessary to alter the state of the medium (solvent) from the initial to the final equilibrium state when the charge of the particle changes by unity.¹⁰⁻¹²

Thus, by virtue of the above analysis,

$$E_{\text{red}}^{\circ} + E_{R,\text{red}} - E_{\text{ox}}^{\circ} + E_{R,\text{ox}} = 0 \quad (6)$$

The quantity F_0 is defined by the relation

$$F_0 = E_{\text{red}}^{\circ} + E_{R,\text{red}} = E_{\text{ox}}^{\circ} - E_{R,\text{ox}} \quad (7)$$

which follows from Eq. (6) and characterizes the change in the free energy of the system considered when an electron is transferred, in an equilibrium manner, from the red particle in the solution into vacuum (or when an electron is transferred, again in an equilibrium manner, from vacuum to the ox particle). Combining Eqs. (6) and (7), we obtain

$$F_0 = \frac{1}{2}(E_{\text{ox}}^{\circ} + E_{\text{red}}^{\circ}) + \frac{1}{2}\Delta E_R \quad (8)$$

where

$$\Delta E_R = E_{R,\text{red}} - E_{R,\text{ox}} \quad \text{and} \quad E_{\text{ox}}^{\circ} - E_{\text{red}}^{\circ} = E_{R,\text{ox}} + E_{R,\text{red}} \quad (9)$$

We note that relation (9) can also be derived if we consider the equilibrium transfer of an electron directly from the red particle to the ox particle within the solution.

In polar liquids, in particular in water, one may assume $E_{R,\text{ox}} = E_{R,\text{red}} \simeq E_R$, especially for the so-called outer-sphere reactions.¹³ In this case, the main contribution to the change in state of the medium is due to repolarization of the solvent caused by long-range electrostatic interactions.

We have then from Eqs. (8) and (9),

$$F_0 = \frac{1}{2}(E_{\text{ox}}^{\circ} + E_{\text{red}}^{\circ}), \quad E_{\text{ox}}^{\circ} - E_{\text{red}}^{\circ} = 2E_R \quad (10)$$

It can be seen from Eq. (10) that, in the simplest case considered here, the characteristic level F_0 lies midway between E_{ox}° and E_{red}° , and the difference between E_{ox}° and E_{red}° is twice the value of E_R .

Thus, using Eqs. (3) and (5) and taking into account that F_0 is calculated per particle, we finally obtain for the electrochemical potential, $\tilde{\mu}_e^{\text{el}}$,⁸

$$\tilde{\mu}_e^{\text{el}} = \mathcal{N}_A F_0 - RT \ln \frac{c_{\text{ox}}}{c_{\text{red}}} \quad (11)$$

where \mathcal{N}_A is the Avogadro number.

Since relation (11) is of fundamental importance, we shall give another, independent derivation of this relation by the methods of statistical mechanics,^{7,9} without using Eq. (5).

Consider a system which is a set of cells whose average number per unit volume is N . These cells contain at most one electron per cell, so that the average number of electrons per unit volume is $n \leq N$. In this case, the free energy of the system with only one electron is F_0 . The free energy of a unit volume of such a system containing n electrons, G , is given by the relation (see, e.g., Ref. 14)

$$G = F_0 n - TS \quad (12)$$

the S is the so-called configurational entropy, equal to

$$S = -k \ln C_N^n = -k \ln \frac{N!}{(N-n)!n!} \quad (13)$$

where k is the Boltzmann constant ($k = R/\mathcal{N}_A$) and C_N^n is the number of ways according to which n particles may be placed in N cells. The electrochemical (chemical) potential of electrons $\tilde{\mu}_e$ per mole of the substance is $\tilde{\mu}_e = \mathcal{N}_A \partial G / \partial n$. Taking into account Eq. (13) and the formula $\alpha(\ln q!)/\alpha q \approx \ln q$ ($q \gg 1$), we obtain for $\tilde{\mu}_e$:

$$\tilde{\mu}_e = \mathcal{N}_A F_0 - RT \ln \frac{N-n}{n} \quad (14)$$

We note that the model system considered here is, in fact, a redox couple in the solution. Indeed, electrons in this system, whose number is, obviously, c_{red} , are distributed over $(c_{\text{ox}} + c_{\text{red}})$ positions. Thus, substituting $N = c_{\text{ox}} + c_{\text{red}}$ and $n = c_{\text{red}}$ into Eq. (14), we obtain an expression which coincides with Eq. (11).

Hence, the electrochemical potential of electrons in the solution can be introduced quite rigorously and consistently within the framework of both the thermodynamic and statistical-mechanical approach.

In analogy with the Fermi level of electrons in solids (calculated per electron), we introduce the quantity F_{redox} , which is defined by the relation $F_{\text{redox}} = \tilde{\mu}_e^{\text{el}} / \mathcal{N}_A$ and represents the electrochemical potential of electrons in the solution, per particle. The quantity F_{redox} is frequently called "the Fermi level of electrons in solution." We note that this term (and more so the term "Fermi level of

solution") should be considered as not quite adequate and often leading to confusion. It should be stressed that the position of F_{redox} in the solution is in no way related to the concentration of "free" electrons in it, but is determined by the presence in the solution of a redox couple, which contains only "bound" electrons. The quantity F_{redox} does not characterize the energy of any particle because no electrons with the energy F_{redox} are present in the solution (unlike, e.g., the case of metals where the Fermi level F_{met} coincides with the energy E_F of electrons at the Fermi surface). Thus, in the course of electrode reactions, electrons can pass neither from the level F_{redox} to the electrode, nor from the electrode to this level; transitions occur with the levels E_{red}° and E_{ox}° involved. At the same time, it is the position of the level F_{redox} , which determines the thermodynamic properties of a redox couple and the interface between the electrode and solution containing this couple. For example, proceeding from the condition of thermodynamic equilibrium in the semiconductor/solution system,

$$F = F_{\text{redox}} \quad (15)$$

(F is the Fermi level of the semiconductor), the condition for an electrochemical reaction to occur can be written in the form

$$F > F_{\text{redox}} \quad (\text{cathodic reaction}) \quad (16a)$$

and

$$F < F_{\text{redox}} \quad (\text{anodic reaction}) \quad (16b)$$

Similar expressions can be used in considering photoelectrochemical reactions (see Section IV.2).

The electrochemical potentials of redox couples in solution are calculated in a known manner from the thermodynamic characteristics of the substances involved. For certain reactions, which proceed with the participation of the semiconductor electrode material, in particular anodic or cathodic decomposition reactions, the values of F_{redox} are as reported in References 15-18.

2. Relationship between the Energy Scale and the Scale of Electrode Potentials

The position of the energy levels E_{ox}° and E_{red}° and the level of the electrochemical potential F_{redox} with respect to the level E_{vac} can

be determined by establishing a quantitative relationship between the "physical" energy scale, in which the energy E_{vac} is taken as the zero reference point, and the electrochemical scale of electrode potentials, which is reckoned from the potential of a certain arbitrarily chosen reference electrode. The relationship between these scales is, in general, of the form

$$F_{\text{redox}} = -e\varphi^0 + \text{const} \quad (17)$$

Here $e > 0$ is the absolute value of the electron charge.

Let us consider such an ox/red couple, for which the equilibrium potential φ^0 is conditionally taken as zero; the junction between the solution of this couple and an inert conductor [i.e., one which does not take part in reaction (1)] is, by definition, the reference electrode. The constant in Eq. (17) coincides then with F_{redox} , thereby representing the change in the free energy in the course of the reaction



In other words, this constant is the change in the free energy in the transfer of an electron from a point in vacuum near the solution surface to the Fermi level of the reference-electrode metal, this change being equal to F_0 for $c_{\text{ox}} = c_{\text{red}}$. The quantity F_0/e is sometimes called the "absolute potential" of an electrode.¹⁹

An attempt at determining this quantity was first made in Reference 19 and then in Reference 20. By analyzing a rather complicated thermodynamic cycle,[†] the author of Reference 20 found that the change in the free energy of the reaction



which is equal to the value of the constant in Eq. (17) for the normal hydrogen electrode (NHE), amounted to -4.5 eV.

The results of Reference 20 have been extensively used in the literature (in particular, in considering the photoelectrochemical method of solar energy conversion) for determining the electrochemical potential level of various redox couples.

[†] This cycle was based on the known value of the standard potential of a silver electrode in a solution of Ag^+ ions relative to the NHE and comprised the following stages: sublimation of metallic silver, ionization of silver atoms thus formed, and hydration of the ions.

It should be noted, however, that the method chosen in Reference 20, as well as in certain subsequent papers (see, e.g., Reference 21) for determining ΔG appears to be unjustifiably complicated and gives lower accuracy. Indeed, in those calculations the values of, for example, sublimation energy and ionization energy were taken into account twice, and with opposite signs, so they cancel out in the final result.

A simple and accurate method of comparing the scales of energies and electrode potentials follows from Reference 22 and lies in the calculation of the work function of a metal, which is in the electrolyte solution at the reference-electrode potential. This is illustrated in Fig. 2, which shows a metal in equilibrium with an ox/red couple in the solution (so that their electrochemical potential levels coincide: $F_{\text{redox}} = F_{\text{met}}$). The change in the free energy of reaction (16) is the sum of the energies of stages c and d of the cycle shown in Fig. 1, that is the quantity F_{redox} (which coincides, as was already noted, with F_0 for $c_{\text{ox}} = c_{\text{red}}$).

It can be seen from the cycle of Fig. 2 that

$$-F_{\text{redox}} = w + e\Delta\psi \quad (20)$$

Here w is the work function of the uncharged metal in vacuum, and $\Delta\psi$ is the Volta-potential difference in the metal/solution system which arises as a result of mutual charging of "free" surfaces of the metal and solution when they are brought into contact.

For a particular case, for example, for the normal hydrogen electrode, it is convenient to perform calculations using data for the Volta-potential difference in the mercury-aqueous solution system²³: $\Delta\psi = -0.07$ eV at zero potential against NHE. Assuming that the work function of mercury in vacuum is²⁴ $w = 4.50 \pm 0.03$ eV,

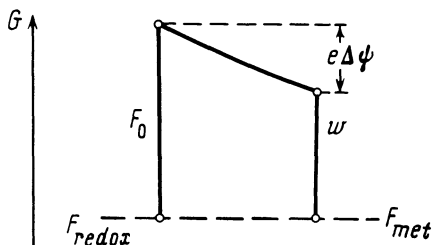


Figure 2. Diagram illustrating the relationship between the "physical" and "electrochemical" scales.

we obtain from Eq. (18)

$$-F_{\text{redox}}(\text{NHE}) = 4.50 - 0.07 = 4.43 \approx 4.4 \text{ eV.}$$

Thus, the level of the electrochemical potential of the normal hydrogen electrode, $F_{\text{redox}}(\text{NHE})$, lies 4.4 eV below the energy level E_{vac} .

Let us recall in this connection that the thermodynamic work function is equal to $w = \chi + |F - E_c|$. Here χ is the electron affinity of the semiconductor, and the position of F relative to the conduction-band bottom, E_c , in the semiconductor bulk is given by the following relations:

$$F - E_c = -E_g/2 + kT \ln(N_v/N_c)^{1/2}, \quad n_0 = p_0 \quad (i\text{-type}) \quad (21a)$$

$$F - E_c = -kT \ln(N_c/n_0), \quad n_0 \gg p_0 \quad (n\text{-type}) \quad (21b)$$

$$F - E_c = -E_g + kT \ln(N_v/p_0), \quad p_0 \gg n_0 \quad (p\text{-type}) \quad (21c)$$

where E_g is the band gap, N_c and N_v are the effective densities of states in the conduction and valence bands, and n_0 and p_0 are thermodynamic equilibrium concentrations of electrons and holes in the semiconductor bulk.

3. Determination of the Reorganization Energy of a Solvent

Using the results presented above, one can suggest a method of determining the reorganization energy from data on photoemission of electrons from solutions into the vapor phase (see review²⁵).

Illumination of a solution containing red particles with light of quantum energy exceeding the electron work function leads to photoemission of electrons into the vapor phase. Since photoionization is a fairly rapid process, an electron passes into the vapor phase from the level E_{red}° , so that the "photoelectric" work function appears to be equal to $-E_{\text{red}}^\circ$, if we take $E_{\text{vac}} = 0$. It follows from Eq. (11) that for $c_{\text{ox}} = c_{\text{red}}$ it differs from the "equilibrium" (thermodynamic) work function, equal to $-F_{\text{redox}} = -F_0$, by the reorganization energy $E_{R,\text{red}}$ (see Fig. 1). Thus, the latter can be found as the difference between the photoelectric work function, $w_{\text{ph}} = -E_{\text{red}}^\circ$, and $-F_{\text{redox}}$ (a similar method for determining $E_{R,\text{red}}$ was

employed previously²⁶ for the case where solvated electrons served as "emitters" in the solution).

The quantity w_{ph} can be found from the dependence of the photoemission current on the light quantum energy by extrapolating it to the zero current. Reference 27 reports the work function as 5.95 eV for photoemission from aqueous solutions of $\text{Fe}(\text{CN})_6^{4-}$. Using the standard potential of the system $\text{Fe}(\text{CN})_6^{4-}/\text{Fe}(\text{CN})_6^{3-}$ as +0.36 V (relative to the normal hydrogen electrode), we obtain for the reorganization energy of water around ferrocyanide/ferri-cyanide ions: $5.95 - 4.4 - 0.36 \approx 1.2$ eV. For the system considered, the electron transfer reaction is an outer-sphere one, so one can take $E_{R,\text{ox}} = E_{R,\text{red}} = E_R$.

We note in this connection that reliable experimental data on the values of E_R are rather scanty.¹⁰ According to Reference 28, in aqueous solutions at room temperatures E_R amounts to about 0.5–2 eV. The problems concerning model calculations of E_R are considered in detail in the review.¹³ Moreover, we have to bear in mind that the "homogeneous" values of E_R (which can be determined, in particular, using electron photoemission from solutions) are, apparently, much higher than the "heterogeneous" values (which can be found, for example, by processing experimental data on tunnel currents flowing from semiconductor electrodes into solutions²⁸). Physical reasons for this discrepancy are mainly related to the fact that in heterogeneous charge transfer processes only the half-space occupied by the solvent is rearranged, and, to a lesser extent, to the contribution of image forces near the surface to the reorganization energy, and also to the effect of specific adsorption, structurization of the solvent near the interface, deformation of solvation shells of reacting particles near the electrode, etc. In the simplest model, the "homogeneous" reorganization energy exceeds approximately twice the "heterogeneous" reorganization energy.^{10,13}

It is of interest that Reference 28 reports for the system $\text{Fe}(\text{CN})_6^{4-}/\text{Fe}(\text{CN})_6^{3-}$ the "homogeneous" value 1.24 eV obtained by model calculation, which agrees well with the value presented above. As for the "heterogeneous" reorganization energy, the same paper reports, as it might be expected, a much lower value (0.4 eV) obtained from tunnel currents measured on heavily doped SnO_2 electrodes.

III. SPECIFIC FEATURES OF THE STRUCTURE OF THE SEMICONDUCTOR/ELECTROLYTE INTERFACE

An electrical double layer arises at the semiconductor electrode/electrolyte solution interface, as in the case of the metal/solution interface. The double layer consists of the "plates" carrying charges of opposite sign, each "plate" being located in one of the phases in contact. In the near-surface region of the semiconductor the charge is formed as a result of redistribution of electrons and holes, while in the solution it is formed as a result of ion redistribution. Under equilibrium conditions, the absolute values of these charges are the same.

1. The Electrical Double-Layer Model

The factors which lead to the formation of an electrical double layer are rather general. First, charges flow across the interface when a thermodynamic equilibrium is established between the phases in contact; second, it is charging processes, which are not generally related to charge transfer across the interface—for example, charging of surface states (see below), certain types of adsorption, etc.

According to the conventional model,^{1,29,30} three regions can be distinguished within the electrical double layer: the space-charge region in the solution, the intermediate region, called the Helmholtz layer, and the space-charge region in the semiconductor.

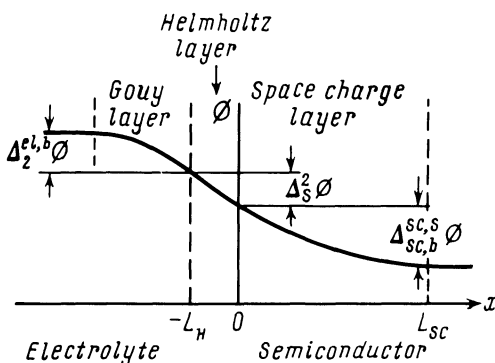


Figure 3. Components of potential drop at the semiconductor/electrolyte interface.

Figure 3 shows schematically (not to scale) the spatial distribution of the interphase potential drop (the Galvani potential) $\Delta_{el}^{sc}\phi$ at the semiconductor/electrolyte interface.

The semiconductor occupies the region to the right of the vertical solid line representing the interface ($x = 0$). To the left of it, there is the Helmholtz layer formed by ions attracted to the electrode surface, and also by solvent molecules; its thickness, L_H , is the order of the size of an ion. The space-charge region in the solution (the Gouy-Chapman layer) is adjacent to the Helmholtz layer from the electrolyte side.

Let us denote the electric potential in the electrolyte solution bulk (for $x \rightarrow -\infty$) by $\phi^{el,b}$ and in the semiconductor bulk ($x \rightarrow \infty$) by $\phi^{sc,b}$. The total potential drop across the interface $\Delta_{sc,b}^{el,b}\phi = \phi^{sc,b} - \phi^{el,b}$ is then

$$\Delta_{sc,b}^{el,b}\phi = \Delta_2^{el,b}\phi + \Delta_s^2\phi + \Delta_{sc,b}^{sc,s}\phi \quad (22)$$

Here $\Delta_2^{el,b}\phi = \phi^{(2)} - \phi^{el,b}$ is the potential drop in the space-charge region in the solution, i.e., between the solution bulk and the outer ("2") Helmholtz plane; this quantity is usually denoted by ψ' ("psi-prime" potential). The second term $\Delta_s^2\phi = \phi^{sc,s} - \phi^{(2)}$ is the potential drop across the Helmholtz layer. Finally, the third term $\Delta_{sc,b}^{sc,s}\phi = \phi^{sc,b} - \phi^{sc,s}$ is the potential drop in the space-charge region in the semiconductor. Below we shall omit, for the sake of brevity, the index "sc" and use the notation $\Delta_{sc,b}^{sc,s}\phi = \Delta_b^s\phi$.

We should note here the following circumstance, important in methodological respects. In electrochemistry, the positive direction of the electrode potential is conventionally the one for which positive electrode charge grows. On the contrary, in the physics of semiconductor surfaces the positive surface potential, which is usually reckoned from $\phi^{sc,b}$, is characterized by the accumulation of electrons in the space-charge region, i.e., the formation of a negative space charge. All this directly follows from the Boltzmann distribution determining the concentration of electrons n_s and holes p_s near the surface:

$$\begin{aligned} n_s &= n_0 \exp[e(\phi^{sc,s} - \phi^{sc,b})/kT], \\ p_s &= p_0 \exp[-e(\phi^{sc,s} - \phi^{sc,b})/kT] \end{aligned} \quad (23)$$

Equation (23) shows that if $\phi^{sc,s} > \phi^{sc,b}$, then $n_s > n_0$ and $p_s < p_0$. Thus, the direction of the potential axis accepted in electrochemistry

is opposite to that accepted in semiconductor physics! This is reflected in the fact that the sign of potential drop in the semiconductor, $\phi^{sc,s} - \phi^{sc,b}$ (which is equal to $-\Delta_b^s \phi$) reckoned from the potential in the bulk $\phi^{sc,b}$, is opposite to the sign of the last term in expression (22) for the Galvani potential. This should always be taken into account in order to avoid confusion in comparing results concerned with the physics of semiconductor surfaces and electrochemistry.

It is to be noted that the positive direction of the potential axis in the semiconductor is in conformity with the direction chosen as positive in the "physical" scale of energy (see Section 2.2). Indeed, in formula (17), the terms characterizing the position of the Fermi level and electrode potential have opposite signs.

When an electrode is polarized, i.e., the electrode potential is varied by $\Delta\varphi$, the Galvani potential changes by $\Delta(\Delta_{sc,b}^{el,b} \phi) = \Delta\varphi$ and, generally, all its three components also change. But in solutions of not very low concentration ($>0.1 M$), which are, as a rule, used in electrochemical experiments, the quantity $\Delta_2^{el,b} \phi = \psi'$ (and hence its change) is negligibly small. Precisely this case is considered below. Thus

$$\Delta\varphi = \Delta(\Delta_s^2 \phi) + \Delta(\Delta_b^s \phi) \quad (24)$$

Besides charge carriers, dipoles at the interface also contribute to the formation of the double layer. Here we mean first of all the dipole moments, which arise in the formation of polar bonds between the semiconductor surface and atoms adsorbed from the solution, and also oriented adsorbed solvent molecules.

The distribution of the dipoles does not contribute to the net electrode charge, but gives rise to a certain additional potential drop included into the quantity $\Delta_s^2 \phi$. Experiment shows that this dipole drop $\Delta_{dip} \phi$ may vary relatively little when the electrode potential changes, but it is usually rather sensitive to preliminary treatment of the electrode surface and to the composition of the surrounding medium.

Variation of the potential $\phi(x)$ with the coordinate in the semiconductor is equivalent, within the framework of the band model, to energy-band bending. The bands are bent downwards if $\Delta_b^s \phi < 0$ and upwards if $\Delta_b^s \phi > 0$. In the latter case, which corresponds to depletion of the near-surface region with electrons, a

depletion layer (the Mott-Schottky layer) is formed in n -type semiconductors if the following inequality is satisfied:

$$kT/e < \Delta_b^s \phi < \frac{kT}{e} \ln(n_0/p_0) \quad (25a)$$

The space charge in this layer is mainly produced by ionized donor impurities of concentration $N_D \approx n_0$. Similarly, in p -type semiconductors, the charge of the depletion layer, which arises in downward band bending in the potential range

$$-\frac{kT}{e} \ln(p_0/n_0) < \Delta_b^s \phi < -\frac{kT}{e} \quad (25b)$$

is mainly produced by an acceptor impurity (that captured an electron) of concentration $N_A \approx p_0$.

The case where a depletion layer is formed is of most importance in practical respects, since in wide-gap doped semiconductors, which are used very extensively in modern electrochemistry of semiconductors, the potential range given by Eqs. (25a) and (25b) is rather large.

If $\Delta_b^s \phi = 0$, the bands remain unbent ("flat") up to the interface, and the space charge in the semiconductor is zero. Under this condition, the potential φ of a semiconductor electrode, measured against a certain reference electrode, is called as the flat-band potential, $\varphi = \varphi_{fb}$. The flat-band potential in the electrochemistry of semiconductors is equivalent to the zero-charge potential (the potential of the zero free charge, to be exact³¹) in the electrochemistry of metals and plays an important role in the kinetics of electrochemical processes occurring on semiconductor electrodes.

It should be noted that at $\varphi = \varphi_{fb}$, when $\Delta_s^b \phi = 0$, the quantity $\Delta_s^2 \phi$ is nonzero, in particular, due to specific adsorption of ions from solution. For example, in the case of oxide semiconductors (TiO_2 , ZnO , etc.) and also semiconductors whose surface is oxidized in aqueous solutions (say, Ge), the concentrations of OH^- and H^+ ions chemisorbed on the surface are not equal to each other, which necessarily gives rise to a contribution to $\Delta_b^2 \phi$. As follows from the conditions of thermodynamic equilibrium between ions adsorbed on the surface and present in the solution bulk, the above contribu-

tion to $\Delta_b^2\phi$ must be a linear function of solution pH. For a certain pH value, dependent on the nature of a semiconductor electrode, the total charge of adsorbed ions appears to be equal to zero. This pH value (or a similar quantity in the case of adsorption of ions of another kind) is characterized by the "point of zero zeta potential" (PZZP, which is sometimes called the isoelectric point) or, according to terminology accepted in Reference 31, by the "potential of zero total charge." At the same time, even at PZZP, $\Delta_b^2\phi$ may, in general, be different from zero because of adsorption of solvent dipole molecules at the interface and also (in the case of oxide semiconductors) because of the dipole character of the bond between a semiconductor atom and oxygen.

In the study of specific features of the semiconductor/electrolyte interface we have to consider surface electron states. (In this case it would be more correct to speak about interface states, rather than surface states; in what follows, the conventional term "surface states" is used to mean "interface states".) These states can be rather important just in semiconductor electrodes, unlike metal ones where they are of no significance because of the enormous number of "free" electrons.

Surface electron states, which exist on atomically pure (ideal) crystal surfaces, are usually called intrinsic. In recent years, considerable progress has been made both in theoretical and experimental methods of studying intrinsic surface states (see, e.g., Refs. 32-34).

Under ordinary conditions, in particular when the electrode material is in contact with an electrolyte solution, adsorbed atoms or even layers are present on the surface; moreover, real surfaces may contain structural defects. They all can exchange electrons with the semiconductor bulk to give rise to surface electron states of kinds and properties other than those inherent to intrinsic surface states. The former play an important role in adsorption and catalysis processes.

Thus, a real semiconductor surface contains various types of surface electron levels, which are characterized by a complicated energy spectrum and may be both donor and acceptor in function. Their concentration depends on the way the surface is treated and may reach values of 10^{14} - 10^{15} cm^{-2} , which approximately coincides with the number of lattice sites per unit surface area of a solid.

Nonstationary methods of investigation reveal both "fast" and "slow" surface states and enable their characteristic relaxation times to be estimated. In most cases, a set of states with different characteristic relaxation times exists on the surface.

The existence of surface energy levels leads to two very important effects. First, electrons and holes can be trapped at the surface to form a surface electric charge layer and thereby induce an opposite charge in the bulk. In particular, the influence of the surface on equilibrium properties of semiconductors is related precisely to this effect. Second, surface energy levels can change significantly the kinetics of processes with electrons and holes involved: on the one hand, they produce additional centers of recombination and generation of charge carriers; on the other hand, they can act as intermediate energy levels in processes of charge transfer across the interface.

It is the existence of surface states that can lead to a considerable change in various electrochemical properties of semiconductors in the course of treatment of their surfaces.

Finally, surface states of a special type arise under conditions of strong band bending. If, for example, $\Delta_b^s \phi < 0$, so that the bands are bent downwards, a potential well for electrons is formed at the surface. If this well is sufficiently deep, bound states can arise in it, and electrons in these states are localized near the surface. The occurrence of such states is one of the manifestations of the surface quantization effect.

All that has been said above is, obviously, valid for holes, with the only exception that in this case a potential well is formed when the bands are bent upwards.

2. Potential Distribution: "Pinning" of Band Edges and/or the Fermi Level at the Surface

Consider now how the total potential drop $\Delta_{sc,b}^{el,b} \phi$ at the interface is distributed between its components $\Delta_s^2 \phi$ and $\Delta_b^s \phi$. According to the well-known electrostatic conditions, the following relation

$$\varepsilon_H \mathcal{E}_H = 4\pi Q_{ss} - \varepsilon_{sc} \mathcal{E}_{sc} \quad (26)$$

must hold at the interface. Here \mathcal{E}_H and \mathcal{E}_{sc} are the values of electric field strength near the interface from the side of the Helmholtz

layer and semiconductor, respectively; ϵ_H and ϵ_{sc} are the static dielectric permittivities, and Q_{ss} is the charge density at surface levels which depends on $\Delta_b^s\phi$; the sign "minus" in the second term of Eq. (26) accounts for the difference in the directions of potential axes mentioned above. For estimates, we can assume that $|\mathcal{E}_H| \approx |\Delta_b^2\phi|/L_H$ and $|\mathcal{E}_{sc}| \approx |\Delta_s^b\phi|/L_{sc}$, where L_H and L_{sc} are the thicknesses of the Helmholtz layer and the space-charge region in the semiconductor, respectively. They are related to the corresponding capacities by $C_H = 4\pi\epsilon_H/L_H$ and $C_{sc} = 4\pi\epsilon_{sc}/L_{sc}$, and depend, in general, on $\Delta_b^2\phi$ and $\Delta_s^b\phi$. If the charge associated with surface states is not too large, then, according to Eq. (26), $|\Delta_s^2\phi| \ll |\Delta_b^s\phi|$, provided

$$\epsilon_{sc}L_H/\epsilon_H L_{sc} \ll 1 \quad (27)$$

It is a simple matter to verify that condition (27) is satisfied for reasonable values of the parameters ϵ_{sc} and ϵ_H . At the same time, for heavily doped semiconductors when the concentration n_0 (or p_0) is sufficiently high, and also for large $|\Delta_s^s\phi|$, the quantity L_{sc} may become so small that inequality (27) will not hold true.

In order to estimate the effect of surface states on the potential distribution, we have to calculate their capacity $C_{ss} = dQ_{ss}/d(\Delta_b^s\phi)$. This calculation appears to be rather simple in the monoenergy model where all surface electron levels are assumed to have the same energy E_{ss} . It can easily be demonstrated (see, e.g., Ref. 7) that if

$$N_{ss} > \epsilon_H kT/\pi e^2 L_H \quad (28)$$

where N_{ss} is the number of surface levels per unit area of the interface, then $|\Delta(\Delta_s^2\phi)| > |\Delta(\Delta_b^s\phi)|$. In other words, if condition (28) is satisfied, the variation of the electrode potential gives rise to a potential change in the Helmholtz layer, which is larger than the corresponding potential change in the space-charge layer. The critical value of N_{ss} (to an order of magnitude), at which inequality (27) becomes equality, is 10^{13} – 10^{14} cm^{-2} .

Thus, since usually $L_H \ll L_{sc}$, then $|\Delta_b^s\phi| \gg |\Delta_b^2\phi|$, and therefore in electrolyte solutions of not very low concentration, $\Delta_b^s\phi$ constitutes, as a rule, the main portion of the interphase potential drop $\Delta_{sc,b}^{el,b}\phi$. If we take into account the above considerations, however, we see that this statement does not hold true in the

following cases:

1. For very strong charging of an electrode when the Fermi level at the surface is in close proximity to the edge of the conduction or valence band ("metalization" of the surface).
2. For high concentration of surface states: the change in the degree of their occupation (charging) leads to a considerable charge and potential redistribution, and can increase noticeably the contribution of the component $\Delta_s^2\phi$ for a fixed value of $\Delta_{sc,b}^{el,b}\phi$.
3. For heavily doped semiconductors, for which the Fermi level in the bulk lies near the majority-carrier band edge (or, as in metals, even lies inside this band).

All that has been said is valid for potential distribution across the interface both under equilibrium conditions and under electrode polarization with the aid of an external voltage source.

Consider now two important extreme cases³⁵⁻³⁷:

1. Suppose that $|\Delta(\Delta_b^s\phi)| \gg |\Delta(\Delta_s^2\phi)|$ when the electrode potential varies. This inequality means that the potential drop across the Helmholtz layer remains practically unchanged ($\Delta\phi = \Delta_b^s\phi$ under electrode polarization). Therefore, the positions of all energy levels at the surface and, in particular, of band edges $E_{c,s}$ and $E_{v,s}$, remain the same with respect to the position of energy levels in the electrolyte solution and reference electrode (Figs. 4a and 4b). In this case, the band edges are said to be "pinned" at the surface.

Band-edge pinning is eventually related to the fact that, as was already noted, the potential drop across the Helmholtz layer, $\Delta_s^2\phi$, is solely determined by the chemical interaction between the semiconductor and solution, and does not depend, to any significant extent, on such external factors as polarization and illumination. Therefore, the band edges $E_{c,s}$ and $E_{v,s}$ have the same position at the surface for all samples of a given semiconducting material, which are in contact with a given redox couple, irrespective of the type and value of conductivity because the chemical nature of the material remains practically unchanged through doping. Experimental determination of $E_{c,s}$ and $E_{v,s}$ for several semiconducting materials (see, e.g., Ref. 38) confirms this conclusion.

2. Suppose, on the contrary, that in electrode polarization $|\Delta(\Delta_s^2\phi)| \gg |\Delta(\Delta_b^s\phi)|$ for one reason or another (mentioned above),

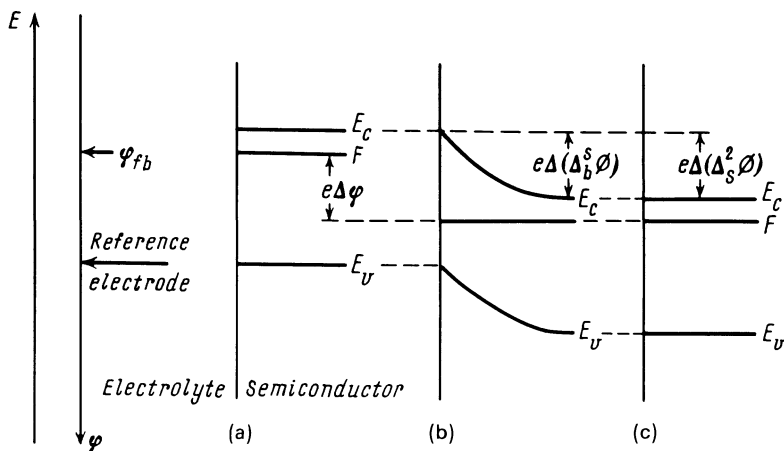


Figure 4. Energy diagram of the interface with an external voltage applied illustrating the band-edge pinning (transition from a to b) or the Fermi-level pinning (transition from a to c) at the surface of a semiconductor electrode. The flatband case is chosen as the initial state.

i.e., it is the potential drop across the Helmholtz layer which mainly changes. Under these conditions (see Figs. 4a and 4c) the energy levels at the surface shift relative to those in the solution by $\Delta\phi = \Delta(\Delta_s^2\phi)$ but relative to the Fermi level in the semiconductor, the band edges $E_{c,s}$ and $E_{v,s}$ retain the positions they had prior to the change in the electrode potential since the quantity $\Delta_b^s\phi$ does not vary. In order to stress the difference between this case and the preceding one, it is said that the bands are “unpinned” from the surface (this effect is sometimes called, though not quite adequately, pinning of the Fermi level with respect to band edges).

Fermi-level pinning leads to the situation that the level F can reach the level F_{redox} even for systems characterized by a rather positive or negative value of the equilibrium potential when the level F_{redox} is beyond the semiconductor band gap. Thus, in the case of Fermi-level pinning, conditions (16a) and (16b) are satisfied, which permit electrochemical reactions to proceed at a semiconductor electrode, while in the case of band-edge pinning these conditions are “unattainable.”

In real systems, an intermediate case often arises, namely, both potential drops $\Delta_b^s\phi$ and $\Delta_s^2\phi$ change in the course of electrode

polarization, so that neither the band edges nor the Fermi level are actually pinned.

Experimental investigation of potential distribution across the double layer on semiconductor electrodes is most frequently performed by differential capacity (see the next section) and photocurrent measurement techniques. A survey of experimental results obtained in this field is beyond the scope of the present review. Certain data illustrating the pinning and more detailed discussion of its origins will be presented in Section IV.2.

3. Determination of the Flat-Band Potential

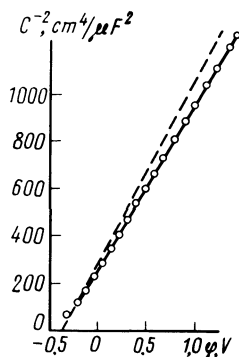
The flat-band potential, as was already pointed out, is one of the most important physicochemical characteristics of a semiconductor electrode. In the electrochemistry of semiconductors this concept has become even more important than the concept of the zero-charge potential in the electrochemistry of metal electrodes. The quantity φ_{fb} appears to be quite essential in the quantitative description of the double-layer structure and the kinetics of electrochemical reactions at semiconductor electrodes. This is especially true for the photoelectrochemistry of semiconductors because considerable photocurrents can only be obtained under efficient separation of light-generated electrons and holes in the space-charge region (for details, see Section IV.2). This separation occurs reliably only for electrode potentials that are more positive (in the case of *n*-type photoelectrodes) or more negative (in the case of *p*-type photoelectrodes) than the flat-band potential φ_{fb} of a semiconductor (though this condition of charge separation, as such, is not sufficient for the occurrence of photocurrent).

The capacity of the space-charge region in a semiconductor C_{sc} , under the formation of a depletion layer, is related to the potential drop in this region $\Delta_b^s \phi$ by¹

$$C_{sc}^{-2} = \frac{8\pi}{eN_D\epsilon_{sc}} (\Delta_b^s \phi - kT/e) \quad (29)$$

(we consider, for specificity, an *n*-type semiconductor). Relation (29) implies that a plot of C_{sc}^{-2} vs. $\Delta_b^s \phi$ should become a straight line (the so-called Mott-Schottky plot—see Fig. 5). If we assume that only the component $\Delta_b^s \phi$ varies with the changing electrode

Figure 5. The Mott-Schottky plot for a zinc oxide electrode (conductivity = $0.59 \Omega^{-1} \text{ cm}^{-1}$) in 1 N KCl (pH = 8.5).³⁹ The dashed line is calculated by Eq. (29).



potential φ and the semiconductor/electrolyte junction capacity C coincides with C_{sc} , the slope of the Mott-Schottky plot gives the concentration of ionized donors and its intercept with the potential axis—the flat-band potential φ_{fb} .

This method has widely been used in electrochemical measurements. It should be stressed, however, that direct application of Eq. (29) to experimental determination of φ_{fb} is based on several assumptions (often accepted without proof) concerning the properties of the semiconductor/electrolyte junction. These assumptions have been analyzed, for example, in Reference 38). Here we formulate the most important of these assumptions:

1. It is assumed that the capacity measured, C , is not distorted due to the leakage effect at the interface, a finite value of the ohmic resistance of the electrode and electrolyte, etc. A correct allowance for these obstacles is an individual problem, which is usually solved by using an equivalent electrical circuit of an electrode where the quantity in question, C_{sc} , appears explicitly. Several measurement techniques and methods of processing experimental data have been suggested to find the equivalent circuit and its elements (see, e.g., Ref. 40).

2. It is assumed that donors (acceptors) in the semiconductor are, first, completely ionized at the temperature of measurements and, second, uniformly distributed in the sample, at least within the space-charge region. (A non-uniformity whose scale is large in comparison with the space-charge region thickness can be determined by a special method; see Section V.4). If the concentrations

N_D and N_A depend on the coordinate, more complicated relations for the dependence of C_{sc} on $\Delta_b^s \phi$ are obtained instead of Eq. (29) (see, e.g., Ref. 41). Deviations from Eq. (29) are also observed in the presence of deep donors (acceptors), which are not ionized in the semiconductor bulk at the temperature of measurements, but become ionized in the space-charge electric field, thereby contributing to the capacity.⁴²

3. The capacity measured is assumed to represent only the capacity of the space-charge region in the semiconductor and not to include, for example, the capacity of surface states, adsorption capacity, etc. In certain cases, this condition is satisfied, for example, on a zinc oxide electrode³⁹; but more frequent is the situation where the contribution of the capacity of surface states is considerable.

4. It is assumed that the electrode capacity measured, C , is not affected by the Helmholtz-layer capacity, C_H . If the dependence of the measured capacity C on the electrode potential φ becomes a straight line in the coordinates $C^{-2} - \varphi$, this fact is frequently interpreted, in accordance with Eq. (29) and the relation $C^{-1} = C_H^{-1} + C_{sc}^{-1}$, as a proof that the following conditions are satisfied:

$$C_{sc} \ll C_H; \quad |\Delta(\Delta_b^s \phi)| \gg |\Delta(\Delta_s^2 \phi)| \quad (30)$$

In other words, it is supposed that: (1) the electrode capacity measured is entirely determined by the capacity of the space-charge region in the semiconductor; and (2) a change in the electrode potential leads only to a change in the potential drop in the semiconductor, while the potential drop across the Helmholtz layer remains constant.

A more detailed consideration⁴³ shows, however, that the effect of C_H is a rather subtle problem which requires thorough analysis. If the change in the potential drop across the Helmholtz layer $\Delta(\Delta_b^2 \phi)$ in the course of electrode polarization is not neglected and nor is the contribution of the capacity C_H to C , we obtain, with due account of Eq. (29), the following relation between C and φ :

$$C^{-2} = C_H^{-2} + \frac{8\pi}{eN_D \epsilon_{sc}} (\varphi - \varphi_{fb} - kT/e) \quad (31)$$

This expression shows that C^{-2} depends linearly on φ , i.e., in the same manner as [according to Eq. (29)] C_{sc}^{-2} depends on $\Delta_b^s \phi$ [or C_{sc}^{-2} on φ , under the assumption that $\Delta_b^2 \phi = \text{const}$ and $\Delta\varphi =$

$\Delta(\Delta_b^s \phi)$]. Moreover, it follows from Eq. (31) that the slope of the corresponding straight line in the coordinates (C^{-2}, φ) is the same as for the straight line $(C_{sc}^{-2}, \Delta_b^s \phi)$ [or the straight line (C_{sc}^{-2}, φ) provided $\Delta_b^2 \phi$ is constant].

But now the straight line intersects the φ -axis at the potential

$$\varphi' = \varphi_{fb} + kT/e - e\epsilon_{sc}N_D/8\pi C_H^2 \quad (32)$$

With respect to the potential determined from Eq. (29), (i.e., when the contribution due to the Helmholtz layer is neglected) this value is shifted by $-eN_D\epsilon_{sc}/8\pi C_H^2$. This shift, especially for heavily doped semiconductors, is by no means small; for example, for TiO_2 it amounts to about -0.12 V at $N_D = 10^{19} \text{ cm}^{-3}$ and $C_H = 10^{-6} \text{ F cm}^{-2}$.

Thus, the linear dependence of C^{-2} on φ , observed experimentally, does not necessarily imply that the effect of the Helmholtz layer on the experimental value of φ_{fb} is insignificant, i.e., the inequalities (30) do hold true. And vice versa, the above considerations show that deviations of the dependence of C^{-2} on φ from a straight line, as such, cannot prove the fact that the inequalities (30) are not valid, i.e., that it is the Helmholtz layer C which is responsible for the deviations.

Finally, it should be noted that in many cases where φ_{fb} is determined by the capacity method uncertainty arises, which is related to the frequency dependence of Mott-Schottky plots. (In particular, the frequency of the measuring current is increased in order to reduce the contribution of surface states to the capacity measured.) As the frequency varies, these plots, as well as the plots of the squared "leakage resistance" R vs. the potential (in the electrode equivalent circuit, R and C are connected in parallel), are deformed in either of two ways (see Figs. 6a and 6b). In most of the cases, only the slopes of these plots change but their intercepts on the potential axis remain unchanged and are the same for capacity and resistance plots (Fig. 6b). Sometimes, however, not only does the slope vary but the straight line shifts, as a whole, with respect to the potential axis, so that the intercept on this axis depends upon the frequency (Fig. 6a).

No comprehensive explanation of the dependences observed has been suggested so far. A model⁴⁴ has been proposed for the case shown in Fig. 6b; according to this model, the semiconductor

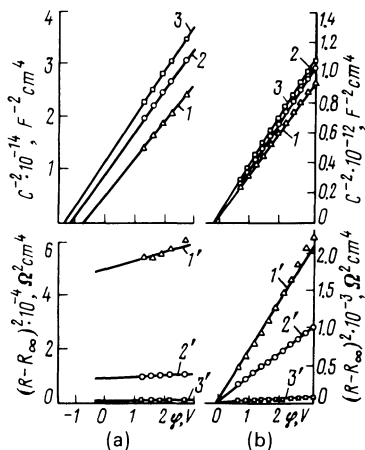


Figure 6. The effect of the measuring current frequency on the Mott-Schottky plot.⁴⁴ C and R are the capacity and resistance in the "parallel" equivalent circuit of the electrode; R_∞ is the value of R extrapolated to infinite frequency. (a) CdSe ($N_D \approx 10^{15} \text{ cm}^{-3}$) in 0.25 M K_2SO_4 + 0.25 M CH_3COOH + 0.05 M CH_3COONa ; frequency: 1–320, 2–2440, 3–7080 Hz and (b) TiO_2 ($N_D \approx 10^{18} \text{ cm}^{-3}$) in 0.25 M K_2SO_4 + 0.1 M $\text{Na}_2\text{B}_4\text{O}_7$; frequency: 1–320, 2–980, and 3–2440 Hz. All the potentials are given against the normal hydrogen electrode.

dielectric permittivity in the space-charge region depends on frequency. It should be noted, however, that this physical explanation seems to be not sufficiently well substantiated and is not the only one possible.

Nevertheless, plots of the type of Fig. 6b are, in fact, used to estimate the flat-band potential by extrapolating them to intersection with the potential axis; apparently, in this case, $N_D(N_A)$ cannot be found from the slopes of these plots, and plots of the type of Fig. 6a are considered to be inapplicable even for determining φ_{fb} .

Besides direct measurements, a method⁴⁵ has been suggested to estimate the flat-band potential φ_{fb} using the properties of the semiconductor and solution.

It follows from Eqs. (21) and (22) that under thermodynamic equilibrium and for sufficiently high electrolyte concentrations, the following relation holds:

$$e(\Delta_s^2 \phi + \Delta_b^s \phi) = F - F_{\text{redox(ref)}} = -\chi + F - E_c - F_{\text{redox(ref)}} \quad (33)$$

where $F - E_c < 0$ is the difference between the level F and the majority-carrier band edge E_c , and $F_{\text{redox(ref)}}$ corresponds to the reference electrode. The electron affinity of the semiconductor appearing in Eq. (33) can be found by semiempirical formulas relating χ to the first ionization potential I_1 and electron affinity A_f of the chemical components that form the semiconductor, and

also to the band gap; for example, in the simplest case of a binary semiconductor MX we have $\chi = \frac{1}{2}(A_f + I_1 + E_g)$. According to Eq. (21), the difference $F - E_c$ can be calculated if the charge-carrier concentrations n_0 and p_0 , the band gap E_g , and the densities of states in the bands N_c and N_v are known. The value of $F_{\text{redox(ref)}}$ is also known (see Section 2.2). Finally, if we assume that at the point of zero zeta potential (PZZP) $\Delta_s^2\phi$ is zero, Eq. (33) yields the band bending $e\Delta_b^s\phi$, whence the flat-band potential can be found.

The quantity $(\text{pH})_{\text{PZZP}}$ corresponding to PZZP can be calculated if the standard electrochemical potentials of reactions with adsorbed ions involved (OH^- and H^+ in aqueous solutions) are known, or it can be determined experimentally by potentiometric titration of a suspension consisting of microparticles of a given semiconductor in the solution of a known ionic strength (for details, see Ref. 45). This permits Eq. (33) to be verified experimentally, at least in part. It was found that for a large number of oxide semiconductors there exists an approximately linear relationship between $(\text{pH})_{\text{PZZP}}$ and χ . A linear relationship was also empirically found between calculated values of χ and measured values of φ_{fb} (see Fig. 7). Using the straight line thus obtained we can calculate, for a given oxide semiconductor, the value of χ and find approximately its flat-band potential.

It is to be noted in conclusion that the existence of a linear dependence between χ and φ_{fb} discussed here is quite analogous to the well-known relationship between the electron work function w and the zero-charge potential in the electrochemistry of metals.³¹ This analogy becomes especially clear if we take into account that for doped wide-gap semiconductors $E_c - F$ is usually rather small (≤ 0.1 eV), so that $\chi \approx w$. In the case of metals, certain experimental

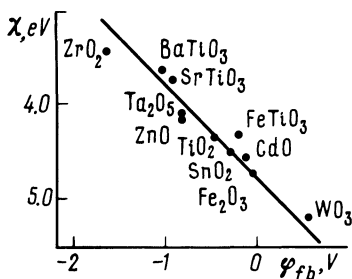


Figure 7. Relationship between the calculated electron affinity and measured flat-band potential (against the saturated calomel electrode) for several semiconductors at their isoelectric points.⁴⁵ (Reprinted by permission of the publisher, The Electrochemical Society, Inc.)

deviations from this linear dependence can be attributed to a difference in the dipole potential drops, which arise due to solvent adsorption on various metals.³¹ A similar effect (though, probably, not well pronounced for semiconductor electrodes of the same nature) should also be observed in the electrochemistry of semiconductors.

IV. QUASITHERMODYNAMIC APPROACH TO THE DESCRIPTION OF PHOTOELECTROCHEMICAL PROCESSES

In this section, we shall consider several photoelectrochemical phenomena which occur in a semiconductor/electrolyte system under illumination. The study of such phenomena is very important, not only from the purely scientific point of view, but also in view of practical applications of electrochemical systems with semiconductor electrodes. Electrode processes are most strongly affected by light of frequencies that are higher than the threshold of the intrinsic (fundamental) absorption of a semiconductor, when the energy of a light quantum absorbed is sufficient for photogeneration of electron-hole pairs. Redistribution of charge carriers in the semiconductor near the interface with the solution, caused by such photogeneration, can change radically not only the rate but also the character of electrochemical processes taking place at the interface.

1. Quasi-Fermi Levels

At present, several methods have been developed to describe photoelectrochemical phenomena. For example, the kinetics of photoelectrochemical processes can be studied theoretically by solving transport equations (with allowance for charge-carrier photogeneration) which are supplemented by certain boundary conditions accounting for the specific features of electrode reactions with electrons and holes involved.⁴⁶⁻⁵⁰ In the simplest cases, this approach enables one to obtain an exact solution of the problem but, with rather complicated boundary conditions, it appears to be somewhat difficult, and the expressions obtained are cumbersome.

At the same time, another approach is quite efficient for qualitative understanding and sometimes for quantitative interpretation; this approach is quasithermodynamic rather than kinetic and is based on the concept of “quasi-Fermi levels.”

We recall that the concept of quasi-Fermi levels, first suggested by Shockley,⁵¹ can be introduced in the following way. Suppose that, in addition to thermal generation, charge carriers in a semiconductor are also generated because of certain external factors, say, illumination. In the steady-state regime, a dynamic equilibrium arises between generation and recombination of electron-hole pairs. As a result, certain steady-state (but not equilibrium) concentrations n_0^* and p_0^* are established in the semiconductor under illumination. Suppose, further, that the lifetimes of excited states are rather large. Then, interaction with lattice vibrations (phonons) gives rise to equilibrium distributions with the temperature of the lattice (the phonon system) separately in electron and hole gases containing the photogenerated particles. However, the electron and hole gases may not, in general, be in equilibrium with respect to each other. Under such conditions, each distribution (electron and hole) is characterized by its own chemical and electrochemical potentials. For electron and hole systems, the latter will be denoted by F_n and F_p , respectively. Unlike the case of complete thermodynamic equilibrium where $F_n = F_p = F$, the quantities F_n and F_p , called the quasi-Fermi levels and corresponding to a partial equilibrium, are not equal to each other (Fig. 8).

Thus, in the quasi-thermodynamic approximation considered here the occurrence of nonequilibrium electrons and holes in the bands can be described as the “splitting” of the initial Fermi level F into two quasi-levels F_n and F_p .

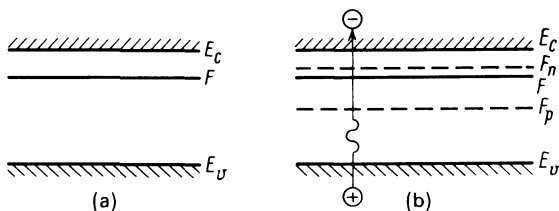


Figure 8. Diagram illustrating the splitting of the Fermi level into quasilevels of electrons and holes (a) in the dark (b) under illumination of the semiconductor.

The quasi-equilibrium concentrations n_0^* and p_0^* are given by

$$n_0^* = n_0 + \Delta n, \quad p_0^* = p_0 + \Delta p \quad (34)$$

and outside the space-charge region $\Delta n = \Delta p$ because carrier photogeneration occurs in pairs.

Substitution of n_0^* and p_0^* into Eqs. (21a)-(21c) yields the quasi-Fermi levels F_n and F_p . For example, in the case of an n -type semiconductor, Eq. (21b) gives $F_n \approx F$, if the condition $\Delta n \ll n_0$ is satisfied. At the same time, since $p_0 \ll n_0$, the condition $\Delta p \gg p_0$ can be satisfied simultaneously; for $F - F_p$ we find then from Eq. (21c):

$$F - F_p \approx kT \ln \frac{\Delta p}{p_0}, \quad \Delta p \gg p_0 \quad (35)$$

Similar relations hold for a p -type semiconductor.

Thus, Eq. (35) implies that a noticeable shift of the electrochemical potential level under photogeneration can only take place for minority carriers. For moderate illumination intensity, the shifts of the quasi-levels, $F_{n,p}$, are proportional to the logarithm of the intensity; as it increases, further growth of the shifts slows down due to enhancement of recombination processes. The ultimate shift of $F_{n,p}$ with increasing illumination intensity, so long as Eq. (35) (and a similar formula for a p -type semiconductor) is valid, is the edge of the corresponding band.

2. Description of the Most Important Types of Photoelectrochemical Reactions

Let us now turn, using the concept of quasi-Fermi levels, to the description of qualitative peculiarities in the occurrence of photoelectrochemical reactions at an illuminated semiconductor/electrolyte interface.^{15,52}

The quasithermodynamic approach employed below relies upon the assumption that an electrode reaction is accelerated under illumination due to the formation of quasi-levels F_n and F_p , which are shifted relative to the equilibrium position F . Conditions (16a) and (16b) should now be modified. Namely, for an anodic process to occur with holes being involved, the following inequality should

be satisfied:

$$F_p < F_{\text{redox}} \quad (36a)$$

and a cathodic process, with conduction-band electrons, requires analogously the fulfillment of the inequality:

$$F_n > F_{\text{redox}} \quad (36b)$$

Let us first consider a semiconductor electrode under open-circuit conditions, an individual particle of a semiconductor suspension in a conducting liquid being an example. Suppose that in a certain potential range, electron transitions across the interface between the semiconductor and solution do not take place in darkness, i.e., the semiconductor behaves as an ideally polarizable electrode. This potential range has an upper and a lower limit, namely, the potential of solvent decomposition and/or the potential of semiconductor decomposition (corrosion). The stationary electrode potential in the region of ideal polarizability is determined by chemisorption processes (in aqueous solutions, it is most often chemisorption of oxygen) or, which is the same in the language of the physics of semiconductor surfaces, by charging of slow surface states. It is these processes which determine steady-state band bending.

Figure 9 shows the energy diagram of a semiconductor, *n*-type as the example, in contact with the solution. Besides the energy levels in the semiconductor, the bottom of the conduction band E_c , and the top of the valence band E_v , the figure depicts the electrochemical potential levels for reactions of anodic dissolution of the semiconductor, $F_{\text{dec},p}$, and cathodic evolution of hydrogen, $F_{\text{H}_2/\text{H}_2\text{O}}$. (We consider the case where semiconductor decomposition with involvement of holes, and water-to-hydrogen reduction, with involvement of conduction-band electrons, are the most probable anodic and cathodic reactions, respectively).

Figure 9 corresponds to the case where a depletion layer is formed in the near-surface region of the semiconductor. Light-generated electrons and holes move in opposite directions in the depletion-layer electric field: holes toward the interface and electrons into the semiconductor bulk. The electric field, which arises as a result of such charge separation, compensates, in part, for the initial field. This is manifested in the decrease in band bending $e\Delta_b^s\phi$ under illumination, i.e., the bands unbend. Band unbending

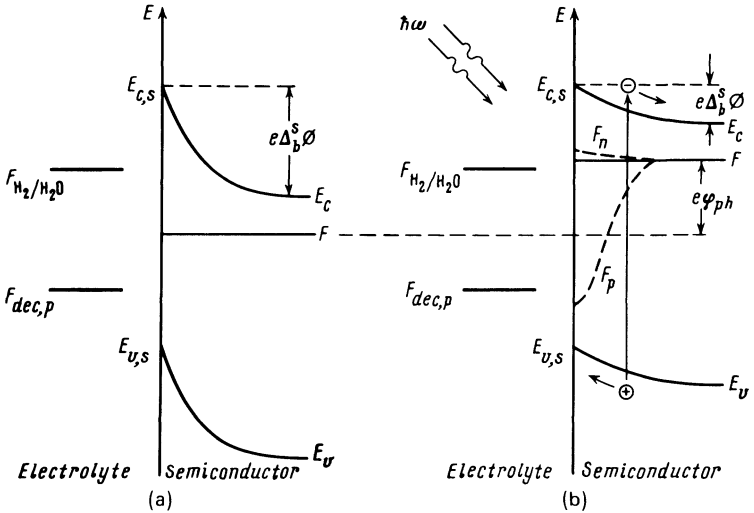


Figure 9. Energy diagram of the semiconductor/electrolyte junction: (a) in darkness and (b) under illumination.

leads in turn to the change in the mutual position of other energy levels in the system. Indeed, suppose for simplicity that the potential drop across the Helmholtz layer does not change under illumination ($\Delta_s^2\phi = \text{const}$), so that the position of the band edges at the surface, $E_{c,s}$ and $E_{v,s}$, is fixed with respect to the reference electrode and, therefore, to energy levels in the solution (band-edge pinning at the surface; see Section III.2). At the same time, the position of the electrochemical potential level of the semiconductor F (the Fermi level) relative to band edges is strictly determined in the semiconductor bulk. Thus, the bands unbend under illumination and “pull” the Fermi level, so that it shifts with respect to its position in the nonilluminated electrode, as is shown in Fig. 9. The shift of the level F under illumination can be measured by a reference electrode. It is this shift, ΔF , which is observed as the photopotential $\varphi_{ph} = \Delta F/e$.

Let us consider the effects related to the formation of quasi-Fermi levels of electrons and holes. For majority carriers (electrons), the shift of F_n with respect to F is very small, as was noted above, and it is usually neglected; on the contrary, for minority carriers

(holes) the quasilevel F_p can shift quite significantly with respect to F .

For a certain illumination intensity, the hole quasilevel F_p at the semiconductor surface can reach the level of an anodic reaction (reaction of semiconductor decomposition in Fig. 9). In turn, the electron quasilevel F_n can reach, due to a shift of the Fermi level, the level of a cathodic reaction (reaction of hydrogen evolution from water in Fig. 9). Thus, both these reactions proceed simultaneously, which leads eventually to photocorrosion. Hence, non-equilibrium electrons and holes generated in a corroding semiconductor under its illumination are consumed in this case to accelerate the corresponding partial reactions.

Simultaneous consumption of nonequilibrium electrons and holes at the semiconductor surface in the course of photocorrosion formally resembles surface recombination. Therefore, processes of this type are referred to as "electrochemical recombination."⁵³

In principle, another anodic reaction can take place instead of semiconductor decomposition (dissolution), for example, oxidation of dissolved substance or oxygen evolution from water. Apparently, in the latter case, the illumination of semiconductor leads to photoelectrolysis of water with the formation of hydrogen and oxygen, that is, conversion of the energy of light into chemical energy of the photoelectrolysis products.

If the whole semiconductor/electrolyte interface is illuminated uniformly, both conjugate reactions proceed at the same rate over the same areas on the interface. The stationary potential of an illuminated semiconductor is thus a mixed potential. If the surface of a semiconductor, homogeneous in its composition and properties, is illuminated nonuniformly, in the illuminated and nonilluminated areas conditions will not be identical for electrochemical reactions. Here the conjugate reactions appear to be spatially separated, so that we can speak about local anodes and cathodes. This situation is deliberately created, for example, for selective light-sensitive etching of semiconductors (see Section V.2).

There is another way of spatially separating anodic and cathodic reactions on an illuminated semiconductor, namely by providing certain regions of the semiconductor surface with different electrochemical (in particular, electrocatalytic) properties. Such regions act as local electrodes, and the entire system as a galvanic

couple. A suspension of platinized strontium titanate in an aqueous solution may serve as an example of such microheterogeneous systems. When it is illuminated, light-generated electrons and holes are separated in the electric field of a depletion layer near the surface (Fig. 10), the holes moving toward the semiconductor surface and the electrons into the bulk where they are transferred across the semiconductor/metal interface. Therefore, hydrogen is evolved on the surface of the metal (platinum in this case) and oxygen on the strontium titanate surface. Such microheterogeneous systems have been widely used in recent years in view of their applications for solar energy conversion.⁵⁴⁻⁵⁶

Finally, a natural extension of this approach would be the creation of a "macroheterogeneous" system: for example, an electrochemical short-circuited cell with a semiconductor photo-electrode and light-insensitive, say, metal, auxiliary electrode (Fig. 11). If a strontium titanate electrode in an aqueous solution is used, illumination of such a cell leads to photoelectrolysis of water, with the gaseous products, hydrogen and oxygen, being evolved on different electrodes of the cell. Reliable and convenient separation of photoreaction products, which is a direct consequence of the separation of primary photogenerated charges, electrons and

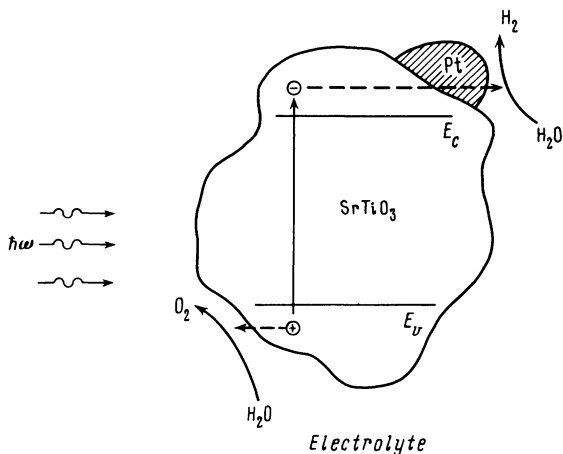


Figure 10. Scheme of water photoelectrolysis on a particle of semiconductor (platinized SrTiO₃) suspension in an aqueous solution.

$F_n \approx F$), so that the whole "acting force" of a photoelectrode is concentrated on the anodic partial reaction taking place with minority carriers (holes) being involved. It is therefore convenient to carry out the cathodic partial reaction (e.g., hydrogen evolution) on a metal electrode, which possesses good electrocatalytic properties for this reaction.

Let us now turn to the case where an equilibrium is established between the semiconductor and solution, even in darkness. This usually takes place when the solution contains a well-reversible redox couple. Then, the semiconductor attains the equilibrium potential of this couple: $\varphi = \varphi_{\text{redox}}^0$ or $F = F_{\text{redox}}$, which is the same.

Considerations similar to those presented above show that illumination of a semiconductor leads to a shift of both the Fermi level and the quasi-levels of holes and electrons, and both the forward and reverse reactions, proceeding according to Eq. (1), are accelerated. In other words, the result of illumination is, above all, the efficient increase of the exchange current in the redox couple⁵⁷; but this is not the only result. If a semiconductor under illumination is an electrode in an electrochemical cell and is connected through a load resistor with an auxiliary electrode, the cathodic and anodic reactions become spatially separated, as in the case of water photoelectrolysis (Fig. 11) considered above. The reaction with the minority carriers involved proceeds on the semiconductor surface, and that with the majority carriers involved, on the auxiliary electrode. Thus, the illumination of a semiconductor electrode gives rise to an electric current in the external circuit, so that some power can be drawn from the load resistor. In other words, the energy of light is converted into electricity. This is the way a photoelectrochemical cell, called "the liquid junction solar cell," operates.

Consider in detail the performance of such a cell for a particular case: *n*-type CdS/alkaline solution of $S_2^{2-} + S_2^{2-}$ /metal cathode (Fig. 12). In darkness, the equilibrium



is established in the cell.

Both electrodes take the equilibrium potential of this redox couple, so that the Fermi levels of the metal and CdS, and the level $F_{\text{redox}} = F_{S^{2-}/S_2^{2-}}$ in the solution, become equal. Good separation of light-generated electrons and holes requires that a depletion layer

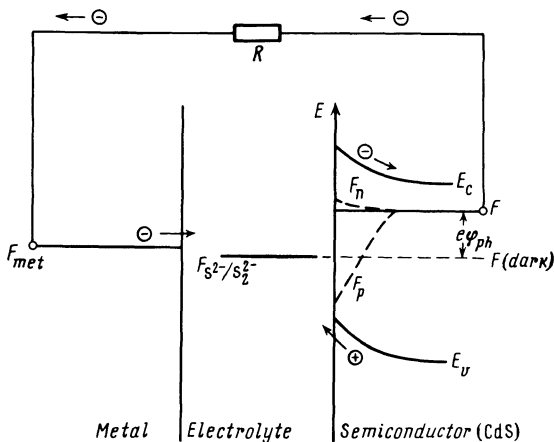


Figure 12. Energy diagram of an illuminated "liquid junction solar cell" with a CdS photoanode and a S^{2-}/S_2^{2-} electrolyte. F (dark) is the Fermi level in nonilluminated CdS.

should be formed in the semiconductor and this, in turn, requires that the equilibrium potential of the redox couple be more positive than the flat-band potential of the semiconductor, i.e. $\varphi_{redox}^0 > \varphi_{fb}$. When the electrode is illuminated, the bands unbend and the Fermi level of the semiconductor F shifts (see Fig. 12), which is manifested as a change in the electrode potential. It can be seen from Fig. 12 that this change in the electrode potential φ_{ph} , i.e., the photopotential, is equal to the shift of the Fermi level of the illuminated electrode relative to the nonilluminated one divided by the electron charge e . In the simplest case (which, as experiment shows, is rather frequent in practice), the potential drop across the Helmholtz layer $\Delta_s^2\phi$ under illumination has the same value as in darkness; moreover, it does not depend on φ_{redox}^0 . In other words, the band edges are pinned at the surface (see Section III.2). Under these conditions, the maximal value of φ_{ph} (which corresponds to the open-circuit photopotential) is equal to the initial (dark) potential drop across the space-charge layer, $\Delta_b^s\phi$, i.e., the difference $|\varphi_{redox}^0 - \varphi_{fb}|$. In order to increase the conversion efficiency, the semiconductor and the redox couple in the solution should be chosen such that this difference be as large as possible.

Next, photogeneration of electron-hole pairs leads to the formation of quasi-levels of minority and majority carriers, F_p and F_n , as shown in Fig. 12. Since, at the surface, $F_p < F_{S^{2-}/S_2^{2-}}$ and $F_n > F_{S^{2-}/S_2^{2-}}$, illumination results in the acceleration of both forward and reverse reactions in a sulfide polysulfide couple. If the circuit is closed on an external load R , the anodic and cathodic reactions become separated: the holes are transferred from the semiconductor photoanode to the solution, so that S^{2-} ions are oxidized to S_2^{2-} , and the electrons are transferred through the external circuit to the metal counterelectrode (cathode) where they reduce S_2^{2-} to S^{2-} . The potential difference across a photocell is $i_{ph}R$, where i_{ph} is the photocurrent, and the power converted is equal to $i_{ph}^2 R$.

In certain cases, however, the potential drop across the Helmholtz layer does not remain constant under illumination or when φ_{redox}^0 changes. As a result, the potential in the double layer is redistributed and the photopotential becomes lower than $|\varphi_{redox}^0 - \varphi_{fb}|$. This occurs, for example, on silicon, gallium arsenide, molybdenum diselenide, and certain other electrodes in solutions of certain redox couples. In other words, band-edge unpinning takes place, which eventually goes over into Fermi-level pinning at the semiconductor surface. This is manifested in the fact that, as the redox couple potential φ^0 gradually changes, the open-circuit

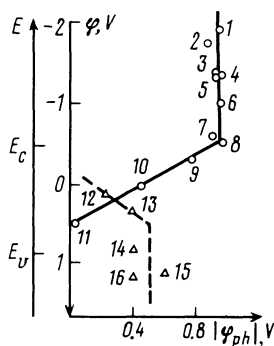


Figure 13. Dependence of the absolute value of the open-circuit photopotential $|\varphi_{ph}|$ on the redox couple equilibrium potential:⁵⁸ WSe_2 photoelectrode (solid line, *p*-type; dashed line, *n*-type) in acetonitrile solutions. Redox couple (figures in parentheses are charge numbers of the ox and red components): (1) anthracene (0/−1); (2) phthalonitrile (0/−1); (3) nitrobenzene (0/−1); (4) 2,2'-bipyridyl complex of ruthenium (+2/+1); (5) azobenzene (0/−1); (6) anthraquinone (0/−1); (7) benzoquinone (0/−1); (8) methyl viologen (+2/+1); (9) tetracyanoquinone-dimethane (+1/0); (10) tetramethyl-*p*-phenylenediamine (+1/0); (11) tetraphenyl-*p*-phenylenediamine (+1/0); (12)

I^-/I_3^- ; (13) Br^-/Br_3^- ; (14) Cl^-/Cl_3^- ; (15) thianthrene (+1/0); and (16) 2,2'-bipyridyl complex of ruthenium (+3/+2). All the potentials are given against the saturated calomel electrode. (Reprinted by permission of the publisher, The Electrochemical Society, Inc.)

photovoltage of the cell φ_{ph} first linearly increases with φ^0 (band-edge pinning) and eventually becomes independent of φ^0 (Fermi-level pinning) (see Fig. 13).

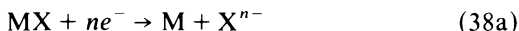
The origins of this phenomenon, which restricts significantly the characteristics of photoelectrochemical cells for solar energy conversion into electricity, have not so far been understood completely. Possible reasons might be the following: (cf. Section III.2): strong charging of a semiconductor electrode on approaching the Fermi level to the band-gap edges, for example, in the formation of an inversion layer in a semiconductor;^{37,59} high density of surface states;^{35,36} and also the shift of the flat-band potential in redox couple solutions because of partial oxidation (reduction) of the semiconductor surface as a result of the chemical action of the components of these couples, so that φ_{fb} becomes dependent on φ_{redox}^0 .⁶⁰ In all these cases, the interphase potential drop is redistributed between the space-charge layer and the Helmholtz layer in favor of the latter.

One may believe that for WSe_2 considered here (see Fig. 13) (and similar relatively wide-band-gap semiconductors), the second and third reasons seem to be the most probable (as far as the second reason is concerned, the assumption that the density of surface states increases on approaching the band-gap edges is quite reasonable). On the contrary, the formation of a developed inversion layer in a sufficiently wide-band-gap semiconductor (hence, the bulk concentration of minority carriers is rather low), when the limiting current of minority carriers flows in it, seems to be less probable. In fact, minority carriers are efficiently extracted from a semiconductor so that their concentration appears to be negligibly low even within the space-charge region and, under such conditions, this region represents an exhaustion rather than an inversion layer.¹

The inversion layer is, in fact, formed in a relatively narrow-gap semiconductor, germanium, in which the equilibrium bulk concentration of minority carriers is sufficiently high. But the main reason for band-edge unpinning in germanium, which is observed practically over the whole potential range accessible,⁶¹ is either a high density of energy-distributed surface states or the change in the dipole potential drop caused by adsorption of water molecules on the electrode surface (for details, see Ref. 1).

3. Photocorrosion and Stability

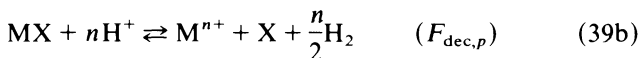
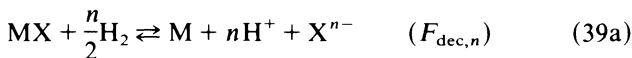
The quasi-thermodynamic approach enables one to obtain a criterion for finding out whether a semiconductor is liable to (photo)corrosion and suggest a way of preventing it.¹⁵ For example, in the case of a binary semiconductor MX (where M denotes the electropositive and X the electronegative components) the equation for a partial electrochemical reaction of cathodic decomposition with conduction electrons involved can be written in the form



and the partial reaction of anodic decomposition with holes involved as



If we choose for the example the hydrogen electrode as reference, the overall reaction in a cell will proceed according to one of the following equations:



(symbols in parentheses denote the corresponding electrochemical potential levels). Calculating the change in the free energy for these reactions we can determine the standard equilibrium potentials $\varphi_{\text{dec},n}^0$ and $\varphi_{\text{dec},p}^0$ of the reactions of semiconductor cathodic and anodic decomposition, respectively (see Refs. 15–18).

The thermodynamic condition for an electrode reaction to take place (including the corrosion partial reaction) can be written in the form [cf. Eqs. (16a) and (16b)]

$$\varphi < \varphi_{\text{dec},n}^0 \quad \text{or} \quad F > F_{\text{dec},n} \quad (40a)$$

for a cathodic reaction with conduction-band electrons involved, or in the form

$$\varphi > \varphi_{\text{dec},p}^0 \quad \text{or} \quad F < F_{\text{dec},p} \quad (40b)$$

for an anodic reaction with valence-band holes involved.

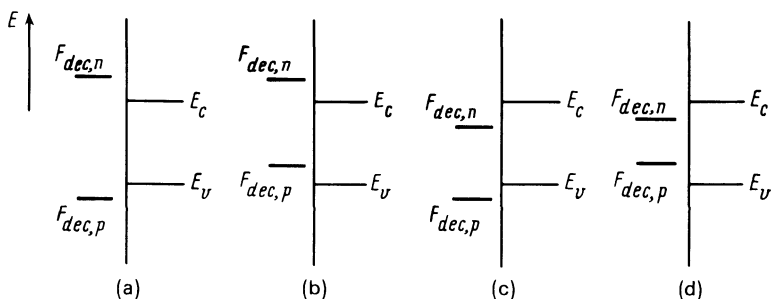


Figure 14. Diagram illustrating the thermodynamic stability of a semiconductor electrode against decomposition in the solution: (a) semiconductor is absolutely stable; (b) stable against cathodic decomposition; (c) stable against anodic decomposition; and (d) unstable.

In order to find out whether a semiconductor is liable to electrolytic or corrosion decomposition in any particular system, let us consider the energy-band diagram which plots the electrochemical potential levels for the decomposition reactions (39a) and (39b).

Figure 14 schematically shows that various situations are possible here. The semiconductor is stable against cathodic decomposition if the electrochemical potential level of the corresponding reaction lies in the conduction band and against anodic decomposition if it lies in the valence band. In both cases, if the whole potential change occurs in the semiconductor (band edge pinning at the surface), this level is "inaccessible" to the Fermi level of the semiconductor.† For example, in the case of Fig. 14a, the semiconductor is absolutely stable because the levels of both decomposition reactions lie outside the forbidden band. However, more frequent are the cases where the semiconductor is stable against only one type of decomposition: cathodic (Fig. 14b) or anodic (Fig. 14c). Finally, if both levels $F_{dec,n}$ and $F_{dec,p}$ lie in the forbidden band (Fig. 14d) the semiconductor can, in principle, suffer decomposition both under anodic *and* cathodic polarization.

In the case of photocorrosion, it is assumed within the framework of the thermodynamic approach that the shift of the quasi-Fermi levels of electrons F_n and holes F_p is the cause of the

† The cases where Fermi-level pinning is observed are an exception.

acceleration of a semiconductor decomposition reaction under illumination. Conditions (40a) and (40b) should, therefore, be modified. The condition for the reaction of cathodic photodecomposition with conduction-band electrons involved is now of the form [cf. Eqs. (36a) and (36b)]

$$F_n > F_{\text{dec},n} \quad (41a)$$

and for the reaction of anodic photodecomposition with holes involved

$$F_p < F_{\text{dec},p} \quad (41b)$$

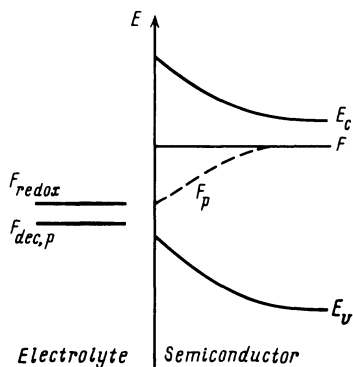
If either (41a) or (41b) is satisfied, the corresponding reactions become thermodynamically favorable.

It should be noted that kinetic restrictions may result in slowing down a reaction. Indeed, in many cases it is the kinetic rather than the thermodynamic specific features of an electrode reaction that determine the corrosion (photocorrosion) behavior of semiconductor electrodes.

While discussing the ways of preventing corrosion (photocorrosion), we have to take into account that other reactions may take place that compete with the photodecomposition process. For example, as the illumination intensity grows, among all the possible cathodic reactions the one that starts first is the reaction whose equilibrium potential is most positive, while among all the possible anodic reactions it is the reaction with the most negative equilibrium potential that starts first. Thus, photocorrosion of a semiconductor may, in principle, be suppressed if appropriate oxidizing or reducing agents are added to the solution. Anodic photocorrosion can be prevented by couples whose redox potentials are more negative than the decomposition potential: $\varphi_{\text{redox}}^0 < \varphi_{\text{dec},p}^0$ (i.e., $F_{\text{redox}} > F_{\text{dec},p}$) (see Fig. 15). As far as stabilization against cathodic photodecomposition is concerned, the corresponding condition is $\varphi_{\text{redox}}^0 > \varphi_{\text{dec},n}^0$ (or $F_{\text{redox}} < F_{\text{dec},n}$).

Such protecting systems are oxidized or reduced, thereby stabilizing semiconductor photoelectrodes, and this effect is used in photoelectrochemical cells for solar energy conversion.⁶²⁻⁶⁵ The solvent (e.g., water) can also act as a protector if it is oxidized (reduced) easier than the semiconductor electrode material. Situations like this arise with many oxide electrodes (TiO_2 , SrTiO_3 ,

Figure 15. Diagram illustrating protection of an *n*-type semiconductor against anodic photodecomposition with the aid of a redox couple introduced into the solution.



etc.) where oxidation of water to oxygen is the most probable anodic photoreaction.

Let us consider, as an example, the photocorrosion behavior of GaAs and GaP in aqueous solutions. The levels of the electrochemical potential of decomposition reactions for these materials are shown in Fig. 16 together with the levels E_c and E_v .

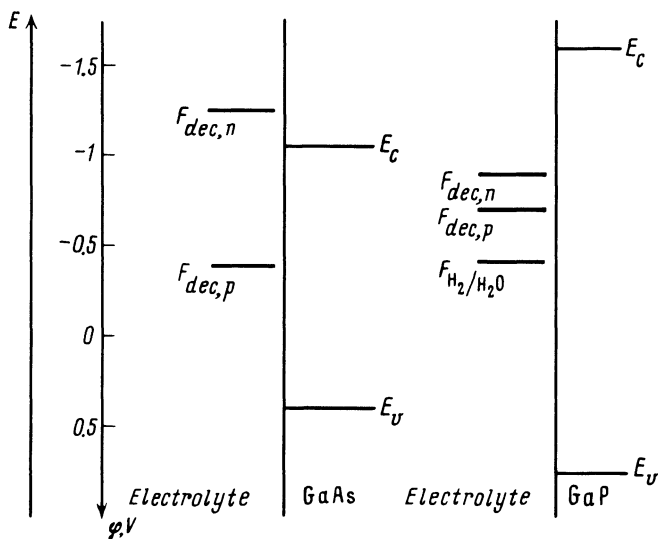


Figure 16. Energy levels at the junction between GaAs, GaP, and an aqueous solution (pH = 7).⁶⁶ All the potentials are given against the normal hydrogen electrode. (Reprinted by permission of the publisher, The Electrochemical Society, Inc.)

For GaAs, $F_{\text{dec},n}$ corresponds to the reaction $\text{GaAs} + 3\text{H}^+ + 3e^- \rightleftharpoons \text{Ga} + \text{AsH}_3$ and $F_{\text{dec},p}$ to the reaction $\text{GaAs} + 5\text{H}_2\text{O} + 6h^+ \rightleftharpoons \text{Ga}(\text{OH})_3 + \text{HAsO}_2 + 6\text{H}^+$. In the case of GaP, $F_{\text{dec},n}$ corresponds to the reaction $\text{GaP} + 3\text{H}^+ + 3e^- \rightleftharpoons \text{Ga} + \text{PH}_3$ and $F_{\text{dec},p}$ to the reaction $\text{GaP} + 6\text{H}_2\text{O} + 6h^+ \rightleftharpoons \text{Ga}(\text{OH})_3 + \text{H}_3\text{PO}_3 + 6\text{H}^+$. Comparison with Fig. 14 shows that the behavior of GaAs corresponds to the case of Fig. 14b, i.e., it is stable against cathodic decomposition, but potentially unstable against anodic decomposition; on the other hand, GaP is potentially liable both to cathodic and anodic decomposition, since the levels of the corresponding reactions lie *in* the forbidden band (the case of Fig. 14d).

4. The Limits of Applicability of the Quasi-Fermi Level Concept in Photoelectrochemical Kinetics: Alternative Approaches

It is clear from the above considerations that the quasithermodynamic approach, based on the concept of quasi-Fermi levels, is sufficiently widespread and what is most important is that it is efficient. Obviousness and simplicity—here are its indisputable advantages. At the same time, it should be noted that the use of the quasi-Fermi-level concept cannot be justified in all cases. At any rate, the applicability of this concept requires that the following inequalities,

$$\tau_c, \tau_v < \tau_{cv} \quad (42)$$

be satisfied. Here τ_c and τ_v are the times of the establishment of a thermodynamic equilibrium separately in an ensemble of electrons in the conduction band and holes in the valence band, and $\tau_{c,v}$ is the time needed for an equilibrium to be established between the electron and hole ensembles. As was already mentioned, the ordinary mechanism through which an equilibrium is attained in the bands is the interaction of excited electrons and holes with phonons; in certain semiconductors this mechanism depends on the interaction between photoexcited and thermalized carriers occurring separately in each band. The values of τ_c and τ_v are of the order of 10^{-12} – 10^{-13} s. The time τ_{cv} is related to the interaction of electrons and holes with one another and, in the simplest case, it coincides with the recombination time. For most semiconductor materials this time is much larger than 10^{-12} – 10^{-13} s so that condition (42) is usually satisfied.

At the same time, these conditions alone are insufficient to describe electron transfer processes at the interface within the framework of the approach discussed. Let us introduce the times $\tau_{n,s}$ and $\tau_{p,s}$, which characterize the time interval between photoexcitation of an electron and a hole, respectively, and consumption of this particle at the surface through, for example, an electrode reaction. Apparently, the concept of the quasi-Fermi levels can be used to describe such processes if only these times are larger than τ_c and τ_v . Otherwise, the quasiequilibrium does not have enough time to be established, and "hot" particles will be directly involved in the electrode process. On the other hand, the times $\tau_{n,s}$ and $\tau_{p,s}$ must be less than τ_{cv} because, if this is not the case, complete equilibrium will be established in the electron-hole system, so that the equality $F_n = F_p = F$ will hold at the interface. Thus, the following two systems of inequalities†:

$$\tau_c < \tau_{n,s} < \tau_{cv}, \quad \tau_v < \tau_{p,s} < \tau_{cv} \quad (43)$$

must be satisfied in order that the concept of the quasi-Fermi levels can be applied effectively to electrons and holes involved in a heterogeneous process at the interface.

In the case of fast consumption of electrons and holes at the surface, the times $\tau_{n,s}$ and $\tau_{p,s}$ coincide with those of the approach of electrons and holes to the interface. Suppose that the penetration depth of light in a semiconductor, α^{-1} , exceeds the thickness L_{sc} of the space-charge region. If L_{sc} is much less than the minority-carrier diffusion length (L_p or L_n), then, by an order of magnitude, $\tau_{p,s} \approx \alpha^{-2}/\mathcal{D}_p$ and $\tau_{n,s} \approx \alpha^{-2}/\mathcal{D}_n$. This implies, in particular, that if α^{-1} exceeds not only L_{sc} but also L_p (or L_n) the condition $\tau_{p,s} < \tau_{cv}$ does not hold for minority carriers. From the physical point of view, this obviously means that if $\alpha^{-1} \gg L_p$ (or $\alpha^{-1} \gg L_n$) an equilibrium is established in a system during the time the carriers approach the interface.

On the contrary, if the condition $\alpha^{-1} < L_{sc}$ applies and when a depletion layer is formed, the time for the carriers to approach the interface is determined by migration in the space-charge field, rather than by diffusion (as before). Under such conditions, τ_{ps} (or τ_{ns}) is of the order of α^{-1}/v , where v is the migration velocity.

† If an electrode reaction proceeds with only one type of carrier involved, it is sufficient that only one system of inequalities be satisfied.

Estimates show that α^{-1}/v is 10^{-13} – 10^{-11} s, so that the inequalities (43) may hold under such conditions.

If the surface process proper cannot be considered infinitely fast, the times $\tau_{n,s}$ and $\tau_{p,s}$ can be limited by the duration of this process; for example, by the duration of an elementary act of an electrode reaction.

Thus, since the time interval between τ_c and τ_{cb} , on the one hand, and τ_{cv} , on the other hand, is sufficiently large (from 10^{-13} to 10^{-8} s), the time characteristics of many electrode processes satisfy conditions (43). Therefore, the concept of quasi-Fermi levels has a rather wide range of application. At the same time, quantitative description (see, e.g., Ref. 67) requires that certain additional conditions should be satisfied. It is necessary, in particular, that the quasi-level behavior in the space-charge region be sufficiently smooth; the latter condition holds true if $\alpha^{-1} \gg L_{sc}$ and recombination in the space-charge region is weak. It is obvious, on the other hand, that if photogeneration of carriers occurs mainly near the surface where a fast electrode reaction takes place, a situation is possible when photogenerated carriers will be extracted from the semiconductor more rapidly than they will come into equilibrium with thermalized carriers in the corresponding band. Under such conditions, they cannot be characterized by quasiequilibrium levels F_n and F_p . Apparently, it would be more correct to consider, in this case, the transition of carriers from the electrode into the solution in a purely dynamical way, as individual independent events, rather than through the quasiequilibrium stage.^{49,68-70}

As an illustration, let us consider an attempt⁷⁰ at a quantitative description of this dynamical process. According to the model used in Reference 70, of major importance are quantum levels which arise near the interface in the case of strong band bending (see Section II.2). Only a fraction of photogenerated electrons (or holes) is thermalized and then they become localized on these quantum levels. Further thermalization proceeds so slowly that an electrode reaction readily takes place before thermalization. This reaction can be described as the tunneling of an electron from a quantum level in a triangular well near the interface through a one-dimensional potential barrier into a one-dimensional square well which simulates the reactant in the solution (Fig. 17). It is assumed that after tunneling has occurred the solvent rearranges around the

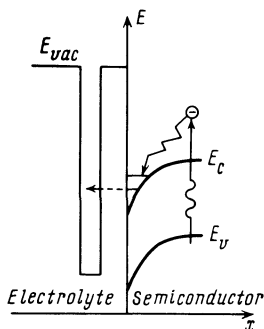


Fig. 17. Diagram elucidating the model for the description of the tunneling of "hot" electrons from the semiconductor to the reactant in the solution.

reactant quite rapidly, so that the reverse electron transition to the electrode is impossible.

One may believe that in certain cases this model describes adequately electron (hole) transitions in doped wide-band-gap semiconductors with a small effective mass for sufficiently strong band bending. At the same time, the model employed is too rough for quantitative agreement with experiment to be expected (especially if we take into account that the description is one-dimensional).

Using experimental data, we can, in principle, decide between two approaches—quasithermodynamic and dynamic—to the description of the kinetics of photoelectrochemical reactions. The first approach (based on the quasilevel concept) predicts the existence of a certain threshold illumination intensity for the case where an equilibrium at the semiconductor/solution interface is not established in darkness. In fact, if an electrode reaction is slowed down in darkness, the levels F and F_{redox} take an arbitrary position with respect to each other. Under illumination, the level F splits into F_n and F_p , so that F_p moves farther away from F as the illumination intensity grows and may reach F_{redox} at a certain threshold value of the intensity. For lower illumination intensities, a photoelectrochemical reaction cannot take place, according to the quasithermodynamic approach. On the contrary, in the dynamic approach a photoreaction does proceed for *any* illumination intensity.

This threshold has not so far been observed experimentally. For example, in the photoevolution of oxygen on TiO_2 the photocurrent grows monotonously with illumination intensity within a very

wide range of intensities (from 10^{-6} to $4 \times 10^2 \text{ W cm}^{-2}$).⁶⁹ On the other hand, until quite recently, investigations have been performed on semiconductors with very wide band gaps and, hence, negligibly low concentrations of minority carriers p_0 (or n_0). For such materials, the threshold illumination intensity, determined by the ratio $\Delta p/p_0$ (or $\Delta n/n_0$), can be too low to be detected in an experiment. Thus, no reliable data are available at present to decide convincingly between the two approaches discussed here. This remains a problem for the future.

V. NEW APPLICATIONS

1. Photoelectrochemical Conversion of Solar Energy

Since semiconductor electrodes are photosensitive, the semiconductor/electrolyte interface is potentially applicable for interconverting the energy of light.⁷¹ In Section IV.2 we have considered in brief the mechanism of the occurrence of photocurrents on a semiconductor electrode for the two most important cases: namely, in the presence of a highly reversible redox couple in the solution and in the absence of such a couple (i.e., under conditions when the electrochemical reaction is slowed down in darkness). In the first case, the energy of the light is converted into electrical energy, and in the second case into chemical energy. Such photoelectrochemical cells are called "liquid junction solar cells" (or photoelectrochemical cells of the regenerative type) and the photoelectrolysis cell, respectively. Among various photoelectrolysis reactions of most interest is photoelectrolysis of water as a possible source of hydrogen fuel and raw material.

The most important advantage of photoelectrochemical cells with semiconductor electrodes, as compared to, for example, solid-state semiconductor solar cells, is a relatively low sensitivity of their characteristics to the crystalline perfection of the semiconductor and the degree of its purification. Polycrystalline semiconductor electrodes in electrochemical "solar cells" exhibit both high absolute and high relative (as compared to single-crystal electrodes) conversion efficiency. This opens, at least in principle, the way of

producing inexpensive and technologically simple solar energy converters.

The mechanism of operation of photoelectrochemical cells and the characteristics of particular systems have been considered in detail in review articles^{52,62-65,69,72-74} and in a monography⁷; therefore, these topics are beyond the scope of the present review. It seems reasonable, however, to concentrate here on the most important problems, which are to be solved before photoelectrochemical cells find extensive practical application.

The main obstacle to creating "liquid junction solar cells" is photocorrosion of semiconductor electrodes, which reduces considerably their lifetime. In order to prevent, for example, anodic photocorrosion, a well-reversible redox couple is introduced into an electrolyte solution, so that the reaction of oxidation of the red component competes for photoholes with the reaction of photodecomposition of the electrode material (see Section IV.2). With the aid of this method, photocorrosion has been practically prevented in certain types of photocells and the duration of their continuous operation has been increased up to about one year. Yet, there are other, more subtle mechanisms of electrode degradation,^{65,75} which has hitherto prevented the lifetime of photoelectrochemical cells from becoming comparable with the 20-year lifetime of solid-state solar cells.

The most essential problem in photoelectrolysis is the "matching" of the energetics of an electrochemical reaction with the spectrum of solar radiation. The energy distribution of photons in the solar spectrum is such that the optimal threshold energy for the quantum conversion process (and it is this type of conversion that is obtained with semiconductor electrodes) lies in the range 1.1-1.4 eV. The change in the free energy of the reaction of electrochemical splitting of water into hydrogen and oxygen is 1.23 eV, i.e., it falls into this range but, in practice, this process proceeds with a considerable overvoltage. If additional inevitable energy losses are taken into account, the energy of a quantum needed for photoelectrochemical decomposition of water increases to about 2 eV,^{72,74} i.e., it exceeds significantly the above value. In other words, only a relatively small fraction of harder quanta in the solar spectrum can be used directly for photoelectrolysis of water. We should stress that this circumstance is in no way an

incidental one. On the contrary, the fact that precisely this situation occurs in nature eventually ensures a relative stability of extremely diverse animate and inanimate systems against solar radiation. However, this obstacle can, in principle, be overcome in several ways.

1. *Realization of the process in the photostimulated electrolysis regime.* In this case, the main fraction of quanta of solar radiation is utilized to generate a photoelectrochemical reaction, and the deficient (for the necessary 2 eV) energy is supplied with the aid of an external voltage source. The greatest progress in this direction has been reached in Reference 76.

2. *Realization of a "two-quantum" type process.* Combining two semiconductor photoelectrodes (an *n*-type anode and a *p*-type cathode) in a single photoelectrochemical cell and choosing appropriately the characteristics of both electrodes, we can obtain an effective summation of photopotentials developed across each of the electrodes and produce the energy sufficient for photoelectrolysis of water.^{77,78}

An alternative way is to divide the overall process of water splitting into two stages, each being conducted in a separate photoelectrochemical cell. Both cells are coupled with the aid of a certain intermediate substance, which acts as a charge transfer agent and is not consumed in the course of the overall process, but only provides the connection in series of the chemical potentials developed in both cells.^{7,79} Apparently, such a scheme imitates the combination of two photosystems in photosynthesis occurring in green plants.

Each of the ways considered above utilizes two photoelectrodes, so that the overall process is formally a two-quantum one, which permits, in principle, the necessary gain in the energetics to be obtained.

3. *Division of the overall process into two stages: production of electricity and water electrolysis proper.*⁸⁰⁻⁸² Let us replace a single photoelectrochemical cell by the combination of a solar cell (solid state or "liquid junction") and an ordinary electrolyzer. In this case, production of electricity and electrolytic decomposition of water, which are combined in a photoelectrolysis cell, appear to be distributed between two specially designed devices. This enables the necessary voltage to be attained by connecting in series several

solar cells and also provides extensive potentialities for choosing the optimal photoelectric and electrocatalytic properties of the electrode materials employed.

4. *Dehydration of inexpensive and readily available organic substances.* Since hydrogen is, in fact, the only desirable final product, this approach is based on giving up the idea that only water should necessarily be utilized in photoelectrolysis. Another electrochemical reaction can be chosen, which is characterized by a lesser change in the free energy, for example, dehydration of industrial waste products. Photoelectrochemical processes of this type have been studied intensively in recent years.^{64,83-87}

Of interest are also systems in which the thermal (IR) portion of the solar spectrum is used besides visible light⁸⁸ and also systems which employ nontraditional processes such as photointercalation of atoms into the crystal lattice of a semiconductor.⁸⁹

One may believe that the current intensive efforts will eventually be crowned with the development of simple, economically reasonable, photoelectrochemical processes capable of competing with other, nonelectrochemical methods of utilizing solar energy.

2. Laser Etching of Semiconductors

An intensive development of quantum optics has led to the emergence of a new field, laser electrochemistry of semiconductors (for reviews see Refs. 90 and 91). It covers the range of problems related to electrochemical processes on semiconductor electrodes stimulated by laser radiation. The greatest progress in this direction has been achieved in the light-sensitive etching of semiconductors by coherent laser radiation, which can be used for recording optical information, for example, for producing holograms.⁹²

Light-sensitive etching with polarization from an external source is called photoanodic etching, and that in an oxidizing solution, photochemical etching.

Light-sensitive etching is based on the change, due to illumination, in the minority-carrier concentration, which determines the rate of anodic dissolution and corrosion of semiconductors. For example, under illumination of an *n*-type semiconductor in the anodic polarization regime, the etching rate can be limited by the rate of hole supply to the electrode surface. In darkness, a certain,

usually low, dissolution rate is established on such electrodes. Illumination is an additional source of holes (photogeneration), so that illuminated areas are dissolved more rapidly than nonilluminated ones.

Illumination of a semiconductor under open-circuit conditions in an etching (oxidizing) solution gives rise to corrosion even in darkness. In the simplest case where the cathodic partial reaction of a corrosion process proceeds exclusively through the conduction band and the anodic one through the valence band, the corrosion rate for specimens of any conductivity type is limited by the minority-carrier supply to the surface and is therefore low in darkness. Illumination accelerates corrosion processes. Comparison with the case considered above shows that here the "chemical" polarization of the semiconductor by an oxidizer introduced into the solution acts as anodic polarization.

In laser etching, the initially flat surface of a semiconductor in an electrolyte solution is illuminated (through the solution) by two coherent light beams of the same intensity and wavelength incident at equal angles and lying in the same plane (Fig. 18). Interference of these beams produces illuminated and dark regions (fringes) at the interface and stimulates nonuniform etching of the surface.

In simple cases but ones that are important for practical applications, the theory of laser etching^{90,93} yields an analytical expression for the characteristics of the relief produced as a function

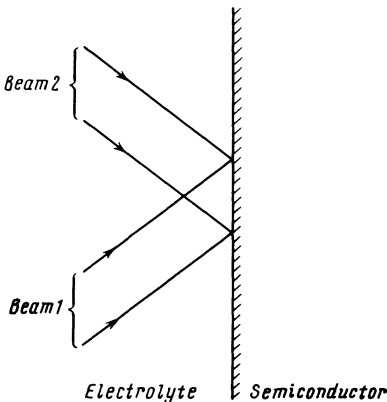


Figure 18. Schematic diagram of the illumination of a surface in laser light-sensitive etching.

of radiation parameters, semiconductor properties, and specific features of the electrode reaction. In brief, the results of the calculations are as follows. The profile of the relief produced (diffraction grating) is rather close to a sinusoidal one. In the case of "surface-absorbed" light (large value of the absorption coefficient) and fast electrochemical reaction (large value of the rate constant) the spatial frequency of the relief d (its dimension is the inverse length) is very high. From the physical point of view this means that if holes are generated in close proximity to the surface and are consumed immediately, the diffusion of photogenerated holes can be neglected beyond the limits of illuminated areas of the surface.

Thus, the resolution of light-sensitive etching, i.e., the maximal value d^{-1} attained, is not determined, in accordance with the above consideration, by the diffusion length L_p , as might be expected *a priori* ($\alpha^{-1} \approx L_p$), but is much higher.

In practice, the laser beam of an appropriate wavelength is first expanded to a diameter of 10–20 mm and then is split (with the aid of two mirrors) into two beams of equal intensity, which intersect at the surface of an electrode immersed in an electrolyte solution (Fig. 18).

The quality of the relief obtained can be evaluated directly in the course of etching because the light reflected from the grating produces a diffraction pattern, which characterizes the depth and shape of the grating profile at any moment. To this end, one simply measures the reflected light intensity. The sensitivity of the method is high: the occurrence of the relief can be observed when its depth is only $\approx 0.01 \mu$.

Light-sensitive laser etching has been employed to produce diffraction gratings on many single-crystal semiconductors (Ge, Si, GaAs, GaP, CdS, CdSe) and also on semiconducting films, including polycrystalline CdSe, CdTe, As_2Te_3 , InSe, GaSe, Cu_2O , and GeO and glassy Ag_2Se_3 .

The profile of the relief etched is usually rather close to a sinusoidal one. The potentialities of the methods can be seen from Table 1, which presents for certain of the aforementioned materials the following parameters: the maximal spatial frequency d_{max}^{-1} attained for the gratings recorded (the maximal number of grooves/mm), the wavelength of the recording light λ , and the diffusion length L_p of minority carriers in the specimens.

Table 1
Characteristics of Diffraction Gratings Produced by the
Light-Sensitive Etching Method

Semiconductor	d_{\max}^{-1} (mm ⁻¹)	λ (nm)	L_p (cm)	References
Photoanodic etching				
CdSe	2600	632.8	10 ⁻⁴	94
CdS	6150	441.6	10 ⁻⁴	95
Si	2500	514.5	10 ⁻²	92
As ₂ Se ₃	2600	632.8	—	96
Photochemical etching				
GaAs	5000–6000	441.6	10 ⁻⁴	93
GaAsP	2700	—	—	97
As ₂ Te ₃	2600	632.8	—	96
Ge	1000	632.8	10 ⁻¹	53

The table shows that the resolution of the photoelectrochemical method of information recording is sufficiently high—more than 6000 mm⁻¹. It should be stressed that for materials with large diffusion lengths, L_p (germanium, silicon), the resolution, as was predicted by the theory, proves to be much higher than might be expected from the values of L_p .

Comparison of light-sensitive laser etching with the most widespread nonelectrochemical methods, such as hologram recording on plates and also photolithography (i.e., etching through a mask produced with the aid of photoresists), shows that resolution of all these methods is approximately the same. As the spatial frequency of the recording light beam increases, the photoetching methods are expected to become more advantageous over, in particular, photolithography, since the relief is produced directly on the semiconductor surface, rather than in an auxiliary photoresist layer. The latter circumstance also makes it easier to obtain a regular sinusoidal profile of the diffraction grating.

Let us note in conclusion that light-sensitive etching is by no means the only problem in the field of laser electrochemistry. It includes, for example, threshold electrochemical reactions stimulated by intensive laser radiation. Such reactions may proceed via new schemes and, therefore, yield new products because both highly excited solution components and a nonequilibrium electron-hole

plasma of the semiconductor are involved. This opens an opportunity for developing unusual processes in chemical technology.

3. The Ion-Selective Field-Effect Transistor

Joining of an ion-selective electrode and a field-effect transistor (FET) in a single device has made it possible to create a new type of ion concentration detector called the ion-selective field-effect transistor (ISFET.) High sensitivity and selectivity, as well as the very small size of this device, have resulted in its constantly growing applications in recent years in industry, medicine, biology, scientific research, etc.

Since the ISFET is based on the field-effect transistor, let us recall briefly how the latter operates (see, e.g., Ref. 98). The field-effect transistor (Fig. 19a) represents the so-called MIS (metal-insulator-semiconductor) structure (hence the abbreviation MIS-FET), i.e., a semiconductor base, onto which an insulating layer and a metal "electrode" (gate) are deposited. The base usually is a *p*-type silicon plate and the insulator, a SiO_2 or Si_3N_4 layer. With a thickness of 100–200 nm, the resistance of this layer is of the order of $10^{13} \Omega$. Two regions are produced in the base by local

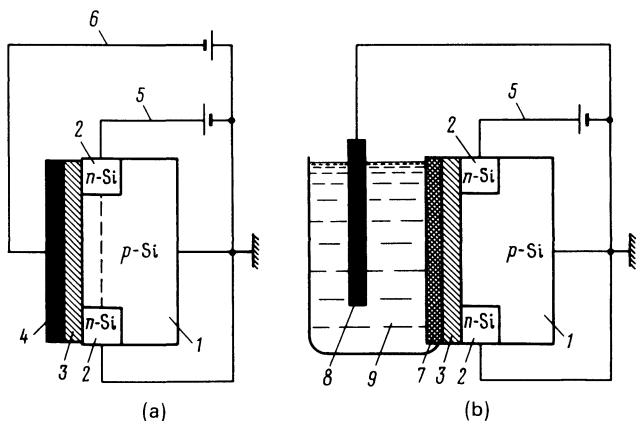


Figure 19. Schematic diagram of the (a) field-effect transistor and (b) ion-selective field-effect transistor: (1) base, (2) source and drain, (3) insulating layer, (4) gate, (5) low-ohmic electric circuit, (6) high-ohmic electric circuit, (7) ion-selective membrane, (8) reference electrode, and (9) electrolyte solution under investigation.

doping with an appropriate impurity, in which the type of silicon conductivity is made reverse. These regions (of n -type) are called source and drain. Connecting external voltage sources to the gate—base and source–drain circuits, as shown in Fig. 19a, we can realize a field effect in the transistor. Namely, with no voltage on the gate, the current in the source–drain circuit is practically absent, since one of the p – n junctions in this circuit is reverse biased. Let us now apply a voltage to the gate of such a polarity and magnitude that an inversion layer is formed in the base near the silicon/insulator interface (in the case of Fig. 19a a positive voltage, with respect to the base, must be applied to the gate). An n -type “channel,” which arises in this case short circuits the source and drain, thereby enabling an electric current to flow in the source–drain circuit whose ohmic resistance appears to be rather low, only several tens of ohms. Thus, by varying the voltage in the high-ohmic gate–base circuit we can efficiently control the current in the low-ohmic source–drain circuit. In other words, this device has a very large current multiplication factor.

This feature of the FET is transformed into high sensitivity in the ISFET. That is, in order to go over from the FET to the ISFET it is sufficient to replace the insulating layer by an ion-selective membrane permeable only to one sort of ion[†] and the metal gate by an electrolyte solution, which contains a reference electrode needed to short circuit the electric circuit (Fig. 19b). The potential, which develops across the membrane in the presence in the solution of that sort of ions for which the membrane is selectively permeable, acts here as an external voltage on the gate. This potential can be determined from Nernst's equation [cf. Eq. (4)]

$$\varphi^0 = \varphi_0^0 + \frac{RT}{z\mathcal{F}} \ln a \quad (44)$$

where a and z are the activity (concentration, in the simplest case) and charge number of potential-determining ions, respectively, and φ_0^0 is the standard potential (i.e., the value of φ^0 for $a = 1 \text{ mol dm}^{-3}$).

With this mechanism of the formation of potential across the membrane, the current in the measuring circuit depends on the ion activity a , which makes the ISFET a very sensitive ion detector.

[†] In certain types of ISFET, the membrane is deposited directly onto the insulating layer, so that we deal with a “four-layer” structure.

Particular types of the ISFET are very diverse, since there is a possibility of widely varying the membrane composition, the type of reference electrode, the mode of operation (e.g., an additional polarizing voltage can be used), etc.

The survey of the most important systems of this type, their characteristics, and possible applications can be found, for example, in the reviews.^{90,100}

4. Characterization of Semiconducting Materials

A certain relationship, which exists between the bulk and surface properties of semiconducting materials and their electrochemical behavior, enables, in principle, electrochemical measurements to be used to characterize these materials. Since 1960, when Dewald³⁹ was the first to determine the donor concentration in a zinc oxide electrode using Mott-Schottky plots, differential capacity measurements have frequently been used for this purpose in several materials. If possible sources of errors that were discussed in Section III.3 are taken into account correctly, the capacity method enables one to determine the distribution of the doping impurity concentration over the surface⁴⁰ and, in combination with the layer-by-layer etching method, also into the specimen depth.^{101,102} The impurity concentration profile can be constructed by this method. It has recently been developed in greatest detail as applied to gallium arsenide crystals and multilayer structures.¹⁰³

Several methods of anodic (photoanodic in particular) etching have been suggested in the literature to reveal various inhomogeneities in the structure and composition of semiconducting crystals (see, e.g., Refs. 104-106).

VI. CONCLUDING REMARKS

It has not been possible in the present review to cover all the diversity of new ideas and approaches that have been developed in the electrochemistry of semiconductors. Therefore, in conclusion we would like to note those directions which seem to us the most interesting and promising (though some of them have not so far been developed extensively because of one reason or another which

are frequently of momentary character); several such directions have been discussed in our monograph.⁷

1. *New systems.* Among new (for electrochemistry) semiconducting materials, those with so-called layered crystal lattices¹⁰⁷ seem to be quite promising in view of their practical applications. It is assumed that, being *d*-semiconductors, they may be more stable against photocorrosion than *sp*-semiconductors that were mainly considered above; moreover, they allow photoelectrochemical reactions of nontraditional types to be realized, for example, (photo)intercalation of atoms from the solution into the semiconductor electrode crystal lattice. As far as materials for photoelectrodes of photoelectrochemical cells are concerned, *d*-band semiconductors are of great interest. Synthesis and investigation of new materials with appropriate photoelectrical and electrochemical properties are important directions in the "electrochemical materials science" of semiconductors (see, e.g., Ref. 108).

Quite promising may be the study of photoelectrochemical properties of microheterogeneous semiconductor systems (porous electrodes, suspensions of different degrees of dispersion up to colloidal solutions), in which photosensitivity inherent in semiconductors is combined with high electrocatalytic activity typical of systems with a developed surface.

Modification of the surface of semiconductor electrodes by catalysts (mediators) "attached" to it¹⁰⁹ also deserves intensive investigation.

Finally, in recent years there has been a new surge of development in the field of thin-film electrochemistry, especially in view of practical applications. The thickness of films in such systems ranges from several angstroms to hundreds of angstroms; in the latter case, the films often possess semiconducting properties.

2. *New methods of investigation.* It may be expected that fresh important information will be gained with the aid of new methods, both developed directly within the framework of the electrochemistry of semiconductors and metals and borrowed from other fields, foremost of which is the physics of surfaces; the latter methods are usually called nontraditional.

Among traditional electrochemical methods we may note the estance method based on the elastic change in surface stress¹¹⁰ (it

has recently been used¹¹¹ to study semiconductor electrodes), and also the method of the rotating ring-disc electrode¹¹² in its various special modifications.¹¹³ In recent years, computer-based measuring devices have been designed for determining various characteristics of semiconductor electrodes.¹¹⁴⁻¹¹⁶

The nontraditional methods are mainly related to the effect of illumination on the interface. Here we should mention foremost phototemperature spectroscopy, which permits one to determine, by measuring the change in the photoelectrode temperature, what fraction of the energy of light absorbed is consumed in a photoelectrochemical reaction and what fraction is converted into heat, and thus permits one to find the "true" quantum yield^{117,118}; high-time-resolution measurement of photocurrents induced by nanosecond laser pulses^{119,120}; and electrogenerated luminescence allowing recombination processes in electrodes to be studied¹²¹ as well as photoemission of electrons from semiconductors into electrolyte solutions²⁵ and electroreflection of light at the semiconductor/electrolyte interface.¹²² To this group of methods we may also refer photoacoustic spectroscopy, which reveals more subtle features of light absorption in semiconductors.^{123,124}

Thus, on the one hand, it may be believed that a more or less adequate picture of the electrochemical behavior of semiconductors has already been established; but, on the other hand, as far as the number and importance of new problems are concerned, the electrochemistry of semiconductors may be considered still a rapidly developing branch of modern science.

REFERENCES

- ¹ V. A. Myamlin and Yu. V. Pleskov, *Electrochemistry of Semiconductors*, Plenum Press, New York, 1967.
- ² J. O'M. Bockris, *Energy: The Solar-Hydrogen Alternative*, Australia and New Zealand Book Company, Sydney, 1975.
- ³ R. A. Smith, *Semiconductors*, Cambridge University Press, Cambridge, 1977.
- ⁴ V. L. Bonch-Bruевич and S. G. Kalashnikov, *Fizika Poluprovodnikov*, Nauka, Moscow, 1977.
- ⁵ H. Gerischer, in *Physical Chemistry, An Advanced Treatise*, Ed. by H. Eyring, Academic Press, New York and London, 1970, Vol. 9, p. 463.
- ⁶ S. R. Morrison, *Electrochemistry at Semiconductor and Oxidized Metal Electrodes*, Plenum Press, New York and London, 1980.
- ⁷ Yu. V. Pleskov and Yu. Ya. Gurevich, *Semiconductor Photoelectrochemistry* (to be published by Plenum Press).

- ⁸ H. Gerischer, *Photochem. Photobiol.* **16** (1972) 243.
- ⁹ Yu. Ya. Gurevich and Yu. V. Pleskov, *Elektrokimiya* **18** (1982) 1477.
- ¹⁰ L. I. Krishtalik, *Elektrodnye Reaktsii, Mechanism Elementarnogo Akta*, Nauka, Moscow, 1979 (to be published by Plenum Press).
- ¹¹ R. R. Dogonadze and A. M. Kuznetsov, in *Progress in Surface Science*, Ed. by S. G. Davison, Pergamon Press, Oxford, Vol. 6, 1975, p. 1.
- ¹² J. Ulstrup, *Charge Transfer Processes in Condensed Media*, Springer-Verlag, Berlin, BRD, 1980.
- ¹³ E. D. German and A. M. Kuznetsov, *Itogi Nauki i Tekhniki, Ser. Kinetika i Katalis*, VINITI, Moscow, 1982, Vol. 10, p. 115.
- ¹⁴ R. Kubo, *Statistical Mechanics*, North-Holland, Amsterdam, 1965.
- ¹⁵ H. Gerischer, *J. Electroanal. Chem.* **82** (1977) 133.
- ¹⁶ A. J. Bard and M. S. Wrighton, *J. Electrochem. Soc.* **124** (1977) 1706.
- ¹⁷ R. Memming, *Electrochim. Acta* **25** (1980) 77.
- ¹⁸ S. M. Park and M. E. Barber, *J. Electroanal. Chem.* **99** (1979) 67.
- ¹⁹ E. Kanevsky, *Zh. Fiz. Khim.* **24** (1950) 1511.
- ²⁰ F. Lohmann, *Z. Naturforsch. A* **22** (1967) 843.
- ²¹ S. Trasatti, in *Modern Aspects of Electrochemistry*, Ed. by B. E. Conway and J. O'M. Bockris, Plenum Press, New York and London, 1979, Vol. 13, p. 81.
- ²² A. Frumkin and B. Damaskin, *J. Electroanal. Chem.* **66** (1975) 150.
- ²³ J. E. B. Randles, *Trans. Faraday Soc.* **52** (1956) 1573.
- ²⁴ V. S. Fomenko, *Emissionnye Svoistva Metallov*, Naukova Dumka, Kiev, 1970, p. 49.
- ²⁵ Yu. Ya. Gurevich, Yu. V. Pleskov, and Z. A. Rotenberg, *Photoelectrochemistry*, Consultants Bureau, New York, 1980.
- ²⁶ Yu. V. Pleskov, *J. Electroanal. Chem.* **105** (1979) 227.
- ²⁷ P. Delahay, *J. Phys. Chem.* **55** (1971) 4188.
- ²⁸ R. Memming and F. Möllers, *Ber. Bunsenges. Phys. Chem.* **76** (1972) 475.
- ²⁹ M. Green, in *Modern Aspects of Electrochemistry*, Ed. by J. O'M. Bockris, Butterworths, London, Vol. 2.
- ³⁰ J. O'M. Bockris and A. K. N. Reddy, *Modern Electrochemistry*, Plenum Press, New York, 1970.
- ³¹ A. N. Frumkin, *Potenzialy Nulevogo Zaryada*, Nauka, Moscow, 1979, (to be published by Plenum Press).
- ³² S. G. Davison and J. D. Levine, *Solid State Physics*, Academic Press, New York and London, Vol. 25, 1970.
- ³³ J. A. Appelbaum and D. R. Hamann, *Rev. Mod. Phys.* **48** (1976) 479.
- ³⁴ A. Ya. Belenky, *Usp. Fiz. Nauk [Sov. Phys.—Usp.]* **134** (1981) 125.
- ³⁵ A. J. Bard, A. B. Bocarsly, F.-R. F. Fan, E. G. Walton, and M. S. Wrighton, *J. Am. Chem. Soc.* **102** (1980) 3671.
- ³⁶ A. B. Bocarsly, D. C. Bookbinder, R. N. Dominey, N. S. Lewis, and M. S. Wrighton, *J. Am. Chem. Soc.* **102** (1980) 3683.
- ³⁷ J. A. Turner, J. Manassen, and A. J. Nozik, *Appl. Phys. Lett.* **37** (1980) 488.
- ³⁸ F. Cardon and W. P. Gomes, *J. Phys. D* **11** (1978) L63.
- ³⁹ J. F. Dewald, *Bell Syst. Tech. J.* **34** (1960) 615.
- ⁴⁰ M. Tomkiewicz, *J. Electrochem. Soc.* **126** (1979) 2220.
- ⁴¹ T. Hirai, I. Tari, and T. Ohzuku, *Bull. Chem. Soc. Jpn.* **54** (1981) 509.
- ⁴² T. P. Brintseva and Yu. V. Pleskov, *Izv. Akad. Nauk SSSR, Ser. Khim.* (1965) 251.
- ⁴³ R. De Gryse, W. P. Gomes, F. Cardon, and J. Vennik, *J. Electrochem. Soc.* **122** (1975) 711.
- ⁴⁴ E. C. Dutoit, R. L. Van Meirhaeghe, F. Cardon, and W. P. Gomes, *Ber. Bunsenges. Phys. Chem.* **79** (1975) 1206.

- ⁴⁵ M. A. Butler and D. S. Ginley, *J. Electrochem. Soc.* **125** (1978) 228.
- ⁴⁶ W. W. Gärtner, *Phys. Rev.* **116** (1959) 84.
- ⁴⁷ H. Reiss, *J. Electrochem. Soc.* **125** (1978) 937.
- ⁴⁸ M. A. Butler, *J. Appl. Phys.* **48** (1977) 1914.
- ⁴⁹ J. O'M. Bockris and K. Uosaki, *J. Electrochem. Soc.* **125** (1978) 223.
- ⁵⁰ W. J. Albery, P. N. Bartlett, A. Hamnett, and M. P. Dare-Edwards, *J. Electrochem. Soc.* **128** (1981) 1492.
- ⁵¹ W. Shockley, *Electrons and Holes in Semiconductors*, Van Nostrand, New York, 1950.
- ⁵² H. Gerischer, in *Solar Power and Fuels*, Ed. by J. Bolton, Academic Press, New York, 1977, p. 77.
- ⁵³ L. V. Belyakov, D. N. Goryachev, L. G. Paritsky, S. M. Ryvkin, and O. M. Sreseli, *Fiz. Tekh. Poluprov. [Sov. Phys.—Semicond.]* **10** (1976) 1142.
- ⁵⁴ H. Reiche, W. W. Dunn, and A. J. Bard, *J. Phys. Chem.* **83** (1979), 2248.
- ⁵⁵ W. W. Dunn, Y. Aikawa, and A. J. Bard, *J. Am. Chem. Soc.* **103** (1981) 3456.
- ⁵⁶ K. Kalyanasundaram, E. Borgarello, and M. Grätzel, *Helv. Chim. Acta* **64** (1981) 362.
- ⁵⁷ R. R. Dogonadze and A. M. Kuznetsov, *Elektrokhimiya* **1** (1965) 1008.
- ⁵⁸ G. Nagasubramanian and A. J. Bard, *J. Electrochem. Soc.* **128** (1981) 1055.
- ⁵⁹ W. Kautek and H. Gerischer, *Ber. Bunsenges. Phys. Chem.* **84** (1980) 645.
- ⁶⁰ H. Tributich, H. Gerischer, C. Clemen, and E. Bucker, *Ber. Bunsenges. Phys. Chem.* **83** (1979) 655.
- ⁶¹ Yu. V. Pleskov and V. A. Tyagai, *Dokl. Akad. Nauk SSSR* **141** (1961) 1135.
- ⁶² J. Manassen, D. Cahen, G. Hodes, and A. Sofer, *Nature* **263** (1976) 97.
- ⁶³ M. S. Wrighton, *Acc. Chem. Res.*, **12** (1979) 303.
- ⁶⁴ A. J. Bard, *Science*, **207** (1980) 139.
- ⁶⁵ A. Heller and B. Miller, *Electrochim. Acta* **25** (1980) 29.
- ⁶⁶ R. Memming, *J. Electrochem. Soc.* **125** (1978) 117.
- ⁶⁷ C. G. B. Garrett and W. H. Brattain, *Phys. Rev.* **99** (1955) 376.
- ⁶⁸ F. Williams and A. J. Nozik, *Nature* **271** (1978) 137.
- ⁶⁹ A. J. Nozik, *Ann. Rev. Phys. Chem.* **29** (1978) 189.
- ⁷⁰ D. S. Boudreaux, F. Williams, and A. J. Nozik, *J. Appl. Phys.* **51** (1980) 2158.
- ⁷¹ A. Fujishima and K. Honda, *Nature* **238** (1972) 37.
- ⁷² H. Gerischer, in *Photovoltaic and Photoelectrochemical Solar Energy Conversion*, Ed. by F. Cardon, W. P. Gomes, and W. Dekeyser, Plenum Press, New York and London, 1981, p. 199.
- ⁷³ A. J. Nozik, Reference 72, p. 263.
- ⁷⁴ Yu. V. Pleskov, in *Progress in Surface Science*, Ed. by S. G. Davison, Pergamon Press, New York, Vol. 15, 1984, p. 401.
- ⁷⁵ A. Heller, *Acc. Chem. Res.* **14** (1981) 154.
- ⁷⁶ A. Heller and R. G. Vadimsky, *Phys. Rev. Lett.* **46** (1981) 1153.
- ⁷⁷ A. J. Nozik, *Appl. Phys. Lett.* **29** (1976) 150.
- ⁷⁸ K. Ohashi, J. McCann, and J. O'M. Bockris, *Nature* **266** (1977) 610.
- ⁷⁹ Z. Takehara and S. Yoshizawa, in *Hydrogen Energy Progress*, Ed. by T. N. Veziroğlu, K. Fueki, and T. Ohta, Pergamon Press, Oxford, 1981, Vol. 2, p. 631.
- ⁸⁰ E. N. Costogoe and R. K. Yasui, *Solar Energy* **19** (1977) 205.
- ⁸¹ M. Ya. Bakirov and D. T. Effendiev, *Geliotekhnika* (1980) 43.
- ⁸² D. Estève, C. Ganibal, D. Steinmetz, and A. Vialaron, in *Hydrogen Energy Progress*, Ed. by T. N. Veziroğlu, K. Fueki, and T. Ohta, Pergamon Press, Oxford, 1981, Vol. 3, p. 1593.
- ⁸³ A. J. Nozik, *Phil. Trans. Roy. Soc. London Ser. A* **295** (1980) 453.
- ⁸⁴ A. Fujishima, T. Inoue, and K. Honda, *J. Am. Chem. Soc.* **101** (1979) 5582.

- ⁸⁵ B. Kraeutler and A. J. Bard, *Nouv. J. Chim.* **3** (1979) 31.
- ⁸⁶ V. Guruswami and J. O'M. Bockris, *Int. J. Energy Res.* **3** (1979) 397.
- ⁸⁷ C. R. Dikson and A. J. Nozik, *J. Am. Chem. Soc.* **100** (1978) 8007.
- ⁸⁸ W. Gissler, in *Hydrogen Energy Progress*, Ed. by T. N. Veziroğlu, K. Fueki, and T. Ohta, Pergamon Press, Oxford, 1981, Vol. 2, p. 653.
- ⁸⁹ H. Tributch, *Appl. Phys.* **23** (1980) 61.
- ⁹⁰ V. A. Tyagai, V. A. Sterligov, and G. Ya. Kolbasov, *Problemy Fizicheskoi Khimii Poverkhnosti Poluprovodnikov*, Nauka, Novosibirsk, 1978, p. 181.
- ⁹¹ L. V. Belyakov, D. N. Goryachev, and O. M. Sreseli, *Problemy Fiziki Poluprovodnikov*, A. F. Ioffe Fiziko-tekhnicheskyy Institut, Leningrad, 1979, p. 5.
- ⁹² A. L. Dalisa, W. K. Zwicker, D. J. De Biteto, and P. Harnack, *Appl. Phys. Lett.* **17** (1970) 208.
- ⁹³ L. V. Belyakov, D. N. Goryachev, S. M. Ryvkin, O. M. Sreseli, and R. A. Suris, *Fiz. Tekh. Poluprov. [Sov. Phys.—Semicond.]* **13** (1979) 2173.
- ⁹⁴ V. A. Tyagai, V. A. Sterligov, G. Ya. Kolbasov, and O. V. Snitko, *Fiz. Tekh. Poluprov. [Sov. Phys.—Semicond.]* **7** (1973) 632.
- ⁹⁵ V. A. Sterligov, G. Ya. Kolbasov, and V. A. Tyagai, *Pis'ma v Zh. Tekh. Fiz.* **2** (1976) 437.
- ⁹⁶ L. V. Belyakov, D. N. Goryachev, Yu. I. Ostrovsky, and L. G. Paritsky, *Zh. Nauchn. Prikl. Fotogr. Kinematogr.* **19** (1974) 54.
- ⁹⁷ Yu. A. Bykovsky, V. L. Smirnov, and A. V. Shmal'ko, *Zh. Nauchn. Prikl. Fotogr. Kinematogr.* **23** (1978) 129.
- ⁹⁸ S. M. Sze, *Physics of Semiconductor Devices*, Wiley, New York, 1969.
- ⁹⁹ J. Janata and R. J. Huber, in *Ion-Selective Electrode Reviews*, Ed. by J. D. R. Thomas, Pergamon Press, Oxford, 1980, Vol. 1, p. 31.
- ¹⁰⁰ Yu. G. Vlasov, *Zh. Prik. Khim.* **52** (1979) 3.
- ¹⁰¹ T. Ambridge, J. L. Stevenson, and R. L. Redstall, *J. Electrochem. Soc.* **127** (1980) 222.
- ¹⁰² C. D. Sharpe and P. Lilley, *J. Electrochem. Soc.* **127** (1980) 1918.
- ¹⁰³ M. M. Faktor, T. Ambridge, C. R. Elliott, and J. C. Regnault, in *Current Topics in Materials Science*, Ed. by E. Kaldis, North-Holland, Amsterdam, 1980, Vol. 6, p. 1.
- ¹⁰⁴ M. T. Pham and J. Hueller, *J. Appl. Electrochem.* **7** (1977) 531.
- ¹⁰⁵ H. Föll, *J. Electrochem. Soc.* **127** (1980) 1925.
- ¹⁰⁶ F. W. Ostermayer and P. A. Kohl, *Appl. Phys. Lett.* **39** (1981) 76.
- ¹⁰⁷ H. Tributch, *Faraday Discuss. Chem. Soc.* no. 70 (1980) 255.
- ¹⁰⁸ J. B. Goodenough, A. Hamnett, M. P. Dare-Edwards, G. Campet, and R. D. Wright, *Surf. Sci.* **101** (1980) 531.
- ¹⁰⁹ M. S. Wrighton, A. B. Bocarsly, J. M. Bolts, M. G. Bradly, A. B. Fischer, N. S. Lewis, M. C. Palazzotto, and E. G. Walton, in *Interfacial Photoprocesses: Energy Conversion and Synthesis*, Ed. by M. S. Wrighton, American Chemical Society, Washington, D.C., 1980, p. 269.
- ¹¹⁰ A. Ya. Gokhshtein, *Poverkhostnoe Natyazhenie Tverdykh Tel*, Nauka, Moscow, 1976.
- ¹¹¹ L. J. Handley and A. J. Bard, *J. Electrochem. Soc.* **127** (1980) 338.
- ¹¹² Yu. V. Pleskov and V. Yu. Filinovsky, *The Rotating Disk Electrode*, Consultants Bureau, New York, 1976.
- ¹¹³ B. Miller, S. Menezes, and A. Heller, *J. Electrochem. Soc.* **126** (1979) 1483.
- ¹¹⁴ T. Ambridge and M. M. Faktor, *J. Appl. Electrochem.* **5** (1975) 319.
- ¹¹⁵ O. V. Romanov, M. A. Sokolov, and S. N. Sultanmagomedov, *Elektrokimiya* **16** (1980) 935.
- ¹¹⁶ B. Miller, *J. Electrochem. Soc.* **127** (1980) 184.

- ¹¹⁷ G. H. Brilmyer, A. Fujishima, K. S. V. Santhanam, and A. J. Bard, *Anal. Chem.* **49** (1977) 2057.
- ¹¹⁸ A. Fujishima, Y. Maeda, K. Honda, G. H. Brilmyer, and A. J. Bard, *J. Electrochem. Soc.* **127** (1980) 840.
- ¹¹⁹ J. H. Richardson, S. P. Perone, and S. B. Deutscher, *J. Phys. Chem.* **85** (1981) 341.
- ¹²⁰ Z. Harzion, N. Croitory, and S. Gottesfeld, *J. Electrochem. Soc.* **128** (1981) 551.
- ¹²¹ A. B. Ellis and B. R. Karas, in *Interfacial Photoprocesses: Energy Conversion and Synthesis*, Ed. by M. S. Wrighton, American Chemical Society, Washington, 1980, p. 185.
- ¹²² V. A. Tyagai and O. V. Snitko, *Elektrootrazhenie Sveta Poluprovodnikami*, Naukova Dumka, Kiev, 1980.
- ¹²³ T. Iwasaki, S. Oda, T. Sawada, and K. Honda, *J. Phys. Chem.* **84** (1980) 2800.
- ¹²⁴ H. Masuda, A. Fujishima, and K. Honda, *Chem. Lett.* (1980) 1153.

Surface-Enhanced Raman Scattering (SERS)

S. Efrima†

*Department of Chemistry, Ben-Gurion University of The Negev, Beer-Sheva, Israel
84105*

I. INTRODUCTION

Surface-enhanced Raman scattering is a phenomenon where the cross section for Raman scattering for molecules adsorbed on some surfaces is enhanced by many orders of magnitude compared to the scattering cross section for the same molecule in the bulk—in solution, for example.

This phenomenon was stumbled upon in the quest of electrochemists for techniques which will allow identification of molecular species in the interphase and which will yield structural information on the molecular level.¹⁻⁴ The initial pioneering work was quickly followed⁵⁻⁷ by the realization that some unexpected behavior was being observed. Imaginations were immediately kindled and much work has been done and reported, most of which was directed to attempts to understand the mechanism (or mechanisms) responsible for the “giant” enhancements of the scattering seen.

In this review it is not the intention to deal with the past *per se*, so no attempt will be made to give an historical presentation of SERS. Rather, a description of the present state of experimental knowledge and theoretical understanding will be given with emphasis on the electrochemical systems studied. The aim is to

† Bat Sheva fellow

present a summary of the experimental results and a simple exposition of the theoretical models, having in mind physical insight rather than rigor. A second part of this review will be devoted to a discussion of possible ways SERS has been used and can be used for the investigation of interfaces and surface processes. We will see that though the main thrust of the field in the past was not in this direction, many interesting results pertaining to structure and chemistry at the interface have been obtained.

The growth of research in the area called today "surface-enhanced Raman scattering (or spectroscopy)" (SERS) has not been a regular one. One may compare it more to an irregular, almost chaotic, deposition from a supersaturated solution rather than to a smooth, epitaxial well-correlated growth. Many groups, from a variety of disciplines, have joined the SERS game in a very short time. This brought to the field the blessing of much interesting work in many different directions. However, this very same "dendritic" activity has led to much confusion and misunderstanding. An epitome of this situation is the very frequent use of the sentence: "... it is a common consensus that ... (... electrochemical pretreatment is an absolute prerequisite ...; or ... the short-range interactions are by far; or ... the major proportion ... originates from the large electromagnetic fields ...)," etc. From a careful screening of the literature, which will be presented here, it will become clear that, as yet, there is no general consensus regarding either the enhancement mechanism or some of the major experimental facts. The closest we are to some kind of consensus is in acknowledging the possibility that several mechanisms may be operative, and that the contribution of the "other" mechanisms (each from his or her point of view) is the minor one.

This review is not intended to put an end to the raging controversy. It is felt that we are still a (long?) way from fully understanding SERS. However, now that some of the dust has settled, it is time to critically review the work done and the theories proposed, and perhaps attain a state of better understanding of what has already been achieved. This article comes to complement and update the reviews already published⁸⁻¹⁹ and the collections of papers dealing with SERS.²⁰⁻²³

This review is updated to early 1984. At the time of proofreading, several excellent papers have appeared in print, which are not

reviewed here. However, by and large, they do not change the general picture of SERS as drawn here.

No doubt, the present author has his own private "consensus" which, in spite of his efforts, may inject itself into the review. In order to offset such an undesirable bias, as much as possible, and perhaps putting the cart before the horse, the author will state here his own conclusions and beliefs: "I am convinced that electric field amplification and enhanced emission near SERS-active surfaces due to resonating metal excitations (surface-plasmon polaritons, plasmonlike modes, shape resonances, or electron-hole pairs) is an active mechanism in most of the systems studied. However, in most systems, this contribution, though an important one, is minor compared to the total enhancement possible in SERS. The major mechanism, in my opinion, must be a resonance mechanism, in the sense of a resonance Raman process, i.e., a mechanism by which a part of the system (molecule, molecule-metal atoms, metal surface) becomes a strong scatterer by virtue of its large resonance polarizability and not as a result of strong fields exerted by the other parts of the system".

This review will emphasize SERS in the context of *electrochemical* systems. The liberty has been taken of including in this category work done on colloids suspended in (mostly aqueous) solutions. Colloids, anyway, have many common features with systems in electrochemistry. Thus SERS at the solid-electrolyte interface is the main question of interest here. Of course, one cannot ignore the work on other systems, nor does one want to. Therefore we will also discuss the other systems, such as various films in ultrahigh vacuum, in air or in tunnel junctions, on specially prepared lithographic structures, on metal clusters trapped in a noble-gas matrix, or on an oxide in catalytic systems, though they will not be at the main focus of this review.

II. SERS EXPERIMENTAL STUDIES

In this section we discuss in a critical manner the experimental evidence accumulated. Discussion of possible enhancement mechanisms will be given only in a later section, so that separation of facts and interpretation, can, as much as possible, be made.

Silver, being the most widely studied metal in the context of SERS, will play the leading role also in this section and in the entire review. Nevertheless, other metals and substrates will also be discussed. The other leading part is played by pyridine—the telltale molecule of SERS. Other molecules will also be discussed, a few in some detail, to introduce new or important behavior not shown by pyridine, or to substantiate some evidence for mechanisms of SERS.

1. Estimate of the Enhancement Factor

(i) *General*

There is no clear definition of what magnitude of enhancement entitles a system to be classified as a SERS-active system. In this review we will arbitrarily set the demarcation line for SERS at a 100-fold enhancement level. Any enhancement higher than that will be considered as SERS, while lower enhancements will be ignored. The reason for this limit is that it is within simple surface coverage effects (roughness factor) and “trivial” enhancements resulting from reflectivity of metal surfaces and possible orientation effects.^{24–26}

The estimate of the degree of enhancement in every one of our experiments is of prime importance for understanding SERS. First, the enhancement factors vary from system to system and that may reflect different contributions of the various possible mechanisms. Second, the sensitivity of the Raman systems has improved; thus, detection of a signal does not necessarily mean that an enhancement of four to six orders of magnitude occurs. Nowadays one can detect signals which are enhanced by a factor of only 100 to 1000 or less.^{27,28} The Raman scattering of dyes adsorbed on surfaces can be detected even without any enhancement at all.

There are four main problems which arise when enhancement factors are evaluated. The first problem is that we generally do not know the amount of material on the surface, especially in electrochemical, colloid, and thin-film studies conducted in the ambient or in solution. There are only a few studies which have used radiochemical techniques for electrodes^{29–32} or colloids.^{33,34} A few studies attempted to measure surface coverages from the

depletion of the concentration in the bulk solution in equilibrium with the surface.^{33,35,36} Such studies may give only a lower limit of the amount adsorbed, especially when the solid and liquid phases are separated in the course of the experiment. Electrochemical techniques are also used, such as reducing or oxidizing the adsorbed species,^{37,38} or also spectroscopical measurements.³⁷ In ultrahigh-vacuum (UHV) systems there are some independent techniques which may indicate the amount of material adsorbed by Auger,³⁹ XPS,^{40,41} and work-function techniques⁴¹ or by using the microbalance.⁴² Such methods, at times, yield information regarding the number of layers but not the amount in a layer.⁴³⁻⁴⁵

The second problem one faces when estimating the degree of enhancement is that the geometry of the SERS system is generally different than that of our reference system. The problem is that we usually cannot see a signal from the reference molecule adsorbed at a SERS-inactive surface of similar geometry, and we have to resort to a measurement at high concentrations in the bulk. This may introduce a large uncertainty in the evaluated enhancements. In UHV systems this is circumvented by comparison with thick layers of the same adsorbant, preserving the same geometry.⁴⁴ Also, in colloid systems, one can, in principle, measure the scattering of the reference in the bulk in the same geometry as that of the colloid measurement itself. However, in this case one generally needs very high concentrations which are detrimental to the stability of the colloid. An alternative, in this case, is to precipitate the colloid or measure a separate liquid sample. But then one needs to correct for the difference in transmittance between the colloid suspension and the clear supernatant or solution. This is the third difficulty in evaluating enhancement factors. It is also of importance for clusters trapped in matrices⁴⁶ and for arrays where the SERS-active metal overlays the adsorbed molecules.^{47,48} For weakly transmitting systems, the uncertainty in the enhancement factor can easily be an order of magnitude if special precautions are not taken.

A fourth, trivial, problem in the determination of enhancements, results from changes in relative band intensities of the adsorbed molecules. Generally, one compares the strongest bands. However, due to the (sometimes large) changes in relative intensities, the real meaning of such an estimate is not altogether clear. This consideration may add to the uncertainty another factor

of 2-5. Thus, at best, enhancement factors can be determined only to an accuracy of one order of magnitude or worse.

A potential difficulty is how to distinguish the signals from the surface and from the bulk in contact with it. It turns out that it is not a problem at all in most cases. The following criteria can be used, in part, or sometimes in full, to distinguish a surface spectrum from a bulk signal:

1. Band-frequency shifts occur;^{49,50}
2. The relative band intensities are different.⁴⁹
3. New bands appear in the surface spectrum.^{49,51,52} These may be vibrational bands of the adsorbed molecule which were weak or forbidden in the bulk^{51,53-55} or may result from chemical changes in the adsorbed molecule, such as, e.g., dissociation.⁵⁶
4. The excitation profiles are different.⁴⁹
5. The surface spectrum is generally depolarized while that from the solution often has a large polarized component (i.e., the depolarization ratio is small).^{5,8,57-60} In fact, using an analyzer which passes the depolarized component only is a neat way to discriminate against the scattering from the bulk in the experiment itself.⁶¹
6. Often using *p*-polarized incident light results in higher scattering intensities from the surface species as compared to *s*-polarization.^{58,62} This does not always work.⁸
7. A high continuous background is associated with the surface scattering.⁶³⁻⁸¹ A long list of references is given here as the continuum will not be discussed in this review due to space limitations.
8. In the case of electrochemical systems, a dependence of the signal on the electric potential may indicate a scattering from an adsorbed molecule;⁸² this may be a result of electric-potential-dependent adsorption and desorption, morphology changes of the electrode, an intrinsic dependence of the scattering process itself on the electric potential, and an electrogeneration of new species. In the latter case, one should consider the possibility of the creation of multilayers or the presence of products in the diffusion layer (which will give a detectable signal if they manifest resonance Raman behavior).

9. For cases of surfaces in contact with a solution, for instance, the concentration dependence of the surface signal is generally different than that of the signal from the bulk species.
10. The surface scattering from a molecule may be affected by the presence of other chemical species in a much different way from that of the same molecule in solution—for instance, the observation of strong dependence of the scattering of pyridine from a silver electrode on the presence and concentration of chloride ions (see Section II.3.(i) or the interdependence of the pyridine signal on the presence of CO coadsorbed on a silver film in UHV conditions^{83,84} or on the presence of cyanide anion in an electrochemical system;⁸⁵ to such a dependence one can add also the dependence on the pH.⁵²
11. Dye molecules adsorbed on metal surfaces generally show only a very weak fluorescence background.⁸⁶

An application of several of these criteria by Campion and Mullins²⁷ showed that the signal they saw was that of a normal scatterer, not the SERS effect. They observed unshifted frequencies, unchanged intensity ratios, linear dependence on coverage, and low depolarization ratios.

A word of caution: in addition to the uncertainties and problems discussed above, one should take note that all the enhancement factors quoted in the literature are merely average values. The average is over the total amount of adsorbed material, be it at submonolayer, monolayer, or multilayer coverages. If there are special SERS-active sites which are a small fraction of the surface, then the “true” intrinsic enhancement factor per molecule may be much larger than the estimated one. We should be aware of this fact when interpretation of results are considered in Section III.

(ii) *Electrochemical Systems*

The original observation and evaluation of the enhancement by Jeanmaire and Van Duyne⁵ inferred an enhancement factor of five to six orders of magnitude. Van Duyne⁸ has improved on that estimate by a careful study of the adsorption and scattering of pyridine compared to an internal reference—deuterated pyridine.

The surface coverage was determined from chronocoulometric measurements of 4-acetylpyridine, which gave 1.95×10^{14} molecules cm^{-2} on an electrochemically treated silver electrode. A special electrode allowed direct comparison of surface Raman scattering and that of the reference. The calculated enhancement factor was 1.3×10^6 . Schultz *et al.*⁸⁷ estimated the enhancement of pyridine scattering at an unanodized, mechanically polished silver electrode with 514.5-nm illumination to be $\sim 10^4 \times$. They based their estimate on the count rate of about 100 cps compared to a count rate of 10^4 cps they usually obtained from anodized surfaces for which they *assume* an enhancement factor of 10^6 . In their experimental results they show (Fig. 2 in their paper) spectra from 3 mm of a 0.5 M pyridine solution which is shown to be superimposed on the surface spectrum (Fig. 3 in their paper). *Assuming* a surface coverage of 5×10^{14} molecules cm^{-2} one can directly derive from these data an enhancement factor of ~ 2000 . If one corrects for the somewhat broader bands in the surface spectrum, a value of 3000 is obtained. Taking a lower value for the surface coverage brings this enhancement factor even closer to their estimates.⁸⁷ After roughening by electrochemical anodization the surface signal increased by a factor of 100 (not shown in the paper), indicating a total enhancement of 10^5 up to 10^6 . A similar work,⁸⁸ for pyridine on copper, using 647.1 nm illumination, gives a factor of 1700 for smooth copper and an additional factor of about 35 after electrochemically roughening the electrode, giving a total enhancement of 6×10^4 .

Albrecht and Creighton⁶ estimated an enhancement factor of approximately 10^5 , based on an adsorption isotherm and the scattering intensity from pyridine in the absence of the electrode. A near-grazing incidence and normal detection configurations were used, which are not the optimal for SERS. Powers of 15 mW were used! Hexter and Albrecht⁸⁹ have estimated the enhancement by measuring the Raman signals in an electrochemical system where the silver electrode was immersed in neat pyridine. Taking into consideration the collection geometry, the focusing of the beam, the surface coverage of pyridine (9×10^{14} molecules cm^{-2}), and a roughness factor of 3.5, they find an enhancement factor of 2×10^4 for 488-nm light. In this case, incidence was at the optimal 70° but the scattering angle was 90° which is not optimal. It is also not

clear whether chloride anions were present. They are known to increase the signals.

Busby and Creighton³⁷ in their investigation of 2-amino-5-nitropyridine (ANP) on silver found, using *in situ* electrochemical methods, which were corroborated by spectroscopical measurements, that an equivalent of many layers of ANP was adsorbed on the electrochemically treated surface. They find enhancement factors of 1.5×10^4 at 647.1 nm. If only the first layer was SERS active (which cannot be determined from this experiment), then the enhancement factor grows to $>10^5$.

Laufer, *et al.*⁹⁰ found for cyanide on copper no dependence of the Raman signal on the number of layers of copper cyanide, at least beyond 10 layers. They estimate an enhancement factor of 100–1000, or 10^4 if only a monolayer is assumed to give enhancement. A disturbing result in their report is an increase of the signal for decreasing wavelengths. This may indicate a bulk and not a copper surface species to be the main scatterer (see Sections II.4 and II.5 for SERS excitation profiles on copper). In this work a relatively large amount of charge was passed in the preparation stage, about 1.2 C cm^{-2} . This should be compared to $10\text{--}25 \text{ mC cm}^{-2}$ which is commonly used (see Section II.2(ii)). Finally, one should note that the electrode preparation consisted of anodization only, without reduction. This further indicates that one is not seeing a surface species but maybe a thick layer.

Bunding *et al.*⁹¹ report an enhancement of $10^4\text{--}10^6$ for methyl pyridines on a silver electrode at 514.5 nm. No detailed estimate is given. Billman *et al.*⁹² report enhancements for cyanide on silver on the order of $10^6\text{--}10^7$. They give no details except a surface coverage of $\sim 10^{15} \text{ molecules cm}^{-2}$, as reported by Bergman *et al.*²⁹ This high value is especially large considering the fact that both the incidence and scattering geometries are normal to the surface. Naaman *et al.*⁹³ studied enhancement of the scattering of pyridine, benzene, and cyclohexane on mercury (mainly a hanging drop); 514.5-nm light was used, with no control over the electric potential. For the electrode in contact with the saturated gas of each of the molecules, a large Raman signal was seen, about 10–20 times more intense than that measured from the gas alone. Assuming monolayer coverage and typical surface concentrations of $\sim 10^{14} \text{ molecules cm}^{-2}$, the enhancement is evaluated as 10^5 , taking into

consideration the volume of the gas contributing to the scattering. There is a high probability for multilayer formation at the pressures used (100–200 Torr), as acknowledged by the authors themselves. A control experiment was conducted with the electrode immersed in neat pyridine. The Raman signal detected was twofold more intense than that of the pyridine liquid alone. This was taken as evidence for the contribution of the adsorbed layer to the scattering. However, it may also be due simply to the beam being reflected from the metal and causing more bulk molecules to scatter. Introducing the electrode into the neat liquid may also easily result in slight geometric and illumination and light-collection changes, which could cause the factor of 2 or so in the measured Raman signal. Note also that there are no shifts in position or changes in intensity ratios of the bands between the electrode and the molecule in the bulk. Furthermore, the bands attributed to the surface do shift between the gas and the solution experiments, fully mimicking the spectra of the bulk. Similar remarks to these above are relevant to the experiments where the electrode was immersed in an aqueous solution and factors of 2 in the scattered intensities, compared to the solutions in the absence of the electrode, were seen.

Blondeau *et al.*³⁰ used radiochemical measurements in conjunction with Raman scattering. They find that the amount of adsorbed pyridine is the equivalent of several layers (based on the assumption of a coverage of 1.5×10^{-9} mol cm⁻², i.e., 9×10^{14} molecules cm⁻²). Even without almost any electrochemical treatment they see about two to three layers, while at typical conditions for SERS (25 mC cm⁻²) the equivalent of eight layers is seen. This, of course, decreases the values calculated for the enhancement factor based on monolayer coverage. For cyanide only a monolayer of Ag(CN)²⁻ ion is seen, emphasizing the large enhancement factors evaluated for this ion.

Tom *et al.*⁹⁴ reported 10^4 enhancement factors for pyridine on a 400-nm-thick film of silver, when the film was given a mild electrochemical treatment and a factor of 10^6 for the usual pretreatment. Their evaluation is based on a comparison with the scattering from the solution before the treatment, but they give no further details. Chen *et al.*⁹⁵ estimate the enhancement by comparing the scattering from neat pyridine at the same configuration as in their SERS studies. They assume monolayer coverage of 4×10^{14}

molecules cm^{-2} and state that they have accounted for the collection volume. They find an enhancement factor of 1.4×10^6 .

(iii) Colloidal Systems

Kerker *et al.*⁹⁶ calculated the enhancement effect for citrate adsorbed on a silver colloid, assuming a uniform size distribution of the colloid and a full-monolayer coverage of the citrate ions. They compared the signal to the intensity of the scattering from the solution in the absence of the colloid. They find values of $<3 \times 10^3$ at 350.7-nm excitation, 3×10^4 at 406.7-nm excitation, and $(3-6) \times 10^5$ in the excitation range of 457.9–647.1 nm. It is not clear how they corrected for the transmittance of the colloid suspensions. Also, taking a full monolayer of the charged anions may be an overestimate, though this is corroborated by a later study.³³ This requires extremely high charges on the 21 nm particles with no electrolyte to reduce the energy of the system. Thus it is probable that the enhancements are even larger than their estimate. A very thorough study of citrate colloids was carried out by this same group.³³ They have investigated several colloids prepared in various manners and have directly determined the amount of adsorbed citrate by radiochemical techniques. By comparison with an external standard and correcting for the absorption of the suspension (details not given) they find essentially the same results as reported earlier,⁹⁶ except at the longer wavelengths. For 647.1-nm excitation, they find 7×10^4 instead of 6×10^5 found before. For several of the preparations the estimated enhancement at 647.1 nm was lower—as low as 2000.

Suh *et al.*⁹⁷ investigated *p*-aminobenzoic acid (PABA) adsorbed on a silver colloid. They assume a specific uniform shape and size of the colloidal particles, from which they calculate a surface area. Then, assuming one-full-monolayer adsorption and estimating the focal volume from which the scattering arises, they deduce an enhancement factor on the basis of comparison with a solution of PABA. They find a value of 4×10^6 . They are well aware of the approximations and assumptions made and therefore claim this value is a lower limit to the enhancement factor.

Creighton *et al.*³⁶ estimated the enhancement of the scattering of pyridine from a copper colloid at 647.1 nm excitation to be

1.5×10^5 . This estimate was based on the determination of the amount of pyridine adsorbed by ultracentrifugation of the suspension and measurement of the amount of pyridine which remained in the supernatant solution. This, of course, assumes that the precipitation of the solid does not release any of the initially adsorbed molecules. Correction for the laser light absorption by the colloid was carried out, though no details are given. The comparison was probably made with respect to a solution of pyridine in a separate experiment.

Estimates of the degree of enhancement were carried out also on metal clusters supported on silica (and other) substrates. As an example, consider the reports of Krasser *et al.*^{98,99} who investigated CO, hydrogen, and benzene adsorbed on nickel particles. For CO in a 1:1 CO-hydrogen mixture they report an enhancement of about 10^4 as deduced from a comparison of the intensities at an exciting frequency which gave the maximum signal (457.9 nm) and at a frequency which gave only a very weak signal. For the 1:4 mixture that maximum was at 488 nm and indicated an enhancement of only two orders of magnitude. The precise meaning of these estimated enhancement factors is unclear. For benzene on Ni⁹⁹ a more detailed estimate of the enhancement was done. The surface intensities were compared to those from neat benzene measured with the same optical arrangement (as far as this is possible). A surface coverage was assumed (no details given) and, from the comparison of the Raman intensities, an enhancement factor of 500 can be obtained (the reported value of 2000 is probably a typographical error). These enhancements, therefore, are not classified as SERS in the present review.

(iv) UHV Systems

UHV systems provided SERS studies with the full power of modern surface techniques. These systems are in principle better controlled and characterized than electrochemical and colloid systems. Thus one can perhaps obtain good evaluations of the coverages and therefore more precise enhancement factors. Another important feature of UHV (and also of film) studies is the possibility of performing experiments where one goes in a controlled manner from submonolayer coverages to multilayers. This can give distance-

dependence information. One can also relatively easily insert spacers between the scattering molecule and the surface, again extracting the distance dependence of the SER effect.

An early effort in that direction was reported by Smardzewski *et al.*¹⁰⁰ In this study the absolute amount of the adsorbed molecules was not known, but there was a good control over the relative amounts, quoted in langmuirs (L). 20 L of perdeuteropyridine was adsorbed on a silver slug and its Raman scattering signal was registered (at 488 and 514.5 nm and after bombarding the surface with argon ions). Then, varying amounts of pyridine were deposited onto the substrate, and the joint Raman signal was measured (the spectra do not overlap and allow a convenient determination of both species simultaneously). The pyridine and deuteropyridine gave equal signals when the coverage of the pyridine was 5000 L, indicating an enhancement of 250 of the molecules closer to the metal over those which are further away. The authors also noticed that the scattering intensity of the perdeuteropyridine did not change between coverages of 5 and 20 L, which indicated an even higher relative enhancement of 1000. This number must also be a lower limit to the absolute enhancement. Similar results are obtained when monitoring the scattered intensity as a function of the amount of pyridine deposited directly on the silver surface. The intensity changes by a factor of 4 between 10 and 3000 L, giving a lower limit of the enhancement of 75. In a later study¹⁰¹ of pyridine on silver, copper, and gold films and single-crystal substrates, a monolayer coverage was assumed when the samples were heated to 230 K, above the sublimation temperature of pyridine (170 K). In this case, an overlayer of (estimated, no details) 10^4 layers of pyridine gave a signal above the detection limit, which was still 10-fold weaker than that of the first layer on pretreated silver. Thus, a relative enhancement factor of 10^5 is indicated. Again this is a lower limit of the enhancement, if the possibility of long-range enhancement is considered. On a sputtered silver single crystal, a 5500 nm-thick layer of pyridine (measured by interferometry) produced a signal two to three times as intense as the surface (frequency shifted) species. Depending on what one takes for the thickness of a monolayer, one can calculate enhancements of 10^4 to 2×10^4 . Rigorously, these are relative enhancements, relative to the thick layer. However, as in a separate experiment no bulk Raman signal

was seen from ~ 40 -nm thick layers; this is probably also the absolute enhancement.

Rowe *et al.*¹⁰¹ studied pyridine on silver roughened by a photochemical reaction with iodine in UHV conditions or, alternatively, electrochemically treated as usual for SERS and then sputtered. They determined surface coverages by Auger spectroscopy (disregarding possible damage to the adsorbed layer; Ref. 43). They found a monolayer has about 3×10^{14} molecules cm^{-2} and that corresponded to a break in the Auger signal *vs.* exposure plot at the 7- to 8-L range. They seemed to use this monolayer value for all their surfaces, smooth as well as rough. Thus they interpret the rise in the 991-cm^{-1} band (bulklike band of pyridine) up to an exposure of 18 L as evidence for a long-range enhancement effect. Alternatively, one may argue that on the rough surface with a reasonable roughness factor of 3 one has not yet completed a monolayer at this exposure. Furthermore, this study proves very nicely that extremely small coverages give exceptionally large signals—the 1006-cm^{-1} band is saturated already at an exposure of ~ 1 L, which is much smaller than a monolayer, even neglecting the roughness factor. This point seems to have been overlooked. This shows conclusively that only a small fraction of the adsorbed molecules can give most of the signal, at least for one of the adsorbed forms of pyridine on the surface in these systems. The form that gives the 991-cm^{-1} band shows a more gradual buildup of the signal, though also for it no real evidence for long-range enhancement is seen.

A further confirmation of this analysis can be found in the interesting study of pyridine and deuteropyridine on silver carried out by the same group.¹⁰² First, they showed that deuteropyridine, like pyridine itself, has two forms on the surface, with slightly different frequencies, at 962 cm^{-1} corresponding to the 991-cm^{-1} band of pyridine, and at 976 cm^{-1} corresponding to the 1003-cm^{-1} band. Then they deposited what they referred to as two monolayers of deuteropyridine on top of a “monolayer” of pyridine. The 976-cm^{-1} band of deuteropyridine did not appear, while its 962-cm^{-1} band was about twice the intensity of the 991-cm^{-1} band of pyridine. They interpret this result as evidence for the deuteropyridine being deposited on a complete monolayer of pyridine, with the same strong enhancement for the second and

third layers as for the first. However, clearly these results can be explained by the deuteropyridine being deposited on the bare metal side by side with the pyridine. In this case the 976 cm^{-1} would not appear as it was shown to saturate at extremely low coverages of either molecule. In addition, one should note that in the results reported¹⁰² there is only a very small change in the signals upon addition of deuteropyridine up to five "monolayers." This shows that there is *no* considerable long-range effect, but merely enhancement of the first monolayer or so.

Essentially similar experimental results were obtained by Pockrand and Otto⁴⁵ for pyridine on silver films, cold deposited. They find the 1006-cm^{-1} mode growing in at very small exposures and saturating at about 2 L. The 994-cm^{-1} band is initially much weaker but grows linearly with exposure (on a silver slug) up to 10^5 L. They interpret their results in terms of short-range effects for the enhancement, and special sites which produce the 1006-cm^{-1} band, which is also enhanced to a large degree. By comparing the 996-cm^{-1} band intensity at large exposures to the 1006-cm^{-1} intensity, an enhancement factor of $>10^4$ is evaluated. Pockrand¹⁰³ has corroborated these results, associating a monolayer in his system to 4.3×10^{14} molecules cm^{-2} or about 11 L. He, too, finds saturation at several langmuirs.

Sanda *et al.*,⁴⁴ in a UHV system, determined the surface coverage by UPS and find a saturation of the signal by the second layer, with some enhancement (about two orders of magnitude less than for the first layer) of the farther layers. One should note that the surfaces they used are smooth single crystals, with only a long-wavelength modulation. Signals from a smooth, unmodulated surface were undetectable, meaning in their system an enhancement of <500 .

Tsang *et al.*⁵⁴ used a similar surface with a grating profile. Using the estimates of Sanda *et al.* for the surface coverages,⁴⁴ they find large enhancements even at six layers. Note that they couple to the surface at the plasmon angle. Comparing to the scattering from a thick layer of benzene, they estimate an enhancement of only ≥ 500 and it is not clear how well the coverages are really known. For pyridine, a surface signal is not seen for less than about a "monolayer" unless some silver is cold deposited onto the grating surface. Then a frequency-shifted signal comparable in intensity to that of about five layers of the bulklike band (the present author's

estimate from Fig. 5 in Ref. 54) is seen. This signal does not change significantly in intensity between 0.5 "monolayer" and seven layers. There is no indication what happens at lower exposures; however, it is clear from the spectra given in the paper that this band saturates at low coverages and is about 40 times more intense than the bulklike band. Thus its enhancement is at least 2×10^4 . This enhancement is what is considered SERS in this review.

Eesley⁴³ investigated pyridine on a silver foil treated by argon ion sputtering. He finds that using Auger spectroscopy with 2–3 keV for monitoring coverages is damaging. Instead, he uses work-function measurements and finds a monolayer at about 4 L. This was confirmed by XPS studies.^{40,41} A saturation of the Raman signal for all the bands, 990, 1002, and 1032 cm^{-1} , is seen at about 0.5-monolayer coverage. Measurements were carried out up to 21 L, i.e., approximately five monolayers.

Bobrov *et al.*¹⁰⁴ find for ethylene on silver films in UHV that an exposure of 1 L leads to a monolayer, based on a kinetic theory estimate, assuming a sticking factor of 1. They see Raman signals already at exposures of 0.03 L which saturate at 2 L. By comparison to the scattering from a crystal of naphthalene (!) they estimate the enhancement as 10^4 – 10^6 (no further details are given).

DiLella and Moskovits¹⁰⁵ find that several butenes on a cold-deposited film of silver show a 2000-fold enhancement relative to a thick (about 200 layers) film of the butene on the same silver surface. This is judged on the basis of a comparison between a surface-frequency-shifted band and a bulklike band. DiLella *et al.*⁵⁸ also investigated CO on cold-deposited silver and found a 10^6 enhancement of the first (frequency shifted) layer compared to the thick overlayer with correction for geometric factors. This group summarizes their findings¹⁰⁶ where they discuss the unique behavior, in general, and enhancement, in particular, of the first adsorbed layer. They emphasize, however, that also more distant layers give enhancement (10^2 fold?).

(v) *Films in Air*

In a series of very elegant studies, spacer techniques were used by Murray *et al.*^{47,48,107} to probe the enhancement from various molecules on silver films. They conclude that large enhancements

are in effect even for molecules located 8–10 nm away from the silver surface and that there is a slow exponential decay of the enhancement upon moving away from the surface. They have essentially two types of experiments. One set uses a spacer, a weak Raman scatterer, poly(methylmethacrylate) (PMMA), to separate *p*-nitrobenzoic acid (PNBA) from a rough silver film. Though studies of possible penetration of the PNBA through the spacer were conducted, the possibility of a small percentage of penetration cannot be ruled out. It is even reasonable to perceive that the degree of penetration will depend (exponentially?) on the spacer thickness. It was already discussed in this review that a small amount of adsorbed molecules is enough to give enormous signals. Also, even though PMMA is a weak scatterer, it is not clear why under the long-range enhancement assumed, and considering the large thickness, it will not contribute to the Raman scattering (or perhaps it does?).

The second set of experiments studied the thickness dependence of the Raman scattering of a layer of poly(*p*-nitrostyrene) (PNNS) on top of which a silver film was deposited. No saturation of the signal was seen to about 40 nm. The authors once again infer a long-range enhancement. However, the possibility of changing the surface area of the silver overlayer due to the different texture of various thicknesses of the PNNS, and as a result the scattering itself, is not considered. Indeed, as the investigators state, the films are of irregular structure and are not easily controlled or well characterized, in spite of the efforts in that direction. These problems are reflected also in the difficulties one has in trying to estimate the absolute enhancements in these systems. Using a strongly model-dependent calculation and estimates of the extinction of the overlayers and the geometric parameters, values of 10^4 – 10^7 are reported. It is reasonable to summarize these studies by saying that they have indicated a possibility of large long-range enhancements; however, they have not excluded the possibility of a short-range mechanism being the main cause of the reported experimental results.

(vi) *Smooth Surfaces*

Another set of studies one should consider is those measuring the enhancement on smooth surfaces. The work of Schultz *et al.*,⁸⁷

which showed large enhancements for "smooth" silver surfaces, was already discussed here. Udagawa *et al.*¹⁰⁸ studied the Raman scattering of pyridine from a silver single crystal oriented in the 100 direction. The substrate was mechanically polished, then mildly sputtered in UHV conditions, followed by high-temperature annealing. The surface was clean under Auger spectroscopy (less than 0.5% impurities) and produced a clearly defined LEED (low-energy electron diffraction) pattern. Using Auger spectroscopy, a monolayer was associated with an exposure of about 5 L. The measured intensity from the 1004-cm^{-1} band was compared to the scattering from gas-phase pyridine at the same geometry setting. The size of the scattering volume from the gas, the area illuminated on the surface, and the number of molecules in one full monolayer (3×10^{14}) were estimated. Thus an enhancement factor of 440 was calculated.

There are four main uncertainties in this evaluation:

1. A monolayer coverage may be different than the assumed 3×10^{14} .
2. The intensity obtained for the 10-L exposure, from which the evaluation of the enhancement was done, may have been reached at lower exposures. As we have previously discussed, the signal often saturates at submonolayer coverages.
3. The scattering volume and illuminated area are only estimates.
4. *s*-polarization was used with both incidence and detection approximately normal to the surface. This highly disfavors scattering from smooth surfaces¹⁰⁹ (not very much from rough ones).

Correcting for the last point alone could increase the estimated enhancement by a factor of about 10–30, giving a total enhancement of 4000– 10^4 (see Ref. 26). Correcting for point (2) would give even higher values. Points (1) and (3) may change the estimated value both ways.

Tsang *et al.*¹¹⁰ have also measured the Raman scattering from pyridine on silver films using an optical multichannel analyzer (OMA). They find an enhancement of about 100 (no details are given as to how this was calculated and what was the geometry of the system). They attribute this enhancement to a "residual" roughness.

Campion¹⁰⁹ also measured the Raman scattering of pyridine from a smooth silver (111) surface by using an OMA. He optimized the geometry, incidence angle, and detection direction. No reference was used. The count rate was directly used to calculate a cross section. For that, assumptions were made regarding the coverage and the efficiency of the detection system was taken from independent experiments. The final score was virtually no enhancement. It should be noted that the spectra Campion recorded was identical to a bulk spectrum (no frequency shifts, no changes in intensity ratios, low depolarization values, linearity with coverage). This is not usual for SERS.

(vii) Summary

There are many other important studies of the degree of the enhancement and its distance dependence, some of which are discussed in various reviews.²⁰⁻²³ We have reviewed here a representative sample, which demonstrates both the results and the problematics related to their extraction. The following points represent a summary of the main findings:

1. Large enhancements are measured for the Raman scattering of molecules adsorbed on (silver) metal surfaces; common enhancement factors are 10^4 - 10^7 .
2. An extremely large enhancement is seen for the first monolayer or fractions of it, of about 10^4 - 10^5 .
3. The scattering from the second layer may be also enhanced, by factors such as 100 or so.
4. The enhancement on smooth surfaces seems to be small, though it can be as high as 10^3 or more. Further work on this point is clearly needed.

2. Surface Preparation

(i) General

From the very first studies of SERS,⁵ it was clear that the morphology of the metal substrate has a significant influence on the SERS activity, much larger than one would expect from the changes in area available for adsorption. Various preparatory

schemes were developed, some of which will be described below, which lead to giant Raman signals.

In spite of the large amount of work directed to the development of SERS-efficient surface morphologies and understanding their role, there is as yet, no general agreement, especially regarding the latter. Disregarding the present author's warning, one can safely say that there is *general consensus that roughening the surface affects the SERS activity, generally favorably (if one does not overdo it)*. However, there is strong disagreement as to the nature of the roughness required for large enhancements; directly related to the controversy over "the" SERS mechanism. We will refer to this question as the "scale-of-roughness" issue.

Let us, for convenience, distinguish between four types of roughness: (1) the atomic scale roughness (ad-atoms and small clusters); (2) the 0.5 to 10-nm range; (3) the 10- to 50-nm size range; and (4) the big structures (microscopic dimensions). The dimension given here is that of some typical dimension of the roughness feature, such as its diameter or height above the smooth plane surface. One should consider the limits given here only as a guide which will provide a framework for thought and understanding. The limit at 50 nm was chosen because that is when retardation effects start to be important, in the sense that fields emanating from different parts of the roughness structure are significantly out of phase with each other. At this size also the dipole approximation seriously fails. The second limit of 10 nm was chosen as that is roughly the mean free path of an electron in silver and also conventional electron microscopy has a resolution of that order of magnitude. Also, silver films at this average thickness begin to be continuous, instead of island films. Obviously, this limit is less sensible for metals other than silver. The lower limit is that of a small cluster or single atom.

Another question one may ask in the present context is whether a roughening pretreatment is an absolute requirement for SERS. Alternatively, one may ask what is the magnitude of SERS from smooth surfaces (as far as these can be produced), and what is the added enhancement upon roughening? We have already discussed this question and found that there is no unambiguous answer to it. The experimental evidence points to a small enhancement (below 100) on a smooth surface, but more work in this direction is required.

(ii) Surface Preparation in Electrochemical Systems

In order to obtain high-quality SERS on silver (as well as on other metals exhibiting SERS) the electrodes have to be electrochemically pretreated. As Schultz *et al.*⁸⁷ and others^{92,111} have shown, this is not an absolute requirement, but it certainly helps in producing extremely large signals.

The treatment generally begins with mechanical polishing with decreasing sizes of alumina (or equivalent). Then an etch with a mixture of ammonia and hydrogen peroxide¹¹¹ or with a solution of sodium cyanide and hydrogen peroxide¹¹² may be carried out. After a further wash with water, the electrode is immersed in the electrolyte solution, sometimes under cathodic potential control (-0.6 to -0.2 SCE). All the electric potentials in this review are referenced with respect to the standard calomel electrode (SCE), unless stated otherwise.

In the next step, an electrochemical treatment is performed, which is basically composed of two distinct stages—an oxidation of the electrode and a reduction. The treatment is therefore often referred to as the ORC—oxidation–reduction cycle. The name remains even though the second step is not always performed, and the treatment can also consist of voltage steps or current pulses instead of cycling the potential.

The ORC calls for a cycle of the voltage between -0.3 V or so, to about $+0.2$ V, where the silver is oxidized to silver ions. In the presence of chlorides in the solution, a layer of silver chloride is formed. On the return to cathodic potentials the silver is reduced back to the metal. In most cases, the charge is fully recovered, indicating a complete reduction of the initially oxidized metal. This holds true, of course, only within the accuracy of the measurement which is on the order of 0.1%. The amount of charge passed in this cycle is of major importance in determining the degree of enhancement of the Raman scattering. A charge of 20 – 50 mC cm^{-2} is optimal. At lower and higher charges, the Raman signals are generally smaller. This optimal charge corresponds to 100 – 200 layers of silver oxidized and then reduced. Upon reduction, a spongelike ultrapure silver surface is created, as determined from SEM studies,¹¹³ with submicron structures approximately ellipsoidal in shape. The true surface area increases by a factor of

~10–15; however, it may be that a large fraction of the adsorbed molecules are not exposed to the light, being shadowed by the deep crevices.¹¹⁴ Blondeau *et al.*³¹ have shown, using radiochemical techniques, that there is an eight-layer equivalent of pyridine on silver treated in the usual ORC. At very high charges, they find the equivalent of 100 monolayers, however, that is at charges $>50 \text{ mC cm}^{-2}$. Hupp *et al.*¹¹⁵ found from lead underpotential deposition (UPD) on silver that the surface roughness factor is only ~1.5–2 at 20 mC cm^{-2} . However, it is not clear that UPD will occur homogeneously on the whole rough electrode. A simple calculation shows that for the concentration of lead ions used and the sweep rates and potential scans employed an amount of about 40 nM lead, per 1 cm^2 *apparent* area, will reach the electrode by diffusion. A surface factor of 10 requires about 15 nM lead for full coverage of the surface. Thus, there is no large ion surplus in the solution to ensure full coverage, even neglecting local differences in ion concentration which can result in a further reduction in the amount of material available to the UPD. Consequently, the estimate for the roughness factor reported by this method is probably a lower limit. There is reason to believe, as will be shown below, that also small clusters and ad-atoms are prevalent on the surface following the electrochemical surface preparation.

The SERS usually, but not always, appears only after the reduction has begun and proceeded to some degree.¹¹⁶ The ORC can be carried out also by stepping the potential to the anodic region and stepping back after the proper amount of charge has passed.

Two types of ORC can be applied.¹¹⁷ The usual way is to carry out the pretreatment in the same solution where the SERS will be measured—the “internal ORC.” Alternatively, one may employ the “external ORC” where the ORC is performed in one solution and then the electrode is transferred to another solution with the molecule studied, or the solution is changed, or an additional molecular species is added. Dornhaus *et al.*¹¹⁴ have shown, for instance, that one could add pyridine after the ORC and still obtain the same intensity as in the “internal” method. Actually, the second “solution” may even be air.¹¹⁸ Blatchford *et al.*¹¹⁹ (see Ref. 39 in their paper) reported that washing off the chloride solution after the ORC still produced SERS from pyridine, following a gradual buildup of the signal.

Kunz *et al.*¹²⁰ found for silver in an azide solution that no ORC was needed to see a Raman signal. The spectrum appeared on the first positive scan as soon as the dissolution of silver began. They estimate that at the early stage of the dissolution, where the signal is already very large, there was not enough dissolved silver to form large structures. Therefore they feel the enhancement, in that case, was due to formation of special (perhaps, atomic size) sites.

Barz *et al.*¹²¹ found that stepping the potential to the region of rapid hydrogen evolution immediately prior to an ORC can result in a further enhancement of the SERS, by almost an order of magnitude as compared to an electrode subjected to ORC alone. They attribute this to an effect the presence of hydrogen bubbles on the electrode have on the surface morphologies created by the ORC. No identification of the precise structures was reported.

ORC was also used for other metals, with the appropriate changes due to the different chemical nature. Copper allows a less anodic sweep, 0 V is quite enough,¹¹⁶ while for gold one must go as high as +1 V or even higher.¹¹⁶

Marinyuk and Lazorenko-Manevich¹²² have shown that a full ORC is not really needed. They electrodeposited silver on a silver electrode and measured strong Raman signals, 100-fold more intense than from the "smooth" surface. The intention was to deposit submonolayer quantities, hopefully creating ad-atoms or small clusters (the actual quantity deposited is not given). Similar results were obtained by them for copper and gold (at 632.8 nm). They also found the spectrum to be stable, even after imposing negative potentials (less than -1.0 V) which are known to irreversibly quench ORC-induced SERS (see below).

Furtak *et al.*¹¹¹ went one step further and have shown that a SERS-inactive gold electrode probed with 514.5-nm light reveals an adsorbed pyridine signal (1008 cm^{-1}) band after one deposits on it submonolayer quantities of silver. The signal disappears after the electrosorption of the silver. They do not give any estimate of the enhancement, but one should note that the spectrum is not intense. From their Figure 2, one can infer a deposition of about 5×10^{14} silver atoms. For a 1-cm^2 electrode this means a monolayer; however, their electrode area is not given. In any case, monolayer or submonolayer quantities cannot form large structures, or even formations on a scale larger than a fraction of a monolayer, especially in this system.¹²³

A very interesting feature of the surface electrochemical preparation is its dependence on illumination. An early report saw no difference in the SERS whether the electrode was illuminated during the ORC or not.¹²⁴ Wetzel *et al.*⁶¹ noticed that illumination was needed during the ORC in order to obtain SERS from EDTA on silver. However, in the absence of the EDTA ("external ORC") illumination did not have any noticeable effect. Cooney *et al.*¹²⁵ suggested that photographitization may play an important role in SERS. Fleischmann and Hill¹²⁶ have proposed that photolysis of silver chloride during the ORC is instrumental in creating SERS-active sites. Macomber *et al.*¹²⁷ have shown that illumination during the ORC results in a 10-fold enhancement over the usual ORC enhancement. The illumination of the electrode during the ORC was especially effective during the reduction stage. They also showed this additional enhancement was apparent even in the absence of pyridine during the ORC. However, they found that the presence of a halide is required to obtain any illumination effect. They felt this indicated photoreduction of the silver halide, perhaps similar to photographic processes. Barz *et al.*¹²⁸ find similar behavior and also showed that the effect is frequency dependent. Green light seemed to be very effective while light of 647.1-nm wavelength was hardly effective at all. Chen *et al.*¹²⁹ again find the additional enhancement due to illumination. They also noted that under illumination, changes occur in the voltammograms, namely, less charge was passed in the reduction stage, indicating, perhaps, photoreduction. Using SEM the illuminated surfaces showed much smoother features than those seen on the areas not illuminated, but which went through the same ORC. Devine *et al.*¹³⁰ have also studied the illuminated surfaces using SEM. They find 200- to 800-nm particles on the irradiated surfaces. They report noticeable effects with a He-He laser and even with regular room illumination! Finally, we note that Fleischmann and Hill¹³¹ have seen illumination effects on the appearance and destruction of chemisorbed pyridine (associated with the 1025-cm^{-1} band); Mahoney and Cooney¹³² discuss metal damage as a result of the illumination; and Stacy and Van Duyne¹³³ report illumination effects.

The story of illumination effects is only at its beginning. Except for the close resemblance to photographic processes, we do not really know enough about the structural changes involved,

especially on the atomic and small cluster range. Further work will certainly be of great importance.

(iii) *Electric Potential Dependence of SERS*

After creating a surface which yields SERS signals, by the proper mechanical, chemical, and electrochemical treatment, one still has the electric potential of the electrode as an independent parameter. This capability is a unique feature of electrochemical systems (and less so of colloids). It gives another very powerful handle to affect and probe the metal-electrolyte interface.

The SERS spectra are all dependent on the electric potential, and both intensity changes and vibrational frequency shifts are seen. A special technique^{8,62,134,135} [potential difference spectroscopy (PDS) or potential modulated spectroscopy (PMS)] takes advantages of the potential dependence to obtain a high surface sensitivity. The electric potential also has an interesting influence on the excitation profiles (see Section II.5).

The electric potential can affect SERS in various ways:

1. By changing the amount of adsorbed materials.
2. By directly affecting the SERS enhancement mechanism itself, whatever that may be.
3. By influencing the structure of the adsorbed molecules.
4. By creating, through electrochemical reactions, new molecular species, products of the molecules initially put into the solution.
5. By changing the surface morphology which then can influence any one of the four factors enumerated above.

This last point is the reason why the electric potential dependence of SERS is included in this section, and the focus of the discussion will be on it. Note that such morphological changes may be associated with irreversible behavior as a function of potential, while one may expect a more reversible dependence for the first three effects. One should keep in mind that it is not always possible to determine which of these above points is operative in a given system.

Fleischmann *et al.*^{1,3} already in their early papers, have noticed the dependence of the spectrum of pyridine on the electric potential. A shift of the band positions to lower values for the more cathodic

potentials was explained in terms of the pyridine being displaced from the electrode by one layer of water. This interpretation was based on the fact that of the two prominent bands of the pyridine (the breathing modes), the lower one at about 1008 cm^{-1} was shifted to 1005 cm^{-1} at -1.0 V , a value identical to the vibrational band seen in an aqueous solution of pyridine. They, however, mention that the shift of the other strong band, from 1036 cm^{-1} to 1033 cm^{-1} , away from the value in solution, 1037 cm^{-1} , does not support this explanation. As we shall see, such interpretations are not straightforward. Fleischmann *et al.* also noted the appearance of a 1025-cm^{-1} band in the SERS spectra and its eventual disappearance at -1.0 V . At this potential all the SERS bands have decreased in intensity. The maximum of intensity occurs at about -0.6 V , which is anodic to the potential of zero charges (PZC) (at -0.95 V). On palladium hydride electrodes a similar behavior was found,¹³⁶ an increase of the pyridine signal up to about -0.6 V , and then an irreversible loss of the Raman signal negative to -0.7 V .

The irreversible loss of signal was noticed earlier by Jeanmaire and Van Duyne,^{5,8} who also reported that different modes had a different intensity dependence on the electric potential. However, all the modes gave a maximum signal at -0.55 to -0.85 V . An important experimental point to note is that such potential-dependent measurements should be, and were, carried out with a wide bandpass of the spectrometer, to allow for the shift of the band positions with potential.

Howard *et al.*¹³⁷ noted the reduction of "graphitic" Raman bands and a simultaneous appearance of bands associated with C-H stretch. At potentials negative to -1.2 V , the C-H bands also disappeared. This was explained in terms of the reduction of surface carbon into hydrocarbons and their subsequent desorption.

Furtak¹³⁸ reported similar behavior for cyanide as well. The Raman intensity maximized at -0.9 V , reversibly decreasing at more positive potentials, and irreversibly slowly decreasing in time. This was an important observation, because cyanide is more favorably adsorbed at the more anodic potentials. Thus, the SERS-intensity dependence is determined by factors other than the surface coverage alone. Furthermore, Furtak *et al.*¹¹¹ have also shown that the signal intensity from cyanide on silver is strongly and irreversibly quenched by potentials negative of -1.4 V . These results were found

also for thiourea.⁵⁷ In spite of its high dipole moment which shifts the PZC to potentials some 400 mV negative of its "usual" position, and its anionic nature in adsorption,¹³⁹ the thiourea produced maximum surface signals on silver at about -1.1 V. There was an irreversible loss of intensity for potentials negative of -1.4 V.

Benner *et al.*¹⁴⁰ followed the development and changes in the SERS of cyanide chemisorbed on a silver electrode as a function of the electric potential. They see a band at 2165 cm^{-1} appear at about -0.1 V, which is replaced by a band at 2140 cm^{-1} cathodically to -0.3 V. This band is eventually replaced by a band at 2110 cm^{-1} . These different bands are associated with AgCN , $\text{Ag}(\text{CN})_2^-$, and $\text{Ag}(\text{CN})_3^{2-}$ or $\text{Ag}(\text{CN})_4^{3-}$, respectively, on the basis of voltammograms and the position of the bands (see also Plieth *et al.*¹⁴¹). At slow sweep rates the cyanide anions have time to diffuse away from the electrode, so the higher complexes are not formed, as indicated by the absence of the relevant bands from the SERS spectrum. Dornhaus *et al.*¹¹⁴ followed in a similar method the development of the signal for pyridine, pyrimidine, and pyrazine on silver. The first showed the usual reversible dependence up to about -1.0 V, cathodic to which an irreversible quench of the signal took place. Pyrimidine was more sensitive to the electric potential, and exhibited the irreversible behavior already at -0.8 V. Pyrazine reaches its maximum of SERS intensity at -0.4 V and was irreversibly quenched at -0.7 V. Potential-dependent frequency shifts of the vibrational bands were also noticed. Benner *et al.*⁷⁴ have followed in a similar fashion the development of SERS bands on a copper electrode as the potential was changed, and associated the various bands seen with possible copper cyanide complexes and copper oxides.

Billmann and Otto⁸⁵ have shown that the potential dependence of SERS depends also on the presence of other constituents beside the Raman scattering molecule. Thus, pyridine produced a lower signal at -0.8 V than at -1.0 V in the presence of cyanide, while in its absence the inverse was seen. Similarly, the cyanide signal (at 2113 cm^{-1}) was higher at -0.8 V than at -1.0 V in the presence of pyridine, and vice versa in its absence. This behavior can perhaps be understood on the basis of competition of the two species over the available surface. The cyanide is more strongly adsorbed at the less cathodic potentials.

Wetzel *et al.*¹⁴² found that SERS of cyanide bands from silver shifted to lower frequencies when the potential changed cathodically to -0.9 V. The shift was of about 17 cm^{-1} for the 2111-cm^{-1} band and about 8 cm^{-1} for the 221-cm^{-1} feature (associated with the metal-cyanide vibration). The spectrum was irreversibly quenched for electric potentials more cathodic to -1.4 V, and showed a reversible behavior with potential up to this limit. Similar results were found for thiocyanate on silver, except that the point of irreversibility was at -0.9 V. The quench at -1.4 V for the cyanide was achieved in less than a second, indicating a fast process. Interestingly, after the quench, if silver cyanide was added to the solution at potentials anodic to -1.2 V, most of the Raman signal was recovered.

Weaver *et al.*¹⁴³ investigated thiocyanate on silver. They estimate the surface coverage by capacitance measurements (which should be considered only as an order-of-magnitude evaluation due to the inherent problems of measuring and interpreting double-layer capacitance of solid electrodes). They find that the thiocyanate saturated at the surface around -0.7 V (*vs.* Ag/AgCl electrode). Its surface Raman signal, though, increased from -0.1 to -0.5 V and strongly decreased at -0.7 V. Part of the decrease was reversible but for times on the order of hundreds of seconds a clear irreversible trend at -0.7 V was apparent. These authors also report frequency shifts ($20\text{--}30\text{ cm}^{-1}$) toward lower frequencies as the potential was changed cathodically. One should remark that not all the modes seen exhibited frequency shifts with potential: the CN and metal-thiocyanate did, while the CS stretch and the NCS bend did not. Does this indicate different adsorption sites with different adsorption configurations? This may be supported by the relatively large width of the bands seen (about 30 cm^{-1}), which may indicate inhomogeneous broadening.

Stacy and Van Duyn¹³³ report time-resolved investigation of SERS of pyridine on silver. They find that at -0.7 V and cathodic to it the signal decays in a biexponential manner, with characteristic times of the order of 0.1 s and tens of seconds. At -0.6 V there is a time-dependent increase of the signal which saturates with the longer time constant.

Sanchez *et al.*¹⁴⁴ studied piperidine adsorbed on silver. They find that the frequencies of most of the bands are independent of

electric potential; however, there are large variations in the intensities. Two groups of bands are noticed—one associated with symmetric vibrations, the other associated with antisymmetric modes. The SERS of the symmetric modes is maximized at -0.7 V, while the antisymmetric modes produced maximum signals at ~ -0.4 V. A rationalization based on the mixing between the modes of different symmetry under the influence of the electric field at the interface was proposed. It is not clear, though, why the different symmetry modes are grouped as they are. This interesting observation should be investigated further.

Hagen *et al.*¹⁴⁵ have shown for *p*-nitrosodimethylaniline (*p*-NDMA) that its surface Raman signal is maximal at -0.3 V and drops strongly for more cathodic potentials. However, it is not clear that this molecule, which is a resonance Raman scatterer, exhibits the usual SERS enhancement [see Section II.3(iii)]. Kotz and Yeager¹⁴⁶ have also reported the dependence of the frequencies of the vibrational modes seen in SERS of pyridine, pyrazine, cyanide, and *p*-NDMA toward lower energies for increasingly cathodic electric potentials. They present a comprehensive discussion of the various explanations proposed for this phenomenon, which is common in SERS, and also add the possibility of changes in the degree of back-bonding.¹⁴⁷ None of the interpretations is fully satisfactory and this point remains for further study.

Hutchinson *et al.*¹⁴⁸ presented interesting results of SERS of pyridine on silver, in contact with a nonaqueous solution of *N,N'*-dimethylformamide (DMF). They find strong signals at cathodic potentials as high as -1.9 V, thus correlating the irreversible quench seen in aqueous solutions with some property of water (perhaps its reduction, or specific interaction with the surface). In addition, the voltage dependence of the intensity of the three main bands (at 1007, 1024, and 1040 cm^{-1}) is strongly dependent on the mode. The 1024- cm^{-1} mode maximizes at -0.2 V, the 1007- cm^{-1} mode shows a minimum of intensity at -0.4 V and the 1040- cm^{-1} mode gives maximum scattering at -0.8 V. Furthermore, on addition of 1% water, this behavior changed dramatically, with all bands giving maximum intensity in the range -0.6 to -0.8 V. No changes in the frequencies themselves were detected.

The electric potential dependence of SERS of pyridine on a copper electrode was investigated by Temperini *et al.*¹⁴⁹ They find (with 647.1-nm excitation) that the bands seen exhibit qualitatively similar dependence on the potential. The behavior depended on the sweep rate. At low sweep rates (1 mV s^{-1}) the signal was constant in the range -1.2 to -0.9 V and decreased monotonously as the voltage was changed to -0.3 V . At a 10-fold-higher scan rate the SERS showed a maximum at about -0.7 V . The ratio between the band intensities did not remain constant, indicating a different quantitative dependence on the potential.

To summarize this section it was found that:

1. SERS intensities depend on the electric potential reversibly and also in an irreversible manner.
2. The reversible dependence cannot be explained on the basis of adsorption and desorption or chemical reactions alone but must reflect also some intrinsic dependence of the SERS mechanism on voltage.
3. The irreversible behavior in the cathodic region is probably a result of changes in the surface morphology. However, there is not enough independent evidence to determine the scale of the structure changes, for sizes smaller than about 10 nm .
4. Different modes may show similar or different behavior as a function of potential. In the irreversible region most behave in a similar fashion.
5. The dependence on electric potential is affected by the presence of different constituents and the solvent.
6. The Raman frequencies are often, but not always, a function of the electric potential, changing to lower energies when the potential is changed cathodically.

(iv) Surface Preparation in Colloidal Systems

The question of “surface preparation” in colloidal systems takes the form of colloid preparation and stability. Several questions are of interest:

1. How to produce the specified colloid with the specified molecule adsorbed on it?

2. What is the size uniformity (or distribution) of the colloid preparation?
3. Is there any aggregation and what are its characteristics and its effect on SERS?
4. How does one stabilize the colloid suspension and slow down time-dependent changes in its state of dispersion, or, alternatively, measure the SERS fast enough?

Some of the questions raised are longstanding ones in the field of colloid science, and they will not be addressed in any detail in this review. Synthesis of the colloids is generally performed (in the context of SERS) by reduction of the metal salt. Specific procedures are to be found in each of the reports which pertain to SERS on colloids. The adsorbed molecule for the SERS study can be present during the reduction stage and even participate in it (citrate on silver,^{33,96} for instance). Alternatively, the adsorption may be carried out after the reduction (pyridine on silver and gold,⁶⁰ for example). The later procedure often causes noticeable changes in the colloid, such as aggregation and precipitation.

There is some experience in preparing monodisperse colloid suspensions,^{150,151} however, most preparations reported in the SERS literature are polydisperse. Siiman *et al.*³³ have used separation methods to obtain suspensions of more well-defined particle-size distributions. The size ranges one often encounters are from a few nm up to several hundreds of nm.

The characterization of the colloids is carried out by several methods:

1. By UV-visible transmission and elastic scattering spectroscopy which can yield information about sizes¹⁵² and changes in it. This is a convenient *in situ* method, which, however, needs elaborate numerical handling to extract quantitative information.
2. By electron microscopy, usually TEM, which yields precise information regarding the distribution of sizes. The problem is that in preparing the sample for microscopy drastic changes may occur in it.
3. Chemical analysis is used to find the composition and quantity of the metal colloid.

Aggregation is a very common occurrence in colloid systems. Any slight change in the composition of the suspension can readily

cause aggregation and precipitation. Thus the colloids studied in SERS are often unstable and time-dependent effects are superimposed on the Raman results. One has to take special care to overcome this problem. One method is to work fast enough on the time scale of the changes in the colloid. An OMA is most beneficial in this respect. One may add stabilizers such as gelatin or agar-agar. Another method is to take advantage of the structural changes and monitor the SERS as a function of time, thus, hopefully extracting the dependence of SERS on the structure in one experiment. Blatchford *et al.*³⁵ studied such time changes upon addition of pyridine to a gold sol produced by the reduction of a gold salt by citrate. They noted a gradual change in the extinction of the suspension—the original band centred at about 520 nm slowly declined while a new band centered at ~ 670 nm grew in. In parallel, the elastic scattering at wavelengths larger than 700 nm grew and produced a band. TEM has shown that chainlike structures were appearing with larger and larger lengths and at the expense of the well-defined 12 to 18-nm spherical particles. Simultaneously, the Raman scattering from the adsorbed pyridine was monitored and showed a gradual increase in intensity, especially for excitations in the neighborhood of the long-wavelength extinction features. This demonstrates the dependence of SERS on the same parameters which determine the extinction of the long chains, i.e., plasmon excitation. Note, however, that the total additional enhancement at 700-nm excitation due to the aggregation is a factor of about 7, even though the number of chains has increased by orders of magnitude. (The present author is tempted to add that this indicates that the enhancement related to plasmon excitation adds, in a multiplicative manner, to a very large enhancement which is due to another, as yet unspecified here, mechanism. However, this is still the purely experimental section, so this remark should be crossed off the protocol!).

Creighton *et al.*³⁶ have measured SERS on copper hydrosols which underwent a slow aggregation affected by the addition of pyridine. Dynamic light scattering revealed a gradual growth in the particles in parallel to the buildup of an extinction band at about 570 nm. Again the SERS signal (evaluated to be enhanced 1.5×10^5 -fold) grew with time, using a 647.1-nm excitation. The total increase in the intensity between 5 and 25 min is large, a factor of

about 50, which may be connected to particle growth, or to the adsorption kinetics of the pyridine, or to both processes. It would be extremely interesting to try and separate these two processes, so that the connection to the colloid morphology and extinction can be carried out on a more rigorous basis.

In a unique experiment Wetzel *et al.*¹⁵³ determined the dependence of SERS of pyridine on a silver sol on the electric potential, which was maintained by a reversible redox system (europium +3, +2) added to the suspension. The relative concentration of the europium ions was maintained by means of an electrode whose potential was controlled with standard electrochemical equipment. They found that the ratio between the two main bands behaved similarly on an electrode and on a sol. Also frequency shifts were seen. They interpreted these results as indicating that the same SERS mechanisms are operative on the sol and in electrochemical systems.

Blatchford *et al.*,¹⁵⁴ in a similar experiment, controlled the potential of a silver sol with sodium borohydride. The effects they saw were correlated with UV-visible extinction measurements. They found that aggregation and disaggregation are important in the changes detected both in SERS and UV-visible spectrum. This would mean that the close resemblance to the electrode behavior seen by Wetzel *et al.*¹⁵³ may be fortuitous. Evidently, more work in this direction is warranted.

In principle, using colloids for SERS studies offers a unique opportunity to study size effects. Ideally, one may consider the colloid as a controlled and characterized "roughness feature without the surface," while in the usual electrochemical and film work one has a surface with a roughness which is generally not well defined. In practice, however, this goal has not been achieved yet.

(v) *Surface Preparation of Substrates in UHV SERS Studies*

In UHV conditions two main different substrates are used: vacuum-evaporated films and single-crystal or polycrystal bulk samples.

One can distinguish between several types of films which exhibit SERS:

1. Island films^{63,155-159}—formed when a small amount of silver is deposited on a substrate. Deposition of up to 8- to 10-nm average width of silver produces this system.
2. Cold-deposited continuous films^{72,75,77,160}, produced when more than about 10-nm-average-width silver is deposited on a substrate cooled to below -190°C .
3. Continuous films deposited on microscopically rough surfaces¹⁶¹ (generally at room temperature).

Smardzewski *et al.*¹⁰⁰ reported SERS studies of pyridine adsorbed on a polycrystalline silver sample treated by argon ion sputtering at 77 K. Prior to introduction to the UHV system, the silver substrate was polished using the mechanical treatment described above. Zwemer *et al.*^{39,101,102} have used iodine vapor illuminated by 488-nm laser light to roughen single-crystal substrates. Using Rutherford backscattering revealed ~ 50 -nm silver particles on the treated surface. For surfaces with larger particles (200 nm), the SERS was weaker by a factor of 10 as compared to the smaller size case. These authors also mention that electrochemical roughening (no details were given) was used to obtain SERS-active surfaces in UHV. In this case argon ion sputtering was used to clean the surface after introduction into the UHV system. A similar electrochemical treatment was used also by Eesley.¹⁶² Pockrand and Otto⁶⁹ mechanically polished their polycrystalline and single-crystal silver substrates and then ion sputtered them. The samples were cooled to 150 K. The polycrystalline sample showed strong signals of “carbonate” structures which reduced in intensity after annealing at 800 K. A single-crystal (110) face was initially annealed at 550 K and did not show any evidence for SERS. The inelastic scattering seen was attributed to thick layers of pyridine. Sanda *et al.*⁴⁴ prepared their single-crystal [(111) face] by mechanical polishing, followed by chemical etching in chromic acid and HCl which was then followed by several UHV sputter/anneal cycles. Finally, a 1000-nm periodic modulation was fabricated using lithographic methods. The completed system was again sputtered and annealed at about 500 K. Eesley⁴³ has used a silver foil, mechanically polished and then sputtered in UHV. He found (using SEM) 100- to 300-nm silver plateaus, between which there were smooth areas covered by silver balls of about 20-nm diameter and fewer balls of 40-nm diameter.

Silver island films are prepared by evaporation of an average thickness of about 10-nm silver on a substrate (quartz, for instance) and was described in detail elsewhere.¹⁵⁷⁻¹⁵⁹ The films are often characterized by their reflection or absorption spectra. Similar to the colloid case one can use Mie theory to understand the optical behavior of the films and its relation to their structure.¹⁵⁵ One can also use electron microscopy.¹⁵⁵ Bergman *et al.*¹⁵⁵ follow the development of a silver film as a function of the average thickness, and monitor, in parallel, also the absorption, the structure (using SEM), and SERS of adsorbed cyanide. They find that the film is composed of hemiellipsoidal islands which grow gradually with the average thickness deposited. The maximum of SERS (for 514.5-nm light) was seen for an average thickness of 6 nm, which gives silver islands of approximately 30 nm diameter. For other film thicknesses, the Raman signal could be as low as three orders of magnitude less than for the maximum. No corrections for difference in coverage of the various film thicknesses were reported. One would expect it to maximize at some intermediate thickness, as a compromise between the amount of silver deposited and its roughness factor. That, of course, would have to be taken into consideration when analyzing the dependence of the Raman signal on film thickness, and probably would result in a less steep dependence of the SERS on the film parameters than that given in the paper. However, without detailed knowledge of the cyanide coverage (or equivalently, the roughness factor) one cannot attempt any further analysis.

Seki⁴² investigated silver island films with pyridine, and found that at 10 K no Raman signal is seen, while warming up to 100 K and cooling back to 10 K, causes intense bands to appear. This indicates that close proximity to the metal surface is not enough for producing SERS. It seems that migration and attachment of the scattering molecules to specific sites is of prime importance for strong SERS in these systems.

The second type of films used in UHV studies of SERS are the films deposited onto cold substrates. Wood and Klein¹⁶³ evaporated silver (unknown thickness) on a copper substrate cooled to 78 K and detected a surface Raman signal at 2134 cm^{-1} (presumably, associated with adsorbed CO or carbonate) which was independent of CO pressure. That band was seen together with

Raman bands from bulk CO. After warming to room temperature this band disappeared.

Wood¹⁶⁴ focused on this phenomenon, by monitoring the film thickness, using a microbalance, and maintaining strict UHV conditions. The cold-deposited silver was deposited on a thick silver film previously annealed at room temperature, which showed no SERS (under the detection sensitivity, of course). Raman signals from adsorbed pyridine were detectable (at 180 K) only after about 15 nm of silver was deposited. This was interpreted as meaning that atomic sizes and small clusters are of limited importance in SERS, and that large structures [size scale (2) and (3) in Section II.2(i)] are dominant in SERS. Note, that no monitoring of the number of adsorbed pyridine molecules was carried out, and thus no corrections for increasing surface roughness were performed. Also, the Raman signal which is measured is relatively poor as compared to the noise. This may mean that the total enhancement is probably small and that small changes near the detection limit become magnified. Wood and Zwemer¹⁶⁵ have shown the utility of these films for detection of ethylene adsorbed on silver.

Wood *et al.*³⁹ compared cold-deposited films of silver (on copper at 100 K) to bulk-roughened surfaces (by a photochemical reaction with iodine). They found that the enhancement on the former was about 5 times larger than on the latter. They also found that with equal exposures to pyridine the evaporated films exhibited predominantly a first-layer enhancement, while the roughened surface showed comparable signals from the first and subsequent layers. These conclusions strongly depend on the absolute coverages on the surfaces and the relative coverages of the two systems studied, both of which are not known precisely.

Pockrand and Otto^{72,77} noted that pyridine on a silver film deposited on copper at 120 K, produced a very large SERS signal which was irreversibly quenched after annealing at 270 K, even though more pyridine was added to compensate for any desorption at the higher temperatures. This behavior was explained as an annealing of atomic-size roughness (ad-atoms and small clusters) at the high temperatures. They further noted that, as a function of temperature, SERS has increased up to about 210 K, while the elastic scattering continued to increase up to about 270 K. The high background seen in the spectrum also had a different temperature

dependence from that of the SERS. The initial increase of the SERS signal is explained as atom migration to steps to create SERS-active sites, together with a growth of the larger surface features, which contributes to the elastic scattering.

This annealing behavior is very similar in nature to the electrochemical "annealing" which produced an irreversible quench of the SERS when cathodic potentials were reached [see Section II.2(ii)].

DelPriore *et al.*¹⁶⁶ have shown that in film deposition, carbon and oxygen impurities may pose a problem, in fact, may cover most or all of the surface (however, Pockrand and Otto,⁷² for instance, have relatively small "cathedral" peaks indicating only slight surface contamination). Monitoring the Raman signal from the impurity bands, combined with SEM, DelPriore *et al.* conclude that strong SERS is seen with a surface roughness scale smaller than 10 nm (their resolution limit).

Results similar to those of Pockrand and Otto were reported for silver by Ladouceur *et al.*,¹⁶⁰ including the irreversible annealing of the silver. For gold and copper the Raman signal remained strong all the way to room temperature. Does this indicate an especially strongly bound pyridine to these metals?

Seki⁷⁵ has carried out a comparative study of silver where he had in the same UHV system an island film (7.5-nm average thickness) deposited at 300 K, a continuous film (30-nm average thickness) deposited at 150 K, and that same continuous film deposited on the island film. At 77 K the first substrate exhibits Raman scattering from pyridine about 10 times stronger than for the continuous film, while the film deposited on the island film showed a comparable intensity to the island films themselves (though not all the bands were seen). Annealing at 200 K and measuring the Raman scattering at 150 K produced an additional enhancement of 20 in the cold films, while the signal from the island films decreased considerably. This is in agreement with the annealing behavior found by Pockrand and Otto. Furthermore, temperature desorption studies (TDS) showed¹⁶⁷ that on the cold films a strongly bound species exists, which is absent on the island films and on a single crystal. Seki attributes this to the presence of cavities, with which he associates especially high enhancements. Albano *et al.*⁴⁹⁵ also discussed the role of pores in cold-deposited films. Mo *et al.*¹⁶⁸

investigated several silver films and found optimal enhancements for silver particles of about 100 nm.

(vi) *Preparation of Miscellaneous Surfaces*

For the sake of completeness, a few other systems which were studied for their SERS activity will be briefly mentioned. Some of these systems were discussed in other sections of this review.

Murray *et al.*^{47,48,107,169} have devised ingenious systems where they used CaF_2 to enforce the roughness. These systems were discussed in the context of range effects and estimates of the enhancement. Tsang *et al.*,¹⁷⁰ in an early paper, have also used the calcium fluoride base for a roughness promoter.

Krasser and Renouprez¹⁷¹ use catalytic systems where the metal clusters are deposited on silica or alumina oxides.

Hart *et al.*¹⁷² produce extremely interesting systems of silver evaporated on polymer microstructures formed by replication of lithographically formed silica surfaces consisting of a well-defined array of holes in a square lattice. Two other unique lithographically produced systems were investigated by Liao *et al.*^{173,174} These systems have the potential of controlling the local microscopic structure, which is very important for the elucidation of the enhancement mechanism.

Evaporated silver films on gratings at room temperature is another interesting layout. It was applied mostly by Tsang *et al.*^{54,170,175,176} As in an ATR (attenuated total reflection) configuration,¹⁷⁷ the gratings provide another controllable parameter of importance—the incidence angle.

Lyon and Worlock¹⁷⁸ produced a system where the behavior of silver islands could be gradually modified. They used a wedge silica spacer to separate silver islands from a graphite substrate. They found that the SERS enhancement decreased strongly as the silver was closer to the carbon. The total effect was of a factor of 300. The role of the graphite is believed to be to quench the silver (plasmonlike) excitations; thus an upper limit of 300 was believed to be found here for the role of these excitations in SERS.

Finally, the modified colloidal system of Goudonnet *et al.*¹⁷⁹ should be mentioned. They formed a system of roughly spherical

coated Teflon particles covered by silver. This offers the opportunity to study SERS in well-defined colloidal systems.

(vii) Summary

In Section II.2 it has been shown that SERS-active systems require a special surface preparation in order to exhibit large enhancements. The preparation consists of roughening the surface in some manner, or creating it already in a rough form. It is not entirely clear what sort of roughness is needed, and what is its scale. The experiments have not been sufficiently conclusive to satisfy everyone's taste. However, it seems clear that large-scale features (tens of nm) induce enhancements, though there are indications that they are limited to a maximum enhancement of two orders of magnitude, in most systems. Small-scale (atomic, small cluster) roughness was shown in many experiments to be of major importance for the extremely large SERS enhancements. The problem is that such small-scale features cannot be seen directly by present techniques, but their existence must be inferred from the temperature dependence, electric potential dependence, etc., of the SERS effect.

3. Some Molecules and SERS Behavior

A large number and variety of molecules have been studied in SERS and a good compilation was given by Seki.¹⁸⁰ As seen there, a large variety of molecules exhibit SERS: nitrogen containing, sulfur containing, aromatic, aliphatic, diatomic, polymers, ionic, neutral, large, small, chemisorbed, physisorbed, organic, inorganic, biological, symmetric, and nonsymmetric. Thus, SERS seems to be rather molecule general. Molecular species which have not shown SERS activity yet, may, under the proper conditions, scatter in an enhanced manner. A classical example for this is the water molecule (see below). This does not mean, of course, that all molecules are SERS active, nor that all the molecules already reported to exhibit SERS have indeed done so. It is clear that the nature of the molecule has an influence on the degree of SERS activity, probably an important one (see, e.g., Ref. 17). However, in this section we shall concentrate only on several selected aspects. Some of the other

aspects are discussed at different places throughout this review and some are to be found in the other excellent reviews published in the past.

Two groups of "molecules" will be discussed in some detail: (1) SERS of halides and their influence on SERS of other molecules; and (2) SERS of molecules which are in resonance with the exciting light, dyes. The former will be discussed primarily because of the central role of halides in SERS and also from the point of view of the utilization of SERS. Dyes will be discussed because they show some special features which strongly bear on the SERS enhancement mechanism. They also have not been reviewed in the past. In addition to these two groups, a specific single molecule will be discussed—the water molecule. It is presumed that no explanation for that choice is needed.

(i) *Halides and SERS*

The importance of chloride ions for SERS was realized in the very first studies.^{5,8} In fact, Jeanmaire and Van Duyne⁵ have studied the dependence on chloride concentration and found that optimal signals were obtained for a halide/pyridine concentration ratio of about 2. This is dependent on the method of surface preparation.¹⁸¹ The role of chloride ions in the ORC, essentially in facilitating the formation of insoluble silver chloride in the oxidation stage, was already discussed in Section II.2(ii).

However, there is the question of whether the chloride has any SERS activity of its own? The only possibility is, of course, that a metal-chloride vibration can be detected. This is of some interest, because, if seen, it would mean that SERS can be extremely useful for surface studies where molecule-metal bonds are created. Van Duyne⁸ has noted a Raman signal at 239 cm^{-1} at potentials positive of -0.4 V , which was "replaced" by a band at 216 cm^{-1} at more cathodic potentials. He associated the first with an AgCl vibration and the last one to an Ag-N stretch vibration. Creighton *et al.*¹⁸² have made similar observations. Bunding *et al.*¹⁸³ associated a similar band to a silver-lutidine vibration, and Venkatesan *et al.*¹⁸⁴ made similar assignments for a series of nitrogen-containing compounds. Venkatesan *et al.* have also tried to rationalize the strong dependence of the band frequency on the electric potential on the

grounds that the changing static electric field interacts to varying degrees with the dipole of the adsorbed molecule.

Pettinger *et al.*¹⁸⁵ have noted that the 240-cm^{-1} band appears in SERS even in the absence of pyridine. Hexter *et al.*^{113,186} have identified the low-frequency band as that of silver chloride and substantiated their assignment by a theoretical evaluation of the expected frequency.¹⁸⁷ Dornhaus and Chang¹²⁴ further showed that the 240-cm^{-1} band gradually evolves into the 216-cm^{-1} band as the electric potential is moved cathodically, thus establishing their association to the same vibrational mode. Marinyuk *et al.*⁷⁶ make a similar association, and remark that it must be a surface AgCl species. Wetzel *et al.*¹⁸⁸ substantiate this conclusion by replacing chloride by other halides. The vibrational band frequency dropped from 246 to 166 cm^{-1} for bromide and to 117 cm^{-1} for iodide, in rough correspondence to the square root of the atomic masses. This result was reproduced by Sanchez *et al.*¹⁴⁴ Does this indicate that the halide is attached to an atom which is an integral part of the surface, rather to an ad-atom?

Regis *et al.*¹¹⁸ see a shift of the band frequency from 233 to 180 cm^{-1} when changing from chloride to bromide. This is a relatively small change. Does it mean that their surface preparation and surface species are different (the spectra are recorded in contact with gas)? In fact, Regis and Corset¹⁸⁹ associate the 227-cm^{-1} feature to a vibrational mode of an anionic chlorine molecule radical. Various gold chloride complexes on a gold electrode, as seen by their Raman scattering, were reported by Loo,¹⁹⁰ but it is not clear whether it is a SERS or simply multilayer scattering arising in the anodic scan employed.

The low-frequency modes associated with the halides were seen also in colloidal systems. Wetzel and Gerischer¹⁹¹ found on a silver sol Raman features at 235 , 163 , and 112 cm^{-1} for chloride, bromide, and iodide. Garrel *et al.*¹⁹² monitored the replacement of chloride by bromide on a silver colloid.

The possibility of detecting metal-molecule vibrations in SERS has induced several studies in the absence of halides. Lombardi *et al.*¹⁹³ have investigated a silver sol and found for adsorbed pyridine a wide band at about 230 cm^{-1} . This band was not seen when acetate or formate ions replaced the pyridine, but, instead, an unresolved feature at slightly higher frequencies (260 cm^{-1}) appeared. They

infer that perhaps also in electrochemical systems there is a contribution from a metal-molecule mode beside the metal-halide. They also tabulate the frequencies seen in the presence of various nitrogen- and oxygen-containing molecules and conclude, on the basis of reduced mass considerations, that indeed a Ag-N or Ag-O mode is seen. They further suggest that one can differentiate between "direct" bonding to the surface as opposed to bonding to an ad-atom, on the basis of this analysis. Recently, Moskovits¹⁹⁴ has pointed out the limitations of this approach.

Loo,¹⁹⁵ basing his conclusion on a comparative study of the low-frequency mode on Cu, Ag, and Au, revived the assignment of this band to a metal-pyridine vibration. The arguments are:

1. A low-frequency mode appears for Cu, Ag, and Au at 241, 237, and 232 cm^{-1} , respectively, i.e., hardly metal dependent.
2. In the absence of pyridine, Cu, for instance, exhibits two bands at 273 and 203 cm^{-1} , which are "too" far from the 241- cm^{-1} band to be considered as having a common origin (similarly for gold).
3. The low-frequency modes in the absence of pyridine disappear at -0.8 V, while in the presence of pyridine the 241- cm^{-1} mode is strong.

These considerations, however, cannot exclude the possibility that a vibration of a pyridine-halide-metal (atom or surface) complex is responsible for the debated Raman feature. This would explain the shift of the frequency from that of a metal-halide frequency, the stability to cathodic potentials¹¹⁷ (and, perhaps, the relative insensitivity to the metal itself). One should mention in this context that Krasser *et al.*¹⁹⁶ reported a band at ~ 240 cm^{-1} in the Raman spectrum of pyridine-silver cluster complexes, which they associate with a pyridine-Ag mode.

This is an appropriate place to mention that besides the low-frequency bands associated with some adsorbed species, there are several other Raman features which are related to the (rough) metal itself. Macomber and Furtak¹⁹⁷ have reported weak and broad features at 160 and 110 cm^{-1} , which they associated with silver bulk phonon scattering. These bands, and, in addition, one at 73 cm^{-1} , have been seen earlier by Pockrand and Otto,^{72,77} in an UHV system.

Another very interesting inelastic scattering was found at the ultralow frequencies of several cm^{-1} . Weitz *et al.*^{68,198,199} noticed the Stokes and anti-Stokes wings of an extremely low-frequency mode. Its frequency depended on the excitation wavelength, and shifted from 4 to 12 cm^{-1} as the light was tuned across the visible range, from the red to the blue. The intensity also depended on the pyridine concentration, growing with it. It was seen on copper and silver and in an electrochemical system and at a sol. They attribute that feature to the inelastic scattering of particles (several tens of nm in size) off their acoustic modes. Fleischmann *et al.*²⁰⁰ also see ultralow-frequency modes at about 8 cm^{-1} , and report their dependence on electric potential and on the cation in the solution.

Returning to halides and their effect on SERS, Birke *et al.*²⁰¹ have investigated that influence for several molecules. They report that chloride affects the intensity of different vibrational modes differently, indicating proximity of the scattering molecule and the chloride. Further evidence for coadsorption of pyridine and chloride was obtained from capacitance and SERS measurements.^{115,202-204}

Halides are not the only chemical species which can influence the SERS of other molecules. Two other examples are CO coadsorbed with pyridine in a UHV system, as reported by Seki,⁸³ and the quenching effect of a small amount of Tl deposited on the surface.¹¹⁷ There are many other examples.

(ii) Summary of Effects

In this section it was shown that: (1) SERS is dependent on the chemical composition of the system, in addition to the dependence on the scattering molecule itself; (2) halides and pyridine seem to have a costabilizing effect and a coenhancing influence; and (3) one can utilize SERS to investigate the bond formed by the adsorbates with the surface.

(iii) SERS of Water

One of the most interesting molecules from the point of view of an electrochemist is the water molecule, which generally constitutes the major component of the solid-electrolyte interphase. Furthermore, it was a great puzzle why SERS from water was not

seen initially. When it finally was seen, the question still remains: Why are very special conditions needed? This, of course, has direct bearing on the SERS mechanism.

Billmann and Otto⁸⁵ have raised the question of the absence of the water signal from SERS. Soon after, several groups managed to see and report the SERS of water. Pettinger *et al.*¹³⁵ have used high salt concentrations (saturated NaCl or 10 M NaBr) in conjunction with potential difference spectroscopy, on a copper electrode. Alternatively, they used an emersion method. They have seen the OH stretch at about 3500 cm^{-1} . Fleischmann *et al.*²⁰⁴ using 1 M salt solutions found the OH stretch at 3498 cm^{-1} , with a noticeably smaller width than that of the analogous bulk water band. Also the water bend at 1610 cm^{-1} was seen. This is a clear indication that a water molecule is involved rather than a hydroxyl species. Pettinger and Wetzel²⁰⁵ found similar results. A further enhancement for water, as well as for pyridine and thiourea, by illuminating the surface during the preparation, was reported by Macomber *et al.*¹²⁷ and by Chen *et al.*¹²⁹ Pockrand,²⁰⁶ in a UHV system, detected Raman signals of water on cold-evaporated silver films. The stretch appears at 3127 cm^{-1} with a shoulder at 3355 cm^{-1} (a similar shoulder was reported also by the earlier workers). The bend was seen at 1611 cm^{-1} . As was noted by other workers the bend is much weaker than the stretch. Fleischmann *et al.*²⁰⁷ detected water SER signals also from 0.5 M cyanide solutions. They discuss a model of electrostatic attachment of water to cyanide in order to explain the shifted and narrow Raman features. At this point, it is not clear how appropriate such a model can be. Chen *et al.*²⁰⁸ have used an OMA to follow the development of the water signal during the ORC in 1 M salt solutions. Essentially, the SERS of water parallels the adsorption and desorption of the anions. Stronger signals were obtained when the anion was known to be specifically adsorbed (such anions also form insoluble salts with silver). Macomber *et al.*¹²⁷ show that the SERS of water is a strong function of the electric potential, the pH, and the concentration of the cations (noticed also by Fleischmann and Hill²⁰⁹). These two groups try to infer the interface structure, from the characteristics of the Raman spectrum. The reader is referred to the original papers for further details.

In general, the SERS of water is analyzed in terms of the structure-breaking nature of the various ions, solvation, and degree

of hydrogen-bond formation. Clearly, this is an important question which warrants further investigation. Blatchford *et al.*¹¹⁹ nicely summarize the reasons for not observing SERS of water under usual SERS conditions. Finally, let us note that according to Seki and Chuang,¹⁶⁷ pores may be of predominant importance in SERS. That, combined with the hydrophobic nature of silver and gold surfaces,²¹⁰ suggests another reason why water does not generally show the SERS effect and why high salt concentrations are needed.

(iv) *Surface Raman Scattering of Dyes*

As is well known,²¹¹ there is a qualitative and quantitative difference between normal Raman scattering (NRS) and resonance Raman scattering (RRS) for molecules in the bulk. The most prominent feature is the intense scattering in the resonance case, as compared to the scattering of a molecule not in resonance. In fact, the signals are so strong that extremely small quantities can be detected in the RRS case, even without the “help” of SERS (e.g., see Ref. 212).

In the early days of SERS, the studies were naturally directed toward molecules which were not in resonance with the incident light. However, a few sporadic investigations of the Raman scattering of dyes adsorbed in SERS-active systems were carried out. These were, generally, aimed at the study of some reaction of interest, or the study of some interesting molecular structure. Only in few cases was the experiment with the dye viewed in the context of SERS and SERS mechanisms. In all these cases it was enough to see that the signal was of “better quality” than for the bulk (better Raman/fluorescence ratios, lower laser powers needed, etc.) in order to proclaim it to be surface enhanced, without any further investigation. Only recently, since 1982, has it become apparent that dye molecules do behave differently than normal Raman scatterers with regard to SERS. Furthermore, this difference in behavior is directly related to the general type of enhancement mechanism active in SERS, and can, perhaps, be employed to elucidate it. At the time of this writing, there is still a heated controversy and a large degree of disagreement over the experimental results (as described below), and their theoretical interpretation in the context of SERS (to be described in Section III).

The aim in the following presentation is to discuss the published results on Raman scattering of adsorbed dyes, from today's perspective, and see whether a clear and unambiguous picture can be reached.

At the risk of triviality, the reader's attention is drawn to the fact that being classified as a dye does not necessarily mean that the molecule will exhibit resonance Raman scattering. A dye is a "homocentric" term used to describe a molecule which absorbs light in some part of the visible spectrum. A molecule may scatter light in a resonance Raman process provided the incident light is in the frequency range of its absorption band. Outside that band only preresonance or normal scattering occurs. This simple observation has been sometimes overlooked in the past, which warrants the remark here.

Jeanmaire and Van Duyne⁵ and Van Duyne,⁸ in their pioneering work, have reported SERS from two dyes, crystal violet and methyl orange, adsorbed on silver. They do not give an estimate for the enhancement, but remark that the surface signal was seen with 5-mW laser power! Compared to the signal intensities they observed for pyridine at 80-mW power, we may estimate the enhancement factor <10 . Correcting for the extinction in the solution may give a somewhat higher value.

Hagen *et al.*¹⁴⁵ studied *p*-nitroso-dimethylaniline (*p*-NDMA) on a silver electrode. *p*-NDMA exhibits a maximum absorbance at 435 nm. In solution it scatters resonantly at 488 nm, but the scattering is 10-fold weaker at 514.5 nm. This indicates that the excitation is very close to the absorption edge. On silver, at +10 mV (electrode pretreatment not specified) a surface signal is seen, which resembles, but is not identical to, the solution spectrum. It is difficult to evaluate the surface enhancement, as only scarce details are given. However, assuming the cross section area of the incident beam is given by A , the length from which the Raman signal in the bulk experiment is collected is given by L (approximately 1 cm), the concentration in solution is C , and the surface concentration at saturation is about 4×10^{14} molecules cm^{-2} , then the ratio between the number of molecules probed in the solution and on the surface turns out to be about $10^6 \times C$. Comparing Figure 1a and Figure 2c of Reference 145 gives an enhancement factor of 100. At 514.5 nm it is 1000. This is substantiated by the results on Pt, where approximately

10-fold-weaker signals were seen at 488 nm and hardly any at 514.5 nm. This enhancement is orders of magnitude smaller than the usual SERS enhancements. Note, however, that the usual SERS surface preparation has not been carried out (or at least reported). Also, such an analysis is very approximate.³⁷ Thus, our qualitative conclusions are:

1. A dye, which in this case is nearly out of resonance, can show surface enhancements.
2. The enhancements are smaller than the usual SERS enhancements on similar systems.
3. The enhancements, in this case, are larger the more the light is out of resonance with the dye.
4. The excitation frequency dependence of the scattering intensity for the adsorbed molecule is radically different than that of the molecule in bulk.

Kotz and Yeager²¹³ investigated cobalt phthalocyanine on a SERS-prepared silver electrode. Strong surface signals were seen, but no estimate of the enhancement was given. Reluctantly, we resort to the approximate analysis used above. Taking $C = 0.01 M$, one finds from the spectra given in this paper a 10^4 enhancement. However, the solution at $0.01 M$ is absorbing while in the electrochemical case $C = 10^{-5} M$. Thus this estimate is probably an upper limit. Note, the excitation wavelengths used are within the transmission window; thus once again the molecule is not fully in resonance.

Pemberton and Buck²¹⁴ studied the adsorption on a silver electrode of diphenylthiocarbazone anion (HDz^-), a dye with its absorption maximum at ~ 470 nm. An ORC was not carried out. Again, the enhancement was not evaluated. However, if one compares the surface spectra obtained, to those reported for a gold electrode²¹⁵ using 488-nm light, it is immediately clear that the Raman scattering is hardly surface enhanced at all on silver, as it is not, at least at this excitation, at gold.

Busby and Creighton³⁷ showed that 2-amino-5-nitropyridine anion (ANP^-) shows enhancement on a properly prepared silver electrode of a factor of 1.5×10^4 . This dye absorbs at 450 nm, but the excitation was at 647.1 nm, very much off resonance. Blatchford *et al.*²¹⁶ noted that the excitation spectrum of "ruthenium red" on the surface of a silver electrode (after ORC) was shifted to 600 nm,

while in solution it peaks at about 530 nm. This was compared to the maximum seen in the excitation spectra of adsorbed pyridine or that of chemisorbed cyanide at 600 nm. They do not give an estimate of the enhancement factor. Furthermore, the electric potential in this measurement was ~ 0 V, while for the pyridine and cyanide it was -0.95 V. As will be shown later, the SERS excitation spectra strongly depend on the potential, a fact that has to be accounted for in any comparison such as above.

Campbell and Creighton²¹⁷ discussed the excitation profile for several dyes adsorbed on a silver electrode. They analyze the data in terms of a *product* of two Lorentzians: one for the resonance enhancement (RR) and the other for the SERS. The *assumption* is that one can have both RR and SERS effects simultaneously. Their conclusion is that the excitation band of the dye on the surface is shifted compared to solution. The effect of the surface is indeed clearly seen. However, the same experimental spectra can be analyzed equally well also in terms of a *sum* of two Lorentzians, meaning that one has either RR or SERS effects. Only a careful estimate can distinguish between these two interpretations of the experimental results.

Cotton *et al.*²¹⁸ report a 10^5 enhancement factor for Cytochrome C adsorbed on a silver electrode, treated by the usual ORC. They do not give details of the estimate. One cannot use the simple scheme we used above in this case, as here are large protein molecules, with a much different surface coverage than that of small molecules. The Raman scattering of myoglobin was also measured, though no estimates of its enhancement were given. Cotton *et al.*²¹⁹ measured the surface Raman spectrum of an even larger protein, Cytochrome C_{dl} . They conclude that its scattering is enhanced similarly to that of the first two molecules. In all the cases, they note the dependence of the intensity on electric potential and the high depolarization ratios, indicating a surface species. However, unless long-range effects are considered, one would require the porphyrin moiety, which is the center of the resonant behavior, to be exposed to the surface, at very close proximity. This may be difficult to realize without denaturation of the proteins. The heme group in Cytochrome C is buried in the center of a nearly spherical protein, 3.4 nm in diameter, and in myoglobin it is in a crevice with a propionate side chain between it and the surface of the protein.²²⁰

Ohsawa *et al.*⁶² investigated the *n*-heptyl viologen monoradical cation adsorbed on a silver (not treated by ORC) and a platinum electrode. They find strong surface Raman signals on both electrodes, and can detect scattering for films as thin as 0.5 nm (judged by the charge passed to reduce the dication parent molecule). The excitation spectrum completely overlaps the absorption band. This is a good example of a resonance scattering seen on silver, without the SERS effect.

Cotton *et al.*,²²¹ studied meso-tetrakis (4-sulfonatophenyl)porphyrine, TSPP, and the 4-carboxy derivative, TCPP, adsorbed on silver. These molecules have a strong absorption at 420 nm and a weaker one at 514.5 nm. An intense surface spectrum was obtained for both molecules. Compared to the scattering intensity from the solid, the enhancement was estimated to be approximately 10^5 . The way that the absorbance of the solid was corrected for was not specified. Note also that at 457.9 nm the molecules are not entirely in resonance. The metalated form (suggested to be one of the surface components) is also not really on resonance at 514.5 nm. The long-wavelength absorption is a weak one. Furthermore, silver is not noted for producing large enhancements at 457.9 nm! This, of course, bears immediately on the spectra observed at 514.5 nm. Obviously, this point needs further clarification.

Itabashi *et al.*²²² also studied TSPP adsorbed on silver, from an acid solution where it is found as a dimer. While the details, dependence on electric potential, for instance, are different, they too conclude that the scattering of the dye is further enhanced by the surface. No details of the estimate are given. This molecule, in its aggregated form, absorbs light at 490 nm and the monomer at 434 nm. Using 488-nm excitation, they see no scattering at 0 V (*vs.* Ag/AgCl), while at cathodic potentials (starting from -0.1 V) strong signals are seen. They conclude that the scattering is enhanced, but do not give any estimate of the degree of enhancement.

Watanabe and Pettinger⁸⁶ estimated the enhancement of the Raman scattering of crystal violet (CV) adsorbed on a silver electrode. They report an enhancement of about a 1000, but give no details of their estimate, though they admit it is a rough one. They felt it could be even larger, in better agreement with the large enhancements reported previously,⁵ which only now we know are not "very large." Furthermore, they have noted that relatively

intense Raman signals from CV adsorbed on smooth silver electrodes are seen. This may indicate an upper bound to the enhancement factor on the rough surface, which is lower than their estimate. One should note that *s*-polarization was used, which is even more detrimental for the scattering from smooth surfaces than it is for roughened ones. The excitation spectrum found for the CV was very similar to that in solution.

McMahon²²³ showed that *t*-1,2-bis-(4-pyridyl)ethylene, (*t*-BPE), adsorbed on a silver electrode exhibits an excitation profile with a definite maximum at about 600 nm, and then increases again toward the red. The intensities were normalized to perchlorate ion scattering. These maxima have no counterpart in the solution absorption spectrum. This is a case of an off-resonance SERS effect.

Stacy and Van Duyne³⁸ studied the Raman scattering of tris(2,2'-bipyridine) ruthenium, TBPR, adsorbed on a silver electrode from an acetonitrile solution (another electrochemical SERS study reported recently is that in Ref. 224). They find that the surface spectra at 457.9 nm (when the molecule is in resonance) and at 647.1 nm (when it is totally out of resonance) are comparable in intensity. As an internal reference one may use the acetonitrile band seen in both of the spectra, assuming it is from the nonadsorbed solvent. At 647.1 nm, an enhancement $> 10^6$ is estimated. The conclusion must be that the enhancement at resonance is orders of magnitude smaller than at the off-resonance situation. An estimate of the difference is not given. An interesting point is that at 457.9 nm the Raman spectrum was identical in band positions and relative intensities to that seen in solution. At 647.1 nm there were large changes in the relative intensities of the bands and several new bands appeared. Another point of interest is that, as reported in the paper, no signal was seen before the ORC (with a solution concentration of $5 \times 10^{-5} M$). This indicates that: (1) this molecule is not a very strong resonance Raman scatterer, and (2) even at 457.9 nm there is some surface enhancement (if one considers 10 cps to be the detection limit, then an enhancement factor of about 250 can be estimated from the figures given in the paper). Further support to these conclusions is supplied by a study of the Raman scattering of TBPR adsorbed on a *n*-GaAs electrode with a silver island overlayer.²²⁵ No Raman signal at 457.9 nm is detected in the absence of the silver; thus point (1) above is substantiated (however,

it also may be that the dye is "baked" by the 100-mW power used, or photoreacted with the photoactive semiconductor). A clear signal is observed in the presence of silver (approximately two orders of magnitude above the detection limit, as judged from the spectra given in the paper). The silver can also protect the dye from a photoreaction.²²⁶

Now we turn to studies of dyes adsorbed on colloids. Lipitsch^{59,227,228} reported surface Raman spectra of several dyes adsorbed on a silver sol (methyl violet, biliverdine, pyrromethanone, and pyrromethane), and claimed they were enhanced, implying the usual large surface enhancement. It is difficult to carry out an estimate of the enhancement as the spectra in solution are dominated by the strong fluorescence.

Bachackashvili *et al.*^{49,229,230} have shown for a series of azo dyes adsorbed on a silver hydrosol that the enhancements were significantly different, smaller, than those exhibited by normal Raman scatterers. They circumvented the difficult problem of the evaluation of the absolute enhancement by *coadsorbing* a dye molecule and a reference molecule which is not in resonance, pyridine for instance. Thus only relative enhancements were determined, the dye compared to the reference molecule. Using competition of the two molecules over the surface they also could extract relative surface concentrations, which are required for the calculation of relative surface enhancements. This substitution experiment also showed that both molecules adsorbed to similar sites on the surface. They find that the reference molecule, pyridine, exhibits enhancements larger than 5×10^5 . Azobenzene, which is almost completely off resonance (maximum of absorption at 422 nm), shows a similar enhancement, perhaps up to a factor of a 100 less. Methyl yellow (absorption maximum at 447.1 nm) gives an enhanced spectrum by a factor of 300 less than coadsorbed pyridine. 4-dimethylamino-2-methylazobenzene (maximum at 453.5 nm) gives enhancement 1000-fold less than pyridine. Methyl orange exhibits an enhancement smaller by 3×10^4 . The scattering of methyl red (maximum of absorption at 515 nm) is enhanced 10^5 less than pyridine. Thus a clear trend evolves: gradually smaller enhancements the more the molecule's resonance. All this is in the presence of another molecule which exhibits the usual large surface enhancement. The excitation profiles of the dyes and the coadsorbed

pyridine are also fundamentally different. While the pyridine signal gains intensity toward excitation in the red, that of methyl red has a maximum around 550 nm. As the excitation profiles are measured simultaneously for both coadsorbed molecules, one can rule out morphological changes (aggregation) as a cause for the difference.

Lee and Meisel²³¹ investigated 4,5-benzoindotricarbocyanine, BICC, which absorbs in the red (one absorption maximum at 700 nm and the other at 800 nm). On a silver colloid they obtained an intense spectrum at 514.5 nm, at which wavelength the dye is a normal scatterer in solution. They also observe intense Raman signals at 647.1 nm when the dye is adsorbed on a gold sol. They do not estimate whether there is any further enhancement in addition to that due to resonance. Significantly, a copper phthalocyanine dye, with absorption maximum at ~ 670 nm, exhibited a weak Raman signal from a gold sol with 647.1-nm excitation, while in solution it produces intense spectra.

Siiman *et al.*^{34,232,233} studied dabsyl aspartate. On a silver colloid in ethanol and in water they report enhancement factors ranging from ~ 20 to 2000, at various wavelengths. This is based on experimental attempts to estimate the surface coverages.

Akins²³⁴ reported an enhancement of about 2000 for cyanine chloride when adsorbed on a silver sol. However, the dye absorption is centered around 530 nm, while for the Raman studies a 564-nm excitation was used, i.e., a slightly off-resonance situation. An absorption feature, not present for the dye by itself or the sol alone, was seen at about 575 nm. Akins interprets it as due to a dye aggregate. However, as will be seen in Section II.5, similar bands are commonplace in SERS systems. In a separate study, Li *et al.*²³⁵ tried to evaluate the enhancement factor for cyanine chloride at 488 nm (in the absorption band) on a silver electrode and on a sol. Their estimate is a factor of about 50 for the colloid and 10^4 on the electrode. One should recall the difficulties inherent in such determinations (see Section II.1).

Kneipp *et al.*⁴⁹⁴ investigated several cyanine and merocyanine dyes adsorbed on a silver sol. The absorption maxima of these dyes were 422, 557, 655, and 468 nm, and they used the 514.5-nm line of an argon ion laser. They found that all these dyes gave intense Raman surface spectra of comparable intensity. It is especially worthwhile to emphasize that the same intensity was registered for

the dye which was, more or less, in resonance and the dyes which were far off resonance. They also report that the dyes, also the dye which was on resonance, exhibited surface enhancements larger than unity. However, they do not report how large or give any details. Surface concentrations are also not reported.

Aroca and Loutfy²³⁶ report surface enhancement from phthalocyanine films with 15-nm silver overlayers. They estimate the enhancement at 1000, but give no details of their method of deriving it. Note, further, that the dye was investigated at a "window"²³⁷ of its absorption spectrum. The dye in a film absorbs at ~ 600 nm, while the surface studies reported were at 488 and 514.5 nm.

Several studies of Raman scattering of dyes from island films have been carried out. Chen *et al.*²³⁸ claim enhancement of fluorescein isothiocyanate scattering, at various wavelengths (at least over the fluorescent background). Full details are not given.

Weitz *et al.*^{239,240} have carried out a systematic study of the behavior of normal Raman scatterers and resonance scatterers on silver islands (incidentally, they also investigated fluorescence as well). They find an enhancement factor of about 1000, for rhodamine 6G and basic fuchsin, considerably smaller than that found for *p*-nitrobenzoate in a similar but not identical experiment. Their estimate of enhancement is based on a comparison with the Raman intensity of the same dye adsorbed on a silica slide, assuming the total coverages are equal. This last point is investigated by comparing the fluorescence from the silver-dye and silica-dye systems. They exhibit the same peak positions for the same preparation procedure. This was taken as evidence that, under similar conditions, both substrates have the same coverage, as fluorescence peaks shift with aggregation. However, this may only prove that coverages per real surface area are equal; the total amount of the adsorbed molecules may still be different. Actually, one expects the silver island system to have more adsorbed molecules due to its roughness. Consequently, the enhancement of 1000 is only an upper limit, and a factor of merely 300–500 would not be surprising. Anyway, this is in agreement with the results found with colloids. The excitation spectrum measured for R6G and for *p*-nitrobenzoate peaked at the same frequency, but the former was much narrower. Both profiles were on the long-wavelength shoulder of the

absorption band of the silver islands. For high dye coverages¹⁵⁷ the absorption band of the system was found to split, exhibiting maxima at about 440 and 590 nm. The Raman excitation profile also showed two peaks, this time very near the absorption peaks.

Nimmo *et al.*²⁴¹ measured the Raman scattering of copper phthalocyanine in pressed silver, KBr, Cu, and Al disks. This is a dye producing intense signals at concentrations as low as 10^{-6} M. The ratio of intensities measured for the four substrates was about 10: <1:1:2, respectively, which indicates (very) small enhancements for silver. Note, however, that the authors did not show that such silver disks exhibit SERS for normal Raman scatterers.

Shoji *et al.*²⁴² investigated a porphyrin and its complexes with silver. The dye is adsorbed to a calcium fluoride substrate and overcovered by silver. In the absence of silver no signal was detected, while in its presence a strong Raman spectrum was seen. This may be due to a surface enhancement, or to a degrading photochemical reaction in the absence of the silver. The degree of enhancement is not given, but judging from the solution and surface spectra, and considering the absorption in the solution, an enhancement factor of less than 1000, probably much less, can be evaluated.

To summarize, it was shown that:

1. Molecules at resonance show a significantly different SERS behavior than "normal" scatterers, especially as regards the surface enhancement.
2. The enhancement of the surface Raman scattering of dyes at their resonance (which may be shifted on the surface as compared to solution) is that of "normal" Raman scatterers.
3. The additional surface enhancement is greater the more the dye is out of resonance.
4. A dye "fully" in resonance exhibits a surface enhancement of up to about two orders of magnitude.
5. The excitation Raman profiles for adsorbed dyes are generally different from those for the dyes in solution, and from that of "normal" scatterers exhibiting the SERS effect.

4. Metals (or Solids) which Exhibit SERS

(i) *General*

It is often wondered whether SERS is a useful tool in the study of solid surfaces in general or, perhaps, it is only a unique property of silver and its family. In the latter case the utility of SERS would be greatly diminished. From the theoretical point of view it is also extremely interesting to know which solid substrates support SERS. This may be an important clue in elucidating the enhancement mechanism itself.

One should keep in mind several points when considering the experimental evidence for SERS activity on various solid substrates, in addition to the considerations mentioned in Section II.1:

1. SERS is strongly dependent on the excitation frequency, a dependence which varies from solid to solid (see Section II.5), and, in addition, for the same substrate, it depends on the surface preparation procedure adopted. Therefore, the practice is to scan for SERS activity throughout the visible range and the near UV, the classical domain of Raman spectral effects.
2. Merely detecting a Raman signal from a solid substrate surface does not necessarily mean that SERS is in effect. Weak signals can be detected due to the improved Raman systems, the larger surface areas on rough surfaces, multi-layer formations, and simple reflectivity considerations.
3. One is bound to find from time to time unique, specific systems where a special mechanism causes an enhancement of Raman scattering. Such a case, for instance, is probably the enhancement of the Raman scattering of oxygen on polydiacetylene.²⁴³ It is thought to originate from a charge transfer mechanism. In this review such systems will be considered SERS active only if several molecules (of different types) show an enhancement.
4. Negative results are generally not reported in the literature and when they are, no details are given. There is always the possibility that the proper experimental conditions were not achieved. As an example, detecting the Raman signal in a normal direction to the surface and using *s*-polarized

incident light discriminates against SERS, especially for a relatively smooth surface.

(ii) *Coinage Metals*

It is senseless to specifically list here the studies done with silver; they are referenced throughout this review. Work on gold and copper is also relatively abundant and full coverage of all pertinent references is not attempted here. To detect SERS from these metals, excitation in the red is required. A surface preparation, ORC for instance, is often needed, as described in Section II.2.

Gold and copper have generally shown weaker maximum intensities than silver. Several examples of studies on gold in electrochemical systems are to be found in References 116, 190, 195, 205, 244, and 245, and for colloidal suspensions see References 35, 60, 78, 191, 246, and 247. Work has also been done on gold films.^{73,79,160,238,248} Several studies on copper as a substrate were carried out in electrochemical systems (see Refs. 53, 88, 90, 116, 135, 149, 195, 205, 244, 245, 249, and 250), on a colloid,³⁶ and on films^{79,160,248} and clusters.^{251,252}

Furtak *et al.*^{111,253} have shown that a gold electrode which shows no SERS activity with 514.5-nm excitation (at least not within the detection limit), exhibits Raman signals from adsorbed pyridine when submonolayer quantities of silver are deposited on it. They note that under those conditions no changes in the optical properties of the substrate are detected. Plieth *et al.*,²⁵⁴ in a similar experiment, reported SERS for cyanide, but only after an ORC was carried out on the deposited silver. It seems that their deposited films were thick, contrary to the conditions of the previous experiment. A series of silver-gold alloys was investigated by Kester and Furtak.²⁵⁵ At 488- or 514.5-nm excitation, adding gold, strongly quenched the SERS signal of pyridine. Starting from gold and measuring at 647.1 nm, increasing the silver content slightly lowered the signal, which increased again as the limit of formation of pure silver was approached. Note that in this case potential difference spectra were reported, which may complicate the interpretation of these results.

Murray²⁵⁶ investigated the effect of gold layers deposited on silver island films on the SERS of cyanide. Gold island films did not support SERS of cyanide (within the detection limit of about

a 1000 enhancement factor) when 488-nm excitation was used. However, the gold-covered silver islands did exhibit SERS of a *gold cyanide* species. The signal decreased with gold thickness, between 0.05 and 1 nm. If one *assumes* a smooth coverage of the gold over the silver, this can mean only that the silver exerts a Raman enhancement effect at a distance (the thickness of the gold layer), and that this effect decreases with distance and perhaps with the change of the optical properties from those of silver to those of gold. Such a layer-by-layer deposition was indeed seen for gold on smooth silver single crystals or oriented films. However, the details of the deposition on the island films is not really known, and there is a possibility that gold starts producing structures of several layers in thickness before completely filling in the first layer. In that case, the Raman results can be explained on the basis of a short-range enhancement mechanism which enhances the scattering of a gold cyanide “molecule” on the silver, just as with pyridine. Thus, a complete layer of gold cyanide will quench the silver cyanide signal, as seen in the experiment at about 0.5-nm thickness, simply because there will be no silver cyanide. As the gold layer grows to 1 nm, cyanide will be too far from the silver to give an enhancement effect. There should be a smooth transition, as is seen in the gradual disappearance of the silver cyanide signal.

(iii) Other Substrates

Other metals have also been investigated as probable SERS-active systems. Platinum, the conventional electrode in many electrochemical studies, was studied by Cooney *et al.*,^{257,258} with electrogenerated iodine as the scattering molecule. Iodine is a resonance scatterer at 514.5 nm and, in addition, the surface was a rough one. Thus, it seems that this result does not indicate a SERS effect. (Is there a possibility that the 174-cm^{-1} band seen in this experiment belongs to a platinum-iodide surface “complex”? Some platinum iodides are insoluble.) As shown by Cooney *et al.*²⁵⁹ the large surface area of platinized platinum is in itself enough to produce (weak but detectable) signals. The authors also note that the intensity of the “iodine” scattering was not sensitive to a frequency change from 514.5 to 488 nm. Heitbaum²⁶⁰ measured the

Raman scattering from the product of the oxidation of phenylhydrazine adsorbed on a slightly platinized platinum electrode. The intensity is large; however, how much of it is the contribution from the solution species is hard to tell. Benner *et al.*^{81,140} saw SERS of silver cyanide from Pt electrodes only after several layers of silver were deposited on them. Loo^{82,261} reported iodine and chlorine SERS from a platinum electrode, even in excitation frequencies removed from the absorption band. He further notes that the excitation profile for coadsorbed iodine and triiodide ion are significantly different, suggesting that SERS is chemistry specific.

Benner *et al.*²⁶² found a small (less than 20) enhancement effect for platinum cyanide on a platinum colloid.

Krasser and Renouprez¹⁷¹ have reported SERS for benzene adsorbed on a dispersed platinum catalyst. They estimate the enhancement to be as high as 2000. This is based on the assumption that 1 cps corresponds to an enhancement factor of unity. They find that the enhancement increases toward shorter wavelengths, up to 400 nm.

Loo²⁶³ has measured Raman scattering from pyridine adsorbed on a cadmium electrode. Pettinger and Moerl²⁶⁴ could not reproduce these results. Loo⁸² has also measured the Raman scattering of iodine and triiodide on palladium. He found a very broad excitation profile, similar to the one he reported for Pt. Fleischmann *et al.*¹³⁶ reported SERS (about 10^4) from pyridine adsorbed on roughened palladium hydride, under very special preparation conditions, including the presence of CO. The intensity at 514.5 nm was higher than at 488 nm. Furtak and Kester²⁶⁵ showed that alloying silver with Pd quenches the Raman signal of adsorbed pyridine already at 5% palladium content.

Two studies^{93,266} report SERS for mercury; however, these experiments have not been repeated. It would be very desirable to have more data for this metal.

Sodium,²⁶⁷ lithium,^{106,268} and indium²⁶⁸ have been reported to be SERS active. In a series of papers, Krasser *et al.*^{98,99,269-271} have reported Raman scattering from CO and benzene adsorbed on high-surface-area Ni catalysts. Stencil and Bradley²⁷² obtained, under relatively high pressures of CO, Raman spectra from nickel single crystals. The spectra were very poor, of about 10 cps. The apparent enhancement factor is unreported. Borov *et al.*²⁷³ also see

acetylene on Ni films, but details of the intensities and coverages are not given.

Yamada and Yamamoto²⁷⁴ reported surface Raman scattering from pyridine adsorbed on sputtered films of Ag, Au, Ni, and Pt. The enhancements are not estimated. There is a strong background which is very steep at about 1000 cm^{-1} . The signal/background ratio in this region is small. Nickel exhibits the strongest spectrum of all! (at 514.5 nm; no signal at 600-nm excitation). In subsequent work,²⁷⁵⁻²⁷⁷ Raman scattering of pyridine adsorbed on evaporated films of Ni, Pd, and Pt was studied. Under SEM no roughness larger than 20 nm was detected. Surface pyridine signals are reported to be seen on all these metals, and judging from the excitation profile, their intensity is comparable to that measured from silver. Pt, Ni, and Pd had maximum scattering in the region 500–550 nm, while on Ag and Au the intensity increased with exciting wavelength. Signals of comparable intensity to that measured on the metals were reported also from single crystals of NiO and TiO₂! A weak scattering from pyridine adsorbed on carbon was also reported. In all these studies the signals were considered to be surface signals due to the measured frequency of $1004\text{--}1014\text{ cm}^{-1}$ which is shifted from the neat pyridine vibrational band at 993 cm^{-1} , and to the fact that the system was evacuated at room temperature to 10^{-5} Torr. However, note, for instance in Reference 275, that before evacuation a signal is seen at 1009 cm^{-1} .

Loo²⁷⁸ investigated Raman scattering of electrogenerated iodine on a titanium oxide electrode. He reports signals at 181, 190, and 360 (weak overtone) cm^{-1} . Also the anti-Stokes transition is seen. The signals were not seen at 488- or 514.5-nm excitation, but only for excitations between 530.9 and 647.1 nm. This strongly indicates resonance scattering. However, that of “free” iodine is at 515 nm, and the band gap of the oxide is 3 eV (415 nm). Thus one must conclude that the interaction of the iodine with the solid shifts the resonance to lower frequencies.

Another semiconductor, *n*-GaAs, was studied by Van Duyne and Haushalter²²⁵; however, it was found to be SERS active only after a deposition of a silver island overlayer. Furthermore, the molecule that was investigated was a dye at its absorbance wavelength. The silver can have a double role: (1) to enhance the scattering, just as it is done on a silver electrode; and (2) to protect

the dye from a destructive photochemical reaction with the incident laser light.

There are claims that also aluminum produces enhancements. Liao and Stern¹⁷⁴ saw Raman scattering of *p*-nitrobenzoic acid adsorbed on oxide-covered (~ 3 -nm thickness) aluminum ellipsoids, which was 500-fold weaker than exhibited on silver. The intensities on aluminum increased by a factor of 3 changing the exciting energy from 2.2 to 2.7 eV, though the optical parameters of aluminum are rather constant in this region. Lopez-Rios *et al.*²⁷⁹ also reported surface Raman spectra from (perhaps) molecular oxygen and carbon oxides adsorbed on aluminum in UHV conditions. No SERS of pyridine was seen.

(iv) Summary of SERS-Active Substrates

To summarize this section, the following points are pertinent:

1. The coinage metals are SERS active in all the systems investigated, provided a proper wavelength is used (for gold and copper, in the red).
2. Other metals have been studied far less extensively, and though there are indications that enhancements are possible, their general applicability has not yet been demonstrated.

One would like to see whether a given metal exhibits large enhancements in various systems (electrochemical, colloid, films, etc.) and for several different molecules.

5. Excitation Profiles

(i) General

Raman scattering, in general, and SERS, in particular, depend on the frequency of the incident light. Normal Raman scattering is characterized by a fourth-power dependence on the frequency. This introduces a factor of approximately 6 between 700 and 450 nm. Resonance Raman scattering in solution has an additional strong frequency dependence stemming from the frequency-dependent molecular polarizability. This generally leads to an excitation profile peaked at the neighborhood of the absorption band and strongly falling off for lower and higher frequencies. Changing the

frequency in a range of 100 nm may result in orders-of-magnitude changes in the Raman scattering intensities.

It was thought that measuring the excitation frequency dependence of SERS may supply unambiguous information which may then be interpreted in terms of a unique enhancement mechanism. In addition, such excitation profile studies could help in finding the best conditions for giant SERS effects, thus facilitating their utilization.

Several specific questions were of interest in such studies:

1. Is there any difference in the SERS excitation profile and that of the same molecule in solution?
2. How does the excitation profile relate to the excitations of the solid as seen in transmission or reflection absorption spectroscopies?
3. Are the SERS excitation profiles of various modes in the same adsorbed molecule different or similar?
4. How do the SERS excitation profiles of different molecules compare, especially for normal scatterers (in solution) in relation to resonance scatterers, e.g., dyes?

Points (1) and (2) above require determination of absolute behavior, in general, in two different environments. Points (3) and (4) call for relative behavior, which is easier to study.

In general, absolute intensity excitation profiles are not measured directly. One needs to correct for the accumulation, dispersion, and detection systems response at the various frequencies. These response functions can be measured and tabulated for future use. However, it is more convenient to use a reference signal to correct for that as well as for laser intensity variations and changes in the system configuration. In an electrochemical system one may measure simultaneously with SERS a Raman signal from a molecule in the solution which is present in a high enough concentration (such as perchlorate ion from the supporting electrolyte^{185,223} or perdeuteropyridine⁸⁸). In film studies an oxygen overlayer was used,²⁶⁷ for example, and in colloids the water signal was employed.²⁶² One can sometimes use the signal from thick layers of the molecule as a reference.^{58,106} In this case one generally assumes that the enhancement is short range.

Another possibility is to have the reference molecule in a separate cell, or an entirely separate experiment conducted just

prior to or after the SERS measurement.^{35,36,60,97,216} This is obviously less desirable. In the case of solutions or suspensions (as with colloids) a spinning technique may be used²⁴⁶ with the reference molecule in one-half of the cell in the absence of the colloid, separated from the colloid suspension located in the other half of the cell. This has the disadvantage of having to correct for the frequency-dependent transmission. Ideally, one would want the reference molecule to have a strong Raman band in the vicinity of those of the SERS-active molecule, but not overlapping, of course.

In some cases, such as for films evaporated on a base which is not SERS active, one may have a free base surface with the adsorbed molecules as a reference for the adjacent metal-covered surface.^{50,106} Though the real surface coverages may differ between the bare base and the metal-covered one, this poses no problem for the excitation spectra (except in extreme cases of highly adsorbing molecules). Of course, for the determination of absolute enhancement factors, this method should be used with caution.

A unique reference signal used sometimes in SERS, is the Rayleigh signal²⁵⁴ or the background continuum.⁸⁶ Normalizing the detected Raman intensity with respect to either of these reference signals corrects for detection response, geometry changes in the system, laser intensity, and even for surface roughness and transmission of the system. Correcting with respect to the Rayleigh scattering has the disadvantage of a very high signal which may call for inserting an attenuating filter between the sample and the entrance to the monochromator, or partially closing the slits. It also has the disadvantage that the normalization is carried out with respect to a frequency some 25–75 nm away from the Raman-shifted frequencies. Referencing to the background or to the Rayleigh scattering may normalize out many effects of the surface which are common to these surface optical processes. This may be a serious fault, especially if absolute behavior is of interest. Otherwise, it is a very convenient method.

(ii) Excitation Profiles in Electrochemical Systems

In an early paper, Pettinger *et al.*¹⁸⁵ measured the excitation profile of SERS together with the reflectivity for pyridine on silver single-crystal electrodes. The Raman profile showed gradual

increase of the signal as the excitation frequency was changed from 457.9 to 647.1 nm, by a factor of about 20 for the 1008-cm^{-1} mode and a factor of about 10 for the 1037-cm^{-1} mode. These profiles were normalized to a perchlorate internal standard. Thus, it is apparent that the SERS profile is different from the excitation behavior in solution, and that each mode has its own dependence. This is especially significant here as the two modes are very close in frequency and both are ring-breathing modes. The reflectance reveals a broad structure, peaking at 750 nm, with a shoulder at 650 nm. Both were absent in the absence of pyridine or before an ORC was performed.²⁸⁰ Thus, at least a circumstantial correspondence between the SERS excitation profile and the dielectric properties of the metal-molecule system was established. The results for the Raman excitation spectrum were measured also by Creighton *et al.*¹⁸² and corroborated by other groups.^{205,281} Tadjeddine and Kolb,²⁸² using surface-plasmon excitation dispersion methods, confirmed the reflectance measurements. Marinyuk *et al.*²⁴⁴ attempted to locate a possible absorption, by analyzing the ratio of Stokes and anti-Stokes scattering. They report a transition at about 650 nm. However, one should note that their analysis considers the frequency dependence to result only from the polarizability, and assumes that the dependence of other system parameters, such as metal reflectivity, is relatively weak.

Blatchford *et al.*²¹⁶ extended the frequency range to about 800 nm and found a maximum of the excitation spectra for adsorbed pyridine, cyanide, and triphenylphosphine. The maximum was at 600 to 750 nm and was somewhat molecule dependent. Replacing the solution by nitrogen gas, made apparent changes in the excitation profile for triphenylphosphine. The peak at 710–740 nm was broadened and in one experiment (out of the two reported) a shift to shorter wavelengths was noted (to about 630 nm).

A very interesting dependence of the excitation spectrum on the electric potential was reported by several groups.^{117,283–286} Otto *et al.*^{283–285} showed for pyridine on silver a gradual shift of the maximum of the excitation profile to higher energies as the electric potential was changed in the anodic direction. The shift was approximately the same for all the bands (1006 , 1215 , and 1594 cm^{-1}), except for the 623-cm^{-1} band which was more weakly affected. The shift is rather large, about $2\text{--}3\text{ eV V}^{-1}$. As shown by

Furtak and Macomber,²⁸⁶ the composition of the solution affected the slope of the maximum frequency/electric potential curves. Higher chloride concentrations resulted in higher slopes (though, perhaps still within the experimental reproducibility) and fluoride exhibited smaller slopes (1.46 eV V^{-1}). Furtak and Roy¹¹⁷ have shown that for coadsorbed chloride and pyridine, or chloride and thiocyanate, each molecule shows its own excitation potential dependence. Another interesting point was that the excitation maximum of one of the molecules was "reflected" in the excitation profile of the other coadsorbed molecule.

It is important to note in this context that electroreflectance measurements on silver electrodes (in the absence of pyridine) have found structures attributed to surface states, which were unusually and strongly dependent on the electric potential.^{287,288} Normally, we would expect the energies of species in the interface to change not more than the change in the electric potential. When these findings are further verified, they may turn out to be very important for understanding SERS and interface problems in general.

The excitation spectrum for SERS from gold and copper electrodes is characterized by a threshold behavior. Wenning *et al.*²⁴⁵ detected SERS of pyridine on gold and copper only at 647.1 nm, while at 568 nm no signal was seen (or a 200-fold-less-intense scattering was measured¹¹⁶). Chang *et al.*⁸¹ measured a strong copper cyanide scattering using 600-nm excitation, which was comparable in intensity to a signal from silver. However, below 575 nm the Raman intensity dropped below the background. Allen *et al.*⁸⁸ report a threshold for SERS detection of pyridine from copper at about 600 nm. Marinyuk *et al.*,²⁴⁴ using the measurements of the anti-Stokes transit as described above, estimated the existence of a transition at 1.77 eV for copper and 1.55 eV for gold, with adsorbed pyridine. Laufer *et al.*⁹⁰ found for copper cyanide a continuous increase of the intensity with decreasing wavelength, between 514.5 and 457.9 nm. As discussed in Section II.1, this result may be due to multilayer scattering. The frequency dependence of SERS on a silver gold alloy²⁵⁵ was described in Section II.4.

A unique frequency dependence was exhibited by the ultralow-frequency feature discussed in Section II.3(i) (see also Ref. 199). In this case the Raman shift itself depends on the excitation

frequency. The higher the excitation energy, the larger is the “vibrational” frequency. This means that changing the excitation causes a coupling to a different entity in the system with a different characteristic vibrational frequency.

(iii) *Excitation Spectra in Colloidal Systems*

Creighton *et al.*^{60,289} measured the excitation spectrum for SERS of pyridine adsorbed on a silver sol. It showed a clearly parallel behavior to that of the extinction of the sol. Following the addition of the pyridine, the colloid with an initial extinction maximum at 400 nm gradually developed a feature at longer wavelengths. This broad extinction peak shifted in time to lower and lower energies. The Raman excitation maximum overlapped with this “red” feature. One should note, however, that throughout these changes the peak at 400 nm remained, by and large. Wetzel and Gerischer¹⁹¹ stabilized their silver colloids, and found the 400-nm peak in the extinction. The excitation profile showed an increase toward the blue, in parallel to the extinction, but in opposition to the previous results discussed above. The reference was internal, pyridine in the suspension, which is “filtered” out by using proper polarizations at incidence and detection. This is a very efficient method to correct for absorption in the sample, besides the detection-system response. Kerker *et al.*^{96,290} found for citrate adsorbed on stable silver increasing SERS intensities toward the red, but an extinction band localized around 400 nm. In later work,³³ different fractions of a citrate silver colloid were investigated. All exhibited Raman excitation maxima at about 500 nm. Some preparations had low shoulders at 500 nm in the extinction spectra, others had only the main peak at 400 nm.

The gold sol of Creighton *et al.*⁶⁰ had a flat extinction response, but the SERS excitation spectrum was characterized by a threshold at about 570 nm, as seen for the electrodes. In a more comprehensive study³⁵ gold colloids exhibited a maximum of absorption at 520 nm, and when pyridine was added a band at longer wavelengths increased gradually and shifted to about 700 nm. TEM studies, conducted in parallel, indicated aggregation of some of the initially spherical single gold particles into chains. The Raman signal of

pyridine appeared with an excitation spectrum closely following the extinction. The absorption of the colloid was explained by dipolar coupling between adjacent gold particles, to produce a longitudinal plasmon excitation in the gold chains. In the stabilized gold sol of Wetzel and Gerischer¹⁹¹ the extinction spectrum retains the band at 520 nm, without any feature at longer wavelengths. The Raman signal of pyridine was higher at about 650 nm than at 675 nm. The citrate gold colloid of Mabuchi *et al.*²⁴⁶ had the usual strong extinction at 520 nm and a barely noticeable shoulder at about 700 nm. The Raman intensity increased from 500 to 670 nm. An external reference was used. Extinction losses were reduced by passing the incident beam close to the flank of the cell; however, this does not totally correct for the losses.

Von Raben *et al.*⁷⁸ investigated several gold colloids, one of which was especially stable and consisted of single spherical particles. The extinction spectrum for this colloid revealed only the 520-nm band; the other two colloids had a shoulder at about 700 nm. The Raman excitation in all the colloids was characterized by an onset at about 530 nm and large intensities at 700 nm. The intensities of the more aggregated samples were up to two orders of magnitude larger than that of the nonaggregated sample. In all cases, an external reference was used. It is not clear how corrections for extinction losses were introduced.

Recently, Creighton *et al.*³⁶ studied a copper colloid, using dynamic light scattering to characterize the size and size distribution. When pyridine is added, the colloid starts to change color and the light scattering shows aggregation processes. However, for up to about 6 min, the average particle radius is not significantly different from that of the colloid in the absence of pyridine (~30 and 5 nm—the two dimensions inferred from the light scattering). In that time the Raman signal of pyridine grows from a very low value to a value which is only five times smaller than the intensity after a long time. This induction time seems to be needed for pyridine adsorption, after which the colloid starts to aggregate, the main growth occurring in the next 6 min or so. The morphological changes bring about only a factor of 5 in the intensity change. Thus, the correlation of the Raman excitation spectrum to the extinction (which is associated with the morphological changes) is relatively weak.

(iv) SERS Excitation Profiles on Films

In this section, a few examples of excitation spectra of SERS on films are discussed.

Moskovits and DiLella^{50,106} measured the excitation spectrum of ethylene adsorbed on a cold-deposited silver film in UHV conditions. Using the Raman signal from a thick layer of ethylene as a reference, they find a monotonous increase of the SERS as one changes the excitation wavelength from 457.9 to 620 nm. In that region the signal changed by a factor of 11. The same behavior was seen also for CO adsorbed on a similarly prepared film. In a different experiment by the same group,⁵⁸ however, CO exhibited a sharp maximum of SERS at about 520 nm. The different behavior can, perhaps, be attributed to minute differences in the silver film. Yet another behavior was observed for CO on a silver film deposited at 120 K on a copper substrate.⁷³ A monotonous increase of the SERS by a factor of about 20 was seen when the excitation changed from 1.9 to 2.6 eV. Incidentally, for CO on gold an opposite behavior was observed. The measurements were corrected for the response of the detection system and the fourth power of the frequency. McBreen and Moskovits²⁹¹ found a broad feature in the reflection spectrum of silver films evaporated on cold substrates with a maximum at ~ 480 nm, which decreased and moved to higher energies with annealing. Thus, it appears there is hardly any correspondence between the optical properties of the film and the observed Raman excitation dependence in these experiments.

Bergman *et al.*¹⁵⁵ reach a different conclusion. They measured the absorbance, Rayleigh scattering, and Raman scattering from adsorbed cyanide on a silver film as a function of the average thickness of the film. A fixed wavelength of 514.5 nm was used. They find a broad absorption centered around 6.7-nm thickness, a peaked Rayleigh band with a maximum at ~ 8 nm, and a Raman band peaking at about 6 nm. The Raman intensity changed by a factor of 5 between 2-nm thickness and the thickness of maximum response. It is not clear whether a correction for the changes in the adsorbed amount of cyanide was made or whether the background was subtracted. Anyway, the authors show a dependence on thickness of their Raman signal and the imaginary part of the effective dielectric constant, calculated from the absorbance, using an

approximate approach. The correlation holds up to a thickness of 5.5 nm. This indicates some relationship between the dielectric properties of the film and SERS; however, due to the points mentioned above, it is not clear how rigorous this correlation is. Certainly, it does not prove any cause-and-effect relationship.

Seki^{75,292,293} found that the excitation profiles for SERS of pyridine on a silver island film and on a cold-deposited film are different and uncorrelated to the absorbance, which is also measured. For instance, CO on rough cold silver exhibits maximum scattering around 500 nm, while pyridine on a similar film (but not coadsorbed) scatters with maximum intensity at about 600 nm.

Pockrand *et al.*^{80,103,248,294} measured SERS excitation profiles for pyridine, oxygen, and ethylene adsorbed on "coldly" evaporated silver films. The reference was a thick film of pyridine adsorbed on a silver surface which was not SERS active. All the spectra maximized around 550 nm. However, it is noted that higher-frequency modes are characterized by maximum scattering at higher excitation frequencies. For instance, the difference between the excitation maximum of the 808- and 3000-cm⁻¹ bands was ~ 0.35 eV, i.e., 2800 cm⁻¹. These shifts are too large to be explained on the basis of optical response alone (see Ref. 294), considering the large widths of the excitation measured. The excitation maxima seem to shift to shorter wavelengths upon annealing. A correlation with measured reflectivity is carried out, and it is found that the Raman maximizes at wavelengths red to the absorption band.

Ladouceur *et al.*¹⁶⁰ find for "coldly" deposited silver, gold, and copper films an overall increase in SERS of pyridine at longer wavelengths, with gold and copper exhibiting a more pronounced behavior. Their reference is a thick layer of pyridine.

Tsang *et al.*¹⁷⁰ find for 4-pyridine-carboxaldehyde adsorbed on a rough silver surface in a tunnel junction layout, that the intensity is constant in the red to green region and strongly decreases in the blue. They use a Raman line of quartz as a reference, but that does not correct for the absorbance in the silver overlayer in this system.

Liao and Stern¹⁷⁴ show a relation of the Raman excitation spectra from silver and gold particle arrays to the same value (see Section III) calculated from experimentally determined absorption spectra.

In this context of excitation behavior and the relationship to the optical properties, it is important to mention the work of Demuth *et al.*,²⁹⁵⁻²⁹⁷ who found new transitions which did not belong to the molecules or the silver substrate alone, but to the molecule-silver surface system. Such transitions were found for pyridine, CO, oxygen, and ethylene. They were seen beside the (slightly perturbed) known transitions of the isolated molecules and the bare surface. These transitions were observed only when the surface was roughened. They were associated with charge transfer transitions. The justification for this assignment was the appearance of a transition for a CO-silver (cluster or atom) system at 3.1 eV compared to 3 eV on the silver surface. Also, for ethylene on a small cluster, a 2.25-eV transition was seen compared to the 2.8-eV transition on the surface. It is extremely difficult in these systems to provide more direct proof for the assignment to a charge transfer transition. An important point is that the experimental data are entirely consistent with the possibility that these new transitions are associated with only a small fraction of the adsorbed molecules.

Finally, one should note that there are many published papers that report the optical behavior of silver films²⁹⁸⁻³⁰⁷; these contributions will not be discussed in detail here, but the reader may find them helpful on the SERS journey.

(v) *Summary of SERS Excitation Profiles*

In spite of the sometimes conflicting experimental results, the four questions which were posed at the beginning of Section II.5 have been answered in full. It was unanimously found that the excitation spectra in SERS are significantly different than those of the molecules in solution. Even for the case of dyes it was found that the surface affects the profile. There is evidence that in many systems the SERS excitation profile does not follow the optical behavior of the system (as observed in absorption or reflection), let alone that of the bare metal. On the other hand, there are systems where such a correlation is apparent. At times the various modes of the same adsorbed molecule exhibit the same dependence on the exciting frequency, while in many other cases, different modes behave differently. The modes may be distinguished on the basis of the vibrational frequency (large, small) or their symmetry.

Various molecules exhibit in some cases similar dependence of their spectra on frequency, but more often than not they appear to have different behavior. This is especially true for resonance scatterers and normal Raman scatterers.

III. THEORETICAL MODELS OF SERS

1. General

In Section II it was shown that there is a large number of experimental studies of SERS phenomena. It is not surprising that there is also an abundance of theoretical models proposed to explain these results. Several excellent reviews^{10,12,16,19,20,308} and, in addition, some more specific papers (see, e.g., Refs. 21-23) have been published. The reader is referred to them for a more complete and rigorous presentation, or for a different point of view. The aim here is to present the theories in as simple terms as possible in order to facilitate comparison of their predictions with the experimental evidence. Also, an attempt is made to point out the strengths of each model and its limitations.

Just as the previous section dealt with experiment alone, trying to exclude theoretical interpretation, thus, in the present section, we try to discuss theory devoid of the experimental results.

Our theoretical sojourn begins with the following expression, which describes the intensity $I_D^s(\omega_s, \Omega_s)$ of the Raman-shifted light with frequency ω_s scattered in direction Ω_s :

$$I_D^s(\omega_s, \Omega_s) = K \text{Av}\{n_s |\mathbf{G}_s(\omega_s, \Omega_s) \cdot \mathbf{a}_s(\omega_s, \omega_i, \Omega_s, \Omega_i) \cdot \mathbf{E}_p(\omega_i, \Omega_i)|^2\} \quad (1)$$

It is given in terms of the local field acting on the scattering center, $\mathbf{E}_p(\omega_i, \Omega_i)$, which depends on the frequency of the incident light, ω_i , its direction Ω_i , and, of course, the characteristics of the system. The scattering intensity also depends on the (Raman) polarizability of the system, $\mathbf{a}_s(\omega_s, \omega_i, \Omega_s, \Omega_i)$, and on the propagator $\mathbf{G}_s(\omega_s, \Omega_s)$, which propagates the scattered light from the scattering zone to the detector. Finally, the measured Raman intensity also depends on the number of scattering centers, n_s . K is a constant, which depends on the frequency, essentially to the fourth power. The $\text{Av}\{\dots\}$ in

Eq. (1) denotes an average over all possible orientations and positions of the species which scatter the light. For instance, we may envisage molecules adsorbed on a heterogeneous surface, each sensing a local field, characterized by a polarizability and associated with a propagator, all of which may be position dependent.

The enhancement of the Raman scattering, R , is given in these terms by the ratio

$$R = (I_D^s / N_s) / (I_D^0 / N_0) \quad (2)$$

where N is the total number of molecules and the index 0 denotes a measurement in the bulk, characterized by \mathbf{a}_0 , \mathbf{G}_0 , n_0 , N_0 , and $E_p = E_n$, when E_l is the laser electric field. For a homogeneous field bulk system, to which we generally make reference, one remains only with the average over the orientations of a *single* molecule:

$$I_D^0 = \text{Av}\{|\mathbf{G}_0(\omega_s, \Omega_s) \cdot \mathbf{a}_0(\omega_s, \omega_n, \Omega_s, \Omega_l) \cdot \mathbf{E}_l(\omega_n, \Omega_l)|^2\} \quad (3)$$

In many cases in the SERS studies one does not have precise knowledge of the number of adsorbed molecules but only an estimate, \bar{N}_s . Consequently, an apparent enhancement factor will be calculated which is different from the actual enhancement by a factor $N_R = N_s / \bar{N}_s$. Obviously, if $N_R \gg 1$, then it will seem that there are surface enhancements. In the inverse case (special active sites) the real enhancements are higher than the apparent ones. In the following we assume that the surface coverage is known exactly.

Any one of the terms in Eqs. (1) and (2) can be different on the surface than it is in the bulk, and thus result in $R \neq 1$. For SERS, as considered here, $R > 100$ and, generally, $R > 10^4$.

The difference between the orientational averages in solution and on the surface can be the reason (or one of them) for the specific angular and polarization properties of SERS.^{24-26,309} However, it can affect the intensity only to an insignificant degree on the scale of the total enhancement. At the most it can cause an enhancement of $3 \times$ for a molecule with only one large Raman polarizability principal axis which is oriented perpendicular to the surface of a planar reflecting metal. Thus, for the sake of simplicity, we disregard the angular average and the vectorial properties of all the quantities involved.

Thus, one must search the three quantities G_s , α_s , and E_p , for the source of SERS. E_p and G_s are essentially electromagnetic in nature and can be obtained by solving the Maxwell equations with

the proper input of the dielectric properties of the various components of the system. Rigorous solutions can be obtained in many model cases. However, these solutions use (sharp) boundary conditions at the face of the solid, which may limit their validity very close to the surface, where a gradual transition from phase to phase is apparent.

The surface changes in the polarizability, α , can be due to electromagnetic interactions, or to “chemical” effects. By electromagnetic interactions is meant interactions given by macroscopic Maxwell equations, or their microscopic modification, when the adsorbed molecules and the substrate retain their own chemical identity and integrity. Chemical interactions involve some overlap of the molecular orbitals and those of the substrate.

One may classify the various proposed models in several ways. One way is to differentiate between models that focus on the role of the electric field E and the emission G terms (these two are related), on the one hand, and those that emphasize the role of changes in the Raman polarizability tensor, on the other. The former discuss the enhancement in terms of amplified fields, due to the presence of the surface, which act on the scattering molecule and its emission being further amplified by the surface. These are the local field and emission enhancement models (LFE). The difference between the various models which belong to this group is in the identification of the specific excitation in the solid which is responsible for the amplification: plasmon polaritons, shape resonances, electron holes, etc.

The second main group of theoretical models associates the SERS effect with a large intrinsic polarizability through a resonance mechanism (RE). The resonating species depend on the specific model and can be the molecule modified by the presence of the metal, the metal itself affected by the molecular vibrations, or some mixed molecule-metal states.

Another classification of the theoretical models can be based on the nature of the interaction: “electromagnetic” *vs.* “chemical” (for which we will be satisfied with the simplistic intuitive definition given above). Of course, one does not always have a clear delineation between these two types of interactions.

One should note that most of the theoretical models suggested are not mutually exclusive, at least not in principle. Thus, it is

possible that the real situation is a composite of several mechanisms. The exact blend is, at present, a matter of dispute. There is also the possibility that this blend changes from system to system.

2. Resonance Models (RE)

To this group belong several models of very different kinds such as the "image" model (RE-IE), the charge transfer (RE-CT) model, the electron-hole excitation model (RE-EH), and the Raman reflectivity model (RE-RF). These models have very little in common except that they all lead to enhancements by virtue of a resonance scattering mechanism. The validity of the last statement is not always realized by people, but it will be shown below to hold true.

An example of the models in this category is that proposed by Moskovits.^{310,311} He proposed that the SERS was a result of a resonance or preresonance Raman scattering, where the resonating moieties are the metal roughness features—the "bumps." The localized, plasmonlike states in these bumps are excited by the incident field, and the vibrations of the molecules which are adsorbed on their surface scatter as if they are in a resonating molecule. Moskovits showed that the characteristic frequencies of the excitations in small coinage metal particles should be in the visible, especially if interactions among them are considered. Thus the special role of silver, gold, and copper was stressed. Moskovits did not specify the mechanism that couples the molecular vibrations to the metallic bump. This mechanism can be any of those described below as resonance mechanisms. However, this same general outline can lead to SERS through enhancements of the local fields, which we classified as a LFE mechanism. This comes to emphasize the point that all the enhancement mechanisms suggested involve some type of resonative process. The difference between them is based on their major effect: large fields (and amplified emission) *vs.* resonance of the scattering center itself.

(i) Renormalization ("Image") Model (RE-IE)

One of the earliest models proposed to explain SERS was suggested and developed by Efrima and Metiu^{24-26,312-315} and also by King *et al.*³¹⁶ It is based on the classical theory of Raman

scattering and on classical electrodynamics. The main idea is that an excited (or virtually excited) molecule can be described by a classical oscillating electric dipole. It is induced by the incoming laser field. This dipole exerts fields on the surroundings. One component decreases as the first power of the distance and is the radiative, scattered field. The other components, the so-called near field,³¹⁷ decrease as the square and the cube of the reciprocal distance. They are extremely small far from the molecule, but can become exceptionally strong at close proximity to the molecule. This field is responsible for energy transfer processes such as the Förster mechanism. The oscillating dipole, near a surface, strongly polarizes the metal which exerts a field back on the molecule, which further polarizes it. The larger molecular dipole induces additional polarization in the metal and so on. The net result is a much larger induced molecular dipole than would be achieved in the absence of the highly polarizable surface. Such a large oscillating dipole scatters much more light which amounts to a measured enhancement. In molecular terms, as will be shown below, this self-polarizing effect means a shift of the molecular levels to attain a state separation which is, under certain circumstances, in resonance with the incident light. Thus the molecule which may be a normal Raman scatterer in solution turns into a resonance scatterer on the surface.

The simplest presentation of this mechanism starts from an expression which gives the induced dipole μ in terms of the total field E_T operating on it:

$$\mu = \alpha_0 E_T \quad (4)$$

where α_0 is the molecular *Rayleigh* polarizability, in the absence of the surface. The total field is composed of the incident laser field (perhaps modified by the surface) E_p and a field exerted by the induced polarization in the metal which is proportional to the dipole moment and falls off as the distance to the surface, Z , cubed:

$$E_T = E_p + \gamma\mu/(2Z)^3 \quad (5)$$

Here γ denotes a metal response function and the factor 2 was written in order to obtain the form of an image interaction. From Eqs. (4) and (5) one obtains:

$$\mu = \alpha_s E_p \quad (6)$$

with the surface polarizability α_s given by

$$\alpha_s = \alpha_0/[1 - \gamma\alpha_0/(2Z)^3] \quad (7)$$

In the absence of the metal, $\gamma = 0$ and $\alpha_s = \alpha_0$. However, in its presence, γ may be large so that the whole denominator becomes very small and the polarizability very large. This is what is generally called the image mechanism. In this form it amounts to calculating γ and checking whether it can be large enough and in the appropriate direction. γ generally has an imaginary part, which remains even when the denominator of Eq. (7) vanishes. This will determine the maximum value of the surface polarizability. For large enhancements, one needs small contributions of the imaginary part. This is also a matter of concern in all calculations of γ .

Before discussing calculations of γ , which is at the core of this mechanism, we show the equivalence of this model to a resonance enhancement mechanism. We take a simple form of the molecular polarizability,

$$\alpha_0 = (fe^2/m)/(\omega_0^2 - \omega^2 - 2i\omega\Gamma) \quad (8)$$

where f is the oscillator strength, e the electronic charge, m the electron mass, ω_0 a self-frequency of the molecule (an electronic transition frequency in a molecule in a quantum-mechanical picture), Γ the transition width, and ω the frequency of the exciting light. Inserting this expression for the polarizability into Eq. (7) one obtains

$$\alpha_s = (fe^2/m)/[\omega_0^2 - \omega^2 - 2\omega\Delta_s - 2i\omega(\Gamma + \Gamma_s)] \quad (9)$$

Here we defined the surface shift Δ_s and the surface width Γ_s as the real and imaginary parts of $(fe^2/m)\gamma/(2Z)^3$, respectively. In the absence of the surface, the resonance condition is attained for $\omega = \omega_0$. On the surface, the resonance condition is approximately

$$\omega = \omega_0 - \Delta_s \quad (10)$$

and the total width has increased by Γ_s . This establishes the connection between the "image" model and a surface-induced resonance Raman process. Incidentally, such a picture was developed even prior to the discovery of SERS by Philpott,³¹⁸ and enhancements were predicted assuming increased widths (not shifts).

The Raman polarizability will be obtained from α_s by differentiating with respect to a vibrational coordinate Q , which gives the leading term in the scattered intensity

$$I_D^s \sim |\alpha_0|^2 / [1 - \gamma\alpha_0 / (2Z)^3]^4 |\partial\alpha_0 / \partial Q|^2 \quad (11)$$

Efrima and Metiu,²⁴⁻²⁶ and King *et al.*³¹⁶ suggested that γ could be calculated on the basis of reflection from a plane metal surface. They find

$$\gamma = 2(\epsilon_M - \epsilon_S) / (\epsilon_M + \epsilon_S) \quad (12)$$

Here ϵ_M and ϵ_S are the frequency-dependent dielectric constants of the metal and the solution, respectively. Using known pyridine polarizability and silver dielectric data,³¹⁹ large enhancements could be obtained (up to 10^7). In terms of the molecular picture, a several-eV decrease of level spacing was involved. This shift, however, strongly depends on the frequency, through the dielectric constant of the metal. This is a dynamic shift and the resonance is really a joint metal-molecule-photon excitation. This is different from a shift of levels under static fields. This point has often been misunderstood.

The consequences of this model are:

1. For realistic molecular polarizabilities a close proximity to the surface is needed. For a normal Raman scatterer, generally only first-layer enhancement is expected (as seen below, roughness can increase this range to 1-2 nm); for a preresonance scatterer, the effect can be at longer distances, however, the enhancement will be smaller than for a NR scatterer.
2. No further enhancement is expected of a molecule which is already in resonance. This is a common feature of all RE mechanisms.
3. Coinage metals will support SERS at appropriate frequencies, due to their dielectric properties. Silver is especially good due to the relatively small imaginary part of the dielectric constant. Other metals may be SERS active, Hg for instance, especially for preresonance scatterers (i.e., when the polarizability is already relatively large).
4. The excitation spectrum should be strongly related to the dielectric response of the metal-molecule system. For a

NR scatterer, the maximum of enhancement should appear on the long-wavelength side of the metal substrate excitation.

5. No direct dependence on surface roughness! (However, note below that roughness does increase the “image” interaction and changes the dielectric response.)
6. The dependence on electric potential stems from the dependence of the dielectric properties on it, and it can be a strong dependence as the enhancement is nonlinear with the dielectric response.

The model has the disadvantage (and advantage) of being extremely simplistic: classical electrodynamics, plane surface, point dipole, etc., concepts are involved. From the point of view of theory, using a classical electromagnetic treatment at a distance of 0.1 nm from the surface can send shudders down the spine of any decent theoretician. Using a point-dipole approximation does not help either. Hilton and Oxtoby³²⁰ indeed criticized this model for the use of the dipole approximation. In a series of papers,³²¹⁻³²³ Maniv and Metiu used a quantum-mechanical RPA (random-phase approximation), infinite-barrier method to investigate the validity of macroscopic electrodynamics at the surface (see also Feibelman³²⁴⁻³²⁶). They find that the macroscopic results, the Fresnel reflectivity, for instance, are exact outside of the metal electronic cloud, are still reasonable about halfway between the infinite barrier and the jellium edge, and for closer distances are simply inapplicable. For a dipole near the surface,³²⁷⁻³²⁹ they find that the simple image interaction is not a good approximation. Outside the electron cloud, it is too small, because of “spillover” effects (the polarizable electrons are closer to the molecule and the “image plane” is closer; see also Efrima³³⁰). As the molecule penetrates the electronic cloud, strong screening sets in and the interaction becomes much smaller than the “image.” Their conclusion is that a corrected image model could still produce, somewhat reduced, but still substantial, enhancements, but only at higher frequencies than those predicted on the basis of the classical image, probably in the blue (for silver). This model still uses the point-dipole approximation and the surface is taken as flat.

Weber and Ford³³¹⁻³³³ introduce finite-size effects and also close-range dispersion for a rough surface in a classical electrody-

dynamic model. To simulate the size, they perform their calculation for a polarizable sphere, and the dispersion is introduced via a Lindhard dielectric function.³³⁴ They find that the “image” enhancement is much reduced, but still considerable, ~ 1000 .

Agarwal *et al.*³³⁵ showed, using a point-dipole, classical electrodynamic calculation, that the image can be considerable near a metal sphere (simulating a roughness feature) of about 2–3 nm and with similar molecule–sphere distances. At such distances the approximations are tolerable, so that their results are dependable. The reason for the increase in the interaction is a coupling to the surface plasmon (or shape resonance), which in the sphere can occur at lower frequencies than for a flat surface.

Incidentally, any mechanism which lowers the plasmon frequency (by shape effects or by interaction between small particles sustaining the local plasmon oscillations) will result in a stronger “image” interaction, provided dissipation does not increase to any large extent. Furthermore, roughness promotes efficient coupling also by providing wavenumber components that help in conserving momentum (i.e., conservation of “crystal” momentum).

Wood³³⁶ notes that the static image interaction with a sphere is smaller than with a plane. Note, however, that the coupling at optical frequencies is stronger due to the effects mentioned above. Gersten³³⁷ showed that at the tip of a *perfect metal* ellipsoid of aspect ratio of 10:1 to 50:1 the “image” is small at any reasonable distance. Gersten and Nitzan³³⁸ show, on the other hand, that at the tip of an ellipsoid conductor characterized by silver dielectric properties, the image can be of importance at distances of 0.1–0.25 nm. Kerker *et al.*³³⁹ remark that in the limit of the small spherical particle (particle radius smaller than the wavelength) the image enhancement is small, but they give no details.

Eesley and Smith³⁴⁰ have carried out a classical electrodynamic calculation, which is essentially an “image” model. They also consider the interaction between neighboring molecules, using a dipole–dipole coupling including images. The most significant result they present is a dependence of the scattered intensity on the *second* power of the incident intensity! No other model has this prediction, and it can easily be checked experimentally. Another point of interest is the coverage dependence, at the submonolayer level. Due to the depolarizing effect of the neighboring molecules,

the Raman cross section should decrease at coverages higher than 0.1–0.3. This effect can also be represented simply by an average dielectric constant of the adsorbed layer, decreasing the field intensity sensed by the individual molecules. However, an increase in the dielectric constant of the surface layer affects the metal excitations as well, a factor which was not considered in this work.

Arunkumar and Bradley³⁴¹ carry out a similar calculation, but include the polarizing and depolarizing effect of the other molecules and the roughness features. They assume that atomic-scale surface roughness can reflect the near field of the molecules that are neighbors to the site of the scattering molecule. If the polarizing effect is larger than the depolarizing effect, then enhancements are expected. Large surface-roughness features are found to increase the contribution of the polarizing reflections (probably due to allowing favorable molecular orientations with respect to each other). The expected enhancements are $>10^5$ for the atomic-scale roughened surface and higher by several orders of magnitude, when microscopic features are present.

Li,³⁴² in a classical treatment based on the Drude equation, considers also nonlinear effects. The model is essentially an “image” model.

There are several theoretical models which are essentially image models, but apply quantum-mechanical treatments. Lee and Birman^{343–345} find “coupled-system eigenstates” created from the electrodynamic interaction of the molecular-induced dipole and the polarizable metal medium, which are analogous to the shifted molecule–metal–photon states of the classical treatment. They include dispersion, which is important at short distances, but still retain a planar surface. Note that they have a sharp boundary, i.e., no allowance is given to the penetration of the polarizable electron cloud outside the positive-charge background of the metal, an effect which generally increases the interaction. They find a peaked dependence of the enhancement on the frequency, near the surface-plasmon excitation or even on the short-wavelength side of it, and a maximum enhancement of a 1000. If surface structure will push the surface excitations into the visible range, then this calculation predicts “image” enhancements of this order of magnitude.

The treatment of Eguiluz³⁴⁶ for the “image” interaction strength also shows that dispersion tends to decrease it.

Ferrell,³⁴⁷ using a simple quantum-mechanical approach to investigate the case of a molecule adsorbed on a small sphere, finds renormalized states, which enable a resonance process to arise at lower energies than in the solution. He predicts an enhancement of 10^4 , but does not state at what molecule-surface distances it is calculated, nor whether such distances which cause a resonance are realizable.

Arya and Zeyher³⁴⁸ develop a general many-body theory for SERS. In the limit of a planar surface and only plasmon contributions to the interactions, they find an enhancement of a factor of 100 for the "renormalization" model and it is relatively weakly dependent on the excitation frequency. This is for silver of course. For Cu or Au, they predict even smaller "image" effects, <10 .

To summarize the "renormalization," "image" enhancement mechanism, it is important to note that all estimates predict maximum enhancements ranging from 100– 10^8 , located at frequencies close to the metal excitations (plasmon or shape resonances or electron hole, for that matter). If such excitations are possible in the visible range, then this mechanism should be an important contributor to SERS. The "image" mechanism, also, contrary to popular belief, is sensitive to surface roughness, and generally favorably so. It therefore can be stronger at specific SERS-active "sites" on the surface. It is also molecule sensitive through the molecular (Rayleigh) polarizability.

(ii) Charge Transfer Models (RE-CT)

Basically, this set of models claims that SERS is a result of a resonance Raman process, where the molecule avails itself of the unoccupied states of the metal, or vice versa. Thus one can envisage a virtual intermediate transition to occur not between pure molecular states, but between a molecular and a metal state. This model has the advantage of a clear chemical picture, but it does not easily lend itself to rigorous calculations leading to quantitative predictions.

Aussenegg and Lippitsch³⁴⁹ have explained Raman scattering enhancements in charge transfer complexes as compared to the separate molecules, on the basis of this charge transfer. They found enhancement factors of about 2, in agreement with experiment.

They suggested that the same model is valid for SERS, where due to the high polarizability of the metal electrons, large enhancements are expected. They also predict that the molecule-metal vibrational mode will be exceptionally intense, as it strongly affects the degree of charge transfer.

King and Schatz³⁵⁰ investigated the effect of charge transfer on the transition dipoles (oscillator strengths) determining the Raman activity. This charge transfer, in their model, is promoted by static electric fields at the surface. For the case of small oscillator strengths, a large enhancement is predicted, due to the strong coupling through the metal states.

Burstein *et al.*³⁵¹ discussed several possible mechanism involving electron-hole pairs and charge transfer (CT). They expect a threshold behavior at a frequency where the photon energy plus the molecular ground-state energy surpass the Fermi level in the solid, for a molecule-to-metal charge transfer. In the case of metal-to-molecule charge transfer, an onset should appear at the frequency that equals the difference between the Fermi level and the lowest unoccupied molecular state (LUMO).

Gersten *et al.*³⁵² treat this model using an Anderson model. They note a threshold behavior, as mentioned above. A dependence on the electric potential is also predicted. When the virtual excited state resides on the molecule (metal-molecule CT), then more positive potentials will require higher excitation frequencies. For molecule-to-metal CT, more positive potentials should be associated with lower frequencies for SERS. The CT model also rationalizes the continuum background as real transitions which occurred and had suffered some decay in the metal.

Ueba *et al.*^{353, 358} have presented a comprehensive treatment of the CT model. Based on a Fano-type formalism they predict an enhancement of ~ 100 for pyridine on smooth silver. When roughness is added, in the form of ad-atoms, the enhancement increases to 1000. The excitation profile exhibits a resonance shape, not an onset. Ueba^{359, 360} applied his model to the Raman scattering of molecules adsorbed on semiconductors and interacting with them via the excitonic states. Persson³⁶¹ and Kirtley *et al.*³⁶² using similar but not identical models predict the same order of magnitude of CT enhancements, ~ 100 . Adrian³⁶³ calculated enhancements of 10-1000, again, provided the threshold conditions discussed above

are attained. Robinson,^{364,365} invoking “exchange dipole interactions,” predicts enhancements of 10^9 – 10^{13} and a distance dependence of R^{-12} . He finds that particles smaller than ~ 50 nm are not expected to give enhancements. A relatively flat excitation frequency dependence is predicted. The reader is referred to these papers for full details.

To summarize the CT model calculations:

1. Most predict maximum enhancements of about a 100.
2. The excitation frequency is related to the energy difference between the metal Fermi level and the molecular LUMO and HOMO, i.e., these models are molecule sensitive.
3. A threshold excitation frequency is predicted or a resonance shape.
4. The continuum background is explained.
5. Roughness of atomic scale favors e-h (electron-hole) coupling and orbital overlap.
6. SERS-active sites are those locations on the surface that have atomic-scale roughness features. Thus the apparent enhancement will consist of an average over the (small? number of) enhanced scatterers at the active sites and the (large number of) molecules adsorbed at smoother parts of the surface, and which do not contribute much to the total signal. The net result should be apparent enhancements that are much smaller than the enhancement per site. This remark is valid for any other model which calls for a limited number of active sites.
7. The dependence on the electric potential is a result of the change in molecule-metal relative energy separation.

(iii) Raman Reflectivity ($RE-RF$)

The “image” models describe SERS in terms of molecular states modified by the surface. The CT model focused on joint molecule-metal states. The Raman reflectivity envisages the scattering as coming from the metal, modified by the presence of the molecule, and its internal vibrations.

Metals, and especially at frequencies near a metal excitation, are strong reflectors and exhibit high luminescence. If the presence of the molecule can modulate any metal property, or accept energy

from the metal into its vibrational modes, then a Raman branch of this emission will be detected. The modulation can be brought about by several mechanisms: van der Waals-type interactions, charge transfer, density fluctuations in the solid due to electrodynamic interactions, etc.

Otto^{366,367} suggested that, as in electroreflectance, where changes in the structure of the interface cause changes in the reflectance, modulations of the interface by the molecular vibrations can change it as well. Thus, the reflectivity R is given by

$$R = A_0^2(1 + 2f_{\text{ER}}\Delta E_n) \quad (13)$$

where A_0 is the amplitude of the incident field; f_{ER} is an electroreflectance coefficient, which can be obtained from independent measurements; and ΔE_n is the change in the normal component of the field. Otto calculated ΔE_n from a model of a layer of oscillating molecules, and from that estimated the SERS enhancement to be $>10^3$. The basic implicit assumption here is that the vibrations are correlated in SERS as they are when excited in the infrared. Thus, all molecules within the coherence distance will produce reflectivity changes in the same direction, thus enforcing each other's effect. However, such an assumption is inappropriate for the optical frequencies of SERS, where the electronic polarizability is driven and there is no phase correlation between the vibrations of different molecules. Consequently, the molecules would modulate the interface at random, resulting in a smaller effect than that estimated above. Otto also mentions that this model cannot explain the special role of silver in SERS.

McCall and Platzman³⁶⁸ suggest that charge transfer between the metal and the chemisorbed molecule modulates the dielectric properties of the metal and thus its reflectance. A similar model was presented by Mal'shukov.³⁶⁹

Burstein *et al.*³⁵¹ discuss mechanisms by which electron-hole pairs (e-h) are generated and, by interaction with the adsorbed molecule, lose energy to it, while the rest is emitted (some also dissipates as heat and some gives the elastic emission and the continuum background). They envisage the e-h excitations to be resonant with the incident light, the roughness relaxing the momentum conservation requirements. An e-h excitation can be transferred to the molecule by coulombic interactions, and then either emitted

directly from the molecule, or transferred back to an e-h excitation in the metal and then emitted, in both cases the molecule retaining the vibrational quantum. Another possibility is similar to the above, except that the coupling to the molecule occurs through wave-function overlap. In the case of strong interactions between the e-h pairs and the molecular vibrations, one can envisage a direct inelastic scattering of the incident light off "e-h polaritons," i.e., dressed e-h excitations.

Maniv and Metiu³⁷⁰ and Maniv³⁷¹ have considered the coulombic coupling mechanisms and find, under RPA and infinite-barrier approximations, a large enhancement of the Raman scattering, of up to 10^4 . However, that is obtained only for unreasonable distances of the molecule from the surface (~ 0.05 nm from the jellium edge). Introducing roughness may increase the range. Maniv⁴⁹⁶ has summarized the results and showed large effects *inside* the metal electron cloud.

To summarize this part, one might say that the Raman reflectivity models, though possible in principle, still need more theoretical substantiation before one can decide regarding their importance in SERS. Certainly, these mechanisms cannot be the whole story.

3. Electric Field and Emission Enhancement Mechanisms (LFE)

In this section, we discuss the theoretical models that associate the SERS mechanism with the enhancement of the electric field sensed by the molecule and the amplification of the fields emitted by it. The key words here will be "surface plasmons." These are collective excitations of the electrons on a nearly free-electron metal. There are bulk plasmons, which are generally very high in energy, compared to photon energies of 1.5–3 eV, which are of interest in the context of SERS. There are also surface plasmons, which are confined to the region of the surface and decay exponentially away from it. Their characteristic frequencies are lower than the bulk plasmons and can be brought into the visible range by confining them in "bumps," i.e., metal particles with sizes ranging between a few nm and hundreds of nm. The characteristic frequencies can be affected also by the interaction between several of these "bumps." For a comprehensive review, the reader is referred to Raether.^{372,373} The theories which center on the role of plasmons automatically

give special importance to the coinage metals, due to their relatively low-frequency plasmons or other dielectric excitations.

(i) *The Lightning Rod Effect*

Gersten³³⁷ suggested that the strong electric fields produced near sharp metallic tips may cause some of the Raman enhancement. For an ellipsoid perfect conductor, the field at its tip can be even 10^3 times larger than the external electric field producing it. This was calculated for a point located 0.1 nm from the tip of an ellipsoid with a major axis of 50 nm and a minor axis of 2.5 nm. Lio and Wokaun³⁷⁴ obtain 10^4 Raman enhancement due to these effects at the tip of an ellipsoid of 3:1 axial ratio. At other points, on or near the ellipsoid, they find the electric field greatly reduced.

These tips are suggested as simulations of the roughness on the SERS-active surfaces. On the average (considering the molecules distributed over the entire surface of the ellipsoid) large enhancements are not expected from this model. There is also nothing special about silver in this respect, and all molecules should exhibit this kind of enhancement, if it is really significant.

(ii) *Surface Electromagnetic Wave Enhancement*

The possibility of utilizing the surface electromagnetic field to enhance the Raman scattering from overlayers on metals in an ATR configuration was proposed before the SERS "era" by Chen, *et al.*^{375,376} They predicted, for silver, enhancements of about 300 when both the excitation and emission were carried out through the coupling prism, and a factor of ~ 100 when only the excitation was thus coupled. Indeed, they reported³⁷⁶ a 75-fold enhancement of benzene on a silver film. These ideas were used by Chen and Burstein³⁷⁷ to suggest that SERS on silver islands was due to the excitation of transverse collective electron resonances, which caused large electric fields and amplified the emission. Their estimate of the enhancement was about 10^6 , which they reduced to about 10^4 , considering inhomogeneous broadening.

Gersten and Nitzan³³⁸ have presented a comprehensive treatment of the electric field and emission enhancement mechanism. In order to illustrate the main physical features of this mechanism a simple model, following Gersten and Nitzan,³³⁸ will be given here.

Let the system consist of a molecule with (Rayleigh) polarizability α_1 , and a metallic body with the polarizability α_2 . Let the external field be E_0 . The moments of the induced dipoles, in the molecule μ_1 and in the metal μ_2 , are given by the product of the polarizability and the total field operating on each moiety. Here one assumes the particles to be much smaller than the wavelength and, for simplicity, the tensorial properties are dropped. Thus,

$$\mu_1 = \alpha_1(E_0 + M\mu_2) \quad (14)$$

$$\mu_2 = \alpha_2(E_0 + M\mu_1) \quad (15)$$

where M is the scalar form for the dipolar field function

$$M = (3\hat{n}\hat{n} - \mathbf{1})/d^3 \quad (16)$$

d is the distance between the two (point) dipoles and \hat{n} is the direction of the radius vector. In Eqs. (14) and (15) the total field is composed of the incident field and the polarization field exerted by the other particle.

Solving these linear equations and summing the total induced dipole in the system, gives an effective polarizability

$$\alpha_T = (1 - \alpha_1 M \alpha_2 M)^{-1} [\alpha_1(1 + M\alpha_2) + \alpha_2(1 + M\alpha_1)] \quad (17)$$

Though written in scalar form, the tensor structure of the equation was retained.

The Raman polarizability of the system is obtained by differentiating Eq. (17) with respect to a molecular vibrational coordinate Q and multiplying by its displacement ΔQ . If one neglects the image term, which is the first term in Eq. (17), then one obtains for the Raman polarizability of the system:

$$\Delta Q \alpha' = \Delta Q [\alpha'_1 + \alpha'_1 M \alpha_2 + \alpha_2 M \alpha'_1] \quad (18)$$

where the differentiation with respect to the vibrational coordinate is denoted by the prime. It is assumed here that the only vibration-dependent quantity is the molecular polarizability. One could include the Raman reflectivity model by allowing α_2 to be dependent on the vibration. Also one could consider the dependence of the coupling matrix M on the vibrational coordinate. M depends on the metal-molecule distance, which certainly varies with the vibration of the molecule against the metal. This term was considered

also by Eesley and Smith³⁴⁰ and predicts a special dependence of the molecule-metal-“bond” Raman scattering.

The three terms of Eq. (18) stand for three distinct processes. The first is the usual scattering of the isolated molecule. The second corresponds to the additional Raman scattering by the molecule due to the local field induced by the polarizable metal. The third term is a Raman reflectivity, where the coupling mechanism is the coulombic interaction [see Section III.2(iii)]. If the term $M\alpha_1$ is $\gg 1$, then enhancements of the Raman scattering are expected.

A further enhancement is expected if one considers the emission process. The Raman-shifted molecular dipole moment μ''_1 is given by

$$\mu''_1 = \mu''_{10} + \alpha_1 M \mu''_2 \quad (19)$$

where

$$\mu''_{10} = (\Delta Q \alpha'_1 + \Delta Q \alpha'_1 M \alpha_2) E_0 \quad (20)$$

and that of the metal “bump” is given similarly by

$$\mu''_2 = \mu''_{20} + \alpha_2 M \mu''_1 \quad (21)$$

with

$$\mu''_{20} = \Delta Q \alpha_2 M \alpha'_1 E_0 \quad (22)$$

We have, for simplicity, assumed that the Rayleigh polarizability at the Raman-shifted frequency is equal to the polarizability at the incident frequency. This approximation can be easily removed. It is important to do so for large Raman shifts, and this predicts smaller maximum enhancements for high wavenumber vibrations than for small wavenumber modes.

Combining Eqs. (19)–(22) gives, for the total Raman-shifted dipole,

$$\mu''_T = (1 - \alpha_1 M \alpha_2 M)^{-1} [\mu''_{10}(1 + \alpha_2 M) + \mu''_{20}(1 + \alpha_1 M)] \quad (23)$$

Once again an image term is apparent (rigorously at the Raman-shifted frequency). In addition, the molecular “Raman” dipole is amplified by the factor $\alpha_2 M$, and to that is added the Raman-shifted scattering of the metal with its “reflection” in the molecule. This constitutes the emission enhancement. The relation between the

field enhancement and the emission amplification is obvious. They arise from the same type of interaction and have the same form, but quantitatively may be different as they are to be evaluated at different frequencies. Recall that the detected intensity is proportional to the square of the Raman-shifted total dipole moment.

Gersten and Nitzan³³⁸ investigated the case of metal ellipsoids and spheres, using classical electrodynamics. They find that at the tip of the ellipsoid large enhancements can occur due to the LFE mechanism. They also find that the largest enhancement occurs at the plasmon frequency of the particle, which is size (and shape³⁷⁸) dependent. This condition is the one that maximizes α_2 . They find that relatively large particles (several tens of nm) can be SERS active. Larger particles would introduce retardation effects, which would adversely affect the enhancement, mainly due to uncorrelated phases of effects from different parts of the particle, and also radiation damping. The preferred aspect ratio, for silver, is about 1:3. For a sphere of comparable dimensions, the calculated enhancements are about two orders of magnitude lower than for an optimized ellipsoid. The range of the enhancement, in terms of distance from the surface, depends strongly on the shape. The larger is the aspect ratio, the shorter range is the effect. For a sphere, the range of enhancement is several nm, as is the case for low aspect ratios. For an aspect ratio of 10, the range is extremely short and the enhancement is to a large degree contributed by the image term. There are many other interesting aspects discussed in this classic paper and the reader should refer to it.

Several approximations and assumptions in these calculations are worth mentioning. The enhancement factors which were calculated are for a molecule located at the tip of the metal roughness feature. The authors argue that due to the large (static) fields at tips the molecules will tend to concentrate there. Even if that was true, then for full coverage still, an average over the protusion area should be carried out to obtain the apparent enhancement factor. Wokaun *et al.*³⁷⁹ estimate the reduction in intensity due to this effect to be a factor of 43, for an ellipsoid with the favorable aspect ratio of 3:1. Also Kotler and Nitzan³⁸⁰ found considerable reductions of the average local intensity in a film. Furthermore, at room temperature there is no preference for adsorption at the tips, as the thermal energy is comparable to, or higher than, the energy gain

by a molecule with a static polarizability of 10^{-2} nm^3 and sitting at a site of an extremely high field, 10^7 V cm^{-1} .

Another matter to consider is radiation damping, i.e., self-induced emission. Wokaun *et al.*³⁷⁹ find that this effect limits the possible enhancement and they calculate a reduction of *five orders of magnitude* of their calculated enhancement of 10^{11} without the damping. Similarly, Mills and Weber³⁸¹ find, near a grating, that the fields are enhanced only by a factor of 5 (i.e., a factor of, at most, 600 for the LFE Raman enhancement). They estimate that these effects start to be important for typical sizes of $\sim 12.5 \text{ nm}$. This is confirmed by calculations of Kerker *et al.*,³³⁹ who find significant enhancements only for particles smaller than 5 nm.

At the small-particle limit, where retardation is unimportant, the LFE enhancement is limited by surface scattering. This means that the dielectric coefficient of the bulk metal is not valid for the small particle. The collisions of the electrons in the small particle with the wall causes dissipation, that is, broadening of the plasmon spectrum. Consequently, the particle excitations are less efficient in producing the large fields needed for LFE enhancement. The process is damped by the surface scattering. Surface scattering starts to be important when the particle size is smaller than the mean free path of an electron in silver, about 10 nm. Wokaun *et al.*³⁷⁹ find that the scattering affects the LFE enhancement significantly already at 20 nm. For a silver ellipsoid of about 10-nm average axis size, the amplification of the square of the electric field is reduced by factors ranging from 10 to 100. Thus the LFE SERS enhancement would be reduced by two to four orders of magnitude; this is out of 10^5 – 10^{11} factors they calculate for the total enhancement at the tip.

Another point which is important to remember when evaluating the LFE is its sensitivity to geometrical factors of the metal "bumps." For example, Gersten and Nitzan³³⁸ show that for a silver ellipsoid with an adsorbed molecule positioned along the major axis, 1 nm away from the surface, the enhancement changes from ~ 200 for both axes of 50 nm to about 8×10^4 for a major axis of 50 nm and an aspect ratio of 5:1. In most of the SERS experiments, the roughness is not uniform. Therefore, averaging over the distribution of protusions should be carried out, which certainly decreases the expected LFE enhancement even further. Another

effect this averaging will have is a broadening of the excitation profile, from a sharp resonance spectrum. McCall *et al.*³⁸² have treated the case of a small sphere. They simulated the distribution of the “bumps” by assuming a distribution of resonant frequencies.

Laor and Schatz^{383,384} considered a distribution of hemispheroids on a flat perfect conductor. The interactions are taken as the dipole coupling of the “bumps,” which is valid for a low-density case. They find for silver (not including retardation and wall scattering) a flat variation with frequency with a drop at ~ 300 nm. The total enhancement is < 100 . This includes a factor of 16 with which they multiplied to account for simple reflectivity from a smooth surface. They did not, however, include emission enhancement (except the trivial reflection factor), arguing that rarely will the incident frequency and the Raman-shifted emission be simultaneously in resonance with the plasmons. If we add the maximum value of such an emission enhancement to their evaluation, we find a total ideal enhancement of ~ 500 . Similar results, though with somewhat smaller values, are calculated for Cu, Au, Hg, and Pt.

Arya *et al.*³⁸⁵ consider a randomly rough metal surface and find a maximum enhancement for silver of 1000 at 400 nm. In the visible the enhancement is smaller (about 100).

Another point worth mentioning is the use of the metal long-wavelength dielectric function. No dispersion was allowed in the model. The wave-vector dependence of the dielectric constant is important at close proximity to the surface as was already remarked in the context of the image calculations. This approximation may be reasonable away from the surface, distances for which the LFE is most appropriate.

Ford and Weber^{331,332} included the effect of dispersion by using a Lindhard formula for the dielectric constant, and included also a constant term to account for the bound-electron contribution. They find that the LFE enhancement is < 1000 and point out the importance of the coupling to e-h.

A further point is neglect of the interaction between the roughness features on the surface. This electromagnetic interaction causes dissipation and broadening of the plasmon excitations, with an adverse effect on the enhancements. Aravind *et al.*³⁸⁶ investigated the case of two metal spheres. They found that the enhancement

is smaller than for a single sphere, except at configurations which monitor the region between the two spheres.

Yamaguchi, *et al.*³⁸⁷ have shown that in addition to broadening due to dipole-dipole interactions between silver particles, additional broadening is brought about by proper treatment of the retardation, beyond the static limit.

The effect of the approximations discussed above, or at least some of them was shown in the work of Moreland *et al.*³⁸⁸ They demonstrated that the efficiency of light emission from silver surfaces excited by ATR was typically small: about 5% for a silver island film, 9% for a calcium fluoride roughened layer, and up to 80% for a silver film evaporated on a holographic grating.

Several other groups have considered the LFE mechanism in a variety of systems with similar models. Aravind and Metiu³⁸⁹ have studied the case of a sphere extended above a flat metal substrate. They find exceptionally high enhancements in the region between the two bodies. Aravind and Metiu³⁹⁰ discuss the role of emission enhancement due to random roughness characterized by a correlation length. They find a maximum enhancement of a 100 for silver, but that is at the plasmon frequency, 3.5 eV. In the visible the enhancement due to this model is <10. For correlation lengths >15 nm, there is an attenuation instead of an enhancement. Adrian³⁹¹ calculated the LFE enhancement for a moderately prolate spheroid in the electrostatic limit. He finds up to 10^7 enhancement for a molecule sitting along the major axis. It is very slightly distance dependent. Rupin³⁹² calculated the electric field enhancement near a hemispheroid on a flat surface. Both have "real" dielectric properties (not perfect conductors). He further assumes the emission enhancement to be equal to the field factor. He finds maximum enhancements of 10^7 along the normal to the flat surface, at the plasmon frequency. Off the plasmon resonance, the total enhancement is typically 1000. The distance dependence is again weak. For a 10-nm bump, the enhancement decreases by a factor of 10 going from the first to the third pyridine layer. Messinger *et al.*³⁹³ considered only the field enhancement and find that the multipolar excitations can be important and will support resonances at frequencies lower than the dipolar resonance frequency. Additional calculations have been made by Gorobei *et al.*,³⁹⁴ Ohtaka and Inoue,³⁹⁵ Numata,³⁹⁶ Agarwal, *et al.*,³³⁵ Sakoda *et al.*,³⁹⁷ Arya and Zeyher,³⁴⁸

Brodsky and Urbakh,³⁹⁸ Barber *et al.*,³⁹⁹ Garcia,^{400,401} and Kirtley *et al.*^{402,403} Regretfully, these papers cannot be discussed in detail here and the reader should refer to the original articles quoted above.

As mentioned above, Kerker *et al.*^{339,404–407} have carried out a rigorous calculation in the classical limit for metal spheres, spheroids, and covered spheres suspended in a liquid support (colloid). They noticed that large particles (>5 nm) exhibit reduced enhancements, probably due to the retardation and radiation damping. For the small particles they find large enhancements ($\sim 10^5$), but only at the maximum of the excitation spectrum, which should be for their colloids (silver citrate) at ~ 400 nm, and not in the visible.

Finally, Weber and Ford⁴⁰⁸ estimate an upper limit of the field enhancement on the basis of conservation-of-energy considerations. They find for silver and a perfect coupler between the radiation and the metal excitations (a grating or a prism) that the maximum enhancement of the square of the field is approximately 300. This is probably the average quantity. For a rough surface they estimate an enhancement on the order of magnitude of unity!

4. Dyes in SERS—Theory

In this section the behavior of dyes, i.e., molecules that are in resonance with the incident light before adsorption on the surface, will be discussed from the theoretical point of view. It is of interest to see whether the study of dyes may not help discriminate between the various mechanisms. Perhaps, this may have also some value for the utilization of SERS.

The strong resonance behavior of dyes may interact with the metal substrate resonances and bring about a behavior which is not a simple superposition of either of the two. Pockrand *et al.*⁴⁰⁹ have shown the orienting effect of a surface on the organization in the dye layer, which affected the formation of dimers or monomers, and also the polarization properties of the dye absorption. In this case, due to the wide absorption bands of the dyes, no resonance-resonance effects were seen.

Glass *et al.*⁴¹⁰ and Craighead and Olson⁴¹¹ have shown experimentally that the resonance of rhodamine 6G (R6G), at about 570 nm, interacts strongly with the excitation resonance of silver

island films (associated with plasmonlike excitations). A double-peak absorbance develops, with the high-energy peak at energies greater than that of the isolated silver film and the lower-energy peak is red shifted compared to that of the dye alone. For silver film thicknesses such that the film is continuous, the R6G spectrum reappears. Similar results were obtained also for rhodamine B and Nile Blue. The luminescence intensity was also measured as function of average film thickness. It was found that the intensity generally peaks at a thickness for which the plasmon resonance of the bare silver coincides in frequency with that of the dye. The luminescence intensity changed by as much as a factor of 20. It was not corrected for the surface coverage which may also change in a peaked way—a small amount of adsorbed material for the low-thickness, low silver-particle density as for the relatively smooth thick films, and in between, the largest adsorbed amount on the rough and dense silver island film. The excitation spectrum (for luminescence) or rhodamine B on a silver film coincided with that measured when this dye was adsorbed on glass.

Garoff *et al.*⁴¹² found similar results for R6G on silver films. They study the optical density of the dye-coated films as a function of dye concentration (in the solution from which it is adsorbed on the silver) and as a function of film thickness. The double peaks appeared and were explained on the basis of Mie formalism. Note that significant changes in the spectrum shape appear only from a concentration of 2.8×10^{-4} M. Also no determination of the amount adsorbed on the surface is reported.

Wang and Kerker⁴¹³ and Chew and Wang⁴¹⁴ have presented a theoretical treatment, based on the electrodynamic approaches used for the SERS problem, and provide a full description of the extinction of the dye-coated spheroids. They also calculated the luminescence enhancement, and find it to be up to 10^4 on silver for optimal wavelengths and particle shapes.

Kotler and Nitzan⁴¹⁵ applied the electrostatic limit to a silver sphere coated with a dye. They found also in this case a double-peak behavior, under certain circumstances. Noteworthy, are the enhancements of the Raman scattering of up to $\sim 10^4$, near the particle plasmon resonance. (For their model of a sphere it is at 3.5 eV but for other shapes it can be brought into the visible range). The enhancement is very weakly dependent on the distance from

the surface, decreasing by an order of magnitude for a layer of 8 nm (for a particle of radius of 10 nm).

However, changes in the absorption spectrum are not the only effects expected and seen in the behavior of dyes on metallic (silver) surfaces. It has been known for some time now that proximity to a silver surface brings about major changes in the lifetimes and quantum yields for fluorescence of molecules. For an early work in that field, see Kuhn⁴¹⁶ and for an excellent theoretical treatment, Chance *et al.*⁴¹⁷ Within the framework of classical electrodynamics, it was shown that the metal opens dissipative channels into which the excited molecule can discharge its energy. The theoretically calculated lifetimes fully agreed with those measured, up to distances of about 10 nm from the surface.

Rossetti and Brus⁴¹⁸ found, for pyrazine on silver, that the classical electrodynamic theory indeed agrees well with the measured decrease of lifetimes. However, at shorter distances the change in lifetime was much more gradual and did not follow the theory. Campion *et al.*⁴¹⁹ and Whitmore *et al.*⁴²⁰ found, for the same molecule, that the classical theory worked agreeably all the way down to 0.5 nm away from the surface, where the lifetime has decreased by a factor of ~ 1000 as compared to the lifetime of the isolated molecule.

Pockrand *et al.*⁴²¹ also find that the decay into the surface plasmons becomes inefficient at distances smaller than 18 nm, when the dye is not in resonance with the plasmon frequency.

Weitz *et al.*^{422,423} studied the fluorescence of europium ions adsorbed on silver islands. They find the lifetime to be about three orders of magnitude shorter than on a bare silica substrate. The emission in this case is resonant with the silver islands at 613 nm.

Gersten and Nitzan⁴²⁴ developed the theory of lifetimes and quantum yields near metal spheroids. They showed that at short distances the expected change in lifetimes should be larger than near a flat surface by several orders of magnitude, when in resonance with the plasmon of the spheroid. When out of resonance, the effect is limited to a factor of about 10. Thus a total of lifetime shortening of about 10^3 is expected.

The two effects discussed above—the enhancement of the fields (and emission) and the shortening of lifetimes—were combined by Weitz *et al.*²⁴⁰ to describe SERS behavior of dyes. The basic claim

is that the LFE mechanism enhances the Raman scattering of the dye, just as it would that of a normal Raman scatterer, i.e., by factors of about 10^5 – 10^6 . However, they continue, due to the shorter lifetimes near the surface, the resonance of the dye is broadened, and a less efficient scattering is exhibited. The net effect would be an enhancement two to three orders of magnitude lower than that for a normal scatterer.

However, the latter argument is not valid for the following reason: typical lifetimes of high-quantum-yield molecules are 10 ns. For a surface effect of even 10^4 (which is a higher factor than that measured on island films), the surface lifetime becomes ~ 1 ps, which is 3 cm^{-1} . This is close to the linewidths associated with vibrational, nonradiative decay rates. Thus, the resonance Raman intensity which is determined by the *shortest lifetime* will *not* change to any significant degree. The *vibrational* lifetimes are clearly not changed to any large degree, as the SERS vibrational bands are only slightly broader than in solution (up to a factor of 2) and part of that is due to inhomogeneous broadening. It must be mentioned that there are claims for larger lifetime changes in several systems, both for electronic and vibrational degrees of freedom (see, for instance, Persson⁴²⁵ and Demuth and Avouris^{297,426}), but that is a separate story. Anyway, in order to affect the resonance Raman intensity to any significant degree, the broadening should be as large as the electronic absorption envelope itself. Champion and Albrecht⁴²⁷ show that there is no difference in the Raman scattering intensity for widths of 10 or 100 cm^{-1} . If indeed the broadenings due to the surface are as large as the absorption band itself, then no typical resonance structure of the SER spectrum of the dye should appear. Thus one would expect the SER spectrum to maximize at the same wavelengths as those for which the SERS of normal scatterers is a maximum (especially if the dye and the normal Raman scatterer are coadsorbed).

Thus, in summary, it appears that the LFE mechanism predicts that for dyes in resonance the Raman spectrum will be enhanced to the same degree as normal scatterers, except when a typical resonance excitation profile is not observed. This conclusion is in contradiction to that expressed in Reference 240. The excessive sensitivity of the model presented there to lifetime changes is, to a large part, due to the simple two-state description of the excited

molecule. One should keep in mind that, on the surface, there may be shifts of the spectra. That still would require the usual large SERS enhancements according to the LFE. A more detailed analysis is given elsewhere.⁴⁹⁷

The resonance mechanisms, by virtue of all of them having a ceiling enhancement determined by the properties of the enhanced moiety, predict that the enhancement effect with dyes in SERS will be orders of magnitude smaller than for a normal scatterer. As a rough rule of thumb, the enhancement will be smaller by a factor comparable to the ratio of the scattering intensity of the dye and normal scatterer in solution.

Thus, study of the surface Raman scattering of dyes can be helpful in pinning down the SERS enhancement mechanism.

IV. WHAT IS "THE" SERS MECHANISM?

1. General

The points to be considered when analyzing the various theoretical models in the light of the available experimental evidence are the following:

1. Can the theoretical model explain *apparent* enhancements $>10^4$ and as high as 10^7 ? This evaluation should have been done after considering the approximations in the models and the effect the removal of these approximations may have on the calculated enhancement.
2. Is the surface morphology required by the model shown to be unquestionably present in the experimental setups?
3. Can the model explain the dependence on the metal substrate?
4. Can the model explain the electric potential dependence?
5. How does the predicted excitation profile agree with the experimental one?
6. Regarding the distance dependence, how does theory compare with experiment?
7. What is the dependence on the molecule?
8. What is expected of the behavior of two different molecules coadsorbed, in terms of intensities and frequency dependence, and what is seen?
9. How are "dye" molecules expected to behave, especially compared to (coadsorbed) normal scatterers?

10. How does the SERS depend on the "solvent," especially as regards the excitation spectrum?
11. What is the dependence of SERS of one molecule on the concentration of other chemical species present?
12. What should be the effect of temperature annealing, and how does it correlate with irreversible behavior under electric potential changes?
13. Regarding the dependence of SERS on the Raman shift, how does the SERS of the various modes in the same molecule compare?
14. How is the dependence of the excitation maximum on the electric potential explained, especially as regards the magnitude of the shift?

Most of these points were addressed in this review, both from the experimental side and the theoretical aspect.

There are several other criteria which we have not mentioned here, or discussed in the main body of this review, such as the polarization dependence, angular dependence, selection rules, the appearance of a continuum, and the dependence on intensity. These topics were not discussed here due to space limitations. It seems that the polarization characteristics, the angular dependence, and the selection rules are less model sensitive and depend more strongly on the metal dielectric properties and the adsorption formation than on the specific enhancement mechanism. The continuum background, which appears in most SERS studies, is perhaps more indicative of the enhancement mechanism, or parallel processes at the surface.

Another topic which was not discussed in this review is the role of graphitic layers in the promotion of SERS. A short exposition will be given in Section V.

This is an appropriate place to acknowledge the contributions of the large number of researchers to the advancement of the understanding of SERS, and to apologize to those whose work has not been adequately covered in this review, as it certainly deserves.

2. "The" SERS Mechanism

This section is left for the reader to fill in!

The experimental facts (and myths) were critically reviewed and exposed here. The theoretical models were discussed.

The present author can only reiterate his conclusion, stated in the Introduction, based on the evaluation of theory and experiment as given above: "There is no 'one' mechanism at the root of SERS; however, there is a mechanism which, in the large majority of systems, is the main contributor to the surface enhancement effect. That mechanism is a resonance mechanism. It is felt there is not enough evidence, yet, to determine which of the mechanisms belonging to this group is the important one, or which can be ruled out. The LFE mechanism certainly has a role, but a more minor one. Note, however, that a minor factor in SERS is a factor of a 100 or so, which may be the difference between a detectable and a nondetectable signal!"

V. SERS—A USEFUL TOOL

It is appropriate to begin this last section by quoting Furtak,¹³⁸ in one of the early SERS papers: "The long sought for experimental tool for detailed chemical characterization of the solid-aqueous electrolyte interface may have at last been found." This was the general feeling or at least the general wish. Has it been realized? What does the future hold for it?

As was shown in this review, the major effort in SERS studies was directed toward understanding this phenomenon, and generally not toward its application and utilization. Nevertheless, some very interesting information was acquired along the way, regarding interfaces and molecules at interfaces, as can be seen from the reports reviewed through this review. An increasing number of studies is carried out now to use SERS as a tool and the proportion can be expected to increase further.

In this section a brief summary of representative studies, which have used SERS for surface studies, is given.

SERS is not the only method to apply Raman techniques to surfaces. There are several other ways of increasing the sensitivity of the Raman technique, and all work together to offer a versatile and powerful instrument. Nowadays, Raman measurements can be performed with the high sensitivity of OMA techniques, which pose no special restrictions on the systems investigated (no specific metal or surface preparation).^{28,110,428}

An alternative is using metal grating surfaces.^{110,170,175,281,429,430} Such surfaces can exhibit enhancements up to two orders of magnitude. Also ATR configurations can be used on a variety of surfaces.^{94,177,431-435} Interference techniques can be applied⁴³⁶ as well as waveguide techniques in 100-nm films.⁴³⁷⁻⁴³⁹ New geometries for surface enhancement were suggested, for instance by Aravind *et al.*⁴⁴⁰

An interesting possibility is inducing SERS activity, in a non-SERS-active substrate, by depositing submonolayer quantities of silver on its surface. Van Duyne and Haushalter²²⁵ used this method to measure Raman scattering from a GaAs semiconductor interface. There was also an experiment to use a silver underlayer to induce SERS in a layer covering it.²⁵⁶

A very important feature of SERS is that it works in "dirty" rough-surface systems, and is relatively insensitive to the phase adjacent to the metal. This allows its use in "real" systems of interest, for instance, to the study of absorption in catalysis.

Another interesting characteristic of SERS is that, as was shown above, in many systems special sites are most efficient in promoting it. Thus, generally, SERS does not "see" all the molecules, but mainly those adsorbed near surface defects. But these same defects and sites may be the center of the chemical activity of the surface. It would be of extreme importance if such a connection could be made, and future research in this direction may prove very fruitful. Knoll *et al.*¹⁵⁶ have shown that IR and SERS are sensitive to molecules in different environments on the same system. Also, Yamada *et al.*²⁷⁷ found for CO on silver that the IR exhibited a band at 1940 cm^{-1} , while in SERS a band at 2112 cm^{-1} was observed. Consequently, these two methods are complementary also on the surface.

SERS provides a means to study adsorbed molecules through their vibrational structure. However, a simple comparison is, alas, not straightforward in most cases. Besides the chemical changes which can occur, we still do not know in what way the enhancement mechanism affects the various vibrational bands, shifts them, and changes their relative intensities. It is established that the selection rules on the surface are different than those which pertain to a bulk situation. Hexter and Albrecht⁸⁹ have analyzed the selection rules by assuming that the metal surface is approximately a perfect mirror,

which adds a symmetry element, imposing some restrictions on the appearance of vibrational bands. However, real (SERS-active) metals at optical frequencies are not perfect conductors and one would not expect a complete disappearance of modes which are parallel to the surface. Furthermore, in Raman scattering the direction of change of the polarizability is the important direction and not that of the vibrational transition dipole, which complicates the analysis even further. Erdheim *et al.*⁵¹ have found that the SERS of pyrazine exhibited asymmetric bands, which in solution are Raman forbidden. Kunz *et al.*¹²⁰ have demonstrated that azide ion adsorbed on silver exhibits SERS of IR-allowed-Raman-forbidden bands. Moskovits and DiLella^{105,441} find similar behavior. Moskovits *et al.*⁴⁴²⁻⁴⁴⁴ analyze this in terms of the existence of electric field gradients at the surface. They show that the bands that appear have the proper symmetry to be explained by this assumption. The possibility of the lowering of the symmetry upon adsorption in a site of a specific symmetry, was also mentioned by them and further discussed by Dornhaus.⁵⁵

The vibrational analysis of the SERS spectrum can be further complicated by the appearance of overtones.⁴⁴⁵ The net result is that extreme care should be exercised when trying to use the vibrational shifts and relative intensities to infer the identity of a surface species and its immediate environment. Nevertheless, such analyses were carried out in the past, and will continue to be performed also in the future, until we have a better understanding of the surface contributions involved.

Allen and Van Duyne⁴⁴⁶ have correlated the Raman intensity for the cyano group in 2-, 3-, and 4-cyanopyridine to its direction with respect to the surface. They found that the molecule for which this group is parallel to the surface exhibits the weakest signal. Creighton⁴⁴⁷ discussed the possibility of determining adsorbate orientation from SERS relative intensities. The conclusion is that it is feasible, unless chemical changes are involved.

SERS was used to determine the structure of adsorbed molecules. Many examples were cited in the various sections of this review, such as the study of adsorbed water, and will not be repeated here. We give here only a few additional examples, most of them very recent.

Fleischmann *et al.*^{209,448} discuss the structure of water in the double layer and adsorbed on a rough silver electrode. They find several bands indicating different forms of water. These are associated with solvated cations. The effect of anions is also studied and it was found that they are coadsorbed with the water. Fleischmann *et al.*,⁴⁴⁹ in a separate study, have inferred from the SERS spectra that quinoline and isoquinoline ions adsorbed as ion pairs when adsorbed from an acidic medium. Bunding and Bell⁴⁵⁰ infer selective hydration of pyridine carboxaldehydes producing carbinols, for the para and ortho derivatives but not for the meta. Pockrand *et al.*⁴⁵¹ identify two forms of acetylene on a silver film. They cannot assign the bands seen to any specific form. Sandroff *et al.*⁴⁵² use tetrathiafulvalene to probe the charge transfer to silver and gold surfaces, monitored by the position and intensity of the vibrational bands.

The possibility of detecting a vibrational band associated with a surface-molecule bond was already discussed. In this context we mention the silver-thiourea bond seen by Macomber and Furtak⁵⁷ and the copper-N vibrations seen on copper colloids.³⁶

Several molecules were investigated because of the applicability in a system of interest. Silver oxide was investigated by Kotz and Yeager⁴⁵³ for the significance of the silver/silver oxide electrode as a cathode in batteries and as a catalyst for oxygen reduction. Mercaptobenzothiazole was studied⁴⁵⁴ for its role as a corrosion inhibitor for several metals. Von Raben *et al.*^{455,456} could follow the adsorption of sulphates and nitrates on a silver powder in the context of catalysis. Sandroff and Herschbach⁵⁶ showed that several disulfides dissociate to the sulfides when adsorbed on silver. This was discussed in relation to lubrication problems. Sandroff *et al.*⁴⁵⁷ investigated the surface conformations of hexadecane thiol as a function of the solvent in contact with silver. This molecule is an amphiphile, of interest in wettability problems.

Reactions were also monitored by SERS. Yamada *et al.*⁴⁵⁸ discussed the reaction of rose bengal adsorbed on a ZnO electrode. This is an example of the use of the resonance enhancement to gain enough sensitivity. Billmann *et al.*⁹² followed the chemisorption of cyanide on silver, and detected the formation of the various cyanides on the surface. Similarly, Loo¹⁹⁰ investigated halide complexes on a gold electrode. Pemberton and Buck²¹⁴ used SERS to see the adsorption of diphenylthiocarbazon and its oxidation into

a disulfide. Itabashi *et al.*²²² looked at the dissociation of porphyrin into its monomers and silver incorporation into the ring. Fleischmann *et al.*⁴⁵⁹ investigated the electropolymerization of phenol on silver.

SERS is important also in the study of catalysis. Here silver itself is of interest such as for the ethylene epoxidation reaction.⁴⁶⁰ Moskovits *et al.*^{46,50,106} showed the usefulness of SERS for the study of the adsorption of simple alkenes on silver. Dorain *et al.*⁴⁶¹ found, using SERS, catalytic formation of sulfites from sulfur dioxide on silver powder, and followed the oxidation by oxygen to sulfates. Pettenkofer *et al.*⁴⁶² report the detection of peroxides and superoxides on silver.

SERS has been used also under high-pressure conditions by Podini and Schnur⁴⁶³ who discuss the reliability of the measured parameters. Sandroff *et al.*⁴⁶⁴ have used high-pressure chambers, too.

Suh *et al.*⁹⁷ demonstrated that SERS could be used to detect "two-dimensional" phase equilibrium between a gaslike phase and a solidlike phase, for *p*-aminobenzoic acid adsorbed on silver.

Competition over surface sites and surface displacement of adsorbates was observed by Garrell *et al.*,¹⁹² who detected replacement of chloride by bromide on a silver colloid. Owen *et al.*⁴⁶⁵ report similar displacements on a silver electrode. Bachackashvilli *et al.*^{49,229,230} have monitored competition of pyridine and several azo dyes over the surface of a silver colloid.

Kinetics of adsorption were investigated by Pemberton and Buck,⁴⁶⁶ who followed the adsorption of dithizone on a rotating-disk silver electrode, on the time scale of a few seconds. Dendramis *et al.*⁴⁶⁷ reported adsorption of cetyltrimmonium on copper in the minute time scale.

An interesting application of SERS was reported by Farquharson *et al.*⁴⁶⁸ They determined the reversible redox potential of osmium ions by monitoring their relative surface concentrations as a function of electric potential.

The investigation of dye molecules or other highly fluorescing molecules can be facilitated by the quenching of the fluorescence by the surface, as noted by Nimmo *et al.*²⁴¹ A good example can be seen in References 59 and 227.

SERS has been used for the study of molecules of biological importance, such as nucleic acid components.^{469,470} The adsorption on a silver electrode was considered in some way similar to the adsorption to the charged membranes in biological systems. The adsorption of a nucleic acid itself was also studied with SERS.⁴⁷¹ We have already discussed the work of Cotton *et al.*^{218,219,221} who studied Cytochrome C and myoglobin. SERS requires only small quantities of material, which is very suitable for biological studies.

Special mention must be made of SERS studies of carbonates, carbon, and graphitic layers on surfaces. Cooney *et al.*^{137,472-475} have reported the appearance of Raman vibrational structures associated with the presence of carbon species on the SERS-active surfaces, in electrochemical systems. They even suggest that a graphitic layer formed on the surface is responsible for the SERS phenomenon itself. Tsang *et al.*⁴⁷⁶ also discuss the broad bands seen in SERS at 1350 and 1550 cm^{-1} in terms of amorphous carbon. In the UHV systems, Pockrand and Otto⁶⁹ report carbonate impurities exhibiting enhanced Raman scattering. They find that these impurities are incorporated into the sample below the surface. DelPriore *et al.*¹⁶⁶ find by XPS several layers of carbon and oxygen on SERS-active vapor-deposited surfaces in the UHV.

Very recently, Efrima⁴⁷⁷ suggested a combination of SERS and optical-activity measurements. Provided large field gradients are present near the metal surfaces, one should measure very large effects. This may provide an easy way to extract chiral information.

Besides the direct utility of SERS and the impact it had on the way we think about metal interfaces, SERS and the SERS mechanisms have suggested many other effects, some of which have already been put to trial. This review would not be complete without mentioning them.

Nitzan and Brus^{478,479} have proposed that photochemical reactions on SERS-active substrates may be also enhanced. Goncher and Harris⁴⁸⁰ reported photofragmentation of several molecules adsorbed on a silver surface, with an incident wavelength of 363.8 nm(!). They attribute the reaction to enhanced singlet-triplet transitions or to multiphoton processes. Chen and Osgood⁴⁸¹ reported enhanced photodeposition on several metals, but not on gold, at 257 nm.

Garoff *et al.*²²⁶ report contrary behavior. They noticed slower rates of photofragmentation on silver islands as compared to an oxide substrate. This is probably due to the efficient dissipative channel for transfer of excess energy of the molecule to the metal, which arises upon adsorption.

Weitz *et al.*²⁴⁰ also noted an effect of SERS-active systems on the fluorescence of molecules. For the molecules they studied, a low quantum yield in the bulk was associated with higher fluorescence on the surface, while efficient emitters exhibited a quenched fluorescence.

Chuang⁴⁸² and Chuang and Seki^{483,484} reported enhanced desorption rates of pyridine from silver when illuminated in the IR near a pyridine vibrational frequency. The rate was nonlinear in the laser intensity and exhibited a definite resonance behavior around the breathing mode of pyridine. Pyridine on KCl gave essentially similar results. It seems that local heating due to the absorbance of the pyridine is important here.

Another phenomenon related to SERS and supposed to be affected by the same mechanisms, is second harmonic generation (SHG). This was seen a long time ago by Lee *et al.*⁴⁸⁵ In a series of papers, Chen *et al.*^{95,486-489} reported enhanced SHG with enhancement factors ranging from 100 to 10^4 . These results have an immediate impact on the validity of the LFE mechanism. However, the role of field gradients has not been considered. SHG was used to monitor changes on a silver electrode during electric potential cycling.⁴⁹⁰

Also coherent anti-Stokes Raman scattering (CARS) was tried in SERS-active systems. Schneider⁴⁹¹ measured the CARS of benzene on a silver film. The degree of enhancement (if any) is not given. Chew *et al.*⁴⁹² have presented a theoretical discussion of the CARS on colloids. Schneider⁴⁹¹ reported that CARS was not seen on colloids, due to a small interaction zone.

Finally, Glass *et al.*⁴⁹³ investigated two-photon fluorescence of molecules adsorbed on silver surfaces, and found an enhancement factor of ~ 150 .

Examples of several of the ways SERS has been utilized were quoted here in order to show the directions of research and application. The validity of the various applications and their results are still an open question, and hopefully will be investigated in future experiments.

As a final note, it is useful to quote Furtak¹³⁸ once again: "We have shown in this report, given the state of understanding as it now exists, that some . . . systems can already be studied in detail using enhanced Raman scattering. If we can develop the technique to its potential, as Auger spectroscopy has been developed in surface-vacuum characterization, understanding of the metal-electrolyte interface will be propelled by a genuine breakthrough." This holds true today, five years later. The *if* is perhaps smaller, but it is still there!

ACKNOWLEDGMENTS

I wish to thank Mr. Hai Cohen for his invaluable help in assembling and cataloging the extensive literature.

REFERENCES

- ¹ M. Fleischmann, P. J. Hendra, and A. J. McQuillan, *Chem. Phys. Lett.* **26** (1974) 163.
- ² A. J. McQuillan, P. J. Hendra, and M. Fleischmann, *J. Electroanal. Chem.* **65** (1975) 933.
- ³ M. Fleischmann, P. J. Hendra, A. J. McQuillan, R. L. Paul, and E. S. Reid, *J. Raman Spectrosc.* **4** (1976) 269.
- ⁴ R. P. Cooney, E. S. Reid, M. Fleischmann, and P. J. Hendra, *J. Chem. Soc., Faraday Trans. 1* **73** (1977) 1691.
- ⁵ D. L. Jeanmaire and R. P. Van Duyne, *J. Electroanal. Chem.* **84** (1977) 1.
- ⁶ M. G. Albrecht and J. A. Creighton, *J. Am. Chem. Soc.* **99** (1977) 5215.
- ⁷ M. G. Albrecht and J. A. Creighton, *Electrochim. Acta* **23** (1978) 1103.
- ⁸ R. P. Van Duyne, in *Chemical and Biochemical Applications of Lasers*, Ed. by C. B. Moore, Academic Press, New York, 1979, Vol. 4, p. 101.
- ⁹ T. E. Furtak and J. Reyes, *Surf. Sci.* **93** (1980) 351.
- ¹⁰ A. Otto, *Appl. Surf. Sci.* **6** (1980) 309.
- ¹¹ J. A. Creighton, in *Springer Series in Chemical Physics Vol. 15, Vibrational Spectroscopy of Adsorbates*, Ed. by R. F. Willis, Springer-Verlag, New York, 1980, p. 145.
- ¹² M. Kerker, *Pure Appl. Chem.* **53** (1981).
- ¹³ H. Yamada, *Appl. Spectrosc. Rev.* **17** (1981) 227.
- ¹⁴ R. L. Birke, J. R. Lombardi, and L. A. Sanchez, *Advances in Chemistry Series No. 201, Electrochemical and Spectrochemical Studies of Biological Redox Components*, Ed. by M. Kadish, American Chemical Society, Washington, D.C., 1982, Chap. 4, p. 69.
- ¹⁵ R. Dornhaus, *Festkörperprobleme XXII* (1982).
- ¹⁶ A. Otto, in *Light Scattering in Solids Vol. 4, Topics in Applied Physics*, Ed. by M. Cardona and G. Guntherodt, Springer, Berlin, 1983.
- ¹⁷ I. Pockrand, *Surface Enhanced Raman Vibrational Studies at Solid / Gas interfaces, Springer Tracts in Modern Physics*, Vol. 104, Springer-Verlag, New York, 1984.

- ¹⁸ R. Mills, *Surf. Interface Anal.* **5** (1983) 43.
- ¹⁹ T. E. Furtak, *J. Electroanal. Chem.* **150** (1983) 375.
- ²⁰ J. L. Birman, H. Z. Cummins, and K. K. Rebane, Eds., *Light Scattering in Solids*, Proceedings of the Second Joint USA-USSR Symposium, Plenum Press, New York, 1979.
- ²¹ W. F. Murphy, Ed., *Proceedings VIIth International Conference on Raman Spectroscopy*, Ottawa, North-Holland, Amsterdam 1980.
- ²² *Proceedings VIIIth International Conference on Raman Spectroscopy*, Bordeaux, North-Holland, Amsterdam 1982.
- ²³ R. K. Chang and T. E. Furtak, Eds., *Surface Enhanced Raman Scattering*, Plenum Press, New York, 1982.
- ²⁴ S. Efrima and H. Metiu, *Chem. Phys. Lett.* **60** (1978) 59.
- ²⁵ S. Efrima and H. Metiu, *J. Chem. Phys.* **70** (1979) 1602.
- ²⁶ S. Efrima and H. Metiu, *J. Chem. Phys.* **70** (1979) 2297.
- ²⁷ A. Champion and D. R. Mullins, *Chem. Phys. Lett.* **94** (1983) 576.
- ²⁸ A. Champion, J. K. Brown, and V. M. Grizzle, *Surf. Sci.* **115** (1982) L153.
- ²⁹ J. D. Bergman, J. P. Heritage, A. Pinzuk, J. M. Worlock, and J. H. McFee, *Chem. Phys. Lett.* **68** (1979) 412.
- ³⁰ G. Blondeau, J. Corset, A. Regis, and N. Jaffrezic, *Thin Solid Films* **82** (1981) 97.
- ³¹ G. Blondeau, J. Zerbino, and N. Jaffrezic-Renault, *J. Electroanal. Chem.* **112** (1980) 127.
- ³² G. Blondeau, M. Froment, J. Zerbino, N. Jaffrezic-Renault, and G. Revel, *J. Electroanal. Chem.* **105** (1979) 409.
- ³³ O. Siiman, L. A. Bumm, R. Callaghan, C. G. Blatchford, and M. Kerker, *J. Phys. Chem.* **87** (1983) 1014.
- ³⁴ O. Siiman, L. A. Bumm, R. Callaghan, and M. Kerker, *Time Resolved Vibrational Spectroscopy*, Academic Press, New York, 1983, p. 387.
- ³⁵ C. G. Blatchford, J. R. Campbell, and J. A. Creighton, *Surf. Sci.* **120** (1982) 435.
- ³⁶ J. A. Creighton, M. S. Alvarez, D. A. Weitz, S. Garoff, and M. W. Kim, *J. Phys. Chem.* **87** (1983) 4793.
- ³⁷ C. C. Busby and J. A. Creighton, *J. Electroanal. Chem.* **133** (1982) 183.
- ³⁸ A. M. Stacy and R. P. Van Duyne, *Chem. Phys. Lett.* **102** (1983) 365.
- ³⁹ T. H. Wood, D. A. Zwemer, C. V. Shank, and J. E. Row, *Chem. Phys. Lett.* **82** (1981) 5.
- ⁴⁰ G. L. Eesley and J. M. Burkstrand, *Phys. Rev. B* **24** (1981) 582.
- ⁴¹ G. L. Eesley and D. L. Simon, *J. Vac. Sci. Technol.* **18** (1981) 629.
- ⁴² H. Seki, *J. Vac. Sci. Technol.* **18** (1981) 633.
- ⁴³ G. L. Eesley, *Phys. Lett.* **81A** (1981) 193.
- ⁴⁴ P. N. Sanda, J. M. Warlaumont, J. E. Demuth, J. C. Tsang, K. Christmann, and J. A. Bradley, *Phys. Rev. Lett.* **45** (1980) 1519.
- ⁴⁵ I. Pockrand and A. Otto, *Solid State Commun.* **35** (1980) 861.
- ⁴⁶ K. Manzel, W. Schultze, and M. Moskovits, *Chem. Phys. Lett.* **85** (1982) 183.
- ⁴⁷ C. A. Murray and D. L. Allara, *J. Chem. Phys.* **76** (1982) 1290.
- ⁴⁸ C. A. Murray, D. L. Allara, and M. Rhinewine, *Phys. Rev. Lett.* **46** (1981) 57.
- ⁴⁹ A. Bachackashvilli, Z. Priel, S. Efrima, and B. Katz, Raman scattering of methyl-*red* adsorbed on silver colloids, unpublished paper.
- ⁵⁰ M. Moskovits and D. P. DiLella, *Chem. Phys. Lett.* **73** (1980) 500.
- ⁵¹ G. R. Erdheim, R. L. Birke, and J. R. Lombardi, *Chem. Phys. Lett.* **69** (1980) 495.
- ⁵² M. Ohsawa and W. Suetaka, *J. Electron Spectrosc. Related Phenomena* **30** (1983) 221.
- ⁵³ C. G. Allen and R. P. Van Duyne, *J. Am. Chem. Soc.* **103** (1981) 7497.
- ⁵⁴ J. C. Tsang, J. R. Kirtley, and T. N. Theis, *J. Chem. Phys.* **77** (1982) 641.

- ⁵⁵ R. Dornhaus, *J. Electron Spectrosc. Related Phenomena* **30** (1983) 197.
- ⁵⁶ C. J. Sandroff and D. R. Herschbach, *J. Phys. Chem.* **86** (1982) 3277.
- ⁵⁷ S. H. Macomber and T. E. Furtak, *Chem. Phys. Lett.* **90** (1982) 59.
- ⁵⁸ D. P. DiLella, A. Gohin, R. H. Lipson, P. McBreen, and M. Moskovits, *J. Chem. Phys.* **73** (1980) 4282.
- ⁵⁹ M. E. Lippitsch, *Chem. Phys. Lett.* **74** (1980) 125.
- ⁶⁰ J. A. Creighton, C. G. Blatchford, and M. G. Albrecht, *J. Chem. Soc., Faraday Trans. 2* **75** (1979) 790.
- ⁶¹ H. Wetzel, B. Pettinger, and U. Wenning, *Chem. Phys. Lett.* **75** (1980) 173.
- ⁶² M. Ohsawa, K. Nishijima, and W. Suetaka, *Surf. Sci.* **104** (1980) 270.
- ⁶³ C. Y. Chen, E. Burstein, and S. Lundquist, *Solid State Commun.* **32** (1979) 63.
- ⁶⁴ R. L. Birke and J. R. Lombardi, *Phys. Rev. Lett.* **43** (1979) 71.
- ⁶⁵ J. P. Heritage, J. G. Bergman, A. Pinczuk, and J. M. Worlock, *Chem. Phys. Lett.* **67** (1979) 229.
- ⁶⁶ J. Timper, J. Billmann, A. Otto, and I. Pockrand, *Surf. Sci.* **101** (1980) 348.
- ⁶⁷ B. Pettinger, M. R. Philpott, and J. G. Gordon II, *J. Chem. Phys.* **75** (1981) 934.
- ⁶⁸ J. I. Gersten, D. A. Weitz, T. J. Garmila, and A. Z. Genack, *Phys. Rev. B* **22** (1980) 4562.
- ⁶⁹ I. Pockrand and A. Otto, *Appl. Surf. Sci.* **6** (1980) 362.
- ⁷⁰ A. Otto, J. Timper, J. Billmann, and I. Pockrand, *Phys. Rev. Lett.* **45** (1980) 46.
- ⁷¹ A. Otto, J. Timper, J. Billmann, G. Kovacs, and I. Pockrand, *Surf. Sci.* **92** (1980) L55.
- ⁷² I. Pockrand and A. Otto, *Solid State Commun.* **37** (1981) 109.
- ⁷³ T. H. Wood and M. V. Klein, *Solid State Commun.* **35** (1980) 263.
- ⁷⁴ R. E. Benner, K. U. Von Raben, R. Dornhaus, R. K. Chang, B. L. Laube, and F. A. Otter, *Surf. Sci.* **102** (1981) 7.
- ⁷⁵ H. Seki, *J. Chem. Phys.* **76** (1982) 4412.
- ⁷⁶ V. V. Marinyuk, R. M. Lazorenko-Manevich, and Ya. M. Kolotyркиn, *Sov. Electrochem.* **17** (1981) 527.
- ⁷⁷ I. Pockrand and A. Otto, *Solid State Commun.* **38** (1981) 1159.
- ⁷⁸ K. U. Von Raben, R. K. Chang, and B. L. Laube, *Chem. Phys. Lett.* **79** (1981) 465.
- ⁷⁹ I. Pockrand, *Chem. Phys. Lett.* **85** (1982) 37.
- ⁸⁰ I. Pockrand, J. Billmann, and A. Otto, *J. Chem. Phys.* **78** (1983) 6384.
- ⁸¹ R. K. Chang, R. E. Benner, R. Dornhaus, K. U. Von Raben, and B. L. Laube, *Springer Ser. Opt. Sci.* **26** (1981) 55.
- ⁸² B. H. Loo, *Solid State Commun.* **43** (1982) 349.
- ⁸³ H. Seki, *J. Vac. Sci. Technol.* **20** (1982) 584.
- ⁸⁴ H. Seki, *Solid State Commun.* **42** (1982) 695.
- ⁸⁵ J. Billmann and A. Otto, *Appl. Surf. Sci.* **6** (1980) 356.
- ⁸⁶ T. Watanabe and B. Pettinger, *Chem. Phys. Lett.* **89** (1982) 501.
- ⁸⁷ S. G. Schultz, M. Janik-Czachor, and R. P. Van Duyne, *Surf. Sci.* **104** (1981) 419.
- ⁸⁸ C. S. Allen, G. C. Schatz, and R. P. Van Duyne, *Chem. Phys. Lett.* **75** (1980) 201.
- ⁸⁹ R. M. Hexter and M. G. Albrecht, *Electrochim. Acta* **35A** (1979) 233.
- ⁹⁰ G. Laufer, T. F. Schaaf, and J. T. Huneke, *J. Chem. Phys.* **73** (1980) 2973.
- ⁹¹ K. A. Bunding, J. R. Lombardi, and R. L. Birke, *Chem. Phys.* **49** (1980) 53.
- ⁹² J. Billmann, G. Kovacs, and A. Otto, *Surf. Sci.* **92** (1980) 153.
- ⁹³ R. Naaman, S. J. Buelow, O. Cheshnovsky, and D. R. Herschbach, *J. Phys. Chem.* **84** (1980) 2692.
- ⁹⁴ H. W. K. Tom, C. K. Chen, A. R. B. de Castro, and Y. R. Shen, *Solid State Commun.* **41** (1982) 259.
- ⁹⁵ C. K. Chen, T. F. Heinz, D. Ricard, and Y. R. Shen, *Phys. Rev. B* **27** (1983) 1965.
- ⁹⁶ M. Kerker, O. Siiman, L. A. Bumm and D. S. Wang, *Appl. Opt.* **19** (1980) 3253.

- ⁹⁷ J. S. Suh, D. P. DiLella, and M. Moskovits, *J. Chem. Phys.* **87** (1983) 1540.
- ⁹⁸ W. Krasser and A. J. Renouprez, *J. Raman Spectrosc.* **11** (1981) 425.
- ⁹⁹ W. Krasser, H. Ervens, A. Fadini, and A. J. Renouprez, *J. Raman Spectrosc.* **9** (1980) 80.
- ¹⁰⁰ R. R. Smardzewski, R. J. Colton, and J. S. Murday, *Chem. Phys. Lett.* **68** (1979) 53.
- ¹⁰¹ J. E. Rowe, C. V. Shank, D. A. Zwemer, and C. A. Murray, *Phys. Rev. Lett.* **44** (1980) 1770.
- ¹⁰² D. A. Zwemer, C. V. Shank, and J. E. Rowe, *Chem. Phys. Lett.* **73** (1980) 201.
- ¹⁰³ I. Pockrand, *Chem. Phys. Lett.* **92** (1982) 509.
- ¹⁰⁴ A. V. Bobrov, A. N. Gass, O. I. Kapusta, and N. M. Omel'yanovskaya, *ZhETF Pis. Red. [JETP Lett.]* **35** (1982) 626.
- ¹⁰⁵ D. P. DiLella and M. Moskovits, *J. Chem. Phys.* **85** (1981) 2042.
- ¹⁰⁶ M. Moskovits and D. P. DiLella, in Reference 23, p. 243.
- ¹⁰⁷ C. A. Murray, in Reference 23, p. 203.
- ¹⁰⁸ M. Udagawa, Chih-Cong Chou, J. C. Hemminger, and S. Ushioda, *Phys. Rev. B* **23** (1981) 6843.
- ¹⁰⁹ A. Campion, *J. Electron Spectrosc. Related Phenomena* **29** (1983) 397.
- ¹¹⁰ J. C. Tsang, Ph. Avouris, and J. R. Kirtley, *J. Electron Spectrosc. Related Phenomena* **29** (1983) 343.
- ¹¹¹ T. E. Furtak, G. Trott, and B. H. Loo, *Surf. Sci.* **101** (1980) 374.
- ¹¹² B. Pettinger and U. Wenning, *Chem. Phys. Lett.* **56** (1978) 253.
- ¹¹³ J. F. Evans, M. G. Albrecht, D. M. Ullevig, and R. M. Hexter, *J. Electroanal. Chem.* **106** (1980) 209.
- ¹¹⁴ R. Dormhaus, M. B. Long, R. E. Benner, and R. K. Chang, *Surf. Sci.* **93** (1980) 240.
- ¹¹⁵ J. T. Hupp, D. Larkin, and M. J. Weaver, *Surf. Sci.* **125** (1983) 429.
- ¹¹⁶ B. Pettinger, U. Wenning, and H. Wetzler, *Surf. Sci.* **101** (1980) 409.
- ¹¹⁷ T. E. Furtak and D. Roy, *Phys. Rev. Lett.* **50** (1983) 1301.
- ¹¹⁸ A. Regis, P. Dumas, and J. Corset, *J. Electron Spectrosc. Related Phenomena* **30** (1983) 203.
- ¹¹⁹ C. G. Blatchford, M. Kerker, and D. S. Wang, *Chem. Phys. Lett.* **100** (1983) 230.
- ¹²⁰ R. E. Kunz, J. G. Gordon II, M. R. Philpott, and A. Girlando, *J. Electroanal. Chem.* **112** (1980) 391.
- ¹²¹ F. Barz, J. G. Gordon II, M. R. Philpott, and M. J. Weaver, *Chem. Phys. Lett.* **94** (1983) 168.
- ¹²² V. V. Marinyuk and R. M. Lazorenko-Manevich, *Sov. Electrochem.* (1980) 283.
- ¹²³ D. M. Kolb, in *Advances in Electrochemistry and Electrochemical Engineering*, Ed. by H. Gerisher and C. W. Tobias, Wiley, New York, 1978, Vol. 11, Chap. 2.
- ¹²⁴ R. Dornhaus and R. K. Chang, *Solid State Commun.* **34** (1980) 811.
- ¹²⁵ R. P. Cooney, M. W. Howard, M. R. Mahoney, and T. P. Mernagh, *Chem. Phys. Lett.* **79** (1981) 459.
- ¹²⁶ M. Fleischmann and I. R. Hill, in Reference 23, p. 275.
- ¹²⁷ S. H. Macomber, T. E. Furtak, and T. M. Devine, *Chem. Phys. Lett.* **90** (1982) 439.
- ¹²⁸ F. Barz, J. G. Gordon II, M. R. Philpott, and M. J. Weaver, *Chem. Phys. Lett.* **91** (1982) 291.
- ¹²⁹ T. T. Chen, K. U. Von Raben, J. F. Owen, R. K. Chang, and B. L. Laube, *Chem. Phys. Lett.* **91** (1982) 494.
- ¹³⁰ T. M. Devine, T. E. Furtak, and S. H. Macomber, *J. Electroanal. Chem.* **164** (1984) 299.
- ¹³¹ M. Fleischmann and I. R. Hill, *J. Electroanal. Chem.* **146** (1983) 353.
- ¹³² M. R. Mahoney and R. P. Cooney, *J. Phys. Chem.* **87** (1983) 4589.

- ¹³³ A. M. Stacy and R. P. Van Duyne, *Time Resolved Vibrational Spectroscopy* Academic Press, New York, p. 377.
- ¹³⁴ W. Suetaka and M. Ohsawa, *Appl. Surf. Sci.* **3** (1979) 118.
- ¹³⁵ B. Pettinger, M. R. Philpott, and J. G. Gordon II, *Surf. Sci.* **105** (1981) 469.
- ¹³⁶ M. Fleischmann, P. R. Graves, I. R. Hill, and J. Robinson, *Chem. Phys. Lett.* **95** (1983) 322.
- ¹³⁷ M. W. Howard, R. P. Cooney, and A. J. McQuillan, *J. Raman Spectrosc.* **9** (1980) 273.
- ¹³⁸ T. E. Furtak, *Solid State Commun.* **28** (1978) 903.
- ¹³⁹ H. Wroblowa and M. Green, *Electrochim. Acta* **8** (1963) 679.
- ¹⁴⁰ R. E. Benner, R. Dornhaus, R. K. Chang, and B. L. Laube, *Surf. Sci.* **101** (1980) 341.
- ¹⁴¹ W. Plieth, B. Roy, and H. Bruckner, *Ber. Bunsenges. Phys. Chem.* **85** (1981) 499.
- ¹⁴² H. Wetzel, H. Gerischer, and B. Pettinger, *Chem. Phys. Lett.* **80** (1981) 159.
- ¹⁴³ M. J. Weaver, F. Barz, J. G. Gordon II, and M. R. Philpott, *Surf. Sci.* **125** (1983) 409.
- ¹⁴⁴ L. A. Sanchez, R. L. Birke, and J. R. Lombardi, *J. Phys. Chem.* **88** (1984) 1762.
- ¹⁴⁵ G. Hagen, B. Simić Glavanski, and E. Yeager, *J. Electroanal. Chem.* **88** (1978) 269.
- ¹⁴⁶ R. Kotz and E. Yeager, *J. Electroanal. Chem.* **123** (1981) 335.
- ¹⁴⁷ A. B. Anderson, R. Kotz, and E. Yeager, *Chem. Phys. Lett.* **82** (1981) 130.
- ¹⁴⁸ K. Hutchinson, A. J. McQuillan, and R. E. Hester, *Chem. Phys. Lett.* **98** (1983) 27.
- ¹⁴⁹ M. L. A. Temperini, H. C. Chagas, and O. Sala, *Chem. Phys. Lett.* **79** (1981) 75.
- ¹⁵⁰ J. Turkevich, P. C. Stephenson, and J. Hillier, *Discussions Faraday Soc.* **11** (1951) 55.
- ¹⁵¹ R. M. Wilenzick, D. C. Russel, R. H. Morriss, and S. W. Mashall, *J. Chem. Phys.* **27** (1967) 533.
- ¹⁵² M. Kerker, *The Scattering of Light and Other Electromagnetic Radiation*, Academic Press, New York, 1969.
- ¹⁵³ H. Wetzel, H. Gerischer, and B. Pettinger, *Chem. Phys. Lett.* **85** (1982) 187.
- ¹⁵⁴ C. G. Blatchford, O. Siiman, and M. Kerker, *J. Phys. Chem.* **87** (1983) 2503.
- ¹⁵⁵ J. G. Bergman, D. S. Chemla, P. F. Liao, A. M. Glass, A. Pinzuk, R. M. Hart, and D. H. Olson, *Opt. Lett.* **6** (1981) 33.
- ¹⁵⁶ W. Knoll, M. Philpott, and W. G. Golden, *J. Chem. Phys.* **77** (1982) 219.
- ¹⁵⁷ D. A. Weitz, S. Garoff, and T. J. Gramila, *Opt. Lett.* **7** (1982) 168; A. Z. Genack, D. A. Weitz, and T. J. Gramila, *Surf. Sci.* **101** (1980) 381.
- ¹⁵⁸ I. Pockrand, A. Brillante, and M. Mobius, *Chem. Phys. Lett.* **68** (1980) 499.
- ¹⁵⁹ W. Knoll, M. R. Philpott, J. D. Swalen, and A. Girlando, *J. Chem. Phys.* **75** (1981) 4795.
- ¹⁶⁰ H. D. Ladouceur, D. E. Tevault, and R. R. Smardzewski, *J. Chem. Phys.* **78** (1983) 980.
- ¹⁶¹ J. C. Tsang and J. Kirtley, *Solid State Commun.* **30** (1979) 617.
- ¹⁶² G. L. Eesley, *Phys. Rev. B* **24** (1981) 5477.
- ¹⁶³ T. H. Wood and M. V. Klein, *J. Vac. Sci. Technol.* **16** (1979) 459.
- ¹⁶⁴ T. H. Wood, *Phys. Rev. B* **24** (1981) 2289.
- ¹⁶⁵ T. H. Wood and D. A. Zwemer, *J. Vac. Sci. Technol.* **18** (1981) 649.
- ¹⁶⁶ L. V. DelPriore, C. Doyle, and J. D. Andrade, *Appl. Spectrosc.* **36** (1982) 69.
- ¹⁶⁷ H. Seki and T. J. Chuang, *Chem. Phys. Lett.* **100** (1983) 393.
- ¹⁶⁸ Y. Mo, I. Morke, and P. Wachter, *Surf. Sci.* **133** (1983) L452.
- ¹⁶⁹ C. A. Murray, D. L. Allara, A. F. Hebard, and F. J. Padden, Jr., *Surf. Sci.* **119** (1982) 449.
- ¹⁷⁰ J. C. Tsang, J. R. Kirtley, and J. A. Bradley, *Phys. Rev. Lett.* **43** (1979) 772.
- ¹⁷¹ W. Krasser and A. J. Renouprez, *Solid State Commun.* **41** (1982) 231.

- ¹⁷² R. M. Hart, J. G. Bergman, and A. Wokaun, *Opt. Lett.* **7** (1982) 105.
- ¹⁷³ P. F. Liao, J. G. Bergman, D. S. Chemla, A. Wokaun, J. Melngailis, A. M. Hawryluk, and N. P. Economou, *Chem. Phys. Lett.* **82** (1981) 355.
- ¹⁷⁴ P. F. Liao and M. B. Stern, *Opt. Lett.* **7** (1982) 483.
- ¹⁷⁵ J. C. Tsang, J. R. Kirtley, and T. N. Theis, *Solid State Commun.* **35** (1980) 667.
- ¹⁷⁶ J. C. Tsang, J. R. Kirtley, T. N. Theis, and S. S. Jha, *Phys. Rev. B* **25** (1982) 5070.
- ¹⁷⁷ R. Dornhaus, R. E. Benner, R. K. Chang, and I. Chabay, *Surf. Sci.* **101** (1980) 367.
- ¹⁷⁸ S. A. Lyon and J. M. Worlock, *Phys. Rev. Lett.* **51** (1983) 593.
- ¹⁷⁹ J. P. Goudonnet, G. M. Begun, and E. T. Arakawa, *Chem. Phys. Lett.* **92** (1982) 197.
- ¹⁸⁰ H. Seki, *J. Electron Spectrosc. Related Phenomena* **30** (1983) 287.
- ¹⁸¹ I. Bernard, private communication.
- ¹⁸² R. M. Creighton, M. G. Albrecht, R. E. Hester, and J. A. D. Matthew, *Chem. Phys. Lett.* **55** (1978) 55.
- ¹⁸³ K. A. Bunding, R. L. Birke, and J. R. Lombardi, *Chem. Phys. Lett.* **54** (1980) 115.
- ¹⁸⁴ S. Venkatesan, G. Erdheim, J. R. Lombardi, and R. L. Birke, *Surf. Sci.* **101** (1980) 387.
- ¹⁸⁵ B. Pettinger, U. Wenning, and D. M. Kolb, *Ber. Bunsenges. Phys. Chem.* **82** (1978) 1326.
- ¹⁸⁶ R. E. Hexter, *Solid State Commun.* **32** (1979) 55.
- ¹⁸⁷ H. Nichols and R. M. Hexter, *J. Chem. Phys.* **74** (1981) 2059.
- ¹⁸⁸ H. Wetzel, H. Gerischer, and B. Pettinger, *Chem. Phys. Lett.* **78** (1981) 392.
- ¹⁸⁹ A. Regis and J. Corset, *Chem. Phys. Lett.* **70** (1980) 305.
- ¹⁹⁰ B. H. Loo, *J. Chem. Phys.* **86** (1982) 433.
- ¹⁹¹ H. Wetzeel and H. Gerischer, *Chem. Phys. Lett.* **76** (1980) 460.
- ¹⁹² R. L. Garrell, K. D. Shaw, and S. Krimm, *J. Chem. Phys.* **75** (1981) 4155.
- ¹⁹³ J. R. Lombardi, E. A. Shields Knight, and R. L. Birke, *Chem. Phys. Lett.* **79** (1981) 214.
- ¹⁹⁴ M. Moskovits, *Chem. Phys. Lett.* **98** (1983) 498.
- ¹⁹⁵ B. H. Loo, *J. Electroanal. Chem.* **131** (1982) 381.
- ¹⁹⁶ W. Krasser, U. Kettler, and P. S. Bechthold, *Chem. Phys. Lett.* **86** (1982) 223.
- ¹⁹⁷ S. H. Macomber and T. E. Furtak, *Solid State Commun.* **45** (1983) 267.
- ¹⁹⁸ D. A. Weitz, T. J. Gramila, A. Z. Genack, and J. I. Gersten, *Phys. Rev. Lett.* **45** (1980) 355.
- ¹⁹⁹ D. A. Weitz, T. J. Gramila, and A. Z. Genack, in Reference 23, p. 339.
- ²⁰⁰ M. Fleischmann, I. R. Hill, and J. Robinson, *Chem. Phys. Lett.* **97** (1983) 441.
- ²⁰¹ R. L. Birke, I. Bernard, L. A. Sanchez, and J. R. Lombardi, *J. Electroanal. Chem.* **150** (1983) 447.
- ²⁰² M. Fleischmann, P. R. Graves, I. R. Hill, and J. Robinson, *Chem. Phys. Lett.* **98** (1983) 503.
- ²⁰³ M. Fleischmann, J. Robinson, and R. Waser, *J. Electroanal. Chem.* **117** (1981) 257.
- ²⁰⁴ M. Fleischmann, P. J. Hendra, I. R. Hill, and M. E. Pemble, *J. Electroanal. Chem.* **117** (1981) 243.
- ²⁰⁵ B. Pettinger and H. Wetzel, *Ber. Bunsenges. Phys. Chem.* **85** (1981) 473.
- ²⁰⁶ I. Pockrand, *Surf. Sci.* **122** (1982) L569.
- ²⁰⁷ M. Fleischmann, I. R. Hill, and M. E. Pemble, *J. Electroanal. Chem.* **136** (1982) 361.
- ²⁰⁸ T. T. Chen, J. F. Owen, R. K. Chang, and B. L. Laube, *Chem. Phys. Lett.* **89** (1982) 356.
- ²⁰⁹ M. Fleischmann and I. R. Hill, *J. Electroanal. Chem.* **146** (1983) 367.
- ²¹⁰ G. Valette, *J. Electroanal. Chem.* **139** (1982) 285.
- ²¹¹ D. A. Long, *Raman Spectroscopy*, McGraw-Hill, New York, 1977.

- 212 K. W. Hipps and J. W. Keder, *J. Phys. Chem.* **87** (1983) 3186.
- 213 R. Kotz and E. Yeager, *J. Electroanal. Chem.* **113** (1980) 113.
- 214 J. E. Pemberton and R. P. Buck, *J. Phys. Chem.* **85** (1981) 248.
- 215 J. E. Pemberton and R. P. Buck, *J. Phys. Chem.* **87** (1983) 3336.
- 216 C. G. Blatchford, J. R. Campbell, and J. A. Creighton, *Surf. Sci.* **108** (1981) 411.
- 217 J. R. Campbell and J. A. Creighton, *J. Electroanal. Chem.* **143** (1983) 353.
- 218 T. M. Cotton, S. G. Schultz, and R. P. Van Duyne, *J. Am. Chem. Soc.* **102** (1980) 7962.
- 219 T. M. Cotton, R. Timkovich, and M. S. Cork, *FEBS Lett.* **133** (1981) 39.
- 220 L. Stryer, *Biochemistry*, Freeman, San Francisco, 1981.
- 221 T. M. Cotton, S. G. Schultz, and R. P. Van Duyne, *J. Am. Chem. Soc.* **104** (1982) 6528.
- 222 M. Itabashi, K. Kato, and K. Itoh, *Chem. Phys. Lett.* **97** (1983) 528.
- 223 J. J. McMahon, in Reference 22, p. 77.
- 224 K. Hutchinson, A. J. McQuillan, and R. E. Hester, *Chem. Phys. Lett.* **98** (1983) 27.
- 225 R. P. Van Duyne and J. P. Haushalter, *J. Phys. Chem.* **87** (1983) 2999.
- 226 S. Garoff, D. A. Weitz, and M. S. Alvarez, *Chem. Phys. Lett.* **93** (1982) 283.
- 227 M. E. Lippitsch, *Chem. Phys. Lett.* **79** (1981) 224.
- 228 M. E. Lippitsch, in Reference 22, p. 65.
- 229 A. Bachackashvilli, S. Efrima, B. Katz, and Z. Priel, *Chem. Phys. Lett.* **94** (1983) 571.
- 230 A. Bachackashvilli, B. Katz, Z. Priel, and S. Efrima, *J. Phys. Chem.* **88** (1984) 6185.
- 231 P. C. Lee and D. Meisel, *J. Phys. Chem.* **86** (1982) 3391.
- 232 O. Siiman, A. Lepp, and M. Kerker, *Chem. Phys. Lett.* **100** (1983) 163.
- 233 O. Siiman, A. Lepp, and M. Kerker, *J. Phys. Chem.* **87** (1983) 5319; O. Siiman and A. Lepp, *J. Phys. Chem.* **88** (1984) 2641.
- 234 D. L. Akins, *J. Colloid. Interface Sci.* **90** (1982) 373.
- 235 X. Li, B. Gu, and D. L. Akins, *Chem. Phys. Lett.* **105** (1984) 263.
- 236 R. Aroca and R. O. Loutfy, *J. Raman Spectrosc.* **12** (1982) 262.
- 237 R. O. Loutfy, *Can. J. Chem.* **59** (1981) 549.
- 238 C. Y. Chen, I. Davoli, G. Ritchie, and E. Burstein, *Surf. Sci.* **101** (1980) 363.
- 239 D. A. Weitz, S. Garoff, J. I. Gersten, and A. Nitzan, *J. Electron Spectrosc. Related Phenomena* **29** (1983) 363.
- 240 D. A. Weitz, S. Garoff, J. I. Gersten, and A. Nitzan, *J. Chem. Phys.* **78** (1983) 5324.
- 241 J. A. Nimmo, A. A. McConnell, and W. E. Smith, in Reference 22, p. 89.
- 242 K. Shoji, Y. Kobayashi, and K. Itoh, *Chem. Phys. Lett.* **102** (1983) 179.
- 243 D. N. Batchelder, N. J. Poole, and D. Bloor, *Chem. Phys. Lett.* **81** (1981) 560.
- 244 V. V. Marinyuk, R. M. Lazorenko-Manevich, and Ya. M. Kolotyркиn, *J. Electroanal. Chem.* **110** (1980) 111.
- 245 U. Wenning, B. Pettinger, and H. Wetzal, *Chem. Phys. Lett.* **70** (1980) 49.
- 246 M. Mabuchi, T. Takenaka, Y. Fujiyoshi, and N. Uyeda, *Surf. Sci.* **119** (1982) 150.
- 247 S. M. Heard, F. Grieser, and C. G. Barraclough, *Chem. Phys. Lett.* **95** (1983) 154.
- 248 I. Pockrand, *J. Electron Spectrosc. Related Phenomena* **29** (1983) 357.
- 249 R. L. Paul, A. J. McQuillan, P. J. Hendra, and M. Fleischmann, *J. Electroanal. Chem.* **66** (1975) 248.
- 250 B. Pettinger, M. R. Philpott, and J. G. Gordon II, *J. Phys. Chem.* **85** (1981) 2736.
- 251 P. S. Bechthold, U. Kettler, and W. Krasser, in Reference 22, p. 91.
- 252 D. E. Tevault and R. R. Smardzewski, *J. Chem Phys* **77** (1982) 2221.
- 253 B. H. Loo and T. E. Furtak, *Chem. Phys. Lett.* **71** (1980) 68.
- 254 W. Plieth, B. Roy, and H. Bruckner, *Ber. Bunsenges. Phys. Chem.* **86** (1982) 273.
- 255 J. J. Kester and T. E. Furtak, *Solid State Commun* **41** (1982) 457.
- 256 C. A. Murray, *J. Electron Spectrosc. Related Phenomena* **29** (1983) 371.

- 257 R. P. Cooney, E. S. Reid, P. J. Hendra, and M. Fleischmann, *J. Am. Chem. Soc.* **99** (1977) 2002.
- 258 R. P. Cooney, P. J. Hendra, and M. Fleischmann, *J. Raman Spectrosc.* **6** (1977) 264.
- 259 R. P. Cooney, M. Fleischmann, and P. J. Hendra, *J. Chem. Soc. Chem. Commun.* (1977) 235.
- 260 J. Heitbaum, *Z. Phys. Chem. Neue Folge, Bd.* **105** (1977) 307.
- 261 B. H. Loo, *J. Phys. Chem.* **87** (1983) 3003.
- 262 R. E. Benner, K. U. Von Raben, J. F. Owen, R. K. Chang, and B. L. Laube, *Chem. Phys. Lett.* **96** (1983) 65.
- 263 B. H. Loo, *J. Chem. Phys.* **75** (1981) 5955.
- 264 B. Pettinger and L. Moerl, *J. Electron Spectrosc. Related Phenomena* **29** (1983) 383.
- 265 T. E. Furtak and J. Kester, *Phys. Rev. Lett.* **45** (1980) 1652.
- 266 L. A. Sanchez, R. L. Birke, and J. R. Lombardi, *Chem. Phys. Lett.* **79** (1981) 219.
- 267 P. A. Lund, R. R. Smardzewski, and D. E. Tevault, *Chem. Phys. Lett.* **89** (1982) 508.
- 268 D. P. DiLella, J. S. Suh, and M. Moskovits, in Reference 22, p. 63.
- 269 W. Krasser, A. Ranade, and E. Koglin, *J. Raman Spectrosc.* **6** (1977) 209.
- 270 W. Krasser, A. Fadini, and A. J. Renuoprez, *J. Catal.* **62** (1980) 94.
- 271 W. Krasser, A. Fadini, E. Rozemuller, and A. J. Renuoprez, *J. Mol. Structure* **66** (1980) 135.
- 272 J. M. Stencel and E. B. Bradley, *J. Raman Spectrosc.* **8** (1979) 203.
- 273 A. V. Borov, Ja. M. Kimel'fel'd, and L. M. Mostovaya, *J. Mol. Structure* **60** (1980) 431.
- 274 H. Yamada and Y. Yamamoto, *Chem. Phys. Lett.* **77** (1981) 520.
- 275 H. Yamada, Y. Yamamoto, and N. Tani, *Chem. Phys. Lett.* **86** (1982) 397.
- 276 H. Yamada and Y. Yamamoto, in Reference 22, p. 73.
- 277 H. Yamada, N. Tani, and Y. Yamamoto, *J. Electron Spectrosc. Related Phenomena* **30** (1983) 13.
- 278 B. H. Loo, *J. Electroanal. Chem.* **136** (1982) 209.
- 279 T. Lopez-Rios, C. Pettenkofer, I. Pockrand, and A. Otto, *Surf. Sci.* **121** (1982) L541.
- 280 D. M. Kolb and R. Kotz, *Surf. Sci.* **64** (1977) 96.
- 281 A. Girlando, J. G. Gordon II, D. Heitmann, M. R. Philpott, H. Seki, and J. D. Swalen, *Surf. Sci.* **101** (1980) 417.
- 282 A. Tadjeddine and D. M. Kolb, *J. Electroanal. Chem.* **111** (1980) 119.
- 283 J. Billmann and A. Otto, *Solid State Commun.* **44** (1982) 105.
- 284 A. Otto, I. Pockrand, J. Billmann, and C. Pettenkofer, in Reference 23, p. 147.
- 285 A. Otto, *J. Electron Spectrosc. Relat. Phenom.* **29** (1983) 329.
- 286 T. E. Furtak and S. H. Macomber, *Chem. Phys. Lett.* **95** (1983) 328.
- 287 W. Boeck and D. M. Kolb, *Surf. Sci.* **118** (1982) 613.
- 288 D. M. Kolb, W. Boeck, K. M. Ho, and S. H. Liu, *Phys. Rev. Lett.* **47** (1981) 1921.
- 289 J. A. Creighton, in Reference 23, p. 315.
- 290 M. Kerker, D. S. Wang, H. Chew, O. Siiman, and L. A. Bumm, in Reference 23, p. 109.
- 291 P. McBreen and M. Moskovits, *J. Appl. Phys.* **54** (1983) 329.
- 292 H. Seki, *J. Electron Spectrosc. Relat. Phenom.* **29** (1983) 413.
- 293 H. Seki, SERS excitation profile of pyridine and CO on silver in UHV, internal report, IBM, 1982.
- 294 I. Pockrand, *Chem. Phys. Lett.* **92** (1982) 514.
- 295 J. E. Demuth and P. N. Sanda, *Phys. Lett.* **47** (1981) 57.
- 296 D. Schmeisser, J. E. Demuth, and Ph. Avouris, *Chem. Phys. Lett.* **87** (1982) 324.
- 297 Ph. Avouris and J. E. Demuth, *J. Chem. Phys.* **75** (1981) 4783.
- 298 R. S. Sennet and G. D. Scott, *J. Opt. Soc. Am.* **40** (1950) 203.

- 299 R. H. Doremus, *J. Appl. Phys.* **37** (1966) 2775.
- 300 S. Yoshida, T. Yamaguchi, and A. Kinbara, *J. Opt. Soc. Am.* **61** (1971) 62.
- 301 S. Yoshida, T. Yamaguchi, and A. Kinbara, *J. Opt. Soc. Am.* **61** (1971) 463.
- 302 T. Yamaguchi, S. Yoshida, and A. Kinbara, *Thin Solid Films* **21** (1974) 173.
- 303 T. Lopez-Rios, Y. Borenztein, and G. Vuye, *J. Phys.* **44** (1983) L99.
- 304 W. Vogel, B. Tesche, and W. Schultze, *Chem. Phys.* **74** (1983) 137.
- 305 H. Abe, W. Schultze, and B. Tesche, *Chem. Phys.* **47** (1980) 95.
- 306 O. Hunderi, *J. Phys. C* **5** (1977) 89.
- 307 O. Hunderi and H. P. Myers, *J. Phys. F* **3** (1973) 683.
- 308 H. Metiu, in Reference 23, p. 1.
- 309 R. G. Greenler and T. L. Slager, *Spectrochim. Acta* **29A** (1973) 193.
- 310 M. Moskovits, *J. Chem. Phys.* **69** (1978) 4159.
- 311 M. Moskovits, *Solid State Commun.* **32** (1979) 59.
- 312 S. Efrima and H. Metiu, *J. Chem. Phys.* **70** (1979) 1939.
- 313 S. Efrima and H. Metiu, *Isr. J. Chem.* **18** (1979) 17.
- 314 S. Efrima and H. Metiu, in Reference 20, p. 509.
- 315 S. Efrima and H. Metiu, *Surf. Sci.* **92** (1980) 427.
- 316 F. W. King, R. P. Van Duyne, and G. C. Schatz, *J. Chem. Phys.* **69** (1978) 4472.
- 317 J. D. Jackson, *Classical Electrodynamics*, Wiley, New York, 1975.
- 318 M. R. Philpott, *J. Chem. Phys.* **62** (1975) 1812.
- 319 P. B. Johnson and R. W. Christy, *Phys. Rev. B* **6** (1972) 4370.
- 320 P. R. Hilton and D. W. Oxtoby, *J. Chem. Phys.* **72** (1980) 6346.
- 321 T. Maniv and H. Metiu, *Phys. Rev. B* **22** (1980) 4731.
- 322 T. Maniv and H. Metiu, *J. Chem. Phys.* **76** (1982) 2697.
- 323 T. Maniv and H. Metiu, *J. Chem. Phys.* **76** (1982) 696.
- 324 P. J. Feibelman, *Phys. Rev. B* **12** (1975) 1319.
- 325 P. J. Feibelman, *Phys. Rev. B* **12** (1975) 4282.
- 326 P. J. Feibelman, *Phys. Rev. B* **14** (1976) 762.
- 327 G. E. Korzeniewski, T. Maniv, and H. Metiu, *Chem. Phys. Lett.* **73** (1980) 212.
- 328 T. Maniv and H. Metiu, *Surf. Sci.* **101** (1980) 399.
- 329 G. E. Korzeniewski, T. Maniv, and H. Metiu, *J. Chem. Phys.* **76** (1982) 1564.
- 330 S. Efrima, *Surf. Sci.* **107** (1981) 337.
- 331 W. H. Weber and G. W. Ford, *Phys. Rev. Lett.* **44** (1980) 1774.
- 332 G. W. Ford and W. H. Weber, *Surf. Sci.* **109** (1981) 451.
- 333 G. W. Ford and W. H. Weber, *Surf. Sci.* **110** (1981) L587.
- 334 K. L. Kliewer and R. Fuchs, *Phys. Rev.* **181** (1969) 552.
- 335 G. S. Agarwal, S. S. Jha, and J. C. Tsang, *Phys. Rev. B* **25** (1982) 2089.
- 336 D. M. Wood, *Phys. Rev. Lett.* **46** (1981) 749.
- 337 J. I. Gersten, *J. Chem. Phys.* **72** (1980) 5779.
- 338 J. I. Gersten and A. Nitzan, *J. Chem. Phys.* **73** (1980) 3023.
- 339 M. Kerker, D. S. Wang, and H. Chew, *Appl. Opt.* **19** (1980) 4159.
- 340 G. L. Eesley and J. R. Smith, *Solid State Commun.* **31** (1979) 815.
- 341 K. A. Arunkumar and E. B. Bradley, *J. Chem. Phys.* **78** (1983) 2882.
- 342 K. H. Li, *Surf. Sci.* **115** (1982) 513.
- 343 T. K. Lee and J. L. Birman, *Phys. Rev. B* **22** (1980) 5953.
- 344 T. K. Lee and J. L. Birman, *Phys. Rev. B* **22** (1980) 5961.
- 345 T. K. Lee and J. L. Birman, *J. Raman Spectrosc.* **10** (1981) 140.
- 346 A. G. Eguiluz, *Solid State Commun.* **33** (1980) 21.
- 347 T. L. Ferrell, *Phys. Rev. B* **25** (1982) 2930.
- 348 K. Arya and R. Zeyher, *Phys. Rev. B* **24** (1981) 1852.
- 349 F. R. Aussenegg and M. E. Lippitsch, *Chem. Phys. Lett.* **59** (1978) 214.
- 350 F. W. King and G. C. Schatz, *Chem. Phys.* **38** (1979) 245.

- ³⁵¹ E. Burstein, Y. J. Chen, C. Y. Chen, and S. Lundquist, *Solid State Commun.* **29** (1979) 567.
- ³⁵² J. I. Gersten, R. L. Birke, and J. R. Lombardi, *Phys. Rev. Lett.* **43** (1979) 147.
- ³⁵³ H. Ueba, *J. Phys. Chem.* **73** (1980) 725.
- ³⁵⁴ H. Ueba and S. Ichimura, *J. Chem. Phys.* **74** (1981) 3070.
- ³⁵⁵ H. Ueba, S. Ichimura, and H. Yamada, *Surf. Sci.* **119** (1982) 433.
- ³⁵⁶ H. Ueba, in Reference 23, p. 173.
- ³⁵⁷ H. Ueba, *Surf. Sci.* **131** (1983) 347.
- ³⁵⁸ H. Ueba, *Surf. Sci.* **129** (1983) L267.
- ³⁵⁹ H. Ueba, *Surf. Sci.* **131** (1983) 328.
- ³⁶⁰ H. Ueba, *Surf. Sci.* **133** (1983) L432.
- ³⁶¹ B. N. J. Persson, *Chem. Phys. Lett.* **82** (1981) 561.
- ³⁶² J. R. Kirtley, S. S. Jha, and J. C. Tsang, *Solid State Commun.* **35** (1980) 509.
- ³⁶³ F. J. Adrian, *J. Chem. Phys.* **77** (1982) 5302.
- ³⁶⁴ G. W. Robinson, *Chem. Phys. Lett.* **76** (1980) 191.
- ³⁶⁵ G. W. Robinson, *Chem. Phys. Lett.* **80** (1981) 404.
- ³⁶⁶ A. Otto, International Conference on Vibrations in Adsorbed Layers, **Julich, 1978.**
- ³⁶⁷ A. Otto, *Surf. Sci.* **92** (1980) 145.
- ³⁶⁸ S. L. McCall and P. M. Platzman, *Phys. Rev. B* **22** (1980) 1660.
- ³⁶⁹ A. G. Mal'shukov, *Solid State Commun.* **38** (1981) 907.
- ³⁷⁰ T. Maniv and H. Metiu, *Chem. Phys. Lett.* **79** (1981) 79.
- ³⁷¹ T. Maniv, *Phys. Rev. B* **26** (1982) 2856.
- ³⁷² H. Raether, *Physics of Thin Films*, Academic Press, New York, 1977, p. 145.
- ³⁷³ H. Raether, *Springer Tracts in Modern Physics*, Springer-Verlag, New York, 1980, Vol. 88, Chap. 10.
- ³⁷⁴ P. F. Lio and A. Wokaun, *J. Chem. Phys.* **76** (1982) 751.
- ³⁷⁵ Y. J. Chen, W. P. Chen, and E. Burstein, *Phys. Rev. Lett.* **36** (1976) 1207.
- ³⁷⁶ Y. J. Chen, W. P. Chen, and E. Burstein, *Bull. Am. Phys. Soc.* **21** (1976) 338.
- ³⁷⁷ C. Y. Chen and E. Burstein, *Phys. Rev. Lett.* **45** (1980) 1287.
- ³⁷⁸ P. C. Das and J. I. Gersten, *Phys. Rev. B* **25** (1982) 6281.
- ³⁷⁹ A. Wokaun, J. P. Gordon, and P. F. Liao, *Phys. Rev. Lett.* **48** (1982) 957.
- ³⁸⁰ Z. Kotler and A. Nitzan, *Surf. Sci.* **130** (1983) 124.
- ³⁸¹ D. L. Mills and M. Weber, *Phys. Rev. B* **26** (1982) 1075.
- ³⁸² S. L. McCall, P. M. Platzman, and P. A. Wolff, *Phys. Lett.* **77A** (1980) 381.
- ³⁸³ U. Laor and G. C. Schatz, *Chem. Phys. Lett.* **82** (1981) 566.
- ³⁸⁴ U. Laor and G. C. Schatz, *J. Chem. Phys.* **76** (1982) 2888.
- ³⁸⁵ K. Arya, R. Zeyher, and A. A. Maradudin, *Solid State Commun.* **42** (1982) 461.
- ³⁸⁶ P. K. Aravind, A. Nitzan, and H. Metiu, *Surf. Sci.* **110** (1981) 189.
- ³⁸⁷ T. Yamaguchi, S. Yoshida, and A. Kinbara, *J. Opt. Soc. Am.* **64** (1974) 1563.
- ³⁸⁸ J. Moreland, A. Adams, and P. K. Hansma, *Phys. Rev. B* **25** (1982) 2297.
- ³⁸⁹ P. K. Aravind and H. Metiu, *Surf. Sci.* **124** (1983) 506.
- ³⁹⁰ P. K. Aravind and H. Metiu, *Chem. Phys. Lett.* **74** (1980) 301.
- ³⁹¹ F. J. Adrian, *Chem. Phys. Lett.* **78** (1981) 45.
- ³⁹² R. Rupin, *Solid State Commun.* **39** (1981) 903.
- ³⁹³ B. J. Messinger, K. U. von Raben, R. K. Chang, and P. W. Barber, *Phys. Rev. B* **24** (1981) 649.
- ³⁹⁴ N. N. Gorobei, I. P. Ipatova, and A. V. Subashiev, *ZhETP Pis. Red.* [JETP Lett.] **34** (1981) 149.
- ³⁹⁵ K. Ohtara and M. Inoue, *J. Phys. C* **15** (1982) 6463.
- ³⁹⁶ H. Numata, *J. Phys. Soc. Jpn.* **51** (1982) 2575.
- ³⁹⁷ K. Sakoda, K. Ohtaka, and E. Hanamura, *Solid State Commun.* **41** (1982) 393.
- ³⁹⁸ A. M. Brodsky and M. I. Urbakh, *Surf. Sci.* **115** (1982) 417.

- ³⁹⁹ P. W. Barber, R. K. Chang, and H. Massoudi, *Phys. Rev. Lett.* **50** (1983) 997.
- ⁴⁰⁰ N. Garcia, *J. Electron Spectrosc. Related Phenomena* **29** (1983) 421.
- ⁴⁰¹ N. Garcia, *Opt. Commun.* **45** (1983) 307.
- ⁴⁰² J. R. Kirtley, S. S. Jha, and J. C. Tsang, *Solid State Commun.* **35** (1980) 509.
- ⁴⁰³ S. S. Jha, J. R. Kirtley, and J. C. Tsang, *Phys. Rev. B* **22** (1980) 3973.
- ⁴⁰⁴ D. S. Wang, H. Chew, and M. Kerker, *Appl. Opt.* **19** (1980) 2256.
- ⁴⁰⁵ D. S. Wang and M. Kerker, *Phys. Rev. B* **24** (1981) 1777.
- ⁴⁰⁶ M. Kerker and C. G. Blatchford, *Phys. Rev. B* **26** (1982) 4052.
- ⁴⁰⁷ H. Chew, D. S. Wang, and M. Kerker, *Phys. Rev. B* **28** (1983) 4169.
- ⁴⁰⁸ W. H. Weber and G. W. Ford, *Opt. Lett.* **6** (1981) 122.
- ⁴⁰⁹ I. Pockrand, J. D. Swalen, R. Santo, A. Brillante, and M. R. Philpott, *J. Chem. Phys.* **69** (1978) 4001.
- ⁴¹⁰ A. M. Glass, P. F. Liao, J. D. Bergman, and D. H. Olson, *Opt. Lett.* **5** (1980) 368.
- ⁴¹¹ H. G. Craighead and A. M. Olson, *Opt. Lett.* **6** (1981) 248.
- ⁴¹² S. Garoff, D. A. Weitz, T. J. Gramilla, and C. D. Hanson, *Opt. Lett.* **6** (1981) 245.
- ⁴¹³ D. S. Wang and M. Kerker, *Phys. Rev. B* **25** (1982) 2433.
- ⁴¹⁴ H. Chew and D. S. Wang, *Phys. Rev. Lett.* **49** (1982) 490.
- ⁴¹⁵ Z. Kotler and A. Nitzan, *J. Phys. Chem.* **86** (1982) 2011.
- ⁴¹⁶ H. Kuhn, *J. Chem. Phys.* **53** (1970) 101.
- ⁴¹⁷ R. R. Chance, A. Prock, and R. Silbey, in *Advances in Chemical Physics*, Ed. by I. Prigogine and S. A. Rice, Wiley, New York, Vol. XXXVII, 1978, p. 1.
- ⁴¹⁸ R. Rossetti and L. E. Brus, *J. Chem. Phys.* **73** (1980) 572.
- ⁴¹⁹ A. Champion, A. R. Gallo, C. B. Harris, H. J. Robota, and P. M. Whitmore, *Chem. Phys. Lett.* **73** (1980) 447.
- ⁴²⁰ P. M. Whitmore, H. J. Robota, and C. B. Harris, *J. Chem. Phys.* **77** (1981) 1560.
- ⁴²¹ I. Pockrand, A. Brillante, and D. Mobius, *Chem. Phys. Lett.* **69** (1980) 499.
- ⁴²² D. A. Weitz, S. Garoff, C. D. Hanson, T. J. Gramila, and J. I. Gersten, *J. Lumin.* **24/25** (1981) 83.
- ⁴²³ D. A. Weitz, S. Garoff, C. D. Hanson, T. J. Gramila, and J. I. Gersten, *Opt. Lett.* **7** (1982) 89.
- ⁴²⁴ J. I. Gersten and A. Nitzan, *J. Chem. Phys.* **75** (1981) 1139.
- ⁴²⁵ B. N. J. Persson, *J. Phys. C* **11** (1978) 4251.
- ⁴²⁶ J. E. Demuth and Ph. Avouris, *Phys. Rev. Lett.* **47** (1981) 61.
- ⁴²⁷ P. M. Champion and A. C. Albrecht, *Ann. Rev. Phys. Chem.* **33** (1982) 353.
- ⁴²⁸ J. C. Tsang, Ph. Avouris, and J. R. Kirtley, *J. Chem. Phys.* **79** (1983) 493.
- ⁴²⁹ A. Giraldo, M. R. Philpott, D. Heitmann, J. D. Swalen, and R. Santo, *J. Chem. Phys.* **72** (1980) 5187.
- ⁴³⁰ W. Knoll, M. R. Philpott, J. D. Swalen, and A. Giraldo, *J. Chem. Phys.* **77** (1982) 2254.
- ⁴³¹ M. Fujihira and T. Osa, *J. Am. Chem. Soc.* **98** (1976) 7850.
- ⁴³² B. Pettinger, A. Tadjeddine, and D. M. Kolb, *Chem. Phys. Lett.* **66** (1979) 544.
- ⁴³³ J. F. Rabolt, R. Santo, and J. D. Swalen, *Appl. Spectrosc.* **33** (1979) 549.
- ⁴³⁴ R. E. Benner, R. Dornhaus, and R. K. Chang, *Opt. Commun.* **30** (1979) 145.
- ⁴³⁵ S. Ushioda and Y. Sasaki, *Phys. Rev. B* **27** (1983) 1401.
- ⁴³⁶ R. J. Nemanich, C. C. Tsai, and G. A. N. Connell, *Phys. Rev. Lett.* **44** (1980) 273.
- ⁴³⁷ Y. Levy, C. Imbert, J. Cipriani, S. Racine, and R. Dupeyrat, *Opt. Commun.* **11** (1974) 66.
- ⁴³⁸ J. Cipriani, S. Racine, R. Dupeyrat, H. Hasmonay, M. Dupeyrat, Y. Levy, and C. Imbert, *Opt. Commun.* **11** (1974) 70.
- ⁴³⁹ M. Menetrier, R. Dupeyrat, Y. Levy, and C. Imbert, *Opt. Commun.* **21** (1977) 162.
- ⁴⁴⁰ P. K. Aravind, R. W. Rendell, and H. Metiu, *Chem. Phys. Lett.* **85** (1982) 396.
- ⁴⁴¹ M. Moskovits and D. P. DiLella, *J. Chem. Phys.* **73** (1980) 6068.

- ⁴⁴² J. K. Sass, H. Neff, M. Moskovits, and S. Holloway, *J. Phys. Chem.* **85** (1981) 621.
- ⁴⁴³ D. P. DiLella, R. H. Lipson, P. McBreen, and M. Moskovits, *J. Vac. Sci. Technol.* **18** (1981) 453.
- ⁴⁴⁴ M. Moskovits and D. P. DiLella, *J. Chem. Phys.* **77** (1982) 1655.
- ⁴⁴⁵ B. Pettinger, *Chem. Phys. Lett.* **78** (1981) 404.
- ⁴⁴⁶ C. S. Allen and R. P. Van Duyne, *Chem. Phys. Lett.* **63** (1979) 455.
- ⁴⁴⁷ J. A. Creighton, *Surf. Sci.* **124** (1983) 209.
- ⁴⁴⁸ M. Fleischmann, P. Graves, I. Hill, A. Oliver, and J. Robinson, *J. Electroanal. Chem.* **150** (1983) 33.
- ⁴⁴⁹ M. Fleischmann, I. R. Hill, and G. Sundholm, *J. Electroanal. Chem.* **158** (1983) 153.
- ⁴⁵⁰ K. A. Bunding and M. I. Bell, *Surf. Sci.* **118** (1983) 329.
- ⁴⁵¹ I. Pockrand, C. Pettenkofer, and A. Otto, *J. Electron Spectrosc. Related Phenomena* **29** (1983) 409.
- ⁴⁵² C. J. Sandroff, D. A. Weitz, J. C. Chung, and D. R. Herschbach, *J. Phys. Chem.* **87** (1983) 2127.
- ⁴⁵³ R. Kotz and E. Yeager, *J. Electroanal. Chem.* **111** (1980) 105.
- ⁴⁵⁴ M. Ohsawa, H. Matsuda, and W. Suetaka, *Chem. Phys. Lett.* **84** (1981) 163.
- ⁴⁵⁵ D. V. Murphy, K. U. Von Raben, R. K. Chang, and P. B. Dorain, *Chem. Phys. Lett.* **85** (1982) 43.
- ⁴⁵⁶ K. U. Von Raben, P. B. Dorain, T. T. Chen, and R. K. Chang, *Chem. Phys. Lett.* **95** (1983) 269.
- ⁴⁵⁷ C. J. Sandroff, S. Garoff, and K. P. Leung, *Chem. Phys. Lett.* **96** (1983) 547.
- ⁴⁵⁸ H. Yamada, T. Amamiya, and H. Tsubomura, *Chem. Phys. Lett.* **56** (1978) 591.
- ⁴⁵⁹ M. Fleischmann, I. R. Hill, G. Mengoli, and M. M. Musiani, *Electrochim. Acta* **28** (1983) 1545.
- ⁴⁶⁰ W. M. H. Sachtler, C. Backx, and R. A. Van Santen, *Catal. Rev. Sci. Eng.* **23** (1981) 127.
- ⁴⁶¹ P. B. Dorain, K. U. Von Raben, R. K. Chang, and B. L. Laube, *Chem. Phys. Lett.* **84** (1981) 405.
- ⁴⁶² C. Pettenkofer, I. Pockrand, and A. Otto, *Surf. Sci.* **135** (1983) 52.
- ⁴⁶³ P. Podini and J. M. Schnur, *Chem. Phys. Lett.* **93** (1982) 86.
- ⁴⁶⁴ C. J. Sandroff, H. E. King Jr., and D. R. Herschbach, *J. Phys. Chem.* **88** (1984) 5647.
- ⁴⁶⁵ J. F. Owen, T. T. Chen, R. K. Chang, and B. L. Laube, *Surf. Sci.* **125** (1983) 679.
- ⁴⁶⁶ J. E. Pemberton and R. P. Buck, *J. Electroanal. Chem.* **136** (1982) 201.
- ⁴⁶⁷ A. L. Dendramis, E. W. Schwinn, and R. P. Sperline, *Surf. Sci.* **134** (1983) 675.
- ⁴⁶⁸ S. Farquharson, M. J. Weaver, P. A. Lay, R. H. Magnuson, and H. Taube, *J. Am. Chem. Soc.* **105** (1983) 3350.
- ⁴⁶⁹ K. M. Ervin, E. Koglin, J. M. Sequaris, P. Valenta, and H. W. Nurnberg, *J. Electroanal. Chem.* **114** (1980) 179.
- ⁴⁷⁰ E. Koglin, J. M. Sequaris, and P. Valenta, *J. Mol. Structure* **60** (1980) 421.
- ⁴⁷¹ J. M. Sequaris, E. Koglin, P. Valenta, and H. W. Nurnberg, *Ber. Bunsenges. Phys. Chem.* **85** (1981) 512.
- ⁴⁷² R. P. Cooney, M. R. Mahoney, and M. W. Howard, *Chem. Phys. Lett.* **76** (1980) 448.
- ⁴⁷³ M. R. Mahoney, M. W. Howard, and R. P. Cooney, *Chem. Phys. Lett.* **71** (1980) 59.
- ⁴⁷⁴ R. P. Cooney, M. W. Howard, M. R. Mahoney, and T. P. Mernagh, *Chem. Phys. Lett.* **79** (1981) 459.
- ⁴⁷⁵ M. W. Howard and R. P. Cooney, *Chem. Phys. Lett.* **87** (1982) 299.
- ⁴⁷⁶ J. C. Tsang, J. E. Demuth, P. N. Sanda, and J. R. Kirtley, *Chem. Phys. Lett.* **76** (1980) 54.

- ⁴⁷⁷ S. Efrima, *Chem. Phys. Lett.* **102** (1983) 79.
- ⁴⁷⁸ A. Nitzan and L. E. Brus, *J. Chem. Phys.* **74** (1981) 5321.
- ⁴⁷⁹ A. Nitzan and L. E. Brus, *J. Chem. Phys.* **75** (1981) 2205.
- ⁴⁸⁰ G. M. Goncher and C. B. Harris, *J. Chem. Phys.* **77** (1982) 3767.
- ⁴⁸¹ C. J. Chen and R. M. Osgood, *Phys. Rev. Lett.* **50** (1983) 1705.
- ⁴⁸² T. J. Chuang, *J. Chem. Phys.* **76** (1982) 3828.
- ⁴⁸³ T. J. Chuang and H. Seki, *Phys. Rev. Lett.* **49** (1982) 382.
- ⁴⁸⁴ H. Seki and T. J. Chuang, *Solid State Commun.* **44** (1982) 473.
- ⁴⁸⁵ C. H. Lee, R. K. Chang, and N. Bloembergen, *Phys. Rev. Lett.* **18** (1967) 167.
- ⁴⁸⁶ C. K. Chen, A. R. B. de Castro, and Y. R. Shen, *Phys. Rev. Lett.* **46** (1981) 145.
- ⁴⁸⁷ T. F. Heinz, C. K. Chen, D. Ricard, and Y. R. Shen, *Chem. Phys. Lett.* **83** (1981) 180.
- ⁴⁸⁸ C. K. Chen, T. F. Heinz, D. Ricard, and Y. R. Shen, *Phys. Rev. Lett.* **46** (1981) 1010.
- ⁴⁸⁹ C. K. Chen, T. F. Heinz, D. Ricard, and Y. R. Shen, *Chem. Phys. Lett.* **83** (1981) 455.
- ⁴⁹⁰ D. V. Murphy, K. U. Von Raben, T. T. Chen, J. F. Owen, R. K. Chang, and B. L. Laube, *Surf. Sci.* **124** (1983) 529.
- ⁴⁹¹ F. W. Schneider, in *Non Linear Raman Spectroscopy and Its Chemical Applications*, Ed. by W. Keifer and D. A. Long, Reidel, Dordrecht, 1982, p. 461.
- ⁴⁹² H. Chew, D. S. Wang, and M. Kerker, *J. Opt. Soc. Am.* **B1** (1984) 56.
- ⁴⁹³ A. M. Glass, A. Wokaun, J. P. Heritage, J. D. Bergman, P. F. Liao, and D. H. Olson, *Phys. Rev. B* **24** (1981) 4906.
- ⁴⁹⁴ K. Kneipp, G. Hinzmann, and D. Fassler, *Chem. Phys. Lett.* **99** (1983) 503.
- ⁴⁹⁵ E. V. Albano, S. Daiser, G. Ertl, R. Miranda, and K. Wandelt, *Phys. Rev. Lett.* **51** (1983) 2314.
- ⁴⁹⁶ T. Maniv, *J. Phys. C* **10** (1983) 321.
- ⁴⁹⁷ S. Efrima, *J. Phys. Chem.*, in press.

Batteries for Vehicular Propulsion

Halina S. Wroblowa

Ford Motor Company, Scientific Research Laboratory, Dearborn, Michigan 48121

I. INTRODUCTION

1. General Remarks

The key part of an electric vehicle (EV) is its power plant. Within 10 years of the invention of the lead/acid battery (Planté, 1860) an electric carriage appeared in England, followed 10 years later by an electric tricycle in France. In America the first electric two-seater was constructed in 1891, and in 1899 electric vehicles captured 60% of the emerging U.S. automobile market. The nickel-iron battery invented by Edison to provide cars with longer range between recharges failed to prevent, however, an early demise of the EV market share. Its abrupt decrease was a result of the invention of the electric self-starter for internal combustion engine vehicles (ICEV) and their improved reliability. A few years after the introduction of the Ford Model K car, the market share of EVs dwindled to some 3%. About the same time, small fleets of electric buses, delivery vans, and cars appeared in Germany. They were powered by somewhat improved versions of the lead-acid system (18 Wh kg^{-1}). Over 20,000 electric trucks were on German roads until the middle 1930s to reappear for about a decade after World War II.¹ Over 200 battery-powered railcars are in operation each day in West Germany.² In Great Britain, fleets of delivery vans (presently over 55,000 units) have been on the road continuously

for the last 70 years. The energy and maintenance costs of electric vans were shown to be 45–60% of their gasoline and diesel-powered analogues.^{3,4} Small fleets of electric buses are in operation in Australia, England, France, Germany, and Japan.^{4,5} For specialized purposes (e.g., indoor, underground, and airport transport of people and cargo; golf carts; forklifts) lead/acid traction batteries are widely used. Only in the USSR they have not completely displaced nickel-iron batteries.

Electric passenger cars cannot presently compete with ICEVs, neither economically nor in terms of user's convenience. Therefore, only a very limited number of two- and four-seater lead/acid-powered passenger EVs have as yet been constructed.^{2,4}

In the 1960s the interest in electric cars—as a remedy against urban pollution—was revived and strengthened in the 1970s by the realization that foreign oil sources can be abruptly shut off, oil supplies will be exhausted in the not-too-distant future, and indeed all fossil-fuel supplies are finite. Intensified research in the area of battery systems, which (at least in the USA) seems to have peaked in terms of funding around 1980, resulted in considerable improvements of previously available systems and in worldwide efforts to develop new batteries better suited for EV applications than lead-acid. The latter still remains the only battery commercially used for specialized traction purposes, while other systems are now at various stages of development. The decrease in the EV battery R&D effort can be related, on the one hand, to the temporary “oil glut” and, on the other, to the inherent range limitation of cars powered by secondary batteries and severe technical difficulties connected with the necessity of *simultaneous* optimization of several battery attributes which are desirable for EV applications. The required battery attributes are closely linked together and improvement of one feature usually has an adverse effect on other properties.

2. Battery Classification

Among rechargeable batteries commercially available today (Table 1), only the lead/acid (Pb-A) and Ni-Fe systems can be considered as potential EV power plants because of the cost and scarcity of materials used in other batteries. The performance of the Pb-A and Ni-Fe systems is, however, inherently limited by their low-energy

Table 1
Commercially Available Rechargeable Batteries

Name	System	Applications
Lead-Acid (SOA)	Pb-H ₂ SO ₄ -PbO ₂	Automotive SLI; traction (specialized vehicles); emergency power
Nickel-Iron (SOA)	Fe-KOH-NiOOH	Traction and lighting of trains (predominantly in USSR)
Nickel-Cadmium	Cd-KOH-NiOOH	Small-size portable power
Silver-Cadmium	Cd-KOH-Ag ₂ O ₂	Aerospace applications requiring nonmagnetic components
Silver-Zinc	Zn-KOH-Ag ₂ O ₂	Military; aerospace

storage capability. Attempts to provide EVs with a range (between recharges) exceeding that of the SOA (state of art) Pb-A traction batteries has led to considerable improvements in the technology of Pb-A ISOA ("Improved" SOA) battery prototypes, "advanced" Pb-A cells, and Ni-Fe batteries, as well as to the emergence of several new systems expected to have a more acceptable range on the basis of their higher theoretical specific energies. With the exception of a few primary batteries (metal fuel cells), the candidate systems are electrically rechargeable. They can be classified in a number of ways, e.g., according to the operating temperature (ambient or high), type of electrolyte (aqueous, organic liquid, molten salt, solid; flowing or stationary), or their relative stage of development. The latter classification, somewhat subjective and labile, divides the candidate systems into three groups: near term, advanced, and exploratory. Very roughly, the development of near-term systems has reached the prototype EV battery stage; of advanced systems, the battery prototype or module stage; and of exploratory systems, the small-module, or cell stage. The list and basic characteristics of near-term and advanced batteries is given in Table 2, along with data pertaining to some exploratory systems.

II. EV BATTERY REQUIREMENTS

Battery characteristics can be described in terms of the desired EV's *performance*-, *cost*-, and *safety*-related factors, as listed in Table 3.

Table 2
Battery Classification

System	Cell voltage (V)	Operating temperature (°C)	Theoretical specific energy (Wh kg ⁻¹)
Near term and advanced			
Lead/Acid	~2.1	Ambient	~177
Nickel-Iron	1.26	Ambient	267
Nickel-Zinc	1.7	Ambient	326
Zinc-Chlorine	2.1	Ambient	460
Zinc-Bromine	1.87	Ambient	433
Lithium-Iron sulfide	1.33	450-500	447
Sodium-Sulfur	1.92 (aver.)	320-350	637 (aver.)
Exploratory			
Calcium-Iron disulfide	~2.0	450-500	790
Lithium-Titanium Disulfide	2.7-1.9	Ambient	480 (aver.)
Iron-Air	0.88	Ambient	525
Zinc-Air	1.65	Ambient	890
Aluminum-Air	2.7	Ambient	2681
Conducting polymer (CP)	≤5.0	Ambient	Several thousands

Table 3
Correspondence between the Vehicle and EV Battery Characteristics

EV parameters	Battery parameters
1. Performance	
Range between recharges	Specific energy (Wh kg ⁻¹) Energy density (Wh liter ⁻¹) Self-discharge rate (percent per day)
Daily range	Charging time (h/C)
Acceleration capability	Specific peak power (W kg ⁻¹) Peak-power density (W liter ⁻¹)
Climbing speed	Specific sustained power (W kg ⁻¹)
Reliability	Ruggedness Insensitivity to ambient conditions, overcharge, overdischarge, shock, vibration, etc. Lack of complexity
2. Cost	Materials Fundamental resource limitations Recycleability Geopolitical distribution Manufacturing, R&D Cycle life Overall energy efficiency Maintenance
3. Safety and environmental aspects	Stationary failure modes Impact failure modes Fire and/or explosion hazard Reactive and/or toxic material release Environmental impact Pollution Mining and processing effects

1. Performance-Related Requirements

(i) *Range between Recharges*

EV range depends primarily on the amount of effective energy stored per unit weight or volume of the battery. The specific energy (Wh kg⁻¹) of secondary batteries delivered to EV wheels is approximately 2–5% of that of gasoline. Volumetrically, the situation is not much better, the energy density being within ~3–7% of the

gasoline value. This explains the inherent gap in the vehicle range between “refueling” of battery- and ICE-powered cars, a gap which cannot be bridged by simply increasing the battery weight. The battery fraction (battery weight/vehicle curb weight) should not exceed $\sim\frac{1}{3}$ to ensure mechanical stability and to avoid the excessive waste of energy spent on propelling the battery itself.

(a) *Specific energy*

The energy available for driving purposes is often somewhat lower than the energy deliverable by the battery. The losses may be due, e.g., to the operation of battery auxiliaries (pumps in flow batteries, shunt-current protection, etc.) The translation of the available specific energy into the EV’s range must take into account the vehicle characteristics including its weight, wind and rolling resistance, and the driving profile⁶ determined by the vehicle’s end use as shown in Fig. 1, based on the average performance of Pb-A-powered vehicles driven in Germany.⁷ The trend shown can be rationalized in terms of slower speeds and acceleration (energy losses are proportional to the square of velocity) of larger German vehicles driven with various driving profiles, depending on their mission. Also the drag due to the frontal wind resistance does not decrease linearly with decreasing vehicle volume. The ordinate values can vary considerably from those shown in Fig. 1. Thus,

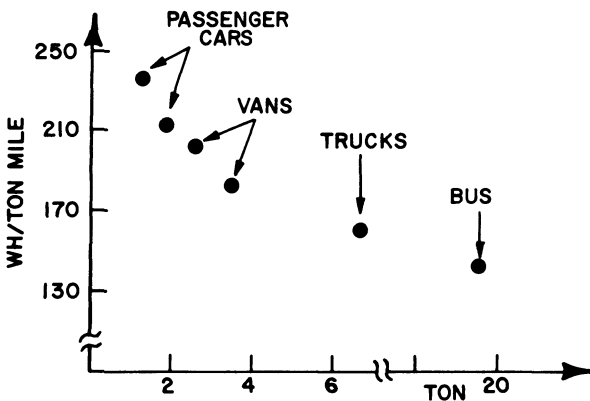


Figure 1. Specific energy of various types of EVs.

e.g., a 1500-kg compact-type EV with $\sim\frac{1}{3}$ battery fraction, driven under urban conditions, as simulated by the U.S. Federal Urban Driving Schedule,⁶ requires only ~ 250 Wh mile⁻¹, or ~ 170 Wh ton⁻¹ mile⁻¹.⁸ The trend, however, correctly indicates that the most demanding is a small passenger car. The packaging constraints are compounded by size effects of the battery itself. Scaling down battery capacity results in a loss of effective specific energy, which is relatively small for simple, ambient-temperature systems and becomes progressively larger with the degree of complexity and number of auxiliary subsystems in flow- and high-temperature batteries. As shown in Fig. 2, the specific energy of complex batteries is severely impaired in the region of 20–30 kWh suitable for small urban cars. The latter require ~ 60 Wh kg⁻¹ to attain a 100-mile range.⁸ This might indicate that, in spite of some more optimistic projections, only simpler systems may prove compatible with compact EVs, while more complex batteries would be more suitable for large family cars, vans, etc.

The effective specific energy of various batteries amounts presently to some 10–25% of theoretical specific energy (defined as the reversible work of the cell reaction per unit weight of reactive electrode materials). The extent of departure from the theoretical value depends on: (1) the weight of nonactive battery components;

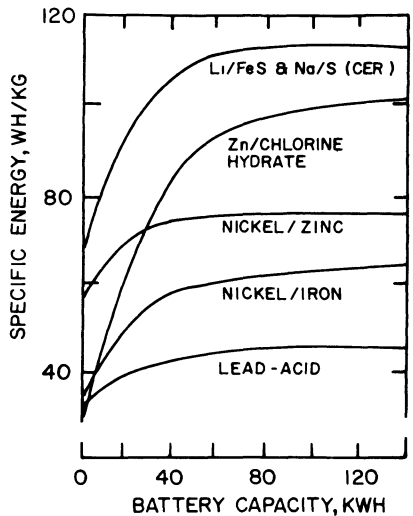


Figure 2. System size effects on specific energy.⁹

(2) reactant utilization; (3) discharge overvoltage (determined primarily by ohmic losses); (4) coulombic losses due to parasitic reactions, self-discharge, and/or shunt currents in series-connected cells with a common electrolyte; and (4) losses connected with operation of auxiliaries.

Efforts to improve the ratio of effective to theoretical specific energy involve, in general: (1) replacement, where possible, of inert grid, container, connector, and current collector materials by light-weight substances; (2) increase of utilization of active materials by improved cell design and/or use of special additives; (3) careful modeling and optimization of current collection; and (4) use of bipolar electrodes.

Although the individual mechanism may differ, the specific energy of batteries decreases, in general, with increasing rate of discharge. For example, the specific energy of a certain SOA Pb-A traction battery varies between 34 and 22 Whkg^{-1} when discharged within 5 and 1 h, respectively.¹ The capacity C_I available at the given discharge current I is often represented for porous-plate simple batteries by the empirical Peukert equation:

$$C_I = KT^{-n}$$

where K and n are coefficients characteristic for the given battery. Any comparisons of battery specific energy or ranges have sense only if the latter are measured for the same value of C/h , where C denotes the rated capacity of the battery and h —the number of hours of discharge.

The EV range is affected by the self-discharge which may occur both during rest and operating periods of the battery. The self-discharge rate depends on the individual battery characteristics, ranging from zero for batteries with solid electrolytes (e.g., Na-S) to considerable values for batteries operated without separators (e.g., zinc-chlorine hydrate). In batteries with separators, self-discharge is determined by the rate of ion transport through the membrane. The most efficient—ion-exchange membranes—are usually too expensive for practical purposes and microporous separators are commonly used.

The EV's range can be somewhat extended by the battery's capability of accepting charge pulses during regenerative braking.

Depending on the battery and driving profile, such recovery may increase the range by some 15–25%.¹⁰

(b) The volumetric energy density

This defines the packaging requirements for the given EV range. For simple, ambient-temperature systems, its numerical value is about double the battery's specific energy. This ratio decreases with increasing volume of auxiliaries, and, for smaller cars, volumetric considerations may become range limiting for rather than the gravimetric effective energy storage capability. This limitation may pertain particularly to bulky batteries which cannot be spatially distributed in the car being designed as a single package (e.g., high-temperature systems enveloped in a vacuum insulation).

Optimal packaging of batteries will require vehicles specially designed to accommodate the given battery.

(ii) Daily Range

In general, fast recharge decreases the energy efficiency (unless the self-discharge rate during charge is considerable, as in the case of the Zn–Br₂ battery) and may cause severe cell damage owing to temperature increases which accompany high charging currents. Therefore, recharging to full capacity requires 6–10 h for most systems and the range between recharges usually defines the daily mileage allowable. Some systems are claimed by their developers to be capable of a 0.5-h recharge to some fraction (e.g., 50%) of the rated capacity. If indeed, the high charging rates would not affect the battery reliability and cycle life, the daily mileage of EVs could be extended to more convenient distances. The demands on the infrastructure of electric utilities would be in this case more severe (although probably not prohibitive) than those anticipated for overnight recharge.

(iii) Acceleration

Specific peak power (W kg^{-1}) of the battery determines the EV acceleration capability. Not only the energy storage but also the power/weight ratio comparisons with ICEs are not favorable for

electrochemical power plants. The obvious reason is the tridimensional character of hot combustion which occurs in the reactor's volume, as opposed to the two-dimensional characteristics of the interfacial electrochemical energy conversion. In spite of the poor power/weight ratio, acceptable acceleration of EVs is more easily attainable than the desirable range.

The specific power passes through a maximum at a voltage corresponding to $\sim 50\%$ of the open-circuit value (OCV). The usable peak power, however, limited in practice to $\sim 85\%$ of the maximum value, is attainable at voltages some 30% lower than OCV. (Higher-voltage departures would severely affect the cost of the present dc motors or ac controllers.) Available data usually refer to the maximum power. Also, published data often refer to peak power averaged over a 15-s pulse, while actually the value of peak power during the next 5 s is as important for EV acceleration.

In general, the specific peak power decreases with the depth of discharge (DOD) (cf. Fig. 3). Therefore, EV battery specification with respect to range and allowable depth of discharge limit should pertain to (whichever comes first) DOD values at which EV becomes incapable of the demanded acceleration, or to which the system

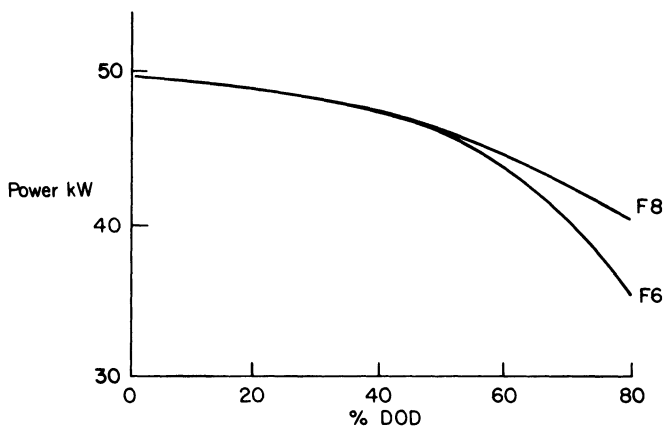


Figure 3. Specific peak-power, averaged over the last 10 s of a 20-s pulse, as a function of the depth of discharge for Lucas-Chloride, ~ 535 kg, 192-V ISDA tubular Pb-A batteries. EV power-train constraints imposed. (Courtesy of Lucas Chloride EV Systems, 1984.)

can be safely discharged without impairing its reliability and lifetime (often $\sim 80\%$ of the rated capacity is required as a limit).

The EV power requirements depend on the car's end use and assumed acceleration demands. For example, the specifications for safe driving in a mixed ICEV and EV urban traffic of a small compact-type EV have been defined as acceleration from 0 to 50 mph in <20 s.⁸ The specific peak-power corresponding to these demands has been calculated as $80\text{--}90 \text{ wkg}^{-1}$ for conditions of optimum use of the AC power train (i.e., for constant-power acceleration following the initial period in which the peak-power is attained at the maximum tractive effort⁸). The majority of near-term and advanced batteries could, at least potentially, meet these demands.

The difference between projected and actual performance of the present prototypes is often very high. Thus, e.g., the potentially "best" performance of the LiAl/FeS battery (Argonne National Laboratory) is compromised at present, primarily by the inadequate current collection which causes substantial power losses due to the high internal resistance.

(iv) Specific Energy–Peak power Tradeoffs

The specific energy to peak power ratio is a key battery-design parameter. Since both cannot be simultaneously increased, the given system can be designed for maximum range at some loss of peak-power capability, or for high-power operation at some loss of the achievable range. The sensitivity of the given system to the power demands is shown in Ragone plots exemplified⁹ in Fig. 4 for projected performance of a number of battery systems. (It should be kept in mind that the data in Fig. 4 differ considerably from those presently attainable and are of comparative rather than absolute value). Ragone plots map the specific energy available from the battery for values of the specific power at which the battery is discharged. The energy/power relations determined in laboratory tests have been successfully used to project EV's performance. An agreement of $\pm 5\%$ has been reported for a number of near-term batteries¹⁰ between the projections based on Ragone plots obtained for small (6–12 V) modules at the Argonne National Laboratory and vehicle ranges obtainable under conditions of urban driving cycle as tested at the Jet Propulsion Laboratory.

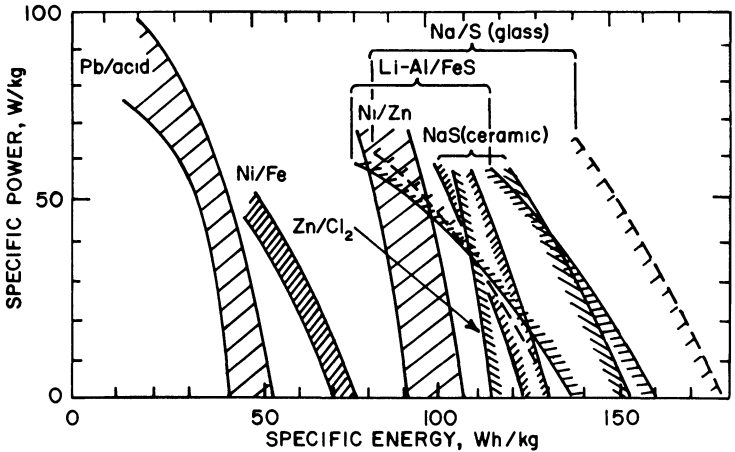


Figure 4. Ragone plots. Characteristics expected for 1990s. Specific power data for 80% DOD.⁹

It would seem that battery-battery hybrids might provide better simultaneous optimization of range and acceleration. However, the overall specific-energy and efficiency losses, cost, and complexity of the hybrid systems seem to militate, at present, against this solution.

(v) Reliability

The probability that a battery will function properly under various kinds of driving and environmental conditions determines its reliability. The latter is an extremely important parameter which may adversely affect public acceptance of electric cars to an even greater extent than their limited range. At present, little is known about the reliability of full systems other than a number of lead/acid traction batteries which are highly reliable. (Thus, e.g., batteries for delivery vans produced by Lucas Chloride EV Systems are presently sold in England with a two-year unconditional and two-year conditional warranty.) Data for other batteries are largely absent since very few have been sufficiently tested even at the module or cell level and hardly any information exists concerning effects of actual driving conditions.

Reliability projections are often based on the probability theory which relates the reliability of the battery with that of the single cell:

$$(1 - P_{BF}) = (1 - P_{CF})^n$$

where P_{BF} and P_{CF} are the probabilities of battery and cell failure, respectively; n is the number of cells; and $1 - P_{CF} = e^{(c/MCBF)}$, where $MCBF$ is the mean number of cycles before cell failure. This approach assumes that a multicomponent system does not introduce additional failure probability due to the interconnection of cells and the influence of their electrochemical behavior on neighboring elements. Physically this assumption corresponds to a situation in which each cell is separately monitored and prevented from overcharge, undercharge, or overdischarge abuse. It is not clear, at present, whether this type of control would be economically viable.

In addition, the presence of auxiliaries may adversely affect the full system's reliability. Simple, ambient-temperature batteries may require little more than some thermal management in the form of free or forced convective air cooling and some insulation. Other systems may involve more extensive thermal management and/or a flowing electrolyte subsystem(s), e.g., the Westinghouse Ni-Fe battery¹² (cf. Section III, Fig. 8) or the Exxon Zn-Br₂ battery¹³ (cf. Section III, Fig. 11); vacuum insulation for high-temperature batteries;¹⁴ operation of a complex chemical plant relying on internal feedback controls of flow rates and the refrigeration subsystem—the EDA zinc-chlorine hydrate battery¹⁵ shown in Figure 10 (Section III); or operation of an even more complex, Lawrence Livermore Laboratory primary aluminum-air battery with five subsystems (cf. Section III, Fig. 14).

Factors affecting the reliability of cells are discussed in Section II.2(ii)(a) together with the cycle life, since both parameters are closely interrelated.

Statistically meaningful data require prolonged cycling of large numbers of (connected) cells. It should be kept in mind that EV technology is at a very immature stage, perhaps comparable to that of the internal combustion engine at the beginning of the century. Attempts are being made to help design appropriate testing methods and achieve high reliability by introducing proper switching methods and sufficient redundancy.¹⁶

2. Cost-Related Requirements

Data concerning battery cost have to be treated with considerable caution. The uncertainty is both objective (changing commodity and labor costs; unknown price of undeveloped components, mass production, recycling, etc.) and subjective (the enthusiasm of battery developers).

Some of the values projected for mass production are reported in Section IV (cf. Table 6). Most of them are close to \$100 per kilowatt-hour, possibly because of the development targets set by R&D funding institutions. Some zinc-based batteries are projected as least expensive^{13,15,17} when fully developed. It seems unlikely that the projected costs of nickel-containing systems will be met in the foreseeable future, although in the case of Ni-Fe the high initial cost may be compensated by low cost per mile due to the anticipated long cycle life and high reliability of the battery. At present, it appears that only the improved Pb-A battery may be available at a cost less than \$100 per kilowatt-hour within the 1980s.

(i) *Initial Cost*

Battery price is calculated on the basis of the material and manufacturing costs. The cost of the active materials is directly related to their availability. With the exception of Na-S, Fe-air, and a few other exploratory systems, all EV battery candidates are based on materials which are either not too abundant worldwide, reside in diluted ores, or can be extracted viably only from ores located geographically in a few areas. The imports may be subject to politically induced shortages or stoppages, in analogy to the gasoline situation. In some cases, even the domestic resource utilization may become prohibitive because of the environmental impact.

Material availability could become a serious problem if one thinks in terms of total conversion to electric cars. On the other hand, a 10% incremental demand on the reserves could support the production of 10^5 - 10^7 batteries per year of each kind listed in Table 4.¹⁸

The potential availability problem might be substantially relieved if battery materials could be efficiently recovered. The development of cheap recycling methods is of primary importance

Table 4
Preliminary Supply Constraint of Battery Materials

Battery type	Material	Battery requirements (kg kW ⁻¹)	Yearly use level (tons × 10 ⁻³)	Battery capacity at 10% of use level (kWh × 10 ⁻⁷)	Number of batteries per year (10 ⁻⁵)
Pb-A	Lead	22	1400	0.64	3
	Antimony	1.6	40.3	0.025	
Ni-Zn	Nickel	3.29	211	0.64	3
	Zinc	1.28	1500	11.7	
	Cobalt	0.055	8.5	1.54	
LiAl-FeS	Lithium	0.25	3.4	0.11	40
	Aluminum	1.0	6175	61.7	
Zn-Cl	Zinc	0.74	1500	13.5	700
	Titanium	0.39	585	15	
	Chlorine	0.80	7640	95.5	

(e.g., the present cost of recycling lead considerably contributes to the cost of commercial lead-acid batteries). The projected battery costs usually assume such methods to have been developed.

(ii) *Cost per Mile*

The most important factor affecting this cost is the battery cycle life; operating costs determined by the energy efficiency of the battery and range losses due to self-discharge will become progressively important with the future increase of energy cost. Maintenance costs vary from relatively insignificant in batteries requiring only water addition (simple near-term systems) to somewhat higher values in more complex batteries.

(a) *Cycle life*

Cycle life of sufficient duration, combined with acceptable specific energy, is the most elusive of the desirable battery attributes. Factors responsible for cycle life and reliability of a single cell vary in different systems; they are connected with the mechanical, structural, and/or chemical changes accumulating in electrodes or other cell components upon cycling. These changes can often be

attributed to electrode reaction mechanisms involving phase changes: redeposition of the solid phase from a dissolved discharge product and/or volumetric expansion/contraction cycles between charged and discharged solid phases. Surface passivation of the active material or decomposition of the (organic) electrolyte may also become a life-limiting factor. Cells with inert electrodes and gaseous or liquid reactants (e.g., zinc-halogen) are less subject to limitations connected with reactant deterioration. Their cycle life may, however, be shortened by electrochemical processes (e.g., corrosion or oxidation) which deteriorate inert cell components or lead to products which affect the normal cell operation, e.g., as with some Na-S systems.

Depending on the system, cells may be sensitive to damage by overcharge, frequent undercharge, overdischarge, extremes of temperature, thermal cycling, and/or mechanical effects of driving conditions, such as change of position, vibration, and/or shock.

Among near-term and advanced systems, the longest cycle life is expected for Ni-Fe systems (sintered iron electrodes have been reported to be capable of ~ 3000 deep discharge cycles); a very short lifetime (at most ~ 300 cycles achieved before 20% loss of rated capacity) is characteristic of simple alkaline Ni-Zn cells. Other near-term and advanced systems have demonstrated battery, module, or cell cycle life of 400–1000 cycles. Further improvements and reliable transfer of the cycle life achieved in modules into full batteries depend, in general, on the feasibility and rate of technical and engineering progress, rather than on scientific breakthroughs as is the case of the simple alkaline Ni-Zn system.

As it has been previously mentioned, statistical projections based on single-cell tests are not sufficient for evaluation of a battery's cycle life and reliability, since a multicomponent system has additional problems connected with the effects exerted by each cell on its neighbors. These effects are due to the nonideally uniform electrochemical behavior of battery cells. Small differences in charge or discharge rates of individual cells may accumulate in cycling, leading to various degrees of overcharge and overdischarge (including cell reversal) which may result in irreversible cell or even battery damage. The latter can also be caused by corrosion due to single-cell(s) leakage. In general, suitable precautions are needed to minimize spreading damage due to the malfunction of a single cell.

Attempts to increase the specific energy usually compromise the battery cycle life as exemplified in Fig. 5 for Pb-A batteries.¹¹ The cycle life is also affected by the depth of discharge. Voss and Huster¹⁹ suggested an empirical equation

$$\log N = -kD/100 + d$$

where N is the number of cycles, D is the depth of discharge, and k and d are coefficients characterizing the given battery. It is assumed here that the battery loses a certain percentage of its capacity in each cycle. The equation has been found valid for a number of batteries, such as Pb-A (cf. Fig. 6), Ni-Cd, Ni-Zn, Ag-Zn,²⁰ and probably Zn-Br₂, although the failure mechanism in the latter case is different than in the case of porous plate batteries and the cycle life of Zn-halogen batteries is much less susceptible to DOD.

These examples illustrate the tremendous technological challenge involved in the simultaneous optimization of several attributes required for a viable EV battery.

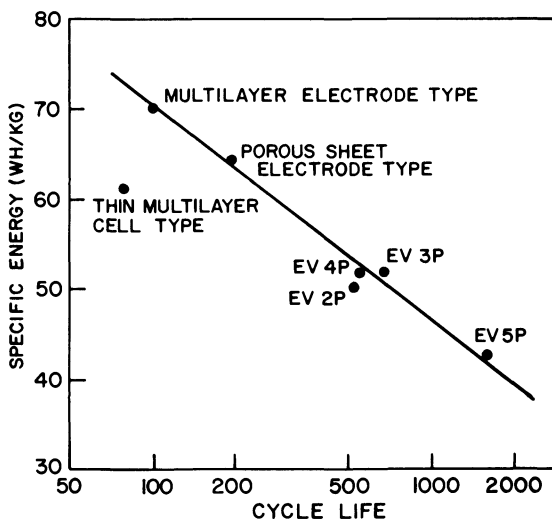


Figure 5. Specific energy vs. cycle life of lead/acid batteries.¹¹

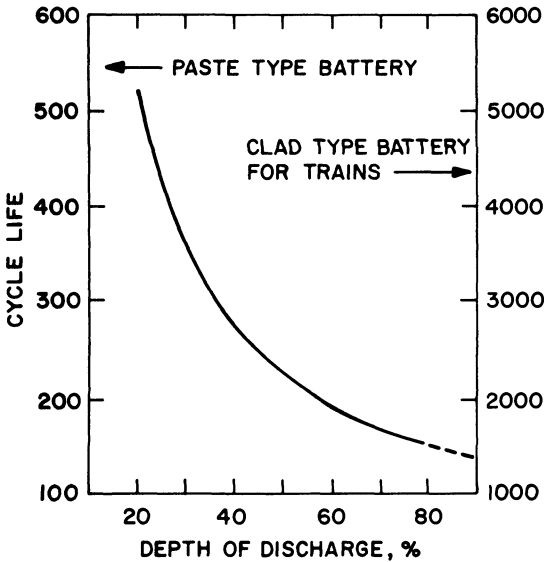


Figure 6. Cycle life of lead/acid batteries as a function of DOD.¹

(b) Energy efficiency

Energy efficiency of batteries is mainly connected with the electric input to output ratio, because the initial energy input required in manufacturing is a relatively small fraction of the total energy consumed during a battery's life.²¹

The main component of voltaic inefficiency is usually the ohmic loss, compounded by mass-transport-related overvoltage. The extent of coulombic losses depends on the system and may be due to parasitic electrode and/or chemical reactions, self-discharge, and/or shunt currents (in flowing systems with a common electrolyte). The efficiency, as measured at battery terminals differs from the effective value if a part of the battery's energy is used to operate auxiliaries (e.g., pumps) or if thermal losses are involved (high-temperature batteries).

Except for zinc-halogen complex and metal-air systems, traction battery prototypes have been shown to operate at 60–75% efficiency (cf. Table 6). Higher values, usually quoted for high-

temperature batteries (Na-S, LiAl-FeS) do not take into account thermal losses, which, among other factors, depend on the type of insulation, assumed EV driving cycle, and mileage per year.

3. Safety and Environmental Impact

(i) *Use of Batteries in EVs*

Hazards connected with the failure (stationary or on impact) of the Pb-A and Ni-Zn batteries are comparatively small and safety precautions may be limited to explosion-arrest devices. In Ni-Fe cells, catalytic reactors are installed to prevent hydrogen fires.

Toxic substances (stilbine and arsine from Pb-A batteries), which may be released during charging as well as, surprisingly, during discharge, seem to require no more than ventilation of the garage and of the battery compartment.²²

A possible destruction upon impact of zinc-halogen batteries might lead to the release of chlorine gas or bromine liquid and vapor. A study²³ of the effects of spilling a full load of chlorine hydrate on hot concrete concluded that the probability of lethal accidents appears to be no more serious than that caused by gasoline fires in ICE-powered cars. The bromine vapor pressure above the organic complex is lower than that of chlorine above chlorine hydrate; its lethal dose, however, is smaller and the spill cleanup and dispersion problems may be more severe.

Among high-temperature batteries, the lithium-iron sulfide systems are reasonably safe, although there are some hazards connected with the 450–500°C operating temperature. The sodium-sulfur-system impact failure hazards are primarily connected with the possibility of SO₂ emissions, sodium oxide dust, and fires resulting from sodium exposure to moisture.

(ii) *Environmental and Health Considerations*

Urban pollution has been shown by Japanese,²⁴ Australian, and U.S. researchers to be primarily due to car exhaust emissions. The U.S. Environment Protection Agency (EPA) reports transportation in the USA to be responsible for ~42% of total emissions, the car being the largest single polluter. Correspondingly, cars in the

USA must conform to the increasingly restrictive federal exhaust emission standards. Transition to EVs supplied by oil-fired power stations would considerably lower the level of hydrocarbons and nitrogen oxides (even in comparison to the present EPA-allowed levels) and almost eliminate carbon monoxide emissions² as shown in Table 5. More realistically, however, this transition may be expected to occur when coal will be the primary energy source. With the exception of CO, the emission levels from coal-fired power stations²⁵ (calculated in g per EV mile) are not superior to those allowed by the EPA (cf. Table 5). The question arises whether the pollution problem is then not simply transferred from the car power plants to the central power facilities. Central, large-scale coal combustion seems to alleviate the problem since the pollutants are well dispersed above ground level being released from tall stacks (~200 m) located away from urban areas. Also, the large-scale central combustion process appears to be better suited economically for the installment of sophisticated pollutant removal, particularly of SO₂ than the distributed small IC engines of mobile vehicles powered by coal-derived fuels.^{2,4} Not only air but noise pollution would also be decreased by use of EVs in urban environments.

Environmental and health hazards connected with mining and milling of raw materials, battery manufacture and recycling have been studied for near-term (lead/acid, nickel-iron, nickel-zinc)²⁶ and zinc-halogen²⁷ batteries. Significant increases in processing lead could result in an increased probability for local (~50-km radius) development of the central-nervous-system response as well as of renal proteinuria due to increased cadmium emissions. Increased levels of mining highly dilute ores might eventually bring

Table 5
Pollutant Levels

Pollutant	EPA standard (g mile ⁻¹)	Emissions from power station (g per EV mile)	
		Oil fired ²	Coal fired ²⁵
Hydrocarbons	0.41	0.03	0.40
NO _x	3.4	0.48	1.48
CO	1.0	Negligible	

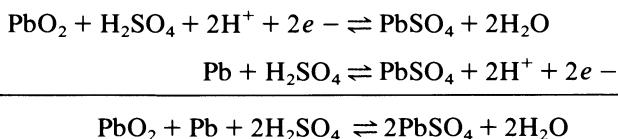
about some pejorative ecosystem effects, which are otherwise considered insignificant.

III. CHARACTERISTICS OF INDIVIDUAL SYSTEMS

1. The Lead/Acid Battery

The development of the lead/acid battery has been steadily progressing since 1860 when Planté²⁸ constructed the first practical device based on the concept of Siemens and Sisteden (1850). The extension of the present traction-battery applications to passenger vehicles requires primarily a substantial increase of specific energy and peak power without compromising cycle-life-related battery characteristics. At present, commercially available traction batteries for forklift-type applications can provide some 2000 cycles and 20–22 Wh kg⁻¹ at the C/6 rate; the higher specific energy of golf-cart batteries (~27 Wh kg⁻¹ at the C/3 rate) has been achieved at the expense of battery life (~400 cycles). Modified batteries for delivery vans and similar uses which do not require specific peak-power levels expected of passenger cars have attained up to 30 Wh kg⁻¹ and 800–1000 cycles.^{29,30}

The electrochemistry of the Pb–A cell can be represented by



Although water decomposition and elemental-lead corrosion reactions are strongly inhibited by the low hydrogen exchange current on lead, overcharge without proper controls may result in severe damage due to the excessive gassing (see below).

The theoretical specific energy of the Pb–A battery varies somewhat with acid concentration and amounts to ~77 Wh kg⁻¹ for traction batteries which utilize more concentrated solutions ($d_{25^\circ\text{C}} = \sim 1.28 \text{ g cm}^{-3}$). In the limits (an ideal system operating without overvoltages at 100% reactant utilization, and containing no inactive materials except for the necessary dilution water and ~30% excess acid) the specific energy would be almost halved to

$\sim 96 \text{ Wh kg}^{-1}$. The specific energy achieved in ISOA modules is $35\text{--}40 \text{ Wh kg}^{-1}$ at the $C/3$ rate.³⁰⁻³² Efforts which have resulted in this improvement and aim at achievement in advanced systems of $\sim 50 \text{ Wh kg}^{-1}$ without compromising the specific power and cycle life³³ have been centered around the following:

1. A decrease of weight of inactive materials used for casing, grids, connectors, terminals, and separators, e.g., by use of carbon fibers, plastics or plastic-lead-alloy materials, lead-coated aluminum positive grids, and/or aluminum terminals and connectors. Attempts to build batteries with bipolar electrodes have resulted, until now, in highly improved power (but not energy storage) characteristics at the penalty of a drastically shortened cycle life due to severe sealing problems.³⁴ The concept is still being pursued, among others, in the form of a lead-boron tetrafluoride system,³⁵ and a new "quasi-bipolar" design, involving a continuous plastic-composite conductive sheet (enveloping connective cells) which can be thermally sealed.³⁶

2. Increased utilization of solid reactants. Even at rates lower than those required in EV operation, $<40\%$ of the solid reactant mass is utilized. The poor utilization of PbO_2 has been blamed on the volume change of the reactant between charge and discharge, changes in its microstructure, appearance of an inactive PbO_2 form, and/or blocking of the pores by the discharge product. With increasing depth of discharge, the growth of PbSO_4 layers impedes the mass transfer of HSO_4^- ions. Simultaneously, the latter become depleted, and water is generated at the interface affecting the reaction kinetics and ohmic resistance. Improvements in reactant utilization are attempted, among others, by optimizing the PbO_2 microstructure,³⁷ electrolyte agitation, or circulation, and/or by decreasing the electrode thickness³⁸ without affecting its mechanical strength. (The positive electrode must combine the ability to withstand stresses introduced by volumetric changes of the reacting solid phases during cycling with sufficient porosity to maximize the interfacial contact with sulfuric acid.)

The EV range is obviously affected by the level of self-discharge. The latter is mainly due to the reduction of PbO_2 by lead of the grid and to the formation of anodic oxidation products (e.g., of Sb) which diffuse to the negative plate. Their deposition decreases the hydrogen overpotential and results in corrosion of

the Pb sponge at OCV and on charge. This process may decrease the rated capacity by some 20–30% per month.

The specific power of the Pb–A battery strongly depends on the depth of discharge³⁹ owing to the previously mentioned mass transfer, kinetic, and ohmic effects. As opposed to the inherently limited range, the acceleration (power) capability of the ISOA prototypes, is close to values required for a small passenger car even at 80% DOD. Apart from the weight decrease, further improvements aim at a decrease of internal resistance by use of better separator materials⁴⁰ and better current collection at both flat⁴¹ and tubular⁴² electrodes. Analysis of current distribution and computer-assisted modeling techniques have resulted in new grid structures and designs which have already considerably reduced the battery weight and internal resistance, and have potential for further improvements. Up to now, the highest specific peak-power values (440 and 220 W kg⁻¹³⁴) have been reported for the previously mentioned short-lived bipolar batteries designed for low specific energies. Combination of high specific power with high (~50 Wh kg⁻¹) specific energy might conceivably be achieved in the future for bipolar systems. At present, these characteristics are computer projected for the Jet Propulsion Laboratory's "quasi-bipolar" cells at a very early stage of laboratory development.³⁶

The battery cycle life is generally limited by the behavior of the positive electrodes. The latter have a tubular or flat design. The more expensive tubular positives seem to provide longer life but lower specific energy than flat electrodes. However, the superiority or either version for EV applications is at present difficult to assess.⁴³ The life limitation is related to shedding of PbO₂ and its inactivation.^{44–48} Both phenomena are ascribed to the changes of volume, structure, and morphology of the positive electrode material which accumulate during cycling.

Although several hypotheses have been proposed, the mechanisms of electrode degradation involved in shedding and inactivation processes are still not clear. The method of material preparation plays a substantial role here. For example, positive material prepared by oxidation of needle like crystals of tetrabasic lead sulfate (4PbO · PbSO₄) maintains the latter's morphology and the electrode's superior performance during cycling of stationary cells.⁴⁹

The material has not been used in traction batteries, presumably owing to its manufacturing cost. The original structure of the active material (and retardation of the appearance of the deleterious coralloid structure⁴⁴) is also reported to be retained longer in gelled electrolyte⁴⁷ used in sealed, maintenance-free batteries. Differences in the electrochemical behavior of α - and β - PbO_2 have been often blamed as a possible cause of inactivation, but see References 37 and 48. Stress and particle subdivision due to the dissolution-precipitation mechanism of cyclic PbO_2 - PbSO_4 reactions and accompanying volumetric changes are thought to cause electrode disintegration, at least in antimonial cells.³⁸

Severe gassing during overcharge considerably accelerates shedding.

The "return to fundamentals" in the recently extended structural studies may help in better understanding of the positive electrode processes and in developing necessary manufacturing and operational improvements.

Another major failure mode is due to corrosion of the positive grid. The formation of corrosion layers at the grid-paste interface depends on the alloy used and determines the extent of the electrode damage. Antimony, used in the lead alloy to improve mechanical strength and castability,²⁹ is now often partly or completely replaced⁵⁰ by other alloying metal additives, primarily Ca or Ca and Sn. The corrodibility and self-discharge rate is thus decreased, and the possibility of toxic stilbine emissions during cycling is avoided.

The desired cycle life of Pb-A batteries depends on their end use. In stationary applications, under conditions of low discharge/charge rates and shallow depths of discharge, up to 4000 cycles have been achieved. The goal assumed to be sufficient for economically viable EV applications is ~ 1000 cycles at a specific energy of $\sim 40 \text{ Wh kg}^{-1}$. This is difficult to attain since the cycle life is adversely affected by several factors, such as:

1. High depth of discharge (cf. Fig. 6). The effect has been ascribed, among others, to the development of a coralloid structure.⁴⁴

2. Increase of specific energy (cf. Fig. 5) achieved, e.g., by use of thinner plates or increased porosity of reactants which leads, in turn, to enhanced grid corrosion and faster shedding of PbO_2 .

3. Gassing due to overcharge which should be limited to the necessary minimum ($\sim 10\%$ of rated capacity^{10,38} Overcharge, otherwise beneficial in preventing, by gassing, stratification of the electrolyte (water generated during discharge rises to the surface, while sulfuric acid produced during charge concentrates at the bottom) accelerates grid corrosion and shedding. Electrolyte agitation and/or circulation has been attempted^{42,51} as a means of preventing stratification and acid depletion. Consequently, conditions are improved for high discharge rates, deep discharge, and reactant utilization. Varta batteries with flow-through porous electrodes (“eloflux principle”) are reported to improve reactant utilization in the middle range of current densities.⁷ Effects on cycle life, however, are as yet unclear. A substantial improvement in the reduction of the overcharge from 20 to 40% to some 5% has been reported by the Globe Battery Division of Johnson Controls due

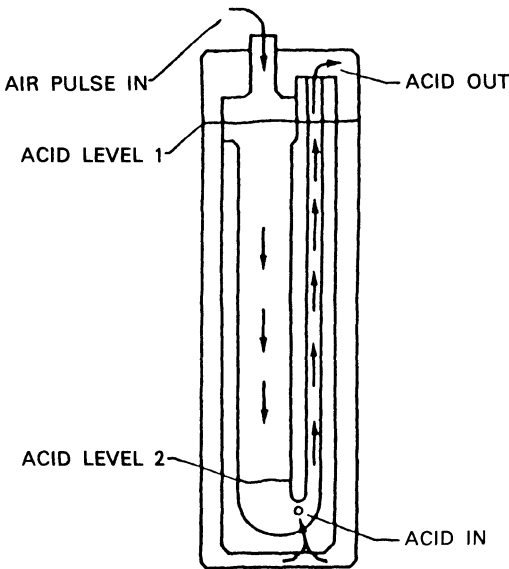


Figure 7. Pulse pump structure: Globe Battery Division, flat Pb-A cell. (Courtesy of Globe Battery Division, Johnson Controls, Mr. D. Thuerk, 1984.)

to incorporation of a light circulation system. It consists of polypropylene insert pumps in each cell^{38,51} (cf. Fig. 7). Apart from the extension of the cycle life, electrolyte circulation is reported to have improved the energy efficiency (>80%), specific energy, and power, to have facilitated the thermal management⁵² and minimized the water loss. Grid corrosion, one of the major failure modes of the positive electrode, has been inhibited, since the decrease of overcharge allows the establishment of charging overvoltage based on the grid alloy composition.

4. Operating temperature, which seems to be at optimum at 30–44°C.^{10,53} The severe loss of cycle life and capacity of the Pb–A battery, particularly at low temperature may require, depending on the driving profile,⁵⁴ some degree of thermal management in terms of forced convection (air cooling), as well as a light insulation to inhibit heat loss during prolonged shutouts.

Owing to the scarcity of data correlating the battery performance with the cycle life under conditions of the EV's driving profiles (which involve, among others, high rate pulses during acceleration and regenerative braking, chopping voltage into rectangular high-frequency pulses by solid-state switches in vehicles with continuous speed control, and frequent stops in urban traffic), the effects of optimizing both specific energy and cycle life under EV driving conditions are presently difficult to assess.

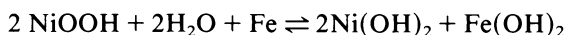
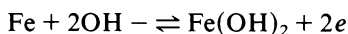
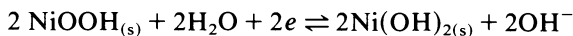
Safety precautions may involve introduction of simple explosion-arrest devices integrated with the watering system.

In spite of its inherently low storage capability, the lead–acid battery seems to be a realistic EV-power-plant candidate owing primarily to the manufacturing and recycling experience, relatively low cost, long cycle life, and reliability. Improvements in the technology due to the EV effort have already been incorporated in commercial traction batteries and are envisaged for introduction in SLI (automotive starting) batteries.⁵⁵

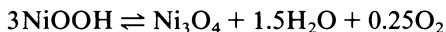
2. The Nickel–Iron Battery

The Ni–Fe system developed by Edison⁵⁶ in 1901 was the predominant commercial secondary battery till the early 1920s. Past applications have been to railcar lighting, mine lamps, mine vehicles, lift trucks, etc.

The electrochemical reactions (limited in the battery to a two-electron redox process on iron) can be represented by

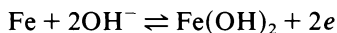
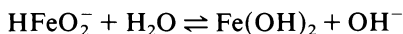


The relatively high exchange current of hydrogen on iron (lowered somewhat by amalgamation already by Edison) results in considerable gassing during charge and in corrosion of iron which shortens the battery shelf life by self-discharge processes such as



The capacity loss due to self-discharge is considerable. It can amount, in a fully charged battery, to $\sim 2\%$ during the first 20 min of open-circuit standtime and exceeds 5%, after 4 h.¹⁰

As opposed to the positive electrode, the redox process at iron does not proceed in the solid phase but via a dissolution-precipitation mechanism⁵⁷ simplified below to



In spite of their low solubility ($\sim 5 \times 10^{-5} M$ litre), HFeO_2^- ions diffuse to the positive electrode and are oxidized to solid FeOOH ²⁰ causing further dissolution of iron and its continuous transfer to the positive electrode. The process is irreversible, the potential of the nickel electrode being too positive, even during discharge, for the reduction of trivalent iron. Further decrease of capacity is caused by the lowering of oxygen overpotential on the nickel oxide in the presence of FeOOH . The self-discharge and iron transfer processes are somewhat inhibited by additives⁵⁸ to the electrode (sulfur) or electrolyte (e.g., lithium and sulfide ions, or hydrazine sulfate).

The theoretical specific energy of the battery is $\sim 267 \text{ Wh kg}^{-1}$; the effective values previously achieved in commercial applications did not exceed some 25 Wh kg^{-1} . In spite of the limited energy

storage and power capability, the battery is under development in the USA,^{59,60} Sweden,⁶¹ Germany,⁶² Japan,⁶³ and the USSR.⁶² The improvements aim primarily at better utilization of active materials and weight decrease of inactive battery components. The positive electrode is life limiting owing primarily to volume difference between charged and discharged phases ($\sim 20\%$).⁶⁴ Therefore, a sufficient mechanical stability of inactive supports must be maintained. Several new designs and materials have been utilized in battery prototypes including, among others, nickel or nickel-coated carbonaceous fibers and cloths of high porosity; nickel hydroxide-graphite mixtures pressed into nickel wire screens; sintered structures; and specially prepared reactant powders (for both electrodes).

The management of water, heat, and evolved gases requires battery designs which allow for easy replacement of water evaporated or decomposed during charge and rest periods, sufficient heat exchange, and prevention of explosion due to accumulating hydrogen and oxygen gases. Designs involving a single watering point and flame arrestor or an auxiliary electrolyte circulating system are under development at Eagle-Picher Industries Inc.⁶⁵ and Westinghouse Electric Corporation,⁶⁶ respectively. In the latter design, cooled electrolyte is flowed into the battery from a reservoir (cf. Fig. 8) which may be placed off-board or on-board at some penalty of decreased specific energy and power.

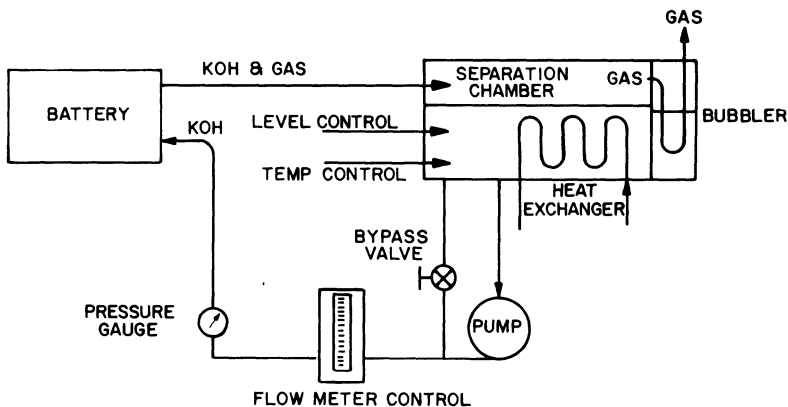


Figure 8. Schematic of the Westinghouse nickel-iron circulating battery.⁶⁶

The Ni-Fe battery rapidly loses its capacity and peaking-power capability with decreasing temperature. Improvements in this area have been significant, particularly in batteries using sintered iron electrodes⁶⁷ developed by the Swedish National Development Company and Eagle-Picher Industries Inc.⁶⁸ They are reported to perform satisfactorily down to some -20°C .⁶¹

The improvements, aimed at a $>60\text{-Wh kg}^{-1}$ system, have to date resulted in EV battery prototypes with specific energies close to $\sim 50\text{ Wh kg}^{-1}$ at $C/3$. Their dynamometer tested range is, at best, some 20% higher than that of the Pb-A EV prototypes.¹⁰

The specific peak power of the battery strongly depends on the depth of discharge; nevertheless, acceptable acceleration seems to be achievable even at 80% DOD (cf. Fig. 3).

The system is expensive owing to the high price of nickel and low operating voltage (1–1.2 V) which necessitates a larger number of cells in this battery than in most other systems. The high initial cost can, to some extent, be offset by the projected long cycle life. Although the extension of the EV range over the Pb-A is marginal, the proven ruggedness, expected reliability, and long life of the Ni-Fe system (~ 900 cycles have been achieved for a van battery cycled with a simulated driving profile without capacity loss¹⁰) has made it attractive to EV battery developers.

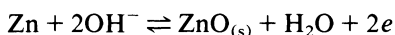
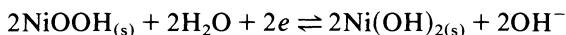
3. Zinc Batteries

(i) *The Nickel-Zinc Battery*

The concept of a rechargeable Ni-Zn battery was first patented by de Michalowski in 1899 and the first railroad battery was constructed in the early 1920s by J. J. Drumm.⁶⁹ Because of its short cycle life, limited by dendritic growth and shape change of the zinc electrode, little work was done on the system until the last few decades when it was realized that the energy storage and power capabilities, coupled with ambient-temperature operation, make the system most desirable for mobile applications. The theoretical specific energy of the battery is $\sim 320\text{ Wh kg}^{-1}$. Extensive R&D effort carried out in several countries^{4,70} resulted in a number of EV battery prototypes with specific energies reaching $>100\text{ Wh kg}^{-1}$ and specific peak power exceeding 140 W kg^{-1} . The cycle life,

however, of these batteries was prohibitively short. Attempts to improve the cycle life resulted in a considerable decrease of specific energy and power without sufficient life extension⁷¹ to compensate for the high initial cost, due primarily to the high cost of nickel. The longest life (300 cycles) reported by General Motors⁷² appears to be insufficient to make the system economically viable.

The electrode and cell reactions can be represented by



The key technical problem of the battery causing its loss of capacity with cycling is the shape change and densification of the zinc electrode.⁷³ (Dendritic growth of zinc during charge, which was the original failure mode of the battery by short circuiting, has been largely overcome in alkaline solutions by use of suitable separators and programmed charging modes, and by limiting the cell capacity by the positive electrode.) Both phenomena are ultimately connected with the high solubility of zinc oxide (cf. the anodic reaction) which results in morphological changes (densification) and/or redistribution during charge of the active material toward the electrode center (shape change). These effects accumulate with cycling, leading to the loss of active surface area and eventually to bulging of the electrode which may even result in a mechanical rupture of the cell. The mechanism of both phenomena, which are not necessarily connected,⁷⁴ is not clear. Neither of the suggested hypotheses can satisfactorily account for the observed cycling behavior of the zinc electrode. Models which have been proposed to explain the center-oriented accumulation of the metal involve:

1. Differences in the kinetics and secondary current distribution between charge and discharge half-cycles, resulting in lateral concentration gradients and material transport due to the resulting concentration cells.⁷⁵
2. Osmotic membrane pumping effect, driving the electrolyte away from the electrode center during charge, and toward

it during discharge, when the electrolyte is more concentrated.⁷⁶ This model seems to require the presence of an electrolyte reservoir. Experimental confirmation of the model is somewhat controversial.⁷⁷

3. Fragmentation of zinc^{78,79} due to anomalous current distribution or a nonuniform cross section of dendritic stems and/or their fracturing during current reversal in the cathodic half-cycle. Electrophoretic motion of small fragments would then account for the shape change.

Recent observation of the opposite cycling effect—denudation at the electrode center and zinc accumulation at the electrode edges⁸⁰—is an additional factor to be taken into account in future attempts at a better understanding of the mechanism of zinc shape change. Without this understanding further semi empirical attempts to extend the cycle life of the Ni-Zn battery without compromising its high-performance capability, seem to have little chance of success.

A number of measures have been tried to prevent the shape change, including the use of binders,⁸¹ the extension of negative plate edges beyond the edges of the positive electrode, the use of specially shaped electrodes and/or additives⁸² to the Zn electrode and electrolyte, and the use of vibrating,⁸³ mechanically wiped, or slurry⁸⁴ negative electrodes. An interesting modification of the Zn slurry electrode of Compagnie Générale d'Electricité⁸⁵ is under development at SEREGIE, France.^{17,86} A circulating system of small Zn-coated plastic spheres brings them intermittently in contact with a horizontal current collector. The low concentration overpotential prevents dendritic growth. About 80% of the zinc is deposited on the spheres. Plating errors on the current collector, at which the balance of zinc is deposited on charge, cannot accumulate since they are corrected upon discharge by complete dissolution of the metal. High reactant utilization of the system is in contrast with that in conventional Ni-Zn cells which require that negative electrodes contain a three- to four-times excess of Zn over the rated capacity. A module containing 28 bipolar cells has been reported to deliver 70 Wh kg⁻¹ (95 Wh liter⁻¹). The peak-power capability of 120 W kg⁻¹,¹⁷ as well as high longevity have been, as yet, reported only for single cells and therefore the merits of this modification cannot be evaluated at the present stage of exploratory develop-

ment. The low cost (\$70 per kilowatt-hours) projected for a mass-produced battery must be treated with caution, in spite of the special, light foam Ni electrode used.⁸⁷

In all Ni-Zn batteries, various techniques aiming at the reduction of the inactive Ni content (e.g., 60% in sintered electrodes) have been proposed. The limited reserves of the metal and the sensitivity of the battery's initial cost to nickel price would require an extremely efficient (~85%) metal recovery program.

The development of an economically viable conventional Ni-Zn battery hinges on a scientific and technological breakthrough which, contrary to expectations, has not yet materialized, causing a drastic drop in the R&D effort in this area.

(ii) Zinc-Halogen Batteries

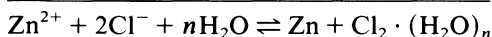
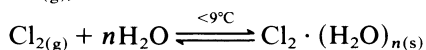
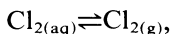
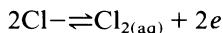
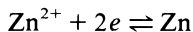
The attractive features of the zinc electrode (relatively low cost and light weight of the metal with highly negative reversible potential and relatively high hydrogen overpotential) stimulated attempts to improve its cycle life by replacement of the alkaline electrolyte by a flowing acid medium. Two systems under development for both stationary and EV applications involve chlorine hydrate and an organic bromine complex as positive electrode reactants in acidic $ZnCl_2$ and $ZnBr_2$ electrolytes, respectively. Owing to the corrosive properties of these media, metals are almost completely excluded as battery components. Advantages of both systems involve their potential longevity; "forgiving" character, e.g., in their relative insensitivity to overdischarge; retention of capacity with cycling; little dependence of performance on the depth of discharge; and potentially low cost. Disadvantages, common to all flow batteries, include complexity and high weight and volume, which affect specific energy and power, as well as performance losses due to the operation of auxiliary subsystems.

(a) The zinc-chlorine battery

Zinc and chlorine were first suggested as battery materials some 150 years ago.⁸⁸ Several efforts were made to build the battery;⁸⁹ the first realistic design based on the concept of using solid chlorine hydrate instead of gaseous or liquid chlorine had

been patented in the USA in 1968. Since then the battery has been under development primarily at EDA (Gulf + Western Company) in USA⁹⁰ for mobile as well as stationary applications, and at the Furukawa Electric Company in Japan.

The reversible processes taking place during the charge \rightleftharpoons discharge cycle are



The electrochemical reactions proceed at catalyst-free graphite comb-like electrodes arranged so that the zinc side teeth interleave with those on the chlorine side of the next comb⁹⁰ (cf. Fig. 9). The low (2 g liter^{-1}) solubility of chlorine in the acidified ZnCl_2 electrolyte allows separator-free operation, but see Reference 91. The electrolyte is circulated between the sump (cf. Fig. 10) and the battery stack. During charge, zinc is deposited on the negative combs while gaseous chlorine, which evolves at the high-surface-area positive electrodes, is transferred to the store tank where it combines with chilled water to form a yellow solid—chlorine hydrate, $\text{Cl}_2 \cdot (\text{H}_2\text{O})_n$ ($n = 6$ or 8).⁹² The latter process occurs below 9.6°C and requires refrigeration. During discharge, the processes are reversed: warm electrolyte is drawn from the sump into the store tank to decompose the hydrate. Evolving chlorine dissolves in the electrolyte and, upon transfer to the battery stack, is reduced passing through the porous flow-through positives. Zinc can be fully dissolved during discharge, thus plating errors accumulated within intermediate-depth discharges can be periodically corrected.

As opposed to the straightforward electrochemistry, the engineering of the battery poses serious problems owing to the complexity of the system and its operational demands relying on internal feedbacks. Thus, e.g., the discharge rate is controlled by monitoring the pressure in the store tank and the rate of injecting the warm electrolyte. About 80 cycles are claimed to have been obtained (without human intervention) in an EDA Zn-Cl₂ battery-

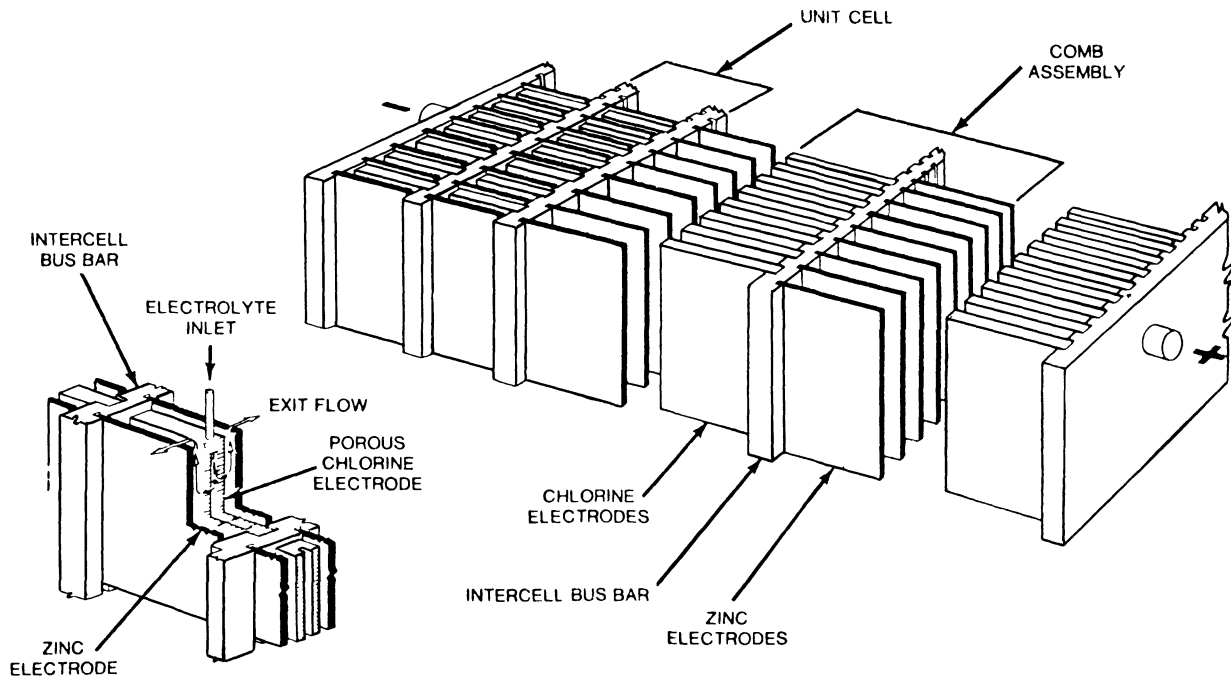


Figure 9. Comb structure of EDA zinc-chloride electrodes. (Courtesy of EDA, Gulf + Western Company, Dr. Peter Carr.)

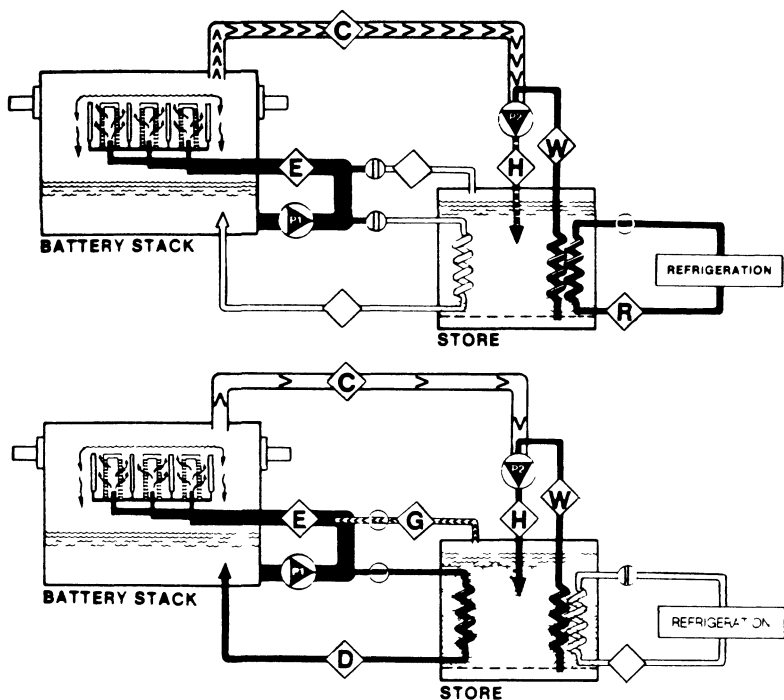


Figure 10. Schematic of the EDA zinc-chloride battery during charge (upper diagram) and discharge (lower diagram). (Courtesy of EDA, Gulf + Western Company, Dr. Peter Carr.)

powered van,⁹³ while over 1600 cycles⁹⁴ have been obtained under laboratory conditions with human assistance.

The theoretical specific energy of the battery is 460 Wh kg^{-1} . Several battery prototypes have been tested in specially modified vans and vehicles.⁹⁵ For example, effective values of specific energy and peak power are reported as 64 Wh kg^{-1} and 59 Wh kg^{-1} , respectively, when tested in a passenger car powered by a 636-kg battery (refrigerating system off-board) and driven at a constant speed.⁹³

The energy efficiency of the EV battery is $<50\%$. The major cause of coulombic inefficiency (10–30%) is the chemical reaction of zinc with dissolved chlorine. Thanks to kinetic inhibitions, only about 1% inefficiency (over the complete cycle) derives from the evolution of hydrogen and carbon oxides. The latter derive from

the graphite positives which oxidize at a rate corresponding to some 10% weight loss in 1000 10-h cycles. Both gases affect the capability of hydrate formation and decrease the solubility of chlorine in the electrolyte. Since the accumulation of hydrogen exceeding 5% may create explosive conditions, a photochemical reactor⁹⁶ is used to recombine hydrogen with chlorine. Hydrochloric acid returns to the sump maintaining pH of the electrolyte at a constant (~ 0.2) level. Inert gases (CO_2 with traces of CO and O_2) are periodically purged or continuously separated from chlorine in a small cell and vented from the system.⁹⁷

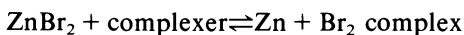
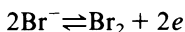
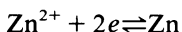
Another source of inefficiency are the shunt currents arising in all series-connected systems with a common electrolyte. In the EDA system, these parasitic currents are minimized to some (model computed) 5% power loss by maximizing the hydraulic resistance.

The relative abundance of reactants and low cost of the battery materials, combined with a potential for long cycle life, make the projected cost of the zinc-chloride battery low in comparison with that of most other systems. The complexity of the system and its reliance on automated controls may cause reliability problems, particularly under conditions of vibrations, shocks, etc. The fleet operation of larger vehicles, with easily available human intervention during recharge, seems more realistic than the use of individual units, but see Reference 98.

(b) *The zinc-bromine battery*

The first U.S. patents for a secondary zinc-bromine battery were awarded in 1880s to C. S. Bradley.⁹⁹ The obvious disadvantages of operating a battery containing elemental bromine—corrosion, high toxicity, high self-discharge rate—did not completely prevent its development, which is still underway, e.g., at GEL Inc.¹⁰⁰ The major effort, however, was directed toward alternative versions of the system, both for mobile and stationary uses. EV applications have been pursued mainly at Exxon Research and Engineering Co¹⁰¹ in the form of a flow battery with two separately circulated electrolytes.

The charge \rightleftharpoons discharge cycle involves the following highly reversible processes:



The complexing agents used at Exxon are quaternary pyrrolidinium and morpholinium compounds.^{101,102} The bromine complex formed upon charge is a heavy insoluble oil which accumulates at the bottom of the catholyte reservoir (cf. Fig. 11) Complexing reduces the vapor pressure of bromine by one to two orders of magnitude, and the self-discharge rate, as well as corrosive bromine attack, are considerably diminished.

The battery stack consists of cells formed by bipolar planar electrodes made of conducting ($\sim 1 \Omega^{-1} \text{ cm}^{-1}$) carbon-plastic composite with a high-surface-area carbon layer on the bromine side. (The Exxon system is unique, in that it is the only EV *bipolar* battery

ZINC-BROMINE CIRCULATING BATTERY

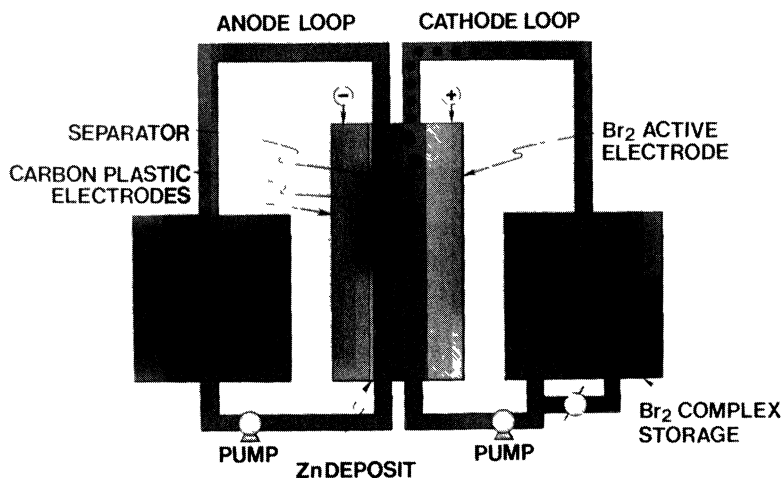


Figure 11. Schematic of the Exxon zinc-bromine complex cell. (Courtesy of Exxon Research and Engineering Company, Dr. R. Bellows.)

developed to the prototype stage.) The electrodes are framed with a filled nonconductive plastic with molded flow channels which separately distribute anolyte and catholyte pumped from their reservoirs into the respective compartments of each cell. A microporous membrane prevents direct mixing of the electrolytes. Higher solubility of the positive reactant (as compared to Cl_2) allows the use of flow-by rather than the flow-through electrodes employed in the Zn- Cl_2 system.

The complexing agent decreases, probably by adsorption, the exchange current of hydrogen evolution on zinc. Mixtures of bromine vapor and small amounts of hydrogen evolved under charge are generally not explosive and not flammable within the operating limits.

The theoretical specific energy of the system exceeds 400 Wh kg^{-1} . The effective values of specific energy and peak power, projected as $\sim 65 \text{ Wh kg}^{-1}$ and $> 115 \text{ W kg}^{-1}$, respectively, have not yet been reached in the 10- to 20-kWh prototypes built to date.¹⁰³

As opposed to other systems the energy efficiency of the Zn- Br_2 battery increases with decreasing charging time owing to decreased self-discharge losses. It is reported as $\sim 65\%$. This value includes losses due to operation of auxiliaries (pumping; shunt-current protection) but does not take into account the extent of self-discharge under EV operating conditions, when at each shutdown the bromine remaining at the electrode desorbs and diffuses through the separator to the zinc electrode. These losses may considerably affect the car range under stop/go conditions.

Shunt currents are minimized in an innovative way by use of a protective current applied from the battery to the common electrolyte flowing through the manifold channels.¹⁰⁴ The energy loss connected with this type of protection is reported as $\leq 5\%$.

The demonstrated cycle life of eight-cell modules has reached 400–640 cycles. The most serious failure mode seems to be the electrode warpage. The potential longevity of the system (stability of the electrolyte has been demonstrated in over 1200 cycles) can only be realized after methods of warpage control have been developed.

The initial cost projected for the battery is lower than for other systems with the possible exception of the SEREGIE Ni-Zn battery.^{17,86} The reactants and inert battery materials are relatively

abundant and inexpensive. The manufacturing methods, already highly developed, seem to be easy and suitable for mass production.

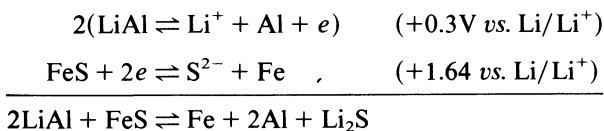
Apart from the electrode warpage and shutdown losses discussed above, certain other technical problems remain to be solved. They include internal leakage, optimization of performance in the low-temperature range, possible startup delays, weight decrease, and packaging capability. It is possible that the bulkiness and weight of this system may limit its potential EV applications to vehicles larger than compact.

4. High-Temperature Batteries

(i) *The Lithium–Sulfur-Based Systems*

The original concept of coupling molten lithium with highly electronegative S, Se, or Te melts, to obtain high-voltage cells with extremely high theoretical specific energies (2566 Wh kg^{-1} for Li–S), resulted in an intensive research and development effort on Li–S-based systems, carried out primarily in the USA (Argonne National Laboratory, Gould Inc., Eagle-Picher, General Motors), England (Admiralty Marine Technology), and West Germany (Varta). Difficulties encountered in operating “all-liquid” cells (in which Li and S melts were contained in porous stainless steel and graphite felt electrodes, respectively, separated by a paste electrolyte of Li halogenides¹⁰⁵) led eventually to the replacement of molten negative electrodes by solid lithium–aluminum¹⁰⁶ or lithium–silicon¹⁰⁷ alloys, and of molten sulfur—by solid metal sulfides.¹⁰⁸ The most advanced systems involve Li–Al alloy coupled with FeS and immersed in a eutectic mixture of molten halides of lithium and (usually) of other alkali metals. The replacement of elemental Li and S resulted in a loss of OCV by some 40% and of the theoretical specific energy by $\sim 84\%$. The operating temperature of the battery is $450\text{--}500^\circ\text{C}$.

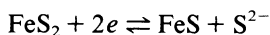
The overall electrode and cell reactions can be represented by



At 450°C the negative electrode is operated between 10 and 48 at. % Li. Within this composition range two solid phases coexist in the melt¹⁰⁹; the open-circuit potential and the operating voltage plateau are constant. In this two-phase region the lithium transport rate is high, presumably owing to a high vacancy concentration.

The lithium-silicon electrodes are under development mainly at Rockwell International and General Motors. Their disadvantage, as compared to the aluminum alloy, lies in several voltage steps over which discharge takes place, owing to a series of compounds which are solid at Li concentrations up to 81%¹¹⁰ (the operating composition range is 50–80 at. % Li). However, the average cell voltage, gravimetric and volumetric theoretical specific energies are higher than for the LiAl system.

The capacity and voltage of the cell can be increased by using FeS₂ as the positive electrode. Partial discharge proceeds then at ~0.3-V-higher upper plateau corresponding to the first (overall) reduction step:



Both positive electrode reactants undergo considerable volumetric changes during cycling, which are more pronounced in the case of FeS₂.

The mechanism of the positive electrode reactions is very complex and even for the lower plateau operation involves numerous electrochemical and chemical steps.¹¹¹ One of the intermediates, the so called “*J*” phase, seems to inhibit the reduction kinetics and limit the cell performance. Measures which eliminate this intermediate bring about some undesirable effects, such as higher corrosion rates, narrowing of operating temperature range, increased cost, and—in the case of the use of Cu₂S as an additive—possibility of short-circuiting due to precipitation of Cu in the separator.

Use of FeS₂ severely complicates the electrochemical sequence of intermediate steps.¹¹² In addition, corrosion problems become even more serious owing to the higher vapor pressure of sulfur over FeS₂. Nevertheless, the higher specific energy and voltage continue to stimulate further R&D effort, particularly on the LiSi-FeS₂ and CaSi-FeS₂ systems.

The composition of the electrolyte is of primary importance owing to the required high ionic conductivity, compatibility with active and inert cell components, wetting characteristics, effects on the course of electrode reactions, and the cell's cost. The optimized electrolyte mixtures consist of alkali-metal halides. An all Li^+ ion electrolyte would be preferred from the point of view of kinetic and transport considerations; however, the decreased specific energy and high cost are then prohibitive.

Cell operation requires the presence of separators which are well wetted by the electrolyte and provide good electronic insulation, high rates of lithium ion transport, and retention of active electrode material. Among materials used, the rather expensive boron nitride felt¹¹³ seems to be superior in terms of performance and cycle life than the much cheaper ceramic powders.¹¹⁴

The electric-to-electric energy efficiency of the battery is very high. Thermal losses must be minimized by use of high-efficiency, preferably vacuum¹⁴, insulation.

The safety considerations involve primarily the consequences of the high temperature of the system. No significant reactions of the battery components with air have been observed under conditions of rupture of cells at the operating temperature. A massive short circuit in a 20-kWh module¹¹⁵ which resulted in generation of ~ 20 kWh of heat did not present any hazard, except for a 100°C increase of the temperature of the vessel.

The limited supply of lithium raises some concern.¹⁸ The total global resources are estimated at $\sim 7.2 \times 10^6$ metric tons—an equivalent of $\sim 3.6 \times 10^8$ 30-kWh batteries. However, the metal is expected to be readily recoverable. An alternative system, using calcium alloys in the negative electrode, is being explored.

The LiAl-FeS system has been developed to an EV-battery-prototype stage.¹¹⁶ Several inherent cell and engineering problems still remain to be resolved. These include, primarily, increased utilization of active materials, prevention of deteriorating effects of volumetric changes of the positive electrode, and development of inexpensive noncorroding materials and of improved designs for efficient current collectors. Ohmic losses in the present design of the battery have lowered the potentially high-power capability to levels unacceptable in mobile applications.

(ii) *The Sodium–Sulfur-Based Systems*

The discovery of a solid conductor of sodium ions by Kummer and Weber¹¹⁷ made possible the construction of sodium–sulfur cells which utilize molten or dissolved reactants separated by the ceramic electrolyte β - (cf. Fig. 12), or, usually, β'' -alumina. The latter ceramic has a three Al–O spinel block structure, a molar ratio of $\text{Al}_2\text{O}_3\text{--Na}_2\text{O} = \sim 5$, and contains 1–4% of MgO or Li_2O . The resistivity of the polycrystalline material at 350°C is about $5\ \Omega\ \text{cm}$, ~ 4 times lower than that of β -alumina. Other recently reported solid Na^+ ion conductors containing phosphorus oxides¹¹⁸ do not seem to be stable in contact with sodium at elevated temperatures.¹¹⁹

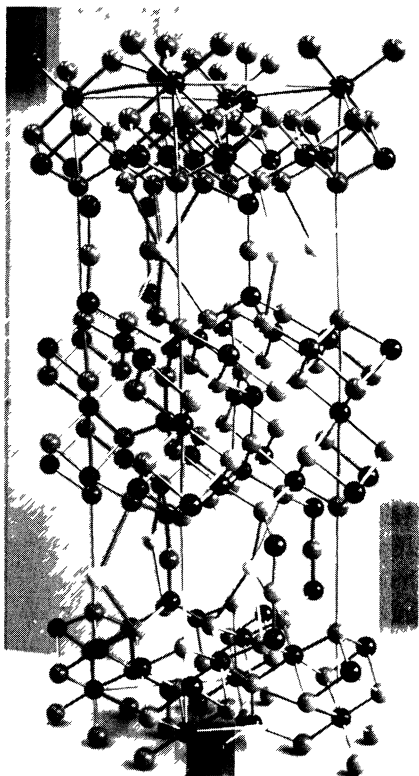


Figure 12. Structure of β -alumina.

Only Na- β "-alumina-S systems operating at 320–350°C have reached the prototype stage envisaged for both stationary and traction purposes. The development is underway at Ford Aerospace and Communication Co¹²⁰ in the USA, the Chloride Group in England,¹²¹ Brown, Boveri, & Cie^{122,123} in Germany, Yuasa Battery Company in Japan,^{122,124} and Compagnie Generale d'Electricite in France.¹²²

A high-temperature Na-S cell consists of a tubular solid electrolyte filled, in the fully charged state, with molten Na (sodium core) or sulfur (sulfur core cell),¹²⁵ the other reactant being contained between the outer wall of the ceramic and the inner wall of a cylindrical container (see Fig. 13). The sulfur electrode compartment is filled with a graphitic felt which serves as the inert electrode.¹²⁵ During discharge, sodium ions produced at the negative electrode are transported through the solid electrolyte to the sulfur electrode compartment in which sulfur is reduced to polysulfide ions. Within the composition range S to \sim Na₂S₅, the melt consists

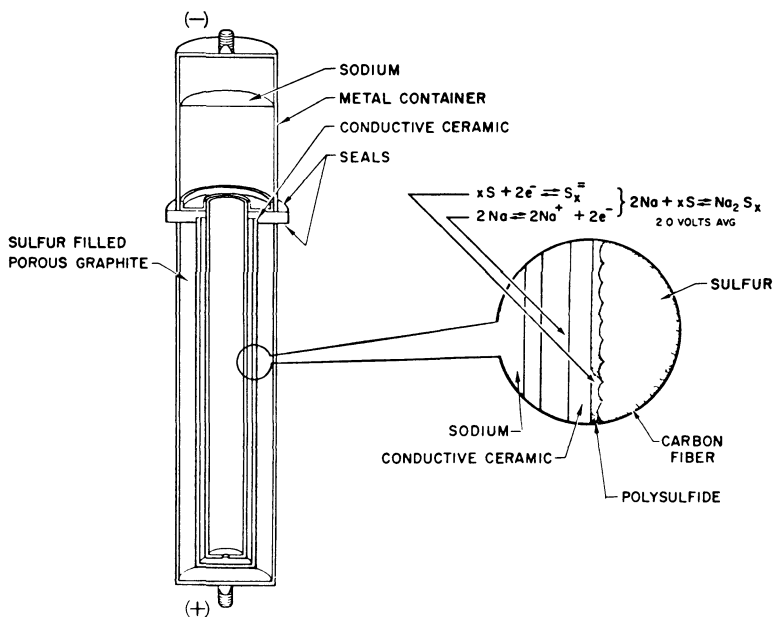
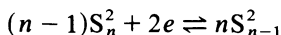


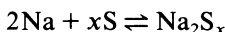
Figure 13 Schematic of Ford sodium-sulfur cell.

of two immiscible phases¹²⁶ and the OCV remains constant (2.07 V at 350°C). Further reduction proceeds in a single polysulfide phase down to the composition $\sim \text{Na}_2\text{S}_3$. Lower polysulfides form solid phases which may block the interface and inhibit the discharge kinetics. Therefore the theoretical 100% capacity is defined on the basis of conversion of S to Na_2S_3 .

In the single-phase region, the OCV decreases with decreasing value of x in Na_2S_x . The OCV-composition plot is much too steep to reflect the Nernstian behavior of the simple



reaction. The observed OCV values may reflect mixed potential behavior of redox reactions of several polysulfides, consecutive (or single) redox equilibria.¹²⁷ The overall cell reaction can be formally represented by



where $x > 3$ under operating conditions.

The kinetics of the polysulfide reactions are also little known (a recent review is available¹²⁸) and difficult to study. At the operating temperature the exchange currents are so high that they have not been reliably determined. The absence of a supporting electrolyte further complicates the interpretation of transient voltammetry.

The voltaic losses of the discharging cell are primarily connected with the resistance of the ceramic. During charge additional losses appear which are determined by the rate of removal of the insulating film of sulfur being evolved at the electrode, and thus by its preferential wettability by conducting polysulfides or sulfur. There are no coulombic losses due to parasitic reactions (unless the positive reactant is consumed in a reaction with the container material) and self-discharge is absent. The high-energy efficiency ($\sim 90\%$ electric-to-electric) is diminished by thermal losses which are determined by engineering design (insulation) and driving characteristics of the EV.

The theoretical specific energy of the system is $\sim 635 \text{ Wh kg}^{-1}$. The effective values of specific energy and peak power strongly depend on the cell geometry. The desired values of $\geq 120 \text{ Wh kg}^{-1}$ at sufficient power capability have not yet been achieved in multicell

batteries. The cell geometry also affects the energy density and packaging capability of the battery which is of primary importance since the range of a Na-S-powered EV may be volumetrically limited.

A number of problems connected with battery construction and operation, such as rechargeability into the two-phase region which requires improvement of sulfur transport away from the solid electrolyte and carbon surface,¹²⁹ and development of sealing techniques and of ceramic mass production, have been to a great extent overcome. The remaining difficulties are primarily connected with the reliability and cycle life of the battery.

One of the issues is the durability of the ceramic electrolyte under operating conditions.¹³⁰ It depends on factors which are not fully understood. The damage occurring at excessive current densities may be interpreted in terms of crack propagation: above a critical charging current density, liquid sodium enters the micro-cracks at a rate faster than it can escape. This tends to cause a buildup of pressure and crack propagation and failure of the ceramic.¹³¹ This hypothesis has some confirmation in the fact that current densities exceeding 15 A cm^{-2} are harmless when elemental sodium forms in a gaseous state at the ceramic interface, as in the case of the sodium heat engine.¹³² Improvements in ceramic durability have been attempted by improving the fracture toughness and decreasing the tensile forces at the crack tips.¹³³

The life-limiting increase of resistance and decrease of capacity of cycled cells is usually attributed to the deteriorating effects of corrosion of the positive current collector—the cell container in the case of sodium core cells or a rod in the case of sulfur core cells. Apart from consuming the active material, corrosion may lead to the deposition of poorly conductive layers at the current collector surface, thus interrupting the contact of the inert electrode fibers with the current collector. Corrosion products may also deposit and block both the solid electrolyte and the electrode surface. The thermodynamic instability of metals in polysulfide melts severely limits the choice of materials interfacing the sulfur electrode.¹³⁴ A fully satisfactory solution has not yet been reported.

Another issue which requires a more satisfactory solution is the capability for thermal cycling of the battery. At present, freeze-thaw cycles cannot yet be repeated with the desired reliability.

The safety of single cells and modules has been extensively tested. Cells were mechanically crushed, exposed to electrically induced failures, and dropped from heights with exposure to open flame. Induced failures have been shown not to spread to surrounding cells nor to lead to a thermal runaway. No data yet exist concerning the level of SO₂ emissions and the probability of fire and/or explosion during a vehicle crash leading to a total destruction of the battery. The possibility of excessive heat generation and explosion by direct chemical reaction of sodium with sulfur is minimized by the cell structure, which allows only a very small amount of sodium to contact the sulfur melt in case of the accidental cracking of the solid electrolyte (cf. Fig. 14).

The system is unique among secondary batteries in that it uses extremely cheap and abundant reactants. The achievable range of a Na-S-powered passenger car may exceed 150 miles. It is possible, however, that the bulkiness of the battery may limit its applications to larger vehicles.

Another, exploratory version of the Na-S system (aimed at present at stationary applications) is under development at Dow Chemical Company. It operates at ~300°C and utilizes hollow sodium borate glass fibers as electrolyte¹³⁵ in the form of thousands of thin hollow fibers sealed at one end and open at the other to a common reservoir of molten sodium. The fibers are wrapped in Mo-coated aluminum foil which serves as a positive electrode for the polysulfide melt, which fills the space between the fiber wall and the Al.

The lifetime of 6-Ah (Ampere hours) cells is reported as 250–300 cycles. The predominant failure mode is extensive breakage of the fibers at their junctions with the tube sheet. The fragility of glass capillaries makes mobile applications of the system doubtful in spite of its very high specific energy and power.

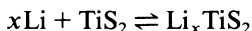
Replacement of the sulfur melt by a solution of sulfur and/or its compounds offers some advantages in that the operating temperature can be lowered, the faradaic utilization of the reactant increased (i.e., the redox reactions of sulfur may involve reduction to lower polysulfide, solid at 350°C, as well as oxidation to positive valences of sulfur), the open-circuit voltage made higher, and the two-phase operation avoided. In exploratory systems which follow this route, use is made of sulfur dissolved in molten chloroalumi-

nates or in organic solvents separated by β'' -alumina membranes from the molten sodium. In the first case,¹³⁶ the positive electrode reactions involve positive, primarily S^{4+} ions. At 220°C small laboratory cells have sustained some 400 cycles when discharged at 35 mA cm⁻². The discharge and charge plateaus were steady at >3.5 and <4.5 V, respectively. In the second¹³⁷ case, various solvents were investigated with respect to their compatibility with the ceramic electrolyte and effects on the cell performance. In general, the power capabilities of these cells may be too low for mobile applications.

5. Rechargeable Lithium Batteries

The high-energy density and very high cell voltage of organic electrolyte cells, in which lithium is coupled with a suitable insertion (intercalation) positive electrode¹³⁸ has stimulated a substantial R&D effort (in the USA mainly at Exxon Research and Engineering Co., and EIC) aimed at the production of an EV battery.¹³⁹ Among a number of lamellar transition-metal dichalcogenides,¹⁴⁰ titanium disulfide has been the most commonly studied material of the positive electrode.¹³⁸⁻¹⁴¹

The cell reaction



during Li insertion is associated with only a slight expansion perpendicular to the basal planes of the positive electrode matrix. This lack of structural change (which often limits the life of electrodes remaining in solid state during cycling) makes the intercalation compounds hopeful candidates for prolonged cycling, although some undesirable changes, which depend on the material/electrolyte combination, accumulate in time.¹⁴²

The potential EV advantages of these systems are very attractive. Nevertheless, several drawbacks have, as yet, prevented the emergence of lithium-dichalcogenide (EV) batteries: rechargeability of lithium negatives seems to be limited to some 150 cycles in known nonaqueous electrolytes¹⁴³ owing to the shape change, dendritic growth, and/or formation of passivating surface layers; lithium cost was given as a reason for termination of the Exxon effort; the high voltages make difficult finding suitable organic

solvent-salt combinations which would not decompose at either (or both) electrodes; the low conductivity of nonaqueous electrolytes makes it difficult to ensure sufficient power capabilities. The most commonly used electrolytic solutions contain LiPF_6 , LiAsF_6 , LiClO_4 , or LiCF_3SO_3 dissolved in propylene carbonate, THF, methyl- or ethyl-substituted THF, sulfolanes, and a few other solvents.

Some of the problems connected with the presence of liquid electrolyte can be avoided in all-solid-state batteries. Previous attempts to produce such systems for EV applications have been unsuccessful.⁴ With the advent of electronically and ionically conducting polymers, new efforts are underway: a Canadian/French "ACEP" project,¹⁴⁴ and the Harwell Laboratory/Danish Odense Technical University¹⁴⁵ collaboration. The cells consist of TiS_2 or V_6O_{13} positive separated from Li negative electrodes by a solid film of polyethylene oxide complexed with LiClO_4 or LiCF_3SO_3 electrolyte. Bipolar design is envisaged for Harwell EV applications.¹⁴⁵ The operating cell temperature is described as 80 to $<200^\circ\text{C}$ depending on the system. The merits of these projects cannot yet be evaluated owing to the very early stage of development.

6. Conducting Polymer Systems

It has been first demonstrated in 1977 by MacDiarmid *et al.*¹⁴⁶ that films of polyacetylene can be chemically doped to semiconducting and metallic states. Shortly thereafter the possibility of electrochemical doping, resulting in highly conducting materials, had been shown not only for polyacetylene but also for a number of other polyenes, polyphenylenes and polychalcogenides.¹⁴⁷

The most generally accepted theory of conductive properties of polyacetylene is based on the existence of solitons.¹⁴⁸ These are thought to appear in the polymer chain at points of imperfection, where chains of *cis*- and *trans*-polyacetylene meet. The resulting rearrangement of valence bonds leaves an extra electron which becomes delocalized over about 15 CH units. A coherent description of the nature of charge carriers in polymers is under development.¹⁴⁹ The enhancement of conductivity by doping (ranging from 10^{-9} or $10^{-3} \text{ S cm}^{-1}$ for polyacetylene and poly(*m*-phenylene), respectively to some 10^3 S cm^{-1}) is usually interpreted in terms of the charge

transfer between the polymer backbone and the dopant resulting in the formation of a polymeric ion and a counterion derived from the dopant. The structure, electronic properties, and proposed mechanisms of polyacetylene conduction have been recently reviewed.¹⁵⁰

Electrochemical doping is reversible and thus polymers which can be successfully cycled between two dopant levels can serve as rechargeable electrodes. Only polyacetylene, poly(*p*-phenylene) and poly(*p*-phenylene sulfide) are both oxidizable and reducible. Other conducting polymers can only be either *p*- or *n*-doped.

The first rechargeable cells described in 1981¹⁵¹ were based on a doped polyacetylene film serving as a positive electrode coupled with the negative lithium electrode in a nonaqueous electrolyte. Later versions included cells constructed of *p*- and *n*-doped polyacetylene films. Since then, several other systems have also been studied for potential battery applications. They include doped derivatives of polyquinoline¹⁵² and poly(*p*-phenylene).^{153,154} The OCV values of the respective cells are very high, up to ~5 V. They depend on the system and doping levels. The advantages of high voltage are, at least presently, countered by the instability of salts and organic solvents used as electrolytes. It appears that, in general, salts decompose at the electrodes faster than the commonly used organic solvents.¹⁵⁵

Potential advantages of lightweight conducting polymer batteries for mobile applications are obvious. It is possible that only systems based on two polymer electrodes might be envisaged. Use of lithium in organic electrolytes seems to preclude cycle life exceeding some 150 cycles.¹⁴³ Projections based on short-term performance of small single cells claim extremely high-power capabilities combined with high specific energies.¹⁵⁶ However, the transition to a practical device may not be easy. The difficulties involve both scientific and engineering problems. These include, among others:

1. Lack of known nonaqueous electrolytes with sufficiently wide stability windows. Without them the necessary cycle and shelf life cannot be obtained.
2. In most cases, difficulties in achieving doping levels which would ensure sufficiently high specific energy.¹⁵⁷
3. Concerns about stability of electrodes under conditions of prolonged cycling.

4. Instability of most doped materials upon exposure to air and/or moisture which may cause problems in economically viable manufacturing of scaled-up electrodes.

Recently, a form of *p*-doped acetylene has been reported¹⁵⁸ to be compatible with aqueous electrolytes and to be reversibly oxidizable by oxygen (and other oxidizing agents). The stability of the material over periods exceeding a few days is not yet known.

Another material—polyaniline in its quinoid-benzenoid-diimine form—has recently been reported to be compatible with aqueous electrolytes both in the oxidized and reduced states.¹⁵⁹ As opposed to the conventional method of *p*-doping organic polymers by oxidative removal of electrons from the polymer π -system, polyaniline can be proton doped in an aqueous protic acid (HCl or HBF₄) to a metallic ($S \approx 5 \Omega^{-1} \text{cm}^{-1}$) iminium salt. Cells constructed with Zn and PbO₂ counterelectrodes, have been reproducibly cycled (~ 1000 cycles) with good utilization albeit at low currents and voltages. The authors do not invoke vehicular applications.

Conductive polymers have a wide spectrum of potential applications, and a large potential for improvements. Their use in batteries has drawn the widest attention.

7. Metal-Air Batteries

Both primary and secondary metal-air batteries have been considered for mobile applications. The metal negatives involve mainly zinc and iron, in rechargeable, and aluminum, in primary systems.

All metal-air batteries share the well-known problems connected with the performance of the air cathode. Additional difficulties are faced in secondary systems, which require a bifunctional^{160,161} oxygen electrode catalyzed to function also as an anode. (An interesting concept aimed at avoiding this complication has been recently proposed for zinc-air-powered fleet operation of electric vehicles. Recharge at the large central facility would be effected at the anode by oxidation of hydrogen locally generated from natural gas or coal¹⁶².)

Discussion of the oxygen electrode performance is beyond the scope of this chapter (recent reviews are available¹⁶³). The main disadvantages introduced by state-of-art air electrodes in EV

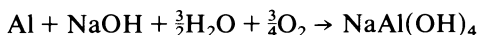
batteries are low electric-to-electric energy efficiency (generally <40%); low specific peak power which may necessitate hybridization with another battery or flywheel; unknown cycle life, particularly under conditions of varying load; and complexity due to the presence of, at least, two subsystems—for air circulation and scrubbing of CO₂—or more.

The merits and disadvantages introduced by iron or zinc negatives have been previously discussed (Sections III.2 and III.3).

The iron-air battery has been under development in Sweden (SNDC, SAB NIFE, KTH¹⁶⁴), the USA (Westinghouse Electric Co,^{160,165} France (SAFT), West Germany (Siemens A.G.¹⁶⁶), and Japan (Matsushita⁶³). The main advantages of this low-voltage, low-power, high self-discharge rate system are the abundant and cheap reactants and long lifetime, ruggedness, and reliability of iron electrodes. The specific energies reported by various developers under nonstandardized conditions have been reported as between 60 and 80 Wh kg⁻¹, and optimistic projections reach even 100 Wh kg⁻¹ combined, however, with power capabilities which are low and do not allow even for a cold start.

The zinc-air system, under development primarily in France (CGE,⁸⁵ Citroen¹⁶⁷), Japan,¹¹ and England (Lucas)¹⁶⁸ seems to be more promising from the point of view of EV performance, particularly if slurry-type^{85,86} zinc electrodes are used. The zinc-air system can also be envisaged as a primary battery of higher-energy efficiency than the alkaline Al-air¹⁶⁹ “mechanically rechargeable” system under development primarily in the USA [Lawrence Livermore National Laboratory (LLL),¹⁷⁰ Lockheed Missiles and Space Company,¹⁷¹ and Eltech Systems Inc.¹⁷²]; its neutral electrolyte version is being studied in Yugoslavia¹⁷³ and Germany.¹⁷⁴

The reactions and mode of operation (cf. Fig. 14) of the LLL Al-air battery are as follows:

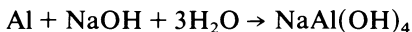


The chemical reaction in the crystallizer¹⁶⁹ produces hydrargillite



which is crystallized under controlled conditions, washed, dried, stored, and periodically removed (while water is added to the system) and shipped to dedicated smelting plants. Electrochemi-

cally recovered aluminum is returned to the service stations. Special cells are necessary for recycling since aluminum must be alloyed with metals (e.g., gallium, indium, thallium, phosphorus) to inhibit the parasitic corrosion reaction



which proceeds at considerable rates both at OCV and under current drain.

Apart from the problems of the air cathode, common to all metal-air cells, the system requires development of all components and processes involved in battery operation and in fast replacement of spent anodes. The most serious drawback of the system is its energy efficiency, much lower than that of most other batteries. This is due primarily to the energy intensive process of aluminum recovery from the discharge product. The energy efficiency can be increased only by considerable improvements in electrowinning of aluminum or by development of thermal recycling methods. In spite of the low energy efficiency the battery is under development for vehicular application owing to its high energy density. The range of an EV powered by this system is claimed to be ~ 1500 km between anode replacement and ~ 400 km between water addition and removal of hydrargillite.

The viability of the Al-air battery vehicular application seems to depend (apart from the successful solution of electrochemical and engineering problems) on the cost of electric power. If, e.g., nuclear or a renewable energy source will ensure in the future abundance of electricity, user's convenience (range, fast refueling, large car powered by a safe system) may become a more important factor than energy savings provided by other potential EV power plants.

IV. COMPARATIVE EV BATTERY CHARACTERISTICS

A very tentative comparison of the quantitative characteristics of EV battery candidates is given in Table 6 for near-term and advanced systems. (Information concerning many exploratory systems is hardly available, even for approximate extrapolations). Values quoted in Table 6 must be treated with considerable caution.

Table 6. Approximate Characteristics of

System ^a	Battery size (kWh)	Specific energy (C/3) (Wh kg ⁻¹)		Energy density (C/3) (Wh liter ⁻¹)		Specific peak power (15 s at 80% DOD) (W kg ⁻¹)	
		Present	Projected	Present	Projected	Present	Projected
A							
Pb-Acid ISOA ^b (Advanced)	20	37-41	45 50	65-72	80 90	~75	85 95
Ni-Fe ^b	25-30	45-48	60	78-95	120	~80 ^c	110 ^c
Ni-Zn ^b	20-30	42-68		75-120		70-120	130
B							
Zn-Cl ₂ ^b	50	~58	64		88		68
Zn-Br ₂ ^h	20-30		65		80		90
LiAl-FeS ^h	30	~55	100	~90	125		100
Na/ β "-alumina/S ^d	35	~65	100	~90	120	~100 ^e	115 ^e

^a System A was tested at NBTL and/or JPL for specific energy and peak power; B is based on developer data.

^b Based on multicell module or prototype battery data.

Near-Term and Advanced EV Battery Candidates

Energy efficiency (%)	Cycle life (80% DOD) Demonstrated in		Projected for battery	Cost projected by developer (\$/kWh)	Auxiliaries	Main developers (some not active presently in the area)
	Cell	Module or battery				
60-75		~800	>1000	60-80	May include air pump in each cell	US: Eagle-Picher, Eltra, ESB, Globe Union, Gould, Westinghouse. Eur.: Lucas Chloride, Varta. Jap.: Japan Storage, Shin-Kobe, Yuasa
60-70	~3000	~900	~2000	~100	May include circulating electrolyte	US: Eagle-Picher, Westinghouse. Eur.: Daimler-Benz, DAUG, INCO, Swed. Nat.'l Dev., NIFE Varta. Jap.: Matsushita.
65-75		100-300		~100		US: Eagle-Picher, ERC, ESB, GM, Gould, Westinghouse, Yardney. Eur.: AGA, CGE, DAUG. Jap.: Furukawa, Japan Storage.
45-50		~1600 with and ~80 without human assistance	>1000	~100	Circulating electrolyte refrigerator; $\text{Cl}_2(\text{H}_2\text{O})_n$ store	US: EDA.
65-70		~400	>1000	~60	Two circulating electrolytes; two tanks	US: Exxon. Austr. & Eur.: Exxon licencees.
~70		>200	~500	~120	Vacuum insulation	US: ANL (AI, CRC, EPI, Gould), GM
~70	>1500		~1000	≤100	Vacuum insulation	US: Ford, GE. Eur.: Brit. Rail, Brown-Boveri, CGE, Chloride. Jap.: Toshiba, Yuasa.

^c 30 s at 50% DOD.

^d Based mainly on cell data.

^e 30 s at 80% DOD.

Very few batteries have been tested for any reasonable period of time and/or under driving conditions. System characteristics are projected on the basis of performance of single cells, or modules. Data quoted by battery developers lack standardization. Often, the reported specific-energy values refer to deliverable rather than available energy and are quoted at unspecified discharge rates and/or at depths of discharge at which sufficient acceleration can no longer be attained. This leaves a considerable margin of uncertainty when quantitative descriptions are attempted. Numbers quoted in the Table as "projected" refer to goals expected by the developers to be reachable in relatively short times and do not reflect limits which might be achievable.

Taking into account the values of specific energy ($\approx 60 \text{ Wh kg}^{-1}$) and of specific power ($\approx 85 \text{ W kg}^{-1}$) required for driving a small (1500 kg) passenger EV in urban, mixed with ICEV's traffic,⁸ it can be seen from Table 6 that among simple systems only Ni-Zn might provide, at sufficient acceleration, a range considered to be acceptable for a marketable small passenger EV. (This range, arbitrarily set at ≥ 100 miles, is of course relative and depends on the driving habits determined by the energy situation at the given time and place⁶.) Unfortunately, the short cycle life of Ni/Zn precludes, at present, its commercialization. The lead-acid battery would require a considerable advancement to approach the 80-mile range, while the nickel-iron system may be closer to the 100-mile goal. The zinc-chloride battery seems to lack sufficient power and can hardly be scaled down to the size demanded by a small passenger car. It is not clear, at present, whether the 100-mile range can be exceeded in small, Zn-Br₂-powered EVs. Only the high-temperature batteries might, in principle, provide ranges of the order of 150 miles, and primary metal-air systems, mileages comparable with ICEVs.

Much higher ranges than those quoted here, often encountered in EV literature,^{2,4,6,11} usually pertain to somewhat unrealistic conditions of cars driven without stops at a constant low speed.

At present, there is hardly a market for widespread EV use. Were it to emerge in the near future, no electrochemical plants would be ready to power electric vehicles, except for the lead-acid battery. The development of candidate systems, capable of better performance, requires a long time and extensive scientific and

engineering effort since the problems still to be overcome are very serious. The product, when perfected, will be inferior in performance to the internal combustion engine but, in general, superior to it in terms of energy conservation and environmental advantages.

ACKNOWLEDGMENTS

The author wishes to thank Dr. N. A. Gjostein and Mr. L. R. Foote for most helpful discussions and constructive criticism.

REFERENCES

- ¹ K. V. Kordesch, Ed., *Batteries*, Marcel Dekker, New York and Basel, 1977, Vol. 2.
- ² J. Jensen, P. McGeehin, and R. Dell, *Electric Batteries for Storage and Conservation*, Odense University Press, Denmark, 1979.
- ³ C. R. Barker, *Electric Vehicles Quant.* (June 1978) 24; J. Johnson, *Commer. Motor* (February 18, 1977); *Electric Vehicle Progr.* 4(13) (July 1, 1982).
- ⁴ D. A. J. Rand, *J. Power Sources* 4 (1979) 101.
- ⁵ *EV Focus*, 1(9) (June 15, 1978).
- ⁶ W. Hamilton, Prospects for Electric Cars, Final Report by General Research Corporation, Contract No. EY-76-C-03-1180 (November 1978); P. C. Butler, Extended Abstracts, Sixth DOE Electrochemical Contractor's Review, Washington, D.C., June 1984, p. 53.
- ⁷ M. Cremer and R. Thomas, *Elektrochemische Energietechnik*, Bundesminister fuer Forschung und Technologie, FRG, 1981, p. 97.
- ⁸ Advanced EV Powertrain Program, Phase I, Technical Report by Ford Motor Company and General Electric Company to DOE, Contract No. DE-ACO8-82NV-10308 (1984), pp. 11-20.
- ⁹ R. Roberts, Status of the DOE Battery and Electrochemical Technology Program II, The MITRE Corporation (December 1980), pp. 12, 13.
- ¹⁰ F. Hornstra, W. H. DeLuca, E. C. Gay, N. P. Yao, Extended Abstracts, Sixth DOE Electrochemical Contractor's Review, Washington, D.C., June 1984, p. 40.
- ¹¹ Condensed account of Japanese EV program, *Lead Power News* (November 1978).
- ¹² Annual Report on Nickel-Iron Batteries, Westinghouse Electric Corporation to DOE, Contract No. 31-109-38-4141 (1979).
- ¹³ Zinc-Bromine Battery Development, Sixth Program Review, Phase III, Exxon Research and Engineering Company to DOE/SANDIA, 16-3187 (May 1984).
- ¹⁴ Insulation and Enclosure Development for High Temperature EV Batteries, Final Report, Union Carbide, Linde Division to DOE, Contract No. DE-ACO2-8DET25426 (May 1982).
- ¹⁵ Development of the Zinc-Chloride Battery for Mobile Applications, Energy Development Associates to DOE, Contract No. DE-ACO2-76ET-20131 (December 1981).

- ¹⁶ R. E. Meredith, Extended Abstract No. 571, 166th Meeting of The Electrochemical Society, New Orleans, La., October 1984.
- ¹⁷ G. Bronoeel, Seventh International EV Symposium, Versailles, France, June 1984.
- ¹⁸ U.S. Bureau of Mines and General Research Report to Environmental Protection Agency (October 1974); R. Singleton, Lithium, Bureau of Mines Commodity Profile, U.S. Department of Interior (September 1979); Battery Technology, TRW to DOE, Report prepared by Inc. Energy Systems Group, Energy Systems Planning Division, McLean, Va (March 1978).
- ¹⁹ E. Voss and G. Huster, *Chem.-Eng.-Tech.* **38** (1966) 623.
- ²⁰ S. U. Falk and A. J. Salkind, *Alkaline Storage Batteries* Wiley, New York, 1977.
- ²¹ D. Sullivan, Life Cycle Energy Analyses of EV Storage Batteries, Whittman Associate Inc. to DOE (December 1980).
- ²² R. Loufty, Stilbine/Arsine Monitoring During EV Operation, Interim ANL Report No. 1, Chemical Engineering Division (June 1980); Health and Environmental Effects Document for Batteries, ANL/ES-105, Argonne National Laboratory to DOE, Contract No. W-31-109-Eng-38 (November 1980).
- ²³ Report on Zinc Chloride Battery Safety, Factory Mutual to DOE (1980).
- ²⁴ *The Japan Times* (July 5, 1976).
- ²⁵ *Elec. Rev. Int. (London)* **200** (1977) 41.
- ²⁶ Health and Environmental Effects Document for Batteries: the Lead/Acid and Zinc-Halogen Batteries, ANL/ES-129, Argonne National Laboratory to DOE, Contract No. W-31-109-Eng-38 (1982).
- ²⁷ Ecological and Biomedical Effects of Effluents from Near-Term Electric Vehicle Storage Battery Cycles, ANL/ES-90, Argonne National Laboratory to DOE, Contract No. W-31-109-Eng-38 (May 1980).
- ²⁸ G. Planté, *Compt. Rend.* **50** (1860) 640.
- ²⁹ C. W. Fleischmann, SAE Paper No. 790158 (1979).
- ³⁰ ANL/OEPM-82-5 Report for DOE, Contract No. W-31-109-Eng-38 (1982); Lucas Chloride EV Systems, Battery Specifications (1984).
- ³¹ M. L. Whitehead, SAE Paper No. 790162 (1979).
- ³² E. N. Mrotek and J. R. Pierson, EVC Paper No. 8033, EV Expo, St. Louis, Mo., 1980.
- ³³ ANL/OEPM-83-9, Annual Report for DOE, Contract No. 31-109-38-4205 (1983).
- ³⁴ D. W. Kassekert, A. O. Isenberg, and J. T. Brown, Proceedings of 11th IECEC, State Line, 1976, p. 411; A. H. Taylor, F. Goebel, and J. Giner, in *Power Sources 4*, Ed. by D. H. Collins, Oriel Press, Newcastle-upon-Tyne, England, 1973, p. 541.
- ³⁵ K. Steininger and K. Kordesch, Extended Abstract No. 34, 166th Meeting of The Electrochemical Society, New Orleans, La., October 1984.
- ³⁶ Bipolar Lead Acid Battery, Jet Propulsion Laboratory Review (July 1980).
- ³⁷ P. T. Moseley and A. D. Turner, Extended Abstract No. 23, Vol. 84-2, 166th Meeting of The Electrochemical Society, New Orleans, La., 1984.
- ³⁸ Globe Battery Division, Annual Report for ANL, Contract No. 31-109-38-4205 (1982).
- ³⁹ D. Corp *et al.*, SAE Paper No. 820178 (1982); P. C. Butler, Extended Abstracts, Sixth DOE Electrochemical Contractor's Review, Washington, D.C., June 1984, p. 53.
- ⁴⁰ J. R. Pierson, C. E. Weinlein, Paper No. 4, International Power Sources Symposium, Brighton, England, 1982.
- ⁴¹ W. Tiedemann, J. Newman, and E. DeSua, in *Power Sources 6*, Ed. by D. H. Collins, Academic Press, London, 1977, p. 15.
- ⁴² A. Winsel and J. Schulz, *Elektrochemische Energietechnik*, Bundesminister fuer Forschung und Technologie, FRG, 1981, p. 129.

- ⁴³ P. Montalenti, Paper No. 6, International Power Sources Symposium, Brighton, England, 1982.
- ⁴⁴ A. C. Simon, S. M. Caulder, and J. T. Stemmler, *J. Electrochem. Soc.* **122** (1975) 461; A. C. Simon and S. M. Caulder, in *Power Sources 5*, Ed. by D. H. Collins, Academic Press, London, 1975, p. 109.
- ⁴⁵ S. M. Caulder, J. S. Murday, and A. C. Simon, *J. Electrochem. Soc.* **120** (1973) 1515.
- ⁴⁶ S. M. Caulder and A. C. Simon, *J. Electrochem. Soc.* **121** (1974) 1546.
- ⁴⁷ A. C. Simon and S. M. Caulder, Extended Abstracts, Vol. 84-2, 166th Meeting of The Electrochemical Society, New Orleans, La., October 1984, p. 49.
- ⁴⁸ H. Nguyen Cong and P. Chartrier, Extended Abstracts of the 35th Meeting of the ISE, Berkeley, Calif., 1984, p. 87; P. T. Moseley and N. J. Bridger, *J. Electrochem. Soc.* **131** (1984) 608; R. J. Hill, Extended Abstract No. 5, 166th Meeting of the Electrochemical Society, New Orleans, La., October 1984.
- ⁴⁹ R. V. Biagetti and M. C. Weeks, *Bell Syst. Tech. J.* **49** (1970) 1305.
- ⁵⁰ U. B. Thomas, F. T. Foster, and H. E. Haring, *Trans. Electrochem. Soc.* **92** (1947) 313; A. Sabatino, *Technology of Maintenance Free Batteries*, Irving-Gould Publ. Co, Lincolnwood, Ill., 1976; H. E. Jensen, Proceedings of the 11th Annual Battery R&D Conference, Fort Monmouth, N.J., 1957, p. 73; Batteries and Chargers for Industrial Lift Trucks, C&D Batteries Division, Eltra, technical pamphlet section 7-200; R. D. Prengman, Extended Abstract No. 17, Vol. 84-2, 166th Meeting of The Electrochemical Society, 1984; H. K. Giess, Extended Abstract No. 20, Vol. 84-2, 166th Meeting of The Electrochemical Society, 1984; H. Jinbo and A. Watanabe, Extended Abstract No. 21, Vol. 84-2, 166th Meeting of The Electrochemical Society, 1984.
- ⁵¹ U.S. Patent No. 4,221,847 (September 1980); D. Thuerk, private communication, 1984; K. Gutekunst and W. Rusch, Paper No. AII-2, International EV Symposium, Versailles, France, June 1984.
- ⁵² B. L. McKinney, G. L. Wierschem, and E. N. Mrotek, SAE Paper No. 830229 (1983).
- ⁵³ K. F. Barber, Extended Abstracts Sixth DOE Electrochemical Contractor's Review, Washington, D.C., June 1984, p. 56; E. C. Gay, J. D. Arntzen, D. R. Fredrickson, C. C. Christianson, F. Hornstra, and N. P. Yao, Extended Abstract No. 39, Vol. 84-2, 166th Meeting of The Electrochemical Society, New Orleans, La., 1984, p. 55.
- ⁵⁴ W. Tiedemann and J. Newman, Extended Abstract No. 30, Vol. 84-2, 166th Meeting of The Electrochemical Society, New Orleans, La., 1984; B. L. McKinney and G. H. Brilmyer, Extended Abstract No. 31, Vol. 84-2, 166th Meeting of The Electrochemical Society, New Orleans, La., 1984.
- ⁵⁵ A. R. Landgrebe, Extended Abstracts, Sixth DOE Electrochemical Contractor's Review, Washington, D.C., June 1984, p. 2; and W. J. Walsh, p. 79.
- ⁵⁶ U.S. Patent No. 678,722 (1901).
- ⁵⁷ J. O'M. Bockris and A. K. N. Reddy, *Modern Electrochemistry*, Plenum Press, New York, 1970, Vol. II, p. 1276.
- ⁵⁸ P. R. Vassie and A. C. C. Tseung, *Electrochim. Acta* **21** (1976) 299.
- ⁵⁹ R. Rosey and B. E. Taber, EVC Paper No. 8030, EV Expo, St. Louis, Mo., May (1980); Annual Report ANL/OEPM-83-8 prepared by Westinghouse Electric Corporation, Contract No. W-31-109-Eng-38 (1983).
- ⁶⁰ Annual Report ANL/OEPM-83-7, Eagle-Picher Industries Inc., Contract No. W-31-109-Eng-38 (1983).
- ⁶¹ B. Andersson, L. Oejefors, and R. Hudson, Paper No. 25, International Symposium on Power Sources, Brighton, England (1980).

- ⁶² G. Kraemer, V. A. Oliapuram, and K. W. Lexow, *Elektrochemische Energietechnik*, Bundesminister fuer Forschung und Technologie, FGR 1981, p. 157.
- ⁶³ R&D of Electric Vehicles in Japan (Agency of Industrial Science, the Ministry of International Trade and Industry, the Society of Automotive Engineers of Japan, Inc.), 1977.
- ⁶⁴ H. Bode, K. Dehmelt, and J. Witte, *Z. Anorg. Allg. Chem.* **366** (1969) 1.
- ⁶⁵ Nickel-Iron Battery System Safety, Final Report prepared by Eagle-Picher Industries Inc. for DOE and JPL, DOE/CS 54209-17 (1984).
- ⁶⁶ R. Hudson, EVC Paper No. 8031, EV Expo, St. Louis, Mo., May 1980.
- ⁶⁷ W. Feduska and R. E. Vaill, Proceedings of the Symposium on Battery Design Optimization, Vol. 79-1, the Electrochemical Society, New York, 1979, p. 299.
- ⁶⁸ U.S. Patent No. 4,109,060.
- ⁶⁹ T. de Michalowski, British Patent No. 15,370 (1899); J. J. Drumm, British Patent No. 365,125 (1930); U.S. Patent No. 1,955,115 (1934).
- ⁷⁰ DOE Battery and Electrochemical Contractor Conference, Arlington, Va., December 1979.
- ⁷¹ N. P. Yao, C. C. Christianson, R. C. Elliott, T. S. Lee, and J. F. Miller, EVC paper No. 8029, EV Expo, St. Louis, Mo. (1980); ANL/OEPM-82-5, Summary Report for DOE, Contract No. W-31-109-Eng-38 (1982).
- ⁷² *Electric Vehicle Progr.* **4** (13) (1982) 3.
- ⁷³ J. McBreen and E. J. Cairns, GMR-2530, General Motors Research Publication (October 28, 1977).
- ⁷⁴ M. Dzieciuch and H. Wroblowa, unpublished results, 1982.
- ⁷⁵ J. McBreen, *J. Electrochem. Soc.* **119** (1972) 1620.
- ⁷⁶ K. W. Choi, D. N. Bennion, and J. Newman, *J. Electrochem. Soc.* **123** (1976) 1616; K. W. Choi, D. Hamby, D. N. Bennion, and J. Newman, *J. Electrochem. Soc.* **123** (1976) 1628.
- ⁷⁷ D. C. Hamby, N. J. Hoover, J. Wirkkala, and D. Zahnle, *J. Electrochem. Soc.* **126** (1979) 2110.
- ⁷⁸ S. Szpak, D. J. Gabriel, and T. Katan, *J. Electrochem. Soc.* **127** (1980) 1063.
- ⁷⁹ T. Katan, J. R. Savory, and J. Perkins, *J. Electrochem. Soc.* **126** (1979) 1835.
- ⁸⁰ F. R. McLarnon, Sixth DOE Electrochemical Contractor's Review, Washington, D.C., June 1984.
- ⁸¹ G. A. Dalin, in *Zinc-Silver Oxide Batteries*, Ed. by A. Fleischer and J. J. Lander, Wiley, New York, 1971, p. 87.
- ⁸² U.S. Patent No. 3,505,115 (1970); U.S. Patent No. 3,493,434 (1969); R. W. Powers, *J. Electrochem. Soc.* **116** (1969) 1652.
- ⁸³ U.S. Patents Nos. 4,015,053 (1977) and 4,052,541 (1977); Statement of Work on Nickel-Zinc Battery for EV Propulsion, ESB Technology C0030-0082-01, ANL, January 1979.
- ⁸⁴ D. S. Adams, in *Power Sources 4*, Ed. by D. H. Collins, Oriel Press, Newcastle-upon-Tyne, England, 1973, p. 347; U.S. Patents Nos. 3,555,032, and 3,560,262; French Patent No. 2,096,046.
- ⁸⁵ A. J. Appleby, J. P. Pompon, and M. Jacquier, Proceedings of the 10th IECEC, Newark, N.J., 1975, p. 811; A. J. Appleby and M. Jacquier, *J. Power Sources* **1** (1976/77) 17.
- ⁸⁶ U.S. Patent No. 4,126,733 (November 21, 1978); D. Doniat, SORAPEC, private communication, 1982.
- ⁸⁷ French Patent No. 2,472,842 (July 3, 1981).
- ⁸⁸ P. C. Symons, Extended Abstracts, 35th ISE Meeting, Berkeley Calif., August 1984, p. 208.

- ⁸⁹ British Patent No. 1,377,722 (May 1921); G. W. Heise, E. A. Schumacher, and N. C. Cahoon, *Trans. Electrochem. Soc.* **94** (1948) 99.
- ⁹⁰ J. W. Rowan, P. Carr, C. J. Warde, and G. L. Henriksen, Proceedings of the 18th IECEC, Orlando, Fla., August 1983; EDA, EPRI Report EM-3136 (June 1983).
- ⁹¹ C. M. Blevins, M. J. Hammond, and P. C. Symons, Proceedings of the Symposium on Battery Design and Optimization, Vol. 78-2, The Electrochemical Society, New York, 1978.
- ⁹² L. Pauling and C. E. Marsh, *Chemistry* **38** (1952) 112.
- ⁹³ P. Carr, EDA, personal information, 1984.
- ⁹⁴ EDA EPRI Report EM1417, 23-1 (1978).
- ⁹⁵ P. Carr, C. J. Warde, A. Lijoi, and B. D. Brummet, Proceedings 30th Power Source Symposium, 1982.
- ⁹⁶ EDA Report for DOE, Contract No. DE-ACO2-76ET-20131 (1981).
- ⁹⁷ EDA Report to DOE, COO-2966-1, Contract No. EY-76-C-02-2966 (January 1978).
- ⁹⁸ P. Carr, Electric and Hybrid Vehicle Systems Assessment Seminar, JPL for DOE, Gainesville, Fla., December 1983.
- ⁹⁹ U.S. Patents Nos. 312,802 (February 1885) and 409,448 (August 1889).
- ¹⁰⁰ R. Zito and D. L. Maricle, Proceedings Second International EV Symposium, Atlantic City, N.J., 1972.
- ¹⁰¹ R. Bellows, H. Einstein, P. Grimes, E. Kantner, and J. Shropshire, Extended Abstracts of The Electrochemical Society Fall Meeting, October 1979, p. 285; R. J. Bellows, P. Grimes, H. Einstein, E. Kantner, P. Malachsky, and K. Newby, *IEEE Trans. Vehic. Technol.* **VT-32**(1) (1983).
- ¹⁰² D. J. Eustace, *J. Electrochem. Soc.* **127** (1980) 528.
- ¹⁰³ Review of EV and Stationary Zn-Br₂ Batteries, Exxon Research and Engineering Company, Linden, N.J., to DOE/SANDIA, May 1984.
- ¹⁰⁴ R. J. Bellows, H. Einstein, P. Grimes, E. Kantner, and K. Newby, Proceedings 15th IECEC, Paper No. 809288 (1980); R. J. Bellows, P. Grimes, J. Shropshire, and M. Zahn, Extended Abstracts, Vol. 80-2, The Electrochemical Society, New York, 1980, p. 328.
- ¹⁰⁵ E. J. Cairns and R. K. Steunenberg, *Progr. High Temp. Phys. Chem.* **5** (1973) 63; E. J. Cairns, C. E. Crouthamel, A. K. Fischer, M. S. Foster, J. C. Hesson, C. E. Johnson, H. Shimotake, and A. D. Tevebaugh, ANL-7316 (1967); E. J. Cairns and H. Shimotake, *Science* **164** (1969) 1347; E. C. Gray, W. W. Schertz, F. J. Martino, and K. E. Anderson, Proceedings of the Ninth IECEC, San Francisco, Calif., 1974, p. 862.
- ¹⁰⁶ N. P. Yao, L. A. Heredy, and R. C. Saunders, *J. Electrochem. Soc.* **118** (1971) 1039.
- ¹⁰⁷ J. Hall, S. C. Lai, L. McCoy, and R. C. Saunders, EPRI Interim Report-116 (1975); R. N. Seefurth and R. A. Sharma, *J. Electrochem. Soc.* **124** (1977) 1207; Z. Tomczuk, J. James, and D. R. Vissers, Extended Abstract No. 116, 166th Meeting of the Electrochemical Society, New Orleans, La., October 1984.
- ¹⁰⁸ D. R. Vissers, Z. Tomczuk, and R. Steunenberg, *J. Electrochem. Soc.* **121** (1974) 665; L. R. McCoy, S. Lai, R. C. Saunders, and L. A. Heredy, Annual Proceedings of the 26th Power Sources Conference, 1974.
- ¹⁰⁹ C. J. Wen, *J. Electrochem. Soc.* **126** (1979) 2047.
- ¹¹⁰ R. A. Sharma and R. N. Seefurth, *J. Electrochem. Soc.* **123** (1976) 1763.
- ¹¹¹ Z. Tomczuk, S. K. Preto, and M. F. Roche, *J. Electrochem. Soc.* **128** (1981) 761.
- ¹¹² Z. Tomczuk, M. F. Roche, and D. R. Vissers, Extended Abstract No. 78, Vol. 80-2, The Electrochemical Society Meeting, Hollywood, Fla., 1980, p. 209.
- ¹¹³ R. B. Swaroop and J. E. Battles, Extended Abstract No. 149, Vol. 79-2, The Electrochemical Society Meeting, Los Angeles, Calif., 1979, p. 385.

- ¹¹⁴ N. Beecher, DOE Annual Review of the Li/FeS Battery Program, Vol. II, ANL, June 1980.
- ¹¹⁵ V. M. Kolba, DOE Report ANL-80-44 (May 1980).
- ¹¹⁶ Argonne National Laboratory Reports: ANL-78-21; ANL-78-45; ANL-78-94; ANL-79-39; ANL 79-94; ANL-80-49; ANL-80-128; W. Borger, D. Kunze, H. S. Panesar, *Elektrochemische Energietechnik*, Bundesminister fuer Forschung und Technologie, FRG, 1981, p. 206; T. D. Kuhn and M. E. Anderson, Extended Abstract No. 113, 166th Meeting of The Electrochemical Society, New Orleans, La., October 1984.
- ¹¹⁷ J. T. Kummer and N. Weber, *Trans. SAE* **76** (1968) 1003.
- ¹¹⁸ J. A. Kafalas and R. J. Cava, *Fast Ion Transport in Solids*, Elsevier, New York, 1979; U. von Alpen, M. F. Bell, and H. H. Hoefler, *Solid State Ionics*, **3/4** (1981) 215.
- ¹¹⁹ G. J. Tennenhouse and G. M. Crosbie, *J. Am. Ceram. Soc.* **67** (1984) 204.
- ¹²⁰ Ford to NSF, Contract No. NSF-C805 (AER-73-07199), Annual Reports 1973-1976; Ford to ERDA, Contract No. E (11-1) 2566 (1976); FORD to DOE Contract No. EY-76-C-02-2566, Reports (1977-1979); Ford to DOE, Contract No. DE-AMO2-79CH10012, Reports (1979-1983).
- ¹²¹ Review of the British Rail Sodium Sulphur Battery Programme, October 1980; R. M. Dell, J. L. Sudworth, and I. Wynn Jones, Proceedings of the 11th IECEC, State Line, 1976, p. 503.
- ¹²² DOE-EPRI Sodium-Sulfur Battery Workshop IV, Heidelberg Germany, October 1980.
- ¹²³ R. Bauer, W. Haar, H. Kleinschmager, G. Weddigen, and W. Fischer, *J. Power Sources* **1** (1976/77) 109.
- ¹²⁴ S. Hatori, M. Yamamura, S. Kimura, and S. Iwabuchi, SAE Paper No. 770281 (March 1977).
- ¹²⁵ J. L. Sudworth and A. R. Tilley, in *The Sulfur Electrode*, Ed. by R. P. Tischer, Academic Press, New York, London, 1983, p. 163.
- ¹²⁶ N. K. Gupta and R. P. Tischer, *J. Electrochem. Soc.* **119** (1972) 1033; E. A. Maiorova, N. M. Romanchenko, and A. G. Morachevskii, *Elektrokhimiya* **17** (1981) 523.
- ¹²⁷ H. S. Wroblowa, Extended Abstract No. 332, The Electrochemical Society Meeting, Detroit, Mich., 1982, p. 534.
- ¹²⁸ D. A. Aikens, in *The Sulfur Electrode*, Ed. by R. P. Tischer, Academic Press, New York, London, 1983, p. 163.
- ¹²⁹ G. Weddigen, Extended Abstracts, 28th ISE Meeting, Drushba, September 1977; G. Weddigen and W. Fischer, *Chem. Eng.-Tech.* **MS** (1977) 472.
- ¹³⁰ M. L. McClanahan, R. W. Minck, Vol. 82-1, No. 724, 161st Meeting of The Electrochemical Society, Montreal, Canada 1982.
- ¹³¹ A. Virkkar and L. Viswanathan, *J. Mater. Sci.* **18** (1983) 1202; L. C. De Jonghe, Extended Abstract No. A1-6, 35th Meeting of the ISE, Berkeley, Calif., 1984, p. 14.
- ¹³² N. Weber, private communication, 1984.
- ¹³³ G. R. Miller, 31st Power Sources Symposium, Cherry Hill, Pa., June 1984.
- ¹³⁴ F. Gross, F. Harbach, R. Knoedler, R. Langpape, S. Mennicke, and L. Weiler, Extended Abstract No. 102, 166th Meeting of the Electrochemical Society, New Orleans, La., 1984; H. Wroblowa, V. Markovac, R. P. Tischer, and G. Crosbie, Extended Abstract No. A5-2, 35th Meeting of the ISE, Berkeley, Calif., 1984, p. 252; G. Crosbie, G. J. Tennenhouse, R. P. Tischer, and H. S. Wroblowa, *J. Am. Ceram. Soc.* **67** (1984) 498.

- ¹³⁵ C. A. Levine, in *The Sulfur Electrode*, Ed. by R. P. Tischer, Academic Press, New York, London, 1983, p. 327; P. Pierini and F. Tsang, Extended Abstract No. 103, 166th Meeting of The Electrochemical Society, New Orleans, La., October 1984.
- ¹³⁶ R. Marassi and G. Mamontov, in *The Sulfur Electrode*, Ed. by R. P. Tischer, Academic Press, New York and London, 1983, p. 210.
- ¹³⁷ U.S. Patent No. 4,018,969 (1977); K. M. Abraham and S. B. Brummer, Extended Abstracts No. 400, The Electrochemical Society Meeting, Philadelphia, Penn., 1977.
- ¹³⁸ J. Bennett, D. Harney and T. Mitchell, Paper No. 839272, Proceedings of the 18th IECEC, Orlando, Fla., 1983, p. 1665.
- ¹³⁹ M. S. Whittingham, *Science* **192** (1976) 1126.
- ¹⁴⁰ K. M. Abraham, *J. Power Sources* **7** (1981) 1.
- ¹⁴¹ M. S. Whittingham, Proceedings of the Symposium of Electrode Materials for Energy Conversion and Storage, Vol. 77-6, The Electrochemical Society, New York, 1977, p. 784.
- ¹⁴² D. W. Murphy and P. A. Christian, *Science* **205** (1979) 651.
- ¹⁴³ S. B. Brummer, V. R. Koch, and R. D. Rauh, in *Materials for Advanced Batteries*, Ed. by D. W. Murphy, J. Broadhead, and B. G. Steele, Plenum Press, New York, 1982.
- ¹⁴⁴ P. Ricoux and M. Gauthier, Meadowbrook Conference on Conducting Polymers, Oakland University, Rochester, Mich., June 1984; M. B. Armand, Extended Abstract No. A1-2, 35th Meeting of the ISE, Berkeley, Calif., August 1984, p. 3.
- ¹⁴⁵ A. Hooper, Meadowbrook Conference on Conducting Polymers, Oakland University, Rochester, Mich., June 1984.
- ¹⁴⁶ H. Shirakawa, E. J. Louis, A. G. MacDiarmid, C. K. Chiang and A. J. Heeger, *J. Chem. Soc., Chem. Commun.* (1977) 578; C. K. Chiang, M. A. Dray, S. C. Gau, A. J. Heeger, E. J. Louis, A. G. MacDiarmid, Y. W. Park and H. Shirakawa, *J. Am. Chem. Soc.* **100** (1978) 1013; S. C. Gau, J. Milliken, A. Pron, A. G. MacDiarmid, and A. J. Heeger, *J. Chem. Soc., Chem. Commun.* (1979) 662; P. J. Nigrey, A. G. MacDiarmid, and A. J. Heeger, *J. Chem. Soc., Chem. Commun.* (1979) 594.
- ¹⁴⁷ G. B. Street, T. C. Clarke, *IBM J. Res. Develop.* **25** (1981) 51; K. J. Wynne, B. G. Street, *I&EC Products Res. & Dev.* (1982) 21, 23; R. H. Baughman, J. L. Bredas, R. R. Chance, H. Eckhardt, R. L. Elsenbaumer, D. M. Ivory, G. C. Miller, A. F. Preziosi, L. W. Shacklette, in *Conductive Polymers*, Plenum Press, New York, 1981, p. 137.
- ¹⁴⁸ W. P. Su, J. R. Schrieffer and A. J. Heeger, *Phys. Rev. B* **22**(4) (1980) 2099; J. L. Bredas, R. R. Chance, and R. Silbey, *J. Phys. Chem.* **85** (1981) 756.
- ¹⁴⁹ A. J. Heeger, Meadowbrook Conference on Conducting Polymers, Oakland University, Rochester, Mi., June 1984.
- ¹⁵⁰ D. Baeriswyl, G. Harbeke, H. Kiess, and W. Meyer, in *Electronic Properties of Polymers*, Ed. by J. Mort and G. Pfister, John Wiley and Sons, New York, Chichester, Brisbane, Toronto, Singapore 1982.
- ¹⁵¹ P. J. Nigrey, D. MacInnes Jr., D. P. Nairns, A. G. MacDiarmid, and A. J. Heeger, *J. Electrochem. Soc.* **128** (1981) 1651.
- ¹⁵² A. H. Schroeder, Y. S. Papir, V. P. Kurkov, Abstract No. 544, 163rd Meeting of The Electrochemical Society, San Francisco, Calif., 1983.
- ¹⁵³ L. W. Shacklette, R. R. Chance, D. M. Ivory, G. G. Miller, R. H. Baughman, *Synthetic Metals* **1** (1979) 307.
- ¹⁵⁴ L. W. Shacklette, R. L. Elsenbauer, R. R. Chance, J. M. Sowa, D. M. Ivory, G. G. Miller, R. H. Baughman, *J. Chem. Soc., Chem. Commun.* (1982) 362;

- T. C. Clarke, K. K. Kanazawa, V. Y. Lee, J. F. Rabolt, J. R. Reynolds, G. B. Street, *J. Poly. Sci.: Poly. Phys. Ed.* **20** (1982) 117.
- ¹⁵⁵ L. W. Shacklette, Meadowbrook Conference on Conducting Polymers, Oakland University, Rochester, Mich., June 1984.
- ¹⁵⁶ A. H. Schroeder, private communication.
- ¹⁵⁷ G. C. Farrington, B. Scrosati, D. Frydrych, and J. DeNuzzio, *J. Electrochem. Soc.* **131** (1984) 7.
- ¹⁵⁸ A. G. MacDiarmid, R. J. Mammone, S. J. Porter, and N. L. D. Somasiri, Abstract No. 92, 165th Meeting of The Electrochemical Society, Cincinnati, Ohio, 1984.
- ¹⁵⁹ A. G. MacDiarmid, Shao-Lin Mu, L. D. Somasiri, and Wanqun Wu, *Mol. Cryst. Liq. Cryst.* (in press); A. G. MacDiarmid, Jin-Chih Chiang, M. Halpern, zWu-Song Huang, Shao Lin Mu, Nanayakkara, L. D. Somasiri, Wanqun Wu, and S. I. Yaniger, *Mol. Cryst. Liq. Cryst.* (in press).
- ¹⁶⁰ A. Gibney and D. Zuckerbrod, Paper No. 11, International Power Sources Symposium, Brighton, England, 1982; E. S. Buzzelli, L. B. Berk, H. Moyes, and D. Zuckerbrod, Extended Abstracts, Sixth DOE Electrochemical Contractor's Review, Washington, D.C., June 1984, p. 191.
- ¹⁶¹ E. Yeager, D. Tryk, and S. L. Gupta, Extended Abstracts, Sixth DOE Electrochemical Contractor's Review, Washington, D.C., June 1984, p. 183.
- ¹⁶² R. Clarke and A. Wasson, Extended Abstract No. A4-10, 35th ISE Meeting, Berkeley, Calif., August 1984, p. 222.
- ¹⁶³ J. O'M. Bockris, B. E. Conway, and E. Yeager, Eds., *Comprehensive Treatise of Electrochemistry*, Plenum Press, New York, 1983, Vols. 3 and 7; see also E. Yeager, *Proceedings of Workshop on Renewable Fuels and Advanced Power Sources for Transportation*, Boulder, Col., June 17, 1982, p. 27, Department of Energy, Washington, D.C. and E. Yeager, in *Electrochemistry in Industry*, Ed. by U. Landau, E. Yeager, and D. Kortan, Plenum Press, New York, 1982, p. 29.
- ¹⁶⁴ O. Lindstrøm, Tekniska Hogskolan i Stockholm, Report No. KTR 84-04 (January 1984); O. Lindstrøm, in *Power Sources 5*, Ed. by D. H. Collins, Academic Press, London, 1975, p. 283; L. Ojerfors and L. Carlsson, *J. Power Sources 2* (1977/78) 287.
- ¹⁶⁵ B. G. Demczyk, W. A. Bryant, C. T. Liu, and E. S. Buzzelli, Proceedings of the 15th IECEC, 1980, p. 1477.
- ¹⁶⁶ H. Cnobloch, D. Groeppel, D. Kuehl, W. Nippe, and G. Siemsen, in *Power Sources 5*, Ed. by D. H. Collins, Academic Press, New York, 1975, p. 261.
- ¹⁶⁷ D. Doniat, K. Beccu, and A. Porta, German Patent No. 2,125,576.
- ¹⁶⁸ D. S. Adams, in *Power Sources 4*, Ed. by D. H. Collins, Oriel Press, Newcastle-upon-Tyne, England, 1973, p. 347.
- ¹⁶⁹ S. Zaromb, *J. Electrochem. Soc.* **109** (1962), 1125; S. Zaromb, Proceedings of the Symposium on Power Systems for EV's, National Center for Air Pollution Control, Cincinnati, Ohio, 1967, p. 225.
- ¹⁷⁰ J. F. Cooper and E. L. Littauer, Preprint UCRL-81178, Proceedings of the 13th IECEC, San Diego, Calif., August 1978; R. V. Homsby, Proceedings of the First International Workshop on Reactive Metal-Air Batteries, Bonn, FGR, July 1979; Aerospace Corporation to DOE, Summary Report on Al-Air Battery Seminar (January 1982); E. Behrin, R. L. Wood, J. D. Salisbury, D. J. Whistler, and C. L. Hudson, LLL Report UCRL-53382 (January 1983); J. F. Cooper, LLL Report UCID-20023 (April 1983); J. F. Cooper and A. Maimoni, Extended Abstracts, Sixth DOE Electrochemical Contractor's Review, Washington, D.C., June 1984, p. 178.
- ¹⁷¹ H. F. Bauman, Proceedings of the First International Workshop on Reactive Metal-Air Batteries, Bonn FGR, July 1979, p. 13.1; E. L. Littauer, R. P. Hollands-

worth, and D. J. Levy, Proceeding of the Second International Workshop on Reactive Metal-Air Batteries, Belgrade, Yugoslavia, September 1983, p. 259.

- ¹⁷² L. A. Knerr, D. J. Wheeler, T. J. Schuhe, W. R. Bennett, and L. J. Gestaut, Extended Abstracts, Sixth DOE Electrochemical Contractor's Review, Washington, D.C., June 1984, p. 181.
- ¹⁷³ D. M. Drazic, Proceedings of the First International Workshop on Reactive Metal-Air Batteries, Bonn FRG, July 1979, p. 7.1; A. R. Despic and D. M. Drazic, Proceedings of the Second International Workshop on Reactive Metal-Air Batteries, Belgrade, Yugoslavia, September 1983, p. 299.
- ¹⁷⁴ G. Hoffmann, M. Ritschel, and W. Vielstich, Proceedings of the First International Workshop on Reactive Metal-Air Batteries, Bonn, FRG, July 1979, p. 2.1.

Structural and Transport Properties of Perfluorinated Ion-Exchange Membranes

Richard S. Yeo†

Pinnacle Research Institute, Cupertino, California 95014

and Howard L. Yeager

Department of Chemistry, University of Calgary, Calgary, Alberta T2N 1N4, Canada

I. INTRODUCTION

1. Historical Background of Ion-Exchange Membrane Cells

Cell separators (or dividers) are generally required in an electrochemical cell in order to prevent both intermixing of anolyte and catholyte, and, possibly, shorting between anode and cathode.^{1,2} In many cases, without a separator, the cell either does not work at all or works at a much lower efficiency and with a shorter cell life. This is particularly true for the chlor-alkali cell³ and the Fe-Cr redox cell,⁴ both of which require membranous separators.

Ion-exchange membranes are widely used in electrochemical cells. These membranes include, in their polymeric structure, many ionizable groups. One ionic component of these groups is fixed into or retained by the polymeric matrix (so-called fixed ion), while the other ionic component is a mobile, replaceable ion (so-called counterion) which is electrostatically associated with the fixed

† Present Address Kimberly-Clark Corporation, 1400 Holcomb Bridge Road, Roswell, Georgia 30076

component. These membranes are permeable to one kind of ion while resisting the passage of direct flow of liquids and ions of opposite charge.

The concept of using an ion-exchange membrane as an "electrolyte" in electrochemical cells was first introduced by Grubb in 1959.⁵ Since then, extensive research and development programs have been undertaken by the General Electric Company and others,⁶⁻⁹ resulting in the present solid polymer electrolyte (SPE) cells in which Nafion[®] serves as the sole electrolyte as well as separator. High voltaic efficiency can be achieved in SPE cells because of the minimum contact resistance between electrode and separator.

2. Requirements of High-Performance Membranes

The success of an electrochemical process can depend critically on the selection of the proper membrane. Yet, general criteria by which a membrane can be selected do not exist. The essential properties of the membrane for electrochemical applications include good permselectivity, high ionic conductivity, no electronic conductivity, adequate chemical and thermal stability, and sufficient mechanical strength under operating conditions.

The membrane is a compromise of properties: the requirement for low internal resistance suggests that the membrane be porous and thin; good separation dictates that the membrane be of low permeability and high fixed charge concentration; and adequate physical strength requires that it be sufficiently thick. At any rate, membranes can generally be "tailor-made," so that their properties can be adjusted to yield optimal cell performance and cell life.¹⁰

Cell efficiency very often improves at elevated temperatures because of better conductivity and improved kinetics. However, hydrocarbon-type membranes are often unstable in such environments. This is particularly true for cells in which oxidizing agents, such as chlorine or peroxide, are present. The membrane degrades due to the cleavage of carbon-hydrogen bonds, particularly the α -hydrogen atom where the functional group is attached.^{11,12} Perfluorinated materials are better for these electrochemical applications because of their excellent chemical inertness and mechanical integrity in hot corrosive and oxidative environments.¹²

3. Development of Perfluorinated Ionomer Membranes

The interest in perfluorinated ion-exchange membranes has increased extensively in recent years because of their industrial importance. A growing body of research concerning their structure and properties has developed.¹³⁻¹⁸³ Much of this work has been summarized in a recent monograph.¹⁸⁴ While perfluorinated anion-exchange membranes have not yet been produced, several perfluorinated cation-exchange types have been synthesized and fabricated into membrane form, as listed in Table 1.

The perfluorinated sulfonate (Nafion) polymer was synthesized and developed by du Pont about 17 years ago.^{154,185,186} It was initially introduced as SPE in fuel cell applications in 1966. It exhibits excellent stability over conventional cross-linked polystyrene sulfonic acid membranes and becomes the unique candidate for this type of application. Subsequently, further development has been made^{79,181} in improving its chemical stability against peroxide

Table 1
Perfluorinated Cation-Exchange Membranes

Structure	Trade name	Producer	References
XF-OCF ₂ CO ₂ H/SO ₃ H		Asahi Chemical	133 134
XF-O(CF ₂) _n CO ₂ H	Flemion	Asahi Glass	145, 146 150-152
XF-OCF ₂ CF ₂ SO ₃ H	Nafion 1000 series	du Pont	49
XF-OCF ₂ CF ₂ SO ₂ NH ₂	Nafion Sulfonamide	du Pont	62 187
XF-OCF ₂ CF ₂ CO ₂ H/SO ₃ H	Nafion 901	du Pont	149 169
XF-O(CF ₂) _n CO ₂ H/SO ₃ H	Neosepta-F	Tokuyama Soda	129 130
XF = -(CF ₂ CF ₂) _x -(CF ₂ CF ₂) _y - <div style="margin-left: 100px;"> $\begin{array}{c} \\ (\text{OCF}_2\text{CF})_m - \\ \\ \text{CF}_3 \end{array}$ </div>			

degradation. Various modifications have been made to a basic Nafion homogeneous polymer film to produce materials with special characteristics. Open weave Teflon fabric can be laminated into the polymer film for increased strength. Also, composite membranes have been made in which layers of two different equivalent weights of polymer film are laminated together. Moreover, surface treatment has been employed to generate membranes in which a thin layer of weakly acidic sulfonamide exchange sites is formed.¹⁸⁷ Thin amine-treated membranes^{29,31} have found applications in chlor-alkali cells, because improved hydroxyl ion rejection is realized when this treated surface faces the catholyte.⁶²

Perfluorinated carboxylate membranes were introduced about seven years ago. These membranes can be synthesized by a variety of methods or by various chemical conversions from the Nafion polymer.^{129,133,150,151} Composite membranes which contain both sulfonate and carboxylate functional groups have also been produced (see Section IV.1 for more details). These carboxylate membranes have been widely employed in the advanced membrane chlor-alkali cells. This major chemical technology is in the process of being revolutionized by the use of these materials, a remarkable accomplishment for such a small group of polymers.¹⁴³

4. Types of Applications

The perfluorinated sulfonic acid (Nafion) membranes have found a great variety of electrochemical applications. These include the SPE water electrolyzers,^{79,80,131,144,181-183} alkaline water electrolyzers,^{82,142,176} hydrochloric acid electrolyzers,^{174,175,181} Na_2SO_4 electrolyzers,⁸⁰ hydrogen-air fuel cells,^{72,181} hydrogen-halogen fuel cells,^{174,175,181} zinc-bromine cells,¹⁵⁸ zinc-ferricyanide redox cells, zinc-ferric redox cells, Donnan dialyzers,^{32,100-102} electrochromic devices,¹¹⁶ chemically modified electrodes,^{26,27,58,89,90,126,127,157} ion-selective electrodes,⁸⁷ and many others. See References 52, 71, and 181 for detailed discussions.

Potential applications of perfluorinated carboxylate membranes have been focused to date on the chlor-alkali process. It has been pointed out previously that these polymers in acid form are not desirable for electrochemical applications because of rather high resistance.¹⁷⁸

Perfluorinated ionomer membranes show considerable promise with respect to their performance characteristics, low resistivity, high permselectivity, and long-term stability. However, the present cost of these membranes is more than \$300 per square meter. The relatively high cost limits their application in many electrochemical cells when cost effectiveness is a major concern.

5. The Scope of this Review

This article aims at describing the microstructure and transport properties of these polymeric membranes from an electrochemical point of view. It is intended to provide some direction for the future development of high-performance membrane cells in industrial electrolytic or separation processes.

Section II deals with the microstructure of the perfluorinated ionomers. These structural properties and their effect on transport properties are currently understood only qualitatively. Although there are diverse opinions on the detailed morphology of these polymers, it is generally agreed that microphase separation and ion clusters do exist. The presence of ion-clustering morphology and the amount of electrolyte in these membranes can strongly affect the transport properties. The ion-clustering theory of Eisenberg will be used to provide a basic understanding about these materials. Since most electrochemical applications of the materials involve electrolytes, the solvation phenomena as well as the concentrations of fixed ions and co-ions in the polymers are of particular interest.

Membrane transport properties in both dilute and concentrated solution environments are presented in Section III. The membrane transport properties under industrial electrolysis conditions will be dealt with in Section IV. For practical cell applications, the conductivity and permeability of the membrane are of great importance. These properties can significantly affect cell performance. These subjects are treated in Section V.

II. MICROSTRUCTURE

1. Structural Studies of Ionomers

Perfluorinated ion-exchange membranes belong to a class of materials called ionomers.¹⁸⁸ These perfluorinated ionomers differ

from conventional ion-exchange membranes in that they are not cross-linked polyelectrolytes but thermoplastic polymers with pendant acid groups (in concentrations below ~ 15 mol %) partially or completely neutralized to form salts. These perfluorinated materials become soluble when the ionic co-monomer exceeds 15 mol % and would be considered as polyelectrolytes.¹⁸⁸

Research on the structure and properties of solid ion-containing polymers has been carried out extensively in several laboratories during the last two decades.¹⁸⁹⁻²⁰¹ The structure of ion aggregates in these polymers, and the modifications which occur on solvation are generally not known quantitatively. The reason for the lack of understanding of the microstructure of ion-containing polymers lies in their complexity. The microstructure of ion-containing polymers, particularly those aspects dealing with micro-phase separation, presents a particularly challenging problem because none of the usual tools of structure characterization are readily applicable. Also, results obtained by these techniques are subject to different interpretations by the various groups working in the field.

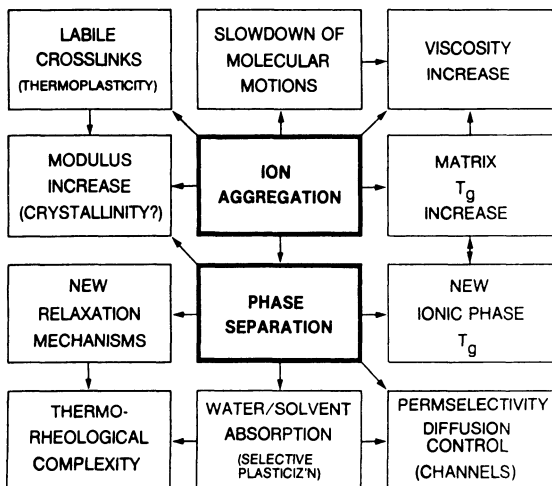


Figure 1. Characteristic ionomer properties and their interrelationships. (Ref. 18; reprinted by permission of the publisher, The Electrochemical Society, Inc.)

It is traditionally considered that for conventional ionic polymers¹⁹⁸⁻²⁰⁰ the ions are dispersed throughout the sample in a very low state of aggregation, either as ion pairs or ion quartets. The evidence to support this concept is derived from nuclear magnetic resonance data,¹⁹⁹ viscosity data,¹⁹⁸ and dynamic mechanical measurements.²⁰⁰ As a recent trend, it is widely accepted that^{43,44,46,119,163,171,173,183,189-193,196} sizable clusters of ions embedded in the surrounding organic medium can also exist in the polymers, the most direct evidence coming from small-angle X-ray scattering.

The presence of these large ion aggregates can influence directly, or indirectly, various properties of these polymers. Such relationships have recently been demonstrated by Besso and Eisenberg¹⁸ and Eisenberg²⁰² and are shown in Fig. 1. In the light of the importance of ion clustering in determining the structural and transport properties of the perfluorinated materials, some theoretical aspects of cluster formation will be briefly described in the following section.

2. Eisenberg's Theory

In 1970, Eisenberg²⁰¹ set forth an initial theory of ionomer structure which contains some concepts of general merit. Two basic types of ionic aggregations have been postulated: small aggregates containing few ion pairs, termed *multiplets*, and larger aggregates, termed *clusters*, which consist of a nonionic backbone material as well as many ion pairs. The structure of the ionomer can thus be broadly described as that of a microphase-separated system in which a matrix of low ion content (due to multiplets) is interspersed with ion-rich domains (clusters). The bulk of the experimental evidence has suggested that only multiplet formation occurs at low ion concentration whereas, beyond a certain ion concentration (which depends on the material), the multiplets may very well aggregate to form clusters.

The formation of ionic domains or clusters is regarded as being a consequence of the thermodynamic incompatibility of the ionic groups with the low dielectric constant organic matrix. The enthalpic advantages of phase separation are obvious but large entropic forces oppose the process. Eisenberg²⁰¹ has analyzed the thermodynamics of phase separation in ionomer systems. He has evaluated

the distances between clusters and the cluster sizes by imposing various geometries on the cluster. The factors involved in this computation are: (1) work done to stretch the polymer chains in cluster formation; (2) electrostatic energy released when clusters collapse; and (3) the temperature threshold T_c where the elastic and electrostatic forces just balance each other. A brief description of his analysis is presented as follows.

The elastic work in cluster formation is related to the energy changes in two different kinds of chain deformations. The first kind is the work of stretching a polymer chain from a distance X_0 to X , the distance corresponding to a cluster size of N . The other kind is the work of contracting a chain from a distance of X_0 to 0. Accordingly, the elastic work per chain in cluster formation is given by

$$W_{\text{ch}} = (3kT/4\bar{h}^2)(X^2 - 2X_0^2) \quad (1)$$

where $\bar{h}^2 = 4\sigma^2 l^2 M_c / M_0$, the mean square end-to-end distance of the polymer chain; σ^2 = chain expansion factor; l = length of repeat unit; M_c / M_0 = degree of polymerization between ionic groups; $X = (NM_c / \rho N_A)^{1/3}$, the average distance between clusters; $X_0 = (N_0 M_c / \rho N_A)^{1/3}$, the average distance between multiplets above T_c ; ρ = density of polymer, and k , T , and N_A have their usual meanings.

The electrostatic energy per ion pair released upon cluster collapse is a function of the geometry of the cluster and the dielectric constant ϵ of the medium. It is given by

$$W' = -\lambda e^2 / \epsilon r \quad (2)$$

where λ = the fraction of energy released, e = electron charge, and r = distance between centers of charge in the ion pair.

The cluster is not infinitely stable. At some temperature T_c the cluster decomposes, and at that temperature the elastic forces and the electrostatic forces just balance each other. Since the elastic force was calculated per chain and the electrostatic force per ion pair, W_{ch} can be set equal to W' at T_c ; thus

$$\begin{aligned} \lambda e^2 / \epsilon r = & (3kT_c M_0 / 16\sigma^2 l^2 M_c) [(NM_c / \rho N_A)^{2/3} \\ & - 2(N_0 M_c / \rho N_A)^{2/3}] \end{aligned} \quad (3)$$

After rearrangement, Eq. (3) yields

$$N = (\rho N_A / M_c) [16 \sigma^2 l^2 M_c \lambda e^2 / 3 k T_c M_0 \epsilon r + 2(N_0 M_c / \rho N_A)^{2/3}]^{3/2} \quad (4)$$

Since, T_c can be determined experimentally and λ calculated for any particular cluster geometry, N and X can be calculated from Eq. (4).

The Eisenberg theory indicates that at low ion concentration, as the distance between multiplets increases, the interaction between multiplets is expected to decrease to the point where the elastic forces become too large to be overcome; below that concentration clustering would not be expected. This is consistent with the experimental findings. This theory has been applied well to both ethylene and styrene ionomers which contain carboxylate groups.¹⁸⁸ Hashimoto *et al.*^{43,44,54} have recently shown that the Eisenberg theory can be used to explain the small-angle X-ray scattering (SAXS) results on various perfluorinated ionomer membranes.

It should be mentioned that the Eisenberg theory is somewhat approximate and should be regarded only as demonstrating feasibility rather than predicting true cluster geometries. The theory has been consulted extensively in many recent models proposed for Nafion membranes (see Section II.4).

3. Ions in Perfluorinated Ionomers

(i) Ion-Exchange Capacity

The amount of ionic groups in these membranes is conventionally expressed in terms of the equivalent weight (EW) of the polymer.⁴⁹ EW is defined as the weight of polymer which will neutralize one equivalent of base. It is inversely proportional to the ion-exchange capacity (IEC) according to the following relationship:

$$EW = 1000 / IEC \quad (5)$$

where IEC is given in terms of milliequivalents per gram of polymer. As for the sulfonate membrane, the range of EW of greatest interest for electrochemical applications is 1100 to 1350, corresponding to 0.741–0.909 meq g⁻¹.

(ii) Ion Clustering

The existence of ion clustering in perfluorinated sulfonate ionomers was first reported by Yeo and Eisenberg in 1975.¹⁷¹ This phenomenon has been subsequently studied for perfluorinated sulfonate and carboxylate ionomers by many others.^{43,46,56,119,163,183} Experimental evidence to support the conclusion that ion clustering occurs in these materials includes thermorheological behavior,¹⁷³ X-ray diffraction results,^{43,44,46,118,139,173} IR data,^{41,55} NMR data,^{22,74} ESR data,¹⁵³ Mössbauer spectroscopic data,^{14,56,120,121,172} fluorescence behavior,^{81,99} neutron scattering spectroscopic data,^{118,119} extended X-ray absorption fine structure (EXAFS) data,¹⁰⁸ electron microscopic data,^{28,46} swelling behavior,¹⁷⁷ acidity,¹⁸³ and transport properties.^{46,63,159,163,183}

Ion clusters are commonly observed in the ionized forms of the perfluorinated membranes. The size of the clusters appears to be larger for sulfonate than for carboxylate membranes.⁴⁴ The size increases in the order H^+ , Na^+ , and Cs^+ and decreases with increasing number of functional groups per chain and with increasing temperature.⁴³ As in the case of ethylene ionomers, the perfluorinated carboxylic acid membranes do not form ion clusters, at least in the dry state.⁴³ The electrostatic interaction may be too weak to form ionic clusters. These observations are expected according to the Eisenberg theory (see Section II.2).

Different ionic environments in Nafion have been indicated from Mössbauer experiments.^{14,56,120,121} Heitner-Wirguin *et al.*¹⁴ suggested the existence of clusters and dimers. Most of the ionic groups are in clusters while the remaining groups are considered to form multiplets or small ion aggregates. The relative amounts of ionic groups which are not present in clusters is difficult to evaluate because of the limitation of available research tools. In addition, the amount changes with the prehistory of the membrane and the environment the membrane encounters. Roche *et al.*¹¹⁹ have made a rough estimate (with an accuracy of $\pm 20\%$) on Nafion in the sodium salt form from small-angle neutron scattering results. They found that the amount of ionic groups in the organic phase is $<60\%$ and $<40\%$, respectively, for N-form and E-form samples [see Section II.5(i) for definitions].

(iii) Ionic Cross-Linking

In contrast to conventional ion-exchange resins or membranes, there is no cross-linking in these perfluorinated membranes. In solvents which might dissolve the nonionic prepolymer, the ionic aggregates are very stable and act as cross-linkage sites. Conversely, highly polar solvents, which interact with the ionic groups, do not solvate the polymer. The crystalline domains originating from tetrafluoro ethylene (TFE) backbone behave like cross-linked points.^{88,177} Also, the clusters of the perfluorinated ionomer membranes never fall apart upon hydration as indicated by SAXS results.⁴³ Thus, either the ionic regions or the nonionic areas act as cross-linkings which make the 1100 and higher-EW materials insoluble, while the 970-EW material, with less TFE content, is too weak for use in the swollen form and is soluble.^{26,27,58,89,95,126,127,157} The high-EW membranes absorb a range of solvents to varying extents^{177,178,180} and exhibit two solubility parameter values. This behavior is referred to by Yeo as "dual" cohesive energy densities of the polymer.¹⁷⁷

High temperatures are required to melt the crystalline domains in the high-EW samples and promote dissolution. Martin *et al.*⁸⁸ have recently found that Nafions with EWs of 1100 and 1200 dissolve in both 50:50 propanol-water and 50:50 ethanol-water, at 250°C and elevated pressure, because the crystallites of the materials are eliminated. McCain and Covitch⁹⁵ have also reported a similar dissolution technique. The ionic membrane was chemically converted into the nonionic precursor (sulfonyl fluoride) form prior to the dissolution process. Due to the nonionic nature of the precursor, it dissolves under relatively mild conditions. These dissolution techniques for Nafion polymers provide an important means for preparation of chemically modified electrodes^{26,58,89,126,157} and membranes of any desired geometry.⁹⁵

4. Structural Models of Nafion

Several structural models of Nafion have been proposed which are based on various transport and spectroscopic properties of the polymer.^{46,60,64,72,122} A detailed picture which is consistent with all

the experimental observations has not yet emerged. Also, the proposed models are either only qualitative or have various adjustable parameters and assumptions.

In 1977, Gierke proposed a phenomenological cluster network model. The concept of ion clustering is adopted in this model, except it is assumed that both the ions and the absorbed solvents are *all* in the clusters. This is only an approximation in view of the more recent spectroscopic observations.^{41,119} The clusters are assumed to be approximately spherical and the cluster size, for varying polymer equivalent weight, has been calculated from solvent absorption data. For sodium-form Nafion of 1200 EW and a water content of 9 wt %, the cluster diameter is about 3 nm. However, based on infrared data, Falk⁴¹ has suggested that the hydrated ion clusters are either much smaller than Gierke estimates, or more likely are highly nonspherical in shape, with frequent local intrusions of the fluorocarbon phase. Extensive intrusions of fluorocarbon material into ion-clustered regions is inferred from these results.⁴¹ The evidence for extensive interaction of the cations with the fluorocarbon phase has also been indicated by Lee and Meisel.⁸¹

Gierke also considered that these clusters are interconnected by short, narrow channels in the fluorocarbon backbone network. The diameter of these channels is about 1 nm estimated from hydraulic permeability data. He further considered that the Bragg spacing (~ 5 nm from SAXS data) can represent the distance between clusters. The cluster-network model is a phenomenological description. Recently, Hsu and Gierke⁶⁴ have derived a semi-phenomenological expression to correlate the variation of cluster diameter with water content, equivalent weight, and cation form of the membrane. They have shown that the short channels are thermodynamically stable.

Hopfinger and Mauritz⁶⁰ and Hopfinger⁶¹ also presented a general formalism to describe the structural organization of Nafion membranes under different physicochemical conditions. It was assumed that ionic clustering does not exist in the dry polymer. This assumption is applicable to the perfluorinated carboxylic acid polymer⁴³ but not the perfluorosulfonate polymers.⁴⁶ They consider the balance in energy between the elastic deformation of the matrix and the various molecular interactions that exist in the polymer.

The calculation depends on many molecular parameters, which are estimated from a combination of experimental bulk thermodynamic data and molecular structure calculations, employing both molecular and quantum mechanics. The model semiquantitatively reproduces water absorption, polymer density, and the number of water molecules per exchange site in these polymers. For a comprehensive description of this work, see References 60, 91, and 92.

Pineri *et al.* have performed a series of investigations^{38,40,118-123,153,155} on the structural properties of Nafion polymers and have derived a three-phase model in which fluorocarbon crystallites, ionic hydrophilic clusters, and an amorphous hydrophobic region of lower ionic content coexist.¹²² The microcrystallites can be eliminated by heating the Nafion-Na sample to 330°C, and then quenching it to room temperature.¹¹⁸ They showed that at high water content (>15 wt %) the quenched Nafion membranes are essentially two-phase systems.¹¹⁹ These phases are rather well separated and most of the water is in the ionic clusters. Samples of lower water content (8 wt %) show deviations from two-phase behavior.¹¹⁹

A structural model, which correlates various spectroscopic and ionic diffusional results, has been proposed recently.¹⁶³ Figure 2 represents a schematic diagram of the model in which three regions are indicated. Region A consists of fluorocarbon backbone material, some of which is in a microcrystalline form, as detected by Pineri *et al.*¹¹⁸ Ion clusters form Region C, in which the majority of sulfonate exchange sites, counterions, and sorbed water exist. The interfacial Region B is seen as one of relatively large fractional void volume, containing pendant side-chain material, a smaller amount of water, some sulfonate exchange sites which have not been incorporated into clusters, and a corresponding fraction of counterions. The relative numbers of ions in Regions B and C would depend on the size, charge density, and hydration energy of the cation. Ions of low charge density or large size, such as Cs⁺ or Ru(bpy)₃²⁺, would prefer Region B, while those of larger charge density and hydration energy would become localized in the more aqueous ionic clusters (within electroneutrality limitations).

Hashimoto *et al.*^{43,44} have recently studied the effects of polymer swelling and deformation on the small-angle X-ray scattering profiles of perfluorinated ionomer membranes. The size of ion clusters appears to be larger for sulfonate than for carboxylate

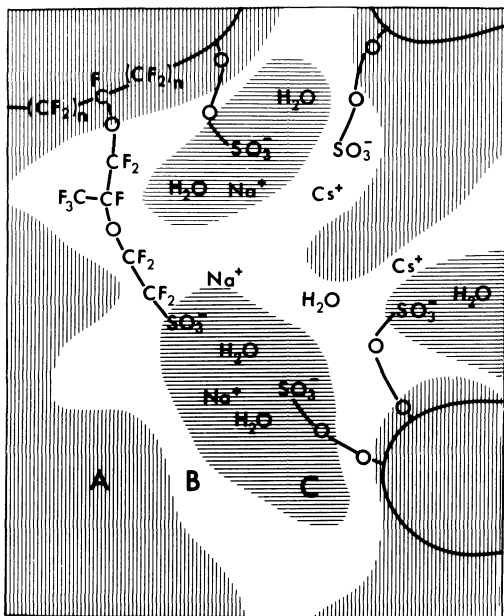


Figure 2. Three-region structural model for Nafion: A, fluorocarbon; B, interfacial zone; and C, ionic clusters. (Ref. 163; reprinted by permission of the publisher, The Electrochemical Society, Inc.)

polymers. The extent of microcrystallinity is less for the sulfonate polymers for a given counterion form. Furthermore, the results have suggested that the microstructure of perfluorinated ionomer membranes can be described better by the core-shell model than the two-phase model. The core-shell model was proposed by MacKnight and co-workers,²⁰³ in which the ionic cluster (i.e., ion-rich core) is surrounded by the fluorocarbon phase (i.e., ion-poor shell). The core-shell particles are dispersed in the matrix composed of fluorocarbon chains and nonclustered ions.

5. Solvation Phenomena

(i) *Electrolyte Uptake*

Various physical and transport properties of these cation-exchange membranes are largely influenced by the amount of elec-

trolyte absorbed. The electrolyte uptake of these non-cross-linked membranes is strongly affected by the polymer functional group, the polymer equivalent weight, the history of pretreatment, and the electrolytic environment.

The amount of water a membrane will initially absorb increases with temperature, as is shown in Fig. 3 for a 1200-EW polymer in the sulfonic acid form. These samples are assigned as normal (N) form or as-received form. It is interesting that a sample, which has been exposed to water at a higher temperature, say 100°C, shows greater water absorption and will continue to retain that same amount of water at room temperature, unless the effect is destroyed by drying at elevated temperatures. These samples are denoted as expanded (E) form. On the other hand, the water absorption can be decreased if the sample is heated in the dry state at elevated temperatures. These samples are denoted as shrunken (S) form. Again, the membrane is particularly sensitive to these treatments if it is in the acid form. As shown in Tables 8 and 9 (Section V),

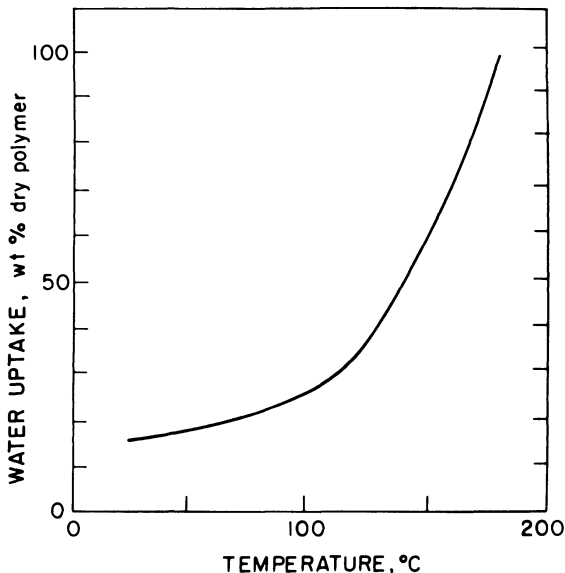


Figure 3. Water uptake for Nafion of 1200 EW as a function of temperature. (Ref. 49; reprinted by permission of the publisher, The Electrochemical Society, Inc.)

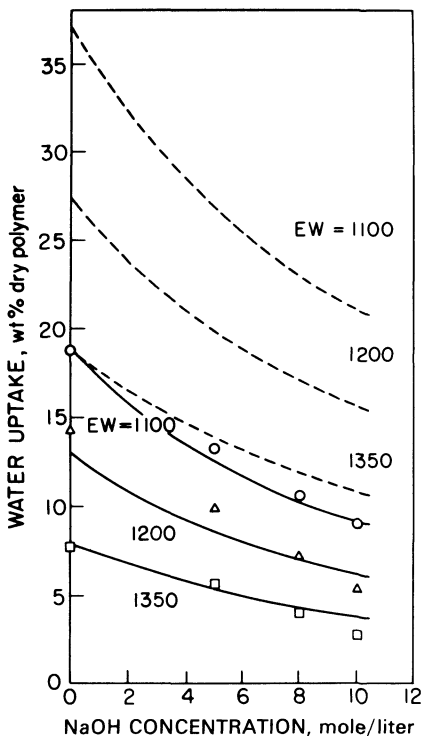


Figure 4. Water uptake for perfluorinated ion-exchange membranes for various EW as a function of NaOH concentration: (---) sulfonate and (—) carboxylate (Ref. 133).

the water content alters appreciably by pretreatment, which is a classical effect with non-cross-linked polymers.

Figure 4 shows the dependence of water absorption on NaOH concentration for the carboxylate and sulfonate membranes. The water absorption of perfluorocarboxylate membranes is much lower than that of perfluorosulfonate membranes. The water absorption decreases with increasing equivalent weight. This can be expected because the higher the equivalent weight, the lower the concentration of ionic groups per unit polymer weight. The data in Fig. 4 can be expressed by the following empirical equations,^{49,133} where Eqs. (6) and (7) represent sulfonate and carboxylate membranes, respectively:

$$W_e = \frac{0.0126AB}{1 + 0.075M} \exp(3980/EW) \quad (6)$$

where W_e is expressed in terms of weight percent of water, based

on the dry polymer weight, M is the molarity of the electrolyte ($0 < M < 14$), A is a constant ($H^+ = 1$, $Li^+ = 0.95$, $Na^+ = 0.79$, $K^+ = 0.57$), and B is a constant dependent on the history of pretreatment of the membrane ($B = 1$ for E-form samples); and

$$W_e = \frac{0.001855}{1 + 0.1065M} \exp(5104/EW) \quad (7)$$

and $1100 < EW < 1400$.

Figure 5 shows the electrolyte uptake of the sulfonic acid membrane as a function of electrolyte concentration for three different acid electrolytes. The electrolyte content of the membrane decreases with increasing acid concentration. As shown in Table 2, both sulfonate and carboxylate membranes sorb large amounts of other solvents as well, particularly alcohols and other protic solvents.^{151,177,180}

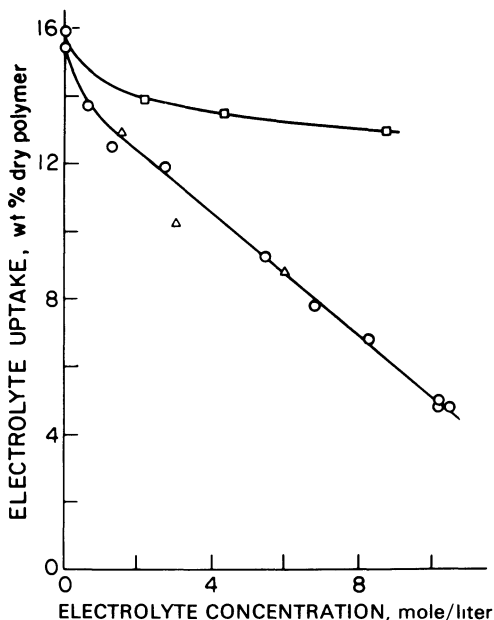


Figure 5. Electrolyte uptake for Nafion of 1200 EW as a function of electrolyte concentration: (○) HCl, (△) HBr, and (□) H₃PO₄. (Ref. 182; reprinted by permission of the publisher, The Electrochemical Society, Inc.)

Table 2
Degree of Swelling for Nafion^b and Flemion Membranes^a

Solvent	Solubility parameter	Nafion acid form	Nafion Li form	Flemion Na form	Flemion ester type
Water	23.4	21	12	14	
Formamide	19.2	56	45		
Glycerol	16.5	56	44		
Ethylene glycol	14.6	66	56	80	
Methanol	14.5	54	48	800	1
Ethanol	12.7	50	45	15	
Propylene glycol	12.6			130	
1-Propanol	11.9	55	47	7	
2-Propanol	11.5	58	32		
Amyl alcohol	10.9	73	75		
Decanol	10.0	70	72		
Acetone	9.9			10	11
2-Ethyl hexanol	9.5		47		
Diethyl amine	8.0	21			
Triethyl amine	7.4	17			

^a From References 151, 177, and 179.

^b Solvent swelling for Nafion (1100 EW) is given in terms of weight percent of dry polymer.

(ii) Sorption Rate of Electrolyte

Good wettability is essential for membranes that serve as separators in electrochemical cells. While fluorocarbon polymers are generally known to be quite hydrophobic substances, these membranes are certainly an exception. They sorb water rapidly even at room temperature. The sorption rates of water and other

Table 3
Apparent Diffusion Coefficients of HCl Electrolytes in Nafion^a

Electrolyte concentration (wt %)	Diffusion coefficient ($\times 10^6 \text{ cm}^2 \text{ s}^{-1}$)
0	1.66
10	1.31
20	0.64
25	0.33

^a From References 182 and 183.

strong electrolytes in Nafion have been reported.^{146,147,183} Table 3 represents the diffusion coefficients of HCl electrolytes in Nafion. The diffusion of these electrolytes in Nafion is very rapid. For dilute electrolytes, it is one order of magnitude smaller than the self-diffusion of water or HCl. The diffusion rate decreases with increasing concentration due to the dehydration of the membrane.

(iii) State of Water in Nafion

Several studies on the state of water in Nafion have been reported recently.^{21,38,41,119,122,136,140,155} A part of the water is associated with the sulfonic acid groups, part interacts with the organic matrix,^{41,119,136} while still another part forms water clusters.^{21,119} Water present in small quantities tends to be preferentially absorbed into the ionic phase.⁴³ The ion clusters in Nafion do not fall apart with water saturation.⁴³ Falk observes evidence for two environments of sorbed water in Nafion from infrared spectroscopic studies.⁴¹ The first environment appears to be aqueous in nature. It is much less strongly hydrogen bonded than water in aqueous salt solutions⁴¹ and it behaves as a liquid which is significantly different in its physical properties from those of bulk water.¹³⁶ In the second environment, the water molecules are not hydrogen bonded and appear to be exposed mainly to fluorocarbon.

In a dielectric relaxation study of Nafion, Yeo and Eisenberg¹⁷³ have observed two dielectric peaks of different energy absorption level. Both of these peaks are highly sensitive to the presence of water in the materials. The activation energies are $\sim 105 \text{ kJ mol}^{-1}$ and $\sim 67 \text{ kJ mol}^{-1}$, respectively, for the peaks appearing at lower and higher temperature.^{22,173} The amount of water in the organic phase is $<24\%$ and $<20\%$, respectively, for N-form and E-form samples, based on neutron scattering data.¹¹⁹ Falk⁴¹ also concludes from infrared data that about three quarters of the water is in the ion cluster.

(iv) Concentration and Acidity of Exchange Sites

The calculation of the concentration of fixed ions (or exchange sites) is complicated by the existence of the ion-cluster morphology in these materials. Recently, an analysis was performed on

Nafion based on ion-cluster morphology and spectroscopic information.¹⁸³

The amount of ionic groups within the hydrated ion clusters is equal to $IEC \times f_i$, where f_i is the fraction of ionic groups in the ion clusters. The volume of the ion cluster is given by $V_w \times f_w$, where V_w is the volume of electrolyte absorbed by the membrane and f_w is the fraction of electrolyte solution in the ion clusters. V_w can be calculated from the electrolyte uptake of the membrane. The concentration of fixed ion (in terms of mol liter⁻¹) is thus given by

$$\bar{C}_f = \frac{IEC f_i}{V_w f_w} = \frac{1000 d_e}{EW W_e} \left(\frac{f_i}{f_w} \right) \quad (8)$$

where W_e and d_e are the weight fraction and density of the electrolyte absorbed by the membrane, respectively. The value of f_i varies between 0.4 to 1.0 whereas the value of f_w varies in the range of 0.76–1.0, based on neutron scattering¹¹⁹ and infrared data.⁴¹ It follows that the ratio of f_i/f_w varies between 0.4 to 1.32. Because of the hydrophilic nature of the ionic groups, it is very likely that the fraction of water in the clusters depends on the fraction of ionic groups in the clusters, i.e., $f_i/f_w \approx 1$.¹⁸³

Figure 6 shows the concentration of fixed ions for Nafion of various EW in equilibrium with water. These concentrations are calculated by assuming $f_i/f_w = 1$.¹⁸³ The concentration of fixed ions increases with EW because the decrease of ionic groups with increasing EW is less significant in comparison with the decrease of V_w , which in turn is related to the water uptake. Another important feature is that membrane pretreatment has a strong effect on the concentration of fixed ions. The concentration of fixed ions is higher for N-form samples than for E-form samples since water uptake increases by boiling the sample in water. It is expected that the concentration of fixed ions in the S-form samples should be higher.

The perfluorinated sulfonic acid membrane exhibits a very strong acidic behavior in water. As shown in Figure 6, the concentration of fixed ion for Nafion of 1200 EW in E-form is equivalent to 13 wt % sulfuric acid. A similar value of 10 wt % sulfuric acid was observed by LaConti *et al.*⁷⁹ The pK_a value is a good indication of the acidity of a material. A recent study has reported that¹⁴⁹ the

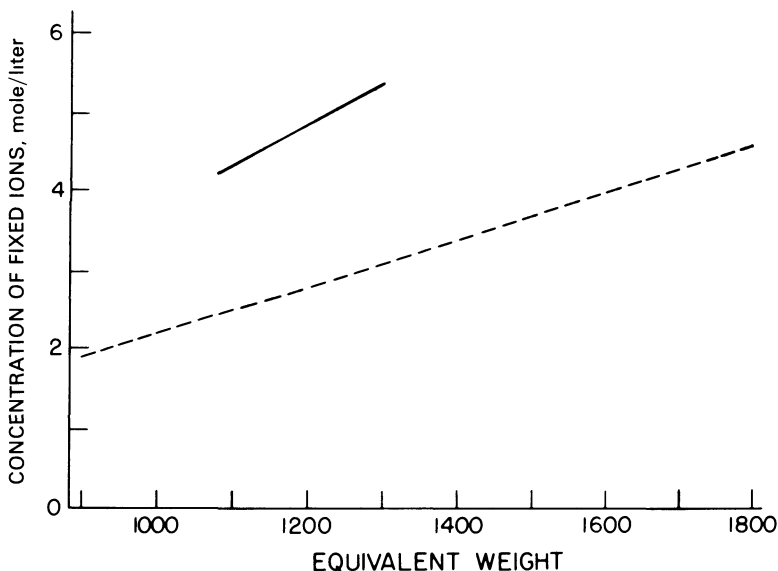


Figure 6. Calculated concentration of fixed ion for Nafion of various EW in equilibrium with water at 25°C. (—) N-form and (---) E-form. (Ref. 183; reprinted by permission of the publisher, The Electrochemical Society, Inc.)

apparent pK_a of the sulfonate and carboxylate membranes are < 1 and 1.9, respectively.

Figure 7 shows the concentration of fixed ions of Nafion. The concentration of fixed ions increases drastically with electrolyte concentration because of the ion-cluster morphology¹⁸³ and the highly dehydrated state of the membrane in concentrated electrolytes, as well as the mass-action effect in counterion activity. Kimoto⁷⁰ has recently shown that in concentrated alkaline solutions the “effective” concentration of fixed ions is less than half of the value calculated from Eq. (8). This decrease is due to the ion-pair formation and strong association in the ion cluster.

(v) Donnan Exclusion Effect and Superselectivity

These perfluorinated membranes, similar to other ion-exchange materials, exhibit a Donnan exclusion effect.^{70,183} Figure 8 shows the concentration of co-ion of N-form Nafion with varying HCl

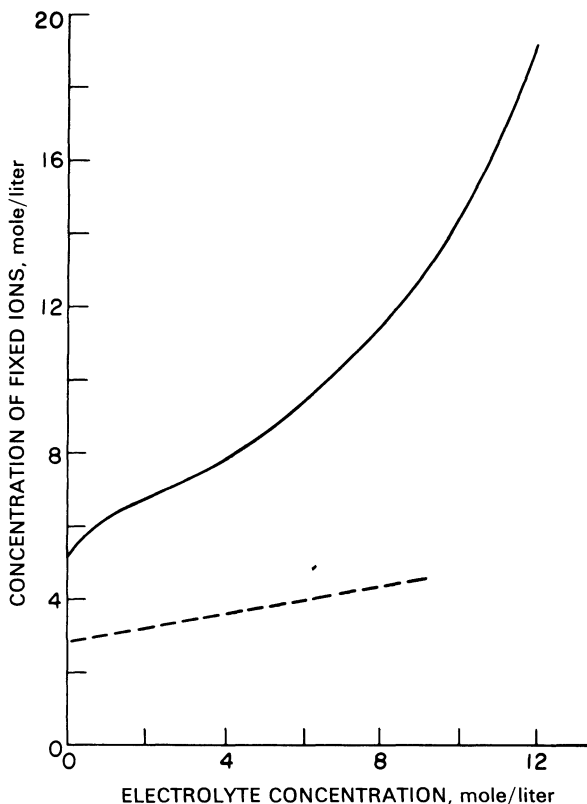


Figure 7. Calculated concentration of fixed ion for Nafion of 1200 EW for varying HCl concentrations at 25°C: (—) N-form and (---) E-form. (Ref. 183; reprinted by permission of the publisher, The Electrochemical Society, Inc.)

electrolyte. The solid curve is calculated from the Donnan equation²⁰⁴:

$$C^2 = \bar{C}_n(\bar{C}_n + \bar{C}_f)(\bar{\gamma}/\gamma)^2 \quad (9)$$

where \bar{C}_f and \bar{C}_n are the concentrations of fixed ion and co-ions, respectively. γ and $\bar{\gamma}$ are the activity coefficients in the external and membrane phase, respectively. The activity coefficient ratio ($\bar{\gamma}/\gamma$) is, for most cases, unity.¹⁸³ The dashed line is for the case in which there is no Donnan exclusion effect for the membrane

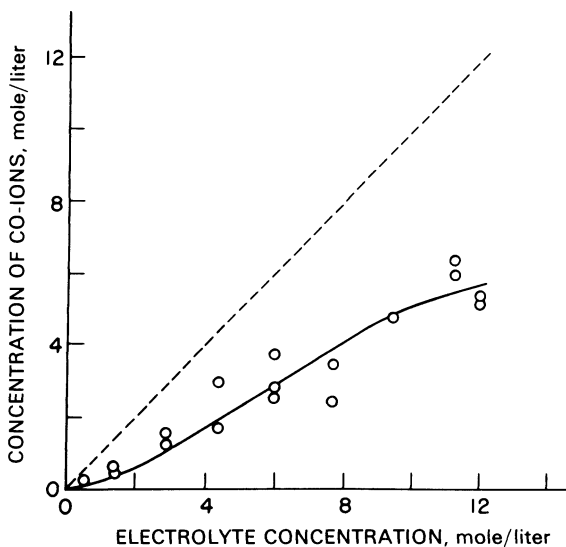


Figure 8. Concentration of co-ion for N-form Nafion of 1200 EW in equilibrium with various HCl electrolytes at 25°C: (---) no Donnan effect and (—) calculated from Eq. (9). (Ref. 183; reprinted by permission of the publisher, The Electrochemical Society, Inc.)

($\bar{C}_f = 0$). The Donnan exclusion effect imparts the permselectivity characteristics to these materials. Good permselectivity generally occurs in dilute solutions while there should be no permselectivity in highly concentrated solutions. However, the permselectivity of Nafion persists beyond the Donnan limit and is referred to as “superselectivity” by Reiss and Bassignana.¹¹⁷ The superselectivity provides enhanced current efficiency beyond the Donnan limit. This extremely valuable property originates from the unusual ion-cluster morphology of these materials.

III. ION AND WATER DIFFUSION

Studies of the diffusional properties of perfluorinated ionomer membranes provide the necessary basic information which is needed for their application in various configurations. Large ionic

diffusion coefficients in the membrane phase are desirable, not only to minimize ohmic losses in electrochemical cells, but also to maximize transport rates for processes driven by concentration gradients such as Donnan dialysis.³² Solvent transport through the membrane may or may not be desirable, depending upon the application. A second goal for the study of diffusion in perfluorinated ionomers is to develop insight into the relationship between the unusual morphology of these polymers and their transport properties. In the latter regard, the determination of self-diffusion coefficients is of particular usefulness. In such experiments the membrane is in equilibrium with the external solution, so that no gradients in internal chemical potential exist. Radioactive tracers can be used to evaluate self-diffusion coefficients which depend upon membrane composition, but are not coupled to chemical potential gradients or the fluxes of other species. These values are therefore more straightforward in their interpretation. Results of such measurements for perfluorinated sulfonate and carboxylate membranes are discussed in this section.

1. Diffusional Properties in Dilute Solution Environments

The self-diffusion coefficients of sodium and cesium ions have been measured for perfluorinated sulfonate (Nafion[®]) and carboxylate membranes of similar structure.^{159,163,165} The exchange-site con-

Table 4
Exchange-Site Concentration and Water Content for Perfluorinated Ionomer Membranes^a

Membrane	Ionic form	Exchange-site concentration ^b mol liter ⁻¹	Mol H ₂ O/mol exchange site	
			N-form	E-form
Sulfonate	Na ⁺	1.20	11.9	18.4
	Cs ⁺	1.35	6.6	11.3
Carboxylate	Na ⁺	1.30	9.5	13.9
	Cs ⁺	1.37	5.0	9.1

^a From Reference 165.

^b N-form samples.

centrations and water-to-exchange-site ratios for these ionic forms of the polymers are listed in Table 4. The exchange site concentrations of the two polymers are quite similar, which is useful for the comparison of their diffusional properties. The water contents strongly depend on the counterion form and pretreatment [Section II.5(i)]; the carboxylate polymer sorbs about 20% less water in all cases. The variability of water content with counterion form is a reflection of the dynamic character of these ion-clustered, non-cross-linked polymers. This is in contrast to conventional cross-linked ion-exchange resins such as the cross-linked polystyrene sulfonates, where water content is largely independent of counterion form for a given counterion charge type.²⁰⁵

Self-diffusion coefficients for sodium ion, cesium ion, and water in these polymers are shown in Fig. 9, as Arrhenius plots from 0 to 40°C.¹⁶⁵ Diffusion of sodium ion and water is remarkably similar

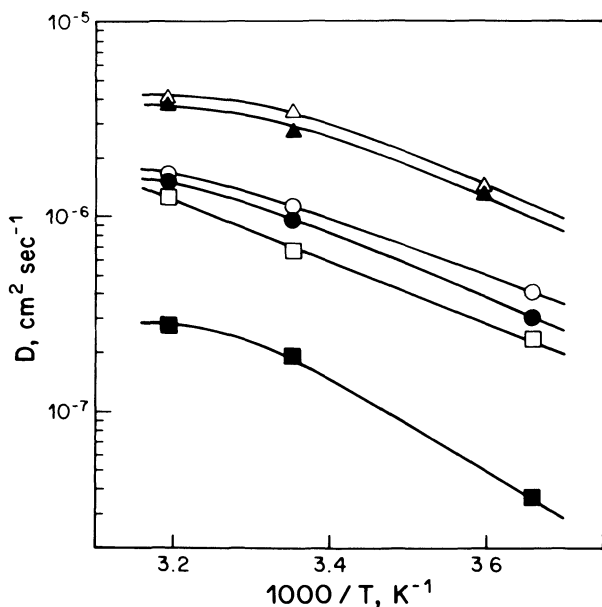


Figure 9. Membrane self-diffusion coefficients vs. the reciprocal of absolute temperature for perfluorocarboxylate (light symbols) and perfluorosulfonate (dark symbols) polymers: (Δ , \blacktriangle) H_2O , (\circ , \bullet), Na^+ and (\square , \blacksquare) Cs^+ . (Ref. 165; reprinted by permission of the publisher, The Electrochemical Society, Inc.)

in the two membranes. Diffusion coefficients are slightly larger for the carboxylate in each case, even though the membrane always contains less water per exchange site. In general, these diffusion coefficients are quite large in relation to the membrane water sorption, about a factor of 10 larger than for polystyrene sulfonate resins of comparable water contents.^{206,207} This is a reflection of the microphase separation of water, exchange sites, and counterions in these ionomers, which produces highly efficient transport paths. Average activation energies of diffusion in these membranes are 24.9 kJ mol⁻¹ for the sodium ion and 23.3 kJ mol⁻¹ for water, which are only marginally higher than their values in pure water, 19.1 and 17.8 kJ mol⁻¹, respectively. Therefore a solutionlike diffusion mechanism for sodium ion and water through a network of ion-clustered regions is indicated for both polymers. The self-diffusion coefficients for cesium ion in these perfluorinated ionomers, which are smaller than those for sodium ion in all cases, are less easily interpreted. Normally, cesium ion has a larger diffusion coefficient than sodium ion in aqueous environments. For example, in water the ratio of D_{Na^+} to D_{Cs^+} is 0.65, and in an 8% DVB polystyrene sulfonate resin the ratio is 0.69.²⁰⁶ For these cases equal amounts of water are present in the diffusing medium though, which is not the case for these ionomers. The values listed in Table 4 indicate that the expanded Cs⁺ form of each membrane has about the same water content as the normal Na⁺ form. A comparison of the sodium ion/cesium ion diffusion coefficient ratios for these cases yields values of 0.71 and 5.3 for the perfluorocarboxylate and perfluorosulfonate polymers, respectively.¹⁶⁵ Thus the apparent anomaly in this ratio is removed if we compare systems with equal water contents for the carboxylate, but not for the sulfonate polymers.

Further anomalies are seen in the diffusional behavior of cesium ion for the perfluorosulfonate membrane. Figure 10 represents the plot of the logarithm of the diffusion coefficient *vs.* the function $v_p/(1-V_p)$, where V_p is the volume fraction of polymer in the water-swollen material¹⁶³ and $1 - V_p$ is the volume fraction of water, as calculated from sorption measurements. This plot corresponds to a test of the equation

$$D = D^\circ \exp[-bV_p/(1 - V_p)] \quad (10)$$

which has been developed by analogy to Cohen and Turnbull's

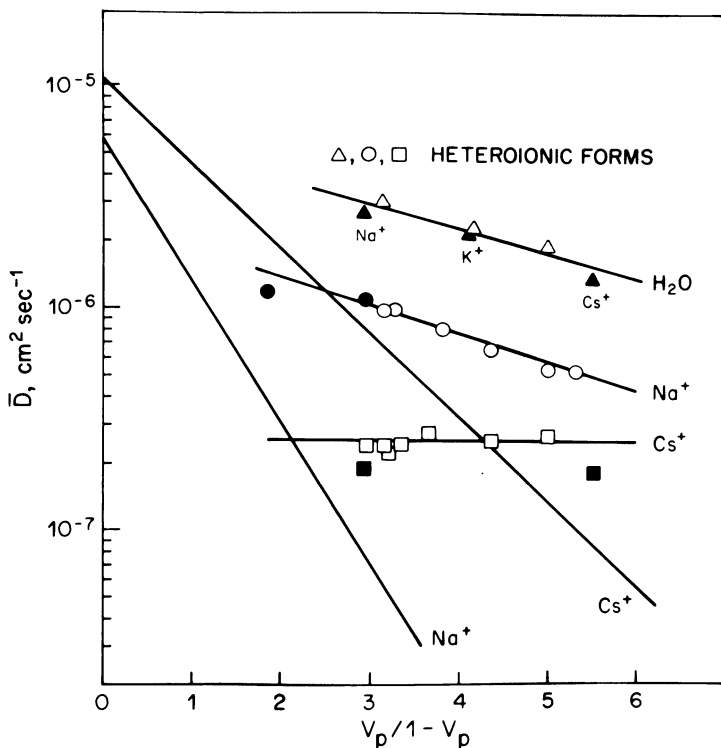


Figure 10. Logarithm of self-diffusion coefficient vs. polymer-fraction function for 1200-EW perfluorosulfonate polymer, at 25°C. Na^+ and Cs^+ lines without data points: polystyrene sulfonate behavior. (Refs. 163 and 207; reprinted by permission of the publisher, The Electrochemical Society, Inc.)

free-volume theory of diffusion.²⁰⁷⁻²⁰⁹ This equation provides an excellent correlation of the self-diffusion coefficients of sodium ion and cesium ion in polystyrene sulfonate resins of varying water content, as shown in Fig. 10.²⁰⁷ The D° intercepts are about one-half of the solution D° values in water, presumably due to electrostatic attractions (Wang effect) exchange sites in the polymer phase. Sodium ion/cesium ion heteroionic forms of the perfluorosulfonate polymer were used to produce samples of varying V_p , in addition to the normal and expanded homoionic forms. No correspondence is seen between the polymer diffusion results for this and polystyrene sulfonates. Most notable perhaps is the complete lack of

dependence of D_{Cs^+} in the perfluorosulfonate membrane on water content. The activation energy for cesium ion diffusion, about 36 kJ mol^{-1} , is largely independent of water content as well. Water diffusion again is similar to sodium ion diffusion, this time in terms of the membrane's water content, with no anomaly seen for the cesium ion form.

The unusual features of cesium ion diffusion in the perfluorosulfonate polymer are related to the microstructure of these polymers. The microphase separation into ion-water and fluorocarbon regions is more complete for the perfluorocarboxylate than for the perfluorosulfonate polymer. For the carboxylate material, stronger hydrogen bonding in the aqueous phase would result due to less fluorocarbon interference with extended intermolecular water interactions. A greater degree of fluorocarbon crystallinity and a smaller fraction of nonhydrogen bonded water for the carboxylate membrane would also be expected consequences of more complete phase separation. Spectroscopic studies of the counterion environments in the perfluorosulfonate polymer provide additional information of interest. The mid- and far-infrared spectra of alkali metal in forms of Nafion perfluorosulfonate films indicate that no ion pairing of counterions to exchange sites occurs, even for completely dehydrated forms.¹⁰⁹ Thus ion pairing is not a relevant factor in the interpretation of small cesium ion diffusion coefficients. A luminescence quenching study of $\text{Ru}(\text{bpy})_3^{2+}$ ($\text{bpy} = 2,2'$ -bipyridine) in Nafion has been performed.⁸¹ The authors conclude that this large, low charge density cation is preferentially situated in a fluorocarbon environment rather than an aqueous one. This suggests that the distinction between ion cluster and fluorocarbon may not be as simple as suggested in various structural models, and that interfacial regions must also be considered.

The less complete degree of phase separation for the sulfonate polymer may well lead to interfacial regions of partly aqueous character and relatively high void volume, as depicted in Fig. 2. A preference of large, low charge density counterions such as $\text{Ru}(\text{bpy})_3^{2+}$ and cesium ions for such regions would help to explain the Cs^+ diffusional anomalies discussed earlier. Diffusion along interfacial boundaries rather than through ion-clustered regions would result in lower bulk diffusion coefficients for cesium ion compared to sodium ion. The lack of dependence of D_{Cs^+} on water

sorption can then be understood by first noting that, as water sorption increases in Nafion, it enters only into ion-clustered regions.⁴¹ Thus tortuosity would not be reduced for a cation diffusion in peripheral regions of the aqueous clusters. Although these interpretations are speculative, it is clear that both spectroscopic and diffusional measurements indicate a more complete microphase separation into aqueous and fluorocarbon regions for the carboxylate compared to the sulfonate polymer.

Self-diffusion coefficients of polyvalent cations in these perfluorinated ionomer membranes have not been reported. It can be inferred from the use of the sulfonate membranes as Donnan dialysis devices that transport of cations such as Cu(II), Mg(II), and Al(III) under a concentration gradient is rapid.^{32,100,210} Also, column chromatographic separation of the alkaline-earth ion is readily accomplished with a powdered Nafion perfluorosulfonate polymer, which is again an indication of facile diffusion of these cations within the polymer phase.¹⁶⁰

Recently, several interesting studies of the electrochemical properties of electrodes coated with thin films of Nafion have been reported.^{26,58,89,126,157} These chemically modified electrodes are prepared using low-EW polymers which are alcohol soluble,^{26,126} or using a solution of a 1100-EW polymer which has been dissolved at high pressure and temperature.⁸⁸ Electrochemical studies for cations such as the $\text{Ru}(\text{bpy})_3^{3+/2+}$ couple yielded estimates of ionic diffusion coefficients in the polymer films. However, results also indicate that these films are far more porous than conventional Nafion membranes, so it is not possible to compare values directly with those discussed above.

2. Diffusion Properties in Concentrated Solution Environments

Industrial applications of perfluorinated ionomer membranes such as the electrolysis of sodium chloride solution to produce chlorine and sodium hydroxide often involve the use of highly concentrated solutions at elevated temperatures. The optimization of these systems depends upon a sound characterization of membrane transport processes under such conditions. Sodium ion is the major current-carrying species through the membrane in a chlor-alkali cell, and

some attention has been focused on its diffusional behavior in these environments.

The self-diffusion coefficient of sodium ion is plotted in Fig. 11 *vs.* the reciprocal of absolute temperature for the perfluorosulfonate and perfluorocarboxylate membranes which were discussed in Section III.1.^{149,168} Here though, the membrane environment consists of concentrated sodium hydroxide solutions of varying concentrations at temperatures of 70–90°C. Under these conditions,

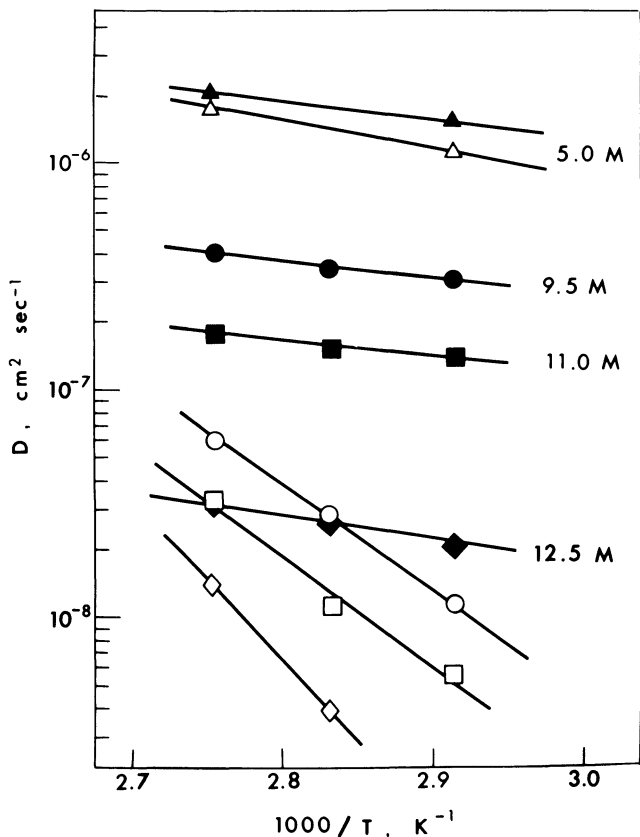


Figure 11. Sodium ion self-diffusion *vs.* the reciprocal of absolute temperature for perfluorocarboxylate (light symbols) and perfluorosulfonate (dark symbols) polymers in concentrated NaOH solution environments. (Refs. 149 and 168; reprinted by permission of the publisher, The Electrochemical Society, Inc.)

major differences between the two types of membrane are also seen, even for sodium ion diffusion, unlike the results for dilute solution environments.

In 5 M NaOH, the carboxylate now shows slightly lower values of the diffusion coefficients compared to the sulfonate membrane. This pattern is repeated for values measured with 4 M and 5 M NaCl solutions as well.¹⁴⁹ At higher NaOH solution concentrations, values for the carboxylate become much smaller, averaging

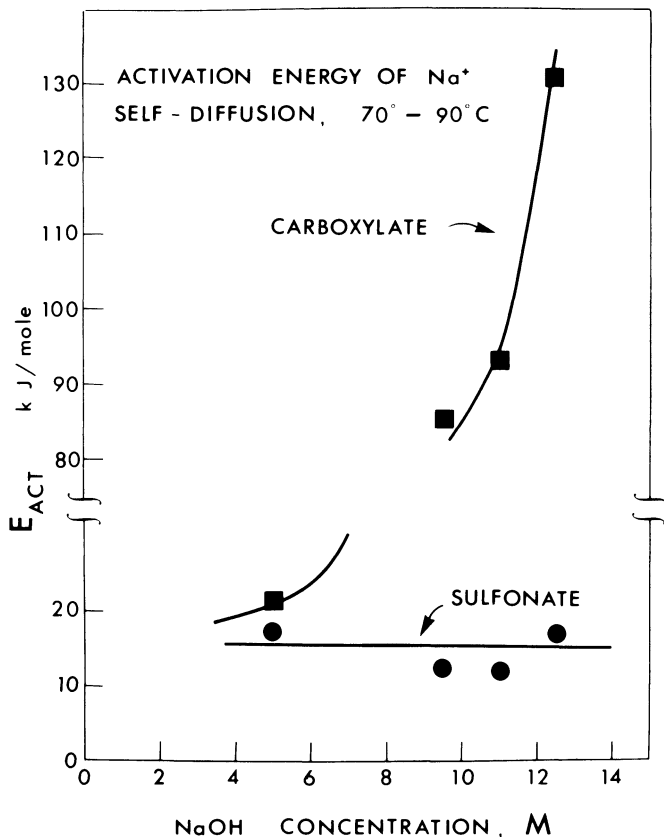


Figure 12. Activation energy of Na^+ diffusion in perfluorinated ionomer membranes vs. NaOH solution concentration, 70-90°C temperature interval. (Ref. 168; reprinted by permission of the publisher, The Electrochemical Society, Inc.)

about an order of magnitude lower than those for the sulfonate membrane. This is accompanied by a pronounced increase in the activation energy of diffusion for the carboxylate polymer, as shown in Fig. 12. It would appear that the mechanism of sodium ion diffusion changes for only the carboxylate polymer over this concentration region.

The results of ion and water sorption measurements for the two polymers under these solution conditions help to explain this difference. Table 5¹⁴⁹ lists the concentrations of various sorbed species and the mole ratio of water to cation/anion in the polymer phase for NaCl and NaOH solution environments. This ratio decreases both in the polymers and in solution with increasing concentration. In solution, the ratio varies from 10.8 to 4.0 over the concentration range of 5–12.5 M NaOH, so that ions in the polymer phase exist in a significantly less aqueous environment compared to the solution phase. As noted by Mauritz and co-workers⁹³ for perfluorosulfonate membranes, these water contents are insufficient to provide even primary hydration spheres for sodium ions, sorbed anions, and exchange sites, and the likelihood

Table 5
Equilibrium Sorption of Sodium Ion, Anion, and Water in
Perfluorinated Carboxylate and Sulfonate Polymers, 80°C^a

Polymer type	Solution	Polymer concentration (mol dm ⁻³)				mol H ₂ O/ mol Na ⁺
		Na ⁺	Cl ⁻	OH ⁻	H ₂ O	
Carboxylate	4.0 M NaCl	2.15	0.7		11.6	5.4
	5.0 M NaCl	2.18	0.7		10.2	4.7
	5.0 M NaOH	2.06		0.6	9.2	4.5
	9.5 M NaOH	3.06		1.6	8.2	2.7
	11.0 M NaOH	2.74		1.2	7.0	2.5
	12.5 M NaOH	3.36		1.9	5.8	1.7
Sulfonate	4.0 M NaCl	1.76	0.4		9.9	5.6
	5.0 M NaCl	1.92	0.5		8.9	4.6
	9.5 M NaOH	2.61		1.2	8.0	3.1
	11.0 M NaOH	2.72		1.3	7.7	2.8
	12.5 M NaOH	2.80		1.4	7.6	2.7

^a From Reference 149.

of ion pairs and higher ion multiples increases with decreasing water levels. The carboxylate polymer generally has even less water available for ionic hydration than the sulfonate, so that the stability of such species would be expected to be even stronger. An additional factor is the relative charge densities of the two types of exchange sites. While the perfluorosulfonate site is well known to be a very strong proton donor, the perfluorocarboxylate has a pK_a of about 2.¹⁴⁹ Thus, it is suspected that strong contact ion pairing in the case of the carboxylate is responsible for the low sodium ion diffusion coefficients and high diffusional activation energies. For the sulfonate, sodium ions that function as exchange-site counterions may be less strongly bound than for the carboxylate case, resulting in more facile sodium ion self-diffusion in the polymer.

Solution pH can also affect the diffusional properties of perfluorinated ionomer membranes. The perfluorosulfonate exchange site possesses very little basicity and thus these membranes can be used even in concentrated acid solutions. However, it has been shown that modified forms, in which the exchange sites are converted to sulfonamide groups, protonate at solution pH values below 13.¹⁶¹ This protonation severely reduces the ability of sodium ion to diffuse through the membrane. The exchange-site acidity of the perfluorocarboxylate membrane is far higher than that of the perfluorosulfonamide of course. Thus no protonation of exchange sites occurs in neutral or alkaline media. Protonation does occur in moderately acidic solutions however. Sodium ion diffusion flux in this membrane in a 5 M NaCl solution environment at 80°C is plotted *vs.* solution pH in Fig. 13.¹⁴⁹ Also plotted is the membrane sodium ion concentration, which begins to fall from the neutral solution value at a solution pH of 2.5. This correlates well with the calculated solution pH of membrane protonation according to the pK_a of the exchange sites. However, the membrane sodium ion diffusion flux drops by over an order of magnitude before this exchange-site protonation is seen. It would appear then that small amounts of protonation, on the order of 1-5% of membrane exchange sites, causes a pronounced loss in the ability of the membranes to transport counterions. Diffusion among clusters is accomplished through interconnecting regions of lower ion and water content, according to the cluster-channel model (Section II.4). If these regions were preferentially protonated, the overall

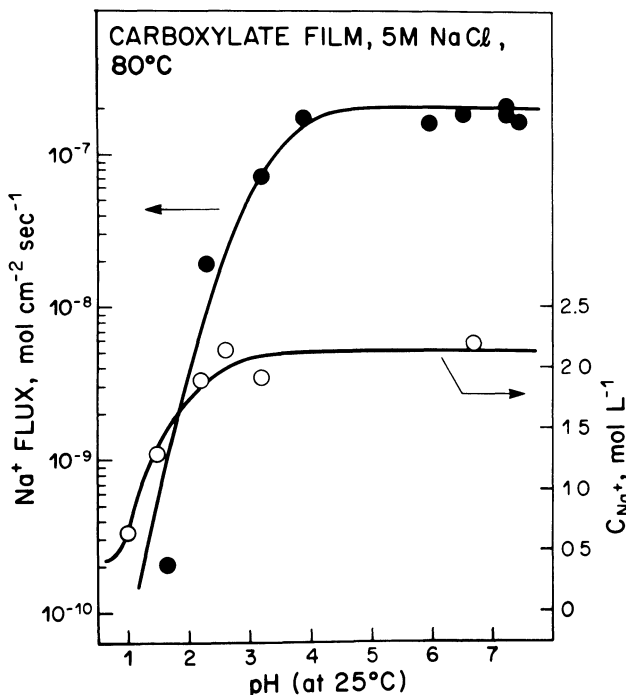


Figure 13. Na⁺ self-diffusion flux in a perfluorocarboxylate membrane and membrane Na⁺ concentration vs. solution pH, 5 M NaCl solution environment, at 80°C. (Ref. 149; reprinted by permission of the publisher, The Electrochemical Society, Inc.)

effect on sodium ion diffusion might well be what is observed experimentally. Although this interpretation is only speculative, it is evident that solution pH is an important consideration in the use of the perfluorocarboxylate membranes.

IV. TRANSPORT PROPERTIES UNDER INDUSTRIAL ELECTROLYSIS CONDITIONS

The most important commercial application of perfluorinated ionomer membranes is currently in the chlor-alkali industry. These materials are used as permselective separators in brine electrolysis cells for the production of chlorine and sodium hydroxide. This

approach to chlor-alkali manufacture is now economically competitive with the two older technologies of asbestos diaphragm and mercury cathode cells. However, developing a sound scientific basis for understanding membrane dynamic properties under industrial electrolysis conditions still presents a formidable challenge as this important technology is brought to full commercialization.

The membrane in a chlor-alkali electrolysis cell experiences rather harsh operating conditions. The anolyte solution consists of 2–5 *M* NaCl solution which is mildly acidic and is mixed with evolving chlorine gas. The catholyte solution contains 6–17 *M* NaOH (20–45 wt %) and hydrogen gas from the reduction of water. Cell temperature and current densities are typically in the ranges of 80–90°C and 0.2–0.5 A cm⁻², respectively. While the perfluorinated sulfonate and carboxylate membranes are indefinitely stable, even under these operating conditions, they are subject to rather severe physical forces during electrolysis. Thus, electrolyte and water sorption, transport properties, and even polymer morphology might be expected to differ from those seen under near-equilibrium, dilute-solution conditions. Also, the slow accumulation of brine impurities within the membrane phase affects its properties. Thus, performance is a function of many variables, some of which are related to cell operating conditions and others which are a function of membrane composition.

1. Characteristics of Perfluorinated Chlor-Alkali Membranes

Through the intense research efforts of a small number of companies over the past 10 to 15 years, several types of high-performance perfluorinated membranes have been developed for chlor-alkali production.^{49–52,62,86,97,98,129,132,133,143,145,146,150,151,211} As discussed in Section I.2, the requirements of these membranes are several: good physical strength, chemical inertness, high rejection of hydroxide transport, and low electrical resistance. The degree to which a given material satisfies these requirements generally depends on cell parameters such as brine and caustic concentrations, temperature, and current density, and no single type has superior performance over all conditions.

Three types of perfluorinated chlor-alkali membranes are noteworthy. The first of these, the homogeneous carboxylate films,

show high current efficiencies, even at the highest concentrations of caustic. Bilayer or multilayer membranes comprise a second type. Here each layer has either sulfonate or carboxylate functionality, with perhaps different equivalent weights of polymer in each layer. For this type, the carboxylate layer is always in contact with the catholyte for effective hydroxide rejection. A third type is related to the second in that a carboxylate layer is combined with a sulfonate layer to yield high current efficiency and strength but low electrical resistance. Here though, the layer is created by chemical treatment of a sulfonate film so that the carboxylate layer is now very thin (on the order of 2–10 μm). This type shows optimum performance at somewhat lower caustic concentrations than the first and second types.

Thus all successful chlor-alkali membranes currently employ a perfluorocarboxylate polymer to lower the rate of hydroxide ion transport. The sulfonate portion of some of these membranes is present mainly to add strength to the thinner carboxylate barrier layer. Fabric backing is also used in some cases to improve physical strength.

Homogeneous or bilayer membranes of only sulfonate functionality can yield reasonably high current efficiencies if a high-EW polymer faces the catholyte. Unfortunately, large electrical resistances also result with such materials. Surface treatment of a sulfonate membrane to yield a layer of sulfonamide exchange sites¹⁸⁷ also produces a membrane with improved current efficiency. However, these sites are slowly hydrolyzed in an operating cell, so that this approach is not commercially viable.

2. Membrane Permselectivity in a Chlor-Alkali Cell

The ability of these perfluorinated ionomer membranes to limit migration of hydroxide ion into the anolyte is of course a central feature of their success in this new technology. However, this phenomenon is a function of many membrane and cell variables, and a satisfactory theoretical description of the nature of this permselectivity has not yet emerged. Certain features of hydroxide rejection are understood though. First, membrane water content shows a strong correlation with permselectivity; those membranes with lower weight percentages of sorbed water under cell operating

conditions invariably show higher current efficiencies. Second, membrane current efficiency shows a pronounced and complicated dependence on sodium hydroxide catholyte concentration. Finally, brine concentration, current density, and temperature also influence membrane performance in a complex manner, but their effects are generally less pronounced than that of catholyte concentration.

Some of these features are illustrated in Figures 14–18. A rather typical literature plot of current efficiency *vs.* sodium hydroxide concentration for perfluorosulfonate membranes is shown in Fig. 14.⁶² Nafion 427 is a 1200-EW sulfonate membrane with fabric reinforcement. Poor hydroxide rejection occurs at catholyte concentrations above 10 wt % but a minimum is seen at higher concentrations, with increasing current efficiency from 28 to 40% caustic (9–14 *M*). The current efficiency of a 1200-EW homogeneous perfluorosulfonate film is shown in more detail over this concentration region in Fig. 15.¹⁷⁰ Sodium ion transport number (t_{Na^+} , mol F^{-1}), which is equivalent to caustic current efficiency, is plotted *vs.* both brine anolyte and caustic catholyte concentration. These values were determined using radiotracer techniques, which have proven to be rapid and accurate methods for the determination of membrane performance.^{24,137,149,164,167,168} A rather sharp maximum is seen at 14 *M* NaOH, and the influence of brine con-

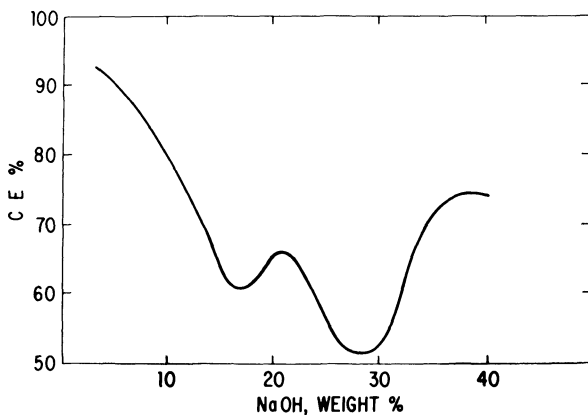


Figure 14. Current efficiency *vs.* catholyte concentration for Nafion 427 perfluorosulfonate membrane. (Ref. 62; reprinted by permission of the publisher, The Electrochemical Society, Inc.)

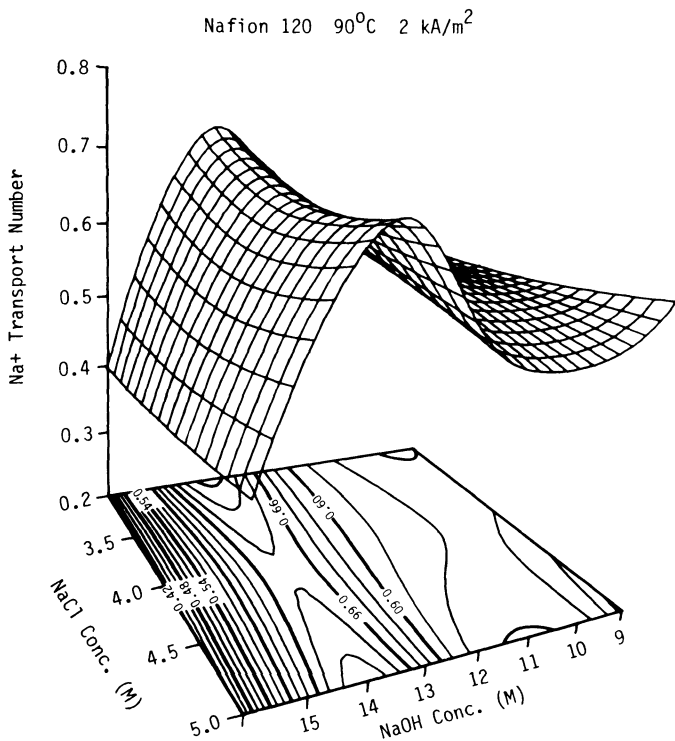


Figure 15. Sodium ion transport number for Nafion 120 vs. brine anolyte and caustic catholyte concentrations (Ref. 170).

centration on the maximum is rather minor. Figure 16 shows results for the same membrane at a higher current density and lower temperature. These parameters affect the maximum value of t_{Na^+} and the overall shape of the surface.

In Figure 17, sodium ion transport number is plotted vs. catholyte concentration for a homogeneous perfluorocarboxylate film. The current efficiency is now higher than 90% over the entire caustic concentration region studied, although a minimum and maximum in performance is again observed. These features are shifted to lower concentration compared to perfluorosulfonate behavior though. Finally, the performance of a sulfonate-carboxylate bilayer membrane, Nafion 901, is plotted in Fig. 18. For such

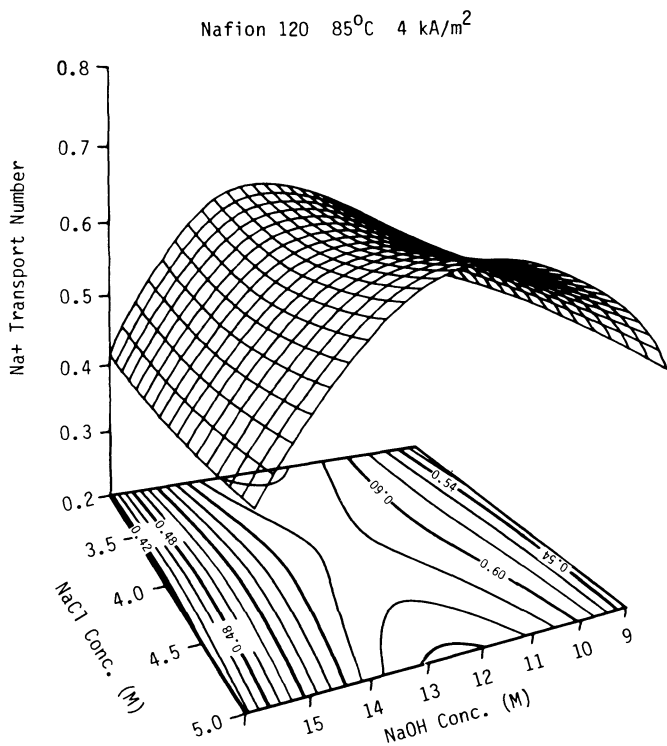


Figure 16. Sodium ion transport number for Nafion 120 vs. brine anolyte and caustic catholyte concentrations (Ref. 170)

a material, the more permselective carboxylate layer faces the catholyte solution. Performance in this configuration should be very similar to that of the carboxylate film alone, according to the treatment by Krishtalik.⁷⁷ Similarities are evident in Figures 17 and 18, in support of this conclusion.

3. Interpretation of Permselectivity as a Function of Membrane Properties and Cell Parameters

Several approaches to the understanding of membrane permselectivity can be taken; these include the use of the Nernst-Planck transport equations,^{72,117,212} irreversible thermodynamics,³⁵ and

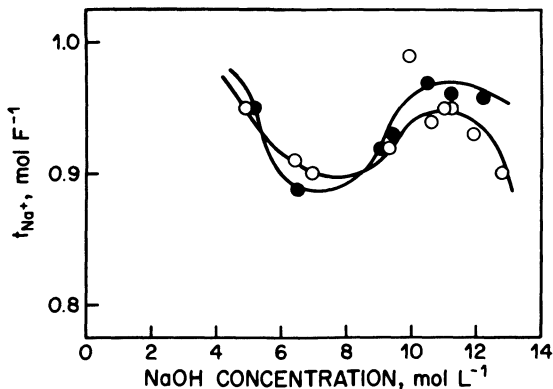


Figure 17. Sodium ion transport number vs. caustic catholyte solution for a perfluorinated carboxylate membrane: (●) anolyte is 5 M NaCl; and (○) anolyte and catholyte are identical concentrations of NaOH. (Ref. 149; reprinted by permission of the publisher, The Electrochemical Society, Inc.)

theories which incorporate morphological and chemical properties of these perfluorinated ionomers to explain performance. Emphasis is placed on the latter type here, for these provide some insight into the molecular basis of permselectivity.

The dependence of current efficiency on polymer structure was first analyzed by Gierke,⁴⁵ based on his cluster-channel model (Section II.4). The current efficiency is given as the ratio of cation flux to total ionic flux. The flux is determined by the ion mobility and the ion concentration in the membrane, and the potential barrier. He calculated the size of the electrostatic potential energy barrier from the Poisson-Boltzmann equation. This barrier energy is added to the activation energy for migration. He employed absolute rate theory to describe the relative reduction in anion mobility. The model correlates well the increase of current efficiency with increase of polymer EW by considering the relative mobilities as a semiempirical and adjustable parameter. Reiss and Bassignana¹¹⁷ have, however, pointed out many shortcomings of Gierke's approach.

Several new developments in interpreting the transport properties, based on the structural parameters, have been reported by Koh

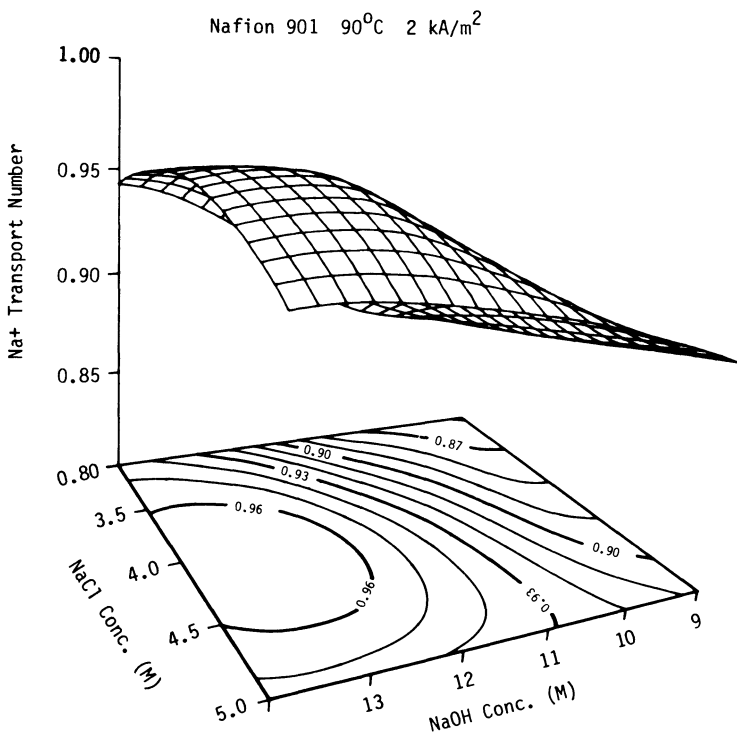


Figure 18. Sodium ion transport number for Nafion 901 *vs.* brine anolyte and caustic catholyte concentrations. (Ref. 168; reprinted by permission of the publisher, The Electrochemical Society, Inc.)

and Silverman,⁷² Reiss and Bassignana,¹¹⁷ and Yeo.¹⁸³ These results generally suggest that the high local concentration of fixed ion (or surface charge density) in these perfluorinated ionomer membranes is the primary factor in providing the extraordinary permselectivity in concentrated solutions.

Mauritz and co-workers^{60,74,75,93,94} and Hopfinger⁶¹ have reported spectroscopic and sorption studies of perfluorosulfonate membranes. Several conclusions drawn in these studies are useful in the interpretation of current efficiencies as a function of caustic solution concentration. Sorption measurements of an 1100-EW film in equilibrium with NaOH solutions from 7.5 to 18 M show that the

NaOH/SO₃Na ratio remains virtually constant at about 0.27. Membrane water content decreases with increasing solution concentration though, so that a steadily decreasing water-to-ion ratio results. This ratio indicates that even the primary hydration requirements of Na⁺, OH⁻, and sulfonate ion-exchange sites are not met within the membrane over most of this concentration range. A continuous infrared absorbance below 3500 cm⁻¹ is assigned to proton tunneling events in the H₃O₂⁻ grouping. For a 1500-EW membrane, this continuous absorbance initially rises with caustic concentration but goes through a maximum at about 10 M. A sharp minimum in absorbance is observed at 14 M solution concentration, followed by an abrupt increase. Thus, the concentration dependence of this infrared absorbance is notably similar to that of current efficiency for a perfluorosulfonate film (Figs. 14-16). If the magnitude of continuous absorption is indicative of the extent of hydroxide transport by a type of Grotthus chain mechanism, then a qualitative explanation for the complicated concentration dependence of current efficiency could be provided.

As discussed by Mauritz and Gray,⁹⁴ the initial rise in infrared absorbance at lower caustic concentration is simply due to the onset of NaOH sorption into the polymer. With increasing solution concentration and membrane dehydration, however, proton tunneling events decrease. In this concentration region, the remaining water molecules would be present mainly in solvent-separated ion pairs. Here the electrostatic field of the ion pair would serve to localize proton position and reduce the frequency of tunneling events. At the highest external solution concentrations, proton transfer processes are suspected to occur between sulfonate groups and the remaining water molecules in the polymer, yielding the final increase in absorbance. Thus the complicated concentration dependence of current efficiency for perfluorosulfonate membranes, referred to above, may be a reflection of the dependence of various proton tunneling mechanisms on the amount of hydration water in the membrane.

An important question is why the perfluorinated carboxylate polymer presents a much more effective barrier to hydroxide ion transport compared to the sulfonate analogue, for any caustic concentration used. There may be several factors involved. First, a more complete phase separation of the ion-clustered regions for

the carboxylate, as inferred from various types of measurements, would be expected to increase the degree of rejection in terms of the cluster-network model. Smaller cluster sizes, larger numbers of interconnecting channels, and less unincorporated exchange sites and water would all lead to more effective hydroxide blockage. Also, the lower inherent water content and higher exchange-site charge density for the carboxylate polymer produce a greater extent of ion pairing. As concluded from infrared studies, this discourages proton tunneling events which enhance hydroxide ion migration. Ultimately though, carboxylate-water interactions would be expected to reduce permselectivity at highest caustic strengths, in analogy to sulfonate-water interactions. Thus a combination of differences in morphology and water sorption are seen as central factors in the relative permselectivities of perfluorinated carboxylate and sulfonate polymer membranes.

Electroösmotic effects also influence current efficiency, not only in terms of coupling effects on the fluxes of various species but also in terms of their impact on steady-state membrane water levels and polymer structure. The effects of electroösmosis on membrane permselectivity have recently been treated through the classical Nernst-Planck flux equations,²¹³ and water transport numbers in chlor-alkali cell environments have been reported by several workers.^{35-37,73,86,149,164,213,214} Even with classical approaches, the relationship between electroösmosis and permselectivity is seen to be quite complicated.²¹³ Treatments which include molecular transport of water can also affect membrane permselectivity, as seen in Fig. 17. The different results for the two types of experiments here can be attributed largely to the effects of osmosis. A slight improvement in current efficiency results when osmosis occurs from anolyte to catholyte. Another frequently observed consequence of water transport is higher membrane conductance,^{133,146,214} which is an important factor in the overall energy efficiency of an operating cell.

V. CONDUCTIVITY AND PERMEABILITY IN MEMBRANES

The perfluorinated ionomer membranes are widely used as separators in electrolytic and fuel cells. A primary consideration

in such applications is the membrane conductivity, because ohmic losses due to membrane resistance can significantly increase energy consumption of the electrolytic cell and energy loss of the fuel cell. Extensive studies of the conductivities of conventional Nafion membranes in various industrially important electrolytes have been carried out in several laboratories in recent years. The conductivity of the carboxylate membranes has been studied only in alkaline electrolytes because of its primary application in the chlor-alkali industry.

1. Conductivity in Pure Water—Solid Polymer Electrolyte Systems

In the dry state Nafion behaves like an insulator.^{63,183} However, the membrane becomes conductive when hydrated. Figure 19 shows the conductivity of hydrated Nafion,¹⁸³ along with that of several polymers containing sulfonic acid groups,^{8,116,215} as a function of water content. The Nafion polymer becomes conductive when it is exposed to the atmosphere and absorbs $\sim 6\text{H}_2\text{O}/\text{SO}_3^-$ of moisture. It has been shown that membranes with this amount of hydration have sufficient conductivity for use as a semisolid proton conductor in WO_3 -based electrochromic displays.¹¹⁶ The water content of the membrane further increases after immersion in water, resulting in higher conductivity. This membrane conductivity is regarded as the intrinsic conductivity because it stems from the strong acidity of the materials [Section II.5(iv)]. The solid curve is calculated from the Bruggemann equation²¹⁶:

$$\kappa = 0.54\kappa_e(1 - V_p)^{1.5} \quad (11)$$

where V_p is the volume fraction of polymer and κ_e is considered as the conductivity of sulfuric acid with concentration equal to that of the sulfonic acid group of the membrane. Equation (11) implies that κ is a strong function of V_p . This is supported by the fact that the conductivity of the E-form membrane is higher than that of N-form samples, despite the fact that the latter has a higher value of κ_e .¹⁸³

Table 6 compares the conductivity of various polymers and electrolytes containing sulfonic acid groups. The intrinsic conductivity of Nafion is high and is very similar to other polymers containing sulfonic acid groups. The activation energy of proton conduction of Nafion is low in comparison with other polymers,

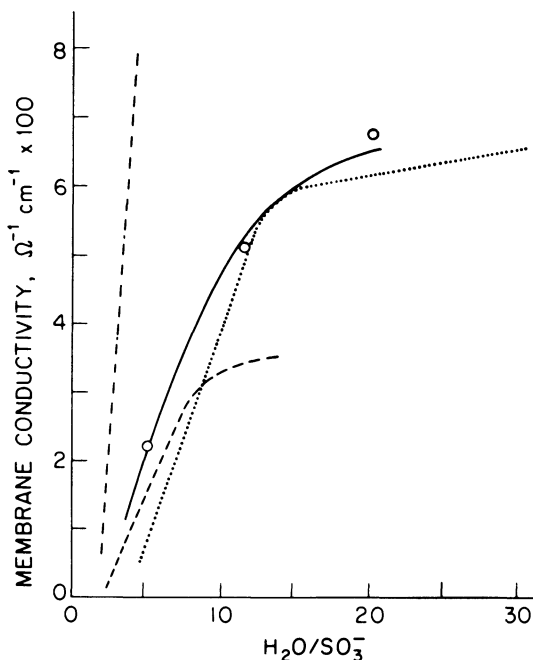


Figure 19. Conductivity of ion-containing polymers as a function of water content: (○) Nafion; (—) calculated from Eq. (11); (···) polystyrene sulfonic acid; (---) poly-2-acrylamido-2-methylpropane sulfonic acid; (-·-) polyethylene sulfonic acid. (Ref. 182; reprinted by permission of the publisher, The Electrochemical Society, Inc.)

presumably because the water in Nafion is not strongly hydrogen bonded [Section II.5(iii)]. This high intrinsic conductivity, together with the strong hydrophilicity [see Section II.5(ii)], makes Nafion an excellent “electrolyte” for many electrochemical applications. At present, this polymer is employed as the SPE in many electrochemical cells.²¹⁷ Besides, many new ideas of using this polymer as electrolyte have been suggested. It has been shown that Nafion has potential for use as a solid “superacid” catalyst for many electroorganic syntheses^{67,103-107} as well as a conductive polymer coating for electrodes.^{26,27,58,89,126,157}

In SPE cells, electrocatalyst particles are bonded to the membrane surfaces. It is important to mention that good bonding

Table 6
Conductivity for Some Ion-Containing Polymers in Water^a

Polymers	IEC ^b	κ ($\Omega^{-1} \text{ cm}^{-1}$)	E_a^c	References
Nafion	0.83	0.06	9.41	183
AMPS ^d	—	0.03	19.25	116
PESA ^e	—	0.08	19.25	116
PSSA ^f	1.97	0.09	—	8
PSA ^g	2.00	0.04	—	8

^a From Reference 182.

^b IEC is the ion-exchange capacity (meq g-polymer⁻¹).

^c E_a is the activation energy (kJ mol⁻¹).

^d AMPS is poly-2-acrylamido-2-methylpropane sulfonic acid (water soluble).

^e PESA is polyethylene sulfonic acid (water soluble).

^f PSSA is polystyrene sulfonic acid.

^g PSA is phenol sulfonic acid.

between electrode and membrane is essential, because any water film and gaseous products which exist between the electrode and membrane surface can produce an extremely high contact resistance. Although deionized water is the only fluid circulated through the SPE water electrolyzer, the environment that the electrodes encounter is highly acidic. The sulfonic acid groups at the membrane surfaces produce an acidity equal to 20 wt % sulfuric acid [Section II.5(iv)]. Because of this acidic medium, acid-resistant noble metals or their oxides are utilized as anode materials,^{156,218} while platinum serves as the cathode material.⁷⁹

The perfluorinated carboxylic acid membrane exhibits a higher resistance than Nafion membranes in SPE water electrolyzers.²¹⁹ This is primarily due to small membrane swelling and slight dissociation of the carboxylic acid group in water or acid electrolyte with a pH < 2.^{178,181}

2. Conductivity in Acidic Electrolytes

The conductivities of Nafion in HCl and HBr have been studied extensively by Yeo *et al.*^{174,175} Results for E-form Nafion in HBr are given in Fig. 20. There are several features noteworthy. First, membrane conductivity is about one order of magnitude less than the electrolyte conductivity due to the large volume fraction of

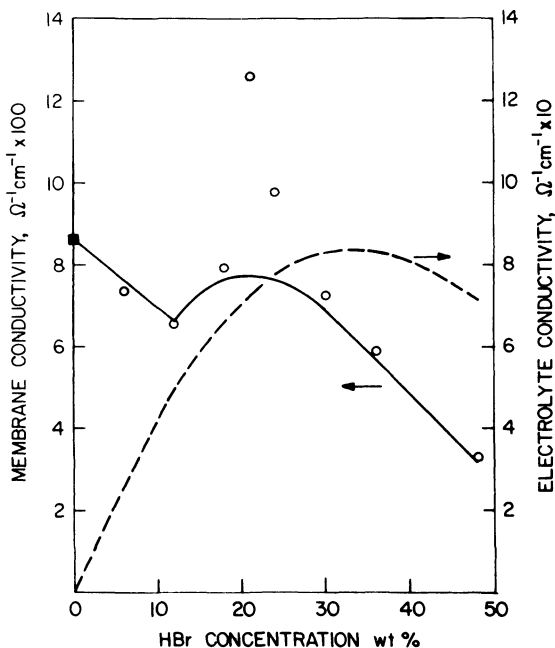


Figure 20. Membrane (—) and free-acid (---) conductivity as a function of HBr concentration: (■) H₂O and (○) HBr. (Ref. 175; reprinted by permission of the publisher, The Electrochemical Society, Inc.)

nonconductive material in the membrane. Second, the membrane has a maximum conductivity at lower acid concentration as opposed to the conductivity maximum for the acids. This maximum conductivity occurs because the hydrogen ion concentration decreases at low acid concentrations and the water content of the membrane decreases with increasing acid concentrations. Another salient feature is that, for electrolytes of less than 0.3 in molarity, the membrane conductivity is higher than the electrolyte conductivity because the intrinsic conductivity of the membrane becomes important.¹⁸³

If one considers that the mobility for diffusion is the same as that for conductance, which is particularly true for the cases of water and dilute solutions, then the diffusivity can be related to the

conductivity by the Nernst–Einstein equation²²⁰:

$$C_i = \frac{1000\kappa RT}{D F^2} \quad (12)$$

where κ is the equivalent conductance and C_i is the concentration of the mobile ions; R , T , and F have their usual meanings. The conductivity of Nafion in varying HCl electrolytes has been reported previously,¹⁷⁴ while the diffusivity data was shown in Table 3. Hence, the concentration of mobile ions in Nafion in equilibrium with various HCl concentrations can be calculated from Eq. (12) and the results are shown in Table 7. The concentration of fixed ions calculated from Eq. (8), based on the ion-cluster model are also included in Table 7 for comparison. It is clear that the transport data support the ion-cluster morphology suggestion for Nafion [Section II.3(ii)].

As expected, the membrane conductivity is improved at elevated temperatures¹⁷⁴ due to the increase in electrolyte uptake and, to a lesser degree, the increase of the electrolyte conductivity. An improvement in the performance of HCl cells by the better membrane conductivity at elevated temperatures has been observed.²²¹ This is an excellent example since the electrode kinetics of the hydrogen and chlorine reactions are fast and the only “overpotential” is ohmic.

The conductivity of these perfluorinated membranes has been found to be affected strongly by the history of treatment of the membrane.^{174,175} As shown in Table 8, the conductivity increases in the order S-form < N-form < E-form. It is apparent that elec-

Table 7
Comparison of Ionic Charge Concentrations Derived from Transport and Uptake Measurements^a

Electrolyte concentration	Calculated from Eq. (8)	Calculated from Eq. (12)
0% HCl	5.21 mol dm ⁻³	8.08 mol dm ⁻³
10% HCl	7.13	12.05
20% HCl	9.40	11.52
25% HCl	11.21	12.76

^a From Reference 182.

Table 8
Effect of Pretreatment on Conductivity
of Nafion Membrane in 24% HBr^a

Sample	W_e	κ
E-form	25.9	0.098
N-form	17.8	0.076
S-form ^b	11.4	0.035

^a From Reference 175.

^b Dried in vacuum at 140°C.

trolyte uptake is an important factor in determining membrane conductivity and the voltaic efficiency of many membrane cells.

Yeo and Chin¹⁷⁵ have observed that the membrane hysteresis effect occurs when the change of electrolyte concentration is faster than the change of concentration in the membrane, which is controlled by the diffusion of electrolyte in the membrane. The electrolyte content in the membrane does not reach its equilibrium value under this condition. The authors have thus suggested various methods for controlling this hysteresis effect and the electrolyte content of the membrane, so that a higher cell efficiency can be obtained.

3. Conductivity in Alkaline Electrolytes

Most studies of membrane conductivity in alkaline electrolytes have been carried out in concentrated solutions.^{63,77,96,133,142,146,176,222} The conductivity of Nafion in concentrated alkaline solutions is generally one order of magnitude smaller than that in pure water or in acid electrolytes, because the membranes absorb far less electrolyte when in neutralized form, as shown by Eq. (6).

The effect of NaOH concentration and temperature on the swelling and conductivity of Nafion has been recently studied by Men'shakova *et al.*⁹⁶ The influence of NaOH concentration on the membrane conductivity is rather similar to the case of acid electrolytes in that a conductivity maximum occurs. The authors found that the conductivity maximum of the membrane is at ~20% NaOH, i.e., close to the concentration where one observes the conductivity maximum of the free electrolyte.⁹⁶ However, the conductivity decrease following the maximum is more drastic in the membranes

than in solutions of the same concentration. The low conductivity of concentrated solutions is ascribed to the less hydrated state of the membrane. It has been pointed out that this is evidence for stronger binding of the mobile ions by the matrix at lower water contents in the matrix.

It has been recently reported¹⁴² that Nafion membranes show an ohmic behavior in 5 M NaOH, while in 10 M NaOH solution the specific conductance of the membranes increases with increasing current density. It is suggested that the passage of high currents at a severely dehydrated membrane may produce morphological changes that alter the character of the ionic conduction paths in the polymer. Hsu *et al.*⁶³ have observed that the membrane conductivity of Nafion in alkaline electrolyte exhibits ion percolation behavior and can be described by

$$\kappa = \kappa_e(1 - V_p - V_T)^{1.5} \quad (13)$$

where V_T is the threshold volume fraction of the aqueous phase and κ_e is the electrolyte conductivity. There is an (ionic) insulator-to-conductor transition in Nafion around V_T . Based on the percolation theory, V_T is 0.15 whereas an experimental value of 0.10 for Nafion in NaOH electrolyte is observed. It is interesting to note that Eq. (13) resembles the Bruggeman equation and Eq. (11) if $V_T = 0$.

The Flemion membrane behaves somewhat differently in that the conductivity maximum appears at a concentration of less than 12 wt % NaOH.¹⁴⁶ The membrane conductivity decreases with increasing caustic concentration; this is ascribed to the decrease in ionic mobility which is caused by the loss of water in the membrane. The very low value of the conductivity and the high value of the activation energy in a 40% caustic solution implies that there exists a strong interaction between counterions and fixed ions in the membrane. Figure 21 compares the conductivity of the sulfonate and carboxylate membranes in NaOH. For the same IEC and electrolyte concentration, the sulfonate membrane is more conductive than the carboxylate membranes,^{133,146} primarily because sulfonate samples absorb more electrolyte. However, the carboxylate membranes of high IEC exhibit higher conductivity than the sulfonate samples because the IEC of the carboxylate materials can be higher than that of the sulfonate polymer in membrane forms.

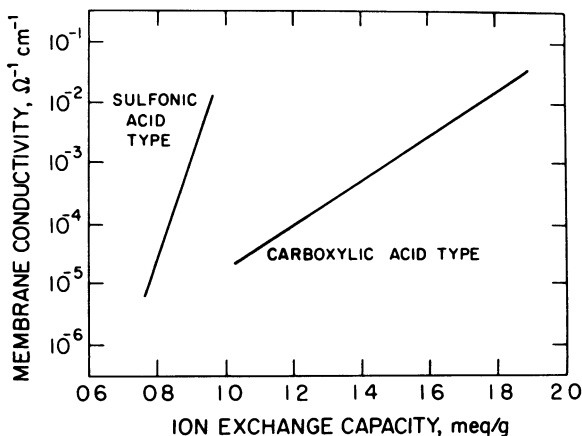


Figure 21. Dependence of membrane conductivity on ion-exchange capacity for perfluorosulfonate and carboxylate membranes, in 35% NaOH, at 90°C. (Ref. 146; reprinted by permission of the publisher, The Electrochemical Society, Inc.)

Yeo *et al.* have reported¹⁷⁶ an analysis of the conductivity of Nafion in different alkaline electrolytes, based on the correlation of membrane conductivity with water content. The analysis reveals that larger conductivities arise when the membranes are equilibrated with NaOH solutions than with KOH solutions of equal molarity. Also, it is shown that better conductivity can be realized with thinner and lower-EW membranes. These effects have been proven in an alkaline-water electrolyzer¹⁷⁶ and in relation to the conductivity

Table 9
Effect of Pretreatment on Conductivity of Nafion
Membrane in 40% KOH^a

Temperature (°C)	Pressure (atm)	W_e (wt %)	κ ($\Omega^{-1} \text{ cm}^{-1}$)
100	1.0	28.2	1.15×10^{-4}
150	4.9	38.8	0.011
150	35.2	86.4	0.046
175	35.2	116.2	0.071
200	703.0	370.0	0.200

^a From Reference 222.

results of Bratin and Tomkiewicz.²³ It has been reported^{142,222} that the conductivity of Nafion membrane can be increased considerably by soaking the membrane in water at temperatures above 100°C and at elevated pressure, as shown in Table 9. The membrane is fully swollen and the electrolyte uptake is high with such pretreatments. In general, membrane conductivity exhibits Arrhenius behavior: the activation energy data for ion conduction of Nafion in various electrolytes are summarized in Table 10, whereas in Table 11 data are compared for carboxylate and sulfonate membranes.

Table 10
Conductivity of Nafion Membrane of 1200 EW in Various Electrolytes^a

Electrolyte concentration	Electrolyte uptake	Conductivity at 25°C ($\times 10^3 \Omega^{-1} \text{cm}^{-1}$)	E_a ^b	References
H ₂ O	7.8	22.8	9.46	183
H ₂ O	17	52.2	9.46	183
H ₂ O	30	68.0	9.37	183
5% HCl	12.9	58.8	10.33	174
10% HCl	11.9	62.5	11.59	174
15% HCl	10.5	46	10.75	174
22% HCl	8.8	23	11.59	174
26% HCl	7.8	14.3	16.95	174
30% HCl	6.8	6.8	13.47	174
37% HCl	4.8	3.9	15.69	174
4.5% KCl	7	3.93	12.07	49
25% NaCl	10	5.3	17.74	49
5.4% KOH	6.0	1.7	25.02	82
0.4% NaOH		5.7	—	77
5% NaOH	12.8	6.0	15.43	96
10% NaOH	12.1	9.3	14.86	96
20% NaOH	9.6	9.7	13.08	96
30% NaOH	8.4	6.0	15.43	96
40% NaOH	8.1	1.0	17.79	96
17% NaOH		—	10.0 ^c	142
30% NaOH		—	10.0 ^c	142

^a From Reference 182.

^b E_a is the activation energy (kJ mol^{-1}).

^c For Nafion of 1150 EW and a temperature range of 100–180°C.

Table 11
Conductivity of Perfluorinated Ionomer Membranes in
35% NaOH^a

Membrane	Ion-exchange capacity (meq g ⁻¹)	Conductivity at 25°C (×10 ⁴ Ω ⁻¹ cm ⁻¹)	Activation energy (kJ mol ⁻¹)
Sulfonate	0.82	1.6	38
	0.91	21	40.6
Carboxylate	1.23	2.3	64
	1.48	8.5	60
	1.70	87	50
	1.88	300	43.5

^a From Reference 146.

4. Conductivity of Nafion in Protic Solvents

The membrane conductivity of Nafion in various protic solvents has been measured in a recent study¹⁷⁹ and the results are given in Table 12. The ratio of the membrane conductivity (κ) to the solvent conductivity (κ_e) is listed in the last column of the table. A plot of the conductivity ratio (κ/κ_e) vs. the solubility parameter of the solvent is shown in Fig. 22. The membrane conductivity is higher than the solvent conductivity in all solvents except formamide,

Table 12
Conductivity of N-form Nafion in Protic Solvents^a

Solvent	Solubility parameter ^c	κ_e (Ω ⁻¹ cm ⁻¹)	κ (Ω ⁻¹ cm ⁻¹)	κ/κ_e
Water ^b	23.4	1.6×10^{-6}	6.8×10^{-2}	4×10^4
Formamide	19.2	4.3×10^{-4}	1.6×10^{-4}	0.4
Glycerol	16.5	4.4×10^{-6}	7.5×10^{-6}	1.7
Ethylene glycol	14.6	1.6×10^{-6}	1.1×10^{-5}	6.9
Methanol	14.5	2.3×10^{-5}	6.8×10^{-5}	2.2
Ethanol	12.7	1.66×10^{-6}	1.94×10^{-5}	11.7
1-Propanol	11.9	1.72×10^{-6}	1.88×10^{-5}	10.9
2-Propanol	11.5	2.7×10^{-6}	1.17×10^{-5}	4.3
<i>i</i> -Amyl alcohol	10.0	1.9×10^{-6}	2.9×10^{-6}	1.5

^a From Reference 179.

^b E-form.

^c Units: (cal/cc)^{1/2}.

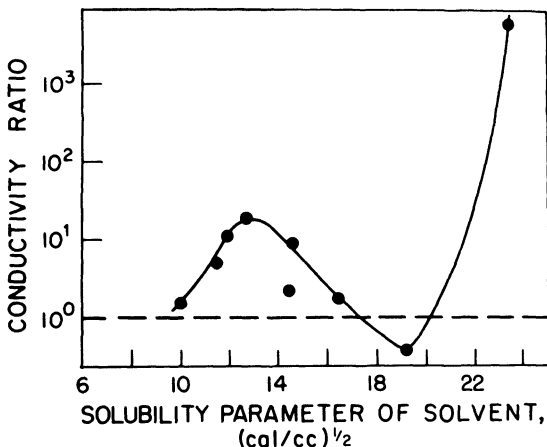


Figure 22. Conductivity ratio (κ/κ_e) of Nafion vs. solubility parameter of solvents. (Ref. 179; reprinted by permission of the publisher, The Electrochemical Society, Inc.)

presumably because of the high dissociation of the ionic groups in these protic solvents and the appearance of the intrinsic conductivity. Also, the membrane exhibits an extraordinarily high conductivity in water. This is the reason why this material is used as an “electrolyte” layer in SPE cells (see Section V.1).

5. Permeation of Molecular Species

The passage of a gas through a membrane takes place via a diffusion mechanism. The gas dissolves in the membrane on the high-pressure side, and desorbs out of the membrane on the low-pressure side. The electrolyte uptake of the membrane plays an important role in gas diffusion since it is primarily in the aqueous phase that the gas dissolves. The coulombic loss in the cell is related to the membrane diffusion current, which is determined by the permeation of the gases and is given by

$$i_D = nFDc_0/L \quad (14)$$

where D is the diffusion coefficient, c_0 the concentration of the

species in the membrane, and L the thickness of the membrane; n and F have their usual meanings.

(i) *Diffusion of Hydrogen and Oxygen in Nafion*

The permeability of hydrogen and oxygen through the membrane contributes to parasitic power loss and may affect long-life performance of cells such as water electrolyzers and hydrogen-oxygen fuel cells. The permeations of hydrogen and oxygen through Nafion have been studied by LaConti *et al.*⁷⁹ The permeabilities of both hydrogen and oxygen increase with increasing temperature and with increasing membrane water content, as shown in Figures 23 and 24. Furthermore, the permeation rates of these molecular species also increase with increasing cell operating pressure²²³ and with thinner membranes.

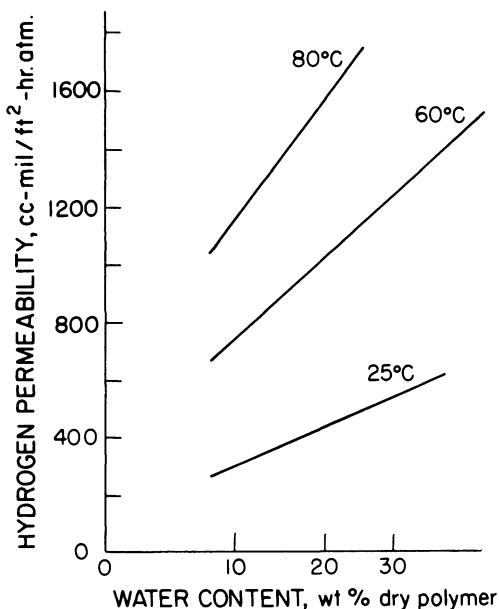


Figure 23. Hydrogen permeability of Nafion as a function of membrane water content. (Ref. 79; reprinted by permission of the publisher, The Electrochemical Society, Inc.)

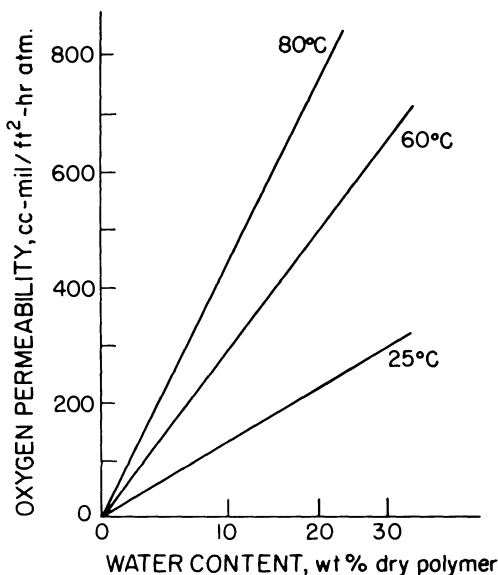


Figure 24. Oxygen permeability of Nafion as a function of membrane water content. (Ref. 79; reprinted by permission of the publisher, The Electrochemical Society, Inc.)

(ii) Diffusion of Chlorine and Bromine in Nafion

Nafion membranes have been used as separators in the hydrogen-chlorine cell,¹⁷⁴ hydrogen-bromine cell,¹⁷⁵ and zinc-bromine cell¹⁵⁸ because of their excellent chemical inertness in these aggressive environments. The function of the separator in these cells, similar to that in a water electrolyzer, is the separation of the molecular species, such as hydrogen, chlorine, bromine, and metallic zinc, which cause self-discharge and efficiency loss when they migrate across the separator.

Yeo and McBreen¹⁷⁴ measured the diffusion coefficients of hydrogen and chlorine in Nafion immersed in HCl solutions, and that of bromine in HCl and HBr solutions as a function of electrolyte concentration and temperature. In concentrated HCl solutions, the order of diffusion coefficients is hydrogen > chlorine > bromine, as expected from the molecular sizes. Activation energies for

diffusion of hydrogen and chlorine in 4.1 M HCl were found to be 21.6 and 23.3 kJ mol⁻¹, respectively, over the temperature range of 25–50°C. These values are very similar to those for water diffusion in the same membrane in dilute solutions (see Section III.1). Figure 25 shows the diffusion coefficients of chlorine and bromine in Nafion for varying acid concentration. The diffusion rate decreases with increasing acid concentration. This is due to the decrease of the electrolyte content, as shown in Fig. 5.

Table 13 presents data for permeation of various diffusants and electrolytes in Nafion. At atmospheric pressure, the permeation rate of chlorine is higher than that of hydrogen even though hydrogen has a much higher diffusivity. This is due to the higher c_0 value for chlorine. In the case of chlorine and bromine in HCl, the c_0

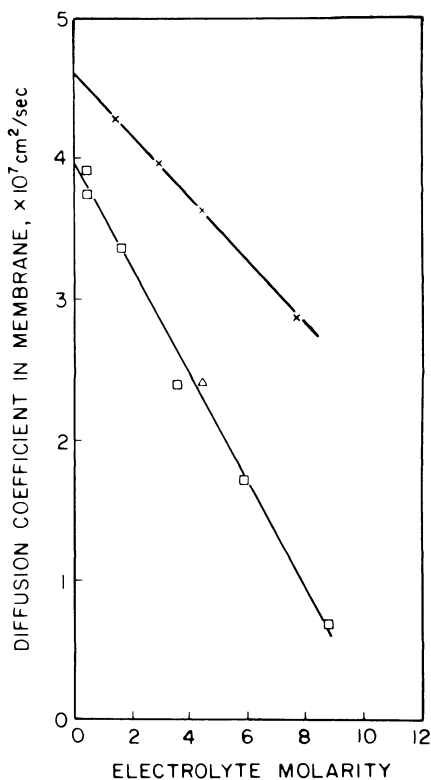


Figure 25. Diffusion coefficients of chlorine and bromine in Nafion of 1200 EW as a function of acid concentration. Diffusant/solvent combinations are: (x) Cl₂/HCl; (Δ) Br₂/HCl; and (□) Br₂/HBr. (Ref. 174; reprinted by permission of the publisher, The Electrochemical Society, Inc.)

Table 13
Permeation of Halogens in Nafion Membrane^a

Diffusant/ Electrolyte	Electrolyte	i_D^b (mA cm ⁻²)	c_∞ (mol dm ⁻³)	c_0/c_∞
H ₂	15% HCl	0.125		
Br ₂	12% HBr	3.57		
Cl ₂ (sat.)/15% HCl	15% HCl	0.2	0.11	1.0
Br ₂ /15% HCl	15% HCl	0.26	0.138	0.99
Br ₂ (sat.)/12% HBr	12% HBr	1.60	2.32	0.27
Br ₂ /3% HBr	3% HBr	0.05	0.148	0.14
Br ₂ /24% HBr	24% HBr	0.25	0.114	0.11
Br ₂ /36% HBr	36% HBr	0.03	0.095	0.23
Br ₂ /48% HBr	48% HBr	0.0135	0.114	0.22

^a From Reference 174.

^b i_D is the steady-state diffusion current [see Eq. (14)].

value is very much equal to the measured concentration in the electrolyte (c_∞). However, in the case of bromine in HBr, c_0 is less than c_∞ . Figure 26 shows a plot of c_0 vs. c_∞ for 12% HBr at 25°C. For this case, c_0 is about 40% of c_∞ . These phenomena occur because of the formation of complex Br_3^- and Br_5^- ions in bromide

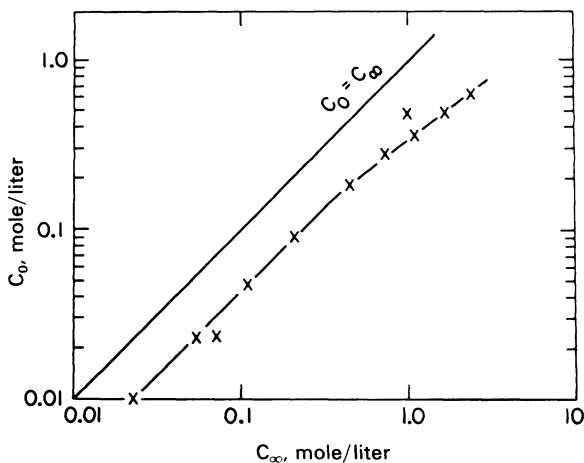


Figure 26. A plot of c_0 vs. c_∞ for bromine in 12% HBr diffusing through Nafion 120 membranes at 25°C. (Ref. 174; reprinted by permission of the publisher, The Electrochemical Society, Inc.)

electrolytes. In HBr, the equilibria (Refs. 224–226) involved are



whereas for Cl_2 in HCl ,^{227,228} it is



The Donnan effect in the cation-exchange membrane inhibits the migration of the negative complex ions. Hence, halogen permeation in Nafion is lower than what might be expected from solubility considerations. In the case of chlorine, the increase of the solubility in HCl at elevated pressures occurs by the formation of Cl_3^- ions so the self-discharge rate of hydrogen/chlorine cells is not expected to increase linearly with chlorine pressure. The coulombic efficiency of the halogen-type cells is over 98%.^{174,175}

The effect of the complex tribromide ion on bromine permeation is also observed in other electrolytes. Will¹⁵⁸ has studied bromine diffusion in Nafion membranes for varying polymer equivalent weight, membrane pretreatment, and solute concentration. The electrolytes used in these experiments were either 2 M ZnBr_2 or 4 M NaBr solutions. The Br_3^- ion is the predominant bromine species in such media, although molecular bromine would appear to be responsible for transport across the membrane. Measured diffusion coefficients of Br_3^- varied from 1×10^{-8} to $5 \times 10^{-7} \text{ cm}^2 \text{ s}^{-1}$ at room temperature. Values increased significantly with decreasing polymer equivalent weight, increasing valency of the cation, and decreasing electrolyte concentrations. The permeation data exhibit a maximum i_D in 35% ZnBr_2 solution. This maximum i_D occurs because the Br_3^- concentration (c_0) decreases at low ZnBr_2 concentrations and the Br_3^- diffusion coefficient (D) decreases with increasing ZnBr_2 concentrations [see Eq. (14)]. Further, the coefficients for diffusion of Br_3^- in the sample pretreated with acid, prior to boiling in water, is higher than that for the sample that was subjected to boiling in water alone (E-form). The E-form sample, in turn, exhibits better diffusivity behavior than that of the N-form samples. This again supports the view that membrane water content is an important factor in determining membrane diffusion coefficients, even for diffusing species that are uncharged.

(iii) Diffusion of Sulfur Dioxide and Sulfides

Kimmerle and Breault⁶⁹ have studied the diffusion of SO₂ in Nafion membranes, considering the possible application in Li/SO₂ cells. Diffusion of SO₂ increases with lower-EW membranes and with thinner samples. D_{SO_2} also varies with residual water content. Diffusion coefficients for acetonitrile-boiled (1 h) membranes were up to twice as great as those ($1\text{--}2 \times 10^{-7} \text{ cm}^2 \text{ s}^{-1}$) observed for membranes boiled overnight. Also, acetonitrile containing 0.5% H₂O yields D_{SO_2} values about twice those observed in dried CH₃CN solution. This is because acetonitrile can replace the water molecules in the membrane, given sufficient time, and subsequent diffusion within the pores is slowed down appreciably. The activation energy of diffusion for SO₂ in Nafion of EW 1100 was found to be 23 kJ mol⁻¹ over the temperature range of 20–60°C.

Bratin and Tomkiewicz²³ have investigated a three-electrode photoelectrochemical storage cell. They studied the transport properties of sulfide and polysulfide through Nafion in Na₂S/NaOH solutions. The diffusion coefficients for sulfide varied from 3×10^{-9} to $1 \times 10^{-7} \text{ cm}^2 \text{ s}^{-1}$, depending on the equivalent weight and thickness of the membrane, and the pH of the solution. The pH of the solution affects the equilibrium between different sulfide species (H₂S, HS⁻, and S²⁻) in the Na₂S solution. It is difficult to determine the actual species diffusing through the membrane. The measured flux and diffusion coefficients of sulfide species include the diffusion of H₂S, HS⁻, and S²⁻, which is the total sulfide. Diffusion coefficients for polysulfide are one order of magnitude lower than those for simple sulfide species, due to the larger size of the diffusing species and to the higher charges on polysulfide ions.

VI. CONCLUSION

The development of perfluorinated ionomers for use as membranes has been noteworthy both in technological and scientific terms. A significant new direction has been given to the electrolytic industries due to the energy savings and environmental impacts that are realized when these membranes are used for electrosynthetic applications. As the leading example, membrane cells can now produce chlorine-sodium hydroxide at less than 2000 kWh per metric ton,

which is not attainable with mercury-cell or diaphragm technologies.¹⁴³ With their cost effectiveness assured, further improvements in membrane conductivity and permselectivity continue to be reported.^{143,211} Also, the use of these polymers as solid polymer electrolytes, and the design of cells which will operate at current densities up to $10,000 \text{ A m}^{-2}$, are further innovations on the horizon in chlor-alkali technology.²¹¹ With these and other applications which exploit the various unusual and novel properties of these materials, they are rapidly becoming a technologically important class of polymers.

In scientific terms, the unusual ion-clustered morphology of the perfluorinated ionomer polymers has provoked much interest. Clearly, the microphase-separated structure that is revealed through various types of experiments is strongly related to their unusual transport properties. It is important to refine our understanding of this relationship in order to exploit these materials in various electrochemical applications.

Nafion is the only commercially available perfluorinated ionomer membrane. Although several other perfluorinated cation-exchange membranes have been manufactured by several Japanese firms (as shown in Table 1), these membranes are not customarily sold without the cell technologies. Thus, the availability of perfluorinated ionomer membranes is rather limited and du Pont is currently the sole source. The relatively high cost of these perfluorinated ionomer membranes precludes their applications in many electrochemical cells where cost effectiveness is a major concern. Besides, the synthesis and fabrication of a corresponding perfluorinated anion-exchange membrane has not been reported yet. Knowledge of the relationship between the unusual ion-cluster morphology and the many unusual properties will be useful for the development of other, less expensive polymer materials for an even wider range of applications. This objective is therefore related to a central goal of membrane science itself: to design polymer membranes with specific dynamic properties from first principles.

REFERENCES

- ¹ R. B. MacMullin, *J. Electrochem. Soc.* **120** (1973) 135C.
- ² T. R. Beck, in *Techniques of Electrochemistry*, Ed. by E. Yeager and A. J. Salkind, Wiley, New York, 1978, Vol. 3, p. 6.

- ³ J. J. Leddy, *J. Chem. Ed.* **57** (1980) 640.
- ⁴ J. S. Ling and J. Charleston, in *Ion Exchange: Transport and Interfacial Properties*, Ed. by R. S. Yeo and R. P. Buck, The Electrochemical Society Softbound Proceedings Series, Pennington, N.J., 1981, p. 334.
- ⁵ W. T. Grubb, *J. Electrochem. Soc.* **106** (1959) 275.
- ⁶ W. T. Grubb and L. W. Niedrach, *J. Electrochem. Soc.* **107** (1960) 131.
- ⁷ E. J. Cairns, D. L. Douglas, and L. W. Niedrach, *AIChE J.* **7** (1961) 551.
- ⁸ L. W. Niedrach and W. T. Grubb, in *Fuel Cells*, Ed. by W. Mitchell, Jr., Academic Press, New York, 1963, p. 253.
- ⁹ H. J. R. Maget, in *Handbook of Fuel Cell Technology*, Ed. by C. Berger, Prentice-Hall, Englewood Cliffs, N.J., 1967, p. 425.
- ¹⁰ R. E. Kesting, *Synthetic Polymeric Membranes*, McGraw-Hill, New York, 1971, p. 291.
- ¹¹ R. B. Hodgdon, J. R. Boyack, and A. B. LaConti, The Degradation of Polystyrene Sulfonic Acid, TIS Report No. 65DE5 (January 1966).
- ¹² V. D'Agostino, J. Lee, and E. Cook, U.S. Patent Nos. 4,107,005 (1978) and 4,012,303 (1978).
- ¹³ E. N. Balko and J. T. Chaklos, *J. Appl. Polym. Sci.* **26** (1982) 1519.
- ¹⁴ E. R. Bauminger, A. Levy, F. Labenski de Kanter, S. Ofer, and C. Heitner-Wirguin, *J. Phys.* **C1** (1980) 329.
- ¹⁵ T. Berzins, Paper presented at AIChE Meeting, Miami Beach, Fla., November 1978.
- ¹⁶ T. Berzins, Paper presented at The Electrochemical Society Meeting, Atlanta, Ga., October 1977.
- ¹⁷ E. Besso and A. Eisenberg, in *Ion Exchange: Transport and Interfacial Properties*, Ed. by R. S. Yeo and R. P. Buck, The Electrochemical Society Softbound Proceedings Series, Pennington, N.J., 1981, p. 197.
- ¹⁸ E. Besso and A. Eisenberg, in *Membranes and Ionic and Electronic Conducting Polymers*, Ed. by E. B. Yeager *et al.*, The Electrochemical Society Softbound Proceedings Series, Pennington, N.J., 1983, p. 1.
- ¹⁹ S. D. Bhakta and D. N. Bennion, Paper presented at AIChE Meeting, Orlando, Fla., February 1982.
- ²⁰ W. J. Blaedel and R. A. Niemann, *Anal. Chem.* **47** (1975) 1455.
- ²¹ N. G. Boyle, V. J. McBrierty, and D. C. Douglass, *Macromolecules* **16** (1983) 75.
- ²² N. G. Boyle, V. J. McBrierty, and A. Eisenberg, *Macromolecules* **16** (1983) 80.
- ²³ P. Bratin and M. Tomkiewicz, *J. Electrochem. Soc.* **129** (1982) 2469.
- ²⁴ S. F. Burkhardt, Paper presented at The Electrochemical Society Meeting, Atlanta, Ga., October 1977.
- ²⁵ D. A. Buttry and F. C. Anson, *J. Electroanal. Chem.* **130** (1981) 333.
- ²⁶ D. A. Buttry and F. C. Anson, *J. Am. Chem. Soc.* **104** (1982) 4824.
- ²⁷ D. A. Buttry and F. C. Anson, *J. Am. Chem. Soc.* **105** (1983) 685.
- ²⁸ J. Ceynowa, *Polymer* **19** (1978) 73.
- ²⁹ M. J. Covitch, S. R. Lowry, C. L. Gray, and B. Blackford, *Polym. Prepr., Am. Chem. Soc., Div. Polym. Chem.* **21** (1980) 120.
- ³⁰ M. J. Covitch, S. R. Lowry, C. L. Gray, and B. Blackford, in *Polymeric Separation Media*, Ed. by A. R. Cooper, Plenum Press, New York, 1982, p. 257.
- ³¹ M. J. Covitch, in *Membranes and Ionic and Electronic Conducting Polymers*, Ed. by E. B. Yeager *et al.*, The Electrochemical Society Softbound Proceedings Series, Pennington, N.J., 1983, p. 31.
- ³² J. A. Cox and Z. Twardowski, *Anal. Chem.* **52** (1980) 1503.
- ³³ S. G. Cutler, in *Ions in Polymers*, Ed. by A. Eisenberg, ACS Advances in Chemistry Series No. 187, 1980, p. 145.

- ³⁴ D. L. DeRespiris and T. J. Gilligan, Paper presented at The Electrochemical Society Meeting, Seattle, Washington, May 1978.
- ³⁵ R. L. Dotson, H. L. Yeager, J. M. Ford, and D. N. Bennion, Paper presented at the Electrochemical Society Meeting, St. Louis, Mo., May 1980.
- ³⁶ R. L. Dotson, R. W. Lynch, and G. E. Hilliard, in *Ion Exchange: Transport and Interfacial Properties*, Ed. by R. S. Yeo and R. P. Buck, The Electrochemical Society Softbound Proceedings Series, Pennington, N.J., 1981, p. 268.
- ³⁷ R. L. Dotson and K. E. Woodard, in *Perfluorinated Ionomer Membranes*, Ed. by A. Eisenberg and H. L. Yeager, ACS Symposium Series No. 180, 1982, p. 311.
- ³⁸ R. Duplessix, M. Escoubes, B. Rodmacq, F. Volino, E. Roche, A. Eisenberg, and M. Pineri, in *Water in Polymers*, Ed. by S. P. Powland, ACS Symposium Series No. 127, 1980, p. 469.
- ³⁹ K. Erdmann and A. Narebska, *Bull. Acad. Polonaise Sci.* **27** (1979) 589.
- ⁴⁰ M. Escoubes and M. Pineri, in *Perfluorinated Ionomer Membranes*, Ed. by A. Eisenberg and H. L. Yeager, ACS Symposium Series No. 180, 1982, p. 9.
- ⁴¹ M. Falk, *Can. J. Chem.* **58** (1980) 1495.
- ⁴² M. Falk, in *Perfluorinated Ionomer Membranes*, Ed. by A. Eisenberg and H. L. Yeager, ACS Symposium Series No. 180, 1982, p. 139.
- ⁴³ M. Fujimura, T. Hashimoto, and H. Kawai, *Macromolecules* **14** (1981) 1309.
- ⁴⁴ M. Fujimura, T. Hashimoto, and H. Kawai, *Macromolecules* **15** (1982) 136.
- ⁴⁵ T. D. Gierke, Paper presented at the Electrochemical Society Meeting, Atlanta, Ga., October 1977.
- ⁴⁶ T. D. Gierke, G. E. Munn, and F. C. Wilson, *J. Polym. Sci., Polym. Phys. Ed.* **19** (1981) 1687.
- ⁴⁷ T. D. Gierke, G. E. Munn, and F. C. Wilson, in *Perfluorinated Ionomer Membranes*, Ed. by A. Eisenberg and H. L. Yeager, ACS Symposium Series No. 180, 1982, p. 195.
- ⁴⁸ T. D. Gierke and W. Y. Hsu, in *Perfluorinated Ionomer Membranes*, Ed. by A. Eisenberg and H. L. Yeager, ACS Symposium Series No. 180, 1982, p. 283.
- ⁴⁹ W. G. F. Grot, G. E. Munn, and P. N. Walmsley, Paper presented at The Electrochemical Society Meeting, Houston, Tex., May 1972.
- ⁵⁰ W. G. F. Grot, *Chem.-Ing.-Tech.* **44** (1972) 167.
- ⁵¹ W. G. F. Grot, *Chem.-Ing.-Tech.* **47** (1975) 617.
- ⁵² W. G. F. Grot, *Chem.-Ing.-Tech.* **50** (1978) 299.
- ⁵³ J. E. Harrar and R. J. Sherry, *Anal. Chem.* **47** (1975) 601.
- ⁵⁴ T. Hashimoto, M. Fujimura, and H. Kawai, in *Perfluorinated Ionomer Membranes*, Ed. by A. Eisenberg and H. L. Yeager, ACS Symposium Series No. 180, 1982, p. 217.
- ⁵⁵ C. Heitner-Wirguin, *Polymer* **20** (1979) 371.
- ⁵⁶ C. Heitner-Wirguin, E. R. Bauminger, A. Levy, F. Labensky de Kanter, and S. Ofer, *Polymer* **21** (1980) 1327.
- ⁵⁷ C. Heitner-Wirguin, in *Ion Exchange: Transport and Interfacial Properties*, Ed. by R. S. Yeo and R. P. Buck, The Electrochemical Society Softbound Proceedings Series, Pennington, N.J., 1981, p. 249.
- ⁵⁸ T. P. Henning, H. S. White, and A. J. Bard, *J. Am. Chem. Soc.* **103** (1981) 3937.
- ⁵⁹ I. M. Hodge and A. Eisenberg, *Macromolecules* **11** (1978) 289.
- ⁶⁰ A. J. Hopfinger and K. A. Mauritz, in *Comprehensive Treatise of Electrochemistry*, Ed. by J. O'M. Bockris, B. E. Conway, E. Yeager, and R. E. White, Plenum Press, New York, 1981, Vol. 2, p. 521.
- ⁶¹ A. J. Hopfinger, *Polym. Prepr., Am. Chem. Soc., Div. Polym. Chem.* **24** (1983) 104.
- ⁶² C. J. Hora and D. E. Maloney, Paper presented at The Electrochemical Society Meeting, Atlanta, Ga., October 1977.

- ⁶³ W. Y. Hsu, J. R. Barkley, and P. Meakin, *Macromolecules* **13** (1980) 198.
- ⁶⁴ W. Y. Hsu and T. D. Gierke, *Macromolecules* **15** (1982) 101.
- ⁶⁵ W. Y. Hsu and T. D. Gierke, *J. Membrane Sci.* **13** (1983) 307.
- ⁶⁶ W. Y. Hsu, *Macromolecules* **16** (1983) 745.
- ⁶⁷ F. Huba, E. B. Yeager, and G. A. Olah, *Electrochim. Acta* **24** (1979) 489.
- ⁶⁸ J. Jorne, *J. Electrochem. Soc.* **129** (1982) 722.
- ⁶⁹ F. M. Kimmerle and R. Breault, *Can. J. Chem.* **58** (1980) 2225.
- ⁷⁰ K. Kimoto, *J. Electrochem. Soc.* **130** (1983) 334.
- ⁷¹ B. Kipling, in *Perfluorinated Ionomer Membranes*, Ed. by A. Eisenberg and H. L. Yeager, ACS Symposium Series No. 180, 1982, p. 475.
- ⁷² W. H. Koh and H. P. Silverman, *J. Membrane Sci.* **13** (1983) 279.
- ⁷³ R. A. Komoroski, in *Ions in Polymers*, Ed. by A. Eisenberg, ACS Advances in Chemistry Series No. 187, 1980, p. 155.
- ⁷⁴ R. A. Komoroski and K. A. Mauritz, *J. Am. Chem. Soc.* **100** (1978) 7487.
- ⁷⁵ R. A. Komoroski and K. A. Mauritz, in *Perfluorinated Ionomer Membranes*, Ed. by A. Eisenberg and H. L. Yeager, ACS Symposium Series No. 180, 1982, p. 113.
- ⁷⁶ L. Kreja, R. Wodzki, and W. Grochowski, *Inzynieria Chemiczna IX* **3** (1979) 663.
- ⁷⁷ L. I. Krishtalik, *Sov. Electrochem.* **15** (1979) 632.
- ⁷⁸ T. Kyu and A. Eisenberg, in *Perfluorinated Ionomer Membranes*, Ed. by A. Eisenberg and H. L. Yeager, ACS Symposium Series No. 180, 1982, p. 79.
- ⁷⁹ A. B. LaConti, A. R. Fragala, and J. R. Boyack, in *Electrode Materials and Processes for Energy Conversion and Storage*, Ed. by J. D. E. McIntyre, S. Srinivasan, and F. G. Will, The Electrochemical Society Softbound Proceedings Series, Pennington, N.J., 1977, p. 354.
- ⁸⁰ A. B. LaConti, E. N. Balko, T. G. Coker, and A. G. Fragala, in *Ion Exchange: Transport and Interfacial Properties*, Ed. by R. S. Yeo and R. P. Buck, The Electrochemical Society Softbound Proceedings Series, Pennington, N.J., 1981, p. 318.
- ⁸¹ P. C. Lee and D. Meisel, *J. Am. Chem. Soc.* **102** (1980) 5477.
- ⁸² R. Leysen and H. Vandendorre, *Mater. Res. Bull.* **15** (1980) 437.
- ⁸³ M. Lopez, B. Kipling, and H. L. Yeager, *Anal. Chem.* **48** (1976) 1120.
- ⁸⁴ M. Lopez, B. Kipling, and H. L. Yeager, *Anal. Chem.* **49** (1977) 629.
- ⁸⁵ S. R. Lowry and K. A. Mauritz, *J. Am. Chem. Soc.* **102** (1980) 4665.
- ⁸⁶ D. E. Maloney and C. J. Molnar, Paper presented at AIChE Meeting, Miami Beach, Fla., November 1978.
- ⁸⁷ C. R. Martin and H. Freiser, *Anal. Chem.* **53** (1981) 902.
- ⁸⁸ C. R. Martin, T. A. Rhoades, and J. A. Ferguson, *Anal. Chem.* **54** (1982) 1639.
- ⁸⁹ C. R. Martin, I. Rubinstein, and A. J. Bard, *J. Am. Chem. Soc.* **104** (1982) 4817.
- ⁹⁰ C. R. Martin and K. A. Dollard, *J. Electroanal. Chem.* **159** (1983) 127.
- ⁹¹ K. A. Mauritz, C. J. Hora, and A. J. Hopfinger, in *Ions in Polymers*, Ed. by A. Eisenberg, ACS Advances in Chemistry Series No. 187, 1980, p. 123.
- ⁹² K. A. Mauritz and A. J. Hopfinger, in *Modern Aspects of Electrochemistry*, Ed. by J. O'M. Bockris, B. E. Conway, and R. E. White, Plenum Press, New York, 1982, Vol. 14, p. 425.
- ⁹³ K. A. Mauritz, K. J. Branchick, C. L. Gray, and S. R. Lowry, *Polym. Prepr., Am. Chem. Soc., Div. Polym. Chem.* **21** (1980) 122.
- ⁹⁴ K. A. Mauritz and C. L. Gray, in *Membranes and Ionic and Electronic Conducting Polymers*, Ed. by E. B. Yeager *et al.*, The Electrochemical Society Softbound Proceedings Series, Pennington, N.J., 1983, p. 151.
- ⁹⁵ G. H. McCain and M. J. Covitch, *J. Electrochem. Soc.* **131** (1984) 1350.

- ⁹⁶ N. I. Men'shakova, V. L. Kubasov, and L. I. Krishtalik, *Elektrokhimiya* **17** (1981) 275.
- ⁹⁷ C. J. Molnar and M. M. Dorio, Paper presented at The Electrochemical Society Meeting, Atlanta, Ga., October 1977.
- ⁹⁸ G. E. Munn, Paper presented at The Electrochemical Society Meeting, Atlanta, Ga., October 1977.
- ⁹⁹ I. Nagata, R. Li, E. Banks, and Y. Okamoto, *Macromolecules* **16** (1983) 903.
- ¹⁰⁰ P. K. Ng and D. D. Snyder, *J. Electrochem. Soc.* **128** (1981) 1714.
- ¹⁰¹ P. K. Ng and D. D. Snyder, *J. Membrane Sci.* **13** (1983) 327.
- ¹⁰² P. K. Ng and D. D. Snyder, in *Transport Processes in Electrochemical Systems*, Ed. by R. S. Yeo, T. Katan, and D-T. Chin, The Electrochemical Society Softbound Proceedings Series, Pennington, N.J., 1982, p. 205.
- ¹⁰³ G. A. Olah and J. Kaspi, *Nouv. J. Chim.* **2** (1978) 531.
- ¹⁰⁴ G. A. Olah and J. Kaspi, *Nouv. J. Chim.* **2** (1978) 583.
- ¹⁰⁵ G. A. Olah, T. Keumi, and D. Meidar, *Synthesis* (1978) 929.
- ¹⁰⁶ G. A. Olah, J. Kaspi, and J. Bukala, *J. Org. Chem.* **42** (1977) 4187.
- ¹⁰⁷ G. A. Olah, G. K. S. Prakash, and J. Sommer, *Science* **206** 4414.
- ¹⁰⁸ H. K. Pan, D. J. Yarusso, G. S. Knappa, and S. L. Cooper, in *Membranes and Ionic and Electronic Conducting Polymers*, Ed by E. B. Yeager *et al.*, The Electrochemical Society Softbound Proceedings Series, Pennington, N.J., 1983, p. 15.
- ¹⁰⁹ S. L. Peluso, A. T. Tsatsas, and W. M. Risen, Jr., Spectral Studies of Ions in a Perfluorocarbonsulfonate (Nafion) Ionomer, Report 1979, Tr-79-01 Order No. AD-A080935 (available from NTIS).
- ¹¹⁰ E. J. Peters and D. R. Pulver, Paper presented at The Electrochemical Society Meeting, Atlanta, Ga., October 1977.
- ¹¹¹ M. Pineri, E. Roche, B. Rodmacq, and F. Volino, in *Ion Exchange: Transport and Interfacial Properties*, Ed. by R. S. Yeo and R. P. Buck, The Electrochemical Society Softbound Proceedings Series, Pennington, N.J., 1981, p. 210.
- ¹¹² M. Pineri, R. Duplessix, and F. Volino, in *Perfluorinated Ionomer Membranes*, Ed. by A. Eisenberg and H. L. Yeager, ACS Symposium Series No. 180, 1982, p. 249.
- ¹¹³ P. N. Pintauro and D. N. Bennion, *IEC Fundamentals*, **23** (1984) 234.
- ¹¹⁴ E. H. Price, Paper presented at The Electrochemical Society Meeting, Atlanta, Ga., October 1977.
- ¹¹⁵ N. E. Prieto and C. R. Martin, *J. Electrochem. Soc.* **131** (1984) 751.
- ¹¹⁶ J. Randin, *J. Electrochem. Soc.* **129** (1982) 1215.
- ¹¹⁷ H. Reiss and I. C. Bassignana, *J. Membrane Sci.* **11** (1982) 219.
- ¹¹⁸ E. J. Roche, M. Pineri, R. Duplessix, and A. M. Levelut, *J. Polym. Sci., Polym. Phys. Ed.* **19** (1981) 1.
- ¹¹⁹ E. J. Roche, M. Pineri, and R. Duplessix, *J. Polym. Sci., Polym. Phys. Ed.* **20** (1982) 107.
- ¹²⁰ B. Rodmacq, M. Pineri, and J. M. D. Coey, *Rev. Phys. Appl.* **15** (1980) 1179.
- ¹²¹ B. Rodmacq, M. Pineri, J. M. D. Coey, and A. Meagher, *J. Polym. Sci., Polym. Phys. Ed.* **20** (1982) 603.
- ¹²² B. Rodmacq, J. M. Coey, M. Escoubes, E. Roche, R. Duplessix, A. Eisenberg, and M. Pineri, in *Water in Polymers*, Ed. by S. P. Powland, ACS Symposium Series No. 127, 1980, p. 487.
- ¹²³ B. Rodmacq, J. M. D. Coey, and M. Pineri, in *Perfluorinated Ionomer Membranes*, Ed. by A. Eisenberg and H. L. Yeager, ACS Symposium Series No. 180, 1982, p. 171.

- ¹²⁴ S. Rondinini, P. Longhi, and T. Mussini, *Ann. Chim. (Paris)* **73** (1983) 193.
- ¹²⁵ S. Rondinini, P. Longhi, and T. Mussini, *J. Membrane Sci.* **16** (1983) 151.
- ¹²⁶ I. Rubinstein and A. J. Bard, *J. Am. Chem. Soc.* **102** (1980) 6641.
- ¹²⁷ I. Rubinstein and A. J. Bard, *J. Am. Chem. Soc.* **103** (1981) 5007.
- ¹²⁸ E. J. Rudd, in *Membranes and Ionic and Electronic Conducting Polymers*, Ed. by E. B. Yeager *et al.*, The Electrochemical Society Softbound Proceedings Series, Pennington, N.J., 1983, p. 214.
- ¹²⁹ T. Sata and Y. Onoue, in *Perfluorinated Ionomer Membranes*, Ed. by A. Eisenberg and H. L. Yeager, ACS Symposium Series No. 180, 1982, p. 411.
- ¹³⁰ T. Sata, K. Motani, and Y. Ohashi, in *Ion Exchange Membranes*, Ed. by D. S. Flett, Ellis Horwood, Chichester, U.K., 1983, p. 137.
- ¹³¹ G. G. Scherer and S. Stucki, Paper presented at the Electrochemical Society Meeting, Montreal, Canada, May 1982.
- ¹³² K. H. Simrock, E. Griesenbeck, J. Jorissen, and R. Rodermund, *Chem.-Ind.-Tech.* **53** (1981) 10.
- ¹³³ M. Seko, S. Ogawa, and K. Kimoto, in *Perfluorinated Ionomer Membranes*, Ed. by A. Eisenberg and H. L. Yeager, ACS Symposium Series No. 180, 1982, p. 365.
- ¹³⁴ M. Seko, A. Yomiyama, and S. Ogawa, in *Ion Exchange Membranes*, Ed. by D. S. Flett, Ellis Horwood Publishers, Chichester, U.K., 1983, p. 121.
- ¹³⁵ V. V. Sitnikova, G. G. Chuvileva, and N. I. Nikolaev, *Zh. Fiz. Khim.* **54** (1980) 1320.
- ¹³⁶ N. Sivashinsky and G. B. Tanny, *J. Appl. Polym. Sci.* **26** (1981) 2625.
- ¹³⁷ P. J. Smith and T. L. Jones, *J. Electrochem. Soc.* **130** (1983) 885.
- ¹³⁸ P. J. Smith, in *Ion Exchange Membranes*, Ed. by D. S. Flett, Ellis Horwood, Chichester, U.K., 1983, p. 151.
- ¹³⁹ H. W. Starkweather, Jr., *Macromolecules* **15** (1982) 320.
- ¹⁴⁰ H. W. Starkweather, Jr. and J. J. Chang, *Macromolecules* **15** (1982) 752.
- ¹⁴¹ A. Steck and H. L. Yeager, *Anal. Chem.* **52** (1980) 1215.
- ¹⁴² A. Steck and H. L. Yeager, *J. Electrochem. Soc.* **130** (1983) 1297.
- ¹⁴³ S. C. Stinson, *Chem. Eng. News* (March 15, 1982) 22.
- ¹⁴⁴ S. Stucki and A. Menth, Paper presented at The Electrochemical Society Meeting, Seattle, Wash., May 1978.
- ¹⁴⁵ M. Suhara and Y. Oda, in *Ion Exchange: Transport and Interfacial Properties*, Ed. by R. S. Yeo and R. P. Buck, The Electrochemical Society Softbound Proceedings Series, Pennington, N.J., 1981, p. 290.
- ¹⁴⁶ M. Suhara and Y. Oda, in *Transport Processes in Electrochemical Systems*, Ed. by R. S. Yeo, T. Katan, and D-T. Chin, The Electrochemical Society Softbound Proceedings Series, Pennington, N.J., 1982, p. 223.
- ¹⁴⁷ T. Takamatsu, M. Hashiyama, and A. Eisenberg, *J. Appl. Polym. Sci.* **24** (1979) 2199.
- ¹⁴⁸ T. Takamatsu and A. Eisenberg, *J. Appl. Polym. Sci.* **24** (1979) 2221.
- ¹⁴⁹ Z. Twardowski, H. L. Yeager, and B. O'Dell, *J. Electrochem. Soc.* **129** (1982) 328.
- ¹⁵⁰ H. Ukihashi, CHEMTECH (February 1980) 118.
- ¹⁵¹ H. Ukihashi and M. Yamabe, in *Perfluorinated Ionomer Membranes*, Ed. by A. Eisenberg and H. L. Yeager, ACS Symposium Series No. 180, 1982, p. 427.
- ¹⁵² H. Ukihashi, T. Asawa, and H. Miyake, in *Ion Exchange Membranes*, Ed. by D. S. Flett, Ellis Horwood, Chichester, U.K., 1983, p. 165.
- ¹⁵³ R. Vasquez, J. Avalos, F. Volino, M. Pineri, and D. Galland, *J. Appl. Polym. Sci.* **28** (1983) 1093.
- ¹⁵⁴ D. J. Vaughan, *Du Pont Innovation* **4** (1973) 10.
- ¹⁵⁵ F. Volino, M. Pineri, A. J. Dianoux, and A. De Geyer, *J. Polym. Sci., Polym. Phys. Ed.* **20** (1982) 481.

- ¹⁵⁶ J. L. Weininger and R. R. Russell, *J. Electrochem. Soc.* **125** (1978) 1482.
- ¹⁵⁷ H. S. White, J. Leddy, and A. J. Bard, *J. Am. Chem. Soc.* **104** (1982) 4811.
- ¹⁵⁸ F. G. Will, *J. Electrochem. Soc.* **126** (1979) 36.
- ¹⁵⁹ H. L. Yeager and B. Kipling, *J. Phys. Chem.* **83** (1979) 1836.
- ¹⁶⁰ H. L. Yeager and A. Steck, *Anal. Chem.* **51** (1979) 862.
- ¹⁶¹ H. L. Yeager, B. Kipling, and R. L. Dotson, *J. Electrochem. Soc.* **127** (1980) 303.
- ¹⁶² H. L. Yeager and A. Steck, in *Ion Exchange: Transport and Interfacial Properties*, Ed. by R. S. Yeo and R. P. Buck, The Electrochemical Society Softbound Proceedings Series, Pennington, N.J., 1981, p. 257.
- ¹⁶³ H. L. Yeager and A. Steck, *J. Electrochem. Soc.* **128** (1981) 1880.
- ¹⁶⁴ H. L. Yeager, B. O'Dell, and Z. Twardowski, *J. Electrochem. Soc.* **129** (1982) 85.
- ¹⁶⁵ H. L. Yeager, Z. Twardowski, and L. M. Clarke, *J. Electrochem. Soc.* **129** (1982) 324.
- ¹⁶⁶ H. L. Yeager, in *Perfluorinated Ionomer Membranes*, Ed. by A. Eisenberg and H. L. Yeager, ACS Symposium Series No. 180, 1982, p. 25.
- ¹⁶⁷ H. L. Yeager, in *Perfluorinated Ionomer Membranes*, Ed. by A. Eisenberg and H. L. Yeager, ACS Symposium Series No. 180, 1982, p. 41.
- ¹⁶⁸ H. L. Yeager, in *Membranes and Ionic and Electronic Conducting Polymers*, Ed. by E. B. Yeager *et al.*, The Electrochemical Society Softbound Proceedings Series, Pennington, N.J., 1983, p. 134.
- ¹⁶⁹ H. L. Yeager, J. D. Malinsky, and R. L. Dotson, in *Transport Processes in Electrochemical Systems*, Ed. by R. S. Yeo, T. Katan, and D-T. Chin, The Electrochemical Society Softbound Proceedings Series, Pennington, N.J., 1982, p. 215.
- ¹⁷⁰ H. L. Yeager, unpublished results.
- ¹⁷¹ R. S. Yeo and A. Eisenberg, *Polym. Prepr.* **16** (1975) 104.
- ¹⁷² R. S. Yeo, Ph.D. thesis, McGill University, 1976.
- ¹⁷³ R. S. Yeo and A. Eisenberg, *J. Appl. Polym. Sci.* **21** (1977) 875.
- ¹⁷⁴ R. S. Yeo and J. McBreen, *J. Electrochem. Soc.* **126** (1979) 1682.
- ¹⁷⁵ R. S. Yeo and D-T. Chin, *J. Electrochem. Soc.* **127** (1980) 549.
- ¹⁷⁶ R. S. Yeo, J. McBreen, G. Kissel, F. Kulesa, and S. Srinivasan, *J. Appl. Electrochem.* **10** (1980) 741.
- ¹⁷⁷ R. S. Yeo, *Polymer* **21** (1980) 432.
- ¹⁷⁸ R. S. Yeo, S. F. Chan, and J. Lee, *J. Membrane Sci.* **9** (1981) 273.
- ¹⁷⁹ R. S. Yeo, in *Ion Exchange: Transport and Interfacial Properties*, Ed. by R. S. Yeo and R. P. Buck, The Electrochemical Society Softbound Proceedings Series, Pennington, N.J., 1981, p. 235.
- ¹⁸⁰ R. S. Yeo, in *Perfluorinated Ionomer Membranes*, Ed. by A. Eisenberg and H. L. Yeager, ACS Symposium Series No. 180, 1982, p. 65.
- ¹⁸¹ R. S. Yeo, in *Perfluorinated Ionomer Membranes*, Ed. by A. Eisenberg and H. L. Yeager, ACS Symposium Series No. 180, 1982, p. 453.
- ¹⁸² R. S. Yeo, in *Transport Processes in Electrochemical Systems*, Ed. by R. S. Yeo, T. Katan, and D-T. Chin, The Electrochemical Society Softbound Proceedings Series, Pennington, N.J., 1982, p. 178.
- ¹⁸³ R. S. Yeo, *J. Electrochem. Soc.* **130** (1983) 533.
- ¹⁸⁴ A. Eisenberg and H. L. Yeager, Eds., *Perfluorinated Ionomer Membranes*, American Chemical Society Symposium Series No. 180, 1982.
- ¹⁸⁵ D. J. Connolly and W. F. Gresham, U.S. Patent No. 3,282,875 (1966).
- ¹⁸⁶ W. G. F. Grot, U.S. Patent No. 3,692,569 (1972).
- ¹⁸⁷ W. G. F. Grot, U.S. Patent No. 3,784,399.
- ¹⁸⁸ A. Eisenberg and M. King, *Ion-Containing Polymers*, Academic Press, New York, 1977.

- ¹⁸⁹ T. C. Ward and A. V. Tobolsky, *J. Appl. Polym. Sci.* **11** (1967) 2403.
- ¹⁹⁰ W. J. MacKnight, L. W. McKenna, and B. E. Read, *J. Appl. Phys.* **38** (1968) 4208.
- ¹⁹¹ B. W. Delft and W. J. MacKnight, *Macromolecules* **2** (1969) 309.
- ¹⁹² M. Navratil and A. Eisenberg, *Macromolecules* **7** (1974) 84.
- ¹⁹³ A. Neppel, I. S. Butler, and A. Eisenberg, *Macromolecules* **12** (1979) 948.
- ¹⁹⁴ A. T. Tsatsas, J. W. Reed, and W. M. Risen, *J. Chem. Phys.* **55** (1971) 3260.
- ¹⁹⁵ C. L. Marx, D. F. Caulfield, and S. L. Cooper, *Macromolecules* **6** (1973) 344.
- ¹⁹⁶ C. T. Meyer and M. Pineri, *J. Polym. Sci., Polym. Phys. Ed.* **16** (1978) 569.
- ¹⁹⁷ R. D. Lundberg and H. S. Makowski, in *Ions in Polymers*, Ed. by A. Eisenberg, ACS Advances in Chemistry Series No. 187, 1980, p. 21.
- ¹⁹⁸ E. P. Otocka, M. Y. Hellman, and L. L. Blyler, *J. Appl. Phys.* **40** (1969) 4221.
- ¹⁹⁹ E. P. Otocka and D. D. Davis, *Macromolecules* **2** (1969) 437.
- ²⁰⁰ E. P. Otocka and T. K. Kwei, *Macromolecules* **1** (1968) 401.
- ²⁰¹ A. Eisenberg, *Macromolecules* **3** (1970) 147.
- ²⁰² A. Eisenberg, Keynote lecture at the Workshop on Structure and Properties of Solid Ion Containing Polymers, Villard de Lans, France, June 29–July 2, 1981.
- ²⁰³ W. J. MacKnight, W. P. Taggart, and R. S. Stein, *J. Polym. Sci.* **C45** (1974) 113.
- ²⁰⁴ F. G. Donnan and E. A. Guggenheim, *Z. Phys. Chem.* **A162** (1932) 346.
- ²⁰⁵ O. D. Bonner, *J. Phys. Chem.* **59** (1955) 719.
- ²⁰⁶ G. E. Boyd and B. A. Soldano, *J. Am. Chem. Soc.* **75** (1953) 6091.
- ²⁰⁷ R. Fernandez-Prini and M. Philipp, *J. Phys. Chem.* **80** (1976) 2041.
- ²⁰⁸ M. H. Cohen and D. Turnbull, *J. Chem. Phys.* **31** (1959) 1164.
- ²⁰⁹ H. Yasuda, C. E. Lamaze, and L. D. Ikenberry, *Makromol. Chem.* **118** (1968) 19.
- ²¹⁰ J. A. Cox and J. E. Di Nunzio, *Anal. Chem.* **49** (1977) 1272.
- ²¹¹ *Chemical Week* (August 25, 1982) 63.
- ²¹² F. Helfferich, *Ion Exchange*, McGraw-Hill, New York, 1962, Chap. 8.
- ²¹³ C. A. Kruissink, *J. Membrane Sci.* **14** (1983) 331.
- ²¹⁴ O. P. Romaskin, M. M. Fioshin, R. G. Erenburg, E. F. Ryabov, V. L. Kubasov, and L. I. Krishtalik, *Sov. Electrochem.* **15** (1979) 553.
- ²¹⁵ C. S. Fadley and R. A. Wallace, *J. Electrochem. Soc.* **115** (1968) 1264.
- ²¹⁶ D. A. G. Bruggemann, *Ann. Phys.* **24** (1935) 636.
- ²¹⁷ P. W. T. Lu and S. Srinivasan, *J. Appl. Electrochem.* **9** (1979) 269.
- ²¹⁸ R. S. Yeo, J. Orehotsky, W. Visscher, and S. Srinivasan, *J. Electrochem. Soc.* **128** (1981) 1900.
- ²¹⁹ B. V. Tilak, P. W. T. Lu, J. E. Colman, and S. Srinivasan, in *Comprehensive Treatise on Electrochemistry*, Ed. by J. O'M. Bockris, B. E. Conway, E. B. Yeager, and R. E. White, Plenum Press, New York, 1981, Vol. 2, p. 1.
- ²²⁰ W. Nernst, *Z. Phys. Chem.* **2** (1888) 613.
- ²²¹ R. S. Yeo, J. McBreen, A. C. C. Tseung, S. Srinivasan, and J. McElroy, *J. Appl. Electrochem.* **10** (1980) 393.
- ²²² R. L. Coalson and W. G. Grot, U.S. Patent No. 3,684,747 (1972).
- ²²³ L. J. Nuttall, *Int. J. Hydrogen Energy* **2** (1977) 395.
- ²²⁴ T. Mussini and G. Faita, *Ricerca Sci.* **36** (1966) 175.
- ²²⁵ D. B. Scaife and H. J. V. Tyrell, *J. Chem. Soc.* (1958) 386.
- ²²⁶ G. Jones and S. Baeckstrom, *J. Am. Chem. Soc.* **56** (1934) 1517.
- ²²⁷ A. Cerquetti, P. Longhi, T. Mussini, and G. Natta, *J. Electroanal. Chem. Interfac. Electrochem.* **20** (1969) 411.
- ²²⁸ G. Zimmerman and F. C. Strong, *J. Am. Chem. Soc.* **79** (1957) 2063.

Index

- Acceleration requirements, for electric vehicles, 379
- Activation energy, Fermi level effect on, 111
- Adsorption, of non-ionic molecules, 84
- Adsorption effects, with ions, 64
- Agar, potential dependence of entropy of activation, 132
- Aluminum-air system, 422
- Anion adsorption
 - at mercury, 157
 - at nickel, 159
- Anions
 - adsorption at gold faces, 73
 - specific adsorption effects on transfer coefficient, 156
- Anion effects, at single-crystal silver faces, 69
- Anodic photodecomposition, protection against, 231
- Apparent activation energy, and Tafel equation, 172
- Apparent and real heats of activation, 175
- Apparent heat of activation, 168

- Back reflection photos, chart for, 14
- Band edges, pinning of, 206
- Barrierless discharge, 155
- Batteries
 - for vehicular propulsion, 371
 - high-temperature, 409
 - lithium-sulfur, 409
 - metal-air, 420
 - nickel-iron, 396

 - Batteries (*cont.*)
 - with conducting polymer systems, 418
 - zinc, 399
 - zinc-halogen, 402
 - Battery, lead/acid, 391
 - Battery classification, 374
 - Battery materials, supply constraints of, 385
 - Battery requirements, for electric vehicles, 373
 - β (symmetry factor), 113
 - BDM theory of solvent orientation, 139
 - Brine anolyte, and sodium ion transport number, 477
 - Bromine evolution, at carbon, 127
 - Brønsted linear free-energy relations, 112
 - b , Tafel slope parameter, 106
 - Butler, energy profiles, 109
 - Butler-Volmer equation, 108

 - Cadmium sulfide, as photoelectrode, 224
 - Capacity curves
 - and growth steps, 79
 - for non-ionic adsorption, 85
 - Carboxylate membranes, 468
 - Cation-exchange membranes, perfluorinated, 439
 - Charge transfer model, of SERS, 332
 - Chemisorption energy, in potential profiles, 109
 - Chlor-alkali cell, membrane selectivity for, 472
 - Clean conditions, for interface studies, 2
 - Close-packed structures, 18

- Coinage metals, and SERS, 308
- Colloidal systems
- excitation spectra for, 317
 - SERS effect from, 263
 - surface preparation in, 282
- Comparison of electric vehicle batteries, 423
- Concentrated solution, diffusion behavior in, 465
- Conducting polymer systems, 418
- Conductivity
- of membranes in pure water, 480
 - in membranes, 479
- Coordination numbers, in unit cells, 18
- Cost factors, in battery development, 384
- Coverage effects, in multistep pathways, 161
- Crystal cutting, 32
- Crystallographic orientation, 10
- Crystallography, of metals, 4
- Crystal polishing, 33
- Crystal structures, defects in, 27
- Crystal surfaces
- and stereographic projection, 6
 - models of, 15
- Cubic crystals, stereographic projection of, 9
- Cubic system
- principal index faces of, 5
 - stepped surfaces in, 22
- Cyanide, adsorption and SERS effect, 279
- Cycle life and depth of discharge, 388
- Cyclic-voltammetry, for single-crystal surfaces, 40
- Defects, 27
- Depth of discharge and cycle life, 388
- Diffusion behavior, in concentrated solutions, 465
- Donnan effect, and ion-exchange membranes, 457
- Double-layer
- at semiconductor interface, 201
 - at single crystals, 1
- Double-layer capacity
- at gold surfaces, 54
 - at silver surfaces, 52
 - curves for, 46
- Dye effects in SERS, theoretical, 344
- Dyes, surface Raman scattering of, 297
- Eisenberg, theory of membranes, 442
- Electrical energy term, in rate equation, 110, 135
- Electric field enhancement mechanism, in SERS, 336
- Electric vehicle batteries
- comparison of, 423
 - near term and advanced, 424
- Electric vehicle battery requirements, 373
- Electrochemical polishing, 34
- Electrochemical potential, of electrons in solution, redox systems, 191
- Electrochemical systems
- excitation profiles in, 314
 - SERS in, 259
 - surface preparation for SERS in, 273
- Electrochemistry, of semiconductors, 189
- Electrode potentials, scale of, 196
- Electrode processes, linear free energy relations for, 111
- Electrodes
- preparation of single-crystal, 28
 - semiconductor, new applications of, 236
 - semiconductor, surface states at, 205
- Electrode surfaces, characterization of, 37
- Electrolysis, with ion-exchange membranes, 470
- Electrolyte systems, solid polymer, 480
- Electron affinities, and flat-band potentials, 215
- Electron and particle transfer, Ulstrup treatment, 147
- Electrons, electrochemical potential of, 195
- Energy efficiency, of vehicular batteries, 388
- Enhancement factor, in SERS, 256
- Enhancement, surface electromagnetic wave, 337
- Enhancement mechanism, of SERS, electric field, 336
- Entropy of activation, 133
- Agar's comments on, 132
 - and solvent dipole orientation, 138

- Entropy of activation (*cont.*)
for hydrogen evolution reaction, 180
for redox reactions, 180
potential dependence of, 133, 181
- Entropy of libration, at electrodes, 140
- Exchange capacity of ion membranes, 445
- Exchange currents, and Tafel slopes, 164
- Exchange sites, acidity of in membranes, 455
- Excitation profiles in SERS, 312
- Excitation profiles on films, 319
- Excitation profiles, summary of SERS, 321
- Excitation spectra, in colloidal systems, 317
- FCC structure, unit stereographic triangle for, 20
- FCC system
higher index faces, 21
models of, 17
- FCC systems, 18
- Fermi-Dirac statistics, in rate equation, 136
- Fermi level effects, at electrodes, 111
- Fermi level pinning, 206
- Field effect transistor, ion selective, 243
- Flat-band potential, 210
and electron affinity, 215
- Ford, sodium-sulfur cell, 413
- Gassing, overcharge, 395
- Gibbs energy of activation, for electrode processes, 110
- Gold
anion adsorption at, 73
hydrogen oxidation at, 42
- Gold electrode, SERS effect at, 308
- Gold surfaces, double-layer capacity at, 54
- Growth of single-crystals, 28
- Growth steps and capacity curves, 79
- Gurney energy profiles, 109
- Halides, and SERS effect, 292
- Halogen, zinc battery, 402
- Halogens, permeation in Nafion, tabulated, 494
- Harmonic potential effects, 150
- HCP systems, 18
- Heat of activation, apparent, 168
- Heats of activation, apparent and real, 175
- Helmholtz layer and temperature, 155
- High-performance membranes, 438
- High-temperature, batteries, 409
- Historical aspects
of ion-exchange cells, 437
of single-crystal studies, 3
- Hydrogen diffusion in Nafion, 491
- Hydrogen evolution
at mercury, 117
at nickel, 120
- Hydrogen evolution reaction, entropy of activation for, 180
- Hydrogen oxidation, at gold, 42
- Industrial electrolysis, ion-exchange membranes in, 470
- Inner-layer capacity, 60
- Interaction, of ions with metal, 62
- Interactions, of neutral molecules at metals, 81
- Interfaces, clean, 2
- Inversion layer, in semiconductors, 227
- Ion and water diffusion, in membranes, 459
- Ion clustering, in membranes, 446
- Ion-exchange capacity, 445
- Ion-exchange membrane cells, historical background of, 437
- Ion-exchange membranes, 437
acidity of exchange sites, 455
and ion diffusion, 459
and water diffusion, 459
clustering in, 446
conductivity of, 479
Donnan effect in, 457
Eisenberg's theory, 443
industrial conditions, 470
ionic cross-linking in, 447
microstructure of, 441
permeability of, 479
self-diffusion in, 463
solvation phenomenon in, 450
sorption of ions and water, 468
- Ionic cross-linking in membranes, 447

- Ions
 adsorption of, 64
 factors in adsorption of, 64
- Ion-selective field-effect transistor, 243
- Iron sulfide, lithium battery, 410
- Isoelectric point, 205
- Laser etching of semiconductors, 239
- Laue method
 for crystal orientation, 12
 X-ray goniometer, 13
- Lawrence Livermore aluminum–air system, 422
- Lead/acid batteries, behavior of, 387
- Lead/acid battery, characteristics, 391
- Levich model, for proton transfer, 145
- Libration, entropy of, at electrodes, 140
- Lightening rod effect in SERS, 337
- Linear free-energy relations, Brønsted, 112
- Linear free-energy relationship, for electrode processes, 111
- Liquid junction solar cell, 225
- Literature, on semiconductor electrodes, 247
- Lithium batteries, rechargeable, 417
- Lithium iron sulfide battery, 410
- Lithium–sulfur batteries, 409
- Mechanisms, of SERS effect, 348
- Membranes
 conductivity in acids, 482
 conductivity in alkali, 485
 high performance, 438
 ion-exchange, 437
 permeability of, 479
 permeation of molecular species, 490
- Membrane selectivity, in chlor-alkali cells, 472
- Mercury
 anion adsorption at, 157
 hydrogen evolution at, 117
- Metal–air, batteries, 420
- Metal/ion interactions, 62
- Metals
 crystallography of, 4
 exhibiting SERS, 307
 structure of, 4
- Metal surfaces
 electronic aspects, 24
 structure of, 23
- Models
 for β , 113
 of crystal surfaces, 15
 of FCC system faces, 17
- Molecules, permeation in membranes, 490
- Mott–Schottky plot, 211
- Mott–Schottky plots, frequency dependence of, 213
- Multistep pathways
 coverage effects in, 161
 Tafel slopes for, 160
- Multistep reactions, Tafel slopes for, 115
- Nafion
 applications of, 440
 conductivity in protic solvents, 489
 conductivity of, 487
 diffusion of chlorine and bromine in, 492
 diffusion of sulfur dioxide and sulfides in, 496
 hydrogen and oxygen diffusion in, 491
 permeation of halogens in, tabulated, 494
 sodium ion transport number in, 474
 state of water in, 455
 structural models of, 447, 450
- Nafion membranes, water uptake in, 451
- Near term and advanced E.V. batteries, 424
- Neutral molecules, metal interactions with, 81
- Nickel
 anion adsorption at, 159
 hydrogen evolution at, 120
- Nickel–iron battery, 396
- Nickel–zinc battery, as optimum system, 426
- Nitro-compounds, reduction of, 130
- Non-ionic adsorbates, 85
- Organic compounds, and SERS effects, 280
- Orientation
 crystallographic, 10
 of single-crystals, 13

- Overcharge, gassing on, 395
Oxygen diffusion in Nafion, 491
Oxygen evolution, at platinum, 127
Oxygen reduction, at platinum, 129
- Particles, photoelectrolysis at, 222
Peak power, specific energy balance, 381
Perfluorinated ion-exchange membranes, 437
Perfluorinated membranes, development of, 439
Performance requirements, for vehicle batteries, 375
Permeability, of membranes, 479
Photoanode, for water splitting, 223
Photoassistance, of water electrolysis, 238
Photocell, for electrolytic water splitting, 223
Photochemical processes, at semiconductors, 216
Photocorrosion, 228
Photoelectrochemical conversion, of solar energy, 236
Photoelectrochemical reactions, important types of, 218
Photoelectrolysis, of water at particles, 222
Photopotentials, open circuit, 226
Pinning of band edges, 206
Platinum
 oxygen evolution at, 127
 oxygen reduction at, 129
Polishing, electrochemical, 34
Polymer systems, conducting, 418
Potential, flat-band at semiconductors, 210
Potential dependence
 of activation entropy, 133
 of entropy of activation, 181
 of reaction rates, 107
 of SERS, 277
 of transfer coefficient, 148
Potential distribution, at semiconductor interfaces, 206
Potentials of zero charge, at single-crystals, 45
Preparation of single-crystal electrodes, 28
Principal index faces, symmetries, 11
Protection of semiconductor interface, 231
Protic solvents, conductivity of Nafion in, 489
Proton transfer
 Bell model of, 146
 Levich model of, 145
Proton tunneling, 143
Purity requirements, for double-layer studies, 2
- Quadratic effects, in Tafel relation, 152
Quasi-Fermi levels, 216
- Ragone plots for specific power versus energy, 382
Raman reflectivity in SERS, 334
Raman scattering, *see* SERS effect, 297
 surface enhanced, 253
Rate equation
 Butler-Volmer, 108
 Fermi-Dirac statistics in, 136
Reaction rates, potential dependence of, 107
Real and apparent heats of activation, 175
Rechargeable batteries, commercially available, tabulated, 373
Rechargeable lithium batteries, 417
Redox couple, electrochemical potential of electrons for, 191
Redox reactions at electrodes, 124
Redox reactions, entropy of activation for, 178
Relative surface energy, at single-crystal surfaces, 48
Reorganization energy, of a solvent, 199
Resonance models, of SERS, 325
Roughness factor, at surfaces, 94
Russian work, on electrochemistry of semiconductors, 189
- Self-diffusion in ion-exchange membranes, 463
Semiconducting materials, characterization of, 245
Semiconductor electrochemistry, literature on, 247
Semiconductor electrodes
 new applications of, 236
 surface states at, 205
 thermodynamic stability of, 229

- Semiconductor interface, double-layer at, 201
- Semiconductor interfaces, potential distribution at, 206
- Semiconductors
- and photocorrosion effects, 228
 - electrochemistry of, 189
 - flat-band potential of, 210
 - laser etching of, 239
 - photoelectrochemical processes at, 216
 - tunneling of hot electrons from, 235
- SERS, 253
- and halides, 292
 - and surface preparation, 271
 - at metals, 307
 - controversy on origin of, 254
 - electric field enhancement mechanism, 336
 - electrode potential dependence of, 277
 - enhancement factor in, 256
 - excitation profiles in, 312
 - experimental studies, 255
 - from UHV systems, 264
 - image model, 325
 - in electrochemical systems, 259
 - lightning rod effect in, 337
 - of water, 295
 - Raman reflectivity in, 334
 - resonance models of, 325
 - uses of, 350
- SERS effect
- from colloidal systems, 263
 - of adsorbed cyanide, 279
 - theoretical models of, 322
 - with organic compounds, 280
- SERS enhancement factor, values of, 256
- SERS excitation profiles, on films, 319
- SERS mechanisms, 348
- SERS model, charge transfer, 332
- SERS studies, surface preparation for, 285
- Silver
- anion adsorption at, 69
 - SERS effect at, 308
 - single-crystal surfaces, double-layer capacity at, 52
- Silver surfaces, inner-layer capacity at, 60
- Single-crystal faces
- isolation of, 34
 - preparation of, 32
- Single-crystal gold surface, double-layer capacity at, 54
- Single crystals
- double-layer at, 1
 - growth from metal vapor, 30
 - growth from solutions, 31
 - growth of, 28
 - orientation procedure for, 13
 - potentials of zero charge at, 45
 - specification of principal index faces of, 11
- Single-crystal studies, historical aspects, 3
- Single-crystal surfaces
- cyclic-voltammetry of, 40
 - double-layer capacity at, 46
 - electrochemical results, 43
 - surface energy of, 48
- Smooth surfaces, SERS effect, 269
- Sodium ion diffusion, in membranes, 466
- Sodium ion transport number in Nafion, 474
- Sodium-sulfur cell, Ford, 413
- Solar cell, liquid junction, 225
- Solar energy, photoelectrochemical use of, 236
- Solid polymer electrolyte systems, 480
- Solids, exhibiting SERS, 307
- Solutions, electrochemical potential of electrons in, 195
- Solvation phenomenon, in ion-exchange membranes, 450
- Solvent
- interaction with metals, 59
 - reorganization energy of, 199
- Solvent dipole libration entropy, 140
- Solvent dipole orientation, and temperature, 138
- Solvent orientation, BDM theory of, 139
- Sorption of ions and water, in ion-exchange membranes, 468
- Specific adsorption, of anions, 62
- Specific adsorption, of anions, and transfer coefficient, 156

- Specific energy, for vehicle batteries, 376
- Specific energy peak power balance, 381
- Specific energy versus power, Ragone plots, 382
- Specific power versus energy, Ragone plots, 382
- Stepped faces, 19
- Stepped surfaces, cubic system, 22
- Stereographic net, Wulff type, 8
- Stereographic projection, 6
for cubic crystals, 9
- Stereographic triangle, 9
- Structural aspects, of ion-exchange membranes, 437
- Structure of metals, 4
- Structure of metal surfaces, 23
- Sulfonate membranes, 468
- Surface electromagnetic wave enhancement, 337
- Surface energy, 26
- Surface enhanced Raman scattering (SERS), 253
- Surface preparation
and SERS effect, 271
for SERS in electrochemical systems, 273
- Surface Raman scattering, of dyes, 297
- Surface Raman signals, distinction of, 258
- Surfaces
roughness factor of, 94
wave functions at, 25
- Surface states
at semiconductor electrodes, 205
Fermi level pinning of, 206
- Symmetries, of principal index faces, 11
- Symmetry factor, β , 113
independence on temperature, 131
relations for, 113
relation to α , 115
- Tafel equation, 105
and temperature effects, 103
real form of, 103
for complete tunneling control, 144
- Tafel slope parameter, b , 106
- Tafel slopes, and electrode area, 167
and exchange currents, 164
- Tafel slopes, and electrode area (*cont.*)
and proton tunneling, 143
and temperature, 103
experimental data as function of temperature, 116
for hydrogen evolution, 118
for multistep pathways, 160
for multistep reactions, 115
- Temperature dependence
conventional behavior of Tafel relation, 107
of Tafel slopes, experimental results for, 116
- Temperature dependence of α ,
conclusions on, 182
theoretical, 132
- Temperature effect, on oxygen reduction, 129
- Temperature effects
on Helmholtz layer, 155
on solvent dipole orientation, 138
on Tafel slopes, 103
- Terraces, 19
- Theoretical, dye effects in SERS, 344
- Theoretical models, of SERS effect, 322
- Thermodynamic stability, of semiconductor electrodes, 229
- Transfer coefficient, α , 115
independence on temperature, 127, 131
potential dependence of, 148
relation to β , 115
- Temperature dependence of β or α
conclusions on, 182
theoretical, 132
- Transport properties
in ion-exchange membranes, 470
of ion-exchange membranes, 437
- Tunneling
of hot electrons at semiconductor, 235
of protons, 143
- Ulstrup treatment, of electron and particle transfer, 147
- Ultrahigh vacuum
preparation of surfaces for SERS, 285
SERS effects in, 264

- Unit cells
 - coordination numbers for, 18
 - number of surface atoms in, 18
- Vehicle and battery characteristics, 375
- Vehicle batteries
 - performance requirements, 375
 - range between recharge, 375
 - cost factors, 384
 - energy efficiency of, 388
 - environmental factors, 389
 - review on, 371
 - safety factors, 389
 - specific energy requirements, 376
- Vehicular propulsion, batteries for, 371
- Volumetric energy density, of batteries, 379
- Water electrolysis, photoassistance of, 238
- Water
 - SERS effect on, 295
 - state of, in Nafion, 455
- Wave functions, at surfaces, 25
- Well defined surfaces, results at, 3
- Wulff stereographic net, 8
- Zinc battery, 399
- Zinc-halogen battery, 402